

annual progress report

2008

VEHICLE TECHNOLOGIES PROGRAM

**ADVANCED VEHICLE TECHNOLOGY
ANALYSIS AND EVALUATION ACTIVITIES
AND HEAVY VEHICLE SYSTEMS
OPTIMIZATION PROGRAM**



**U.S. Department of Energy
Energy Efficiency and Renewable Energy**

Bringing you a prosperous future where energy is clean, abundant, reliable, and affordable

**U.S. Department of Energy
Vehicle Technologies Program
1000 Independence Avenue, S.W.
Washington, DC 20585-0121**

FY 2008

Annual Progress Report for

Advanced Vehicle Technology Analysis and Evaluation Activities and Heavy Vehicle Systems Optimization Program

Submitted to:

**U.S. Department of Energy
Energy Efficiency and Renewable Energy
Vehicle Technologies Program
Advanced Vehicle Technology Analysis and Evaluation**

Lee Slezak, Technology Manager

CONTENTS

I. INTRODUCTION.....	1
II. MODELING AND SIMULATION.....	9
A. PSAT Model Validation	9
B. Simulation Runs to Support GPRA/PDS.....	14
C. DOE and FreedomCAR Technical Team Support	24
D. PSAT Maintenance and Enhancements.....	28
E. Plug-and-Play Software (Cooperative Research and Development Agreement with General Motors).....	31
F. Validation of the Through-the-Road (TTR) PHEV	34
G. Impact of Drive Cycles on PHEV Component Requirements.....	36
H. Component Technology Impact on PHEV Fuel Efficiency	42
I. Comparison of Powertrain Configuration for Plug-in HEVs on Fuel Efficiency	46
J. Development of Models for Advanced Engines and Emission Control Components.....	51
K. PHEV Value Proposition Study.....	58
L. Enabling High Efficiency Ethanol Engines (Delphi PHEV CRADA)	65
M. Plug-In Hybrid Vehicle Systems Analysis	70
N. Evaluating Route-Based Control of Hybrid Electric Vehicles (HEVs).....	74
O. Renewable Fuel Vehicle Modeling and Analysis.....	77
P. Integrated Vehicle Thermal Management Systems Analysis/Modeling	81
Q. Medium-Duty Plug-in Hybrid Electric Vehicle Analysis	87
R. PSAT Heavy-Duty Vehicle Modeling and Simulation	91
S. Heavy Truck Duty Cycle (HTDC) Project	94
III. INTEGRATION AND VALIDATION	105
A. Battery Hardware-in-the-Loop Testing	105
B. MATT/Component Hardware-in-the-Loop Testing	110
C. Active Combination of Ultracapacitors with Batteries for PHEV ESS.....	140
D. PHEV Development Platform — Through-the-Road Parallel PHEV	151
IV. LABORATORY TESTING AND BENCHMARKING	169
A. Benchmarking and Validation of Hybrid Electric Vehicles	169
B. Benchmarking of Plug-In Hybrid Electric Vehicles.....	177
C. PHEV Test Methods and Procedures Development.....	183
D. Advanced Hydrogen Vehicle Benchmarking	187

CONTENTS (CONT.)

E. Maintain an On-Line HEV Test Results Database	193
V. OPERATIONAL AND FLEET TESTING.....	197
A. Hybrid Electric Vehicle Testing	197
B. Plug-in Hybrid Electric Vehicle Testing by DOE's Advanced Vehicle Testing Activity (AVTA)	203
C. Hydrogen Internal Combustion Engine (ICE) Vehicle Testing	225
D. Neighborhood Electric Vehicle Testing	228
E. Advanced Technology Medium and Heavy Vehicles Testing	231
VI. AERODYNAMIC DRAG REDUCTION.....	239
A. DOE Project on Heavy Vehicle Aerodynamic Drag	239
B. Investigation of a Trailer Underbody Fairing for Heavy Vehicle Aerodynamic Drag Reduction.....	241
VII. THERMAL MANAGEMENT	251
A. Efficient Cooling in Engines with Nucleate Boiling	251
B. Erosion of Materials in Nanofluids.....	261
C. Integrated Underhood and Aerodynamic Analysis.....	265
D. CoolCab – Truck Thermal Load Reduction Project.....	268
VIII. FRICTION AND WEAR.....	277
A. Boundary Lubrication Mechanisms.....	277
B. Parasitic Energy Loss Mechanisms	283
C. Superhard Coatings.....	290
D. Residual Stresses in Thin Films.....	295

I. INTRODUCTION

On behalf of the U.S. Department of Energy's Vehicle Technologies (VT) Program, I am pleased to submit the Annual Progress Report for fiscal year 2008 for the Advanced Vehicle Technology Analysis and Evaluation (AVTAE) team activities.

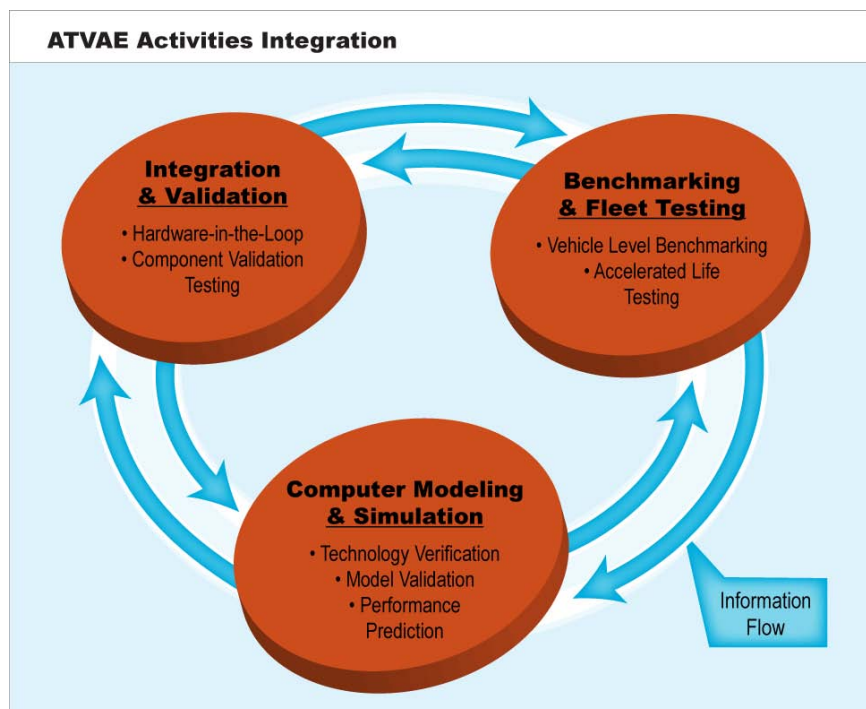
Mission

The AVTAE team's mission is to evaluate the technologies and performance characteristics of advanced automotive powertrain components and subsystems in an integrated vehicle systems context, covering light to heavy platforms. This work is directed toward evaluating and verifying the targets of the VT technology R&D teams and to providing guidance in establishing roadmaps for achievement of these goals.

Objective

The prime objective of the AVTAE team activities is to evaluate VT Program targets and associated data that will enable the VT technology R&D teams to focus research on areas that will maximize the potential for fuel efficiency improvements and tailpipe emissions reduction. AVTAE accomplishes this objective through a tight union of computer modeling and simulation, integrated component testing and emulation, and laboratory and field testing of vehicles and systems. AVTAE also supports the VT Program goals of fuel consumption reduction by developing and evaluating the enabling of vehicle system technologies in the area of light vehicle ancillary loads reduction.

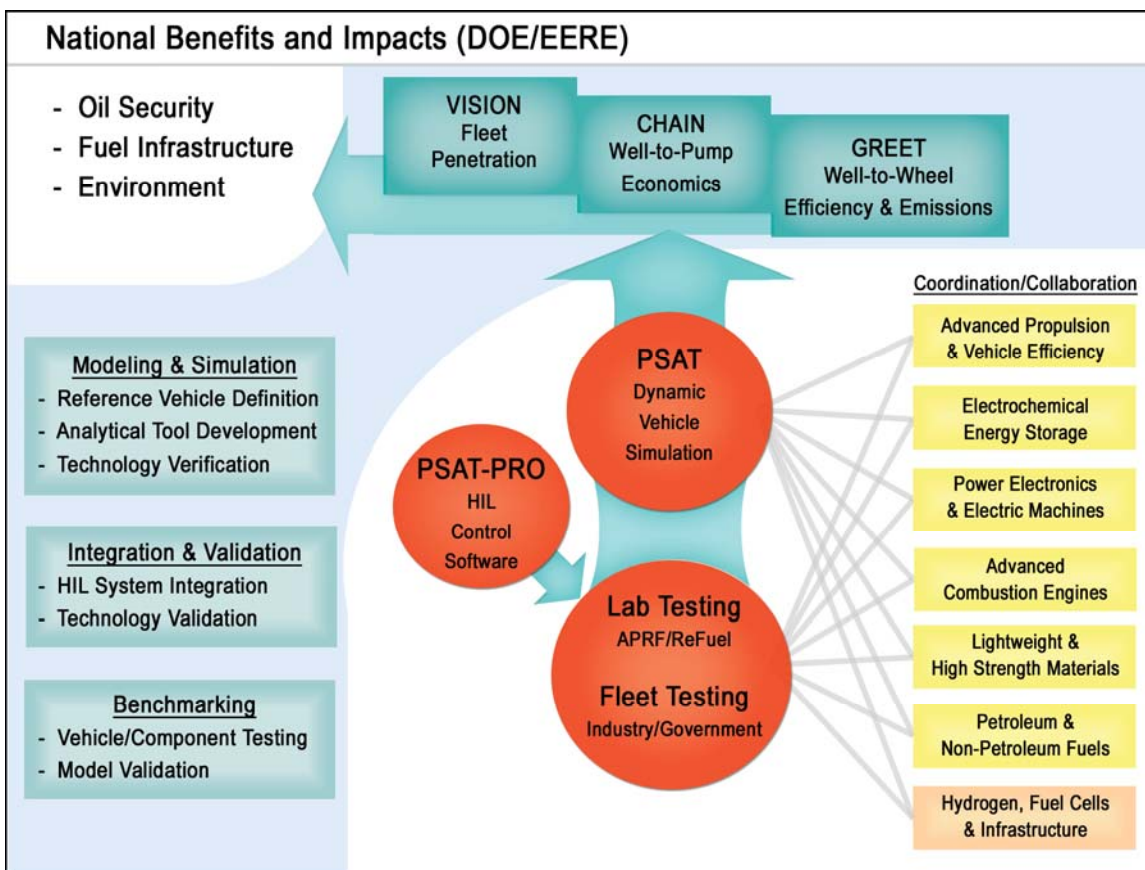
The integration of computer modeling and simulation, hardware-in-the-loop testing, vehicle benchmarking, and fleet evaluations is critical to the success of the AVTAE team. Each respective area feeds important information back into the other, strengthening each aspect of the team. A graphical representation of this is shown in the figure below.



Integration of AVTAE Computer Modeling and Testing Activities

FY 2008 AVTAE Activities

AVTAE provides an overarching vehicle systems perspective in support of the technology R&D activities of DOE's VT and Hydrogen, Fuel Cells & Infrastructure Technologies (HFCIT) Programs. AVTAE uses analytical and empirical tools to model and simulate potential vehicle systems, validate component performance in a systems context, verify and benchmark emerging technology, and validate computer models. Hardware-in-the-loop testing allows components to be controlled in an emulated vehicle environment. Laboratory testing then provides measurement of progress toward VT technical goals and eventual validation of DOE-sponsored technologies at the Advanced Powertrain Research Facility for light- and medium-duty vehicles and at the ReFUEL Facility for heavy-duty vehicles. For this sub-program to be successful, extensive collaboration with the technology development activities within the VT and HFCIT Programs is required for both analysis and testing. Analytical results of this sub-program are used to estimate national benefits and/or impacts of DOE-sponsored technology development, as illustrated in the figure below.



AVTAE Activities Providing Estimates of National Benefits and Impacts of Advanced Technologies

AVTAE is comprised of the following seven (7) main focus areas, each of which is described in detail in this report:

1. Modeling and Simulation

A unique set of tools has been developed and is maintained to support VT research. VISION, CHAIN, and GREET are used to forecast national-level energy and environmental parameters including oil use, infrastructure economics, and greenhouse gas contributions of new technologies, based on VT vehicle-level simulations that predict fuel economy and emissions using the Powertrain System Analysis Toolkit (PSAT) modeling tool. Dynamic simulation models (i.e., PSAT) are combined with DOE's specialized equipment and facilities to validate DOE-sponsored technologies in a vehicle context (i.e., PSAT-PRO control code and actual hardware components in a virtual vehicle test environment). Modeling and testing tasks are closely coordinated to enhance and validate models as well as to ensure that laboratory and field test procedures and protocols comprehend the needs of coming technologies.

PSAT (Powertrain System Analysis Toolkit) allows dynamic analysis of vehicle performance and efficiency to support detailed design, hardware development, and validation. A driver model attempts to follow a driving cycle, sending a torque demand to the vehicle controller, which, in turn sends a demand to the propulsion components (commonly referred to as "forward-facing" simulation). Dynamic component models react to the demand (using transient equation-based models) and feed back their status to the controller. The process iterates on a sub-second basis to achieve the desired result (similar to the operation of a vehicle). The forward architecture is suitable for detailed analysis of vehicles/propulsion systems, and the realistic command-control-feedback capability is directly translatable to PSAT-PRO control software for testing in the laboratory. Capabilities include transient performance, efficiency and emissions (conventional, hybrid, plug-in hybrid, and fuel cell vehicles), development and optimization of energy management strategies, and identification of transient control requirements.

PSAT-PRO (PSAT rapid control PROtototyping software) allows dynamic control of components and subsystems in Rapid Control Prototyping (RCP) or hardware-in-the-loop (HIL) testing. Hardware components are controlled in an emulated vehicle environment (i.e., a controlled dynamometer and driveline components) according to the control strategy, control signals, and feedback of the components and vehicle as determined using PSAT. The combination of PSAT-PRO and RCP/HIL is suitable for propulsion system integration and control system development, as well as rigorous validation of control strategies, components, or subsystems in a vehicle context (without building a vehicle). Capabilities include transient component, subsystem, and dynamometer control with hardware operational safeguards compatible with standard control systems.

2. Integration and Validation

Hardware-in-the-loop (HIL) simulation provides a novel and cost effective approach to evaluating advanced automotive component and subsystem technologies. HIL allows actual hardware components to be tested in the laboratory at a full vehicle level without the extensive cost and lead time for building a complete prototype vehicle. This task integrates modeling and simulation with hardware in the laboratory to develop/evaluate propulsion subsystems in a full vehicle level context.

In this initiative, a versatile Mobile Automotive Technology Testbed (MATT) has been developed. MATT serves as a unique HIL platform for advanced powertrain technology evaluation in an emulated vehicle environment. The flexible chassis testbed allows researchers to easily replace advanced components or change the architecture of the powertrain in various hybrid configurations. MATT has been developed to assist DOE in validating advanced technology. As the VT Program matures, the need to evaluate newly developed technology in a vehicle system context will become critical. Through the FreedomCAR and Fuels Partnership Vehicle System Analysis Technical Team (VSATT), MATT facilitates interactions between each of the other technical

teams by providing a common platform for component integration and testing. Each specific set of technical targets and their impacts on the vehicle system can easily be studied using the MATT platform.

High energy traction battery technology is important to the successful development of plug-in hybrid electric vehicles. In support of plug-in hybrid electrical vehicle (PHEV) research, Argonne National Laboratory (ANL) has developed and implemented a battery hardware-in-the-loop simulator to test potential battery packs in vehicle level operating conditions. In FY 2008, the battery HIL was used to complete evaluation of a JCS 41 amp*hr lithium ion battery. Evaluation of hydrogen internal combustion engine (H₂-ICE) technology potential within hybrid vehicle architectures was performed using MATT starting in FY 2006. In preparation, ANL expanded its hydrogen engine testing and calibration capabilities by building a hydrogen engine test cell. Work is underway to adapt and optimize the engine control to the hybrid vehicle environment, providing a sound integration and enabling this technology to be validated in a suitable hybrid vehicle context.

3. Laboratory Testing and Benchmarking

This section describes the activities related to laboratory validation of advanced propulsion subsystem technologies for advanced vehicles. In benchmarking, the objective is to extensively test production vehicle and component technology to ensure that VT-developed technologies represent significant advances over technologies that have been developed by industry. Technology validation involves the testing of DOE-developed components or subsystems to evaluate the technology in the proper systems context. Validation helps to guide future VT programs and facilitates the setting of performance targets.

Validation and benchmarking require the use of internationally accepted test procedures and measurement methods. However, many new technologies require adaptations and more careful attention to specific procedures. ANL engineers have developed many new standards and protocols, which have been presented to a wide audience such as FreedomCAR partners, other government laboratories, and the European Commission.

To date, more than 100 PHEVs, HEVs, fuel cell vehicles, and propulsion subsystem components have been benchmarked or validated by ANL staff. The propulsion system hardware components (batteries, inverters, electric motors, and controllers) are further validated in simulated vehicle environments to ensure that they will meet the vehicle performance targets established by the government-industry technical teams.

The major facility that supports these activities is the Advanced Powertrain Research Facility (APRF), a state-of-the-art automotive testing laboratory operated by ANL. A multi-dynamometer facility for testing components (such as engines and electric motors), it has a four-wheel vehicle dynamometer that allows accurate testing of all types of powertrain topologies. During 2004, the quality of lab data was validated by correlating results with Ford's Allen Park vehicle test facility using one of their Ford Explorer correlation vehicles. ANL now has its own correlation vehicle for test repeatability.

4. Operational and Fleet Testing

The Advanced Vehicle Testing Activity (AVTA), working with industry partners, accurately measures real-world performance of advanced technology vehicles via a testing regime based on test procedures developed with input from industry and other stakeholders. The performance and capabilities of advanced technologies are benchmarked to support the development of industry and DOE technology targets. The testing results provide data for validating component, subsystem, and vehicle simulation models and hardware-in-the-loop testing. Fleet managers and the public use the test results for advanced technology vehicle acquisition decisions. Idaho National Laboratory (INL) conducts light-duty testing activities in partnership with an industry group led by Electric Transportation Applications (ETA). Accelerated reliability testing provides reliable benchmark data of the fuel economy, operations and maintenance requirements, general vehicle performance, engine and component (such as energy storage system) life, and life-cycle costs.

The AVTA performs three types of tests depending on the vehicle technology, end-use application, and the needs of the testing partner; the tests are described below.

Baseline Performance Testing

The objective of baseline performance testing is to provide a highly accurate snapshot of a vehicle's performance in a controlled testing environment. The testing is designed to be highly repeatable. Hence it is conducted on closed tracks and dynamometers, providing comparative testing results that allow "apple-to-apple" comparisons within respective vehicle technology classes. The APRF at ANL is utilized for the dynamometer testing of the vehicles.

Fleet Testing

Fleet testing provides a real-world balance to highly controlled baseline performance testing. Some fleet managers prefer fleet testing results to the more controlled baseline performance or the accelerated reliability testing.

During fleet testing, a vehicle or group of vehicles is operated in normal fleet applications. Operating parameters such as fuel-use, operations and maintenance, costs/expenses, and all vehicle problems are documented. Fleet testing usually lasts one to three years and, depending on the vehicle technology, between 3,000 and 25,000 miles are accumulated on each vehicle.

For some vehicle technologies, fleet testing may be the only available test method. Neighborhood electric vehicles (NEVs) are a good example. Their manufacturer-recommended charging practices often require up to 10 hours per charge cycle, while they operate at low speeds (<26 mph). This makes it nearly impossible to perform accelerated reliability testing on such vehicles.

Under fleet testing, idle reduction demonstration and evaluation focuses on data collection, cost reduction, and education and outreach activities to overcome barriers to the implementation of idle reduction technologies in heavy-duty trucks. Data collection and demonstration activities include evaluation of fuel consumption, cost, reliability and durability, engine and accessory wear, and driver impressions. Cost reduction activities are focusing on development and evaluation of advanced idle reduction technologies for on-line, factory installation.

Accelerated Reliability Testing

The objective of accelerated reliability testing is to quickly accumulate several years or an entire vehicle-life's worth of mileage on each test vehicle. The tests are generally conducted on public roads and highways, and testing usually lasts for up to 36 months per vehicle. The miles to be accumulated and time required depend heavily on the vehicle technology being tested. For instance, the accelerated reliability testing goal for PHEVs is to accumulate 5,400 miles per vehicle. The testing goal for HEVs is to accumulate 160,000 miles per vehicle within three years. This is several times greater than most HEVs will be driven in three years, but it is required to provide meaningful vehicle-life data within a useful time frame. Generally, two vehicles of each model are tested to ensure accuracy. Ideally, a larger sample size than two would be tested, but funding tradeoffs necessitate testing only two of each model to ensure accuracy.

Depending on the vehicle technology, a vehicle report is completed for each vehicle model for both fleet and accelerated reliability testing. However, because of the significant volume of data collected for the HEVs, fleet testing fact sheets (including accelerated reliability testing) and maintenance sheets are provided for the HEVs.

5. Aerodynamic Drag Reduction for Heavy Duty Vehicles

The primary goal is to reduce Class 8 tractor-trailer aerodynamic drag for a significant impact on fuel economy while satisfying regulation and industry operational constraints. An important part of this effort is to expand and coordinate industry collaborations for DOE and establish buy-in through CRADAs and to accelerate the introduction of proven aerodynamic drag reduction devices to public.

The Lawrence Livermore National Laboratory (LLNL) approach to drag reduction is through the control of the tractor-trailer flow field and tractor-trailer integration. This will be achieved with geometry modifications, integration, and flow conditioning. These are essential components to develop and design the next generation of aerodynamically integrated tractor-trailer.

To accomplish this goal, we have established a unique team of experts from industry, university, and government laboratories to perform a full-scale (80'x120') wind tunnel test at NFAC/NASA Ames research facility. The number of drag reducing aerodynamic devices/concepts will be tested in addition to aerodynamic impact of low rolling resistance super single tires from Michelin. Three flow regions around the heavy vehicle are explored: trailer base, underbody, and tractor-trailer gap for application of drag reducing add-on devices. Many add-on devices will be tested, with two different tractors (standard and long sleeper) and three different trailers (28', 53', and 53' drop frame) for their individual performance and in combination with other devices.

6. Thermal Management for Heavy Duty Vehicles

Thermal management of heavy vehicle engines and support systems is a technology that addresses reduction in energy usage through improvements in engine thermal efficiency and reductions in parasitic energy uses and losses. Fuel consumption is directly related to the thermal efficiency of engines and support systems. New thermal management technologies with the potential for high impact on energy reduction are investigated and developed under this program. Technologies are targeted that can increase the percentage of mechanical work extracted from the combustion process and decrease the heat rejection to the environment. Some technologies affect thermal efficiency directly while others reduce energy usage including, but not limited to, such areas as: reduction in weight, reduced size of auxiliary engine systems, reduction in power consumption of auxiliary systems, and reduced aerodynamic drag.

Components of this interrelated program, which are briefly described in the following paragraphs, include development and characterization of nanofluids, experimental measurements and theoretical analysis of heat transfer characteristics of nanofluids, investigation of the erosion effects of nanofluids, and work on evaporative cooling. ANL collaborators include Michelin, Saint Gobain, Cummins, PACCAR, and TARDEC.

Development and Characterization of Nanofluids

The aim of this project is to develop the required chemistry to produce nanofluids with the largest enhancement of thermal conductivities. Addition of nanoparticles to a coolant (typically 50/50 ethylene glycol/water mixture) increases viscosity so that considerable effort is devoted to viscosity modifications. Additionally, the effects of nanoparticle material, size, volume concentration, suspension properties, and shape are explored because these properties determine the effectiveness of the coolant. These properties are investigated over a range of temperatures. Experimental results are compared with existent theories that are modified if necessary.

Heat Transfer

The most important property of a coolant is most likely its heat transfer coefficient. The heat transfer coefficients are determined for turbulent flow in a unique ANL-designed and built horizontal stainless steel tube apparatus. The experimental turbulent Reynolds number typically ranges from 3,000 to 13,000 with a Prandtl number range of 4.6 to 7.1, a velocity range of 1.8 to 5.4 m/s, and a nanofluid temperature range of 34 to 57°C. Results are compared to predictions from standard correlations for liquids, and the correlations are modified if necessary.

Erosion

Nanofluids could potentially erode radiator materials. This experiment is designed to measure the material wastage of typical radiator materials and an automotive pump using very controlled conditions. Additionally, the power required to pump nanofluids can be measured and compared to power required to pump coolants without nanoparticles.

Nucleated Boiling

It is well known that boiling heat transfer coefficients are much higher than the convective heat transfer coefficient of the same fluid. However, in order to use boiling fluids for cooling a truck radiator, the critical heat flux (CHF) must be avoided or severe damage would occur. Hence, this program is designed to measure the heat transfer coefficient and CHF of several possible coolants, compare the results to theories, and transfer the data to industry.

7. Friction and Wear for Heavy Duty Vehicles

Parasitic engine and driveline energy losses arising from boundary friction and viscous losses consume 10 to 15 percent of fuel used in transportation, and thus engines and driveline components are being redesigned to incorporate low-friction technologies to increase fuel efficiency of passenger and heavy-duty vehicles. The Friction and Wear Project, within the Heavy Vehicle Systems Optimization Program, supports research agreements/projects that focus on the development of advanced technologies required to improve the fuel efficiency and reliability of critical engine and driveline components, notably:

- Activities to experimentally investigate fundamental friction and wear mechanisms to provide the understanding required for developing advanced low-friction, fuel-efficient technologies.
- Activities to model and validate, component-by-component, the impact of friction on overall vehicle efficiency.
- Activities to develop advanced low friction technologies (materials, coatings, engineered surfaces, and advanced lubricants) required to improve engine and driveline efficiency and reliability/durability.

Boundary Layer Lubrication

Researchers at ANL made significant progress on the development of modeling scuffing phenomena and the formation of protective tribofilms. In the first task, material pairs with a high CSI (contact severity index – a measure of resistance to scuffing) were evaluated. The mechanisms for scuffing in these material pairs were elucidated, providing a pathway for further improvement in scuffing resistance. The development of materials with enhanced scuffing resistance will facilitate the development of high-power-density components and systems. The second task involved characterization of low-friction boundary films produced from a model lubricant and fully formulated lubricant. Post-test analysis of the films by SEM, EDX, and FIB is ongoing. These analyses will provide information on the thickness, composition, and structure of highly desirable low-friction boundary films.

Parasitic Energy Losses

At ANL, researchers continued to use computer simulations of parasitic energy losses in diesel engines to guide fundamental research on low friction coatings and additive treatments. Work is underway to experimentally validate the models by tests with a fired, single-cylinder diesel rig outfitted with an instrumented fixed-sleeve to measure the friction forces continuously as a function of crank angle. A piston component test rig was developed and brought on-line to validate the friction coefficient data used to model the parasitic friction losses, as well as to optimize advanced surface modification technologies for engine applications. Tests are underway to evaluate two technologies: a boric-acid-based lubricant additive and a surface texturing technique.

Laboratory tests using the ring-on-liner rig indicated that friction can be significantly reduced by using boric-acid based additives.

Hard/Superhard Nanocomposite Coatings

Researchers at ANL focused their effort toward further optimization and scale-up of ANL's superhard coating technology. In collaboration with a commercial coating company, ANL researchers produced superhard coatings on commercial-scale deposition systems and performed extensive tests to determine their mechanical and tribological properties. They also performed surface and structure analytical studies on the coatings produced on the commercial system to determine their structural morphology and chemical compositions. Tribological tests of such coatings at ANL confirmed their extreme resistance to wear and scuffing. Near-term future activities

will focus on applying the coatings to a large variety of engine components (tappets, valve lifters, fuel injectors, piston rings, etc.) and testing them in actual engines.

Major projects conducted by the national laboratories in support of these areas in FY 2008 are described in this report. A summary of the major activities in each area is given first, followed by detailed reports on the approach, accomplishments, and future directions for the projects. For further information, please contact the DOE Project Leader named for each project.

Future Directions for AVTAE

Near-term solutions for reducing the nation's dependence on imported oil, such as PHEV, will require the development of vehicle components, subsystems, and support systems. These solutions will require exploration of high capacity energy storage and propulsion system combinations to get the most out of hybrid propulsion. Analysis and testing procedures at the national labs will be enhanced to enable the study of these advanced powertrains with simulation tools, component/subsystem integration, and hardware-in-the-loop testing. DOE-sponsored hardware developments will be validated at the vehicle level, using a combination of testing and simulation procedures.

In FY 2009, the AVTAE will continue to expand activities in the area of PHEV simulation and evaluation, including further baseline performance testing of conversion and original equipment manufacturer (OEM) PHEVs and validation of simulation models for PHEVs tested in the APRF. Field and laboratory testing will continue to be integrated with modeling/ simulation tools. Fleet evaluation of PHEV conversion vehicles will continue; however, emphasis will be placed on establishing evaluation fleets of OEM production PHEVs. In FY 2008, DOE VT issued a solicitation for the purpose of establishing a PHEV demonstration fleet consisting of large volume manufacturers and OEMs as participants. This program will launch in FY 2009 and last for approximately four years. Deviation of test procedures for PHEVs will be completed. Work will focus on validation of these procedures. Heavy vehicle systems optimization work in the areas of aerodynamics, thermal management, and friction and wear will continue. Work on a revised vehicle cost model incorporated into PSAT will continue in FY 2009. Although the development of light vehicle simulation models will be essentially completed, the vehicle and component models, as well as their respective control strategies, will continually be updated and enhanced to reflect the progress of technology in the transportation sector. Validation of VT technologies for advanced power electronics, energy storage, and combustion engines will be ongoing as each technology progresses towards the targeted performance.

Inquiries regarding the AVTAE activities may be directed to the undersigned.



Lee Slezak

Technology Manager

Advanced Vehicle Technology Analysis and Evaluation

Vehicle Technologies Program

II. MODELING AND SIMULATION

A. PSAT Model Validation

Namdo Kim (Project Leader), Aymeric Rousseau

*Argonne National Laboratory
9700 South Cass Avenue*

*Argonne, IL 60439-4815
(630) 252-7261; arousseau@anl.gov*

DOE Technology Manager: Lee Slezak

(202) 586-2335; Lee.Slezak@ee.doe.gov

Objectives

Use test data to develop a controller in PSAT for the GM Tahoe Hybrid models that replicates the observed vehicle behavior.

Approach

Gather component test data.

Determine validation criteria.

Tune each component model by using vehicle test data.

Use test data and various curve fitting, clustering, and optimization methods to force the simulated controller to replicate the behavior of the vehicle.

Understand the limitations on the accuracy of the modeling technique.

Accomplishments

Integrated component models into PSAT.

Developed control strategy on the basis of vehicle test data.

Validated vehicle model by using several driving cycles.

Future Directions

Continue to validate PSAT by using test data from Argonne National Laboratory's Advanced Powertrain Research Facility.

Introduction

Argonne National Laboratory's (ANL) Advanced Powertrain Research Facility (APRF) is the principal U.S. Department of Energy (DOE) facility for assessing advanced and hybrid electric vehicle (HEV) technologies for the Vehicle Technologies (VT) Program. The APRF is an integrated multi-dynamometer vehicle and component facility used for testing conventional and hybrid vehicle

propulsion systems and vehicles (two- or four-wheel drive), using a variety of fuels (including hydrogen), in a precise laboratory environment. The facility is used to assess powertrain technology for light- and medium-duty propulsion systems with state-of-the-art performance and emissions measurement equipment and techniques.

PSAT is designed to serve as a single tool that can be used to meet the requirements of automotive

engineering throughout the development process, from modeling to control. Because of time and cost constraints, engineers cannot build and test each of the many possible powertrain configurations for advanced vehicles. PSAT, a forward-looking model, offers the ability to quickly compare several powertrain configurations.

Vehicle Test Data Analysis

To validate the vehicle model, a generic process described in Figure 1 has been used. First, the test data from a text file are imported into a Matlab environment following a PSAT format. Then, each parameter is analyzed, the redundant signals are compared, and the missing signals are calculated.

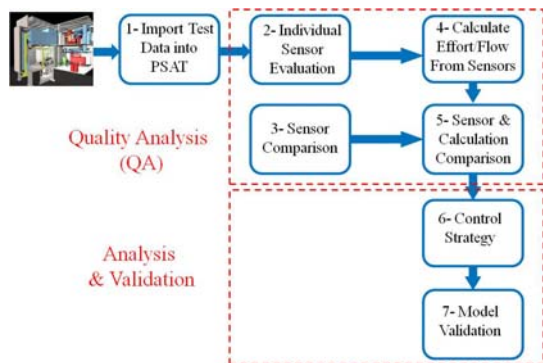


Figure 1. Test Data Analysis Process

Figure 2 shows the main parameters used for the validation process, as well as their origin: sensor, CAN, calculated, and dynamometer. The main issue related to the validation process was the torque and current of both electric machines. Because this information is located on a different bus in the vehicle, it was not accessible during testing.

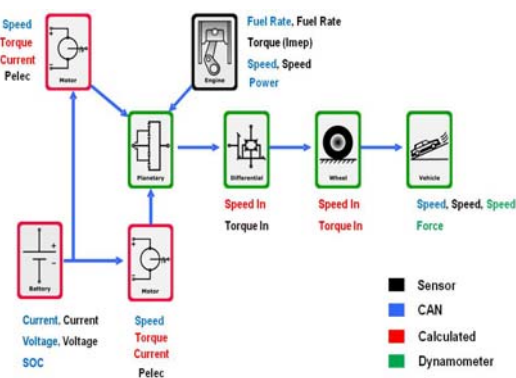


Figure 2. Main Sensor List and Source

To calculate these critical parameters, several options were investigated. First, an algorithm was developed to minimize the losses of the electric machines at every test point. Depending on each mode, calculations were performed on the basis of torque loss maps. The results were consistent with our expectations, and the comparison with the electrical battery power was acceptable.

A second option considered was the use of the power ratio of the Yokagawa instrument. The Yokagawa was used to measure the electrical power of both electrical machines, but the raw measurement could not be used because of a lack of transients. However, the split between the electrical powers was consistent with our expectations. Figure 3 shows the comparison between the calculated electrical power and measured battery power for both electric machines.

Because both approaches showed similar behavior, the last one was chosen because we used an estimated electric machine torque loss map.

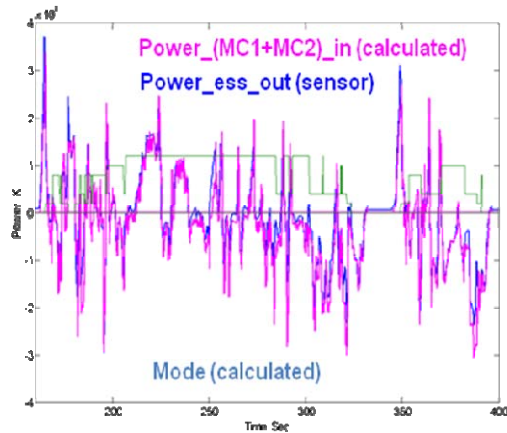


Figure 3. Comparison between Calculated Electrical Power for both Electric Machines with Measured Battery Power

Control Strategy Development

One of the major challenges of the two-mode control strategy is to properly select the operating mode. Although instantaneous optimization is used in the Tahoe, a rule-based approach was used. Because we do not currently have all of the component data, we assumed it would be more accurate to use that approach until more information is gathered.

Figure 4 shows the operating mode from ANL's APRF test data. The vehicle operates in the input split mode (Lo Mode) and compound mode (Hi Mode), as well as on the four fixed gear ratio.

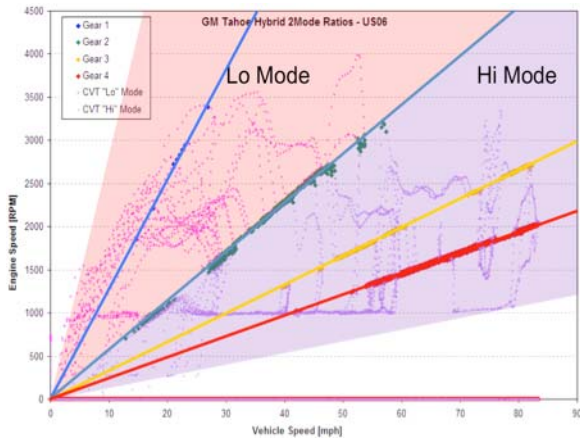


Figure 4. Operating Mode from Test Data

The first step of the validation process was to define the mode in which we were operating at any particular time. Once this analysis was performed, a control logic was defined to select the proper mode on the basis of the operating conditions of the vehicle. Figure 5 shows the comparison between the mode calculated from test data and the ones from PSAT simulations.

As shown in Figure 4, it is important to notice that, while in a particular mode, only a few options are available. For example, when operating in input split, only the first gear can be selected, unless the vehicle speed increases, and then the second gear or the compound mode can be used. The main parameters used to define the transitions between each mode are:

- Torque demand at the wheel
- Engine speed
- Vehicle speed
- Mechanical points

The transition between one mode to the next is performed only if the logic is true for a specific duration to avoid any oscillations. Figure 5 shows the comparison between the modes during test and simulation.

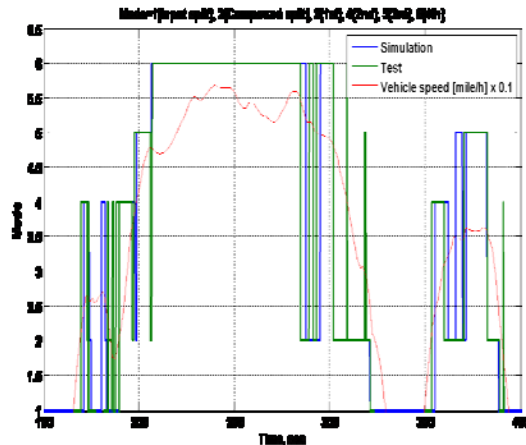


Figure 5. Operating Mode Comparison - UDDS

Comparison between Simulation and Test Data

As for any validation process, we started by comparing the operating conditions of each component, assuming that if the torque and speeds of the engine and both electric machines match the test data, the simulated fuel consumption and the battery state-of-charge would match the vehicle test data.

Figure 6 shows the measured and simulated engine speed on a portion of the urban dynamometer driving schedule (UDDS). Note that both speeds are close, with the main discrepancies occurring during input and compound modes.

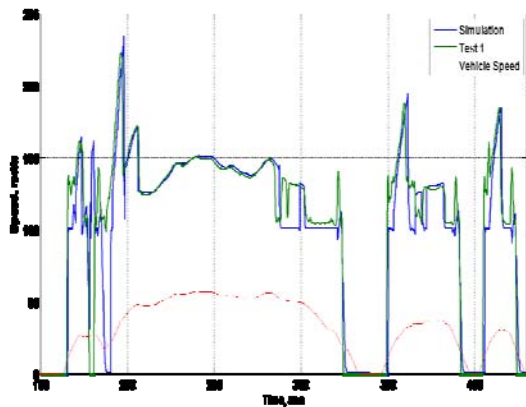


Figure 6. Engine Speed Comparison - UDDS

Figure 7 compares both engine torques. Although the general behaviors are consistent, the test data yielded higher transients. This behavior will be investigated because higher torque transients would increase emissions.

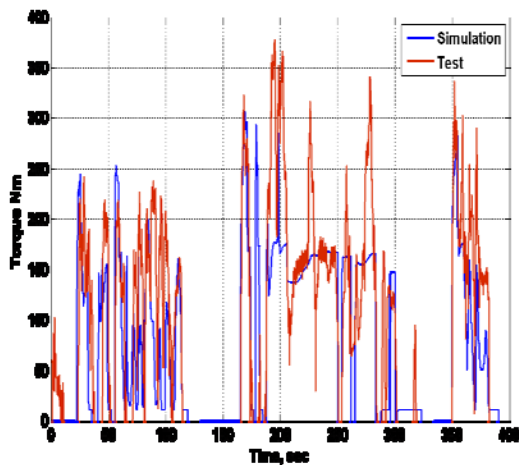
**Figure 7. Engine Torque Comparison - UDDS**

Figure 8 shows both simulated and measured speeds of motor 1. Because the modes are properly matched and the engine speed matches the test data well, the motor speed behavior is expected to be close to the test data.

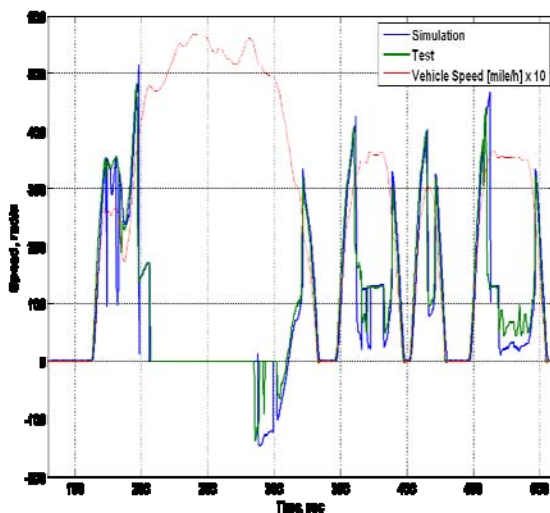
**Figure 8. Motor 1 Speed Comparison - UDDS**

Figure 9 provides the motor 1 torque comparison. This graph, along with the torque validation of motor 2, should be carefully examined because the values from the test data were estimated and not measured. However, with the exception of several spikes occurring from mode changes, both values correlate well.

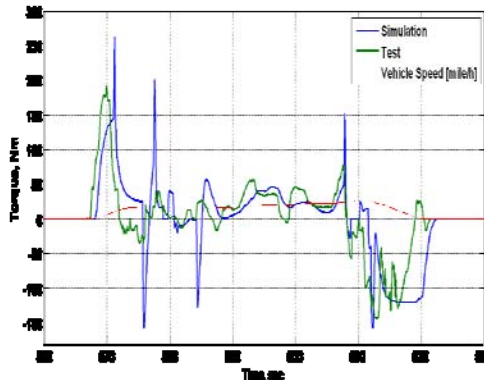
**Figure 9. Motor 1 Torque Comparison – UDDS**

Figure 10 shows close correlation between the simulated and measured speeds of motor 2.

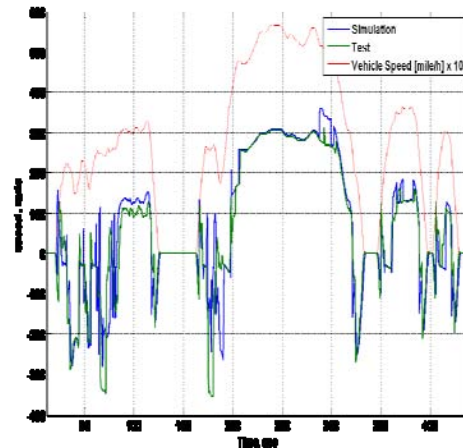
**Figure 10. Motor 2 Speed Comparison - UDDS**

Figure 11 shows the torque comparison for motor 2. This parameter highlights some differences, but it shows good agreement, especially during negative events.

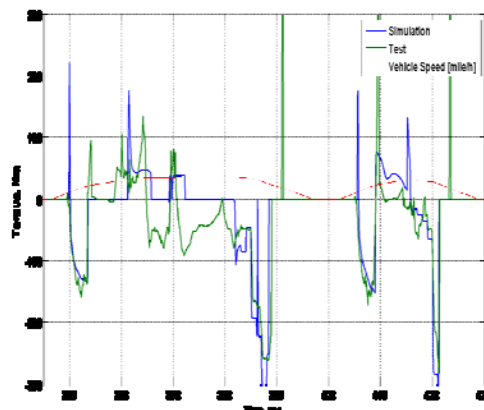
**Figure 11. Motor 2 Torque Comparison - UDDS**

Figure 12 shows the behavior of motor 1 during regenerative braking. Note that the vehicle operates in compound mode up to 20 mph before switching to input mode.

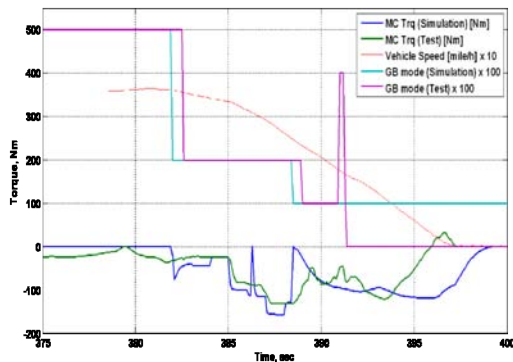


Figure 12. Regenerative Braking – Motor 1 - UDDS

Figure 13 shows the operating conditions of motor 2 during deceleration. Although motor 2 is used to charge the battery in compound mode, it is not used during the input mode.

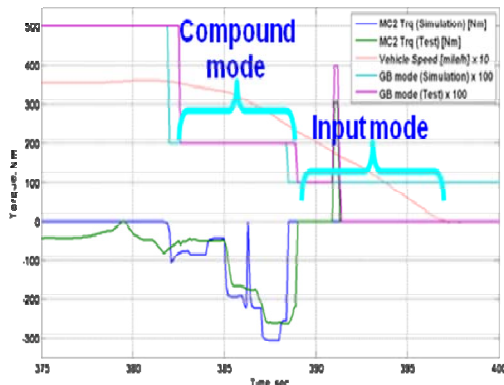


Figure 13. Regenerative Braking – Motor 2 - UDDS

The fuel economy obtained from simulation is 27.9 mpg, with an initial SOC of 56.5 percent and a final value of 60.4 percent. The number of modes enables the two-mode system to displace large amounts of fuel, even though the components are smaller than those for the input split. The consequence is, however, a system that is more complicated to control and validate. Because several component data were estimated (e.g., electric machine torque loss) and critical signals were calculated (e.g., torque and current of both electric machines), it is difficult to understand the origin of the remaining differences between the test and the model.

Conclusion

The GM Tahoe HEV was instrumented and tested at ANL's Advanced Powertrain Research Facility. The test data were analyzed to define the component data. The transmission model was developed on the basis of a bond graph representation of each mode generated from the original schematic of the system. The operating mode logic selection was defined on the basis of the test data, and the component operating conditions within each mode were developed.

The vehicle-level control strategy was developed. Comparison between the measured and simulated engine and electric machine torque and speed showed good correlation. However, some discrepancies remain regarding the fuel economy, most likely the result of uncertainties in component data combined with the control strategy.

Future activities will focus on refining the existing control and developing an instantaneous optimization algorithm to be able to evaluate the potential of the powertrain configuration for other vehicle platforms and component technologies

Publications/Presentations

Kim, N., Carlson, R., Jehlik, F., Rousseau, A., "Tahoe HEV Model Development in PSAT," SAE 09PFL-0612, SAE World Congress, April 2009.

Kim, N., Rousseau, A., "Tahoe HEV Model Development in PSAT," DOE Presentation, Washington DC, June 17 2008.

Kim, N., Rousseau, A., "Tahoe HEV Model Development in PSAT," FreedomCAR Presentation, Detroit, October 1 2008.

B. Simulation Runs to Support GPRA/PDS

Aymeric Rousseau (Project Leader), Antoine Delorme, Sylvain Pagerit, Phil Sharer

Argonne National Laboratory

9700 South Cass Avenue

Argonne, IL 60439-4815

(630) 252-7261; arousseau@anl.gov

DOE Technology Manager: Lee Slezak

(202) 586-2335; Lee.Slezak@ee.doe.gov

Objectives

Simulate multiple vehicle platforms, configurations, and timeframes to provide fuel economy data for analysis in support of the Government Performance and Results Act (GPRA).

Approach

Validate component and vehicle assumptions with DOE National Laboratories and FreedomCAR Technical Teams.

Use automatic component sizing to run the study.

Accomplishments

Simulated and sized more than 700 vehicles.

Simulated new vehicles when assumptions or platforms were revised or when additional configurations or timeframes were requested.

Future Directions

Continue to provide analytical data to support GPRA in 2008.

Introduction

Through its Office of Planning, Budget and Analysis (PBA), the U.S. Department of Energy (DOE) Energy Efficiency and Renewable Energy (EERE) provides estimates of program benefits in its annual Congressional Budget Request. The Government Performance and Results Act (GPRA) of 1993 provides the basis for assessing the performance of Federally funded programs. Often referred to as “GPRA Benefits Estimates,” these estimates represent one piece of EERE’s GPRA implementation efforts—documenting some of the economic, environmental, and security benefits (or outcomes) from achieving program goals. The Powertrain System Analysis Toolkit (PSAT), Argonne National Laboratory’s (ANL) vehicle system analysis tool, was used to evaluate the fuel economy of numerous vehicle configurations

(including conventional vehicles, hybrid electric vehicles [HEVs], plug-in HEVs [PHEVs], and electric vehicles), component technologies (gasoline, diesel, and hydrogen engines, as well as fuel cells), and timeframes (current, 2010, 2015, 2030, and 2045). The uncertainty of each technology is taken into account by assigning probability values for each assumption.

Methodology

To evaluate the fuel efficiency benefits of advanced vehicles, the vehicles are designed on the basis of the component assumptions. The fuel efficiency is then simulated on the urban dynamometer driving schedule (UDDS) and Highway Federal Emissions Test (HWFET). The vehicle costs are calculated from the component sizing. Both cost and fuel efficiency are then used to define the market penetration of each

technology to finally estimate the amount of fuel saved. The process is highlighted in Figure 1. This paper will focus on the first phase of the project: fuel efficiency and cost.



Figure 1. Process to Evaluate Vehicle Fuel Efficiency of Advanced Technologies

To properly assess the benefits of future technologies, several options were considered, as shown in Figure 2:

- Four vehicle classes: midsize car, small SUV, medium SUV, and pickup truck;
- Five timeframes: current, 2010, 2015, 2030, and 2045;
- Five powertrain configurations: conventional, HEV, PHEV, fuel cell HEV, and electric vehicle; and
- Four fuels: gasoline, diesel, ethanol, and hydrogen.

Overall, more than 600 vehicles were defined and simulated in PSAT. The current study does not include micro- or mild hybrids and does not focus on emissions.

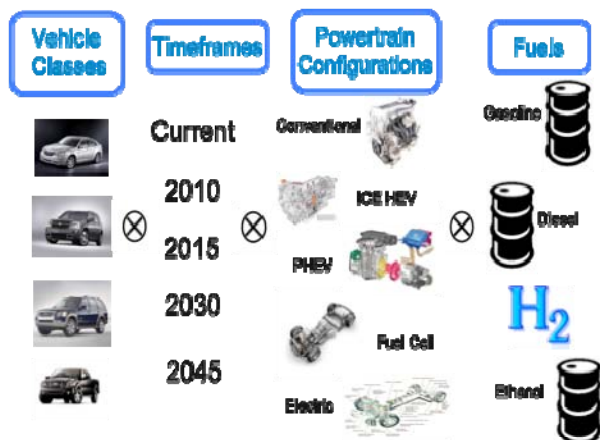


Figure 2. Vehicle Classes, Timeframes, Configurations, and Fuels Considered

To address uncertainties, a triangular distribution approach (low, medium, and high) was employed, as shown in Figure 3. For each component, assumptions were made (e.g., efficiency, power density), and three separate values were defined to represent (1) the 90th percentile, (2) 50th percentile, and (3) 10th percentile. A 90 percent probability means that the technology has a 90 percent chance of being available at the time considered. For each vehicle considered, the cost assumptions also follow the triangular uncertainty. Each set of assumptions is, however, used for each vehicle, and the most efficient components are not automatically the least-expensive ones. As a result, for each vehicle considered, we simulated three options for fuel efficiency. Each of these three options also has three values representing the cost uncertainties.

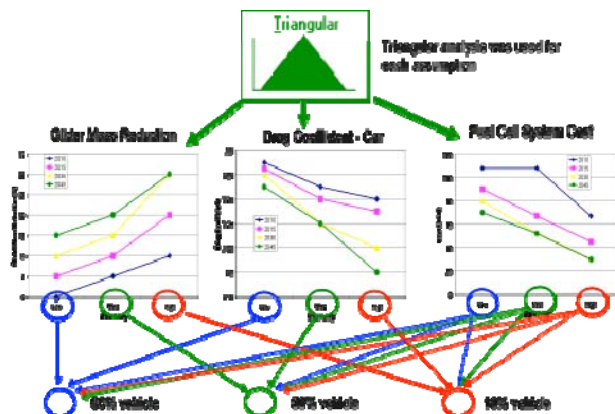


Figure 3. Uncertainty Process

The following describes the assumptions and their associated uncertainties for each component technology.

Vehicle Technology Projections

Engines

Several state-of-the-art engines were selected for the fuels considered: gasoline, diesel, E85 FlexFuel, and hydrogen. Automotive car manufacturers provided gasoline, diesel, and E85 FlexFuel engines used in current conventional vehicles. The port-injected hydrogen engine data were generated at Argonne. The engines used for HEVs and PHEVs are based on Atkinson cycles, generated from test data collected at Argonne's dynamometer testing facility.

Different options were considered when estimating the evolution of each engine technology. Although

linear scaling was used for gasoline and E85 (HEVs application only) and diesel engines, direct injection with linear scaling was considered for the hydrogen-fueled engine, and nonlinear scaling based on AVL's work was used for gasoline and E85 (conventional applications). For the nonlinear scaling, different operating areas were improved by different amounts, which resulted in changing the constant efficiency contours. The peak efficiencies of the different fuels and technologies are shown in Figure 4.

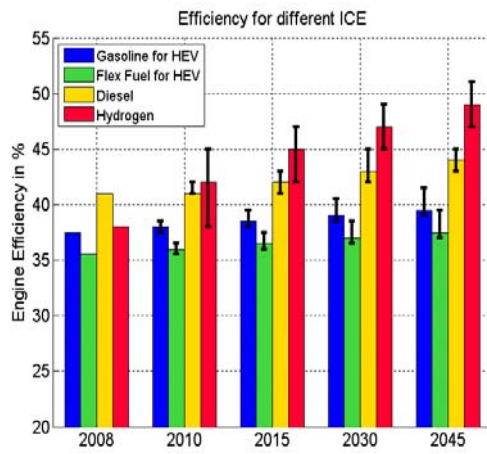


Figure 4. Engine Efficiency Evolution

Fuel Cell Systems

The fuel cell system model is based on the steady-state efficiency map. The values shown in Figure 5 include the balance of plant. The system is assumed to be gaseous hydrogen. In simulation, the additional losses due to transient operating conditions are not taken into account.

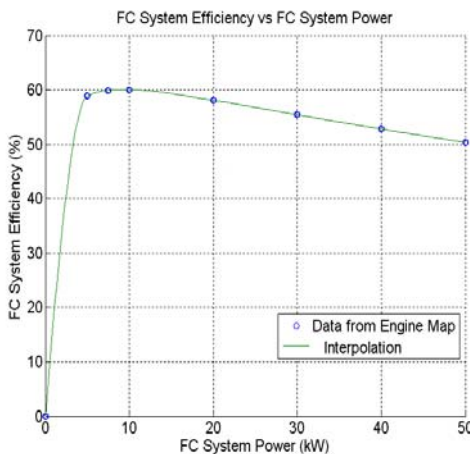


Figure 5. Fuel Cell System Efficiency versus Fuel Cell System Power from the System Map

Figure 6 shows the peak efficiencies of the fuel cell system and its cost. The peak fuel cell efficiency is assumed to be currently at 55 percent and will rapidly increase to 60 percent by 2015. The value of 60 percent has already been demonstrated in laboratories and therefore is expected to be implemented soon in vehicles. The peak efficiencies remain constant in the future as most research is expected to focus on reducing cost. The costs are projected to decrease from \$108/kW currently (values based on high production volume) to an average of \$45/kW in 2030 (uncertainty from \$30/kW to \$60/kW).

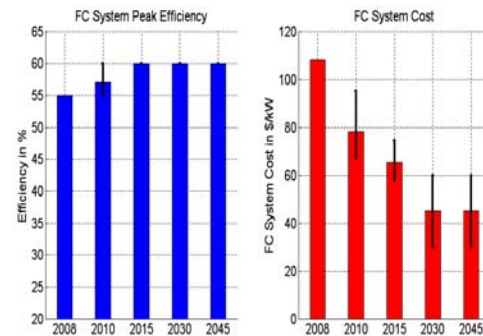


Figure 6. Fuel Cell System Efficiency and Cost

Hydrogen Storage Systems

The evolution of hydrogen storage systems is vital to the introduction of hydrogen-powered vehicles. Figure 7 shows the evolution of the hydrogen storage capacity.

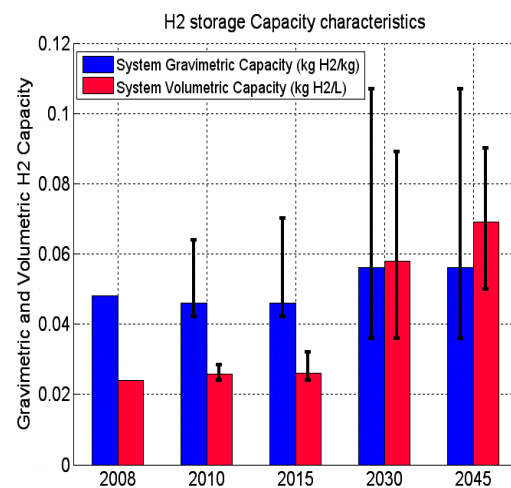


Figure 7. Hydrogen Storage Capacity in Terms of Hydrogen Quantity

One of the requirements for any vehicle in the study is that it must able to travel 320 miles on the combined driving cycle with a full fuel tank. If we wanted to simulate current vehicles with a hydrogen storage system allowing a drive of 320 miles, the amount of hydrogen needed, and thus the corresponding fuel tank mass, would be too large to fit in the vehicles. As a result, different ranges were selected:

- Reference, 2010, and 2015: 190 miles
- 2030 and 2045: 320 miles

Electric Machines

Figure 8 shows the electric machine peak efficiencies considered. The values for the current technologies are based on state-of-the-art electric machines currently used in vehicles. The electric machine data from the Toyota Prius and Toyota Camry were used for the power-split HEV applications, while the Ballard IPT was selected for series fuel cell HEVs. Because the component is already extremely efficient, most of the improvements reside in cost reduction, as shown in Figure 9.

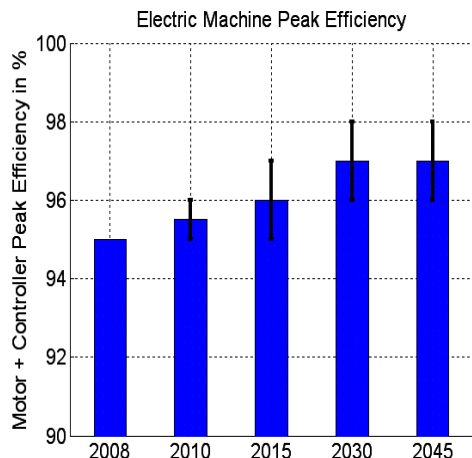


Figure 8. Electric Machine Peak Efficiency

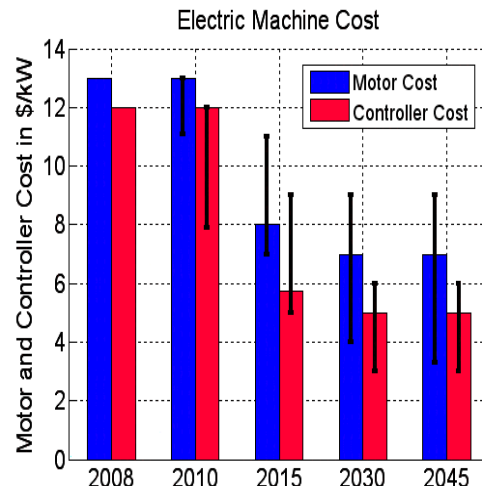
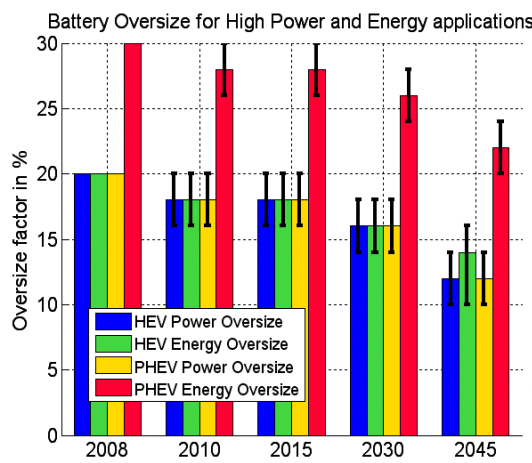
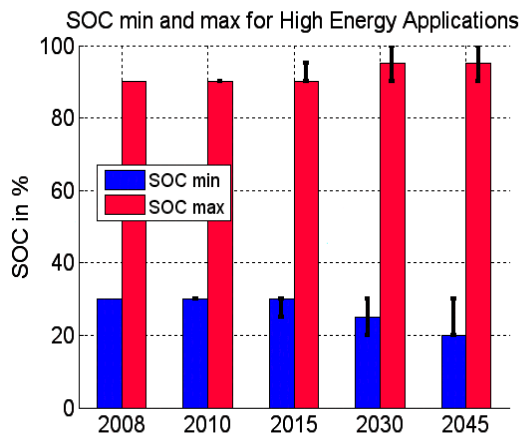


Figure 9. Electric Machine Cost

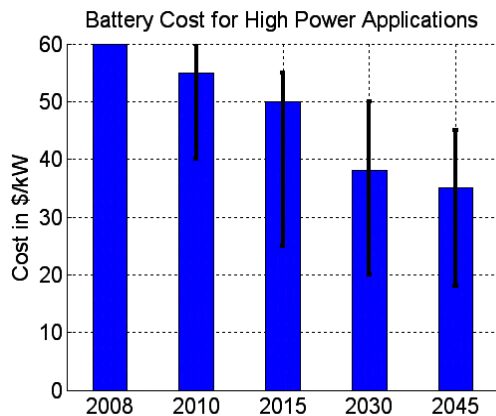
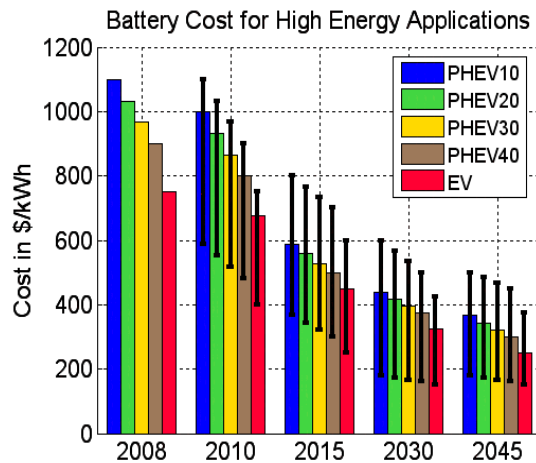
Energy Storage System

Energy storage systems are a key component in advanced vehicles. Although numerous studies are being undertaken with ultracapacitors, only batteries were taken into account in the study. All current vehicles are defined by using NiMH technology. The Li-ion technology is introduced for the high case in 2010 and for the medium and high case in 2015 before becoming the only one considered for later timeframes. For HEV applications, the NiMH is based on the Toyota Prius battery pack, and the Li-ion is based on the 6-A•h battery pack from Saft. For PHEV applications, the VL41M battery pack from Saft has been characterized. Because each vehicle is sized for both power and energy in the case of a PHEV, a sizing algorithm was developed to design the batteries specifically for each application.

To ensure that the battery has similar performance at the beginning and end of life, the packs were oversized both in power and energy, as shown in Figure 10. In addition, for PHEV applications, the State-of-Charge (SOC) window (difference between maximum and minimum allowable SOC) increases over time, allowing a reduction of the battery pack, as shown in Figure 11.

**Figure 10. Battery Oversizing****Figure 11. Battery SOC Window**

Figures 12 and 13 show the cost of the battery packs for both high-power applications (\$/kW) and high-energy applications (\$/kWh).

**Figure 12. High-Power Battery Cost Projections****Figure 13. High-Energy Battery Cost Projections**

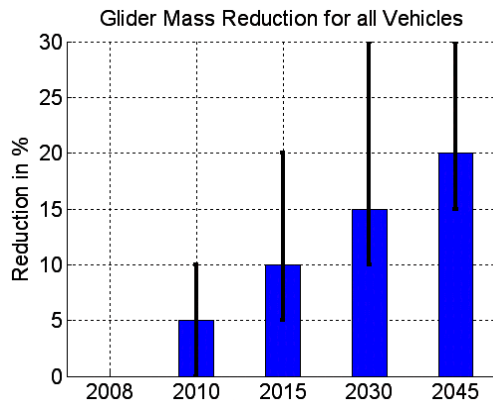
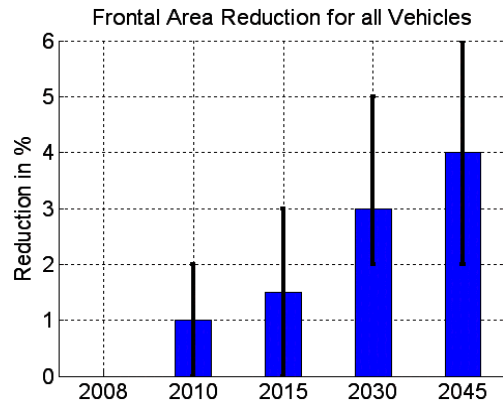
Vehicle

As previously discussed, four vehicle classes were considered, as shown in Table 1.

Table 1. Vehicle Characteristics for Different Vehicle Classes

Vehicle Class	Glider Mass (Ref) (kg)	Frontal Area (Ref) in (m ²)	Tire	Wheel Radius (m)
Midsize Car	990	2.2	P195/65/R15	0.317
Small SUV	1000	2.52	P225/75/R15	0.35925
Midsize SUV	1260	2.88	P235/70/R16	0.367
Pickup	1500	3.21	P255/65/R17	0.38165

Because of the improvements in material, the glider mass is expected to significantly decrease over time. The maximum value of 30 percent was defined on the basis of previous research that calculated the weight reduction that could be achieved by replacing the entire chassis frame with aluminum. Although frontal area is expected to differ from one vehicle configuration to another (i.e., the electrical components will require more cooling capabilities), the values were considered constant across the technologies. Figures 14 and 15 show the reduction in both glider mass and frontal area.

**Figure 14. Glider Mass Reductions****Figure 15. Frontal Area Reductions**

Vehicle Powertrain Assumptions

All the vehicles have been sized to meet the same requirements:

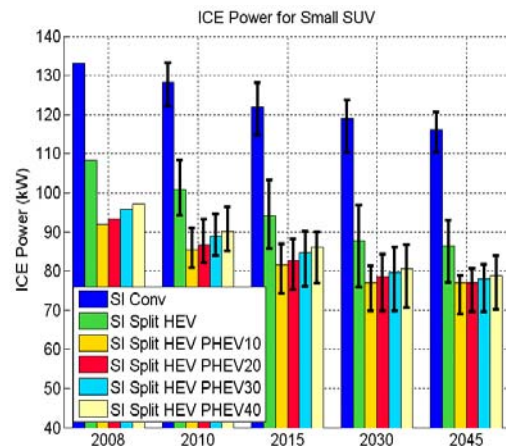
- Zero to 100 km/h in 9 s +/- 0.1
- Maximum grade of 6 percent at 105 km/h at Gross Vehicle Weight
- Maximum vehicle speed of greater than 160 km/h

For all cases, the engine or fuel cell powers are sized to perform the grade without any assistance from the battery. For HEVs, the battery was sized to recuperate the entire braking energy during the UDDS drive cycle. For the PHEV case, the battery power is defined as its ability to follow the UDDS in electric mode, while its energy is calculated to follow the trace for a specific distance. Because of the multitude of vehicles considered, an automated sizing algorithm was defined.

Input mode power split configurations, similar to those used in the Toyota Camry, were selected for all HEV and PHEV applications using engines. The series fuel cell configurations use a two-gear transmission to be able to achieve the maximum vehicle speed requirement. The vehicle-level control strategies employed for each configuration have been defined in previous publications.

Component Sizing

As shown in Figure 16, the engine power for all of the powertrains decreases over time. The power-split HEV is the one with the highest reduction in engine power: 20% from reference to 2045 average case, whereas power for the conventional engine decreases only by 13%. The engine power is higher when the all-electric range (AER) range increases because the power is sized on the basis of acceleration and grade and because the different PHEVs (for the same fuel) only vary from one to the other by having a bigger battery (and thus a heavier car).

**Figure 16. Engine Power for Gasoline Powertrains for Small SUV**

The ICE (internal combustion engine) power linearly changes with the vehicle mass, as shown in Figure 17. The hydrogen and diesel points are on the same line, but they do not cover the same mass range. Also, if the hydrogen had the same travel distance range as the other fuels, its line would be shifted up and left. Two points from the hydrogen series remain on the same line as the gasoline engine. These two points correspond to the 2008 and 2010 low-case values in which the ICE used does not employ direct injection. Consequently, the ICE power is higher for these two cases. For every 100 kg less on the vehicle

mass, the engine power decreases by approximately 10 kW.

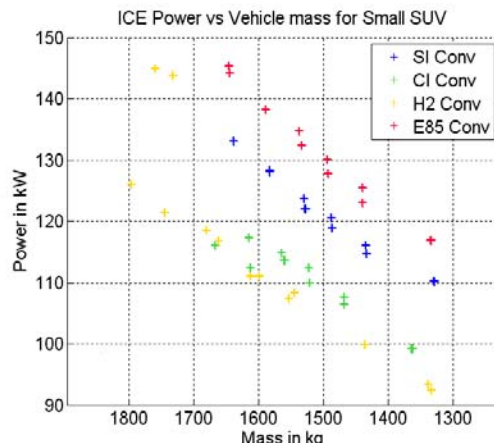


Figure 17. ICE Power as a Function of Vehicle Mass for Conventional Vehicle

Figure 18 shows the electric machine power for the gasoline HEVs and PHEVs. Note that PHEVs require higher power because one of their requirements is the ability to follow the UDDS in electric mode. Note that the vehicles can be driven in electric mode in the UDDS, and the control strategy employed during fuel efficiency simulation is based on blended operation. However, the power in PHEVs does not increase significantly in comparison with HEVs because the input mode power-split configuration was considered. A decrease of 10 to 20 kW can be expected by 2045 as a result of improvements in components.

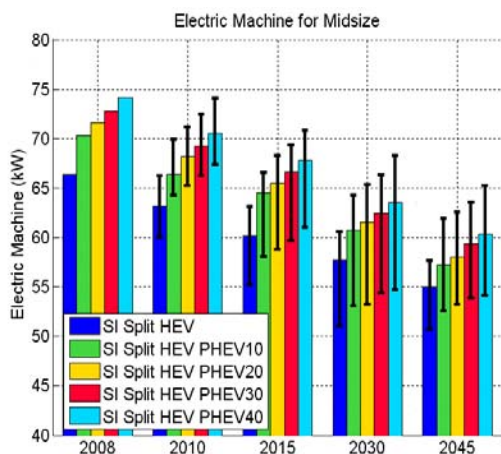


Figure 18. Electric Machine Power for Gasoline HEV and PHEVs for Midsize Vehicle

Figures 19 and 20 show the battery power and energy requirements for HEV, PHEV, and EV applications.

The sensitivity of battery power to vehicle mass increases with the degree of electrification (i.e., higher for EV, then PHEV, and finally HEVs). From an energy point of view, every 100-kg decrease for a PHEV40 (i.e., 40 miles on electric only on the UDDS) results in a decrease in energy requirements by approximately 2 kWh.

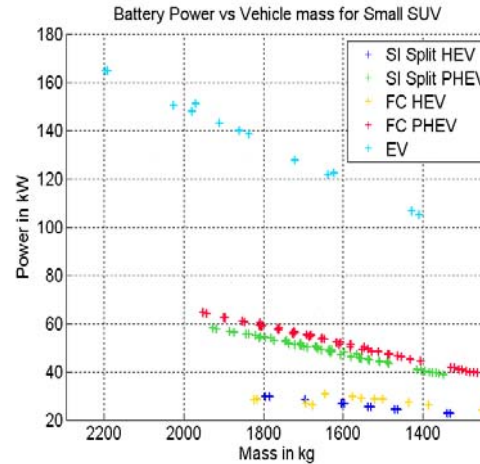


Figure 19. Battery Power

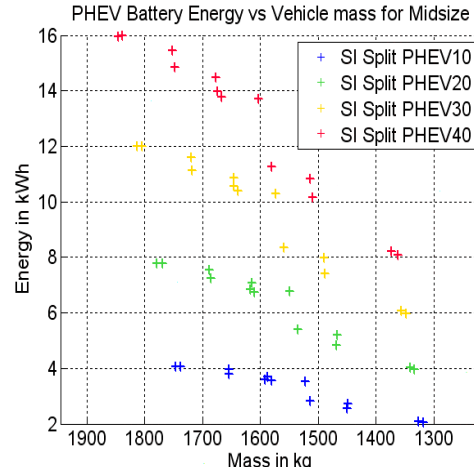


Figure 20. Battery Energy

Results of Vehicle Simulation

The vehicles were simulated on both the UDDS and HWFET drive cycles. The fuel consumption values and ratios presented below are based on unadjusted values. The cold-start penalties were defined for each powertrain technology option on the basis of available data collected at Argonne's dynamometer facility and available in the literature. The following cold-start penalties (on the 505 cycle at 20°C) were maintained constant throughout the timeframes:

- Conventional: 15 percent
- Split HEV: 18 percent
- Split PHEV: 14 percent
- Fuel Cell HEV: 25 percent
- Fuel Cell PHEV: 15 percent
- Electric Vehicle: 10 percent

Impact of Different Fuels on Conventional Vehicles

Figure 21 shows the evolution of the fuel consumption for different fuels on a conventional midsize vehicle. All of the results are presented in the gasoline fuel equivalent. As expected, the diesel engine achieves better fuel efficiency than the gasoline engine, but the difference between both technologies narrows with time as greater improvements are expected for gasoline engines.

Hydrogen engines are penalized by the additional weight of the hydrogen storage system. With the introduction of direct-injection hydrogen engine technology combined with improved storage, hydrogen engines can compete with other fuels. It is, moreover, important to notice the large uncertainty related to hydrogen vehicles. Finally, the hydrogen storage efficiency is assumed to be 100 percent.

Ethanol engines are being designed to run on several fuels. When specifically designed to run on ethanol, the vehicles running on ethanol have the potential to achieve the best fuel efficiency.

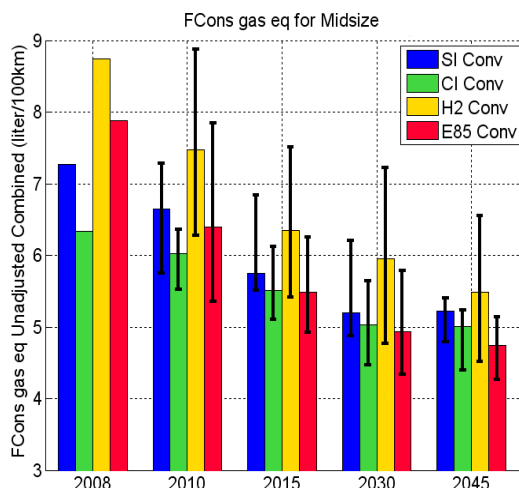


Figure 21. Fuel Consumption Gasoline-Equivalent Unadjusted for Conventional Midsize Cars

Figure 22 shows the vehicle cost ratios between the different fuels for conventional vehicles. Diesel engines are expected to remain more expensive than their gasoline counterparts, while vehicles with hydrogen engines become competitive in the long term because storage will be less expensive.

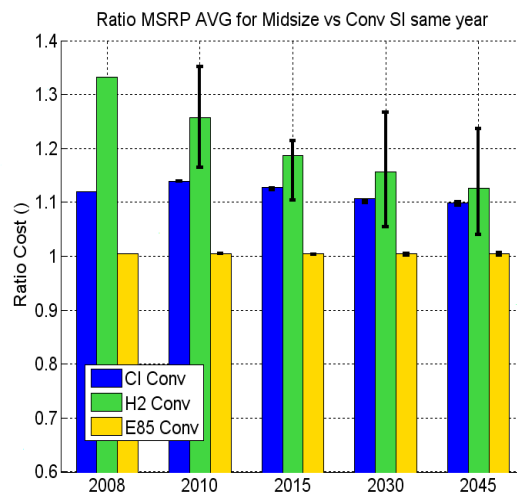


Figure 22. Conventional Vehicle Cost Ratio Compared to Gasoline Conventional Vehicles of the Same Year

Evolution of HEVs vs. Conventional Vehicles

The comparisons between power-split HEVs and conventional gasoline vehicles (same year, same case) in Figure 23 show that the ratios stay roughly constant for diesel, gasoline, and ethanol. Indeed, the gasoline HEV consumes between 25 and 28 percent less fuel than the gasoline conventional vehicle, whereas the diesel HEV consumes between 35 and 38 percent less fuel and the ethanol HEV consumes between 19 and 21 percent less fuel. However, the hydrogen case shows more significant variations. In 2008, the hydrogen power-split vehicle consumes roughly 25 percent less fuel than the gasoline conventional vehicle, but in the 2045 average case, this advantage rises to 43 percent and even 47 percent in the high case. This analysis confirms that hydrogen vehicles will benefit more from hybridization in the future than will comparable conventional vehicles. In summary, the advances in component technology will equally benefit conventional vehicles and HEVs, except for the hydrogen engine, because of the additional benefits of hydrogen storage.

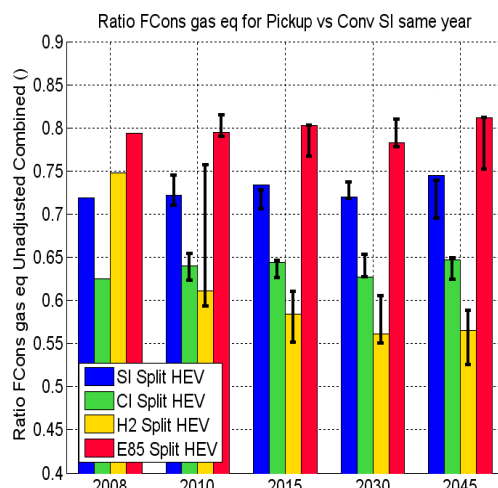


Figure 23. Ratio of Fuel Consumption Gasoline-Equivalent Unadjusted Combined in Comparison to the Conventional Gasoline Same Year, Same Case, for Pickup

Figure 24 shows the vehicle cost ratio between HEVs and conventional vehicles. As expected, HEVs remain more expensive than conventional vehicles, but the difference significantly decreases because costs associated with the battery and electric machine fall faster than those for conventional engines.

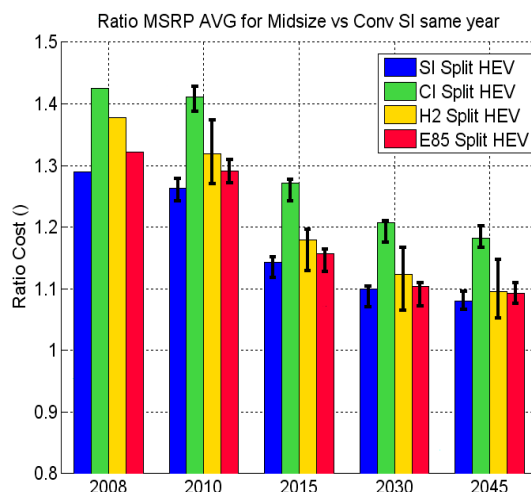


Figure 24. HEV Vehicle Cost Ratio Compared to Gasoline Conventional Vehicle of the Same Year

Evolution of HEVs vs. FC HEVs

Figure 25 shows the fuel consumption comparison between HEVs and FC HEVs for the midsize-car case. First, note that technology for fuel cell vehicles will continue to provide better fuel efficiency than the technology for the HEVs, with ratios above 1.

However, the ratios vary over time, depending upon the fuel considered. The ratio for the gasoline HEV increases over time because most improvements considered for the engine occur at low power and consequently do not significantly impact the fuel efficiency in hybrid operating mode. Both diesel and ethanol HEVs follow the same trend as the gasoline.

Because of the larger improvements considered for the hydrogen engine, the hydrogen power split shows the best improvement in fuel consumption in comparison to the fuel cell technology. Indeed, in 2008, the hydrogen HEV vehicle consumes nearly 40 percent more fuel than the fuel cell HEV vehicle, but in the 2045 average case, this difference is reduced to 10 percent. If we consider the UDDS fuel consumption instead of the combined values, we find that the hydrogen power split consumes only 2.5 percent more fuel than a fuel cell HEV in the 2045 high case.

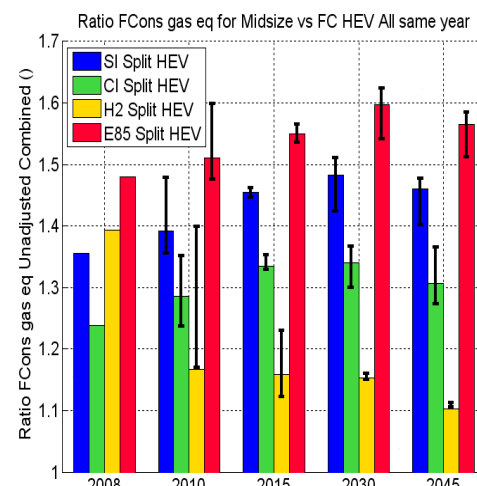


Figure 25. Ratio of Fuel Consumption Gasoline-Equivalent Unadjusted Combined in Comparison to the Fuel Cell HEV Same Year, Same Case for Midsize Vehicles

Figure 26 shows the vehicle cost comparison between HEVs and FC HEVs. Note that the cost difference between both technologies is expected to decrease over time, with a ratio between 0.9 and 1 in 2030 and 2045.

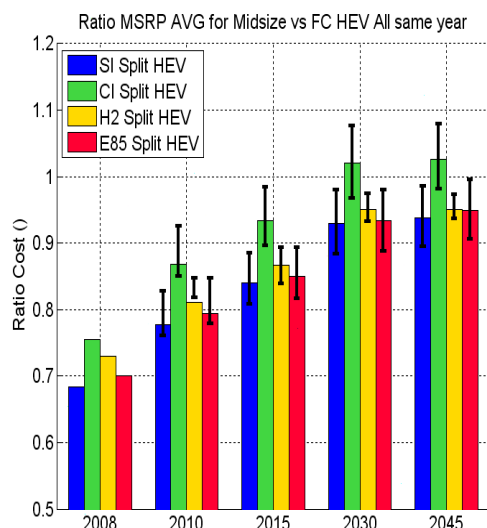


Figure 26. HEV Vehicle Cost Ratio Compared to FC HEV Vehicle of the Same Year

Evolution of Hydrogen-Fueled Vehicles

As shown in Figure 27, in 2008, fuel cell HEVs consume about 49 percent less fuel than gasoline conventional vehicles, and this difference in fuel consumption increases in subsequent timeframes to reach 54 percent in the 2030 average case. In 2045, the trend is changing. In the 2045 average case, the fuel cell vehicle will consume 51 percent less fuel than the conventional gasoline vehicle. This value is still higher than that for the reference year, which means that the conventional gasoline vehicle will not improve its fuel consumption faster than the fuel cell HEV.

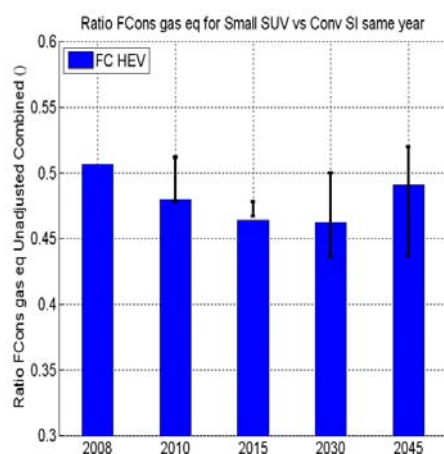


Figure 27. Ratio of Fuel Consumption Gasoline-Equivalent Unadjusted Combined in Comparison to the Gasoline Conventional Same Year, Same Case, Small SUV

Conclusions

More than 700 vehicles were simulated for different timeframes (up to 2045), powertrain configurations, and component technologies. Both their fuel economy and cost were assessed to estimate the potential of each technology. Each vehicle was associated with a triangular uncertainty. The simulations highlighted several points:

- The discrepancy between gasoline and diesel engine for conventional vehicles is narrowing with the introduction of new technologies, such as VVT and low temperature combustion.
- From a fuel-efficiency perspective, HEVs maintain a relative constant ratio compared to their conventional vehicle counterparts. However, the cost of electrification is expected to be reduced in the future, favoring the technology's market penetration.
- Ethanol vehicles will offer the lowest fuel consumption among the conventional powertrains in the near future, which is driving the interest in biofuels development.
- Fuel cell HEVs have the greatest potential to reduce fuel consumption.
- Hydrogen engine HEVs, through direct injection, will offer significant fuel improvements and, because they offer lower cost than fuel cell systems, appear to be a bridging technology, which would help the infrastructure.

Publications/Presentations

Delorme, A., Pagerit, S., Rousseau, A., "Fuel Economy Potential of Advanced Configurations from 2010 to 2045," IFP Conference, Paris, Nov 2008.

Rousseau, A., "Update on GPRA 2009 Study," FreedomCAR Presentation, Detroit, May 2008.

Rousseau, A., "Light Duty Vehicle Fuel Efficiency and Cost," DOE Presentation, Washington DC, July 2008.

C. DOE and FreedomCAR Technical Team Support

Aymeric Rousseau (project leader)

Argonne National Laboratory

9700 South Cass Avenue

Argonne, IL 60439-4815

(630) 252-7261; arousseau@anl.gov

DOE Technology Manager: Lee Slezak

(202) 586-2335; Lee.Slezak@ee.doe.gov

Objectives

Evaluate fuel efficiency potential of hydrogen-powered vehicles.

Define engine power requirements for plug-in hybrid electric vehicles.

Assess impact of steady-state vehicle speed on fuel consumption.

Approach

Gather component assumptions required for the specific study.

Size the components for each option considered.

Run simulations.

Compare results.

Accomplishments

Demonstrated fuel efficiency potential of both hydrogen engine and fuel cell systems.

Defined impact of vehicle speed on vehicle consumption.

Future Directions

Refine fuel efficiency comparison when updated component data are available.

Introduction

With advanced vehicle technologies research moving at a constantly increasing speed, it is necessary to be able to regularly assess the potential of specific options. The following report details the fuel efficiency potential of hydrogen vehicles, as well as updates related to component requirements for plug-in hybrid electric vehicles (PHEVs) and the impact of steady-state vehicle speed on fuel consumption.

Evaluate Fuel Efficiency of Hydrogen-Powered Vehicles

To try to accelerate the development of a hydrogen economy, some original equipment manufacturers

(OEM) in the automotive industry have been working on a hydrogen-fueled internal combustion engine (ICE) as an intermediate step. Despite its lower cost, the hydrogen-fueled ICE offers, for a similar amount of onboard hydrogen, a lower driving range because of its lower efficiency.

This report compares the fuel economy potential of hydrogen-fueled vehicles to their conventional gasoline counterparts. To take uncertainties into account, the current and future status of both technologies were considered. Although complete data related to port fuel injection were provided from engine testing, the map for the direct-injection engine was developed from single-cylinder data. The fuel-

cell-system data represent the status of the current technology and the goals of FreedomCAR. For both port-injected and direct-injected hydrogen engine technologies, power split and series hybrid electric vehicle (HEV) configurations were considered. For the fuel cell system, only a series HEV configuration was simulated.

As discussed previously, uncertainties were taken into consideration for each technology simulated. The graphs discussed in the following paragraph highlight the fuel economy of the different vehicles, as well as the ratios.

Figure 1 and 2 show, respectively, the gasoline-equivalent vehicle fuel economy and the ratio compared to the reference gasoline. Note that the fuel economy drops when a hydrogen ICE (H_2 -ICE) is used in a conventional vehicle. This drop in fuel economy is due to, in part, the additional weight of hydrogen storage. The other likely cause of the reduction in fuel economy is the shifting transmission, which might need to be further optimized for the H_2 -ICE.

When comparing both H_2 -ICE hybrids, note that the series configuration achieves lower fuel economy than the input split. In fact, the series configuration cannot compensate for the additional mass and losses due to additional component efficiencies (90 percent for the generator and 81 percent for the electric machine). Both HEV configurations studied allow the vehicle load to be decoupled from the engine load. As the engine speed is independent of the vehicle speed, similar engine average efficiencies are achieved on the drive cycles (i.e., approximately 31 percent for port injection and approximately 41.5 percent for direct injection on UDDS [urban dynamometer driving schedule]).

In addition, even though the batteries for each configuration have been sized to capture all of the regenerative braking on the UDDS, a lower efficiency path from the wheel to the battery further penalizes the series. This penalty is explained by the lower efficiency of the electric machine compared to the power split configuration. For example, if we recuperate 10 kW from the wheel, a 50-kW electric machine will operate at a higher efficiency point than a 100-kW electric machine.

The fuel cell vehicle, because of its high system efficiency, achieves the highest fuel economy of the hydrogen-powered vehicles (ratio of 2.46 for future technology). The fuel cell system achieves efficiencies of ~47 percent for the current case and ~51 percent for the future case on the UDDS driving cycle.

Both the hydrogen engine and the fuel cell would achieve significantly higher fuel economy than the conventional gasoline (ratios are respectively 2.2 and 2.4).

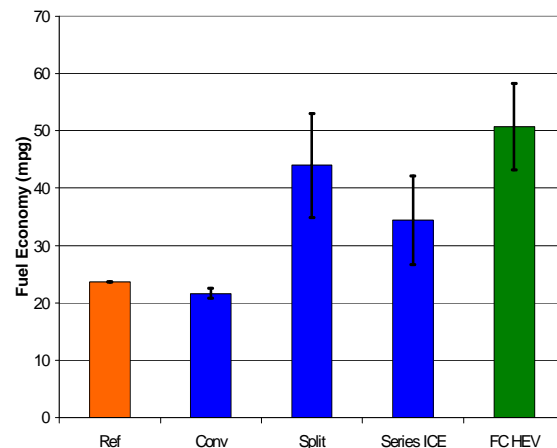


Figure 1. Vehicle Fuel Economy Gasoline Equivalent – Combined Drive Cycle - EPA 2008 Corrections

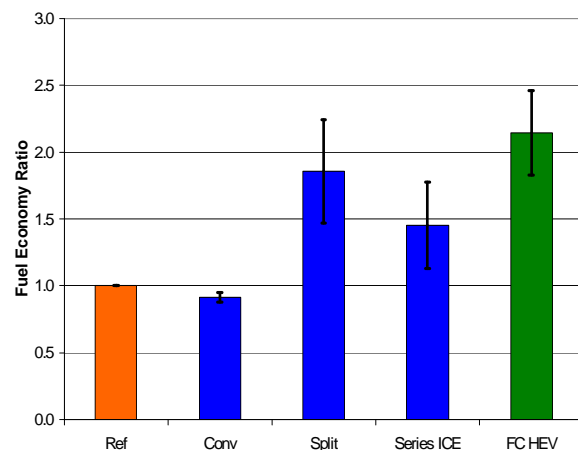


Figure 2. Vehicle Fuel Economy Gasoline Equivalent Ratio – Combined Drive Cycle - EPA 2008 Corrections

Figure 3 shows the fuel economy ratio on the UDDS driving cycle. Note that the power split and fuel cell configuration achieve similar fuel economy when future technologies are considered.

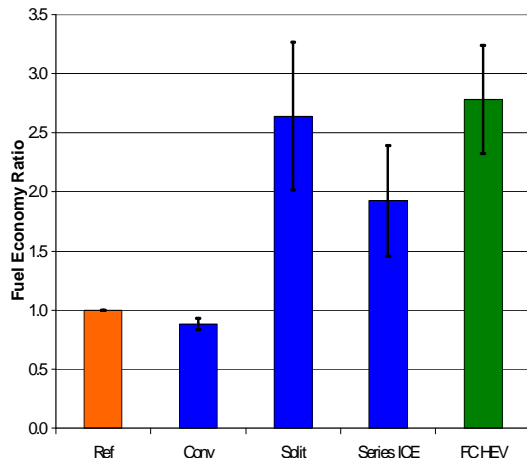


Figure 3. Vehicle Fuel Economy Gasoline Equivalent Ratio – UDDS

Figure 4 shows the fuel economy ratio on the HWFET (Highway Federal Emission Test) driving cycle. First, as one expects, the fuel economy ratio is lower than that for the UDDS driving cycle (maximum of 2.1 on the HWFET instead of 3.2 on the UDDS for the future fuel cell technology). Another interesting finding is that the power split hybrid achieves a lower fuel-economy ratio than does the fuel cell, which explains the overall difference. Note that using a dual-mode power split rather than a one-mode power split would improve the power split fuel economy at high vehicle speed by decreasing the amount of electricity that goes through the series path.

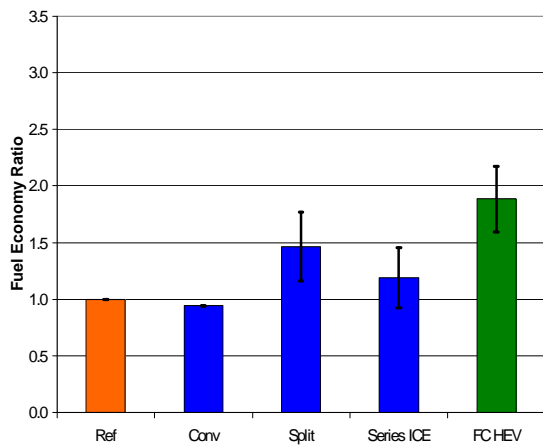


Figure 4. Vehicle Fuel Economy Gasoline Equivalent Ratio – HWFET

Define Engine Power Requirements for PHEVs

The engine power requirements were defined for several vehicle classes, as shown in Figure 5. Since the engine power is defined by the gradeability requirements, the power increases with vehicle weight.

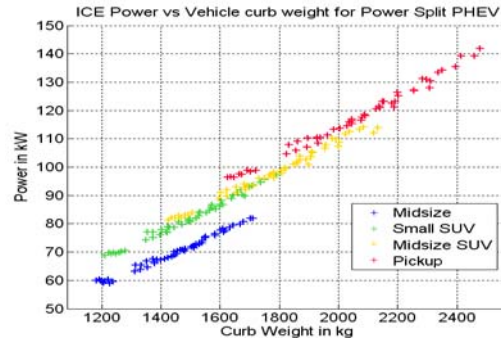


Figure 5. Engine Power as a Function of Vehicle Weight

Figure 6 shows the influence of the all-electric range (AER) on the requirements. Note that, because of the high specific power of the Li-ion battery, the AER does not significantly impact the relationship of engine power to vehicle mass.

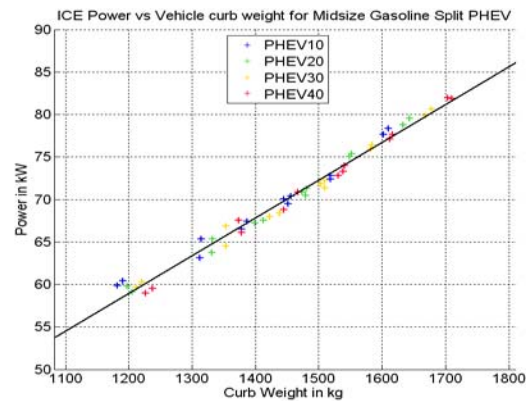


Figure 6. Engine Power as a Function of Vehicle Weight for Different AER

Figure 7 shows the impact of the powertrain configurations on the requirements. Because of the additional losses, the series configuration has higher requirements. However, this impact is not significant either.

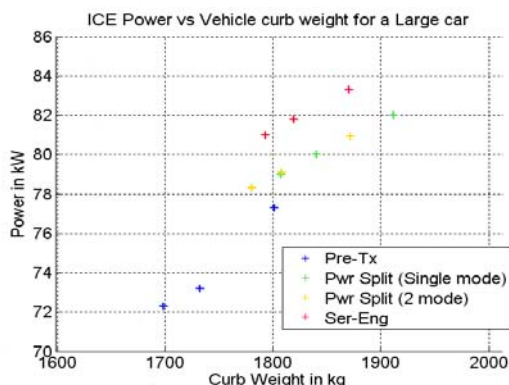


Figure 7. Impact of Vehicle Powertrain Configurations

Assess Impact of Steady-state Vehicle Speed on Fuel Consumption

The impact of steady-state vehicle speed was analyzed from both test and simulated data for different vehicle speeds (45 to 75 mph).

For conventional vehicles, the results demonstrated a fuel consumption increase from 11 to 18 percent for vehicle speeds from 55 to 65 mph. The results were similar for vehicle speeds from 65 to 75 mph (12 to 20 percent).

For HEVs, the results demonstrated a fuel consumption increase from 14 to 18 percent for vehicle speeds from 55 to 65 mph. The results were higher for vehicle speeds from 65 to 75 mph (12 to 30 percent).

Conclusions

The fuel efficiency of several technologies was evaluated. In the process, the study confirmed DOE's position that while fuel cell vehicles achieve the highest fuel economy, the H₂-ICE is a bridging technology and might help in the development of the infrastructure needed for hydrogen fuel.

Regarding the PHEV component requirements related to real world driving, the following conclusions can be drawn:

- Aggressive driving will put limits on all-electric-vehicle range, which, in turn, favors a blended mode operational strategy.
- The real-world drive cycles are generally more aggressive than the UDDS, resulting in higher energy requirements to drive the same distance.

- LA92 seems to better represent current drive-cycle aggressiveness.

Publications/Presentations

Delorme, A., Pagerit, S., Rousseau, A., Sharer, P., Wallner, T., "Evolution of Hydrogen Fueled Vehicles Compared to Conventional Vehicles from 2010 to 2045," 09PFL-0612, SAE World Congress, April 2009.

Rousseau, A., "Hydrogen Hydrogen Fueled Vehicles Efficiency and Cost Assessment," DOE Presentation, Washington DC, August 2008.

Rousseau, A., Wallner, T., Pagerit, S., Lohse-Busch, H., "Prospects on Fuel Economy Improvements for Hydrogen Powered Vehicles," SAE 2008-01-2378, SAE World Congress, Detroit, April 2008.

Rousseau, A., "Prospects on Fuel Economy Improvements for Hydrogen Powered Vehicles," DOE Presentation, Washington DC, April 2008.

Rousseau, A., "Engine Requirements for PHEVs," DOE Presentation, Washington DC, September 2008.

D. PSAT Maintenance and Enhancements

*Aymeric Rousseau (project leader), Shane Halbach, Sylvain Pagerit, Phil Sharer, Dominik Karbowski, Jason Kwon, Ram Vijayagopal
 Argonne National Laboratory
 9700 South Cass Avenue
 Argonne, IL 60439-4815
 (630) 252-7261; arousseau@anl.gov*

*DOE Technology Manager: Lee Slezak
 (202) 586-2335; Lee.Slezak@ee.doe.gov*

Objectives

Enhance and maintain Powertrain System Analysis Toolkit (PSAT) as needed to support the Department of Energy (DOE), the user community, and hardware-in-loop/rapid control prototyping (HIL/RCP) projects. This effort includes development of updates for the latest Matlab/Simulink version(s) and an annual release of the software with the latest models and data.

Approach

Use the feedback from PSAT users to implement new features.

Enhance PSAT capabilities to support DOE studies.

Accomplishments

Released PSAT V6.2 in January 2008.

Released PSAT V6.2 SP1 in July 2008.

Improved the graphical user interface.

Added new powertrain configurations.

Future Directions

Continue to enhance PSAT on the basis of DOE needs and user feedback.

Introduction

To better support the U.S. Department of Energy (DOE) and its users, several new features have been implemented in the Powertrain System Analysis Toolkit (PSAT). Some of the most significant accomplishments are described below.

Results

The Vehicle Systems Analysis Team at Argonne National Laboratory (ANL) released two versions of its vehicle simulation modeling software in January (V6.2) and July (V6.2 SP1) 2008. The latest version, PSAT V6.2 SP1, includes many new features and

improvements. These changes were made on the basis of feedback from users in industry and at universities, as well as the needs expressed by staff at DOE and Argonne. The PSAT V6.2 runs with Matlab R2007b and R2008a.

Graphical User Interface

Numerous enhancements have been included in the graphical user interface (GUI). Some examples are described below.

A specific interface was developed to allow users to build their own trips, as shown in Figure 1. This

capability allows users to test their control strategies on longer drive cycles than the standard ones.

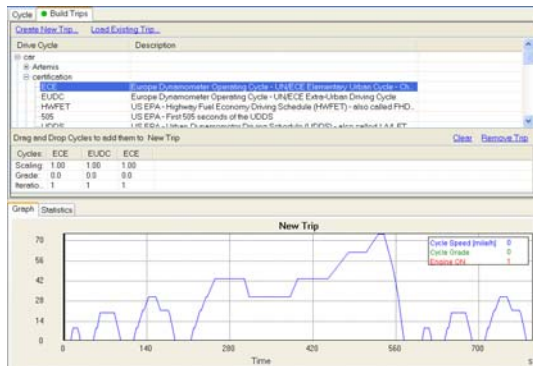


Figure 1. Building Trip GUI

Several testing procedures were modified, including the new EPA 5 cycles, which now include penalties related to cold start at 20°C and -7°C. These values were selected on the basis of test data for several vehicles. Users have the ability to modify the parameters or develop a control strategy and models that take temperature into account.

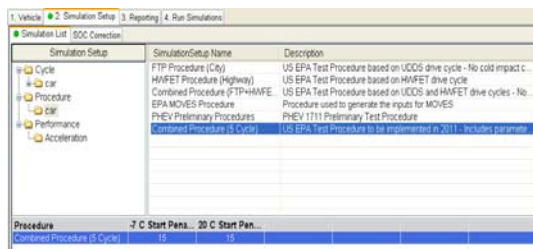


Figure 2. EPA 5 Cycles Test Procedure

Additional Powertrain Configurations

Several new powertrain configurations were implemented on the basis of specific user requests. In addition, two configurations currently in production were added:

- Aisin system
- 2Mode system with four fixed gears

Component Models

The component models in PSAT are continuously being improved to support specific studies.

The energy storage system model and its initialization files were modified to be able to handle both series and parallel arrangements of cells. This

improvement was necessary to support plug-in hybrid electric vehicle (PHEV) activities.

The electric machine models were modified to be able to change the continuous to peak power ratio. This parameter has a significant impact on component sizing and cost. Although the ratio is low for series configurations, it would be higher for power split.

The wheel models and initialization files were modified to include the theoretical wheel radius. Two different parameters now describe the wheel radius (theoretical and real) to avoid confusing users.

A low-pass filter is now used for engine, electric machine, and fuel cell systems to represent their time response rather than a rate limiter block.

Component Data

State-of-the-art component data were implemented from both universities and companies.

For example, DOE national laboratories provided the GM 1.9-L diesel engine from Argonne's dynamometer testing facility and the Camry electric machine from Oak Ridge National Laboratory. The companies using PSAT also provided engine (i.e., ethanol, twin turbocharger), battery, fuel cell, and electric machine data.

In addition, several drive cycles from both light- and heavy-duty vehicles were added, including JC08, HHD65, and CSHVR. Argonne also worked with the U.S. EPA to use real-world drive cycles from Kansas City.

Control Strategies

Default control strategies for most of the configurations were developed and released to simulate PHEVs. To do so, the battery state-of-charge controls were modified both in the Simulink and in the initialization files.

In addition, two control strategies were developed to simulate the 2Mode system, with and without a fixed gear ratio. This work is ongoing, and additional information is provided in the section related to HEV Model Validation.

Vehicles

At the request of several users, including OEMs (original equipment manufacturers), several HEV vehicles were developed and released. Because test data were not available for thorough validation, these vehicles were only correlated. The vehicles include the Ford Escape HEV and the Toyota Camry HEV.

Conclusions

The latest versions of PSAT were released with numerous new features, on the basis of feedback from DOE and the user community. These enhancements are focused on the GUI, component model and data, and control strategies.

Publications/Presentations

PSAT V6.2 Documentation, 1200 pages, January 2008.

E. Plug-and-Play Software (Cooperative Research and Development Agreement with General Motors)

Aymeric Rousseau (project leader), Shane Halbach, Sylvain Pagerit, Phil Sharer, Dominik Karbowski, Ram Vijayagopal, Jason Kwon, Namdo Kim

*Argonne National Laboratory
9700 South Cass Avenue
Argonne, IL 60439-4815
(630) 252-7261; arousseau@anl.gov*

*DOE Technology Manager: Lee Slezak
(202) 586-2335; Lee.Slezak@ee.doe.gov*

Objectives

Develop software architecture and environment to Plug-and-Play hardware and software models to include control system design in the upfront math-based design and analysis.

Approach

- Enable efficient, seamless math-based control system design process.
- Enable efficient reuse of models.
- Enable sharing of modeling expertise across the organization.
- Establish industry standard for architecture and model interfaces.

Accomplishments

- Defined common nomenclature for model (i.e., organization, nomenclature).
- Developed new extensible markup language (XML) database management.
- Developed the prototype of a new graphical user interface.
- Validated new organization with existing Powertrain System Analysis Toolkit (PSAT) and General Motors (GM) models.

Future Directions

- Generate a Beta version of the new software.
 - Test the version at Argonne National Laboratory and with GM internal programs.
 - Refine and complete development of the tool.
 - Release the tool by the end of fiscal year 2009.
-

Introduction

While most companies have developed models of plants and controllers, few have had the resources to set up a process allowing reusability of the models from one program to another. Moreover, because most automotive manufacturers have adopted their

own specifications, it is not unusual for suppliers to develop models several times for the same hardware, which leads to the loss of significant amounts of time and money.

Detailed models also help companies properly evaluate the benefits of a technology early (i.e., in the

development stage) rather than waiting for the hardware testing stage. The new tool will allow users to select different levels of modeling.

Software Requirements

The software is based on three main areas (shown in Figure 1), which include:

- 1) Models and data
- 2) Graphical user interface (GUI)
- 3) Database

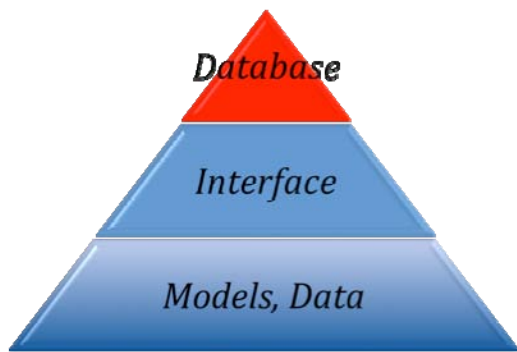


Figure 1. Main Software Requirements

For each area, several requirements were defined.

Models and Data

One of the key requirements is to maximize model reusability. To do so, existing models, controls, and data need to be integrated automatically. In addition, all models for a specific area of expertise reside in a single location. Finally, system duplication will be avoided by using Matlab API.

Because many combinations of system models and control should be used, the software should be flexible. And, in addition to building powertrain configurations, the software should have the capability to build any system automatically. Users should also be able to add their own configurations as well as simulate single components or entire vehicles.

To be able to select different levels of complexity, a common nomenclature (i.e., naming and model) should be defined. Model compatibility should also be included.

Finally, the software should be code neutral. Even if the main environment is Matlab/Simulink/StateFlow, the software should be able to handle models developed in any type of language.

Graphical User Interface

The first step in establishing the GUI is to set up the simulation. Users should be able to select the architecture, model, and data as well as to check compatibilities and simulation type (i.e., fuel efficiency, performance).

Processes should be defined to guide the users to perform different tasks (e.g., calibration, validation tuning). While users need to run single sets of simulations, they also need to be able to launch pre-defined sets of simulations (i.e., drive quality) or use optimization algorithms.

Database

To provide software companywide, a proper structure and process for handling file database management must be developed.

First, user control should be provided to prevent unauthorized users from accessing restricted or proprietary data while also allowing authorized users to download all necessary files related to a project.

Version control is included to maintain traceability of all changes while keeping linked files together through the entire vehicle process (i.e., design, simulation, and test).

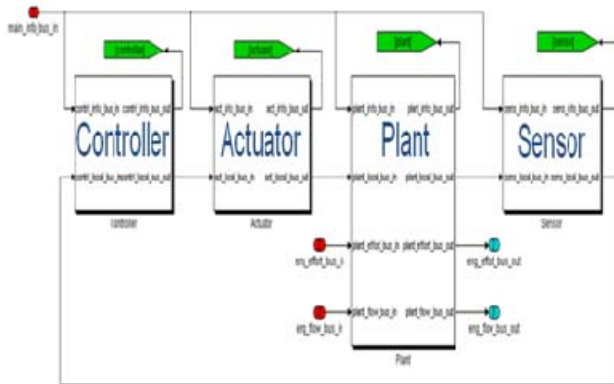
Finally, a keywords function is used to enable the search of data, models, and control related to specific projects. This enables finding the correct model quickly with the correct fidelity of modeling and all its related files.

Accomplishments

Common Nomenclature

A common nomenclature was defined for each main piece of the software, including for parameter naming, system models, and data files organization.

Figure 2 shows the main block composing the system, which includes a controller, actuator, plant, and sensor.

**Figure 2. System Organization**

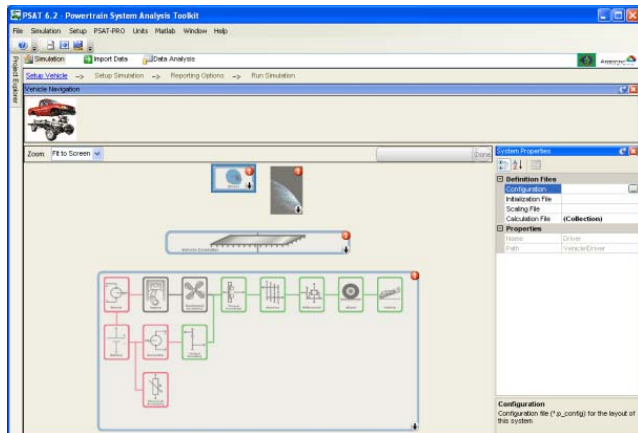
Building Algorithm

A new building algorithm was developed to allow users to select the organization of any system or subsystem.

The new process also allows users to implement their own architectures through XML files.

Graphical User Interface

Figure 3 shows the new GUI that was developed to meet the software requirements as well as to handle the building algorithm.

**Figure 3. New Graphical User Interface**

Conclusions

The software requirements were defined to support both automotive research and production needs. The software architecture and GUI were designed based on the goals. While much work remains to be completed prior to release of the software, the foundations have been laid.

Publications/Presentations

Rousseau, A., "Plug&Play Software Architecture," DOE Presentation, Washington DC, February 2008.

Rousseau, A., "Plug&Play Software Architecture – Year One Review," GM Presentation, Detroit, July 2008.

F. Validation of the Through-the-Road (TTR) PHEV

Dominik Karbowski (project leader)

Argonne National Laboratory

9700 South Cass Avenue

Argonne, IL 60439-4815

(630) 252-7261; arousseau@anl.gov

DOE Technology Manager: Lee Slezak

(202) 586-2335; Lee.Slezak@ee.doe.gov

Objectives

Use test data to validate the model of Argonne National Laboratory's (ANL) Through-the-Road (TTR) vehicle model.

Approach

Gather component test data.

Determine validation criteria.

Tune each component model by using vehicle test data.

Use test data and various curve fitting, clustering, and optimization methods to force the simulated controller to replicate the behavior of the vehicle.

Understand the limitations on the accuracy of the modeling technique.

Accomplishments

Developed and implemented generic data-quality analysis process for the Hymotion Prius.

Integrated component models into the Powertrain System Analysis Tool (PSAT).

Developed control strategy on the basis of vehicle test data.

Validated vehicle model on several driving cycles, including the urban dynamometer driving schedule (UDDS).

Future Directions

Evaluate the change in control strategy between different versions of the Hymotion Prius and compare it with other aftermarket power-split plug-in hybrid electric vehicles (PHEVs).

Introduction

The objective of this project is to validate the model of Argonne's Through-the-Road (TTR) plug-in hybrid electric vehicle (PHEV) vehicle. Because a vehicle-level control strategy was developed and implemented in the vehicle, the main efforts were focused on the powertrain validation.

Vehicle Description

The vehicle used for the validation is a TTR configuration based on the Saturn Vue Greenline.

Figure 1 shows the main characteristics of the different components.

Model Validation

The first phase of the validation process consisted of implementing the data files describing each component. Although the manufacturer provided some test data, other data had to be developed.

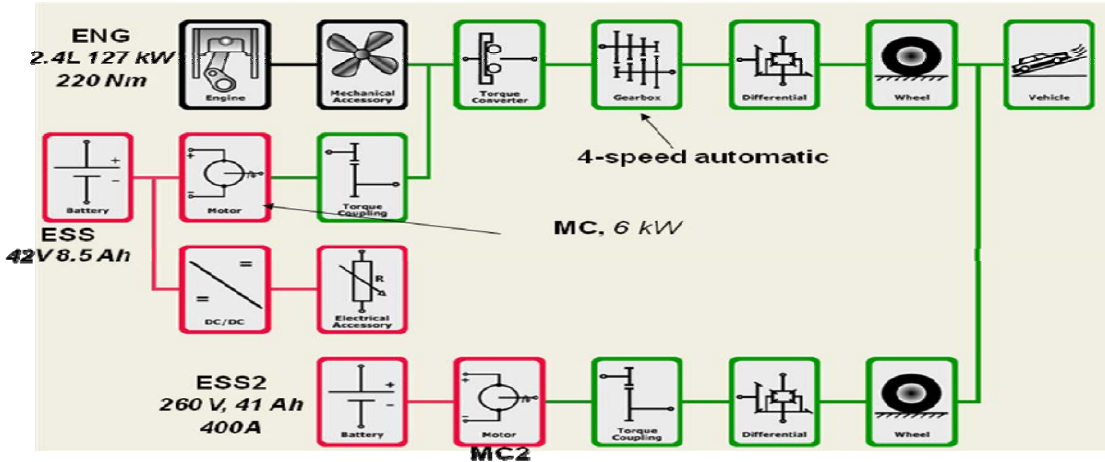


Figure 1. Vehicle Characteristics

One issue affecting the validation process was that the full control strategy developed in PSAT could not be implemented in the vehicle. The main problem was related to the transmission gear, which cannot be controlled. Because the gear ratio of the transmission cannot be directly controlled, the parameters of the shifting logic had to be tuned to reproduce the vehicle behavior.

By using test data from the Advanced Powertrain Research Facility (APRF), the vehicle model was validated. Figure 2 shows the comparison between measured and simulated battery state-of-charge (SOC). Note that both signals track well.

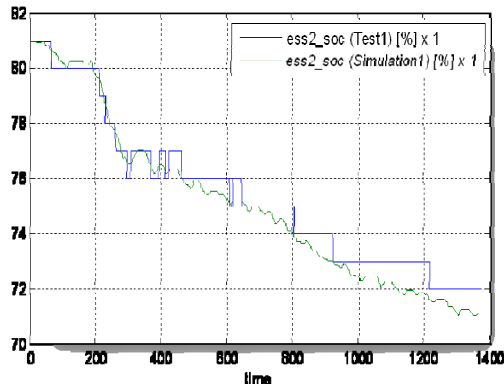


Figure 2. Battery SOC Comparison

Figure 3 shows the engine torque comparison. Note that the engine starts at the same time, and that the behavior of the simulation is consistent with the test data.

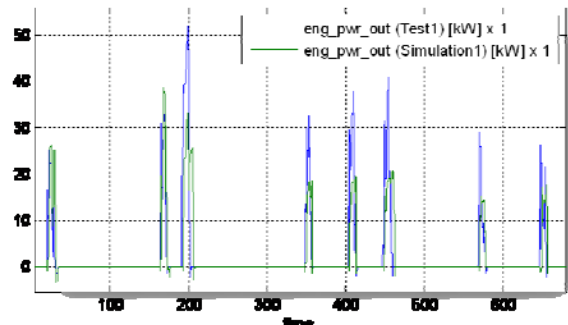


Figure 3. Engine Torque Comparison

Conclusions

Using data from suppliers and APRF, the components were modeled. A control strategy was then developed and implemented in ANL's TTR. The powertrain model was validated using the test data.

G. Impact of Drive Cycles on PHEV Component Requirements

Aymeric Rousseau (project leader), Sylvain Pagerit

Argonne National Laboratory

9700 South Cass Avenue

Argonne, IL 60439-4815

(630) 252-7261; arousseau@anl.gov

DOE Technology Manager: Lee Slezak

(202) 586-2335; Lee.Slezak@ee.doe.gov

Objectives

Evaluate the impact of real-world drive cycles on component requirements.

Approach

Develop component models representing the technologies.

Create complete models for several battery packs based on vehicle requirements.

Define the vehicle and the control strategies.

Analyze the electrical and fuel consumptions on several drive cycles.

Accomplishments

Evaluated the impact of real-world drive cycles on both power and energy.

Demonstrated increased electrical consumption compared to standard cycles.

Future Directions

Evaluate the impact of additional real-world drive cycles.

Evaluate uncertainties of additional vehicle characteristics.

Introduction

In this study, we will describe the methodology used to size the midsize plug-in hybrid electric vehicle (PHEV) on the basis of California Air Resources Board (CARB) requirements over the UDDS (urban dynamometer driving schedule) cycle. We will also assess the impact of various drive cycles on the power and energy requirements.

Vehicle Description

The vehicle class used represents a midsize sedan. The main characteristics are defined in Table 1.

Table 1. Main Vehicle Characteristics

Glider Mass (kg)	990
Frontal Area (m^2)	2.2
Coefficient of Drag	0.29
Wheel Radius (m)	0.317
Tire Rolling Resistance	0.008

The vehicle configuration selected is an input split with a fixed ratio between the electric machine and the transmission, similar to the Camry HEV.

Description and Analysis of Drive Cycles

The U.S. Environmental Protection Agency (EPA) has measured real-world drive cycles. In 2005, more than 100 different drivers in Kansas City participated in the study. Although several measurements were taken, only vehicle speed was used as part of this analysis. Figure 1 shows an example of real-world drive cycles. The maximum acceleration and decelerations of each trip were analyzed to ensure data validity.

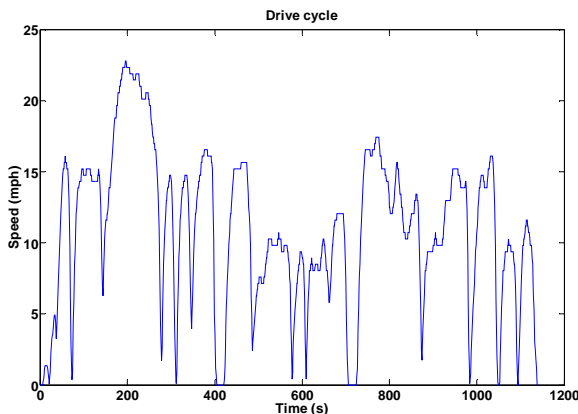


Figure 1. Example of Real-World Drive Cycle

Figure 2 shows the distribution of the distance during daily driving. Note that 50 percent of the drivers drive more than 40 miles per day. The red curve shows the cumulated driving distance computed from the National Household Travel Survey (NHTS) data. It appears that a greater number of trips of shorter distance characterize the NHTS curve.

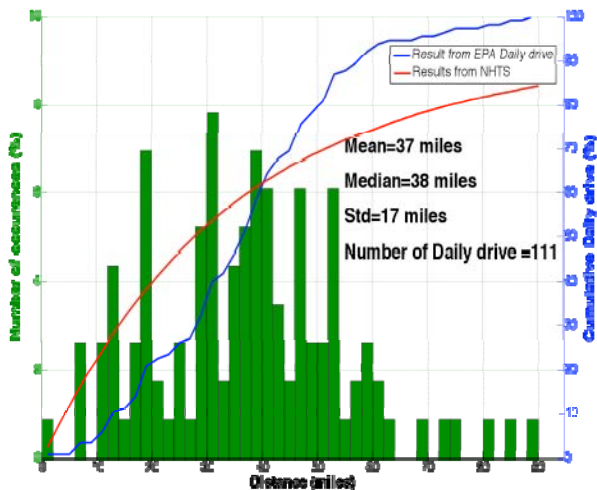


Figure 2. Distance Distribution of Daily Driving

Daily driving can be split into several trips. A trip is defined by events where the driver turns the ignition ON and OFF. Figure 3 shows the distance distribution of each trip. On average, a trip is 11 miles.

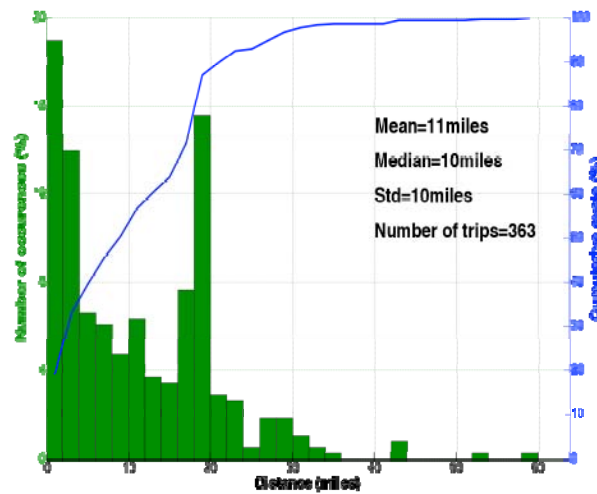


Figure 3. Distance Distribution of Each Trip

Figure 4 shows the relationship between maximum vehicle speed and trip distance. The maximum vehicle speed increases with distance. A similar trend is noticed for the average vehicle speed. This trend is expected because people often choose where to live on the basis of maximum commute time. Drivers close to a highway would then be more inclined to live farther than those who only drive in the city.

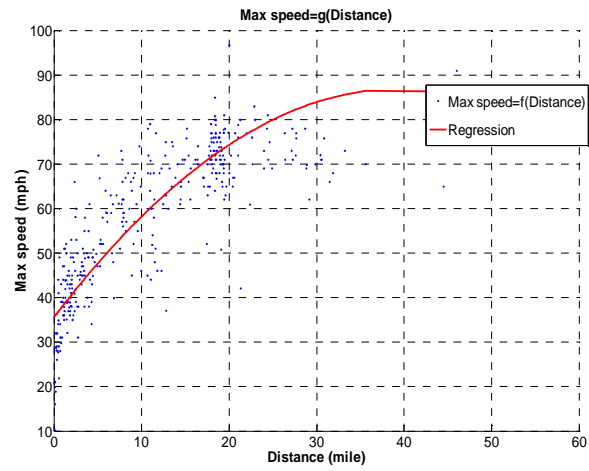


Figure 4. Relationship between Max Speed and Trip Distance

Figure 5 shows the relationship between trip duration and distance. The average daily driving time is 1.1 hours. Considering that most people have two major trips (to and from work), each trip to work lasts an average of 30 minutes.

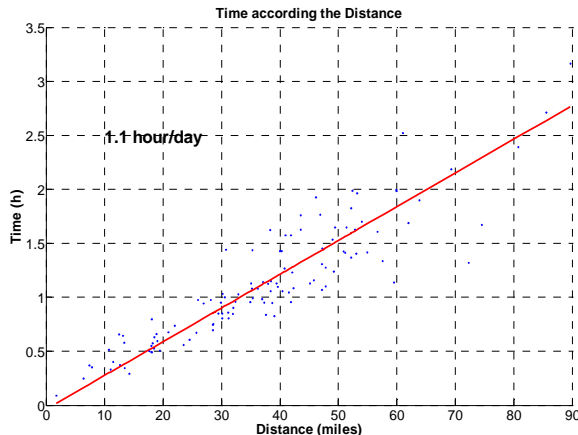


Figure 5. Relationship between Trip Duration and Distance

Battery Calculation Definitions

The maximum battery power was calculated on the basis of several assumptions. The following describes the terms:

Pess Max Sizing – Maximum battery power from component sizing over the entire trip/cycle at 20 percent battery state-of-charge (SOC). This value is usually greater than Pess Max Simu because it should be achieved at any time in the trip. Each trip has a single value.

Pess Max Simu – Maximum battery power obtained from the simulation over the entire trip/cycle. Each trip has a single value.

Pess Max Per Hill – Maximum battery power obtained from the simulation for each hill. A hill is defined by a vehicle speed trace in between two stops. Each trip has several values.

Pess All Points – Battery power distribution for every point of the drive cycle (second by second). Each trip has n values.

Both battery power and energy will be analyzed at different levels in the following paragraphs: daily driving, trips, hill, and continuous.

Analysis of Battery Discharging Power

The first parameter to be analyzed is the discharging battery power. Figure 6 shows the distribution of discharging peak power per trip and a comparison of the standard drive cycles. The trip average peak value is 78 kW. If we size the component on the UDDS, 22 percent of the trips can be completed because of power limitation. As a consequence, the engine will start on most trips on the basis of the current component requirements.

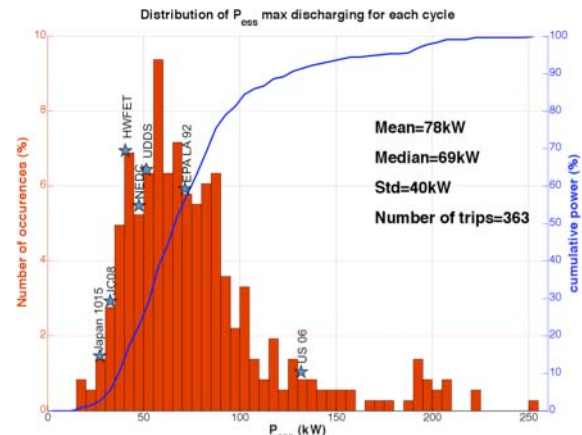


Figure 6. Distribution of Discharging Peak Power per Trip

Figure 7 shows the distribution of discharging peak power for all of the cycle points. Although we notice in Figure 6 that most cycles required greater peak power than the one defined for the UDDS, the cycles can be driven more than 98 percent of the time in electric-only mode on the basis of power limitation. As a result, we can conclude that, even if the events occur frequently, they do not last a long period.

Figure 8 confirms the above-mentioned statement. In fact, 80 percent of the demands greater than 50 kW last only between one and two minutes. If a control strategy based on maximum charge depleting is used, emissions during engine cold start should be monitored carefully.

One of the main issues with any vehicle is related to emissions during the first engine start. Figure 9 shows when the starts should occur if the battery is sized on the UDDS drive cycle (50 kW peak). Note that the first excess battery power occurs only between two and three minutes 50 percent of the time. This period would be the time allowed to, for example, warm the catalyst with an electrical load.

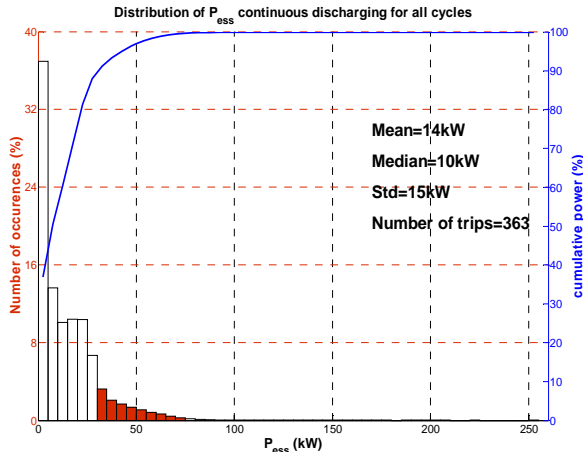


Figure 7. Distribution of Discharging Peak Power for All Points

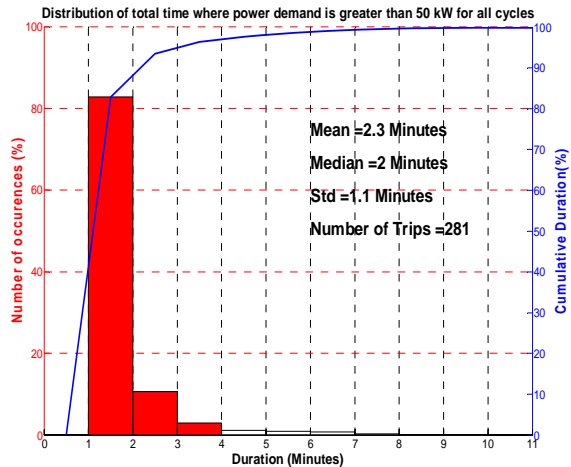


Figure 8. Distribution of the Duration of Battery Power > 50kW

Because the drive cycle has a major influence on the power demand, one also needs to analyze when the high power events occur. Figure 10 shows that most of the battery power demands above 50 kW occur at high vehicle speed. It is assumed that most of these events represent drivers merging on a highway, a process that requires rapid acceleration.

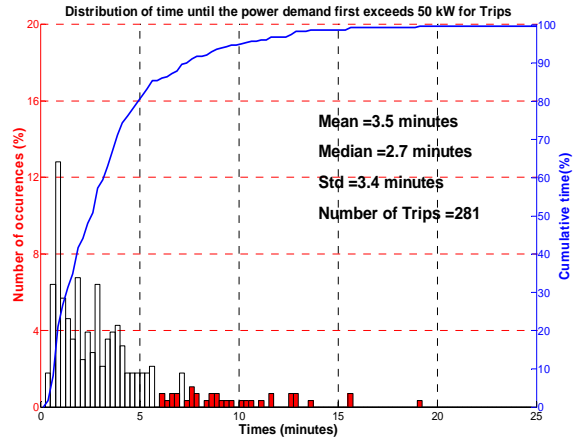


Figure 9. Distribution of the First Occurrence of Battery Power > 50kW

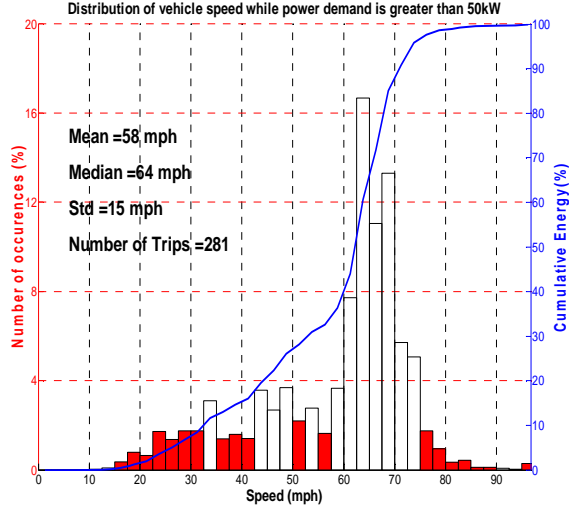


Figure 10. Distribution of the Vehicle Speed at which Battery Power > 50 kW

Analysis of Battery Charging Power

During the simulation, the maximum value of the battery power during deceleration events is also measured. Figure 11 shows the distribution of the charging peak power per trip and a comparison with additional standard drive cycles. If we size on the basis of the UDDS, 21 percent of the cycles can fully recover the energy.

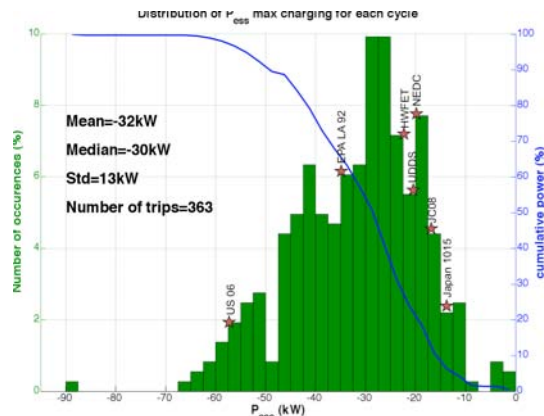


Figure 11. Distribution of Charging Peak Power per Trip

However, what matters for the regenerative braking events is the percentage of energy that can be recuperated. Figure 12 shows that, for every point during deceleration, 92 percent of the energy can be recuperated when we size the battery on the basis of the UDDS. The additional 8 percent would actually require significant additional power (up to 50 kW).

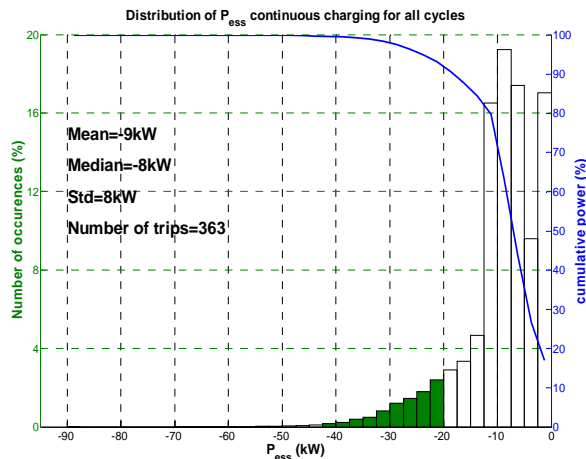


Figure 12. Distribution of Charging Peak Power for All Points

Battery Energy Analysis

In addition to power, energy is the major parameter characterizing the battery. Figure 13 shows the distribution of the usable battery energy for daily driving, and Figure 14 shows the distribution of vehicle speed while power demand is greater than 50 kW. To complete 50 percent of the driving, 12 kWh of usable power is required. The current short-term requirement for DOE (3.4 kWh) would allow 6.3 percent of the trips, while the long-term goal of 11.6 kWh would provide for 47 percent.

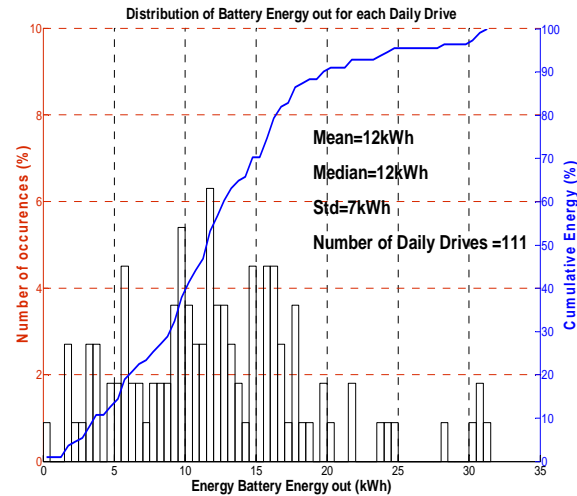


Figure 13. Distribution of the Battery Energy for Daily Driving

Because most people drive two trips per day, charging at work would allow the current long-term requirements to fulfill more than 98 percent of the trips. The short-term requirements would encompass 45 percent of the trips.

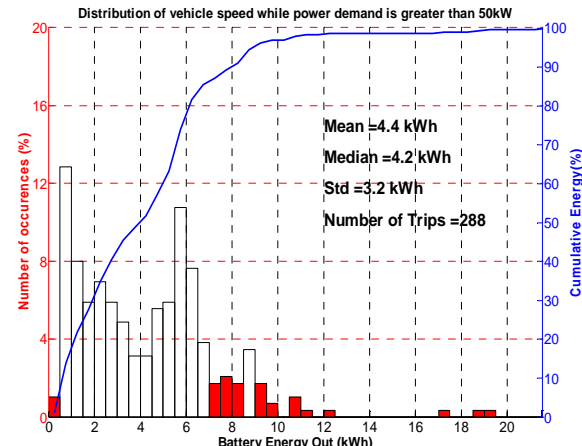


Figure 14. Distribution of the Battery Energy for Trips Longer than Two Miles

Figure 15 shows the usable energy as a function of distance for daily driving. Each point represents a trip. The UDDS (bottom – 230 Wh/mi), LA92 (middle – 330 Wh/mi) and US06 (top – 400 Wh/mi) are also drawn. Note that almost all of the real-world drive cycles are more aggressive than the UDDS. The US06 appears on the other side to represent the maximum limit. Finally, the LA92 seems to properly characterize the drivers from the data set. As a consequence, depending on the aggressiveness of the

cycle, a vehicle with 10-kWh usable power will have an all-electric distance varying from 25 to 42 miles.

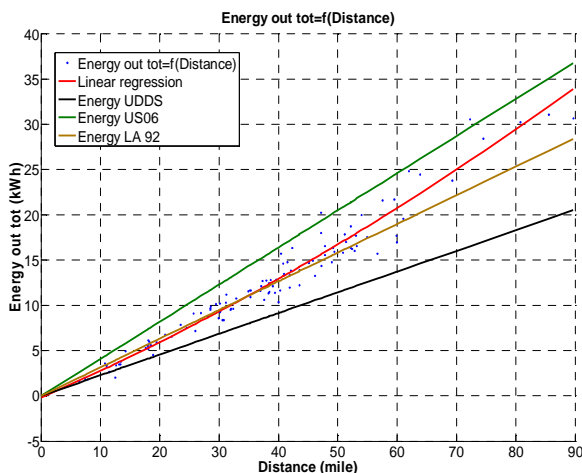


Figure 15. Comparison of Electrical Energy Consumption of Real-World Drive Cycles to Standard Cycles

Figure 16 shows the electrical energy distribution for each trip. Note that 90 percent of the trips have higher energy consumption than the UDDS.

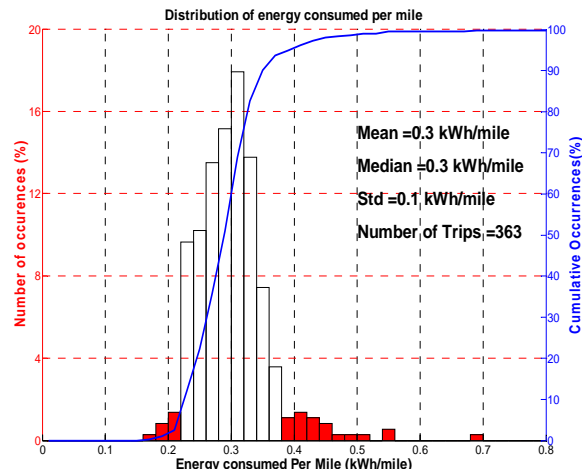


Figure 16. Electrical Energy Consumption Distribution

Conclusions

Real-world drive cycles for more than 110 drivers from Kansas City were used to assess the impact of trips on PHEV component requirements. The PHEV requirements analysis is only valid for the set of drive cycles considered and should not be generalized to the U.S. market. Several points can be drawn from this analysis:

- Aggressive driving will put limits on all-EV range, which, in turn, favors a blended mode operational strategy.
- When the battery is sized for the UDDS,
 - Power requirements are sufficient 97 percent of the time and
 - 1.5 percent (short-term goal) and 50 percent (long-term goal) of the daily driving can be completed in EV because of energy limitation.
- The real-world drive cycles are generally more aggressive than the UDDS, resulting in larger energy requirements to drive the same distance.
- LA92 seems to better represent current drive-cycle aggressiveness.

In the future, additional real-world drive cycles will be considered from different locations. Moreover, other parameters will be analyzed (such as air-conditioning) to evaluate their impact on the component requirements. Finally, a trade-off analysis will be performed between fuel efficiency and cost to maximize fuel displacement while minimizing cost.

Publications/Presentations

Fellah, M., Singh, G., Rousseau, A., Pagerit, P., "Impact of Real World Drive Cycles on PHEV Battery Requirements," SAE 09PFL-0612, SAE World Congress, April 2009.

Rousseau, A., Shidore, N., Carlson, R., "PHEV Battery Requirement - Uncertainty Based on Real World Drive Cycles and Impact on Fuel Efficiency," ANL Li-ion Battery Conference, September 2008.

Fellah, M., Singh, G., Rousseau, A., Pagerit, P., "PHEV Battery Requirements Uncertainties due to Real World Drive Cycles," DOE Presentation, Washington DC, September 2008.

H. Component Technology Impact on PHEV Fuel Efficiency

Aymeric Rousseau (project leader), Antoine Delorme

Argonne National Laboratory

9700 South Cass Avenue

Argonne, IL 60439-4815

(630) 252-7261; arousseau@anl.gov

DOE Technology Manager: Lee Slezak

(202) 586-2335; Lee.Slezak@ee.doe.gov

Objectives

Evaluate the impact of different technologies on plug-in hybrid electric vehicle (PHEV) efficiency.

Approach

Develop component models representing the technologies, including uncertainties.

Develop control strategies.

Define vehicles to fulfill the requirements.

Analyze the electrical and fuel consumption levels on several drive cycles on the basis of the latest J1711 test procedure.

Accomplishments

Evaluated different component technologies for PHEV applications on several all-electric range (AER) options.

Assessed fuel efficiency potential for each timeframe.

Future Directions

Evaluate each component technology independently.

Define technology characteristics that have the greatest impact on fuel efficiency.

Introduction

The objective of the study is to evaluate the impact of different component technologies on plug-in hybrid electric vehicles (PHEV). To do so, Argonne National Laboratory's (ANL) Powertrain System Analysis Toolkit (PSAT) was used to simulate vehicles having differing design assumptions. The study demonstrates potential fuel efficiency improvements related to component technology enhancements.

Assumptions

The assumptions for each component technology were defined for several timeframes (2008 to 2045). For each timeframe, uncertainties were considered by

using a triangular distribution (low, medium, and high case). While this approach is better than using a single value, it considers all assumptions to be correlated, which is usually not the case. For this reason, Monte Carlo analysis will be used to address the issue.

In the following section, each main components' assumptions are described in greater detail.

Engines

Several fuels were considered in the study, including gasoline, diesel, and ethanol, as well as a hydrogen engine. A different approach was used for the hydrogen engines compared to the other fuels.

Indeed, while a linear scaling based on the peak efficiency was assumed for gasoline, diesel, and ethanol, different technologies were used for the hydrogen engine (port injected and direct injected).

Fuel Cell Systems

The fuel cell system assumptions were derived from the FreedomCAR targets. The fuel cell system model is based on the steady-state efficiency map. The values shown in Figure 1 include those for the balance of plant. The system is assumed to be gaseous hydrogen. In simulation, the additional losses resulting from transient operating conditions are not taken into account.

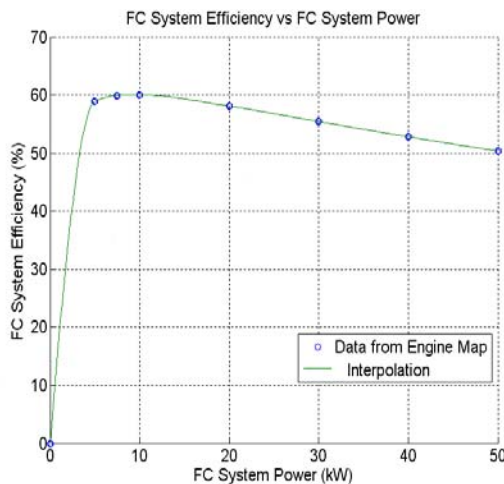


Figure 1. Fuel Cell System Efficiency versus Fuel Cell System Power from the System Map

Electric Machines

Similar to the fuel cell systems, a linear scaling based on the peak efficiency was used to represent the improvements of the electric machine. The electric machine data from the Toyota Prius and Toyota Camry were used for the power-split HEV applications, while the Ballard IPT was selected for series fuel cell PHEVs. Figure 2 shows the electric machine peak efficiencies considered, including the inverters.

Energy Storage Systems

Energy storage systems are a key component in advanced vehicles. Although there are numerous studies being conducted with ultracapacitors, only batteries were taken into account in the study. The VL41M battery pack from Saft has been

characterized. Because each vehicle is sized for both power and energy in the case of a PHEV, a sizing algorithm was developed to design the batteries specifically for each application.

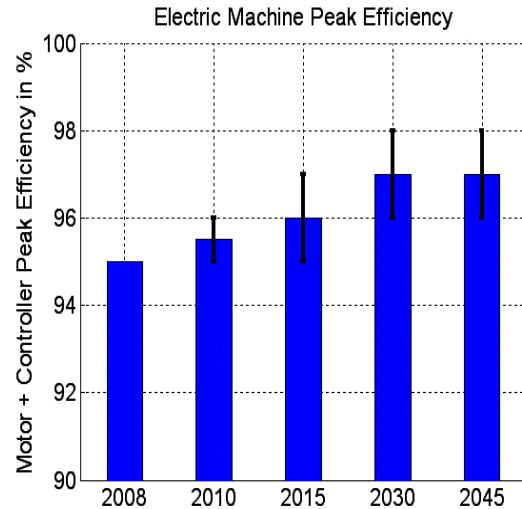


Figure 2. Electric Machine Peak Efficiency

To ensure that the battery has similar performance both at the beginning and end of its life, the packs were oversized both in power and energy. In addition, for PHEV applications, the state-of-charge (SOC) window (i.e., the difference between the maximum and minimum allowable SOC) increases over time, allowing a reduction of the battery pack.

Vehicle

As previously discussed, four vehicles classes were considered, as shown in Table 1.

Table 1. Vehicle Characteristics for Different Vehicle Classes

Vehicle Class	Glider Mass (Ref) (kg)	Frontal Area (Ref) (m ²)	Wheel Radius (m)
Midsize Car	990	2.2	0.317
Small SUV	1000	2.52	0.35925
Midsize SUV	1260	2.88	0.367
Pickup	1500	3.21	0.38165

Because of the improvements in material, the glider mass is expected to significantly decrease over time. The maximum value of 30 percent was defined on the basis of previous studies that calculated the weight reduction that one could achieve when replacing the entire chassis frame with aluminum.

Vehicle Simulation Results

Evolution of Engine PHEVs Fuel Efficiency

Figure 3 shows the impact of improved component efficiencies (e.g., efficiency, specific power) on fuel efficiency. All the values were calculated on the basis of the latest methodology from J1711, which was based on the two U.S. Environmental Protection Agency (EPA) drive cycles (i.e., urban dynamometer driving schedule [UDDS] and the Highway Fuel Economy Test [HWFET]).

As one notices, the fuel efficiency is significantly enhanced as a result of improvements in component technologies. For example, the power-split gasoline configuration designed for a 10-mile all-electric range (AER) on the UDDS sees its fuel consumption decrease from 3.4 l/100 km in 2008 to a range of between 2.8 and 2.1 l/100 km in 2045.

When considering different fuels, the hydrogen engine benefits the most from the technology improvements because of the fact that a change from a port-injected to a direct-injected engine is assumed. As a consequence, its fuel consumption drops from 3.6 l/100 km in 2008 to a range of from 1.6 to 2.3 l/100 km in 2045. As a result, the technology is expected to perform better than its gasoline counterpart at that time.

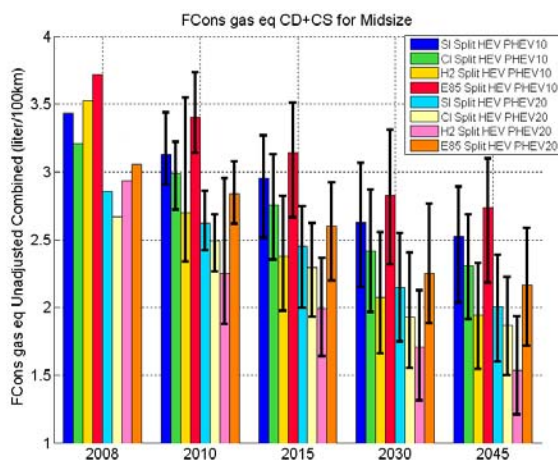


Figure 3. Fuel Consumption, Gasoline-Equivalent, Unadjusted, Combined for Split PHEV 10- and 20-mile Midsize Cars (Note: All the Fuel Consumption values are CD+CS.)

Figure 4 shows the fuel economy ratio of each fuel compared to the gasoline of the same year. Note that

the ratios between the different fuels remain constant, with the exception of the hydrogen engine. This result occurs because a change in technology was considered (port to direct injected) unlike in the case of the other fuels.

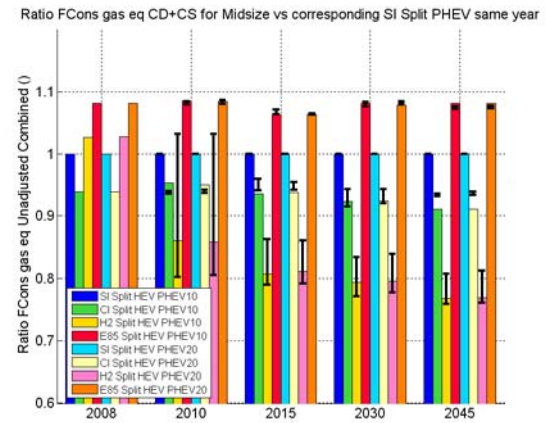


Figure 4. Ratio of the Fuel Consumption (Gasoline Equivalent, Unadjusted, Combined) in Comparison to the Gasoline PHEV with the Matching AER Range (Same Year, Same Case)

Figure 5 shows the electrical consumption of the midsize gasoline PHEV for different AERs. Note that the values slightly decrease over time. While numerous factors influence the results (e.g., frontal area, drag coefficient, rolling resistance, efficiencies), the main reason is related to the vehicle mass as shown in Figure 6. For every 200 kg, the weighted electrical consumption increases by 40 Wh/mi.

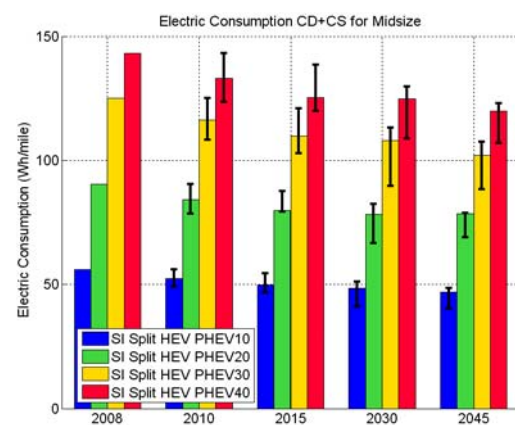


Figure 5. Electric Consumption in CD+CS for Gasoline Power-split PHEV Midsize Vehicles

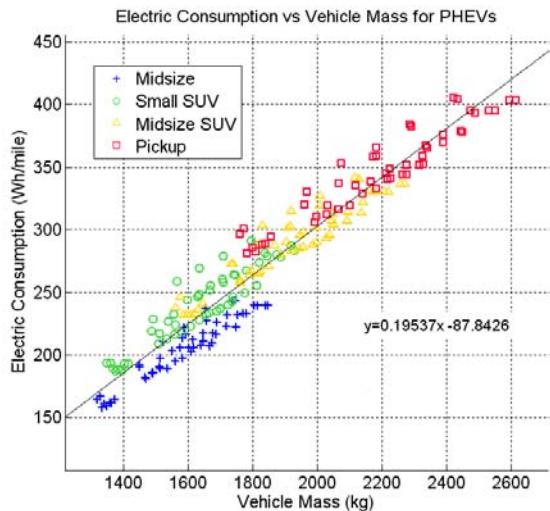


Figure 6. Electric Consumption as a Function of Vehicle Mass

In addition to having significant impacts on fuel efficiency, improved component technologies also lead to lower component requirements. Figure 7 demonstrates the impact on the battery energy. As one notices, the energy could be reduced by as much as a factor of two because of a combination of lighter vehicles and improved efficiency.

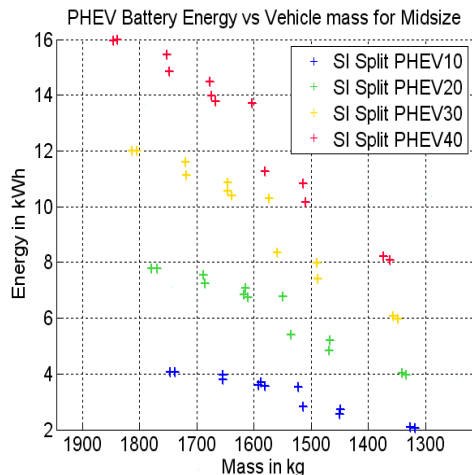


Figure 7. Battery Energy as a Function of Vehicle Mass for Gasoline PHEVs

Evolution of Fuel Cell PHEVs' Fuel Efficiency

The results for fuel cell PHEVs are similar to the power-split PHEVs in terms of data evolution from one AER range to another. However, the fuel consumption decreases at a slower rate than for the engine PHEVs. This result is because the fuel cell system is already very efficient. From 2008 to 2045

for the average case, the consumption decreases by 32 percent.

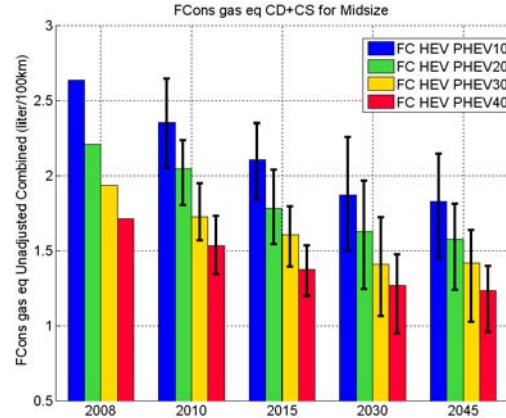


Figure 8. Fuel Consumption (Gasoline Equivalent, Unadjusted Combined) for Fuel Cell PHEVs Midsize Cars (Note: The Fuel Consumption Values are CD+CS)

Figure 9 shows the evolution of the electric consumption for the fuel cell PHEVs. While the consumption decreases with improved component technologies, it does so at a slower rate than for the engine PHEVs.

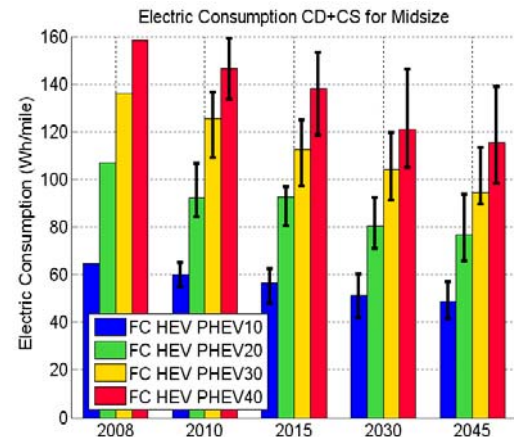


Figure 9. Electric Consumption in CD+CS for FC PHEVs Midsize Vehicles

Conclusions

The impact of component technologies on fuel efficiency for different timeframes has been evaluated. The simulation results demonstrated that significant fuel efficiency gains could be achieved by combining several enhancements. Future studies will focus on the improvement potential of each technology to define future research priorities.

I. Comparison of Powertrain Configuration for Plug-in HEVs on Fuel Efficiency

Dominik Karbowski (project leader)

Argonne National Laboratory

9700 South Cass Avenue

Argonne, IL 60439-4815

(630) 252-7261; arousseau@anl.gov

DOE Technology Manager: Lee Slezak

(202) 586-2335; Lee.Slezak@ee.doe.gov

Objectives

Compare different powertrain configuration options for plug-in hybrid electric vehicles on the basis of component sizes and fuel economies.

Approach

Select most promising powertrain configurations.

Develop control strategies by using similar philosophy to allow fair comparison.

Size the component to match the same vehicle-level requirements.

Compare the levels of electric and fuel consumption on several drive cycles.

Accomplishments

Compared component sizes for each configuration.

Compared fuel economy for each configuration.

Future Directions

Evaluate additional drivetrain configurations.

Refine the component sizing process.

Introduction

Plug-in hybrid electric vehicles (PHEVs) use electric energy from the grid rather than fuel energy for the majority of the time on short trips, thereby drastically reducing fuel consumption. Different configurations can be used for PHEVs. In this study, the parallel pre-transmission, series, and power-split configurations are compared by using global optimization. The latter allows a fair comparison between different powertrains. Each vehicle is indeed operated optimally to ensure that the results are not biased by non-optimally tuned or designed controllers. All vehicles were sized to have a similar all-electric range (AER), performance, and towing capacity. Several driving cycles and distances were

used. The advantages of each powertrain are discussed in detail.

Vehicle Description

Vehicle

To properly compare different configurations, it is important that they meet the same design requirements. A major difference could lead to biased results. The vehicles used in this study meet or exceed the following requirements. They:

- Perform the U.S. Environmental Protection Agency (EPA) urban dynamometer driving schedule (UDDS) cycle in the all-electric mode.

- Reach a battery state-of-charge (SOC) of 30 percent after 10 miles in all-electric mode on the UDDS, after starting at 90 percent of SOC.
- Sustain a 6 percent grade at 65 mph at gross vehicle weight on thermal energy alone.
- Reach 60 mph (96.6 km/h) in at least 9.3 s.
- Reach a top speed greater than 110 mph (177 km/h).

Components

All three vehicles share a common chassis that corresponds to a midsize or full-size car comparable to a Hyundai Sonata, with a glider mass of 1,142 kg. The drag coefficient is 0.28, while the wheel radius is 0.332 m.

The battery model is based on the test data of the Johnson Controls-Saft VL41M cell, which is a 3.6-volt 41-Ah cylindrical lithium-ion cell.

The mechanical components' characteristics are summarized in Table 1.

Table 1. Electric Machines and Engine Characteristics

Component	Peak Efficiency	Remarks
Engine	36%	Gasoline, spark-ignited
MG (parallel), Generator (series)	93.5%	Permanent magnet, top speed 6,000 RPMs
MG1 (split), MG (series)	93.5%	Permanent magnet, top speed 10,000 RPMs
MG2 (split)	95%	Permanent magnet, top speed 14,000 RPMs

The transmission used in the parallel configuration is a 6-speed automatic (4.2, 2.6, 1.8, 1.4, 0.8), with a final drive ratio of 3.32. That same final drive ratio is used in the series and split configuration. In those two configurations, the electric machines are coupled to the final drive with an additional ratio of 1.96. The planetary gearbox used in the power-split configuration has the same teeth number as the one in the Toyota Camry (30 at the sun, 78 at the ring).

There is an additional electric load of 250 W, corresponding to basic electric accessories.

Sizing Routine

Vehicles are sized by using an automated sizing routine that employs Argonne's Powertrain System Analysis Toolkit (PSAT), a forward-looking model. In the first step, the battery and electric machine power is sized to perform the UDDS. The number of cells is defined by an arbitrary voltage (215 V) that is within the voltage range of the electric machines under consideration. The battery capacity is then sized to meet the 10-mile AER on the UDDS. Next the engine must be sized in order to meet the grade requirements. If the vehicle does not meet the 0 to 60 mph requirement, the engine power is increased (as well as the motor power in the series and split).

The outcome of the sizing routine is summarized in Figure 1.

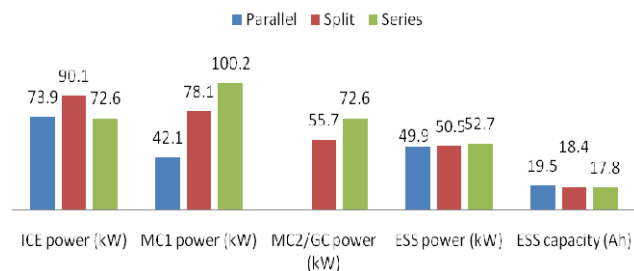


Figure 2. Power and Battery Capacity of Components

Engine power is 73 kW for the series and the parallel configuration, while it is 90 kW for the split. This setting is because of the 0 to 60 mph requirements. Because the engine speed is proportional to the vehicle speed and the MG2 maximal speed, it reaches its peak power only at high vehicle speed, while it can be reached earlier in the other configurations. The battery size is similar from one configuration to another. The total masses of the vehicles are 1,782 kg for the parallel, 1,824 kg for the split, and 1,793 kg for the series.

Optimization Problem

A hybrid system can be considered to have two degrees of freedom: engine speed and torque. For the parallel configuration, the engine speed is defined by the gear ratio and the vehicle speed. In that case, the command is engine torque and gear number.

In the case of the series and the power-split configurations, the transmission is continuous; using torque and speed as commands would result in too

many combinations to consider. Therefore, the command for the series (resp. power-split) is the generator electric power (resp. engine power). The generator set (resp. engine) is assumed to operate along its best efficiency line: for a given generator of electric power (engine mechanical power), the engine speed and torque are such that the engine fuel rate is minimal.

For all configurations, the operating points of the other components can be known by using the models described previously.

We define the state of the system as the battery state-of-charge (SOC). The optimization problem aims at finding the command u and the resulting states that minimize the function J defined in Equation 1. It is the sum over the cycle of fuel power P_{fuel} and a penalty function P_{pen} used to penalize aggressive changes in the command. In other words, we look for a command that will minimize the fuel use, while resulting in acceptable behavior of components.

$$J(SOC, u) = \int_0^{t_{end}} (P_{fuel}(SOC, u) + P_{pen}) dt$$

Equation 1

Because the time derivative of the SOC is proportional to the battery current, state and command are linked by equation (2).

$$\frac{dSOC}{dt} = -\frac{I_{ess}(P_{ess}(u, SOC))}{Q_{ess}}$$

Equation 2

The initial condition is an SOC value between the maximal and minimal limits, or 91 percent and 25 percent, respectively. Furthermore, the system has to operate under several constraints:

- Vehicle follows cycle vehicle speed;
- Final SOC is 30 percent;
- Engine and electric machines operate within their speed and torque limits; and,
- SOC stays between the upper and lower bound defined previously.

Optimal Control

One run of the global optimization algorithm has this output of optimal results for the following combination of initial and final states:

- $SOC_{min} \leq SOC(t=0) \leq SOC_{max}$
- $SOC(t=t_{end}) = SOC_{final}$

It is therefore possible to analyze the data for a broad range of SOC swings, that is, for a wide range in rates of electric consumption. An electric consumption rate of zero corresponds to a charge-sustaining mode, and the higher its value, the closer it is to the maximal battery depletion.

Figure 2 shows the power at the wheels above which the engine is ON 95 percent of the time. Such a parameter can be compared to an engine ON threshold, which triggers an engine start in a rule-based control. For all three configurations, this parameter follows an increasing trend. At high depletion rates (i.e., high electric energy consumption), the engine starts at higher loads. That “engine start triggering” road load is similar for the power-split and the parallel, while it is higher for the series configuration: at the zero rate of electricity consumption (i.e., charge-sustaining), it is 3.5 kW and 4 kW for the split and parallel, as compared to 6.3 kW (50 percent more).

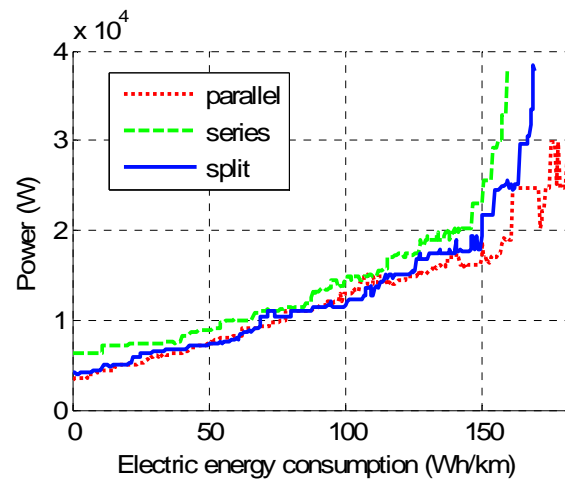


Figure 2. Power at the Wheels, Above Which the Probability of the Engine Being ON Is Above 95 percent (UDDS x1)

Figures 3 and 4 illustrate, respectively, the average engine efficiency and the average engine power when it is on. Both parameters follow the same trends. In the parallel case, there is a clear increasing trend for both the engine power and efficiency, as higher loads allow the engine to operate in more efficient areas. The engine efficiency in the split configuration is higher and relatively constant owing to the ability of the planetary gear to make the engine operate in efficient areas. The efficiency, however, is not as high as for the series (35 percent versus 35.8 percent) because a potential gain in engine efficiency would have resulted in worse overall system efficiency as a result of higher recirculation and/or charging rates. In the series configuration, the engine operates very closely to its maximal efficiency at a 16-kW level.

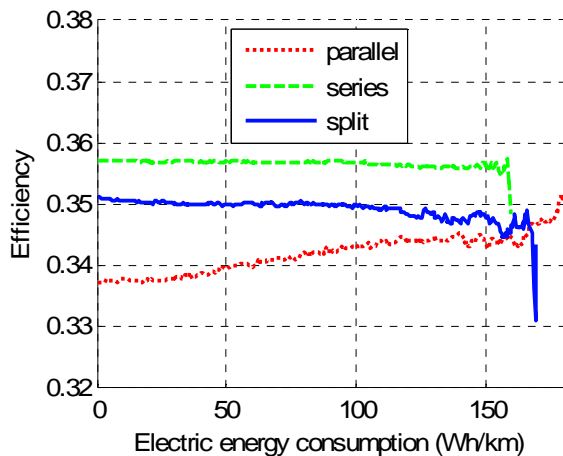


Figure 3. Average Engine Efficiency (UDDS x1)

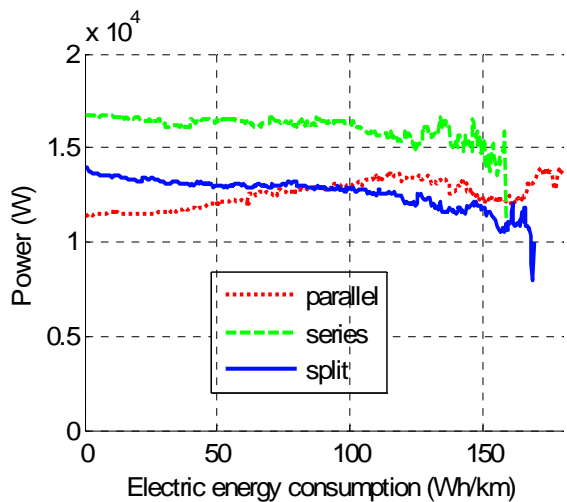


Figure 4. Average Engine Power When On (UDDS)

The series configuration also tends to have the engine charging the battery, as depicted in Figure 5, which displays the share of the total engine mechanical energy that is used to charge the battery. In charge-sustaining mode, more than 10 percent of the engine output is directed to the battery, as opposed to 6 percent for the split and 4 percent for the parallel. This change can be explained by the fact that charging is not as much penalizing for the series as it is for the two other configurations. All the engine output has to be converted through the generator, whether it goes to the wheels or the battery. Directing the engine energy to the battery instead of the motor results in battery losses. In the other configurations, the engine power does not have to be converted into electrical energy first to be used to propel the vehicle; however, it does have to be converted in order to charge the battery. Therefore, the motor losses (both ways) come on top of battery losses; in the best-case scenario — that is, assuming maximum motor/generator efficiency both ways (0.95 for the split using MG2, 0.935 for the parallel) — that would add 10 percent to 15 percent losses in the generating path, which means that additional gains in engine efficiency would not offset the induced conversion losses.

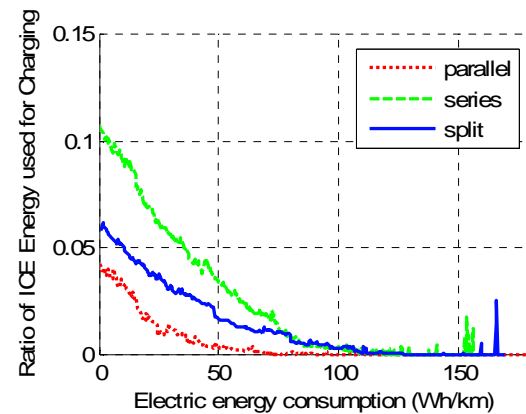


Figure 5. Share of the Engine Energy Used to Recharge the Battery (UDDS)

To summarize, in the parallel configuration, the engine power is oriented for the most part directly to the driveline — all the more so when the use of the engine is low (i.e., battery depletion is high). At higher depletion rates, the engine is started at higher road loads, leading to higher engine loads and increased efficiency.

In the series configuration, the engine is always operated at high efficiency and higher engine load. At low depletion rates, especially in charge-sustaining mode, it translates in battery charging from the engine.

The split configuration also achieves good efficiency (although not as good as the series' level) independently from the battery depletion rate. There is, however, less battery charging from the engine.

Energy Consumption

Figure 6 shows the trade-off between fuel and electricity use for one UDDS.

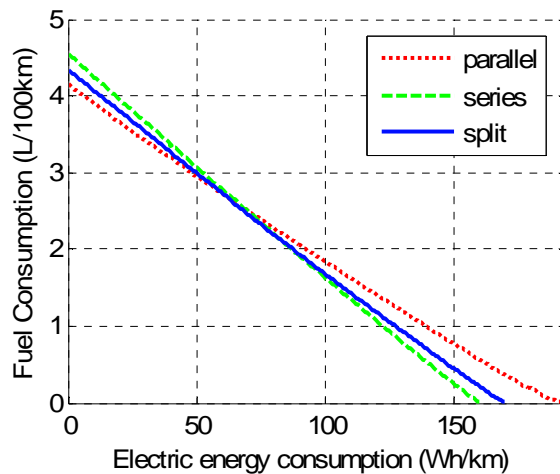


Figure 6. Fuel Consumption (UDDS x1)

In EV-mode, the series is the more efficient configuration, with 160 Wh/km plug-to-wheel (i.e., taking into account the charger efficiency). The transmission is only composed of the final drive and the torque coupling, which makes it very efficient. In the power-split configuration, the planetary gearbox, because of its high efficiency, accounts for the slightly higher electric energy consumption (169 Wh/km). The parallel configuration consumes more electric energy (195 Wh/km) because of its transmission, the bidirectional efficiency of which is 88 percent. It is slightly compensated by a better motor efficiency: 89.2 percent versus 87.5 percent for the series and 87 percent for the power-split.

In charge-sustaining mode, the parallel configuration appears to be the most fuel-efficient (4.1 l/100 km). The series configuration is the least efficient (4.5 l/100 km) because of the inherent inefficiency of the hybrid transmission as the engine output power is

first converted into electrical power by the generator before being converted back into mechanical power by the motor. The efficiency of the path between the engine and the input of the final drive is, at best: $\eta_{Gen} \times \eta_{MG} \times \eta_{tc} = 85$ percent, which assumes that both electric machines work at peak efficiency and that there is no battery buffering. It is actually lower than 80 percent. The power-split configuration's fuel consumption (4.3 l/100 km) is slightly worse than the parallel one because of the inefficiency induced by the recirculation.

Conclusions

A global optimization algorithm was used to compare three different powertrain configurations.

For electric operations, the results demonstrated a higher efficiency for the series configurations, reinforcing the fact that this mode should be used with high-energy batteries.

For charge sustaining, the parallel configuration demonstrates the best results. It is, however, important to mention that drive quality factors, such as number of shifting events and engine ON/OFF, could influence these results.

For the blended mode, all configurations demonstrate similar efficiencies, which would put parallel and power-split configurations at an advantage from the perspective of cost as compared to the series configuration.

J. Development of Models for Advanced Engines and Emission Control Components

Stuart Daw (Principal Investigator)

Oak Ridge National Laboratory

National Transportation Research Center

2360 Cherahala Boulevard, Room L-04

Knoxville, TN 37932-6472

(865) 946-1341; dawcs@ornl.gov

DOE Program Manager: Lee Slezak

(202) 586-2335; Lee.Slezak@ee.doe.gov

Objectives

Ensure that computer simulations using the Powertrain System Analysis Toolkit (PSAT) have the necessary components to accurately reflect the drive performance, cost, fuel savings, and environmental benefits of advanced combustion engines and aftertreatment components as they could potentially be used to optimize leading-edge hybrid electric and plug-in hybrid electric vehicles (HEVs and PHEVs).

Apply the above component models to help the Department of Energy (DOE) identify the highest HEV and PHEV research and development priorities for reducing U.S. dependence on imported fuels.

Approach

Develop and validate low-order, physically consistent computational models for emissions control devices including oxidation catalysts (OCs), lean NO_x traps (LNTs), diesel particulate filters (DPFs), and selective catalytic reduction reactors (SCRs) that accurately simulate HEV and PHEV performance under realistic steady-state and transient vehicle operation;

Develop and validate low-order, physically consistent computational models capable of simulating the power out and exhaust characteristics of advanced diesel and spark-ignition engines operating in both conventional and high efficiency clean combustion (HECC) modes;

Develop and validate appropriate strategies for combined simulation of engine, aftertreatment, and exhaust heat recovery components in order to accurately account for and compare their integrated system performance in conventional, HEV, and PHEV powertrains;

Translate the above models and strategies into a form compatible with direct utilization in the PSAT framework;

Leverage the above activities as much as possible through inclusion of experimental engine and aftertreatment data and models generated by other DOE activities.

Accomplishments

Generated Saab 2-L BioPower flex-fuel engine maps for both gasoline and ethanol fueling.

Validated the Saab engine maps with cold and hot start vehicle chassis dynamometer data.

Generated the first public map for the GM 1.9-L research diesel engine that is capable of HECC combustion and is being used as a common reference engine by the national labs and several universities.

Added and validated external heat loss and thermal transient models to PSAT that can account for these effects on hybrid vehicle performance.

Documented the LNT PSAT model as a template for future lean-exhaust aftertreatment components.

Constructed a new three-way catalyst model for PSAT to be used to account for catalyst light-off and extinction on stoichiometric hybrid vehicles.

Tested preliminary DPF and SCR lean exhaust aftertreatment models for PSAT.

Demonstrated a preliminary thermoelectric generator (TEG) model for simulating thermoelectric exhaust heat recovery.

Demonstrated comparisons between stoichiometric and lean engine based HEVs using PSAT.

Demonstrated the usefulness of PSAT for making leading-edge integrated engine-aftertreatment concepts evaluations to the Crosscut Lean Exhaust Emissions Reduction Simulation (CLEERS) Focus Groups and the DOE Diesel Crosscut Team.

Future Directions

Continue refinement and testing of the PSAT 3-way catalyst model and apply it to assessments of the impact of operating and control strategies on HEV and PHEV fuel efficiency and emissions performance.

Begin development of a refined engine transients model that includes the effect of coolant thermal storage.

Demonstrate HEV simulations with lean direct-injected gasoline combustion.

Continue comparisons of diesel and gasoline HEV and PHEV fuel efficiency and emissions.

Implement and demonstrate DPF particulate matter (PM) control in PSAT for diesel HEV.

Demonstrate Urea-SCR NO_x control in PSAT for diesel HEV.

Investigate possibility of updating PSAT algorithms for engine scaling to include emissions.

Define reference HEV cases for evaluating the impact of exhaust heat recovery by means of thermoelectrics, thermochemical recuperation, and Rankine bottoming cycles.

Close coordination with Combustion MOU, ACEC, DCC Team, and CLEERS to ensure access to the latest engine/emissions technology information and industry needs

Introduction

Accurate systems simulations of the fuel efficiency and environmental impact of advanced vehicle propulsion and emissions control technologies are vital for making informed decisions about the optimal use of research and development (R&D) resources and DOE programmatic priorities. One of the key modeling tools available for making such simulations is the Powertrain System Analysis Toolkit (PSAT) maintained by Argonne National Laboratory (ANL). A distinctive feature of PSAT is its ability to simulate the transient behavior of individual drivetrain components as well as their combined performance effects under realistic driving conditions. However, the accuracy of PSAT simulations ultimately depends on the accuracy of the individual component sub-models or maps. In some cases of leading-edge technology, such as with engines utilizing high efficiency clean combustion (HECC) and lean exhaust particulate and nitrogen oxide (NO_x) controls, the availability of appropriate component models or the data to construct them is very limited.

Oak Ridge National Laboratory (ORNL) is a collaborator with ANL on the vehicle systems analysis technical team (VSATT) and is specifically tasked with providing data and models that augment PSAT's capabilities. Specifically, ORNL's role has focused on the experimental measurement of performance data from advanced diesel engines and emissions controls components and the incorporation of that data in the form of maps or low-order transient models into PSAT. In fiscal year 2008, the ORNL team concentrated its efforts in the following areas:

Measurement and validation of engine maps for the Saab BioPower 2-L flex-fuel engine;

Generation of the first public map for the GM 1.9-L research diesel engine, including HECC combustion capability;

Addition of external heat loss and thermal transient models to PSAT that can account for engine start/stop on HEV performance;

Documentation of the PSAT LNT NO_x control model;

Preliminary testing of DPF and SCR aftertreatment models;

Simulation of thermoelectric exhaust heat recovery in PSAT; and

Demonstration of PSAT simulations for comparing lean and stoichiometric engines in HEVs.

Approach

Most current HEV and PHEV engines utilize stoichiometric engines, which are the predominant technology in most passenger cars in the U.S. today. In these engines, the fuel and air are balanced so that there is no excess oxygen present in the exhaust. With stoichiometric engines the emissions can be very effectively controlled with three-way catalyst aftertreatment technology. The greatest needs for improving simulations of hybrid vehicles utilizing stoichiometric engines involve development of engine maps and models that accurately predict emissions and exhaust temperature as functions of speed and load under the highly transient conditions in normal drive cycles. Also, improved models are needed to capture the effects of start/stop transients in hybrid vehicles on the functioning of three-way catalysts, since the latter have been developed for more consistent engine operation than what occurs in hybrids.

More advanced combustion engines offer the potential for significantly increasing the fuel efficiency of hybrid vehicles. These engines rely on lean combustion conditions (i.e., conditions where air is present in significant excess) and novel combustion states (e.g., HECC) where there is little or no flame present. While beneficial in reducing emissions, such lean combustion also involves larger and more drastic transient shifts in engine operation as driving demands change. Even though emissions are significantly reduced, they are still present in sufficient amounts to require exhaust aftertreatment subsystems for removing NO_x and particulate matter (PM).

Both NO_x and PM removal from lean exhaust involve complex transient and hysteretic interactions with the engine. The demands on the engine

operation are further heightened by the need to periodically denitrify and desulfate LNTs and oxidize the carbonaceous particulate matter in DPFs. Simulation of such complicated behavior makes it necessary to build more sophisticated component models that exploit the known physics and chemistry of these devices as well as the best available experimental data.

Considering the above, the ORNL modeling team is building stoichiometric and lean aftertreatment component models for PSAT utilizing proven approaches for simulating transient chemical reactors. The basic elements of these models include:

Detailed time resolved information on the flows, species, and temperatures entering the device;

Differential, transient mass balances of key reactant species;

Localized surface and gas-phase reaction rates;

Differential, transient energy balances and temperatures within the device;

Time resolved flow, species, and temperature for the gas stream exiting the device.

As much as possible, the descriptions of the internal reaction and transport processes are simplified to account for the dominant effects and physical limits while maintaining execution speeds acceptable for typical PSAT users. For example, there are no cross-flow (i.e., radial) spatial gradients accounted for in the devices, and the kinetics are defined in global form instead of elementary single reaction steps. This ‘in-between’ level of detail still allows for faithful simulation of the coupling of the after-treatment devices to both upstream and downstream components (arranged in any desired configuration). With the above information it is also possible for PSAT to determine both instantaneous and cumulative performance for any desired period.

Due to the greater complexity of engines, it is not practical to develop models with the same level of dynamic detail as in the aftertreatment component models. Instead, the usual approach for engine modeling relies on tabulated ‘maps’ developed from steady-state or pseudo-steady-state experimental engine-dynamometer data. Recently, it has been

possible to develop maps that extend over both conventional and HECC operating ranges. Another key feature remaining to be added is an engine control sub-model that determines how the engine needs to operate (e.g., make transient shifts in combustion regime) in order to accommodate the needs of aftertreatment devices downstream. Typically this also involves development of sensor models that indicate the state of the aftertreatment devices.

In future work, it is anticipated that experimental engine data can be supplemented with engine cycle simulations using large and complex engine simulation codes such as GT Power, which can account for many different effects and operating states that may be difficult to measure experimentally. It is expected that the results from these codes can be captured in more sophisticated formats (e.g., neural networks) than is possible with simple tabulated maps.

Results

Engine Mapping. Using steady-state engine-out emissions measurements for the Saab BioPower flex-fuel vehicle reported last year, we constructed corresponding emissions maps for both gasoline and E85 fuels for PSAT. A highly simplified dynamic transform was then developed to relate the steady-state emissions values from the maps to what would occur under transient conditions based on past history. Figure 1 illustrates a comparison between engine-out NO_x predictions made using this dynamic algorithm and experimental measurements made for the Saab vehicle fueled by gasoline and operating under an Urban Dynamometer Driving Schedule (UDDS) initiated by a cold start. The predicted net emissions of 4.5 g NO_x/mi, 1.9 g hydrocarbons (HC)/mi, and 12.6 g carbon monoxide (CO)/mi are in good agreement with the experimental values of 4.3 g NO_x/mi, 2.1 g HC/mi, and 12.0 g CO/mi. Similar good agreements between the PSAT transient engine-out predictions and experiments have now been demonstrated using this same dynamic algorithm.

We also developed a similar dynamic transform algorithm to predict transient engine-out exhaust temperatures based on steady-state maps. Figure 2 illustrates the agreement between the resulting engine exhaust temperature predictions and experimental measurements for the Saab BioPower vehicle fueled

by E85 and operating over the UDDS cycle after initiation with a cold start. Subsequent improvements to the thermal transient transform have improved the agreement even further.

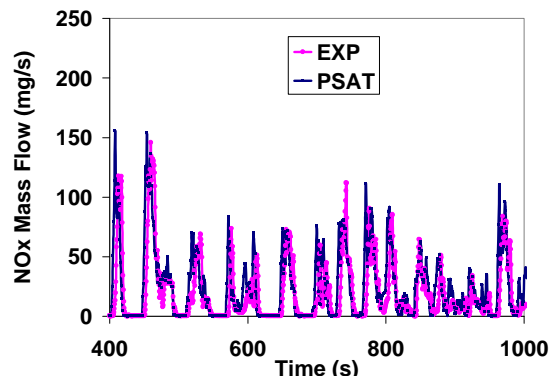


Figure 1. Example comparison between experimental measurements of engine-out NO_x for the Saab flex-fuel vehicle (fueled with gasoline) and transient adjusted map-based predictions from PSAT. For visibility, the plot shows only a 600-second interval from a cold start UDDS drive cycle.

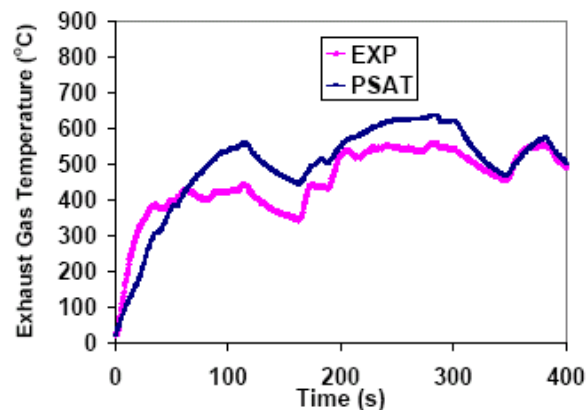


Figure 2. Comparison between experimental measurements of engine exhaust temperature for the Saab flex-fuel vehicle (fueled with E85) and map-based predictions from PSAT. For visibility, the plot shows only the first 400 seconds of a cold start UDDS drive cycle.

Accurate prediction of the engine exhaust composition and temperature during typical drive cycle transients is especially important for HEV and PHEV simulation because of the frequent engine shutdowns and restarts that occur as battery state of charge is managed over time. For both stoichiometric and lean exhaust engines, the transients resulting from engine shutdowns and startups translate into catalyst de-ignition and re-ignition events in the

aftertreatment devices. These events can significantly impact aftertreatment performance as illustrated in the discussion below.

In addition to refining and applying the emissions and temperature maps for the Saab 2-L engine, we generated the first public maps for the GM 1.9-L diesel research engine. This engine has become a standard reference engine among the national labs and universities involved in researching advanced diesel combustion, including the so-called HECC mode. While the present maps are based on a non-standard engine calibration, they provide the first available public reference point for developing PSAT simulations based on more current HECC-capable engine designs. It is anticipated that future versions of these maps (based on different calibrations) will become available as research efforts using this engine intensify.

Aftertreatment Modeling and Hybrid Vehicle Simulations.

Three-way catalysts are used to simultaneously reduce emissions of NO_x , CO, and HC in stoichiometric engine exhaust. Because most current HEVs and PHEVs utilize stoichiometric gasoline engines, it is important to have accurate three-way catalyst models to simulate their emissions. We spent considerable effort this year in developing and validating a three-way catalyst model suitable for general implementation in PSAT. Although three-way catalysts have been available now for over three decades, accurately modeling their dynamic characteristics is a considerable challenge because of their complex chemistry. The modeling challenge is further compounded by the need to minimize the integration time in the PSAT environment so that simulations including three-way catalyst effects do not involve significantly longer run times.

Figure 3 illustrates example results from including three-way catalyst emissions effects in a PSAT HEV simulation. In this case the simulated vehicle is a mid-size parallel HEV powered by a 2-L Saab engine and operated from a cold start through a UDDS drive cycle. Without the catalyst, the net tailpipe emissions are 1.03 g/mi HC, 7.06 g/mi CO, and 3.13 g/mi NO_x . With the catalyst, net emissions drop to 0.29 g/mi HC, 1.14 g/mi CO, and 0.21 g/mi NO_x .

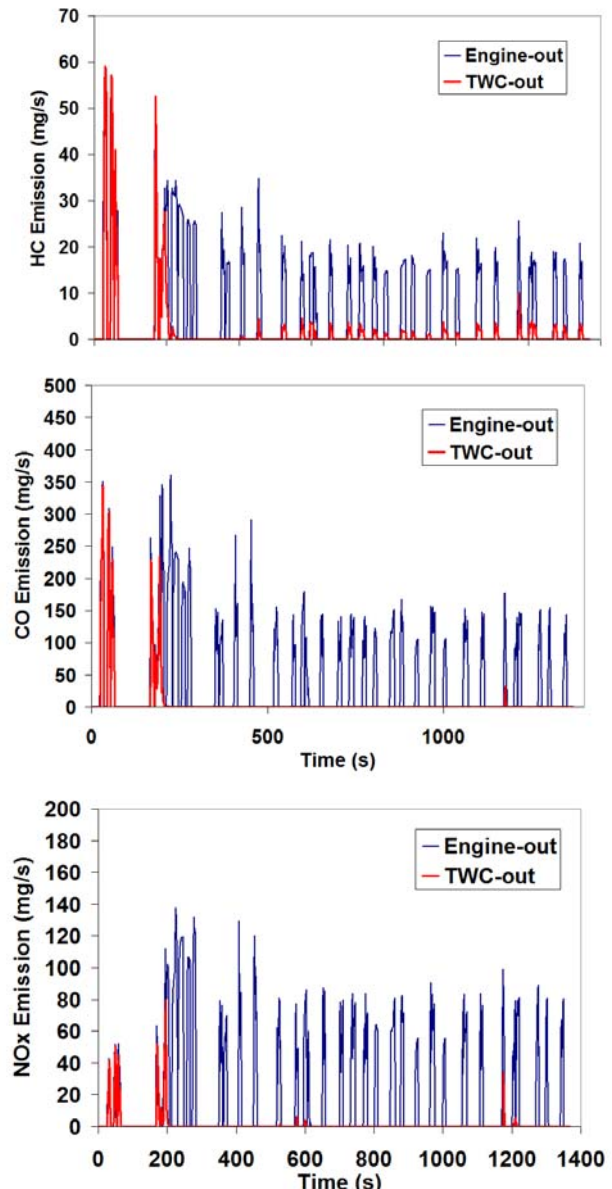


Figure 3. Example PSAT HEV simulation results illustrating the impact of a 3-way catalyst on emissions. Blue indicates the engine out level and red indicates the catalyst out (tailpipe) level. The catalyst reduces cycle average emissions from 1.03 g HC/mi, 7.06 g CO/mi, and 3.13 g NO_x /mi to 0.29 g HC/mi, 1.14 g CO/mi, and 0.21 g NO_x /mi.

Figure 4 illustrates how a three-way catalyst can affect HEV emissions control depending on the battery charge management strategy used. In this example, the battery management strategy adjusts the time interval that the engine must remain on once it is restarted to maintain battery charge. The vehicle and engine specifications are the same as in Figure 3 in this case. As the specified engine on-time is decreased, fuel consumption also decreases because the battery is more effectively used. However, the three-way catalyst performance begins to suffer with increased restarts due to light-off delay. In this case cycle average emissions reach a minimum at a reduced fuel economy. Recognition of this kind of competition between fuel efficiency and emissions in simulations of current HEVs would not be possible without a reliable three-way catalyst model.

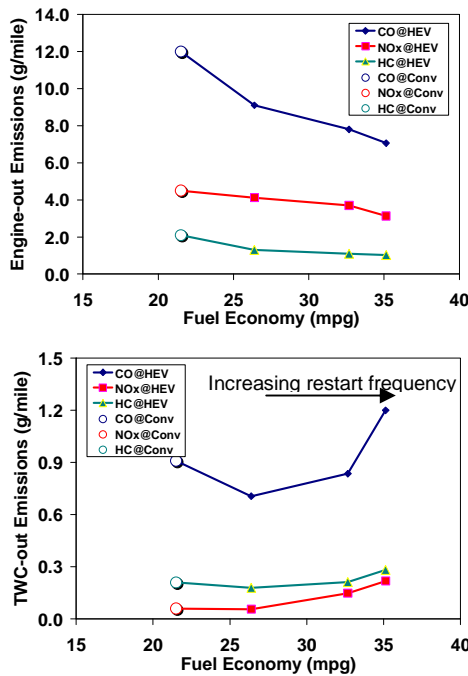


Figure 4. Example PSAT HEV simulation results illustrating the effect of repeated engine starting on fuel economy and emissions. Cycle average emissions reach a minimum at an intermediate restart frequency where fuel economy is reduced.

To quantify the potential benefits of utilizing lean combustion engines (e.g., diesels or direct-injected gasoline engines) for HEVs and PHEVs, we have begun utilizing PSAT to simulate the emissions and fuel efficiency differences between stoichiometric and lean engine HEVs and PHEVs. Figure 5 illustrates example comparisons between a Civic

configuration vehicle powered by a 1.5-L Prius engine (gasoline fueled) and a similar vehicle powered by a scaled down 1.7-L Mercedes diesel. Both HEVs are operated through a UDDS cycle beginning with a hot start. The plotted points indicate instantaneous efficiency at different times in the drive cycle. As expected, the diesel engine exhibits some efficiency advantage. The estimated diesel peak engine efficiency is 41 percent compared to 37 percent for the gasoline engine. Overall cycle average efficiencies are lower (36 percent versus 34 percent, respectively), reflecting the fact that both engines are required to operate away from their peak efficiencies due to the cycle demands. Because diesel fuel has a higher energy density, the mileage estimates for the two vehicles exhibit even greater differences (84.2 mpg versus 71.2 mpg, respectively).

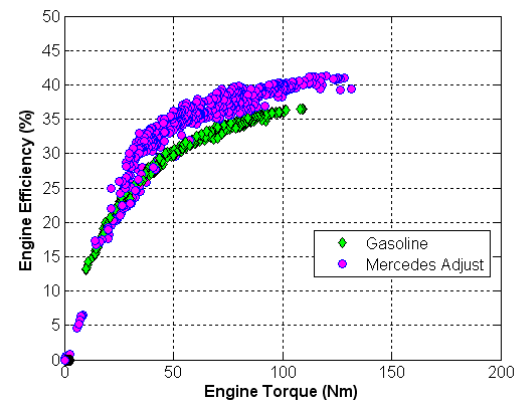


Figure 5. Simulated engine efficiency comparison for diesel and gasoline HEVs. The points indicate instantaneous efficiency at different times in the drive cycle. The estimated diesel peak engine efficiency is 41% compared to 37% for the gasoline engine. Cycle average efficiencies are 36% versus 34%, respectively.

We actually expect that the diesel efficiency advantage described above may be conservative if a more current diesel engine map is considered (the Mercedes engine is now considered somewhat outdated). We plan to investigate this further in the future using the GM 1.9-L engine measurements as a basis for updated simulations.

However, in Figure 6, we see that the diesel efficiency advantage may also be reduced because of the need to utilize lean NO_x aftertreatment instead of a 3-way catalyst. The results in Figure 6 are from a simulation that includes an LNT for lean NO_x control. The simulated vehicle and drive cycle are

the same as in Figure 5. The LNT reduces NO_x emissions by 87 percent but also creates a two percent fuel penalty. Further penalties are expected when particulate emission and diesel oxidation catalyst controls are added.

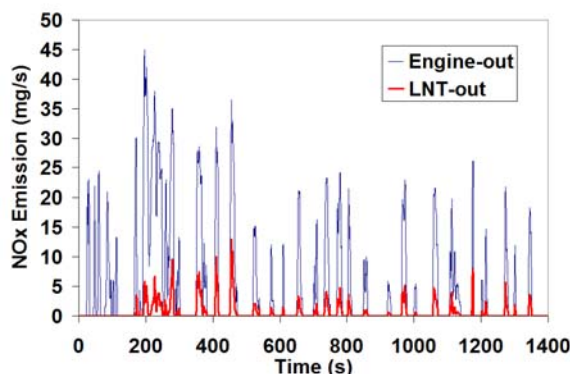


Figure 6. Simulated impact of lean NO_x control using an LNT on diesel HEV emissions. The LNT reduces NO_x emissions by 87% but also results in a 2% fuel penalty.

Conclusions

The transient engine-out emissions and temperature predictions of the Saab 2-L BioPower engine are well described by the dynamic transform combined with the steady-state maps developed for PSAT for both gasoline and E85 fuels. It appears that this approach for handling the effects of transients on aftertreatment can be adapted to other engines as well.

A simplified three-way catalyst model has been developed for PSAT and validated against three-way catalyst measurements on the Saab BioPower vehicle.

HEV simulations that include the three-way catalyst effects on emissions reveal competing trends between fuel efficiency and emissions control performance as the engine restart interval is shortened.

HEV simulations comparing diesel and conventional gasoline-power vehicles indicate that diesel vehicles will have modest efficiency advantages. However, the extent of these advantages may be reduced when the full fuel penalty for lean emissions controls is accounted for.

FY 2008 Publications/Presentations

“An Update on Lean NO_x Trap Modeling in PSAT,” K. Chakravarthy, 11th CLEERS Workshop, May 13-15, 2008, <http://www.cleers.org>.

K. PHEV Value Proposition Study

R. DeVault

*Engineering Sciences & Technology Division
Oak Ridge National Laboratory
(865) 574-2020, devaultrc@ornl.gov*

*DOE Program Manager: Lee Slezak
(202) 586-2335; Lee.Slezak@ee.doe.gov*

Objectives

The Oak Ridge National Laboratory (ORNL), with the support of Sentech, Inc., the Electric Power Research Institute (EPRI), and General Electric (GE), will conduct a study of the benefits, barriers, technical and infrastructure requirements, opportunities, and challenges of grid-connected, plug-in hybrid electric vehicles (PHEV) in order to establish potential value propositions that will lead to commercially viable PHEVs.

Approach

Phase 1 consists of:

Identification of potential propositions through a workshop with a guidance committee and other stakeholders;

Down-selection of business cases for further study;

Development of the analytical toolset using current technical research and industry-recognized models of vehicle design,

Battery controls and electric utility grid operation; and

Evaluation of the first down-selected value proposition using the toolset to identify the conditions under which the value to the owner will justify the cost or investment.

Phase 2 will continue the process with other value propositions as well as identify technical and market barriers that must be overcome to achieve market success, and apply the results of the evaluations to national and regional assessments.

Accomplishments

Held a PHEV Value Proposition Workshop with stakeholders from automotive suppliers, original equipment manufacturers (OEMs), utilities, transmission and distribution companies, government, regulators, and automotive dealerships.

Integrated data and models that are highly regarded by industry. These data and models aggregated the technical and economic impact of 17 PHEV value propositions on vehicle components and systems, facility owners, transmission and distribution systems, and utility power generation plants for a baseline case study of Southern California in 2030.

Coordinated laboratory meetings for collaborating PHEV activities among the DOE national laboratories.

Reported on the findings of the PHEV Value Proposition Study Workshop, data and model building, and assessment results.

Milestones

Completed Phase 1 of study (September 2008), with the exception of one final round of comments/reviews for the Phase I report.

Tasks 1 and 2 of Phase 1 have been completed. Task 3 (Technical Requirements and Procedure for Evaluation of One Scenario) has been completed.

Revised the report for Task 4, Phase I PHEV Value Proposition Study Interim Report, which incorporates the comments and edits made by Department of Energy (DOE) staff and members of the Guidance and Evaluation Committee (September 2008).

Sent the revised report in September for a final review with comments due by October 17, 2008.

Future Directions

Since the Phase I evaluation for Southern California likely displays the most favorable scenario for the introduction of PHEVs, future case studies will investigate alternative geographic settings to account for the nation's diverse range of generation mixes, climates, and other variables. Possible candidates for future locations include the primarily coal-fired generation mix of the Tennessee Valley and the highly diversified mix of the colder Northeast region. A scenario that represents a location with a high nuclear generation mix may also be analyzed to quantify potential benefits resulting from significantly reduced CO₂ emissions.

More extensive sensitivity analyses are also planned for future phases in order to provide a more comprehensive market outlook. Phase 2 will include the following anticipated additions to the "baseline" model:

Advanced ancillary services for vehicle-to-grid (V2G) operation (e.g., spinning reserves, regulating reserves, volt/var support,).

Enhanced responsive load (e.g., regulating the charge for an aggregation of PHEVs at a parking facility,).

Increased utilization of renewable energy generated on-site through enhanced vehicle-to-building (V2B) capability.

Business models for battery leasing, third party ownership, and battery buy-back/recycling programs.

Along with the refinements to the baseline model and the assessment of additional geographic regions, Phase II will include:

Identification of the technical requirements and evaluation procedures needed to analyze the additional case studies.

Technology risk assessment of the value propositions.

Continuation of the laboratory coordination meetings.

Based on feedback on Phase I, a Market Introduction Study will be conducted in fiscal year (FY) 2009 to identify actions items that are critical to creating and sustaining a market for PHEVs. The impact of potential action items will be assessed, and possible pinch points during market growth will be identified. Results will be used to recommend an action plan aimed at successfully transitioning what began as a grassroots industry into a thriving market between now and 2030.

Introduction

Project Overview

Oak Ridge National Laboratory (ORNL), Sentech, Inc., General Electric (GE) Global Research, Electric Power Research Institute (EPRI), and the Center for Automotive Research at Ohio State University (OSU-CAR) have completed Phase 1 of an in-depth study that investigates the benefits, barriers, opportunities, and challenges of grid-connected plug-in hybrid electric vehicles (PHEVs) in order to establish

potential value propositions that will lead to a commercially viable market. During this initial phase of the study, business scenarios were developed based on economic advantages that either increase the consumer value or reduce the consumer cost of PHEVs to assure a sustainable market that can thrive without the aid of state and Federal incentives or subsidies. Once the characteristics of a thriving PHEV market have been defined for this timeframe, market introduction steps, such as supportive policies, regulations, and temporary incentives,

needed to reach this level of sustainability will be determined.

The primary value of PHEVs to the consumer is their potential to markedly reduce fuel cost by substituting gasoline with electricity. This alone may not be enough to offset the increased purchase price of the PHEV when the consumer makes a buying decision. Thus, other potential advantages of PHEVs were identified and, to the extent possible, their values were quantified. Candidate value propositions for the initial case study were chosen to enhance consumer acceptance of PHEVs and/or compatibility with the grid. Potential benefits of such grid-connected vehicles include the ability to supply peak load or emergency power requirements of the grid, enabling utilities to size their generation capacity and contingency resources at levels below peak. Different models for vehicle/battery ownership, leasing, financing and operation, communications, and vehicle infrastructure needed to support the proposed value-added functions, were explored during Phase 1. Rigorous power system, vehicle, financial, and emissions modeling were utilized to help identify the most promising value propositions and market niches to focus PHEV deployment initiatives.

A Guidance and Evaluation Committee composed of representatives from various stakeholder organizations contributed expertise throughout Phase 1 of the study. Committee members include executives and entrepreneurs from the automotive, energy storage, utility, and finance arenas. In addition, participation was sought from several national laboratories, including Pacific Northwest National Laboratory (PNNL), National Renewable Energy Laboratory (NREL), and Argonne National Laboratory (ANL).

Purpose of Study

PHEVs have attracted increased interest over the past decade for several reasons, including their high fuel economy, convenient low-cost recharging capabilities, potential environmental benefits, and reduced use of imported petroleum, potentially contributing to President Bush's goal of a 20 percent reduction in gasoline use in ten years, or "Twenty in Ten." PHEVs have also been suggested as an enabling technology to improve the reliability and efficiency of the electric power grid. However,

PHEVs will likely cost significantly more to purchase than conventional or other hybrid electric vehicles (HEVs), in large part because of the cost of batteries. Despite the potential long-term savings to consumers and value to stakeholders, the initial cost of PHEVs presents a major market barrier to their widespread commercialization. The purpose of this project is to identify and evaluate value-added propositions for PHEVs that will help overcome this market barrier. The conclusions of this analysis will help ensure effective utilization of past research and development (R&D) innovations and will be used as a basis for investment decisions in the future. The U.S. Department of Energy (DOE) also expects to utilize the results of this study to develop future R&D strategies and to help formulate policy recommendations.

Approach

Over 120 representatives from the automotive, battery, utility, and supplier industries attended the PHEV Value Proposition Workshop held at the L'Enfant Plaza Hotel in Washington, D.C. on December 11-12, 2007. The objective of the workshop was to bring together experts from a full range of stakeholders to brainstorm potential business models that would lead to a commercially viable PHEV market and supporting infrastructure. The outcome of this workshop was an extensive list of potential value propositions, assumptions, and a consensus vision of 2030. Forecasts included anticipated regulatory changes, technology breakthroughs, infrastructure characteristics, nature of fuel supply, and more. Key assumptions included in the PHEV Value Proposition Study:

A 10 percent market penetration rate in 2030 to observe maximum effects on the grid.

A tax associated with carbon emissions at \$30 per ton of carbon dioxide (CO_2) in current dollars.

Most first generation PHEV chargers will only be capable of charging at 110V. Over time, dual voltage chargers will be introduced to accommodate quick charging, vehicle-to-building (V2B) and eventually vehicle-to-grid (V2G) applications.

Battery recycling capabilities will be in place due to regulations.

The DOE cost targets through 2030 will be met for all powertrain components (e.g., battery, power electronics).

Thirty percent of transportation fuel will be cellulosic ethanol (approximated by an E30 blend).

Vehicles are anticipated to have a ten-year lifetime (~150,000 miles).

PHEVs analyzed in this study will have an all-electric range (AER) equivalent of 30 miles in 2030 although a variety of electric ranges will exist for PHEVs.

PHEVs enhance energy security and reduce environmental impact by:

- Reducing gasoline consumption by 70 percent and 80 percent compared to HEVs and conventional vehicles, respectively.
- Emitting 1/4 less CO₂ and total GHG emissions than conventional vehicles.
- Consuming 10 percent and 40 percent less total energy than HEVs and conventional vehicles, respectively.
- Potentially increasing utilization of domestic renewable resources.

Technical Progress

Phase 1 Case Study Results

To reach commercial viability, the reduced operating costs attainable with PHEVs must match or outweigh their initial price premium over conventional vehicles or HEVs. Based on the results from the Phase 1 case study set in Southern California, the reduced operating costs of PHEVs accrued over its ten year lifetime (~15,000 vehicle miles traveled annually) do indeed result in significant net cost savings over both conventional vehicles and HEVs.

Case study results show that liquid fuel and electricity costs for a PHEV-30 are projected to be approximately 6¢ per mile. This compares to a projected conventional vehicle fuel cost of more than twice that, about 13.5¢ per mile and a projected HEV fuel cost of about 1.5 times that, about 9¢ per mile. Over the lifetime of the vehicle, this reduced cost per

mile more than outweighs the anticipated ~\$5,300 price premium relative to the conventional vehicle. An anticipated recycling credit of approximately \$1,000 for an “end-of-life” Li-ion battery pack also increases the PHEV’s competitive edge. Furthermore, these savings are prior to additional value-added propositions, such as benefits to auto manufacturers, utilities, or government agencies.

Table 1.

Monetary Value	Conventional	HEV	PHEV 30
Purchase Costs	\$21,400	\$22,600	\$26,675
Glider ¹	\$14,400	\$14,400	\$14,400
Powertrain Costs	\$7,000	\$8,200	\$12,275
Engine ²	\$4,250	\$2,500	\$2,500
Transmission ³	\$2,750	\$2,625	\$2,625
Motor/Inverter ³	-	\$875	\$875
Battery ³	-	\$2,200	\$5,600
Charging Plug ²	-	-	\$675
Operating Costs	\$28,325	\$20,450	\$15,725
E30	\$20,625	\$13,775	\$4,250
Electricity	-	-	\$5,350
Maintenance	\$6,600	\$5,925	\$5,275
Carbon Tax	\$1,100	\$750	\$850
Ownership \$ Benefits	-	-	(\$1,000)
Battery Recycle Credit	-	-	(\$1,000)
COST	\$49,725	\$43,050	\$41,400

The price sensitivity chart in Figure 1 demonstrates the impact of varying retail prices of E30 and electricity used to power the three vehicle types, assuming all other factors held constant. PHEVs appear to have the lowest overall cost volatility primarily because the effects of price changes can be

¹ MSRP of 2009 Toyota Camry SE Base Model (2.4L 4-Cyl.) minus total powertrain costs.

² Graham, R. et al. “Comparing the Benefits and Impacts of Hybrid Electric Vehicle Options.” Electric Power Research Institute. Report Number 1000349. July 2001.

³ FCVT Multi-Year Program Plan. U.S. Department of Energy. April 20, 2008.

shared between two fuel types, which is not an option for conventional vehicles or HEVs.

Variations in carbon tax rates are also displayed in this chart; all vehicle types are similarly affected by fluctuations in the rate, which result in small changes in operating cost.



Figure 1.

More specifically, Figure 2 shows the estimated retail price thresholds for E30 and electricity rates at which PHEVs become the most economic choice with respect to total vehicle ownership cost. With all other parameters held constant, PHEVs are the most economic choice compared to conventional vehicles as long as E30 prices exceed \$2.22 per gallon and electricity rates are below \$0.47/kWh (including transmission and distribution). HEVs, on the other hand appear to be the most financially responsible purchase unless E30 prices exceed \$3.72 per gallon and electricity rates are below \$0.24/kWh, in which case PHEVs become most financially appealing.

In addition to monetary benefits, PHEVs offer significant benefits to society, including reduced imported oil and decreased greenhouse (GHG) emissions. PHEVs are able to dramatically decrease dependence on foreign oil by substituting the majority of it with electricity. Case study results show that, on average, a single PHEV-30 will consume approximately 80 percent less gasoline than conventional vehicles (~250 less gallons annually) and 70 percent less gasoline than HEVs (~150 less gallons annually). With 60 percent of oil imported from foreign lands, the Southern California fleet of one million PHEVs has the potential to reduce imported oil by approximately 8 million barrels (150 million gallons) annually if the PHEV fleet substituted for conventional vehicles or by

approximately 4.5 million barrels (90 million gallons) annually (if the PHEV fleet substituted for HEVs).

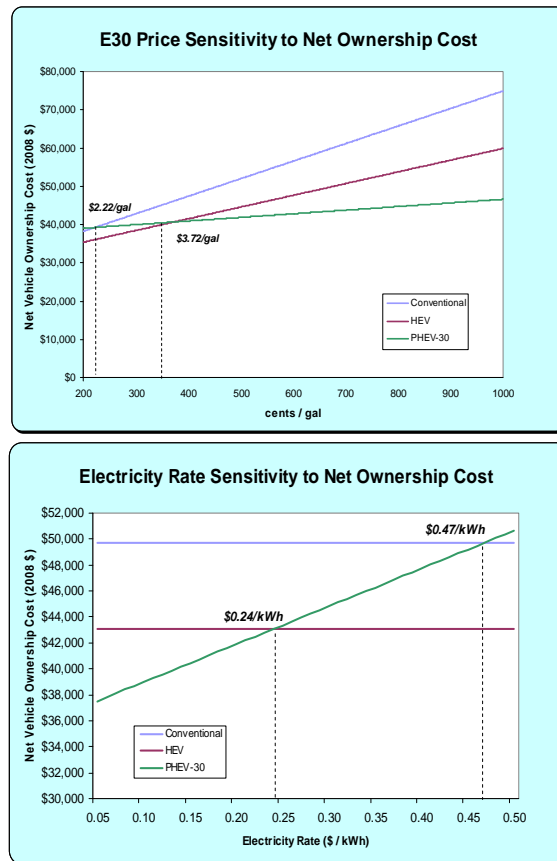
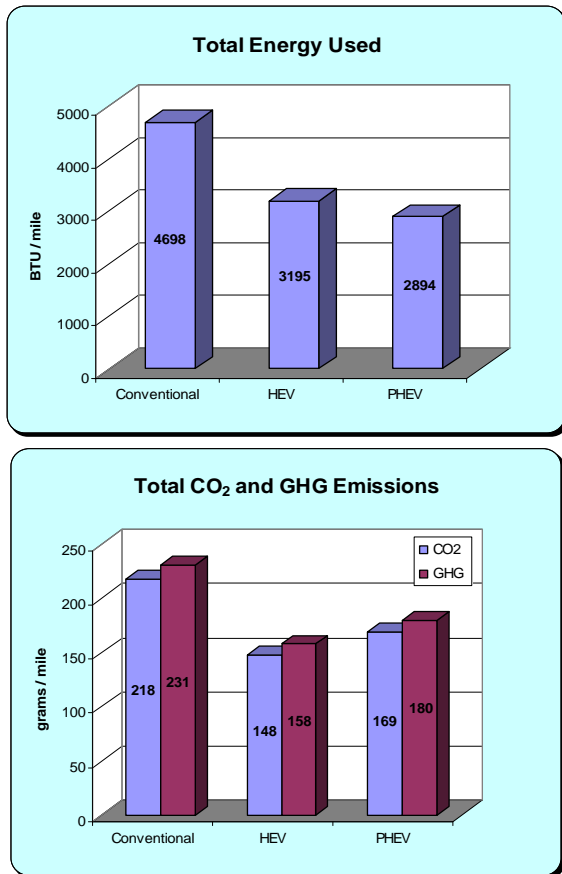
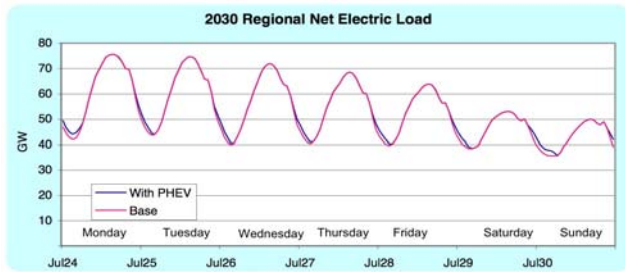


Figure 2.

As shown in Figure 3, PHEVs also demonstrate significant improvements in GHG emissions reductions in some cases. Relative to conventional vehicles, PHEVs reduce both CO₂ emissions and overall GHG emissions by nearly one quarter primarily due to less petroleum burned. PHEVs also use approximately 40 percent and 10 percent less total energy compared to conventional vehicles and HEVs, respectively. CO₂ and GHG emissions for PHEVs and HEVs appear to balance out, depending on the ethanol blend used and the weight of the vehicle. When an E30 blend is used on a lighter weight vehicle (as shown below), PHEV emissions are slightly higher. When an E10 blend is used on a vehicle of traditional weight, however, HEVs have slightly higher emissions.

**Figure 3.**

The relatively slow penetration of PHEVs in the market in combination with smart charging that shifts demands to off-peak times leads to very little impact on overall peak demands while providing the utility with additional sales during off-peak times (see figure below). The benefits to the utility include increased sales from existing generating capacity, thereby providing the potential to recover more of its fixed costs. If all PHEV owners choose to charge their vehicles in the evening (5:00 p.m. to 6:00 p.m.), however, resulting peak demands could have a negative effect on the grid. Such effects clearly show the benefit to the utility of providing incentives for customers to shift their charging times to nighttime. PHEV owners must, therefore, be educated on what hours offer the highest financial benefits and understand why charging during peak hours is discouraged by the utilities.

**Figure 4.**

Commercial building owners may also benefit from allowing their employees to plug in at their workplace upon arrival in the morning. By charging the batteries when demands at the building are below peak, commercial building owners can use the power stored in the batteries towards reducing peak billing demand and thereby lowering their electric bill. At the same time, some of their electricity purchases could be shifted from afternoon peak prices to morning mid-peak prices, saving additional funds. However, the total savings is dependent on the load shape of the facility. Also, the vehicle owners will expect some form of compensation, either monetary rebates or non-monetary incentives (e.g., preferred parking spaces), for wear and tear on the battery. The net savings to the building will need to be sufficient to justify the capital costs and ongoing operations cost for the program.

For a large office building with a 1.5 MW peak demand and up to 50 PHEVs available, the building's owners could purchase extra power in the morning to recharge the batteries to full charge. Then in the afternoon, the building could withdraw that power, squaring off each day's peak as shown below. In this example, PHEVs began plugging in at 8 AM, charged through the morning, and then released the same amount of energy in the afternoon. This dropped the peak demand roughly 60 kW. Using current Southern California Edison and Los Angeles Department of Water and Power commercial tariffs, the savings from both reduced demand charge and lower cost energy purchases was \$1000 to \$2000 per month. By 2030, the amount will likely increase, but the amount of savings depends on the building's rate structure.

**Figure 5.**

Conclusions

Are PHEVs Commercially Viable?

The primary objective of this PHEV Value Proposition Study is to establish potential value propositions that will collectively lead to commercially viable PHEVs, meaning that the reduced operating costs attainable with PHEVs must match or outweigh their initial price premium over conventional vehicles or HEVs. Based on the results from the Phase 1 case study set in southern California, the reduced operating costs of a PHEV accrued over its ten year lifetime (~15,000 VMT annually) do indeed result in significant net cost savings over both conventional vehicles and HEVs.

FY 2008 Publications/Presentations

“Plug-In Hybrid Electric Vehicle Value Proposition Study - Summary Report for December 2007 Workshop.” Sentech, Inc. ORNL/TM-2008/002. January 2008.

Task 3 paper on “Value Propositions Selection,” was completed in May 2008.

A presentation of the project and initial results was made on June 20 at the ESG meeting in Dearborn MI for DOE management including Andy Karsner.

The Phase I interim report (Task 4) was completed and presented to Lee Slezak of DOE on June 30, with subsequent presentations to other DOE personnel on July 2.

Revised report for Task 4, Phase I PHEV Value Proposition Study Interim Report was completed in September.

L. Enabling High Efficiency Ethanol Engines (Delphi PHEV CRADA)

Principal Investigator: Robert M. Wagner

Oak Ridge National Laboratory (ORNL)

National Transportation Research Center

2360 Cherahala Boulevard

Knoxville, TN 37932

(865) 946-1239; fax: (865) 946-1354; e-mail: wagnerrm@ornl.gov

CRADA Partner: John A. MacBain, Keith Confer

Delphi Automotive Systems

(865) 451-3739; e-mail: john.a.macbain@delphi.com

DOE Technology Development Manager: Lee Slezak

(202) 586-2335; e-mail: lee.slezak@ee.doe.gov

ORNL Program Manager: Mitch Olszewski

(865) 946-1350; fax: (865) 946-1262; E-mail: olszewskim@ornl.gov

Objective

To explore the potential of ethanol-based fuels for improvements in drive-cycle efficiency and emissions based on simulation and experiments.

Approach

Make use of direct injection (DI) multi-cylinder engine with advanced powertrain components and controls for exploring the efficiency opportunities of ethanol and ethanol-blend fuels.

Construct representative vehicle model(s) for evaluating the efficiency of ethanol-based engines.

Develop advanced powertrain and component models in collaboration with Delphi Automotive Systems for integration into the Powertrain System Analysis Toolkit (PSAT) environment.

Simulate conventional and advanced powertrain systems for relevant drive cycles using engine data from an advanced ethanol engine developed for use with this activity.

Major Accomplishments

Multi-cylinder engine cell for evaluating ethanol efficiency potential and enabling technologies is near completion.

Ethanol engine build is underway with expected delivery to the Oak Ridge National Laboratory (ORNL) in early fiscal year (FY) 2009.

Engine maps from a Saab Bio-Power vehicle were validated for gasoline and ethanol fuels.

Parallel hybrid electric vehicle (HEV) and plug-in hybrid electric vehicle (PHEV) vehicle model development is underway for use with Saab data.

Models are being used to simulate conventional and advanced powertrains over relevant drive cycles.

Future Direction

Install advanced ethanol engine at ORNL.

Baseline ethanol engine over speed/load range for use in PSAT powertrain simulations.

Simulate conventional and advanced powertrains using Saab Bio-Power data (gasoline and ethanol) in split and parallel HEV models for relevant drive cycles.

Simulate conventional and advanced powertrains using data from advanced ethanol engine developed for this Cooperative Research and Development Agreement (CRADA).

Introduction

Ethanol has become of increasing interest in recent years because it is a large domestic energy resource with a potential to displace a significant portion of petroleum imported into the United States. The substantial subsidies and tax breaks for ethanol production and consumption reflect the desire of the U.S. government to increase ethanol production as a way to make the country's energy portfolio more diverse and secure. Cellulosic ethanol may provide an additional step-change in reducing petroleum consumption by greatly expanding the quantity of feedstock available for ethanol production, and would also reduce the anthropogenic CO₂ emissions per vehicle mile that contribute to global warming due to the lower energy inputs associated with this technology.

Improved utilization of ethanol will require significant technical progress toward enabling higher efficiency. ORNL has considerable experience with non-traditional fuels and improving engine system efficiency for the next generation of internal combustion engines. Delphi Automotive Systems has extensive knowledge and experience in powertrain components and subsystems, along with real-world issues associated with the implementation of ethanol-based fuels. Partnering to combine ORNL and Delphi knowledge bases is key to improving the efficiency and implementation of ethanol-based fuels.

This CRADA makes use of a direct-injection L850 engine, which has advanced Delphi components including a flexible valve train and open controller. This engine will be used in combination with modeling to improve the fundamental understanding of efficiency opportunities associated with ethanol and ethanol-gasoline blends.

This activity is co-funded by the Vehicle Technologies Fuels Utilization Subprogram. The Vehicle Systems portion of this CRADA will focus on drive-cycle estimations of efficiency and emissions based on simulation and experiments. Estimations will be performed for ethanol and ethanol blends with conventional and advanced

powertrains to assess the full merit of the proposed research across a wide spectrum of powertrain technologies. To fully understand the value of the research, overall vehicle efficiency impacts will be considered. PSAT will be the vehicle level modeling environment and allows for the dynamic analysis of vehicle performance and efficiency to support detailed design, hardware development, and validation.

Approach

Engine System Experiments

An advanced engine system has been developed to evaluate the efficiency potential of ethanol and ethanol blends through the use of advanced technologies developed by Delphi. The engine is currently at the Delphi technical center in Rochester, NY, and will be moved to ORNL in early FY 2009. Engine maps developed with this engine will be used as input to vehicle systems modeling to characterize the potential of ethanol and ethanol blends with advanced engine and powertrain components.

Vehicle System Modeling

An essential aspect of the research is to evaluate the potential of optimized ethanol engines and their impacts on conventional and advanced powertrains. The vehicle modeling portion of the project is structured utilizing four principal tasks: (1) model development of a reference conventional vehicle and ethanol engine model, (2) development of advanced powertrain models utilizing gasoline and ethanol engine maps, (3) simulation of all respective vehicle models over pertinent drive cycles, and (4) development of a detailed final report including complete analysis and comparison of the results. These tasks are summarized below.

Development of representative mid-sized conventional vehicle model. A set of vehicle performance attributes, based on a 2007 Saab 9-5 BioPower sedan, were used as the basis to create the complete conventional vehicle model. The results from this task established a reference for conventional vehicle performance, using both

gasoline and ethanol (E85), for subsequent advanced powertrain variations to be compared against. The vehicle specifications used for creating the vehicle model are outlined in Table 1.

Table 1. Main Specifications of the Saab BioPower Vehicle

Component	Specifications
Engine	Gasoline and E85 based on Saab BioPower data
Transmission	5-speed manual Ratios: [3.38, 1.76, 1.18, 0.89, 0.66]
Frontal Area	2.204 m ²
Final Drive Ratio	4.05
Drag Coefficient	0.290
Rolling Resist	0.009 (plus speed-related term)
Wheel Radius	0.3056 m

An integral part of this task was to create an ethanol engine model, based on laboratory data collected at both the ORNL Fuels, Engines, and Emissions Research Center (FEERC) and the Transportation Research Center (TRC). A Saab Bio-Power vehicle was available and has been tested at FEERC. Data from these tests were used to develop the ethanol engine model (map), and also provided a means of model validation. The Saab ethanol engine map also provides a secondary basis for comparison, i.e., the current production “state-of-the-art” for optimized flex-fuel engines.

Development of mid-sized advanced powertrain vehicle models. In order to gain a broad understanding of the potential merits of the optimized ethanol engine, advanced powertrain models, such as HEVs and PHEVs, were identified and developed. Such powertrain configurations represent the most viable means of maximizing fuel economy in the near term.

Utilizing available component data from ORNL and industry, hybrid vehicle models that satisfy the Saab BioPower vehicle performance attributes were developed. The gasoline and ethanol engine models used for the conventional case were scaled in each powertrain application in order to approximate the performance of the conventional vehicle. These powertrains reflect the current technology available (in the case of HEVs), as well as proposed (in the

case of PHEVs). The control system for each powertrain configuration was “optimized” so that a good estimation of the performance of each configuration could be determined. The base control strategy approach was to maximize the efficient use of the engine, since this component is typically the weakest link in the “efficiency chain.”

Simulation of conventional and advanced powertrains over pertinent drive cycles. In order to understand the operational characteristics of the engine in different configurations, the models were exercised over drive cycles of various degrees of aggressiveness and transient characteristics. The drive cycles selected were the Urban Dynamometer Driving Schedule (UDDS), the Highway Federal Emissions Test (HWFET), and the US06 Supplemental Federal Test Procedure. A comparison of all data to the baseline conventional vehicle will then be performed.

Results

The conventional vehicle, based on the 2007 Saab 9-5 BioPower sedan, was modeled and validated against actual test data collected at the ORNL and TRC. Table 2 shows a comparison of the gasoline and ethanol fuel economy results for each drive cycle. An interesting observation from the data set is that US06 fuel economy is actually higher than for the Federal Test Procedure (FTP). Since the US06 is a much more aggressive cycle than the FTP, this was not anticipated. However, the vehicle model predicted this trend with very good agreement.

Table 2. Fuel Economy Comparison for Conventional Model Validation

Facility	Fuel	Fuel Economy (MPG)		
		FTP	HWFET	US06
ORNL	Gasoline	23.2	39.8	26.5
	E85	17.2	29.8	20.0
TRC	Gasoline	22.7	39.0	25.6
	E85	17.3	28.6	19.3
PSAT Conventional	Gasoline	22.4	40.0	25.4
	E85	17.2	29.7	18.4

Although the vehicle model predicted the fuel economy adequately, the focus of the study is on optimizing the engine. Therefore, the performance of the engine model itself required a closer look. Second-by-second data were available from the chassis dynamometer testing that was performed at FEERC.

Figure 1 represents a comparison of the actual versus simulated engine speed for a portion of the UDDS. This shows the vehicle control system is functioning correctly, and the transmission is shifting very close to the shift schedule used by the test operator. The discrepancies in the plot are due to mismatch in the automated shift schedule used by PSAT and the actual shift schedule used by the operator during testing. The engine speed correlation allows a direct comparison of other pertinent engine model variables, such as engine torque and fuel use.

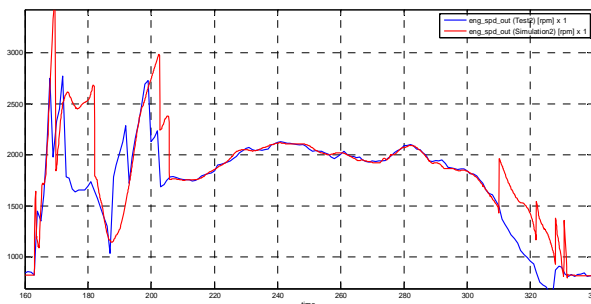


Figure 1. Conventional Vehicle Engine Speed Comparison (test data in blue, simulated data in red)

Figure 2 represents a comparison of predicted versus simulated engine torque for the same portion of the UDDS. It should be noted here that the engine torque based on chassis dynamometer testing is estimated using assumed gear efficiencies and known final drive and transmission gear ratios. Good correlation is shown between “actual” and simulated engine torque.

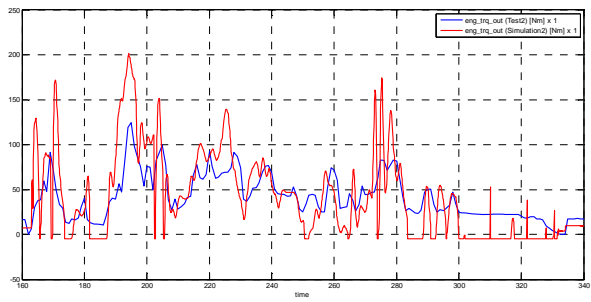


Figure 2. Conventional Vehicle Engine Torque Comparison (test data in blue, simulated data in red)

The other critical element of the engine model is its ability to predict fuel use. Figure 3 represents a comparison of the instantaneous fuel use rate for the same portion of the UDDS. Here, the fuel rate for the test vehicle is calculated using two approaches. The first approach is based on determining the fuel rate based on the measured air-fuel ratio (AFR) during the test. The second method is based on CO₂ measurements taken during the test. The results in Figure 3 suggest that during low engine loads, the model underestimates the fuel rate. However, since the vehicle model predicts overall fuel use reasonably and the methods for determining the test fuel rate are not exact, the results are acceptable for the purposes of this study.

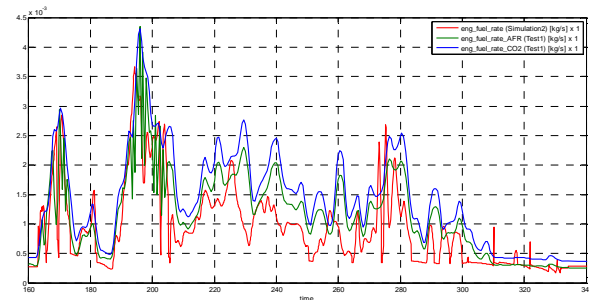


Figure 3. Conventional Vehicle Engine Fuel Rate Comparison (AFR-based test data in blue, CO₂-based test data in green, simulated data in red)

In order to provide useful information for calibration of the “optimized” ethanol engine in subsequent phases of this project, the operating region of the engine should be established. Examples of the conventional baseline (UDDS driving cycle) engine speed and torque operating are shown in Figures 4 and 5, respectively. These graphs provide a basis for comparison of how the engine will operate when advanced powertrains are implemented in the model.

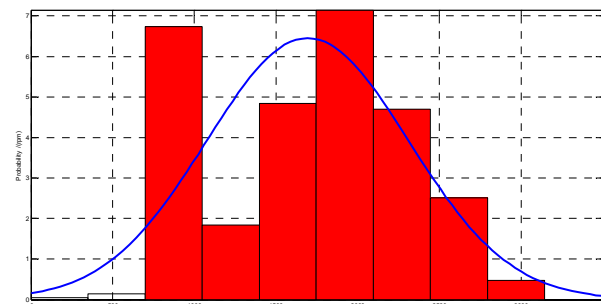


Figure 4. Example of Conventional Vehicle Engine Speed Histogram (UDDS)

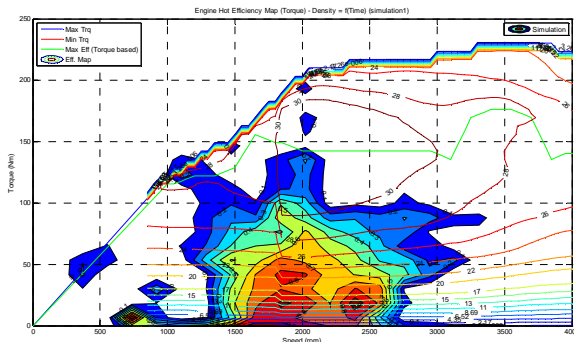


Figure 5. Example of Conventional Vehicle Engine Torque Operating Region (UDDS)

Development of HEV and PHEV models is in progress. For these advanced powertrain cases, the following architectures will be examined based on the 2007 Saab 9-5 BioPower vehicle:

Power-split HEV.

Pre-transmission parallel HEV.

Pre-transmission parallel PHEV.

Conclusions

The first year of the CRADA focused on establishing the tools for use in evaluating the efficiency potential of ethanol-fueled engines in combination with advanced powertrain systems. The CRADA is on schedule with the engine build near completion and transition to ORNL scheduled for early FY 2009. The vehicle base model has also been developed and verified with chassis dynamometer data from ORNL with advanced powertrain architecture development in progress.

M. Plug-In Hybrid Vehicle Systems Analysis

*Tony Markel (Principal Investigator), Jeffery Gonder, Aaron Brooker, Kevin Bennion, Matthew Thornton
National Renewable Energy Laboratory
1617 Cole Boulevard
Golden, CO 80401-3393
(303) 275-4478; tony_markel@nrel.gov*

*DOE Technology Manager: Lee Slezak
(202) 586-2335; Lee.Slezak@ee.doe.gov*

Objective

Objectively evaluate plug-in hybrid electric vehicle (PHEV) technology options, advise on the larger Department of Energy PHEV development effort, and complement activities at other national laboratories through innovative research.

Approach

Collect and assemble information and conduct analysis to enhance understanding of the benefits and barriers of PHEV technology.

Accomplishments

Developed an alternative vehicle economic scenario analysis worksheet to be used to find market conditions and design scenarios that may lead to broad market adoption of PHEVs.

Completed first set of simulations of PHEV storage control that account for real-world driving behavior and initiate smart charging tied to wind variability.

Used real-world travel data from Los Angeles to show that a PHEV10 with opportunity charging provides more fuel savings benefit than a PHEV20 with evening charging.

Published and presented results from travel survey simulations at several venues including EVS-23, CRC On-Road Emissions Workshop, Plug-in 2008, and Advanced Automotive Battery Conference.

Collaborated with Energy Storage program to assess the impact of battery design parameters on the tradeoff between cost and life while meeting performance requirements.

Participated in SAE Committee to revise J1711 test procedures to better address PHEV technology.

Expanded the travel survey database with data from Austin and San Antonio to increase diversity of metropolitan areas and geographic location.

Future Directions

Build and use a Travel Behavior Repository by documenting data processing methods for simulation, provide access to others, and complete simulations with multi-day datasets.

Use exhaust thermal test stand to explore PHEV emissions reduction strategies.

Expand PHEV economic scenario analysis to include alternative end of life scenarios and ancillary services tradeoffs.

Define “smart charging” scenarios that lead to a low CO₂ path for vehicles using renewables

Contribute to the refinement of PHEV test procedures through the Society of Automotive Engineers (SAE), the Environmental Protection Agency (EPA), and the California Air Resources Board (CARB).

Assess the impact of ancillary loads on PHEV benefits.

Introduction

The National Renewable Energy Laboratory's (NREL) plug-in hybrid electric vehicle (PHEV) analysis activities made great strides in fiscal year (FY) 2008 to objectively evaluate PHEV technology, advise on the larger DOE PHEV development effort, and complement activities at other national laboratories with innovative research, while sharing technical knowledge with the vehicle research community and vehicle manufacturers through the FreedomCAR Vehicle Systems Technical Team and the Electrochemical Energy Storage Technical Team.

The NREL research team has participated in many key industry meetings, and NREL research has been documented in several presentations and technical papers. This report highlights important insights that emerged from NREL's PHEV systems analysis efforts.

Real-World Duty Cycle Database Provides Vehicle Analysis Foundation

PHEVs differ significantly from existing vehicles in that they consume two fuels (petroleum and electricity) at rates depending on the distance driven between recharge events and the aggressiveness of the cycle. NREL has contributed to the Department of Energy (DOE) mission by developing a database of real-world personal vehicle duty cycles that form the core input for vehicle systems simulation efforts. In FY06, a database of full day driving profiles for 227 vehicles from the St. Louis metropolitan area was created. Simulation results in FY07 using this data showed the potential fuel consumption benefits of HEV and PHEV technology in real-world applications.

Figure 1 provides an FY08 status report on the travel survey data sets that have been accessed and that are in process. The travel survey data were collected by other entities and NREL focused on processing the data into a format that can be used for simulation. Many of the data sets include only a single day of data per vehicle while some of the data sets provide multiple days of data per vehicle. The multi-day data will be the focus of future analysis as they provide some insight into the consistency or variability in consumer travel behavior. The data collected to date includes more than 2,000 unique vehicles.

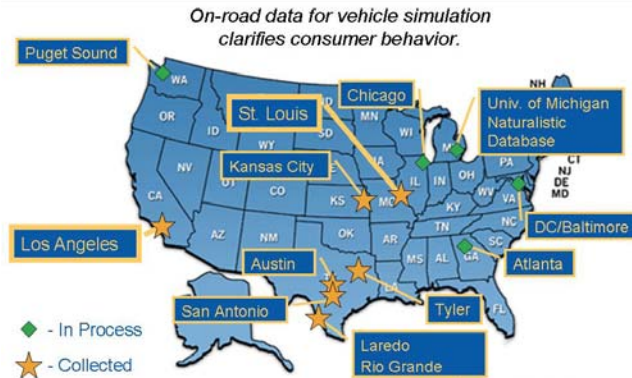


Figure 1. Travel Survey Database provides more than 2000 Consumer Driving Days from Various Regions

The value of the travel survey data presents itself when the data are used for vehicle systems simulation. Figure 2 provides the results from a fleet simulation based on the travel survey data from Los Angeles. Shown is the relative fuel consumption of the fleet if all of the more than 1000 vehicles in that data set were of the specific powertrain. The PHEV20 has 20 miles of energy capacity and is charged only at the end of the day, while the PHEV10opchg has one half the battery capacity of the PHEV20 but is charged whenever the vehicle is parked. The fuel savings and vehicle cost reductions are significant, while the battery wear implications of additional cycling are yet to be determined.

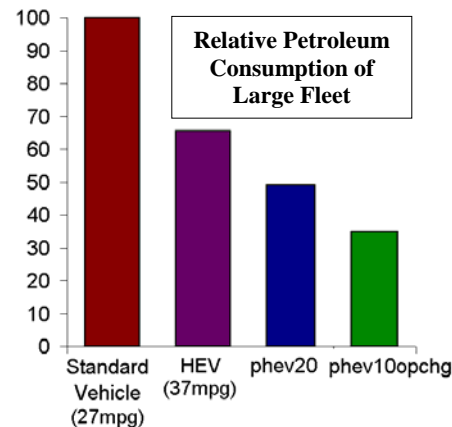


Figure 2. Comparing Relative Petroleum Consumption addressing both Vehicle Design and Consumer Travel Behavior

Economic Analysis Highlights Challenges for Market Penetration of PHEVs

Reducing the initial cost of the PHEV is a critical challenge toward market penetration. NREL's work on economic analysis of PHEVs has evolved into a parametric tool providing a comparison of the net present cost of multiple technologies given a set of evolving input assumptions. A net present cost analysis compiles the lifetime costs into a single number accounting for the relative value of dollars in the future. Some of the inputs include the changing price of gasoline and electricity over time and the trip distance distribution of vehicles based on national statistics.

Figure 3 is an example of the type of output that is provided by the tool. The net present cost of the several electric range assumptions are compared based on initial purchase cost and lifetime fuel savings. Given the assumptions, in this case, a PHEV with 20 to 30 miles of electric range capacity provides the lowest net present cost.

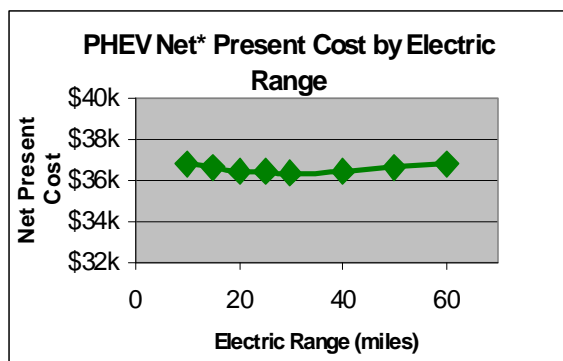


Figure 3. Net Present Cost Comparison for PHEVs Assuming Cost Reductions are Achieved

The economic analysis of PHEVs will continue in FY09 by focusing on quantifying the values of aspects other than petroleum savings. These may include battery replacements, charging scenarios, battery sizing, and grid services.

PHEV Interaction with Renewables

Integration of PHEVs with renewables has the potential to dramatically reduce transportation CO₂ emissions. Renewable generation has a significant amount of intermittency that is in conflict with a utility operator's desire to tightly control generating units to match a load that is varying. Intermittency is

one element slowing the adoption of greater renewable generation in the grid. Vehicle usage is also intermittent. The energy storage system of plug-in vehicles might then have a potential to act as a renewables buffering system thus reducing CO₂ emissions and leading to expansion of renewable electricity generation.

To consider the potential interaction of PHEVs with renewables, NREL analyzed the vehicle intermittency based on travel survey data with generation data from real wind farms to assess the opportunity for PHEVs to firm wind.

Three charging scenarios, three battery capacities, and three vehicle fleet sizes composed the analysis matrix. The goal of the analysis was to understand the fuel consumption and battery wear impacts of the scenario spectrum. If the battery is used for both driving and utility services, there is likely to be reduced life due to additional cycling. However, the analysis suggests that under several scenarios, the battery was used for grid services with only a small reduction in life and increase in petroleum consumption relative to a baseline opportunity charging scenario. Further analysis is needed to determine if these vehicle impacts are worth the value of expanded renewables on the future electricity grid.

PHEV Energy Storage Trade-off Analysis

Understanding the performance, life, and cost of the energy storage system for a PHEV is critical for guiding future development programs. Vehicle systems analysis and energy storage systems analysis are performed in concert to assess the impact of design parameters and usage profiles on the resulting component cost and life.

Under the direction of the DOE Energy Storage activity, models for performance, cost, and life have been developed. Future systems analysis work will use these models, combined with vehicle usage based on travel survey data and grid interaction strategies, to find the best possible solution for long life, cost effective energy storage for plug-in vehicles that bring the most value to the consumer.

Conclusions

NREL's assessment of PHEV technology continues to add value to the DOE Vehicle Technologies

Program. The efforts support the President's Advanced Energy Initiative in the goal of developing a plug-in hybrid vehicle with 40 miles of electric range as a means of changing the way we fuel our vehicles. The PHEV research completed in FY08 continued an exploration of the potential benefits and implications of PHEV design and operating scenarios on real-world travel profiles.

In FY09, NREL's vehicle systems analysis will support creating a travel behavior repository with existing travel survey data by documenting data processing methods and working on shared access for others. Other key items will include contributing to the development of test procedures for PHEVs and further analysis of PHEV economic scenarios incorporating the value attributes of a PHEV beyond its petroleum consumption benefit. Finally, the impacts of ancillary loads on PHEV performance will be assessed.

FY08 Publications

T. Markel, K. Bennion, A. Brooker, J. Gonder, and M. Thornton. "NREL PHEV Analysis Activities Summary." FY08 Milestone Report. September, 2008.

Markel, T. "Simulating Real-World PHEV Operation." Presented at Plug-in 2008. San Jose, CA. 2008.

Bennion, K., Thornton, M., Markel, T. "PHEV Engine Starts and the Impacts on Vehicle Emissions." Presented at 18th CRC On-Road Vehicle Emissions Workshop. 2008.

Markel, T., Pesaran, A., Kelly, K., Thornton, M., Nortman, P. "Research Experience with a Plug-in Hybrid Electric Vehicle – EnergyCS Conversion of a Toyota Prius." To be presented at EVS-23. October 2007. NREL CP-540-42365.

Markel, T., Pesaran, A., Smith, K. "PHEV Energy Storage Performance/Life/Cost Tradeoff Analysis." Presented at Advanced Automotive Battery Conference. 2008.

R. Sioshansi, P. Denholm. "The Value of Plug-In Hybrid Electric Vehicles as Grid Resources." submitted for publication in Environmental Science and Technology 2008.

R. Sioshansi, P. Denholm. "Emissions Impacts and Benefits of Plug-in Hybrid Electric Vehicles and Vehicle to Grid Services." submitted for publication in Environmental Science and Technology 2008.

Prior Year Publications

J. Gonder and A. Simpson. "Measuring and Reporting Fuel Economy of Plug-In Hybrid Vehicles." 22nd Electric Vehicle Symposium. October, 2006. NREL CP-540-40377 and JA-540-41341.

J. Gonder and T. Markel. "Energy Management Strategies for Plug-In Hybrid Electric Vehicles." SAE 2007-01-0290. NREL CP-540-40970.

Parks, K.; Denholm, P.; Markel, T. "Costs and Emissions Associated with Plug-In Hybrid Electric Vehicle Charging in the Xcel Energy Colorado Service Territory." NREL TP-640-41410. 2007.

Markel, T. (2007). "Platform Engineering Applied to Plug-In Hybrid Electric Vehicles." SAE 2007-01-0292. NREL Report No. CP-540-41034.

A. Simpson. "Cost-Benefit Analysis of Plug-In Hybrid Electric Vehicle Technology." 22nd Electric Vehicle Symposium. October, 2006. NREL CP-540-40485 and JA-540-40969.

J. Gonder, T. Markel, A. Simpson, M. Thornton "Using GPS Travel Data to Assess the Real World Driving Energy Use of Plug-In Hybrid Electric Vehicles (PHEVs)." *TRB 86th Annual Meeting*. January 2007. NREL CP-540-40858.

T. Markel and A. Pesaran. "PHEV Energy Storage and Drive Cycle Impacts." *Advanced Automotive Battery Conference*. May, 2007. NREL PR-540-42026.

M. P. O'Keefe and T. Markel. "Dynamic Programming Applied to Investigate Energy Management Strategies for a Plug-In HEV." 22nd Electric Vehicle Symposium. October, 2006. NREL CP-540-40376.

T. Markel, K. Bennion, A. Brooker, Paul Denholm, J. Gonder, and M. Thornton. "NREL PHEV Analysis Activities Summary." FY07 Milestone Report. September, 2007.

N. Evaluating Route-Based Control of Hybrid Electric Vehicles (HEVs)

Jeffery Gonder (Principal Investigator), Matthew Thornton

National Renewable Energy Laboratory

1617 Cole Boulevard

Golden, CO 80401-3393

(303) 275-4462; jeff_gonder@nrel.gov

DOE Technology Manager: Lee Slezak

(202) 586-2335; Lee.Slezak@ee.doe.gov

Objective

Evaluate the potential to increase hybrid electric vehicle (HEV) fuel efficiency by using information about the upcoming driving route to inform control decisions.

Approach

Build on previous work to evaluate the range of potential adaptive control approaches, and to begin implementing a novel approach in a generic simulated HEV platform.

Refine approach implementation and report on results in a conference paper.

Explore industry interest in validating the modeling-predicted fuel savings in commercial vehicle hardware.

Accomplishments

Refined application of novel route-based HEV control approach in a simulation environment.

Documented and presented the analysis results in a paper delivered at the 2008 SAE World Congress.

Engaged with potential industry partners to line up collaborative demonstration of in-use route-based control fuel savings on a commercial HEV platform.

Potential Future Directions

Execute the commercial hardware route-based HEV control demonstration in fiscal year (FY) 2009.

Use the approach to enhance fuel savings on a plug-in hybrid electric vehicle (PHEV) platform.

Investigate other potential HEV/PHEV benefits of route-based control, such as extending battery life or reducing vehicle emissions.

Introduction

Today's hybrid electric vehicle (HEV) controls do not necessarily provide maximum fuel savings over all drive cycles. This fact has prompted National Renewable Energy Laboratory (NREL) to evaluate the additional fuel savings achievable from a route-based control approach. The analysis at NREL began a couple of years ago by investigating a range of different adaptive control approaches and considering the strengths and weaknesses of each. In the end, NREL identified the category of look-ahead control

strategies (using input from "on-the-fly" route predictions) as an area meriting further analysis. The next step involved developing a novel implementation approach and evaluating it over several drive cycles. The analysis included the important task of rigorously identifying the best-fixed baseline control settings to minimize fuel use during general driving. Objectively measuring the fuel savings delivered by route-based HEV control requires comparison against such an optimized baseline. The increasing prevalence of GPS devices in vehicles plus the sole requirement of software

modifications to implement route-based controls suggest that this advancement could be realized with relatively little incremental cost [1].

Approach

Along with refining the process in this fiscal year, the novel route-based control approach and analysis results were documented in a paper delivered at the April 2008 SAE World Congress [2]. The paper included simulation results from a general midsize car HEV platform. Given the importance of comparing efficiency improvements against a sound baseline setting, the baseline controls were first optimized for driving on the New European Drive Cycle (NEDC—which has been shown to provide a good general control tuning [3]). Route-based control settings for different types of driving were then determined through a similar computationally intensive off-line optimization process, and applied based on real-time predictions about the upcoming driving route.

As described below, the simulation results for the generic HEV platform have looked promising, but the approach must be implemented in commercial hardware in order to confirm the achievable fuel savings and pave the way for implementation in large numbers of vehicles. Therefore, the other major thrust in this fiscal year was to engage with potential industry partners interested in evaluating route-based control fuel savings on their particular HEV designs.

Results

Overall, the simulation results in the SAE publication demonstrated two to four percent additional fuel savings from route-based control relative to HEV operation with controls optimized for general driving. Though this may at first seem small, if the approach were to be applied across many vehicles driving thousands of miles per year, the aggregate fuel savings become quite significant. For instance, a three percent across-the-board reduction in HEV fuel use would save nearly 6.5 million gallons of fuel annually in the United States (and these estimated savings will increase further as HEVs achieve greater market penetration). Other ways to achieve comparable fuel savings (e.g., use of exotic lightweight parts, more expensive advanced components,) carry recurring material costs and thus a less attractive cost-benefit ratio.

Figure 1 illustrates route-based control fuel savings over a particular driving segment type relative to two different ‘optimized’ baseline control settings. One comparison shows as much as an 11 percent improvement. The other showing a three percent benefit was taken to be the more robust baseline comparison to retain through the rest of the SAE paper, but even that represents a significant gain to realize from control adjustments alone.

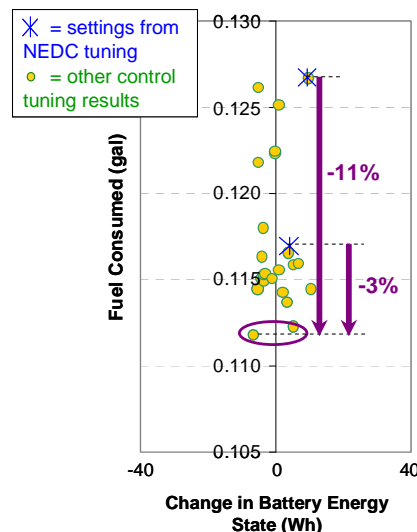


Figure 1. Example Charge-Sustaining Parametric Control Tuning Results over a Low-Speed, Stop-and-Go Driving Segment

Figure 2 shows the overall fuel savings achieved during a drive cycle with multiple driving segment types. The comparison is also expanded over a range of both charge-sustaining (CS) and non-charge-sustaining hybrid battery operation. As indicated in the figure, the route-based control approach achieves a consistent two percent improvement across the range of battery operation.

In discussions with prospective industry partners, HEV bus developers have voiced significant interest in verifying the anticipated fuel savings in their particular transit bus platforms. A hybrid transit bus would provide an ideal test bed for this initial demonstration as these vehicles run on very predictable and repeatable routes and are operated by fleet managers who would greatly value the aggregate fuel (and hence dollar) savings. Successful demonstration in this prime application could also

pave the way for integration into higher volume light-duty hybrid vehicles, further propagating the fuel saving benefit.

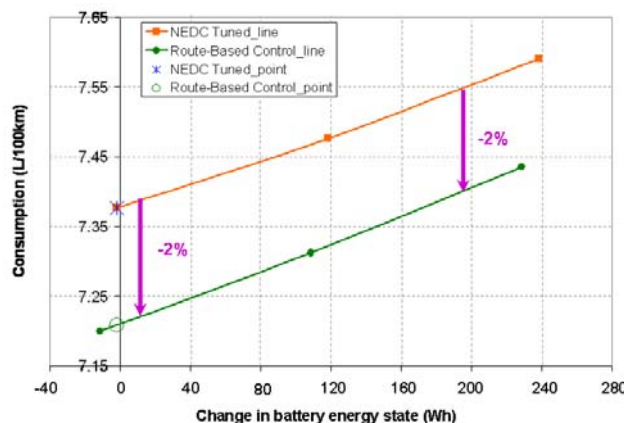


Figure 2. Fuel Savings Resulting from Route-Based Control over a Multi-Segment Drive Cycle

NREL is presently in the process of setting up a CRADA agreement with one such commercial partner. The collaborative project will focus on evaluating route-based control fuel savings in the partner's HEV platform, but as time and budget allow, battery life and emissions impacts may also be considered. The primary tasks included in the drafted work statement for this (FY09) effort include:

- 1) Determining drive cycles to use for route-based control evaluation.
- 2) Developing/modifying a platform-specific model for use in deriving route-based control parameter tunings.
- 3) Applying route-based control optimization to the vehicle model.
- 4) Implementing the identified control variations onto a physical bus controller.
- 5) Testing the route-based control fuel efficiency benefit on board the HEV bus.
- 6) Reporting results.

Conclusions

Route-based HEV control has the potential to further extend hybrid technology fuel savings by leveraging information about a vehicle's driving route. The expanded prevalence of GPS navigation devices in new vehicles provides an opportunity for widespread adoption of the approach. While the HEV transit bus application makes sense for an initial demonstration, success will also pave the way for integration into light-duty hybrid platforms. A few additional challenges exist for light-duty vehicle integration, but that market provides the greatest opportunity for expanding fuel savings across large numbers of vehicles.

Other possible areas of future work include exploring the logistics of translating GPS map routes into representative driving cycle predictions and further investigating the results' sensitivity to variations within the predicted cycle. The approach may also be applied to expanding fuel savings on a plug-in hybrid electric vehicle (PHEV) platform. Even beyond its direct fuel savings potential, the route-based control approach may serve as an enabling technology for increasing HEV (and PHEV) market penetration if it can be used in such a way to extend the life of the traction batteries and/or reduce vehicle emissions.

References

- [1] J. Gonder. "Route-Based Hybrid Electric Vehicle (HEV) Control Strategy Report." *FY07 Milestone Report*. July, 2007.
- [2] J. Gonder. "Route-Based Control of Hybrid Electric Vehicles." *SAE 2008 World Congress*. April, 2008.
- [3] K. Wipke, T. Markel and D. Nelson. "Optimizing Energy Management Strategy & Degree of Hybridization for a Hydrogen Fuel Cell SUV." *EVS-18*. October, 2001.
- [4] J. Gonder. "Route-Based HEV Control Strategy Report." *FY08 Milestone Report*. June, 2008.

O. Renewable Fuel Vehicle Modeling and Analysis

Aaron Brooker (Principal Investigator), Matthew Thornton

National Renewable Energy Laboratory

1617 Cole Boulevard

Golden, CO 80401-3393

(303) 275-4392; aaron_brooker@nrel.gov

DOE Technology Manager: Lee Slezak

(202) 586-2335; Lee.Slezak@ee.doe.gov

Objective

Evaluate the use of renewable fuels in advanced vehicles, such as E85 in a plug-in hybrid electric vehicle (PHEV), on vehicle petroleum use and marketability.

Approach

Link the critical models and test data to optimize and compare several advanced vehicle architectures' impact on fuel use and marketability. A battery wear model, component cost model, Idaho National Laboratory (INL) and Argonne National Laboratory (ANL) plug-in hybrid electric vehicle test data, the Environmental Protection Agency (EPA) conventional and flex-fuel fuel economy data, the National Household Travel Survey (NHTS) driving statistics, and Johnson Controls battery life data were all linked. The models and data were used to optimize the battery size to minimize the net present cost of hybrid electric (HEV) and PHEV powertrains. These vehicles were then compared along with conventional vehicles for differences in petroleum use, E85 use, and cost.

Accomplishments

Expanded the cost/benefit analysis tool to:

Evaluate advanced vehicles using both petroleum and renewable fuels.

Compare advanced vehicle petroleum impacts using multiple production levels of renewable fuels.

Compared the vehicle and fuel net present cost of conventional vehicles, HEVs, and PHEVs.

Evaluated petroleum impacts using today's renewable fuel production, unlimited production, and the Renewable Fuels Standard (RFS) production mandates.

Found:

Conventional flex-fuel vehicles can reduce petroleum use between 60 percent and 80 percent, but require far more E85 than produced today or is mandated in the RFS.

The cost of E85 needs to be lower relative to gasoline than it has been historically in order for it to be cost effective.

Flex-fuel HEVs require lower long term E85 production levels and provide greater petroleum reductions at the same or lower cost than other options when gasoline is over \$4.10 per gallon.

Future Directions

Add other renewable fuel options for comparison:

Mid-level ethanol blends (10, 15, 20).

Dedicated E85 vehicles.

Biodiesel (B20).

AER PHEV 40.

Expand analysis detail using the Technical Target Tool approach:

Trade-off performance, vehicle cost, and fuel cost to find the consumer preferred vehicles.

Estimate petroleum reductions based on those preferences.

Introduction

Renewable fuels and advanced technology vehicles offer some of the most promising pathways to reduce our dependence on foreign oil. Renewable fuels directly displace petroleum while advanced technology vehicles improve the efficiency to reduce the amount of fuel needed. The combination of the two may have even greater benefits than either could provide individually.

Approach

The most critical models and data need to be linked to determine the benefits of combining renewable fuels and advanced vehicle technologies. These include a battery wear model, renewable fuel data, component cost models, fuel economy data, and driving statistics, as seen in Figure 1.

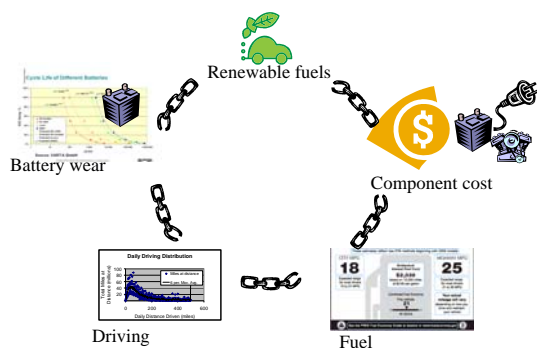


Figure 1. Linked Critical Models and Data

Linking the battery wear model with driving statistics is one of the most critical aspects of the analysis for PHEVs. The number of cycles a battery can sustain depends on the depths of discharge. The depths of discharge depend on daily trip lengths, the control strategy, and the size of the battery. Therefore, the driving distance statistics and battery life model need to be combined to find the best size battery — the size that minimizes the present vehicle and fuel cost.

The present vehicle and fuel cost are used to gauge the marketability of the advanced vehicle and renewable fuel combinations. A present cost

approach compares the options in terms of an investment; the lower the cost, the better the investment. This approach is supported by JD Power surveys in 2002 and 2008 that suggest most consumers will only buy an advanced vehicle if it will be a good investment [0][0].

Assumptions

Long-term perspective.

E85 has 85 percent ethanol. (In reality it is often less.)

Conventional vehicles meet the new CAFE standard of 35 mpg.

\$4.10/gallon gasoline (EIA 6/30/08).

\$3.34/gallon E85 (e85prices.com 7/8/08).

E85 flex-fuel consumption increase: 33 percent. (This was averaged from several vehicles using EPA fuel economy differences.)

\$0.10/kWh electricity (EIA 2007 average).

8 percent discount rate (This is the average long-term stock market adjusted for inflation.)

15-year vehicle life (BTS).

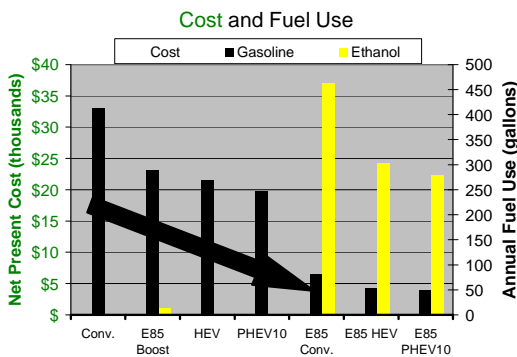
12,375 miles/year (FHWA).

235 million vehicles (BTS).

Ethanol boost efficiency and cost claims [0].

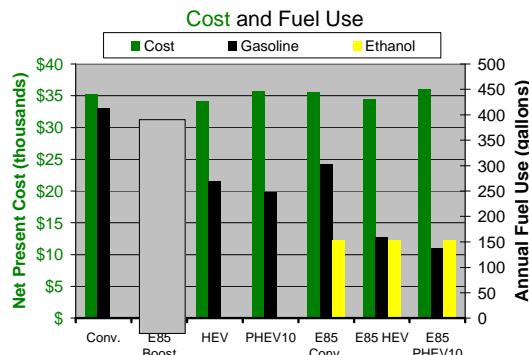
Results

Renewable fuels have the potential of reducing petroleum consumption significantly. Each conventional flex-fuel vehicle using E85 can reduce petroleum consumption 60 percent to 80 percent by directly displacing gasoline.

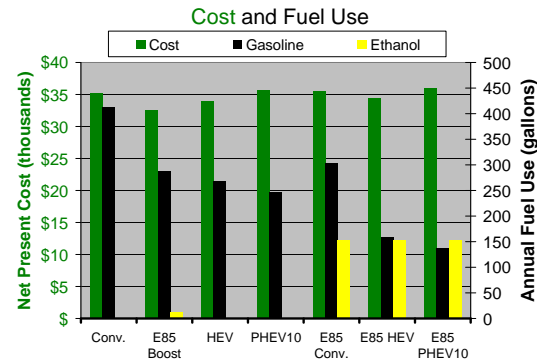
**Figure 2. E85 and Gasoline Use**

Achieving the large reductions in gasoline use across the fleet from flex-fuel conventional vehicles requires more E85 than is currently produced in the U.S. or is planned for production by the RFS. In 2007, the United States produced 6.5 billion gallons of ethanol [0]. By 2022, the RFS mandates 36 billion gallons per year. A fleet of conventional flex-fuel vehicles would use over 100 billion gallons per year. Therefore, the RFS would supply renewable fuels for only 1/3 of the vehicles.

Advanced vehicles could stretch the renewable fuel supply to more vehicles. If the entire fleet were HEVs, the ethanol could supply the necessary E85 for half of the fleet. Not only do flex-fuel HEVs require less ethanol, but they are the same or more marketable than other options as seen in Figure 3.

**Figure 3. Cost and Fuel Use**

According to claims by Ethanol Boosting Systems LLC, an ethanol boost strategy may be even more marketable and have lower ethanol production requirements. However, the ethanol boost system is not expected to reduce petroleum use as much as seen in Figure 4.

**Figure 4. Ethanol Boost**

Conclusions

Renewable fuels have great potential to reduce transportation petroleum use. If enough ethanol is produced, flex-fuel conventional vehicles could reduce light-duty vehicle petroleum consumption 60 percent to 80 percent. Flex-fuel HEVs can reduce petroleum consumption further, at less cost, and with lower ethanol production requirements.

Next Steps

The next steps may include using a consumer preference driven approach and adding other renewable fuel options for comparison:

- Mid-level ethanol blends (10, 15, 20).
- Dedicated E85 vehicles.
- Biodiesel (B20).

References

EIA Annual Energy Review 2007, Report No. DOE/EIA-0384(2007), Table 10.3. Posted June 23, 2008. <http://www.eia.doe.gov/emeu/aer/renew.html>

Duvall, Mark, "Batteries for Plug-In Hybrid Electric Vehicles." The Seattle Electric Vehicle to Grid (V2G) Forum, June 6th, 2005. http://www.ocean.udel.edu/cms/wkempton/kempton-v2g-pdffiles/PDF_percent20format/Duvall-V2G-batteries-June05.pdf

J.D. Power and Associates Reports: "Interest in Hybrid Technology is High, Especially Among Women." March 6, 2002. <http://www.jdpa.com/pdf/2002016b.pdf>

"J.D. Power Survey Says: Yes to Hybrids, No to E85, Maybe to EVs." July 17th, 2008. <http://gm-volt.com/2008/07/17/jd-power-survey-says-yes-to-hybrids-no-to-e85-maybe-to-evs/>

“Ethanol Turbo Boost For Gasoline Engines. Diesel and Hybrid Equivalent Efficiency at an Affordable Cost.”
Presented at the National Research Council Committee,
November 27, 2007.
http://www.ethanolboost.com/EBS_Overview.pdf

P. Integrated Vehicle Thermal Management Systems Analysis/Modeling

Kevin Bennion (Principal Investigator), Matthew Thornton

National Renewable Energy Laboratory

1617 Cole Boulevard

Golden, CO 80401-3393

(303) 275-4447; kevin_bennion@nrel.gov

DOE Technology Manager: Lee Slezak

(202) 586-2335; Lee.Slezak@ee.doe.gov

Objective

Investigate current technologies for improved vehicle thermal management, waste heat utilization, and integrated cooling.

Propose areas of focus for research in waste heat utilization and integrated cooling that apply to advanced vehicle propulsion systems.

Develop initial concepts of new waste heat utilization techniques and integrated cooling.

Approach

Conduct review of thermal management challenges and technologies across multiple vehicle propulsion technologies.

Identify potential areas for research and development (R&D) specifically related to:

Waste heat utilization.

Integrated systems.

Propose R&D concepts that:

Maximize benefit with least change to vehicle systems.

Have wide application to multiple advanced vehicle propulsion technologies.

Accomplishments

Completed review of thermal management challenges and technologies.

Proposed concepts for waste heat utilization and integrated cooling.

Completed initial steady-state thermodynamic analysis of integrated cooling and waste heat utilization concepts.

Future Directions

Complete detailed modeling and analysis.

Develop industry partnership and initiate hardware design for validation.

Complete hardware demonstration and testing.

Publish results for industry review.

Introduction

Vehicle thermal management is critical in terms of safety, reliability, performance, and passenger comfort. However, in addition to these standard functions vehicle thermal management system (VTMS) technologies are receiving more attention with the increasing demand for energy efficiency. These demands arise from vehicle consumers, vehicle regulations, national energy security concerns, and environmental concerns.

Developments in VTMS technologies reduce energy use in three general areas. The first is through reducing the energy required for the VTMS to function. This is possible by focusing on thermal load reduction, efficient delivery, and efficient equipment. All of this has been part of an active research task at the National Renewable Energy Laboratory (NREL) with industry support [1, 2].

The second area in which VTMS technologies reduce energy use is through waste heat utilization. Examples include utilizing waste heat in engine coolant for cabin heating, and using waste heat in the exhaust for enabling emissions control devices. Significant effort through the years has also been focused on recovering waste heat from exhaust and engine coolant to provide additional power using various waste heat recovery techniques [3-7]. Waste heat utilization also includes storing waste heat to use when needed. For example, to improve engine warm-up time during multiple starts of hybrid electric vehicles (HEVs), stored warm coolant can be used to decrease the engine warm-up time [8].

The third area in which the VTMS enables reductions in fuel use is through integrated VTMS. As the number of vehicle components that require active thermal management increase, so do the costs in terms of dollars, weight, and vehicle packaging. This is particularly true for advanced vehicle powertrains in HEVs and plug-in hybrid electric vehicles (PHEVs) that contain additional critical components that require active cooling. Examples include batteries and power electronics. Integrated vehicle thermal management reduces fuel use by enabling advanced vehicle technologies that reduce energy use. It does this by reducing costs and components. The potential weight reduction of integrated vehicle thermal management also enables energy efficiency improvements.

The objective for 2008 focused on three main areas. First, we investigated current technologies for improved vehicle thermal management, waste heat utilization, and integrated cooling. With this information, areas of focus were proposed for research into waste heat utilization and integrated cooling that apply to advanced vehicle propulsion systems. Finally we developed initial concepts of new waste heat utilization techniques and integrated cooling.

Approach

The Integrated Vehicle Thermal Management Systems task in 2008 emphasized waste heat utilization and integrated thermal management with a focus on the application towards advanced propulsion technologies involving electric drive systems. To investigate the potential for waste utilization or integrated cooling, it was first necessary to take a step back and survey the challenges associated with vehicle thermal management across multiple powertrain configurations.

The challenges associated with vehicle thermal management vary significantly depending on the type of powertrain, external environment, and driver behavior. However, for this analysis we focused on challenges related to transitioning away from conventional vehicle powertrain systems to more efficient systems less reliant on internal combustion engines (ICEs) such as PHEVs and EVs. The first challenge for this transition is related to the variable or limited waste heat from the propulsion system as compared to conventional powertrains. The second challenge arises from the increased number of components requiring thermal control.

Through comparing potential technologies to address the thermal management challenges, it was possible to identify potential applications that could apply to multiple advanced vehicle propulsion technologies involving electric drive systems. With the emphasis on electric drive systems and in particular power electronics thermal management, two potential applications were selected for further review and analysis.

Results

Figure 1 and Table 1 highlight the challenges related to waste heat availability. With an internal

combustion engine (ICE), the actual power output (brake power) of the engine is only a fraction of the available fuel energy. A significant amount of energy is transferred to the coolant and exhaust as heat. This is true not only for spark ignition (SI) gasoline engines but also compression ignition (CI) diesel engines. As one transitions away from using an ICE as the primary propulsion source, the quantity (heat kW) and quality (temperature °C) of the waste heat decreases as shown in Table 1.

Table 1. Waste heat quantity and quality comparison.

	Output Power [kW]	Coolant Waste Heat [kW]	Coolant Temp. [°C]	Exhaust Waste Heat [kW]	Exhaust Temp. [°C]
ICE Engine	120 (28%)	111 (26%)	100	171 (40%)	390 [10]
Electric Drive	120 (80%)	30 (20%)	70	NA	NA
Electric Drive	50 (80%)	12.5 (20%)	70	NA	NA

Note: Values within () highlight the percentage of input energy.

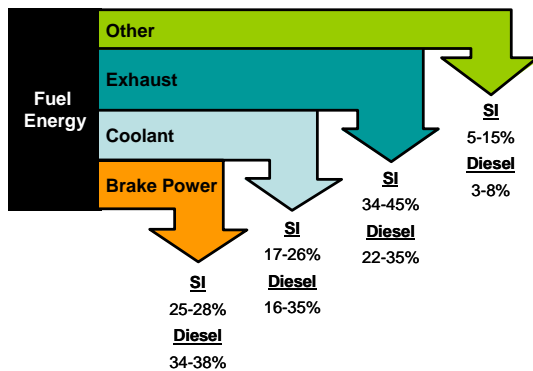


Figure 1. ICE Energy Balance [10,11]

The decrease in the quantity and quality of the waste heat affects the ability to utilize heat for common vehicle functions such as cabin heating and catalyst warm up. It also affects ongoing efforts to generate additional power in conventional vehicles from waste heat to improve the overall vehicle efficiency. This includes thermoelectric devices and Rankine cycle power generation [9].

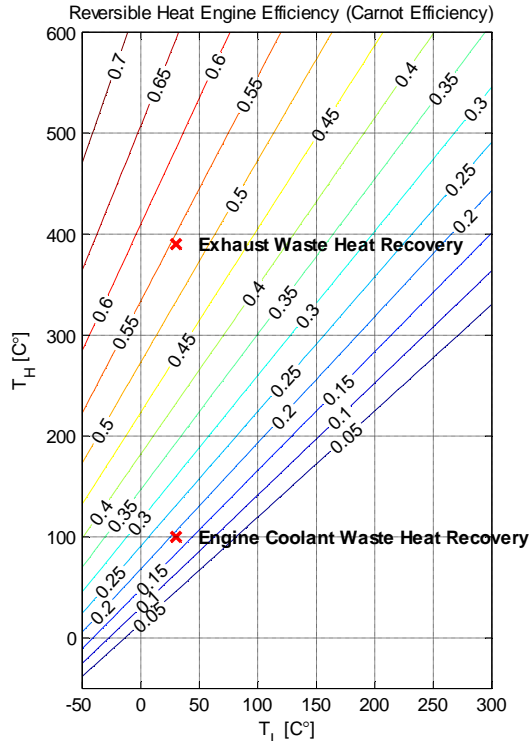


Figure 2. Ideal Carnot Heat Engine Efficiency

Figure 2 highlights the challenges of using alternate heat sources to generate power from waste heat. The figure compares the ideal efficiency (Carnot efficiency) of a heat engine operating between two temperatures. It is the maximum efficiency any engine could obtain while operating between two temperature reservoirs. The thermal efficiency relates the amount of heat produced to the heat input as shown in equation 1 below. The maximum Carnot efficiency applies to both Rankine and thermoelectric power generation cycles.

$$\eta_{th} = \frac{W_{net}}{Q_{in}} \quad (1)$$

Figure 2 highlights the ideal thermal efficiency for two cases. The first highlights the thermal efficiency based on recovering waste heat from an exhaust stream of an ICE powertrain, while the second highlights the drop in efficiency when recovering heat from engine coolant at 100°C. With the move towards electric drive systems, the thermal efficiency not only decreases with lower coolant temperature but also less waste heat is available.

Heat pumps have received significant attention as a method to provide cabin heat in systems with reduced waste heat. Heat pumps operate using a vapor compression cycle similar to a refrigerator with a compressor, but the objective is to transfer heat from a low temperature source to a higher temperature sink. The performance of a heat pump is determined by the coefficient of performance (COP_{HP}) as shown in equation 2. As seen in Figure 3 the COP_{HP} increases as the temperature of the high temperature sink decreases or as the temperature of the low temperature source increases. A higher COP_{HP} indicates the ability to transfer the same amount of heat with less compressor power.

$$COP_{HP} = \frac{Q_H}{W_{in}} \quad (2)$$

Commonly proposed vehicle applications for heat pumps retrieve heat from outside air to improve cabin warm up during cold starts. This application is highlighted on the graph by the label *HP: Air to Cabin Heating* assuming an air temperature of -20°C . One challenge associated with air heat pumps is the potential for ice to form on the evaporator [12]. For this reason some have investigated the potential of using engine coolant, but this brings the challenge of increasing the warm-up time of the engine coolant [12]. Operating a heat pump off of the power electronics coolant would make use of the waste heat in the power electronics system and result in a higher COP_{HP} that would depend on the temperature of the coolant. For comparison, the COP_{HP} of a heat pump transferring heat to warm up a catalyst is also shown to highlight that it would not be practical in a real system where the COP_{HP} would be even lower than the ideal case shown in Figure 3.

As mentioned previously, storing waste heat for later use is another method to utilize waste heat. One example of the impact is seen in batteries. Previous work [13] has looked at the impact of preheating batteries to improve performance at low temperatures. Table 2 illustrates the power or energy needed to heat a 40 kg NiMH battery pack by 20°C in five minutes. It also compares the energy to the energy capacity of the Toyota Prius battery which weighs about 45 kg [14]. The ability to use waste heat to provide the heating energy could reduce the

need to provide it through other means such as electrical heating.

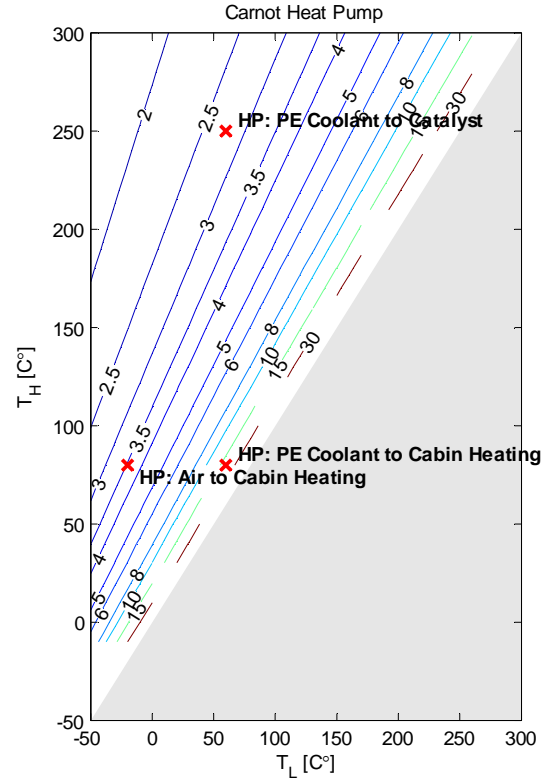


Figure 3. Carnot Heat Pump Coefficient of Performance

Table 2. Energy required to heat a 40 kg NiMH battery pack by 20°C in 5 minutes.

Required Heat [kW]	Required Energy [Wh]	Percent of HEV Energy Capacity (1.3 kWh) [14]
2.6	217	17%

Figure 4 highlights the impact of thermal control throughout the vehicle system and provides a summary of the number of components and subsystems requiring active thermal management. As the demands for improved performance and vehicle efficiency continue to increase, the thermal management challenges will also increase. Also, as the complexity of vehicles increases the ability to use separate thermal management systems for each subsystem becomes cumbersome and costly. The cost not only increases in terms of dollars, but also component count, weight, and packaging space. For this reason it is important to investigate opportunities

for integrated thermal management that enable multiple subsystems to utilize common thermal management systems. An example of how this is occurring in current HEVs is the integration of cabin cooling with air-cooling of batteries. This is one example, but it demonstrates a need to investigate how new vehicle technologies can be integrated into an overall vehicle thermal management scheme.

Components/Systems	Active Heating	Active Cooling	Passive Cooling
Engine	x	x	
Turbocharger		x	x
Engine Oil	x	x	x
Transmission	x	x	x
Charge Air		x	
Brakes		x	x
Electronic Controls		x	x
Alternators		x	x
Passenger HVAC	x	x	
EGR		x	
Electric Machines		x	
Battery	x	x	
Fuel Cells	x	x	
Power Electronics		x	
Emissions Hardware	x	x	x

Figure 4. Selection of Thermal Management Needs [15]

Another potential example of integrated vehicle thermal management could include the power electronics used within electric drive systems and vehicle air conditioning systems. Figure 5 shows the temperature versus entropy diagram from a model of an automotive air conditioning system using HFC-134a. Looking at the condenser region of the figure (states 4-7) one is able to see a temperature similarity with the current coolant used within power electronics cooling for HEVs.

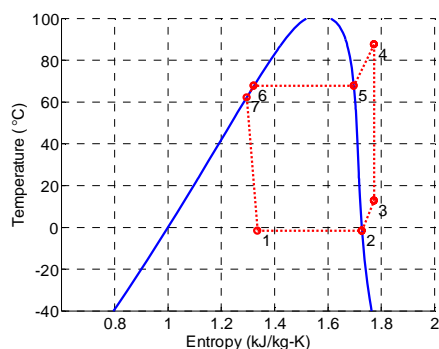


Figure 5. r134a Automotive Refrigeration Cycle

Conclusions

This project was initiated as a response to questions related to the use of power electronics waste heat in advanced vehicle technologies such as PHEVs. It was shown that the use of waste heat from the power electronics is limited due to the decreased quantity and quality of the waste heat as compared to the waste heat available in the coolant and exhaust of ICEs. However, the potential to use waste heat from the power electronics with heat pumps for cabin heat was identified as an area for future research. The need for integrated thermal management was also highlighted, and a method of integrating the power electronics cooling with the air conditioning system was identified for additional research.

Although the project arose out of specific questions related to power electronics, the analysis should be extended to other components such as energy storage. As the complexity and number of vehicle components requiring thermal management increases, it is necessary to look at integrated vehicle thermal management as a method to enable new vehicle technologies by reducing cost, complexity, and mass.

References

- J. Rugh and R. Farrington. *Vehicle Ancillary Load Reduction Project Close-Out Report*. NREL milestone TP-540-42454, January 2008.
- D. Bharathan, L. Chaney, R. Farrington, J. Lustbader, M. Keyser, and J. Rugh. *An Overview of Vehicle test and Analysis Results from NREL's A.C. Fuel Use Reduction Research*. VTMS 8, May, 2007.
- K. Smith and M. Thornton. Feasibility of Thermoelectrics for Waste Heat Recovery in Hybrid Vehicles. EVS-23, December, 2007.
- E. Doyle. Installation of a Diesel-Organic Rankine Compound Engine in a Class 8 Truck for a Single-Vehicle Test. SAE 790646, 1979.
- H. Oomori. Waste Heat Recovery of Passenger Car Using a Combination of Rankine. SAE 930880, 1993.
- Green Car Congress. *Honda Researching Advanced Hybrid Drive with Rankine Cycle Co-Generation*. Available: <http://www.greencarcongress.com/2008/02/honda-researchi.html>.

Green Car Congress. *BMW Developing Steam Assist Drive Base on Waste Heat Recovery*. Available:
http://www.greencarcongress.com/2005/12/bmw_developing_.html.

Toyota Technical Training. *Section 4 Engine*. Available:
<http://www.autoshop101.com/forms/Hybrid04.pdf>

K. Bennion. Integrated Vehicle Thermal Management Systems Analysis/Modeling. NREL milestone, May, 2008.

J. Haywood. Internal Combustion Engine Fundamentals. 1988.

R. Chammas. *Combined Cycle for Hybrid Vehicles*. SAE 2005-01-1171, 2005.

L. Scherer. On-Vehicle Performance Comparison of an R-152a and R-134a Heat Pump System. SAE 2003-01-0733, 2003.

Pesaran, A. Vlahinos, and T. Stuart. *Cooling and Preheating of Batteries in Hybrid Electric Vehicles*. 6th ASMR-JSME Thermal Engineering Conference, 2003.

Wikipedia. *Toyota Prius*. Available:
http://en.wikipedia.org/wiki/Toyota_Prius.

D. Allen. Thermal Management Evolution and Controlled Coolant Flow. SAE 2001-01-1732, 2001.

Q. Medium-Duty Plug-in Hybrid Electric Vehicle Analysis

Robb Barnitt (Principal Investigator), Matthew Thornton

National Renewable Energy Laboratory

1617 Cole Boulevard

Golden, CO 80401-3393

(303) 275-4489; robb_barnitt@nrel.gov

DOE Technology Manager: Lee Slezak

(202) 586-2335; Lee.Slezak@ee.doe.gov

Objective

Assess the potential benefit of a medium-duty (MD) plug-in hybrid electric vehicle (PHEV) platform.

Identify advantages of an MD PHEV platform, and frame project direction based upon an MD vehicle segment analysis.

Approach

A robust vehicle segment analysis will aid in targeted development of the most appropriate vehicles that will yield the largest fuel reduction.

Public data sets were mined to characterize the MD vehicle segment, evaluating its potential for PHEV application.

Accomplishments

The MD vehicle segment has been characterized according to key metrics, including annual and daily vehicle miles traveled (VMT), body type and vocation, and liquid fuel market share.

The breadth of vocation-specific drive cycles in the MD segment underscores the value of custom drive cycle data to allow more accurate modeling of potential PHEV platforms.

Several MD vehicle applications, including multi-stop delivery and utility/bucket, have been identified as having the largest potential for PHEV application, and are slated for further analysis.

Future Directions

Expand drive cycle database to ensure accuracy of modeling efforts.

Model currently available HEVs for PHEV retrofit.

Model range of platforms/vocations for PHEV prototype.

Down selection of vocations/platforms for retrofit and prototype efforts.

Partner with industry, leverage cost-share opportunities to develop one or more ground-up PHEV prototypes.

Initiate in-use vehicle demonstration utilizing NREL analysis, data collection, and chassis dynamometer test capabilities.

Develop MD PHEV test-bed.

Introduction

Classes 3 through 6 typically represent medium-duty vehicles, with a gross vehicle weight rating (GVWR) range of 10,000 to 26,000 pounds. There has been considerable research focus on PHEV technology in the light-duty (LD) vehicle segment, which, due to its large volume of fuel consumed and well-matched user driving behaviors, make it an excellent application for PHEV technology. While also large fuel consumers, heavy-duty vehicles typically do not exhibit characteristic drive cycles (transient intensive), that render them appropriate for PHEV application. The MD vehicle segment has received less scrutiny for PHEV application, despite several compelling attributes:

Many transient intensive drive cycles conducive to PHEV application.

Fleet-based vehicles, which return to a home base, facilitating overnight charging.

Potential for significant fuel savings per vehicle.

Attractive value proposition, given potential for reduced maintenance costs, longer period of vehicle ownership, and social pressures to green corporate image.

Approach

Understanding the nature of the vehicle segment can aid in targeted development of the most appropriate vehicle platform and vocation, which will yield the largest reduction in fuel consumption. While prioritizing MD vocations that are large fuel consumers would be ideal, no comprehensive data set exists to support this approach. The vehicle segment analysis utilized data sets from the Vehicle Inventory and Use Survey (VIUS) 2002 [1], as well as data compiled by U.S. Department of Transportation (DOT) and the Federal Highway Administration (FHA) [2]. These data aid in characterizing MD segment vehicle types and their utilization and driving behaviors to better assess the applicability of PHEV technology to this vehicle segment.

Results

The vehicle body type with the largest MD segment population is multi-stop delivery. These vehicles represent 29 percent of the MD vehicle population.

Figure 1 illustrates the distribution of vehicle GVWR across the MD segment, which is skewed toward lower and higher payload capacity vehicles.

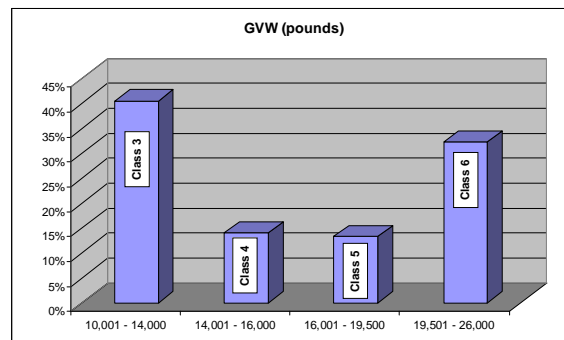


Figure 1. MD Vehicle Segment Class Distribution

Figure 2 indicates the near equal representation of gasoline and diesel engines employed by the MD segment. 48 percent of MD vehicles are fueled with gasoline, while 47 percent are fueled with diesel. This fact underscores the utilization of lower payload capacity vehicles with lesser low-end torque requirements in the segment, primarily a function of vocation.

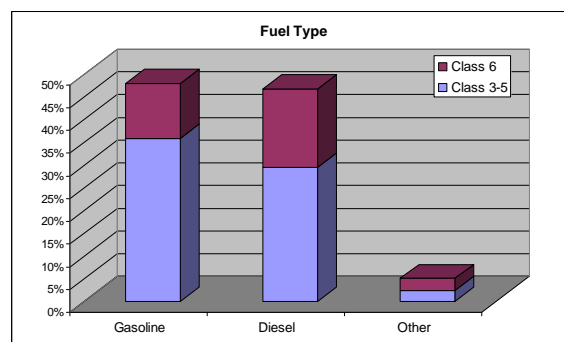
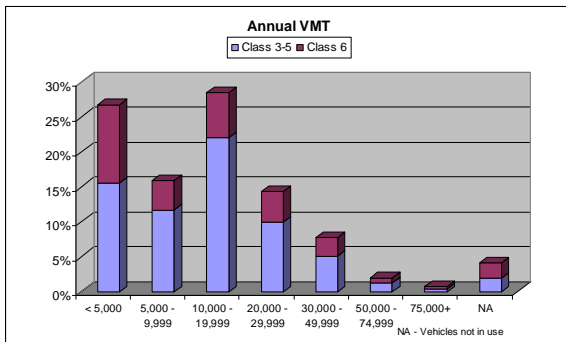


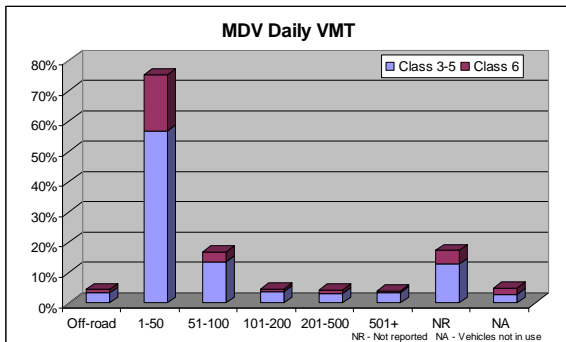
Figure 2. MD Vehicle Segment Fuel Utilization

The acceptability of lower cost gasoline engines for these vocations provides a better cost-benefit ratio for hybridization than would a diesel engine baseline.

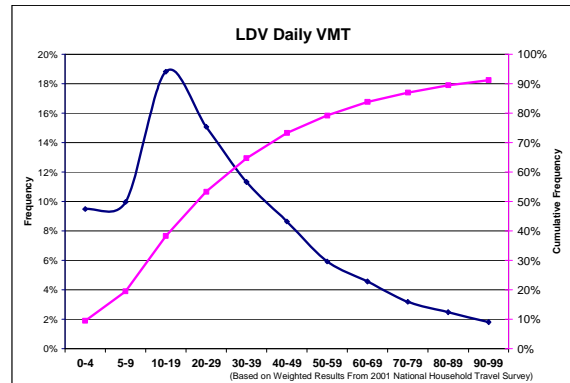
Figure 3 presents annual VMT for the MD vehicle segment, and indicates that 71 percent of MD vehicles travel less than 20,000 miles per year. Relatively low annual mileage indicates lower fleet vehicle turnover – vehicles are owned and driven for 15 or more years. This represents a potential hybridization advantage, in that higher capital costs can be spread over many years of operation, and the payback period for this technology is longer.

**Figure 3. MD Vehicle Annual VMT Distribution**

Daily driving behaviors, including daily VMT, are a dominant factor to be considered when evaluating the potential of PHEV application. Figure 4 presents the daily VMT distribution for the MD segment – 75 percent of MD vehicles travel 50 miles or less per day.

**Figure 4. MD Vehicle Daily VMT Distribution**

A low daily VMT is preferred in order to maximize the benefit of hybridization, while not exceeding the capabilities and cost limitations of a traction battery pack. Indeed, the daily VMT metric is one fundamental to the focus on LD vehicles for PHEV application. Figure 5 illustrates the similarities in daily VMT between MD and LD vehicles [3]. Eighty percent of LD vehicles travel 50 miles or less per day.

**Figure 5. LD Vehicle Daily VMT Distribution**

Analyzing the feasibility of PHEV technology to MD vehicles will require evaluation of many criteria, namely vocation, opportunity and overnight charge logistics, component packaging constraints, and perhaps most important – drive cycle. Consideration of many stock drive cycles available for simulation reveals little compatibility with MD vocations. Custom drive cycles, and those composite drive cycles developed with industry insight, may prove most valuable when simulating the performance and feasibility of PHEV applications in the MD vehicle segment.

Conclusions

Medium-duty vehicles consume a large volume of petroleum fuel, by virtue of low fuel economy, aggressive drive cycles, and/or large accessory power requirements. MD vehicles are diverse in configuration, vocation, and drive cycle, making them compelling candidates for PHEV application. Multi-stop delivery vehicles dominate the MD vehicle population, and are characterized by less than 50 miles driven per day. The breadth of vocation-specific drive cycles in the MD segment underscores the value of custom drive cycle data to allow more accurate modeling of potential PHEV platforms. Significant petroleum reductions can be realized by applying a PHEV configuration to the appropriate platform, vocation, and drive cycle.

In upcoming years, efforts will focus on expanding the in-use MD vehicle duty cycle database and on modeling of potential PHEV configurations for the MD vocation. The ultimate goal will be to identify vocations/platforms for retrofit and prototype development and partnering with industry in order to leverage cost-share opportunities to develop one or more ground-up PHEV prototypes.

References

1. U.S. Census Bureau, 2002 Census Vehicle Inventory and Use Survey. December 2004.
2. <http://www.fhwa.dot.gov/policy/ohim/hs06/htm/vm1.htm>
3. 2001 NHTS Data (<http://nhts.ornl.gov/2001/index.shtml>).

R. PSAT Heavy-Duty Vehicle Modeling and Simulation

Aymeric Rousseau (project leader)

Argonne National Laboratory

9700 South Cass Avenue

Argonne, IL 60439-4815

(630) 252-7261; arousseau@anl.gov

DOE Technology Manager: Lee Slezak

(202) 586-2335; Lee.Slezak@ee.doe.gov

Objectives

Develop heavy-duty Powertrain System Analysis Toolkit (PSAT) capabilities.

Gather component and vehicle data information.

Validate several vehicle classes.

Approach

Collaborate with national laboratories, universities, and industry to collect component and vehicle data from existing projects.

Accomplishments

Collaborated with West Virginia University to validate several heavy-duty and medium-duty vehicle classes on the basis of dynamometer data.

Supported original equipment manufacturers (OEMs) by integrating specific drivetrain configurations in PSAT.

Future Directions

Complete the validation of several heavy-duty vehicle classes on the basis of West Virginia University and Oak Ridge National Laboratory (ORNL) vehicle test data.

Extend collaboration with OEMs to support the 21st Century Truck Partnership (21st CTP) activities.

Introduction

The goal of this task is to support the 21st Century Truck Partnership (21st CTP) activities by extending the heavy-duty capabilities of the Powertrain System Analysis Toolkit (PSAT).

Model Validation

To validate a vehicle model, test data from a dynamometer are required. Collaboration was initiated with West Virginia University to validate several vehicle classes on the basis of previously collected data. Researchers from the West Virginia University Center for Alternative Fuels, Engines, and Emissions (CAFE) supported Argonne National

Laboratory (Argonne) in identifying and quantifying parameters that are critical to the accurate modeling of heavy-duty vehicle performance and fuel economy.

The objective of this project, in its first phase, was to obtain information and prepare a set of heavy-duty component parameters for use in PSAT. Phase 1 work was centered on a conventional over-the-road tractor, for which several operational data sets were available. The Peterbilt truck used for the modeling is owned by WVU/CAFE, has a non-EGR 550-hp Caterpillar 3406 engine, 18-speed Roadranger manual transmission, and a tandem axle drive.

Figure 1 shows the Peterbilt truck used in this research. Table 1 presents the details of the vehicle configuration.



Figure 1. Peterbilt Truck

Table 1. Details of the vehicle and of test conditions used to gain data for this report.

WVU Test Reference Number	WVU-Peterbilt-D2-TEST_D
Vehicle Type	Tractor
Vehicle Manufacturer	Peterbilt
Vehicle Model Year	1996
Gross Vehicle Weight (lb)	46,000 (tractor only) 80,000 (assumed value with trailer)
Vehicle Tested Weight (lb)	56,000
Odometer Reading (mile)	44,1097
Transmission Type	Manual
Transmission	18 speed
Engine Type	Caterpillar 3406E
Engine Model Year	1996
Engine Displacement (liter)	14.6
Number of Cylinders	6
Primary Fuel	D2
Test Cycle	UDDS (also termed TEST_D)
Test Date	4/21/06

A torque map for the truck was fitted to a curve and has been used in subsequent modeling work. The researchers examined the ability to acquire fuel efficiency data by using broadcast percent load and instantaneous fuel consumption calculated from the CO₂ emissions collected from the Peterbilt truck during prior testing. Background correction for CO₂ was also required.

Efficiency maps were prepared, but they need to be refined to account for diffusion of analyzer data. The transmission ratios were documented, and losses were considered to be due to oil churning, gear meshing, and lubricant pump operation. Through calculation, efficiency maps are available for each selected gear.

Auxiliary loads have been considered and an approach has been developed to predict the fraction of time that the fan is engaged for cooling. This fraction can then be combined with the fan load, as a function of engine speed, to predict the cooling power demand. The subsystems typically include the engine fan, alternator, air brake compressor, and power steering pump. A wealth of information is becoming available on these power demands as a result of research on initiatives to reduce idling of trucks at truck stops and electrification of auxiliary loads. Data have been gathered to provide input to PSAT. In the Peterbilt truck with a 550-hp engine, the maximum of the auxiliary load (without fan) is about 11 hp. The fan load is usually far greater than other loads when the fan is engaged and has received separate attention. Figure 2 shows the nature of a fan curve.

Early heavy-duty vehicles used permanently fixed drive fans that were wasteful of energy. The Peterbilt truck employed this type of fan. The fan power loss can be simply expressed as a function of engine speed multiplied by the percentage of the time fan is on. The difficulty is in creating a reliable algorithm to predict either when the fan is engaged or the fraction of time for which the fan is engaged. The investigators have made progress with a model, which considers the following variables: load history, ambient air temperature, an aerodynamic term (approximated by the difference between vehicle speed and wind speed and simply taken as vehicle speed for the generic case when wind speed is not known), and fan operation history.

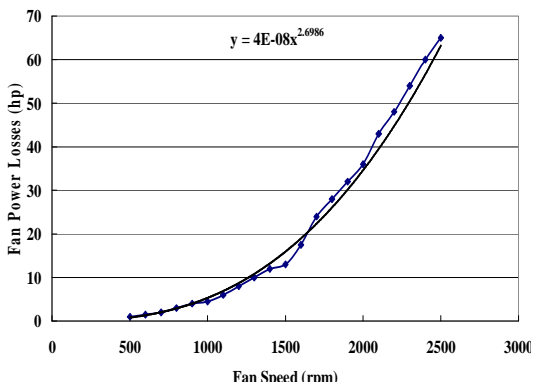


Figure 2. Engine Fan Power Losses as a Function of Fan Speed

Integration of Component Data

Several component models were integrated into PSAT to simulate several technologies. Several engine and electric machine data from an OEM were integrated in PSAT to simulate several vehicle classes, including bus, garbage truck, delivery, and utility.

Support of Existing Activities

Several powertrain configurations were added to support internal development from several manufacturers. Numerous questions from the PSAT users were answered regarding control strategy, graphical user interface usage, and component sizing.

Collaboration with the U.S. Environmental Protection Agency (EPA) continued to support the SmartWay activities. The main goal is to be able to quantify the benefits of a series of advanced technologies (i.e., aerodynamic, single tire).

Conclusions

Several component models and data sets have been integrated to meet the specific requirements of heavy-duty vehicles. The validation of several vehicle classes and powertrain configurations will continue.

S. Heavy Truck Duty Cycle (HTDC) Project

Helmut E. (Bill) Knee (Principal Investigator)

Oak Ridge National Laboratory

National Transportation Research Center

2360 Cherahala Boulevard, Room J-14

Knoxville, TN 37932-6472

(865) 946-1300; kneehe@ornl.gov

DOE Program Manager: Lee Slezak

(202) 586-2335; Lee.Slezak@ee.doe.gov

Objectives

Collect duty cycle data and performance measures for class-8 heavy trucks, and for selected vocations of class-6 and class-7 medium trucks, from real world operating environments.

Assess the fuel efficiency impacts of new commercial off-the-shelf (COTS) technologies.

Analyze the collected data for various perspectives to assess the fuel efficiencies of heavy and medium trucks operating in real-world environments.

Establish a real-world-based heavy and medium truck performance database capable of supporting the needs of the Department of Energy (DOE), researchers, and private industry.

Support Argonne National Laboratory (ANL) by providing data and information for the development and validation of Powertrain System Analysis Toolkit (PSAT) modules for heavy and medium trucks.

Seek strong involvement of private industry and other Federal agencies in the conduct of this program.

Approach

Identify relevant duty cycle and performance measurement data that supports ANL's PSAT development, as well as other major research programs such as DOE's 21st Century Truck Partnership (21st CTP) and the Environmental Protection Agency's (EPA) SmartWay program.

Identify sources of the duty cycle and performance measurement data from existing onboard sensors/databus, and identify any additional sensors that are necessary, affordable, minimally invasive, and do not disrupt normal business activities of the fleets.

Seek private industry fleet partners that would allow data collection from their vehicles at no charge to the program.

Develop and maintain six data acquisition systems (DASs) used to collect data from the test trucks.

Instrument up to six heavy/medium trucks (test trucks) at one time and collect 60 channels of information (heavy truck) and 30 channels of information (medium truck) at 5 Hz for 12 months for each vehicle to obtain a detailed profile of heavy and medium truck operations in real-world environments.

Download data on a bi-weekly basis from the class-8 test trucks by traveling to the facilities of the fleet partner (Schrader Trucking) and extracting the data from the DASs. For the class-6 and class-7 data collection effort, wireless, remote, near-real-time data downloading will be utilized (to start in early calendar year [CY]-2009).

Develop, test, and incorporate the wireless data download capabilities into the DASs for the class-6 and class-7 data collection efforts.

Review the collected data as they are obtained to identify any problems related to the sensors, DAS, or the data.

Enter the reviewed data into a heavy truck/medium truck (HTMT) database residing at the Oak Ridge National Laboratory (ORNL).

- Develop a prototype Duty-Cycle Generation Tool (DC-GenT) capable of statistically generating duty cycles based on characteristics specified by the user and for a user-specified duty-cycle duration period.
- Develop a data search tool that can be utilized by non-ORNL staff to extract data files of interest to the user.
- De-instrument the test trucks upon completion of field testing.
- Identify fuel efficiency studies that can be conducted utilizing the collected data and select and conduct one or more studies for the heavy/medium trucks.
- Support ANL in data needs for development and/or validation of PSAT.
- Seek the partnership of other Federal agencies (i.e., the Department of Transportation's [DOT] Federal Motor Carrier Safety Administration [FMCSA], and EPA) in leveraging funds and resources.
- As possible, support DOE's 21st Century Truck Partnership.
- As possible, be responsive to data and information requests received by ORNL and/or DOE.
- Keep DOE informed of program progress through monthly/quarterly/yearly progress reports, and project review meetings.
- Prepare final reports for the Heavy Truck Duty Cycle (HTDC) and Medium Truck Duty Cycle (MTDC) efforts.

Accomplishments

- Class-8 data collection efforts were completed in December 2007.
- De-instrumentation of the class-8 test vehicles was accomplished between late October 2007 and February 2008.
- Dynamometer testing of one of the class-8 test trucks was planned and carried out at West Virginia University (WVU) for nine days in December 2007. WVU provided ORNL with a report of the effort in February 2008.
- WVU also conducted (in December 2007) coast-down testing of the test truck to assess drivetrain losses.
- ORNL conducted an analysis of the WVU data and confirmed the dependence of the powertrain losses on the square of the speed with a value of 0.016 watt/rpm² for the gear box in the neutral position, referenced to the speed of the engine's output axle.
- Communication with EPA concerning partnering and for the collection of emissions data for the class-6 and class-7 efforts to be conducted in fiscal year (FY) 2009 conducted throughout FY 2008. Although considerable enthusiasm was displayed, EPA has made no commitments.
- In December 2007, ORNL finalized the processing of the raw data collected for the class-8 test vehicles. During the more than 12 months of data collection effort, almost 200 Gigabytes of data were collected and processed resulting in 1,710 files; each one contained the activities of one day of the participating six class-8 trucks, with an average of 285 days per truck.
- In November/December 2008, contacted Lawrence Livermore National Laboratory (LLNL) regarding the possible collection of aerodynamics data on the test vehicle that was to be sent to WVU. The aerodynamics data, in conjunction with the dynamometer data and the field operational testing, would have provided an extremely rich database of data for one of the class-8 test trucks. Unfortunately, the offer of free wind tunnel testing that was made in early FY 2007 was no longer available, and aerodynamics data were not collected.
- In December 2007, ORNL provided a courtesy debriefing of the class-8 data collection efforts and results to ORNL's class-8 fleet partner, Schrader Trucking. It was reported that: 1) fuel efficiencies using the new generation single wide-based tires (NGSWBTs) were consistently better than those when standard dual tires (SDTs) were utilized throughout the field test; 2) as the payload weight increased, the fuel efficiency margin of the NGSWBTs compared to SDTs also increased (at 80,000 lbs, the margin was greater than 10 percent); and 3) the NGSWBTs were more fuel efficient than SDTs for every speed interval.
- In March, ORNL also developed a class-8 weight model based on data and information gathered in the HTDC efforts. This model allows the estimation of the total truck weight by merely knowing the tractor weight as measured by the onboard AirWeigh device that was mounted on the six class-8 tractors participating in the

program. The weigh model will be used to determine the weight of un-instrumented trailers (i.e., only ten out of more than 150 trailers were instrumented).

In March 2008, ORNL provided a phone briefing to FMCSA staff in Washington, DC about the MTDC project and the project's potential in exploring wireless data transfer as a means of collecting duty cycle data. FMCSA has indicated a willingness to draft a letter to be sent to DOE in support of the DOE MTDC project.

In March 2008, ORNL staff traveled to the Mid-American Truck Show in Louisville, KY to interact with class-6 vehicle manufacturers in order to gain insight into the vehicle's data bus structure, vehicle class application, and to look for technology germane to the MTDC project.

ORNL completed a vocational assessment of the U.S. class-6 operations in May 2008. This report was electronically sent to the DOE sponsor in June 2008.

In spring, 2008, ORNL engaged in establishing fleet partnerships. The following fleets accepted a partnership in the program based on the vocations that they represent, and a formal partnership-signing event is scheduled for February/March 2009.

Dillard-Smith Construction.

Electrical Line Utility Bucket Trucks – typically has approximately 8 hours per/day of bucket operation and very low vehicle miles (typically 50 miles/day). They operate locally, regionally, and nationally (storm response). Location: New Market, TN.

Fountain City Wrecker Company. Location: Knoxville, TN.

Knoxville Area Transit (KAT) – operates on suburban and urban routes. Location: Knoxville, TN.

H. T. Hackney – is an institutional food and grocery supplier and operates straight and combination trucks (dry-box and refrigerated). The company engages in local and tri-state delivery. Location: Roane County, TN.

The first draft of the HTDC Final Report was completed in June 2008 and sent to DOE and industry partners for review. The report included a major section that focused on an energy efficiency-based data analysis.

In June 2008, ORNL purchased a Raven X cellular model to test its function and compatibility with the eDAQ DAS to be utilized in the MTDC efforts.

ORNL provided a presentation of the HTDC efforts and results to the 21st CTP held at Volvo Trucks of North America facilities in Greensboro, NC on June 10, 2008.

In August 2008, ORNL staff visited the Knoxville Area Transit (KAT) to present the MTDC project to them, to gain a better understanding of their operation, and to interface the MTDC DAS with one of their fleet vehicles. They agreed to be fleet partners in the MTDC efforts.

In August and September 2008, ORNL conducted fuel consumption testing with the H.T. Hackney Company to obtain one month of fuel records for four vehicles. This was done in order to compare the actual gallons of fuel used with the QualComm-reported fuel usage values from the databus. A strong correlation was found between the QualComm-reported fuel used (in gallons) and the actual fuel used based on driver fueling logs.

A list of the signals available from one of the class-7 H.T. Hackney vehicles is presented in Table 1.

ORNL initiated data analysis of the information collected in the HTDC project to determine the effect of speed change (55 mph vs. 65 mph) in fuel efficiency.

In September 2008, ORNL received a request for a long-haul heavy truck duty cycle from FEV, Inc. (North American Technical Center, 4554 Glenmeade Lane, Auburn Hills, MI 48326-1766). ORNL generated the duty cycle for a trip from Knoxville to Salt Lake City and back and provided the information to FEV.

Future Directions

ORNL will collect class-6 and class-7 duty cycle and performance data for a minimum of four vocations from FY 2009 into FY 2011.

As funding allows, specialized studies will be conducted regarding the fuel efficiency characteristics of the class-6 and class-7 test vehicles.

As funding allows, a comparison of the HTDC class-8 field data with class-8-PSAT module results and Easy-5 results will be conducted.

As possible (and as funding allows), ORNL will work with private industry to evaluate energy efficiency technologies during the MTDC efforts.

Continue to seek sponsorship for class-6/7 duty cycle efforts from EPA, and work with EPA to define any emission data collection requirements.

Initiate the collection of duty-cycle data on class-6/7 vehicles.

As possible, refine the DC-GenT.

Seek stronger alignment with the 21st Century Truck Initiative, the DOE “Super Truck” concept, and the National Transportation Research Center, Inc.’s (NTRCI) “Safe Truck” concept.

Seek integrative energy efficiency and safety research including cross-agency (DOT) research.

Seek opportunities to collect real-world operations experience from fleets utilizing heavy hybrid technologies.

Table 1 - J-1939 Signals Available from the H.T. Hackney Vehicle

Signal	Name	Sample Rate	Available
OutShaftSp	Output Shaft Speed	N (100 Hz)	Y
AccPdlPos	Accelerator Pedal Position	N (20 Hz)	Y
PctLoadISp	Percent Load at Current Speed	N (20 Hz)	Y
ActEgPctTq	Actual Engine - Percent Torque	N? (variable)	Y
DrvDmEgPctTq	Driver's Demand Engine - Percent Torque	N? (variable)	Y
EgSp	Engine Speed	N? (variable)	Y
IGr	Current Gear	N (10 Hz)	Y
SelectedGr	Selected Gear	N (10 Hz)	Y
ActGrRatio	Actual Gear Ratio	N (10 Hz)	Y
FrNoWipSw	Front Non-operator Wiper Switch	N (5 Hz)	N
FrOpWipSw	Front Operator Wiper Switch	N (5 Hz)	N
RearWipSw	Rear Wiper Switch	N (5 Hz)	N
FrOpWipDyCtl	Front Operator Wiper Delay Control	N (5 Hz)	N
FrNoWipDyCtl	Front Non-operator Wiper Delay Control	N (5 Hz)	N
RearWipDyCtl	Rear Wiper Delay Control	N (5 Hz)	N
FanDrSt	Fan Drive State	N (1 Hz)	Y
FAxSp	Front Axle Speed	N (10 Hz)	Y
HResTotVehDt	High Resolution Total Vehicle Distance	N (1 Hz); use 5Hz	N
ACHiPrFanSw	AC High Pressure Fans Switch	N (1 Hz)	Y
TotPTOhr	Total Power Takeoff Hours	Use 0.1 Hz	Y
EgOilTmp	Engine Oil Temperature	N (1 Hz)	Y
FuTmp	Fuel Temperature	N (1 Hz)	N
PTOSetSp	Power Takeoff Set Speed	N (10 Hz)	Y
PTOSp	Power Takeoff Speed	N (10 Hz)	N
CruAccSw	Cruise Control Accelerate Switch	N (10 Hz)	N
CruActive	Cruise Control Active	N (10 Hz)	Y
CruCoastSw	Cruise Control Coast Switch	N (10 Hz)	N
CruEnSw	Cruise Control Enable Switch	N (10 Hz)	N
CruResSw	Cruise Control Resume Switch	N (10 Hz)	N
CruSetSw	Cruise Control Set Switch	N (10 Hz)	N
CruSetSp	Cruise Control Set Speed	N (10 Hz)	Y
FuRate	Fuel Rate	N (10 Hz)	Y

InsFuEcon	Instantaneous Fuel Economy	N (10 Hz)	Y
BarPr	Barometric Pressure	N (1 Hz)	Y
AirInlTmp	Air Inlet Temperature	N (1 Hz)	N
AmbAirTmp	Ambient Air Temperature	N (1 Hz)	?
NetBatI	Net Battery Current	N (1 Hz)	N
AltV	Alternator Voltage	N (1 Hz)	N
BatVSwtd	Battery Voltage, Switched	N (1 Hz)	Y
ElecV	Electrical Voltage	N (1 Hz)	Y

Introduction

Nearly 80 percent of U.S. domestic freight revenue involves the use of heavy trucks. Current trucking industry issues encompass a fine balance of concerns related to the economical, safe, and secure operation of heavy trucks on our highways. In order to move toward an effective solution-set that optimally balances such concerns, a firm understanding of the nature and characteristics of heavy and medium truck driving and their associated duty cycles in the US is critical.

The trucking industry in the US involves considerable use of heavy trucks (class-8 and class-6 being the classes which consume the most fuel), operates in relatively small fleets (50 percent of the fleets in the United States are less than 100 trucks, and 25 percent of the fleets in the United States are less than 10 trucks), operates on small profit margins, and is faced with considerable regulatory and economic pressures (e.g., issues related to hours-of-service, and reduction of truck idling time). Making heavy trucks more efficient through new technologies or congestion avoidance protocols is a goal that would contribute to larger profit margins and would also contribute to a reduced dependence on oil and reduced emissions. Since efficient systems are also typically more inherently safe, lives could also be saved.

A practical dilemma involves knowing what the true benefits of new energy efficient technologies are. Most benefit assessments are based on existing information on heavy truck operation. Much of this information is stylized and based on duty cycles that are meant to test various emission or fuel economy measurements. For example, the FTP Transient Cycle is a transient engine dynamometer cycle for heavy-duty truck and bus engines. It includes segments designed to simulate both urban and

freeway driving and is used for emissions certification testing of heavy-duty diesel engines in the United States. Another example is the Urban Dynamometer Driving Schedule (UDDS), which is an EPA transient chassis dynamometer test cycle for heavy-duty vehicles. While cycles such as these are based on an understanding of the vehicle technology and how best vehicles might be tested to assess emissions and fuel economy, they do not really reflect real world driving and the real demands placed on the vehicle, driver, or vehicle systems.

Despite common beliefs, how trucks actually operate on our highways is not well known. With hours-of-service rules, recurring congestion in urban environments, anti-idling regulations, differing fleet management philosophies, weather, the need to deal with incidents of non-recurring congestion, and various topological conditions, only the most highly experienced heavy truck driver has a true situational awareness of the characteristics of driving on our nation's highways. A better understanding of the effects of these impacts on driving, as captured via a field test of heavy vehicle driving, would provide a valuable asset to DOE, other Federal agencies, as well as the trucking industry in evaluating technologies for energy efficiency, safety, emissions, fleet management, etc.

For DOE, such data and information would provide a basis on which to make decisions related to new technologies being developed to reduce fuel consumption, provide alternative power sources (e.g., hybrid engine technologies and fuel cells), transition to alternative fuels, and reduce emissions. In particular, a database that reflects true driving experiences across various parameters such as geographic terrain, fleet size, fleet type, driving environment, and driving protocols, can provide a rich source of information that could be utilized to

make sound energy efficiency-based technology decisions.

These and similar complementary data needs of various agencies of the Department of Transportation (DOT), the Environmental Protection Agency (EPA), and the trucking industry require data and information on how trucks are actually utilized and driven in real-world environments, the geography over which they are operated, information related to the driving situation, and the protocols and regulations that govern their operation. In addition, much of the current thinking and research related to long haul and urban/city driving are based on anecdotal information. A quantitative profile of the driving behavior of heavy trucks does not currently exist. A thorough understanding of the operation of heavy trucks within duty cycles that reflect real-world conditions is an asset that would have great benefit to DOE, other Federal agencies, and the overall trucking industry.

Approach

This program involves efforts to collect, analyze, and archive data and information related to heavy-and-medium truck (classes 8, 7, and 6) operation in real-world driving environments. Such data and information will be usable to support technology evaluation efforts, and provide a means of accounting for real-world driving performance within heavy truck analyses. Additionally, the data collected will generate data, information, and duty cycles that will support Argonne National Laboratory's (ANL) development of their Powertrain System Analysis Toolkit (PSAT). Industry partners in this program to date have included Michelin Americas Research and Development Corporation, of Greenville, SC; Dana Corporation of Kalamazoo, MI; and Schrader Trucking of Jefferson City, TN. Class-6 and -7 partners include: Dillard-Smith Construction (e.g., electrical line utility bucket trucks) of New Market, TN; Fountain City Wrecker Co. of Knoxville, TN; Knoxville Area Transit (KAT) of Knoxville, TN; and H. T. Hackney (e.g., straight and combination trucks (dry-box and refrigerated)). These partners are interested in the vehicle dynamics of real world driving in order to support their interests in fuel efficiency and improved operations, and to support future investment decisions.

The program partners have provided significant in-kind contributions, including: no-cost access to test vehicles, test equipment, and engineering services; and six sets of new tires for class-8 testing. Figure 1 shows a typical class-7 H.T. Hackney delivery truck with non-refrigerated, refrigerated, and frozen compartments that will be used in the Medium-Truck Duty Cycle portion of the program.

The program has involved a Pilot Test, class-8 data collection and analysis, and currently, a class-6/7 data collection and analysis effort. During FY 2008, the class-8 data collection and analysis effort was completed, and initial efforts to support class-6/7 data collection effort were initiated.



Figure 1. Typical Class-7 H.T. Hackney Delivery Truck with Non-Refrigerated, Refrigerated, and Frozen Compartments

Completion of the Class-8 Heavy Truck Duty Cycle Data Collection and Analysis

During FY 2008, the Heavy Truck Duty Cycle (HTDC) Data Collection and analysis effort was completed. This effort included data collection from six class-8 long-haul tractors and ten trailers that were owned and operated by the program's HTDC partner, Schrader Trucking of Jefferson City, TN. Figure 2 shows one of the Schrader tractors utilized in the HTDC portion of the program.



Figure 2. One of Six Class-8 Tractors Owned by Schrader Trucking Used in the HTDC Field Test

Sixty channels of data were collected at 5 Hz for each of the test vehicles over a 12-month test period. Nearly 200 Gigabytes of data were collected. These data relate to engine performance, vehicle performance, location, topology, weather conditions, and road conditions. The tractors and trailers engaged in normal Schrader-based vocational activities. Half of the instrumented portion of the test fleet used new Michelin NGSWBs while the other half used new Michelin standard dual tires. The routes traveled by Schrader trucking provided a diversity of topology (city, urban, and rural highways) and experienced a variety of weather and road conditions.

The data were reviewed for errors and entered into the heavy and medium truck database. In FY 2008 two prototype data management and analysis tools were developed to allow users to interface with the data: the Duty Cycle Generation Tool (DC-GenT) and the data access tool.

The Duty Cycle Generation Tool (DCGenT)

The DC-GenT prototype allows a user to specify characteristics of interest related to the collected data and to compile all data collection segments in the database that meet the specified characteristics. Users may specify “AND” and “OR” Boolean operations during the search. Characteristics can, for example, relate to road grade, tires, time-of-day, weather, speed, and location (urban, rural, metro, etc). Characteristics related to payload will be added in the future. For the applicable segments, velocity

and acceleration histograms are generated and statistical integration is performed to generate a single characteristic duty cycle that reflects the velocity and acceleration profiles of the applicable segments. In the extremes, users can generate a duty cycle for one specific segment traveled by an individual test tractor-trailer (on one extreme), or can generate a single duty cycle for all segments of the data within the database. More likely will be the generation of a duty cycle that relates to a selected set of characteristics. The user can also specify the desired duration of the duty cycle.

The Data Access Tool

In order to allow users to utilize the database for purposes other than duty cycle generation, a prototype data access tool was developed that allows for the extraction of all of the raw data associated with user-specified performance characteristics. The resulting compilation of raw data segments can then be utilized by users for specialized analyses.

Dynamometer Testing

Drive torque data is a performance characteristic that was identified as being important for utilization within ANL’s PSAT. Because this characteristic was not identified until after class-8 field testing was underway, and because of the difficulty in collecting drive torque data during testing, dynamometer testing at West Virginia University (WVU) was undertaken on one of the six Schrader instrumented tractors. For this testing, three duty cycles were defined for execution on the dynamometer. The three cycles were: 1) a real-world segment in which the truck on the dynamometer engaged in during the field testing, 2) a standard EPA long-haul duty cycle, and 3) a duty cycle designed to extract information related to the truck’s engine map. For each of these duty cycles, the dynamometer testing generated drive torque data, fuel usage data, and emissions data. Coast-down data to identify drivetrain losses were also obtained. Since all of the six tractors utilized in the field tests were similar, drive torque data can be generated from the dynamometer data, which will be accomplished when resources are available.

Fuel Efficiency Study – NGSWBTs vs. Standard Dual Tires

In order to demonstrate the value of the collected data for purposes other than duty-cycle generation, a special study was conducted to compare the fuel consumption of the test trucks with NGSWBTs to that of the trucks with standard dual tires. Details and results of the study are provided in the Heavy Truck Duty Cycle Final Report. For this study, the fuel consumed by the test tractors with NGSWBTs was compared to the fuel consumed by the test tractors with standard dual tires. Only segments with similar characteristics (e.g., weather, congestion) were compared. Overall (without regard to payload or speed), the tractors with NGSWBTs provided 6 percent better fuel efficiency than the tractors with standard dual tires. When the data were segmented into speed-bins, the tractors with NGSWBTs consistently were more fuel-efficient than the tractors with standard dual tires. The only case in which the standard duals outperformed the NGSWBTs was for very high-speed bins (greater than 65 mph), perhaps due to the test tractor traveling on downgrades. When the data were segmented into low-, medium- and high-payloads, the fuel efficiency margin for the NGSWBTs increased with increasing payload. For the fully loaded 80,000-lb. tractor-trailer, the margin was greater than 10 percent. Because of the large amount of data in the database, these margins were statistically significant. A number of other studies capable of being conducted with the data in the database have been identified and a special study relating to performance at 55 mph and 65 mph will be conducted in FY 2009.

Initiation of Medium-Truck Duty Cycle Data Collection Efforts

As the HTDC efforts concluded, focus was turned toward the collection of class-6 duty cycle data, especially since class-8 trucks are the second largest user of truck fuel. The medium-truck class-6 fleet consists of many vocations, and initial efforts were addressed in identifying the class-6 vocations of interest for the Medium-Truck Duty Cycle (MTDC) data collection effort. Initial efforts to identify class-6 vehicle usage were problematic. Class-6 vehicles are present in rental fleets (i.e., Ryder, Hertz, U-Haul), towing/recovery, farm use, and single truck applications, but for the vocational fleets that ORNL

contacted, all use class-7 vehicles. The scarcity of class-6 vehicles seems to contradict the 2002 Vehicle Inventory and Use Survey. The census data indicated that there were approximately ten times as many class-6 vehicles as class-7 vehicles in 2002. Thus, it was assumed that most delivery trucks, school buses, and utility trucks were class-6 vehicles. However, in seeking out partners from these vocations, ORNL found that most of these industries use very few (if any) class-6 vehicles. In talking to potential partners, ORNL found that “typical” utility vehicles, refrigerated delivery trucks, beverage delivery trucks, and school buses, were all class-7 (and occasionally class-8) vehicles. In fact, ORNL found it difficult to locate any class-6 vehicle fleets, locally, in these vocations. Because in the state of Tennessee a class-6 vehicle may be used for commercial purposes without a CDL, it was suggested that the majority of class-6 vehicles were single trucks run by owner-operators. Based on the conflict in this information and the lack of actual class-6 vehicles, ORNL recommended to DOE that a “vocational approach” to the MTDC effort be taken. By focusing on vocations, duty cycle data of interest can be collected independently of the vehicle class. ORNL received concurrence with this approach at a meeting with our DOE sponsor. A Vocational Assessment Report was completed in late June 2008, and a copy of this report was electronically sent to the DOE sponsor.

Class-6/7 Medium Truck Fleet Partners

ORNL engaged in efforts to identify willing partners for the MTDC effort. A number of vocations were addressed, including bucket trucks, tankers, school busses, wrecker services, beverage delivery trucks, transit busses, and dry-box and refrigerated delivery trucks. Four initial fleets have agreed to partner with ORNL on the MTDC effort. The four vocations are described below.

Dillard-Smith Construction: Dillard-Smith Construction utilizes electrical line utility bucket trucks, typically has approximately eight hours per/day of bucket operation, and engages in very low vehicle miles (typically 50 miles/day). The company operates locally, regionally, and nationally, and is located in New Market, TN.

H.T. Hackney Company: H.T. Hackney is an institutional food and grocery supplier and operates

straight and combination trucks (dry-box and refrigerated). It engages in local and tri-state delivery and is located in Roane County, TN.

Fountain City Wrecker Company: Fountain City Wrecker operates class-7 wrecker trucks and is located in Knoxville, TN.

Knoxville Area Transit: KAT operates several types of transit busses on suburban and urban routes and is located in Knoxville, TN. A KAT bus is shown in Figure 3.

Initial MTDC Efforts

In June 2008, ORNL purchased a Raven X cellular model to test its function and compatibility with the eDAQ DAS to be utilized in the MTDC efforts. The Raven X will be used to download the field operational test data wirelessly and remotely from our partners' vehicles. ORNL subsequently tested wireless data upload capabilities both in the laboratory and in over-the-road situations. Complete control of the data acquisition system via the Internet (including data upload, real-time channel monitoring, and test setup) was demonstrated. The Raven X model is shown in Figure 4.

In August and September 2008, ORNL conducted fuel consumption testing with the H.T. Hackney Company to obtain one month of fuel records for four vehicles. This was done in order to compare the actual gallons of fuel used with the QualComm-reported fuel usage values from the databus. A strong correlation was found between the



Figure 3. Typical Class-7 KAT Transit Bus



Figure 4. Instrumentation of Van for Road Testing of DAS

QualComm-reported fuel used (in gallons) and the actual fuel used based on driver fueling logs. There was, however, not a correlation between the two mpg values. This difference will be further investigated in FY 2009.

Leveraging of Resources

In order to leverage the resources of the HTDC and MTDC efforts, and to broaden their applicability to DOE, researchers, and private industry partnerships with other Federal agencies and private industry were sought.

Environmental Protection Agency: Communication with EPA concerning partnering and for the collection of emissions data for the class-6 and class-7 efforts to be conducted in FY 2009 was initiated in early FY 2008. Discussions included the identification and collection of performance measures to support EPA's SmartWay program. Communication efforts with EPA continued throughout FY 2008 with an enthusiastic response. In March 2008, ORNL provided a phone briefing to EPA staff in Ann Arbor, MI, about the MTDC project and its goal of collecting duty cycle data. Also in March, an ORNL staff member participated in the EPA SmartWay Test Protocol Workshop held in Washington, DC. The two-day meeting stressed the need for class-8 and class-6/7 duty cycle information and associated data (e.g., grade, weather, congestion). Contact was made with Cheryl Bynum (EPA), and a presentation was provided that discussed the data that had been collected on class-8 tractor-trailers and the data to be collected on class-6/7 vocational vehicles. The workshop also stressed test-track and dynamometer testing for SmartWay

certification. ORNL suggested that field operational, real-world testing should be added to the suite of testing protocols. Cheryl Bynum expressed significant interest in the HTDC data. A conference call was conducted with Cheryl Bynum and other representatives of EPA on September 2 to discuss the tentative list of signals to be collected in the MTDC effort. EPA expressed an interest in any temperature and emissions-related signals that might be available on the databus. Efforts to include EPA continued, and although considerable enthusiasm was displayed, no commitments have been made.

Federal Motor Carrier Safety Administration (FMCSA): The FMCSA is concerned with the safety and inspection of class-8 vehicles operating on our nation's highways. Inspections of the class-8 vehicles for safety and appropriate credentialing can take 45 minutes per vehicle, and as a result, less than 10 percent of the U.S. class-8 fleet receives a full Level-1 inspection. In order to increase this percentage, FMCSA has designated a 70-mile stretch of Interstate in east-Tennessee (I-40 at Campbell Station Road to the I-81 Inspection Station in Greene County, TN) as a permanent Commercial Motor Vehicle Roadside Technology Corridor (CMVRTC) managed by ORNL. This corridor is being utilized to test new and emerging commercial motor vehicle safety and inspection technologies. One major FMCSA project in this corridor that is conducted by ORNL is the Wireless Roadside Inspection (WRI) project wherein data regarding the fleet, vehicle, and driver are automatically downloaded to the inspection station as a truck pulls in and linked to various back-office databases maintained by the Federal and state government. Safety and traffic violations, out-of-service periods, licensing, certification, credentialing issues, etc., are provided to the inspector so that a timely and thorough inspection can take place. The manual compilation of such data is very time consuming and offers considerable opportunities to reduce inspection times.

The FMCSA has agreed to allow ORNL to utilize the radios used in the WRI for wirelessly transmitting data and information from each vehicle directly to a server at ORNL. This approach saves considerable labor because the download of data does not require the physical presence of ORNL researchers at each fleet partner each weekend, and allows the data to be available for quality assurance purposes in near real

time. FMCSA is interested in the performance of the wireless radios.

Fleet Partners: Throughout this program, the no-cost contributions of the fleet partners (Dana Corp., Schrader Trucking, H.T. Hackney, KAT, Fountain City Wrecker, and Dillard Smith Construction), have made this effort feasible. Free access to vehicles in their fleets and the time provided to help support this program are significant and critical. Without such support, this program would not have been possible.

Michelin Americas Research and Development Corporation (MARC):

Michelin has been a strong and supportive program partner since the start of this program in 2004. The company provided new free tires (NGSWBTs and standard duals) for the Pilot Test and the class-8 efforts. It has also provided significant input to understand the tire-road interface and in assessing the fuel efficiency benefits of their NGSWBTS. The research experience with MARC has added considerable depth to the program and has facilitated a demonstration of the value of the HTMT database.

Future Directions

This program will provide a valuable asset for making heavy truck energy efficiency technology decisions based on real-world performance data. In particular, it will provide input for developing, calibrating, testing and evaluating ANL's PSAT, and will result in the development of a prototype duty-cycle generation tool capable of generating custom duty cycles for various user-specified long-haul characteristics. Future directions for this work will be to enrich the database with data that provide greater breadth and depth to enhance its applicability to fuel efficiency analyses. This includes collecting and analyzing data on class-6/7 vocational applications, situational circumstances, operational protocols, etc. Such a capability supports the establishment of a national data archive for heavy/medium truck performance data, and would be a valuable national asset for heavy truck energy efficiency research. Inclusion of safety data and information might also be a long-term goal that could receive cross-agency attention and support. Lastly, a future goal is to gain a deeper understanding of heavy truck operations on our nation's highways.

Data for the HTMT database should continue to be added and analyzed. Additional data in the post-MTDC era should be accomplished by piggybacking data collection on other national truck-based programs, including programs by other Federal agencies (e.g., DOT's FMCSA).

Analyses should also become a major thrust of this program. Special studies such as the fuel efficiencies of 55 mph vs. 65 mph, utilizing data from the HTMT database, should be conducted.

The availability of a national data archive of heavy truck performance data could support the establishment of a Center of Excellence in Heavy Truck Performance Research.

Lastly, many COTS technologies make fuel efficiency claims that are unsubstantiated. This program should support the laboratory, test-track, and/or field testing of these technologies. If viable, the testing could support greater adoption of these technologies by the private industry.

III. INTEGRATION AND VALIDATION

A. Battery Hardware-in-the-Loop Testing

Neeraj Shidore (Project Leader)

Argonne National Laboratory
9700 South Cass Avenue

Argonne, IL 60439-4815
(630) 252-7416; nshidore@anl.gov

DOE Technology Manager: Lee Slezak

(202) 586-2335; Lee.Slezak@ee.doe.gov

Objective

Evaluate advanced prototype batteries for plug-in hybrid applications by using the concept of hardware-in-the-loop (HIL)/software-in-the-loop.

Approach

Build a battery test stand in which the battery is connected to a bi-directional power supply that acts as a power source/sink.

Control the bi-directional power supply to source/sink power to/from the battery, so that the instantaneous battery power is equivalent to the instantaneous battery power in a plug-in hybrid vehicle running a drive cycle.

Use Powertrain System Analysis Toolkit-PRO (PSAT-PRO) computer simulation software to emulate a plug-in hybrid vehicle and control the DC power supply, so the battery can be evaluated in a closed-loop, real battery-virtual vehicle scenario (concept of HIL).

Accomplishments

Completed setup of a refined battery HIL test facility (Battery HIL v2).

Completed study: Impact of low battery temperature on PHEV all-electric range and battery performance.

Initiated new study in collaboration with Johnson Controls-Saft (JCS) to investigate the trade-off between PHEV fuel economy and battery capacity/power retention. The vehicle sizing and modeling exercise is complete.

Continued support to the ultracapacitor/battery HIL experiment.

Future Directions

Complete the study of the trade-off between PHEV fuel economy and battery capacity/power retention.

Use of battery HIL as a tool for developing battery management system parameter tuning against real-world drive cycles.

Investigate setting up an industry standard test procedure for battery evaluation in a systems context/battery comparison.

Consider possible studies with an air-cooled battery pack to include:

- Low battery temperature — vehicle energy management for a quick rise in battery temperature; impact of such energy management strategies on vehicle fuel economy.
 - High battery temperature — vehicle energy management to control battery usage to limit rise in battery temperature; investigate impact of such energy management strategies on fuel economy.
-

Introduction

Plug-in hybrid electric vehicles (PHEVs) have been identified as an effective technology to displace petroleum because they draw significant off-board energy from the electrical grid through regular charging. When compared to current production charge-sustaining hybrids, the rechargeable energy storage systems of PHEVs (e.g., batteries) have a much larger energy capacity. This larger energy storage system can be utilized by powering a significant all-electric range (AER) or by selectively powering low-load portions of the driving demand. The battery's response to variations in control choices will have a significant impact on vehicle-level performance. The needs of the battery under these control scenarios are of critical interest to battery developers. As such, emulation, modeling, and hardware-in-the-loop (HIL) testing techniques for a plug-in battery system have been developed to support the acceleration in the development of PHEVs for a mass market.

The most significant technical barrier to commercially viable PHEVs occurs in the energy storage system. The challenge resides in developing batteries that are able to perform the requirements imposed by a PHEV system while achieving market expectations in terms of cost and life. In this context, a vehicle systems approach becomes necessary to investigate the operational requirements specific to PHEV technology. Vehicle-level investigations determine the relationship between component technical targets and vehicle system performance and the potential of the entire system design to displace petroleum use. Battery HIL is an important tool in this vehicle-level investigation of the PHEV battery.

Approach

In Battery HIL, the battery is connected to a DC power source, which is controlled by a real-time simulation model that emulates the rest of the power train, for PHEV operation (Figure 1). The vehicle model is derived from a simulation model developed by using the Powertrain System Analysis Toolkit (PSAT).

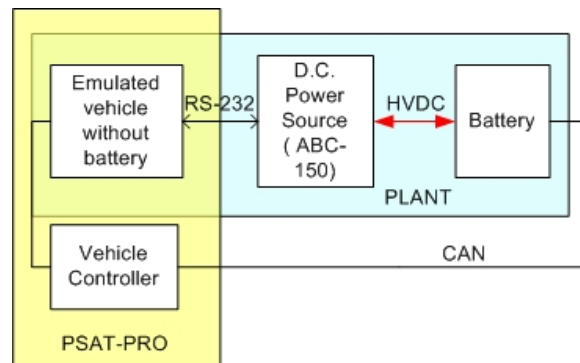


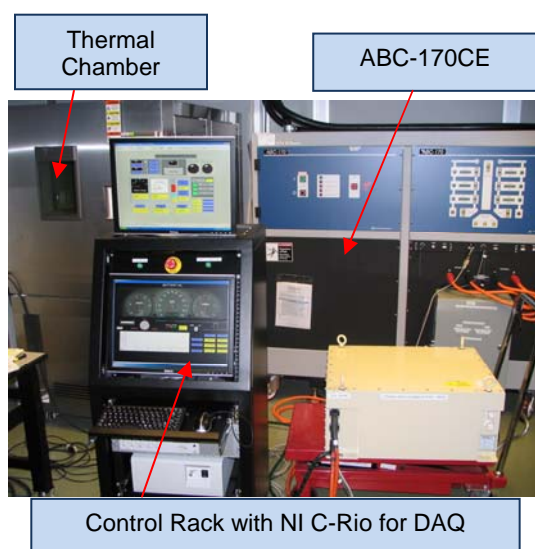
Figure 1. Battery HIL Represented as a Closed-Loop Plant-Controller-Feedback System

Accomplishments

1. Completed setup of a refined Battery HIL test facility (BHIL2).

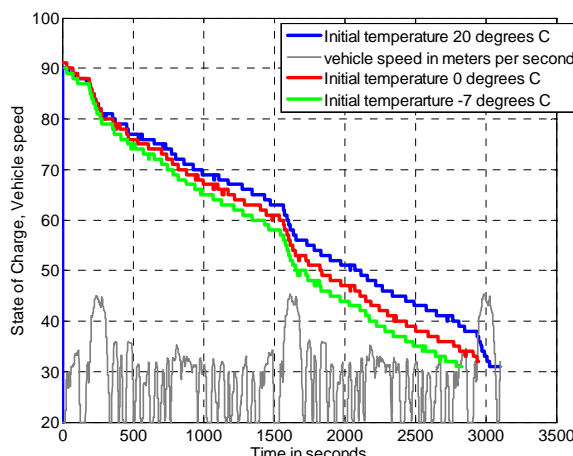
Phase II of the battery HIL test bench was built in FY 2008. Figure 2 shows the new Battery HIL test bench. The following advancements can be seen in BHIL2 as compared to BHIL1:

1. Battery cycler has better response time and more power capability: The ABC-170CE has an extra 20 kW of regen power as compared to the ABC-150. Response time is much improved with the latest power electronics in use in the DC and AC side of the ABC-170. This results in higher accuracy in the actual battery current and lower lag time.
2. Communication between the ABC-170CE and the virtual vehicle in dSpace is via high-speed CAN. Use of CAN in BHIL2 results in higher accuracy and lowers the communication lag between the virtual vehicle model and the ABC-170CE.
3. An ESPEC environmental chamber enables researchers to perform experiments involving extreme battery temperature. This is important because battery performance at extreme temperature is a critical issue facing PHEV batteries.

**Figure 2. Battery HIL2 Test Facility**

2. Completed investigation: Impact of cold battery temperature on vehicle AER (UDDS) and battery performance.

Cold temperature performance is a critical issue facing Li-ion PHEV batteries. This investigation studies the impact of cold initial battery temperature on the AER of a vehicle for three different initial temperatures: -7, 0, and 20°C (Figure 3). The battery was cooled down to the initial temperatures through the coolant loop. The parameters for the virtual vehicle used in the experiment are listed in Table 1.

**Figure 3. Drop in State of Charge for the Three Initial Temperatures over Consecutive Urban Cycles.****Table 1. Specifications of the virtual vehicle**

Vehicle Configuration, Vehicle Class	Pre-transmission parallel, SUV
Vehicle Mass	2049 kg
Vehicle Battery	JCS SAFT -VL41M
Transmission	Five speed manual
Vehicle Coefficient of Drag, Frontal Area	0.41, 2.88 m ²

As expected, a lower initial temperature is related to a lower AER of the vehicle (Table 2). Higher internal resistances at low temperature resulted in an increase in the heat generated — hence, the lower the initial temperature, the higher the rise in temperature (Table 3). It should also be noted that no coolant was circulated through the system when performing the test at -7 and 0°C, to enable the battery to heat up as fast as possible.

Table 2. Decrease in AER with decrease in temperature

Initial Battery Temperature (°C)	AER from 90% to 30% SOC on the UDDS	% drop in AER
20	17.4 miles	0
0	15.7	9%
-7	15.0	13%

Table 3. Decrease in kWh delivered by the battery with decrease in initial temperature

Initial Temperature (°C)	Battery kWh	ΔkWh
20	6.2	0
0	5.6	0.6
-7	5.5	0.1

This decrease in battery kWh at low temperature could be attributed to three reasons:

1. Battery power restrictions at low temperature.
2. Increase in internal resistance.
3. Other losses that could not be accounted for/explicitly measured were lumped together under the term “other losses.”

Table 4 shows the contribution of each of the above-mentioned losses to decrease in battery kWh delivered to the vehicle.

Table 4. Contribution of each loss to the total reduction in Battery kWh to the vehicle

Temperature (°C)	ΔWh compared to Wh delivered at 20°C	$\Delta Regen$ as % of ΔWh	$\Delta I^2 R_t$ as % of ΔWh	$\Delta Other$ losses as % of ΔWh
0	530	34	8	58
-7	730	34	12	54

The test at 0°C was repeated for more aggressive driving (i.e., UDDSX1.2) to study the impact of aggressive driving on the battery rise in temperature. Table 5 shows the comparison between the UDDS 1.2 and UDDS for an initial temperature of 0°C.

Table 5. Contribution of each loss to the total reduction in Battery kWh to the vehicle – difference between UDDSX1 and UDDSX1.2

Cycle	ΔWh compared to Wh delivered at 20°C	% of $\Delta Regen$ ΔWh	$\Delta I^2 R_t$ as % of ΔWh	$\Delta Other Loss$ as % of ΔWh
UDDS	530	34	8	58
UDDSX1.2	600	20.3	22	57.7

The following observations can be made from a review of Table 5:

1. The contribution of to the reduction in battery Wh transferred to the vehicle is much lower with aggressive driving. This can be attributed to a faster rise in battery temperature in the case of UDDS X1.2 (again, no cooling), which removes the temperature-related restrictions on battery charge/discharge power.
2. With an increase in the aggressiveness of the cycle, there is an increase in the $\Delta I^2 R_t$ losses of the battery.
3. The “other losses” from the battery, which cannot be quantified by this experiment, remain roughly the same, as a percentage of the total losses. This may be because the faster rise in battery temperature negates any increase in percent of contribution of these losses.

3. New study in progress: Sensitivity of trade-off between vehicle fuel efficiency and battery cycle life to different vehicle system parameters.

Battery cycle life depends on battery utilization in a vehicle; in other words, it depends on the following factors:

1. Energy management
2. Driving pattern
3. Overnight charging algorithm
4. Temperature
5. Vehicle configuration/class

The first phase of the study considers the sensitivity of the trade-off between vehicle fuel efficiency and battery cycle life to just one system level variable: energy management.

A virtual vehicle will be subjected to different energy management strategies, and the trade-off between fuel economy and estimated battery life will be determined. The battery utilization data will be sent to SAFT for battery life estimation. This study is based on the following:

1. Vehicle sizing will be determined on the basis of performance requirements.
2. Representative vehicle drive cycles will be selected.
3. A pre-prototype level energy management strategy will be incorporated.
4. Actual testing will yield data on battery utilization for different energy management strategies.
5. SAFT will estimate battery capacity fade and battery power fade for those different energy management strategies (capacity, power fade as a function of number of deep discharge cycles).
6. Fuel economy will be calculated at the different battery capacities (over the number of deep discharge cycles), and trade-off between battery capacity and fuel economy for different energy management strategies will be determined (Figure 4).

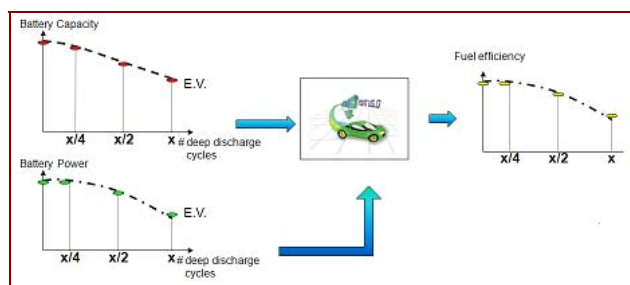


Figure 4. Calculation of fuel efficiency based on battery capacity and power fade data provided by SAFT.

The virtual vehicle for the experiment has been sized on the basis of the following requirements:

1. Acceleration: 0 to 60 mph in 9.3 seconds.
2. Six percent grade at 65 mph.
3. UDDS in EV only.
4. EV range of 20 miles on the UDDS.
5. Configuration: Power split.

The sizing results for the vehicle based on the above goals are listed in Table 6.

Table 6. Sizing Results for Virtual Vehicle

Engine Power (kW)	90
Motor Power (kW)	82
Generator Power (kW)	65
Battery Power (A•h) and Capacity (kW)	41 and 60
Vehicle Mass (kg)	1920

Conclusion

Version 2 of the BHIL test bench has been installed and made operational in FY 2008. Both of the BHIL test benches will now be used for battery HIL and ultracapacitor/battery HIL projects. A WFO project was conducted for a battery company for about five month in FY 2008.

The impact of cold battery temperature on battery performance and vehicle AER revealed that the decrease in vehicle AER is primarily due to the decrease in inherent battery capacity. A new experiment that studies the impact of different vehicle system factors on battery capacity/power fade and in-turn on vehicle fuel economy is being conducted with active collaboration from SAFT.

Papers/Presentations

Neeraj Shidore and Ted Bohn, "Evaluation of Cold Temperature Performance of the JCS-VL41M PHEV Battery Using Battery HIL," presented at the SAE 2008 World Congress conference at Detroit, MI, USA, April 2008.

Neeraj Shidore et al., "Quantifying PHEV All Electric Range and Fuel Economy in Charge Sustaining Mode for Low SOC Operation," poster at the EVS-23 Conference, California, USA, Dec. 2008.

Aymeric Rousseau, Neeraj Shidore, and Richard "Barney" Carlson, "Impact of Battery Characteristics on PHEV Fuel Economy," presented at the Advanced Automotive Batteries Conference (AABC), Orlando, FL, July 2008.

Aymeric Rousseau et al., "PHEV Battery Requirement - Uncertainty Based on Real World Drive Cycles and Impact on Fuel Efficiency," presented at the First Li-ion Battery Conference, Argonne, IL, September 2008.

Neeraj Shidore and Henning Lohse-Busch, "Power Train Component and Subsystem Evaluation at Argonne National Laboratory," invited presentation at the dSpace user's conference, Livonia, MI, USA, September 2008.

B. MATT (Modular Automotive Technology Testbed)/Component Hardware-in-the-Loop Testing

Henning Lohse-Busch

Argonne National Laboratory
9700 South Cass Avenue
Argonne, IL 60439-4815
(630) 252-9615; HLB@anl.gov

DOE Technology Manager: Lee Slezak

(202) 586-2335; Lee.Slezak@ee.doe.gov

Objectives

Evaluate powertrain components in a hybrid vehicle environment.

Use Modular Automotive Technology Testbed (MATT) as a tool to investigate special studies to support the plug-in hybrid electric vehicle (PHEV) test procedure development.

Evaluate the impact on fuel economy and emissions on control strategies in PHEVs

Approach

In the past year, MATT was built as a flexible powertrain evaluation tool; this year, it finally reached maturity and a certain reliability level.

The approach is to use MATT as a tool to evaluate physical components and their impact of the system, evaluate energy management strategies and their impact on fuel economy and emissions, and use the open controller to run different hybrid strategies for specific tests.

Accomplishments

Operated MATT with a high degree of reliability.

Implemented a new automatic transmission, which solved the shift problems encountered with the manual transmission.

Completed the conventional vehicle baseline assessment, including fuel economy and emissions results and detailed analysis.

Developed a hybrid strategy in Powertrain System Analysis Toolkit (PSAT), which was run on MATT. Iterations between simulation and hardware were made to assess the impact of the strategy on emissions and fuel economy for PHEVs. The baseline tests and their analysis have been completed.

Performed a number of studies to support the SAE J1711 hybrid vehicle standard test procedure development, such as:

- The highway cold start correction method for PHEVs and
- Impact of soak time sensitivity between tests for PHEVs.

Generated data from MATT for a few other programs, such as drive cycle sensitivity investigation for PHEVs.

Future Directions

Finish determining the impact of control strategies on fuel economy and complete emission study.

Evaluate further powertrain components.

Support other DOE programs by generating data to answer specific hardware questions.

Concept and Hardware Modules

The concept of the modular powertrain component testbed is addressed, as well as the existing modules that serve the current hybrid configuration.

The Concept of the Modular Automotive Technology Test Bed

The Automotive Component “Bread Board” Test Bench

A modular component powertrain testbed is an alternative solution for testing different technologies in a hybrid vehicle environment while keeping the cost and required resources relatively low. At the center of this report is the Modular Automotive Technology Testbed (MATT). This testbed consists of physical hardware component modules, including an internal combustion engine and a transmission, as well as emulated component modules (such as an energy storage system). Figure 1 shows the modular concept of MATT.

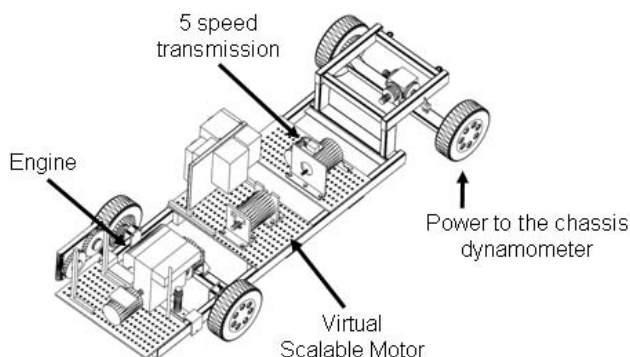


Figure 1. Illustration of the Modular Automotive Technology Testbed

MATT can be compared to an automotive “erector set.” The base is a frame with wheels. Different component modules are bolted to the frame and connected with shafts to construct the hybrid powertrain. The modules are built on a 0.75-inch-thick steel plate with a bolt-hole pattern for mounting. Each module consists of the main component, as well as all the support systems required for its operation. For example, the engine powertrain module has an engine with its ECU (engine control unit), wiring, cooling system, clutch actuation system, and extensive instrumentation.

These modules can be “real” physical components, such as an engine, or they can emulate some hardware, such as a battery pack and electric motor combination. The real components capture those effects that simulation may not represent easily, such as variable losses in components based on temperatures and/or emissions from the engine. The emulated components are defined by models running in a real-time simulation based on physical inputs from sensors. These emulated components then use physical hardware to add or subtract torque from the driveline on the basis of the real-time simulation and the energy management strategy. For example, a single electric motor is used to emulate a multitude of energy storage systems of different capacities and an electric traction motor model.

The components and subsystems on the modules are easy to instrument since all parts are open and are not constrained by packaging constraints or sheet metal. The instrumentation is specific to the module and can be put in place before implementing the new module on MATT. The minimum instrumentation includes a means to measure torque, and speed sensors are installed between each component so that the torque speed performance and the losses of each module can be assessed on transient drive cycles. MATT is tested on a chassis dynamometer with emissions equipment at Argonne National Laboratory’s (ANL) Advanced Powertrain Research Facility (APRF).

The high-level controller that interfaces with all of the modules, including their subsystems, commands the components according to an energy management strategy. The controller has the three functions:

- *Lower level component control.* The purpose of the lower level component control is to interface with the actuators of the different modules to assure their proper operation. An example of lower-level component control is the dry clutch actuator to enable the launch in a conventional vehicle.
- *Energy management and torque split strategy.* The energy management strategy can also be referred to as the hybrid control strategy. This part of the controller decides how to split the torque request from the driver between the engine and hybrid system.
- *Component emulation.* In some modules, the controller also computes a real-time simulation

by using modes for energy storage systems and electric machines. These simulations use sensor inputs and generate outputs that are added to the driveline by using physical hardware.

MATT has been used to test vehicles of different sizes through the use of a modern chassis dynamometer. Specific vehicle characteristics (such as test weight and losses) enable chassis dynamometers to apply appropriate forces at the wheels, as shown in Equation 1. The vehicle is tested by using coast-down techniques on a level test track to derive the vehicle loss coefficients. On the dynamometer, the coast-down test is repeated, and the dynamometer controller adjusts to accurately represent the vehicle as tested on the track.

$$F_{dynamometer} = m \times \frac{\partial(V)}{\partial t} + (A + B \times V + C \times V^2)$$

where m is the vehicle test mass; A , B , and C are the vehicle loss coefficient, and V is the vehicle speed.

Equation 1

In summary, the modular approach makes it possible to test different technologies and combinations without having to rebuild the entire vehicle. The physical elements provide an additional advantage in that they can be incorporated to test emissions and thermal effects, the testing of which is limited in computer simulations. All of the components can be instrumented to a high level since the modules are open on the testbed and the packaging is not limited by a vehicle body shell. The high-level controller is open and can be programmed to any hybrid energy management strategy. On the dynamometer, MATT can be tested as vehicles of different sizes enable another degree of freedom.

Purpose and Goals of MATT

MATT is a flexible and unique automotive powertrain tool that enables:

- The study of physical components in a hybrid vehicle system environment on transient drive cycles.
- The validation of some simulation work or provision of supplemental information (emissions and losses).

- The evaluation of torque split and energy management, including emissions and thermal-related losses of components.
- The generation of hardware based data for a wide range of very specific studies.

MATT has proven useful in terms of providing plug-in hybrid test data to the SAE J1711 Hybrid test procedure committee, among others.

Pre-Transmission Parallel Hybrid Architecture

The current configuration of MATT is a pre-transmission parallel hybrid electric vehicle. The current setup consists of a conventional gasoline-powered 2.3-L gasoline engine, an emulated electric propulsion system, and a five-speed automatic transmission. Figure 2 shows a picture of MATT's current configuration.

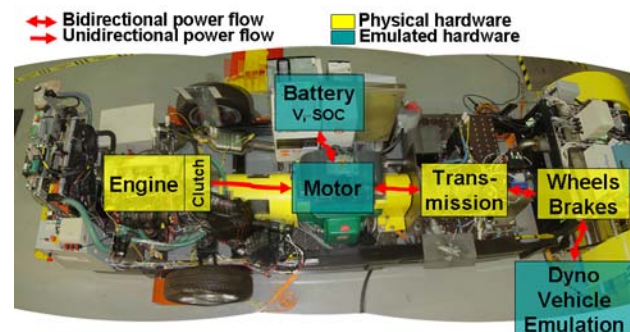


Figure 2. Top view of MATT with component schematic overlay

The engine has a conventional dry clutch and thus can be disengaged from the rest of the driveline. The physical electric motor is only used to provide torque based on the real-time simulation of an energy storage and traction motor model. The automatic transmission has been modified to transfer reverse torque for regenerative braking and to allow electric launch with the motor only. All of these components put together enable different vehicle operating modes.

MATT operating modes are:

- *The conventional vehicle.* MATT operates as a conventional gasoline vehicle by using the engine, the conventional clutch, and the transmission and by bypassing the motor. The conventional vehicle set the baseline for fuel

economy and emission data to enable comparisons with hybrid operation.

- *The electric vehicle.* By disengaging the engine with the clutch, MATT does operate as a pure electric vehicle. Using the emulation hardware's small and large motors (as well as different battery technologies), capacities and power levels can be emulated. MATT can emulate an electric vehicle with a small to infinite range.
- *The hybrid electric vehicle.* By using the virtual scalable motor emulation, different types of hybrids can be emulated from a mild assist hybrid with engine start-stop to a full EV-capable hybrid. A plug-in hybrid mode is also possible since MATT can easily emulate the large battery pack required.

The following sections describe the different powertrain modules that compose MATT.

The Hardware Modules

The Gasoline Engine Module

The engine module consists of a gasoline engine, the ECU, an exhaust after treatment, a coolant system, a clutch actuator, a 12-V starter, and instrumentation. The engine module layout is presented in Figure 3. Table 1 shows the engine specification. The engine size is used in small sedans or small crossover SUVs.

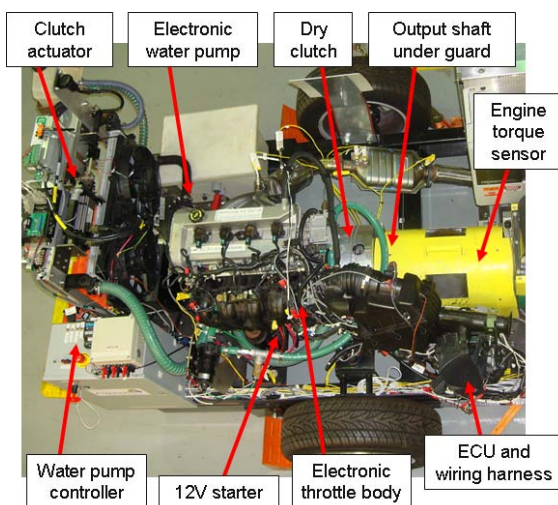


Figure 3. Top View of the Gasoline Engine Module

Table 1. Engine specifications

Displacement	2.3 L
Engine Type	Inline 4-cylinder 16-valve DOHC (no variable valve timing)
Family	DURATEC
Fuel	Gasoline (certification fuel)
Calibration	Stock calibration
Throttle Control	Electronic throttle control
Exhaust	Two stock catalysts
Max Torque	180 Nm @ 4000 rpm
Max Power	100 kW @ 5000 rpm

The engine is a production engine with its stock ECU. The electronics throttle is controlled by the ECU on the basis of the position of the accelerator pedal and engine feedback. MATT's high-level controller commands engine torque by sending the pedal position signal to the ECU. The engine uses a standard automotive 12-V starter for cranking. That starter is wired to be computer controlled. The crank time is limited in software to prevent hardware damage. The controller switches the ignition to the ECU for engine start and stop. In hybrid mode, the engine can also be bump-started by engaging the clutch while the electric motor is already spinning.

The coolant system is set up to work with different engines with and without an internal water pump. On the coolant system, a variable flow pump pushed the water glycol mixture through the system. The pump controller uses a temperature probe to vary the flow to achieve a target temperature. During a cold start, when the engine needs to warm up fast, the flow is slowly pulsed, while the pump will operate at a high flow if the engine is already hot and under high flow to reject more heat. To ensure that the temperature probe for the controller measures an appropriate temperature, an auxiliary pump flows coolant just through the engine block. This is important during cold start; otherwise, the coolant flow may be so slow that the probe might only register the hot coolant after the coolant in the block overheats. In the test cell, a vehicle wind simulator fan provides airflow across the radiator. In case more heat rejection is required, there are two automotive pull fans on the radiator that are triggered by a thermal switch at the radiator inlet. Figure 4 illustrates the setup of the coolant system. The gasoline engine used on MATT does not have an internal belted water pump. The

target temperature of the variable flow coolant pump is set to 90°C. The fans are set to turn on at 95°C.

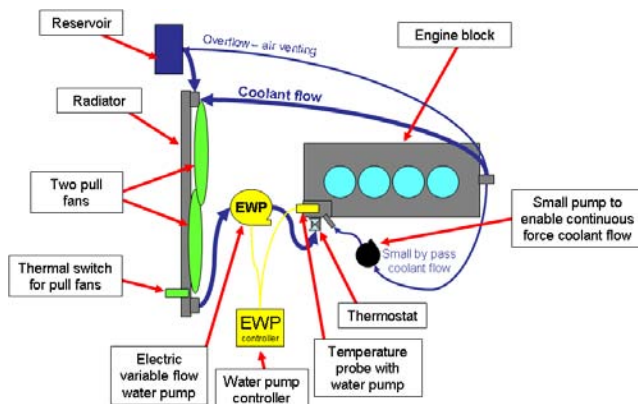


Figure 4. Schematic of Coolant System for the Engine

The engine exhaust system is built with all of the components used in a production vehicle. From the exhaust headers, the gases run through two catalytic converters, then through the exhaust pipe under the vehicle, and finally through a silencer and muffler before coming out at the end of the testbed. The catalytic converters are instrumented with thermocouples and a wide-band oxygen sensor. The exhaust setup is presented in Figure 5.

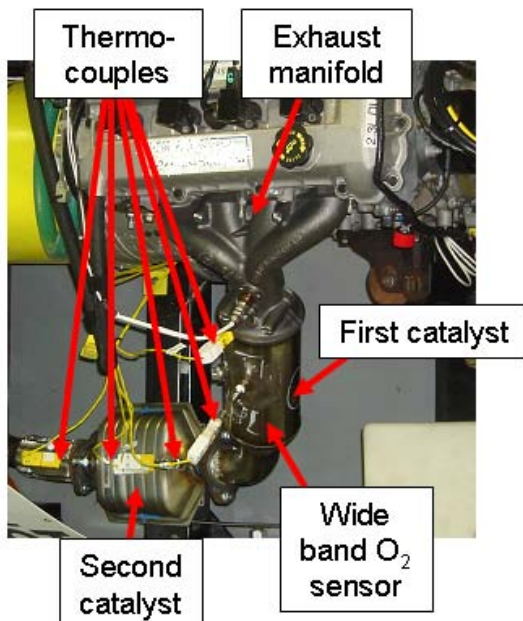


Figure 5. The Engine Exhaust Setup and Instrumentation

During the tests, the exhaust gases are collected and analyzed in a Pierburg AMA 4000 5 gas analyzer.

During the test, diluted exhaust gases are sampled to fill the exhaust sample bags. At the end of the test, the bags are analyzed to provide the total emissions and the carbon balance fuel economy. The exhaust gases are also continuously analyzed during a test, thereby providing modal information that provides insight into the transient engine emissions behavior. This becomes increasingly important for hybrid operation and, especially, plug-in hybrid operation in which the engine starts several times in cycles and may not reach operating temperature rapidly.

The fuel is provided by a stock vehicle fuel pump to ensure proper delivery pressure. A positive-displacement fuel scale measures the volume of gasoline delivered to the engine. The instantaneous fuel flow complements the modal information from the calculated fuel flow by the bench. The flow measured captures transients and dynamics of the fuel flow more accurately. Along with the engine torque and speed sensor mounted on the output shaft of the engine, the quasi-instantaneous engine efficiency can be measured. Figure 6 shows an example of calculated instantaneous brake thermal engine efficiency.

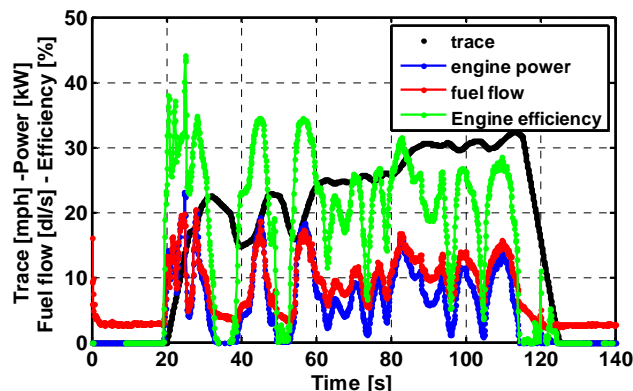


Figure 6. Engine Data from the First Mod of the UDDS in Conventional Vehicle Operation

The data in Figure 6 are from MATT running an urban daily driving schedule (UDDS) as a conventional vehicle with the launch by using the dry clutch and shifting with the five-speed automatic. During gear shifts, the inertia of spinning elements becomes significant and causes torque spikes that are reflected in the calculated engine power data, thus creating short spikes of calculated brake thermal efficiencies higher than 35 percent, which is not engine efficiency.

Additional instrumentation includes an in-cylinder pressure sensor installed in cylinders 1 and 3. The crank speed position is resolved with an encoder. A high-speed data acquisition system records the pressure traces for individual combustion cycles in both cylinders. With this system, indicated mean effective pressure, also known as indicated torque, is calculated. With these data, the mechanical engine losses are inferred. Engine catalyst warm-up behavior is also observed by using the pressure traces.

Table 2 summarizes the instrumentation on the engine module.

Table 2. Summary of engine module instrumentation

	Element Measured	Sensor
Power Input	<ul style="list-style-type: none"> ▪ Fuel flow ▪ Fuel use from carbon balance 	<ul style="list-style-type: none"> ▪ Positive-displacement fuel scale ▪ Emissions bench
Power Output	<ul style="list-style-type: none"> ▪ Engine brake torque and output speed 	<ul style="list-style-type: none"> ▪ High-accuracy torque and speed sensor
Module Specific	<ul style="list-style-type: none"> ▪ Indicated mean effective pressure 	<ul style="list-style-type: none"> ▪ In-cylinder pressure sensor with indicating system
	<ul style="list-style-type: none"> ▪ Engine emissions 	<ul style="list-style-type: none"> ▪ Emissions bench
	<ul style="list-style-type: none"> ▪ Other elements to understand operation 	<ul style="list-style-type: none"> ▪ Thermocouples, pressure sensors, wideband O₂ sensor, flow sensor. ECU-provided data, among others

Another major subsystem on the engine module is the clutch-actuation mechanism. The engine is equipped with a standard automotive dry clutch. That clutch serves two functions. It is the launch device for the vehicle in conventional operating mode, and it disconnects the engine from the rest of the driveline during shifting or in hybrid operation. The first function requires the clutch actuator to perform a position control problem, which involves finding the clutch engagement point and then slowly engaging the clutch to transfer engine torque to launch the vehicle forward. The second function requires the actuator to perform a fast disengagement and reengagement of the clutch so that the shift time is as short as possible. The actuator pushes directly on the master cylinder, thus eliminating the mechanical advantage of the clutch pedal. Thus, the actuator needs to be a position-control device that can push

400 pounds of force over 1 inch in less than a half second. The third and final iteration of the clutch actuator, which fulfills the above requirements, is shown in Figure 7.

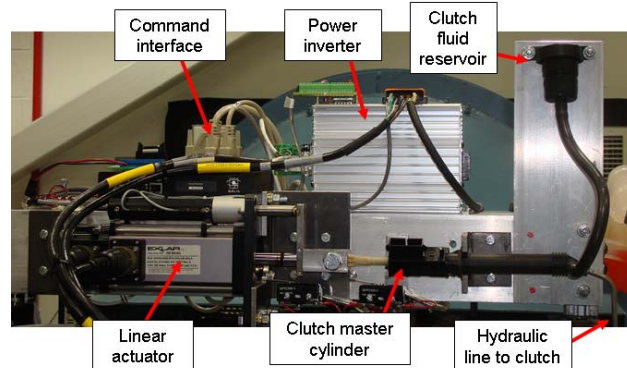


Figure 7. Position control actuator system for the hydraulic clutch

The Virtual Scalable Energy Storage System and Motor Module

A key feature of MATT is the virtual scalable inertia motor module. A physical motor on the module provides positive or negative torque to the driveline as it would in a hybrid powertrain. But the physical motor drives obtain their power from the power grid in the test facility instead of from a battery pack, which is the power source in most hybrids. The motor is an AC induction machine selected for its fast transient response. The motor was modified to be double-ended so that the engine is coupled to the input of the shaft and the transmission is directly coupled to the output. Figure 8 shows a picture of the physical hardware of the motor module.

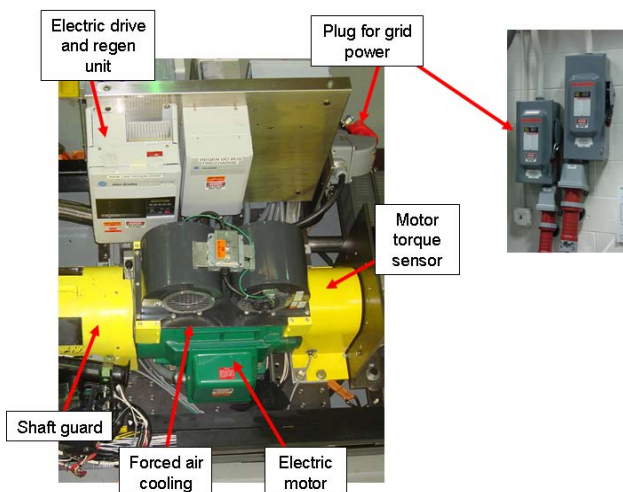


Figure 8. Top view of virtual scalable motor module

The virtual energy storage system and the virtual motor are defined in a real-time simulation in the hybrid vehicle controller. The principles of component hardware-in-the-loop are used here. The hardware interacts in parallel with a real-time simulation of component models. Figure 9 illustrates this interaction. When the energy management system requests a given torque from the motor, the controller first verifies that the virtual motor and the virtual battery pack can provide the requested current and the torque. The controller then sends the torque command or the maximum available torque command to the physical motor. Next, the virtual current is derived from the commanded torque on the basis of the motor model. That current is applied to the virtual battery pack model, where the controller tracks voltage and state-of-charge.

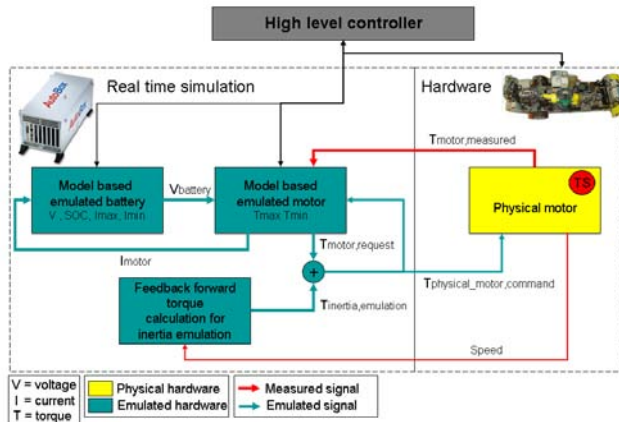


Figure 9. Component hardware-in-the-loop logic for the virtual scalable motor module

Note: Only the electric traction load is shown, and the ancillary loads are omitted for simplicity sake

Another aspect to the virtual scalable motor module is the motor inertia emulation mode. The controller measures motor speed and speed change to calculate the torque required to cancel the physical motor's inertia, as well as the resistive torque that inertia of the virtual motor would add to the driveline. The inertia emulation brings the virtual scalable motor module a step closer to reality. During extremely fast transients, such as gearshifts, the inertia torques—both physical and emulated—are too high for the physical motor to always accurately execute the emulation.

The limitation of the virtual scalable energy storage system and motor module rests with the capability of the physical motor. The physical motor is an AC

induction limited to a maximum torque of 200 Nm and a base speed of 2880 rpm. The maximum electric power from the test facility is 48 kW. To return power to the grid, a regenerative unit is used, which is limited to 36 kW. By using these constraints, the operating regions of the physical motor are defined in Figure 10. Motor torque-speed data points from an actual test of MATT emulating a full electric vehicle version of a 3750-lb small crossover SUV with a single gear on a UDDS are also shown in the graph.

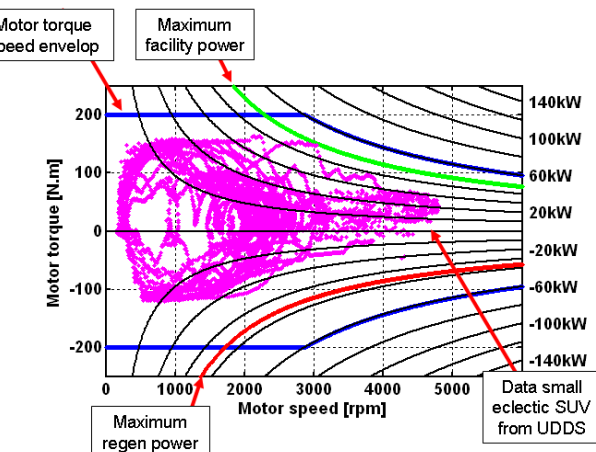


Figure 10. Limits of the physical motor overlaid with the motor torque speed requirements for a small SUV on a UDDS

The current hardware is sized to emulate an electric vehicle like a small SUV on the UDDS. The propulsion system cannot quite supply enough power for the US06, which is the most aggressive cycle in the standard selection. Although the motor is not rated for a continuous 60 kW, the propulsion system is adequate since the drive cycles are transient in nature. In other words higher power demands only occur during high-speed accelerations. For the example given in Figure 10, the peak power is close to 50 kW, which occurred during the high-speed acceleration of the 2nd mod on the UDDS, but the average positive propulsion power on the cycles is 10 kW of the small SUV, which is well within the continuous rating of the physical electric machine.

The virtual scalable energy storage system and motor module can actually emulate a motor that is larger than the physical as long as the torque speed profile is within the operating envelope of the physical machine. That torque speed envelope is determined mainly by the vehicle characteristics and the drive cycle.

An essential element of the emulation is based on the simulation and the fidelity of the component models. The real-time simulation occurs in the controller that manages the higher-level energy management and torque split strategy, as well as the lower-level component control. The code is based on PSAT, which is a forward-looking vehicle simulation tool. The electric motor is based on a UQM 75 motor, and the energy storage system model emulates a 41-A•h lithium ion battery pack intended for plug-in hybrid applications. Both models are been validated against physical hardware. The models include efficiency maps and the constraints that limit the component operation to the limits of the physical hardware. The whole electric vehicle emulation has been correlated to hardware in ANL's APRF.

The key feature of this virtual inertia scalable motor module is the flexibility to emulate different battery technologies and electric motors. The energy storage system can be changed to different technologies and capacities in software without having to change any hardware. The motor emulation ranges from no motor or a small hybrid-assist motor to a full EV-capable electric machine. This module is extremely useful for PHEV studies.

Some other benefits beyond the flexibility are as follows:

- *Instant recharge.* The virtual battery system is recharged from any SOC at the click of a button. For most plug-in hybrid vehicles, the charge time ranges from a few hours to a full night, depending on the battery capacity and the charger used. This considerably shortens the time in the test cell between tests.
- *Start SOC repeatability.* The charging is not only instantaneous but repeatable. The battery can be charged to the exact same SOC for several tests in a row. This is practical for studies where minimum variability from test to test is crucial (see discussion on soak time application).
- *Lack of degradation.* The virtual battery does not experience degradation over time, or, in other words, it cannot be damaged, even if extremely deep discharge cycles are put on the battery.

The instrumentation on this electric propulsion module consists of an input torque speed sensor shared with the engine and an output torque speed

sensor. The rest of the power and energy flow information is collected from the real-time simulation. Table 3 summarizes the instrumentation on the virtual scalable energy storage system and motor module.

Table 3. Summary of motor module instrumentation

	Element Measured	Sensor
Power Input	▪ Input torque	▪ High-accuracy torque and speed sensor
Power Output	▪ Output torque ▪ Output speed	▪ High-accuracy torque and speed sensor
Module Specific	▪ Battery	<ul style="list-style-type: none"> ▪ Voltage ▪ Current ▪ SOC ▪ Maximum discharge current ▪ Maximum charged current
	▪ Motor	<ul style="list-style-type: none"> ▪ Torque command ▪ Maximum propulsion torque ▪ Maximum regenerative braking torque

The Manual Transmission Module

The first transmission module is a manual transmission module. It is a five-speed manual transmission that was modified to be shifted by computer. Because of the mechanical integration complexity, a clutch is not used in this transmission. The electric motor is therefore directly coupled to the transmission input shaft. The transmission is transverse but used in a longitudinal application; thus, the differential is welded up, and only one output is used connect to the rear end. The rear end is a high-efficiency bevel gear box with a one-to-one ratio. Automotive half shafts connect the bevel gear box to the wheel hubs and wheels. A 5000-Nm torque speed sensor is installed between the transmission output and the bevel gear box input. The hardware is shown in Figure 11 and defined in Table 4.

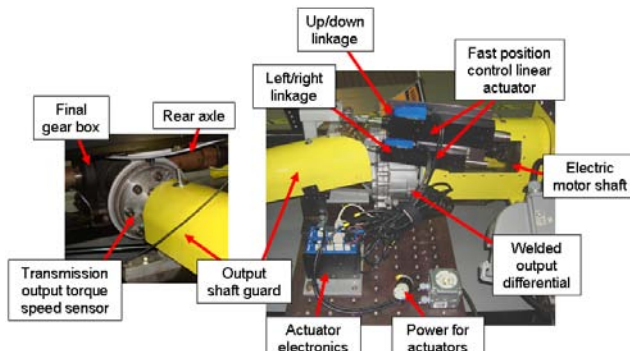


Figure 11. Manual Transmission Hardware

Table 4. Manual transmission characteristics

Transmission Type	5-speed manual	
Family	Ford MTX	
Architecture	Transverse	
Automation	Computer shifted via linear actuators acting on the shift linkage (version 2)	
Mechanical Modification	Welded internal differential and single output used	
Gear #	Ratio	Vehicle Speed at 1000 rpm
1 st	13.11	5.2 mph
2 nd	8.21	8.1 mph
3 rd	5.56	12.1 mph
4 th	3.95	17.3 mph
5 th	2.95	23.5 mph
Final Drive Ratio	1	

The lack of clutch at the input of the transmission requires using the motor during shifting. When the shift is requested in the conventional vehicle mode, the clutch needs to be disengaged. To shorten the torque hole, the throttle command is zeroed once the clutch is partially disengaged. As soon as there is no torque transfer across the transmission, the transmission is forced to neutral, and then the electric motor is used to spin the transmission input shaft to the speed required by the next gear. Once speed match is detected, the linkage is forced to engage the next gear, and then the clutch is reengaged. Once the clutch reaches a certain engagement point, the throttle is reapplied. The process is summarized in Figure 12.

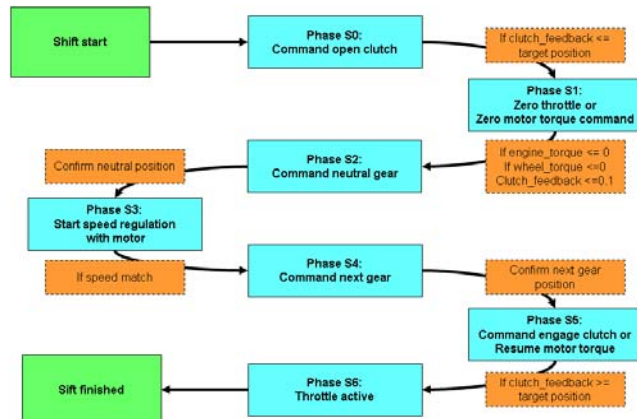


Figure 12. Manual Transmission Lower-Level Shifting Algorithm

The process is simplified in electric operation because the throttle or clutch steps do not apply. The speed match is performed using a PID control loop that is calibrated for each gear number. The shift time is the limitation with the manual transmission module due to the time required to accomplish the shift steps. The longest shift is the 1 to 2 shift since the input speed is the largest to match all of the gears. The initial shift time of about 2 seconds created a shift torque hole that was so long that the vehicle would not meet the trace within the required boundaries. After optimizing the process and the calibration, the shift time was reduced to 1.4 seconds in conventional operation. In hybrid or electric operation, the vehicle is launched in 2nd gear, which eliminates the 1 to 2 shift.

The instrumentation on the manual transmission module of an input torque speed sensor is shared with the electric motor and an output torque speed sensor. Further instrumentation includes a thermocouple in the transmission oil pan and one in the transmission case. Table 5 summarizes the instrumentation on the manual transmission module.

Table 5. Summary of motor module instrumentation

	Element measured	Sensor
Power input	<ul style="list-style-type: none"> ▪ Input torque ▪ Input speed 	<ul style="list-style-type: none"> ▪ High-accuracy torque and speed sensor
Power output	<ul style="list-style-type: none"> ▪ Output torque ▪ Output speed 	<ul style="list-style-type: none"> ▪ High-accuracy torque and speed sensor
Module specific	<ul style="list-style-type: none"> ▪ Oil temperature ▪ Case temperature 	<ul style="list-style-type: none"> ▪ Thermocouples

The manual transmission module was intended as a starter transmission module because it offered the easiest implementation and could debug the other hardware. After the initial manual transmission module was finished, an automatic transmission module was started. The manual transmission module is upgraded with a dry clutch at the transmission input to overcome the shortcoming in shift time.

The automatic transmission module

This module uses a 5-speed automatic transmission. For the electric vehicle and hybrid application on MATT, the automatic transmission is modified to accommodate two additional functions:

- *Electric vehicle launch.* An automatic launches the vehicle by using the torque converter with the engine idling. In the electric launch mode, it would be very inefficient to run the motor at 1000 rpm and launch the vehicle by using the torque converter. The converter was thus removed. An auxiliary pump now provides the pressure required to close the clutches required to hold the gear until the input shaft spins, and so the internal pump spins fast enough to provide the transmission line pressure.
- *Reverse torque transmission during regenerative braking.* To allow reverse torque transfer all the way to zero, some modifications to vehicle speed were implemented to enable regenerative braking in 3rd, 4th, and 5th gear.

With a longitudinal transmission, the differential with the final drive is located in the rear end. On MATT, a solid rear axle belongs with the automatic transmission module. A 5000-Nm torque speed sensor is installed between the transmission output and differential input. Figure 13 shows the hardware implementation of the automatic transmission module. The transmission specifications are detailed in Table 6.

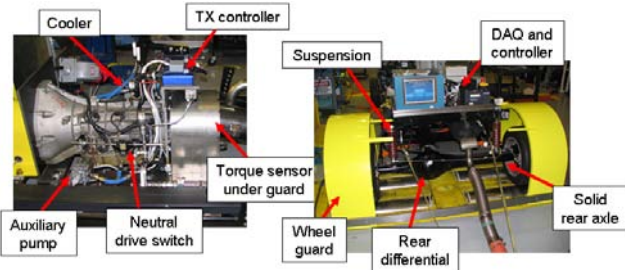


Figure 13. Automatic Transmission Module and Rear End Hardware

Table 6. Manual transmission characteristics

Transmission type	5-speed automatic	
Family	Ford 5R55	
Architecture	Longitudinal	
Automation	Aftermarket controller with calibration tables	
Mechanical Modification	No torque converter for EV launch Auxiliary pump to pressurize the fluid for launch Mechanical modification for reverse torque	
Gear #	Ratio	Vehicle Speed at 1000 rpm
1 st	3.22	6.2 mph
2 nd	2.41	8.8 mph
3 rd	1.55	12.5 mph
4 th	1	19.1 mph
5 th	.75	25.8 mph
Final Drive Ratio		3.55

The aftermarket transmission controller has digital inputs for the upshift and downshift commands. Thus, the lower-level control of the transmission is much easier and faster. During shifts, the control forces the torque from the motor or the engine to be reduced to 15 percent of the driver request to facilitate the shift. When the engine is engaged, the clutch is partially disengaged so the engine is pulled to the transmission input speed, but since the clutch slips, the inertia forces are softened. Shift times with the automatic transmission are above 400 ms with continuous lower-torque transfer. As a safety feature, the transmission mechanical switch needs to be actively shifted to drive by using a little air solenoid. In case of an emergency stop or power loss, the transmission will automatically return to neutral.

The transmission controller requires a torque input signal to adjust the clamping pressure on the appropriate clutches to hold the torque transferred across the transmission. Since MATT has two power sources with the engine and the motor, the signal sent

to the transmission controller is the sum of the torque requests. During braking, the signal is the regenerative torque requested from the motor. In some extreme regenerative braking at lower input speeds, the transmission fluid pressure was not high enough to maintain the required clamping force on the clutches. This problem was solved by increasing the turn-on threshold of the auxiliary pump and, if needed, mechanical braking to reduce the regenerative braking. This step is only necessary on aggressive cycles, such as the US06.

Table 7 summarizes the instrumentation on the automatic transmission module.

Table 7. Summary of motor module instrumentation

	Element measured	Sensor
Power Input	<ul style="list-style-type: none"> ▪ Input torque ▪ Input speed 	<ul style="list-style-type: none"> ▪ High-accuracy torque and speed sensor
Power Output	<ul style="list-style-type: none"> ▪ Output torque ▪ Output speed 	<ul style="list-style-type: none"> ▪ High-accuracy torque and speed sensor
Module Specific	<ul style="list-style-type: none"> ▪ Oil temperature ▪ Case temperature ▪ Line pressure 	<ul style="list-style-type: none"> ▪ Thermocouples ▪ Pressure sensor

Figure 14 shows a comparison on the shift times between the manual transmission and the automatic transmission. The data show that MATT operated as a conventional vehicle on the 5th mod of the UDDS, which is one of the more aggressive accelerations from a stop. This data set for the manual transmission is one of the early slow calibrations to show the contrast between the manual and automatic transmissions. During the shift from one to two, the

manual transmission vehicle loses the trace since the engine did not transfer any torque, as seen in the torque data. Once the shift is complete, the driver requests high torque to catch up with the trace. In contrast, the automatic transmission data show an average engine torque while the vehicle meets the trace without a problem. The smooth, more averaged torque request is much better for the emissions behavior of the engine. The revised manual transmission module with clutch should rectify the shift time problem. The automatic transmission module behaves realistically, as in an actual vehicle.

The Mechanical Brake System

The mechanical brakes are not considered a powertrain module because of their low-technology aspect for hybrid vehicles. The mechanical brake system on MATT is a traditional automotive brake system. Since MATT is a single-axle vehicle, the brake is oversized to stop the entire vehicle inertia on one axle. Brake pads are pushed onto the brake rotors by single piston calipers. The hydraulic line is pressurized by a standard master brake cylinder, which is actuated by a pneumatic air solenoid. The pressure on the air solenoid is dictated by a variable pressure regulator, which is computer controlled. Thus, the computer controls the braking force. The computer can use an infrared temperature sensor to adjust the brake pressure on the basis of the rotor temperature. The computer translates a wheel brake torque into a hydraulic pressure on the basis of an empirical relationship. Figure 15 shows the hardware that composes the mechanical braking system.

The automatic transmission module and the manual transmission modules do not share the same rear axle; thus, the brake hardware is not identical, but it is composed of similar components, has the same layout, and has the same operating strategy.

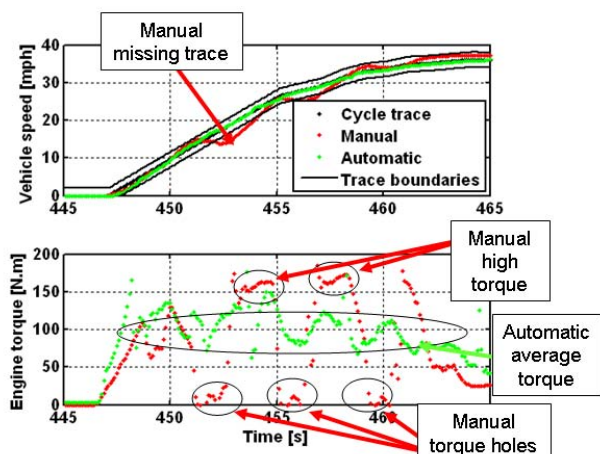


Figure 14. Comparison of the Manual to the Automatic Transmission in Conventional Operation

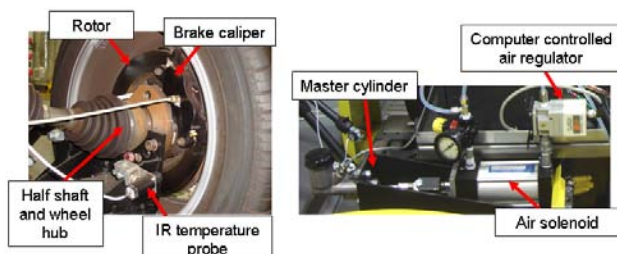


Figure 15. Mechanical Brake Hardware

To establish a relationship between computer command and brake torque, a couple of special tests were performed. MATT was set in a cruise control mode and operated at different steady-state speeds. At each steady-state speed, the brakes were ramped in and out at different rates. The wheel torque sensor records the torque between the brakes and the motor applying torque to maintain the steady-state vehicle speed. Figure 16 provides the results for such a test. A linear relationship with an offset is derived as the default brake command to wheel brake torque conversion. The offset is explained by the minimum pressure to move and apply the pads to the rotor. The data were taken starting in 3rd gear, then 4th, and finally 5th gear at different speeds for each gear. Brake fading is apparent in the data set for 5th gear, where the wheel brake torque is weaker for a given break command.

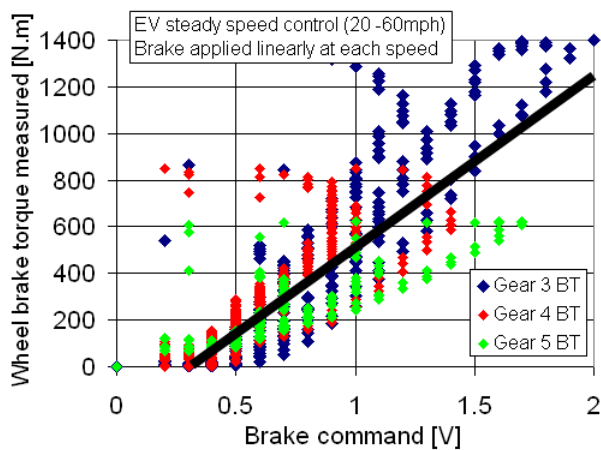


Figure 16. Wheel Brake Torque Data for Steady State Speed Data

For the conventional vehicle, the mechanical brakes work well and the control is relatively simple. In hybrid operation, the braking is shared between the electric propulsion system and the mechanical brakes. On MATT, both the motor and the mechanical brake can be commanded independently, which provides flexibility to test different strategies and calibrations. Typically, most of the braking effort is regenerative braking when possible to maximize the capture of the kinetic energy into electric energy. In some cases (such as aggressive decelerations or a fully charged energy-storage system), the mechanical brakes supplement the regenerative braking when the

electric motor cannot physically provide enough braking torque or the battery cannot accept the electric power. At lower vehicle speed, the regenerative braking fades and the mechanical brakes are used instead to come to a standstill.

The Data Acquisition System and Instrumentation Summary

Most of the instrumentation has been covered in the module-specific sections. The data collection from a single test comes from the instrumentation on MATT, data saved in the high-level controller (control data and emulated component data), the dynamometer data, the test cell data, the emissions bench, and an optional system (such as the engine pressure trace indicating system). The facility data acquisition system, as well as MATT's, is designed to be very flexible in adding instrumentation. Another great advantage is the open-component module approach, which makes easy access for instrumentation. The APRF main host computer records most of the data and some information is merged in post-processing after the test.

The sensors on MATT are wired into signal conditioning boxes. These boxes condition the incoming signal to a standard isolated 0–5-V signal. Each signal has two output connectors in order to share the signal between the high-level controller and the data acquisition system. The high-level controller uses the signal for component control and energy management strategies. The data acquisition system is dedicated to record the data.

Beyond investigations into individual components, the major goal is to understand the performance and the efficiency of the components in a hybrid vehicle system environment and their effect on the system. A requirement of the instrumentation is to be able to track power and energy in the driveline throughout and over the test cycles. Figure 17 summarizes the instrumentation that enables this analysis. The data are also used to debug, understand, and recalibrate the component control, as well as the energy management strategies.

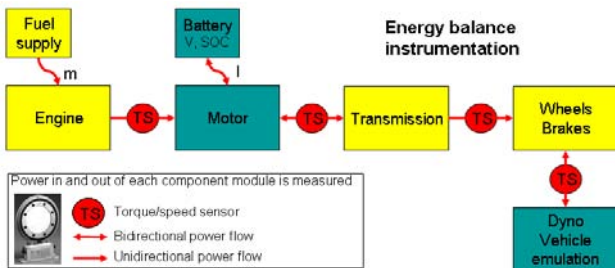


Figure 17. Instrumentation Summary with Respect to Power and Energy Flows between the Module

This concludes the hardware description of the report.

The Software and Safety Functions

The High-Level Controller Hardware and Software

The high-level controller is an Autobox from dSpace with an analog output board, a digital output board, and an analog input board. That controller runs the lower-level component control and the higher-level energy management strategy, as well as the real-time simulations, which emulate the virtual components (such as energy storage).

PSAT-Pro is the software used in the controller. ANL developed it as a companion to PSAT, ANL's automotive simulation tool. The software has been and is used in ANL's HIL experiments, which range from a diesel CVT hybrid powertrain to the battery HIL setup. The software uses the simulation code structure with supplemental layers of code for safety purposes and hardware interfaces. The parallel to the simulation software enables energy management development in simulation before transferring the strategy to the hardware for testing. The hardware results can then be used to improve the model's fidelity and gain additional insight (such as impact of engine operation on emissions).

Since the code in the controller is based on simulation software, it uses physical component signals to feed the real-time simulation and translates the simulation commands to physical component commands. For example, in the powertrain section of the code, the engine model is bypassed with a throttle command output to the hardware and an engine speed and torque signal from the hardware.

Driving MATT

A PID (proportional–integral–derivative) loop is used to emulate a driver. A pre-programmed drive cycle starts once the virtual key is turned. Once started, the PID loop adjusts the driver torque request to minimize the speed difference between the wheel speed and the drive trace. The gains for the PID loops have different calibrations at lower and high vehicle speed. The PID loop does look ahead on the trace by one second. Only the driver PID loop looks ahead; it is not used to influence the energy management strategy. In a real vehicle tested on a dynamometer, a driver also looks ahead and can anticipate the trace. The PSAT-Pro "driver" has extra features that include cruise control from any target speed and a "pulse and glide" mode. The pulse and glide mode was developed to emulate and investigate hypermiler driving techniques.

A final useful feature is a pedal set that can replace the PID loop driver in the code. A user can use an accelerator pedal and a brake pedal to drive MATT. This capability is very useful during initial troubleshooting phases when a new hardware module is put in place. It is also useful to compare input from a human driver to input from the PSAT-Pro PID driver to ensure that the computer driver is realistic.

The driver, be it the virtual driver or a human driver, ultimately closes the loop on powertrain torque control to meet the desired vehicle speed dictated by the drive cycle.

The Energy Management and Torque Split Shell

The energy management and torque split strategy is in a state-flow diagram form. The input is the driver torque and any vehicle information available. The output is simplified to the following:

- *Engine on or off:* The lower-level code enables the ECU ignition and starts the engine with the 12-V starter at a stop, or it can use the clutch to bump start the engine if the drivetrain is already spinning.
- *Engine torque command:* The engine torque command can only be positive. In conventional mode, the engine torque command would be a function of the driver torque request at the wheels and the gear engaged in the transmission. In hybrid mode, the engine torque command and the motor command need to be equal to the total

driver torque request as a function of gear engaged.

- *Motor torque command:* In electric-only mode, the motor torque command would be a function of the driver torque request at the wheels and the gear engaged in the transmission. The motor torque would be positive in propulsion and negative during regenerative braking. In hybrid mode, the motor torque and the engine torque need to relate the driver's torque request.
- *Wheel brake torque command:* In conventional mode, the wheel brake torque is equal to the negative driver torque demand. In hybrid mode, the brakes are typically used to provide stopping torque, with the motor or battery limited in its regenerative braking power. The mechanical brakes are also used to at lower vehicle speed to bring MATT to a stop.

The state flow code is a shell to test different energy management codes easily. One of MATT's key features is this open-control approach, which enables the user to test any energy management strategy, from the very simple to the complex (Figure 18).

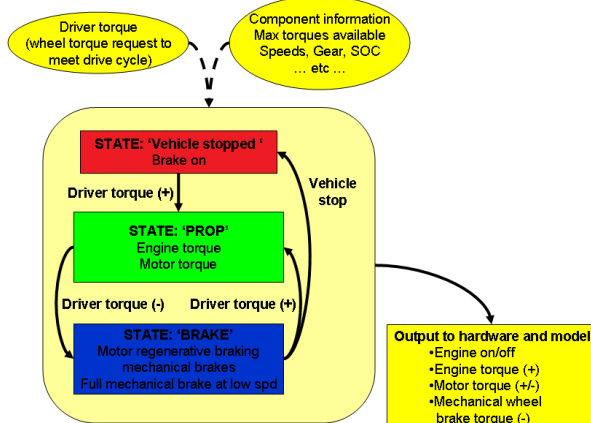


Figure 18. Illustration of the Energy Management Strategy Shell

The lower-level control code translates the commands from the energy management strategy at the component level while protecting the hardware. For example, the conventional vehicle launch using the clutch and throttle are managed in the lower-level control for the component.

The User Interface

During testing, the user has access to the visual feedback and calibration possibilities in the control desk interface. Any control parameter can be calibrated in real time as MATT is running a test. The interface has two modes. The first is the actual test mode, in which a virtual key is turned to start the automated drive cycle test with the current energy management strategy. The second is a manual override mode, in which the user can command all of the actuators on MATT independently. The second mode allows access to a special section in the code that allows the user to override the output commands to components in order to test individual operation of actuators for debugging purposes. Figure 19 shows the user interface.



Figure 19. Screen shot of MATT's Test Mode Interface

The Safety System

To protect the hardware, safety functions are built in the code that can trigger an emergency stop for the hardware, if required. All of the ranges of input sensor are verified continuously and can trigger a shutdown if any reading is outside of the expected operating boundaries. For example, if the engine speed exceeds 6000 rpm, the controller will stop the experiment, zero the throttle command, open the clutch, zero the motor torque, shift to neutral, and let the wheel coast to a stop. The facility emergency stop is triggered as well. The controller also monitors the hardwired emergency stop system on MATT. That emergency stop system consists of a series of physical mash-type switches on each hardware module and throughout the cell test and the control room. The power to the fuel injectors, the power to keep on the electric drive system, and the power to the transmission drive switch are all physically interrupted, thus isolating any power source in the driveline. The other safety features are the saturation

of all of the command signals before they are sent out to the components. The guarding of rotation parts through heavy guards is MATT's passive safety system and final protection.

Summary of MATT's Key Features:

The key features that make MATT a flexible tool and help it accomplish its aforementioned goals are:

- *Modular hardware approach:* MATT enables the testing from a system perspective of different powertrain components in a flexible hybrid vehicle environment.
- *The virtual scalable energy storage system and motor module:* This special hardware module can emulate different battery types and capacities, as well as different traction motors. The side benefits for this module are the ability to recharge the energy storage system instantaneously and to a specific and repeatable state of charge.
- *Open controller for energy management and torque split strategy:* Any energy management strategy can be tested on the hardware, from a conventional vehicle operation to an electric vehicle to a large number of hybrid control strategies. Special investigations require some specific hybrid behavior that may not be optimal, and because MATT is an open-controller tool, it can accommodate that situation.
- *Flexible driver options:* Having an automatic driver provides a good test for evaluating repeatability in all operating modes. The physical pedal set provides more flexible driver input beyond just completing a drive cycle.
- *Test facility:* The APRF dynamometer enables the vehicle emulation capability, data acquisition, and emissions recording.

This concludes the description of MATT. The next section describes some of the applications and results of the tool.

Different Applications of MATT and Their Results

The first operating mode presented here is the conventional vehicle. The conventional vehicle is the most difficult operating mode for MATT because it requires the vehicle to be launched by using the

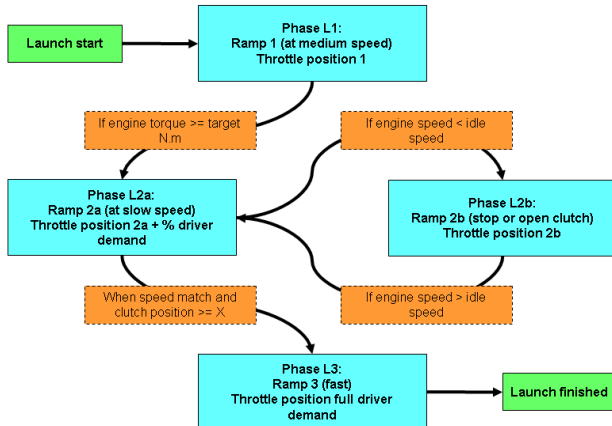
clutch and throttle and good shift time to obtain reasonable fuel economy and emissions. The conventional vehicle is also the baseline for comparisons of all of the other operating modes. The electric vehicle operation is then presented. It is the opposite of the conventional vehicle. And, finally, some specific plug-in hybrid investigations that demonstrate MATT's usefulness as a tool are described.

The Conventional Vehicle Operation

For simplicity, all of the conventional results presented here are based on the use of the automatic transmission module.

Launching a Conventional Vehicle by using a Dry Clutch

The lower-level control code actuates the clutch during the conventional vehicle launch. The process consists of three phases. The first phase is a clutch engagement at medium speed until the point of clutch engagement is determined when the engine torque sensors measure some torque spike. At the same time, a minimum throttle command is sent out to lift the engine speed above idle. The second phase is the critical launch phase. The clutch is further engaged at a slow speed while the engine-based throttle command is increased and an additional throttle command is sent on the basis of the driver's torque request. If the engine speed is pulled below the idle speed, a recovery state is entered in which the clutch engagement is stopped or slowly reopened while more throttle is applied until the engine speed is above idle. Now that the clutch engagement calibration is optimized, the recovery state is almost never used. The final phase starts when the engine speed and transmission input speed match, and the clutch is engaged. In the final phase, the clutch is fully engaged as fast as possible, and the throttle command is directly linked to the request from the energy management strategy. Figure 20 illustrates the conventional vehicle launch logic. If, during a launch, the vehicle speeds up faster than the drive cycles, the launch is aborted and restarted; thus, MATT stays within the drive cycle boundaries.

**Figure 20. Conventional Vehicle Launch Logic**

General Conventional Vehicle Operating Strategy

The energy management strategy is relatively simple. Once the vehicle is launched, the positive driver wheel torque request is translated into the engine torque request by dividing it by the ratio of the current gear. The negative torque request is turned into a brake command to the mechanical wheel brakes. During a stop, the engine idles and the mechanical brakes are engaged. The shift schedule is predetermined as it is done for manual transmission vehicles.

Conventional Vehicle Results on the UDDS

Summarized test results for UDDS

The standard certification cycle is the UDDS (Urban Dynamometer Driving Schedule). For certification purposes, a cold-start UDDS test is performed followed by a 10-minute soak and then another UDDS. The test results are summarized in Table 8. The cold-start test requires that the vehicle be subjected to an ambient temperature condition of 25°C for at least 12 hours and is started for the first time at the start of the UDDS. MATT as a conventional vehicle achieves PZEV.

Table 8. Conventional vehicle UDDS test results (as a mid-size sedan)

Parameter	UDDS (cold start)	UDDS (hot start)	Hot-Cold weighted
Fuel Economy Bag (mpg)	25.5	27.2	26.5
THC (g/mi)	0.010	0.001	0.006
NO_x (g/mi)	0.007	0.001	0.005

Argonne's correlation vehicle, which MATT is emulating, achieves 26.6, 27.5, and 27.1 mpg on a cold-start UDDS, a hot-start UDDS, and the hot-cold weighted. Those fuel economy results are comparable. The difference comes from the hardware. The correlation vehicle uses a 2-L engine and a 5-speed automatic transmission. Since the purpose of the correlation vehicle is to verify fuel economy and emissions measurements of the APRF on a regular basis, the correlation vehicle is not a PZEV.

Data from UDDS cycle in time domain

During these drive cycles, the driver followed the trace at all times within the required boundaries. Figure 21 shows the entire drive trace, the vehicle speed, and different temperature information. All of the temperatures start at 25°C, which indicates the cold-start conditions. The engine coolant and the catalytic converter reached operating temperatures by the start of mod 2 (also known as hill 2). The engine oil and transmission temperature steadily increase throughout the test and almost reach a steady-state temperature.

By using the instrumentation on MATT, the power flow is calculated from the fuel input to the wheels at all times. Figure 22 shows the power levels on the first mode of the UDDS to illustrate the details of the transients. The fuel power is calculated by using the fuel flow measurement and the net heating value of the certification fuel. The indicated engine power is based on the indicated mean effective pressure (IMEP) measurements converted to indicated torque and the engine speed. The engine brake power is calculated with the engine torque and speed sensor. In a similar way, the torque speed sensor of the transmission is used to compute that power. The dynamometer power is calculated on the basis of the reported tractive force and dynamometer speed. All power measured between the components shows the losses of each component. The biggest loss is in the fuel conversion to the engine crankshaft torque and speed. Most other conversion processes are more efficient.

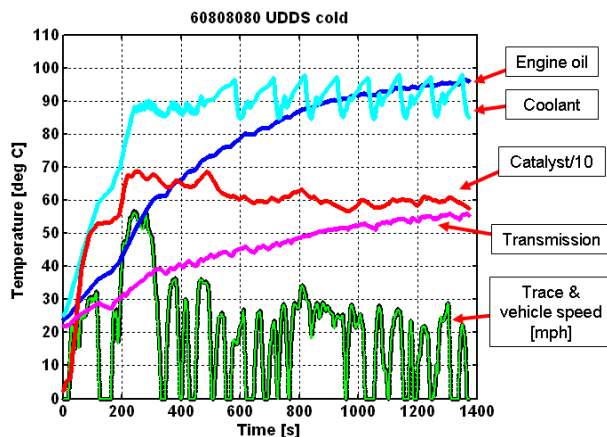


Figure 21. Trace and Temperature Information for the Conventional Vehicle on Cold Start UDDS

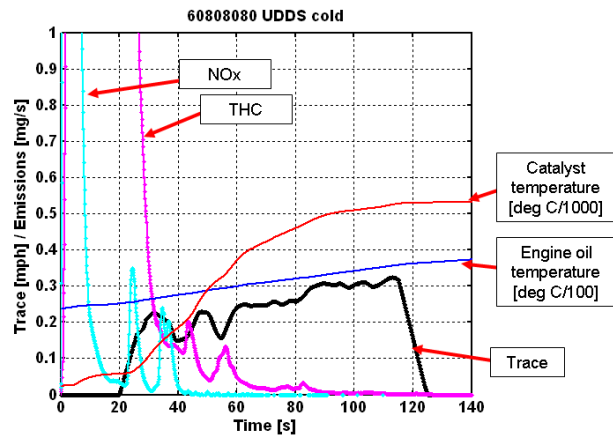


Figure 23. Emissions Measurement for the Conventional Vehicle for the Cold Start

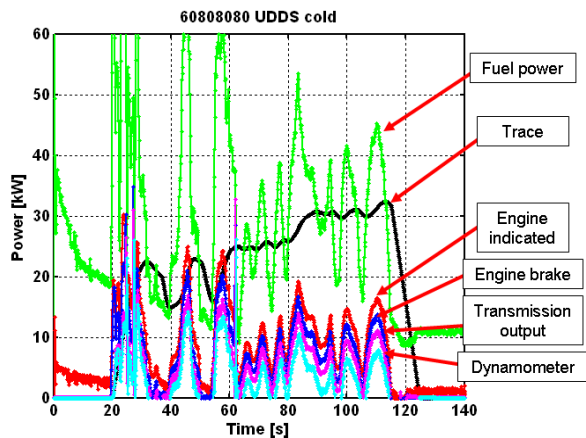


Figure 22. Power Calculation Based on Input from the Sensors for the Conventional Vehicle

Another important piece of information is the modal emission data. Figure 23 shows the cold-start emissions of the first engine start while the catalyst is cold. The catalytic converter is far from light-off temperature and thus cannot convert the excess hydrocarbons caused by the engine still operating in an open loop. Note that by the end of the first mode, over 95 percent of emissions are generated. Figure 24 shows the same engine start and mode 1 of the UDDS test cycle after a 10-minute soak following the end of the cold-start UDDS. The hot-start emissions for the engine are significantly lower since the converter is already at 300°C. Thus, the conversion efficiency is already high and the engine is already operating in a closed loop at stoichiometric operation.

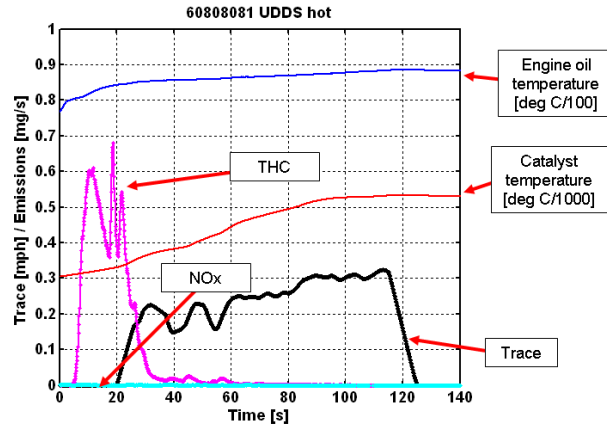


Figure 24. Emissions Measurement for the Conventional Vehicle for a Hot Start

Component performance on cold-start and hot-start UDDS test cycles

From the recorded data, the total energies for each component are calculated from the entire cycles. The dynamometer energy calculation is based on the integration of the positive dynamometer power only. All of the other components only experienced positive torque in the conventional mode. Table 9 summarizes these results.

Table 9. Total positive energy measured for the components during the drive cycles

Parameter	Energy Measured (MJ), UDDS (cold start)	Energy Measured (MJ), UDDS (hot start)
Fuel	34.50	31.90
Engine Indicated	10.26	9.26
Engine Crankshaft	8.61	8.09
Transmission	6.52	5.76
Dynamometer	4.50	4.51
Braking (possible regen)	2.22	2.22

As shown in Table 9, eight percent more fuel is used to complete the UDDS on a cold start in comparison with the hot start. During the cold-start test, more energy went through every component in comparison to the hot-start test. While the components are operating at room temperatures, they are less efficient. In general, friction losses are higher at lower temperature. Some energy is also used to bring components up to operating temperature. The engine during its own warm-up phase will typically retard spark to exhaust more heat, thereby lowering the mean effective pressure (MEP). Thus, more energy was put into the transmission to meet the drive cycle during the cold start, and even more fuel was used by the engine as a result of increased mechanical losses.

A closer look at the engine data

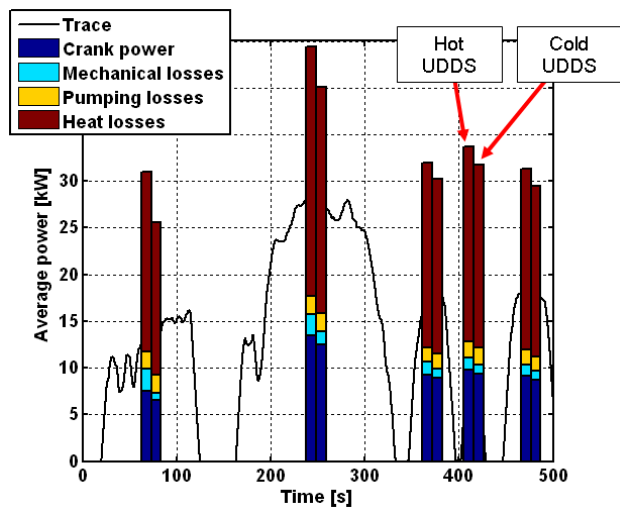
For each component, its average efficiency for the drive cycle is computed in Table 10.

Table 10. Average component efficiency over test cycles

Average Cycle Efficiency (%)	UDDS (cold start)	UDDS (hot start)
Engine Indicated	29.7	29.0
Engine Brake	24.9	25.3
Transmission	75.8	78.4

The average indicated efficiency is higher for a cold-start test even though the brake thermal efficiency is lower. During the cold start, the engine has to produce more energy through the cycle; thus, it operated at a higher average power, which yields a higher average-indicated efficiency. The brake thermal efficiency includes the mechanical losses, which, during the cold start, are so significant that despite the higher indicated efficiency, the brake thermal efficiency is lower. Figure 25 compares the average power losses from the fuel input to the engine crankshaft per UDDS mode for the first 505 seconds for the cold start and hot start.

The crank power is higher for the cold start for each hill but as the components warm up, that difference diminishes. The mechanical losses are four times as high for the cold start on the first hill, and only 50 percent greater on hill 5, thus demonstrating that the frictional losses are proportional to temperature. At the same time, the pumping losses are lower for the cold start because the engine is required to produce more torque at the crank, and thus the throttle is wider open on average on cold start, thus reducing the pumping losses. The “heat losses” label represents mainly the heat losses due to the exhaust gases and heat wall losses, but it also includes unburned fuel. Those heat losses are also bigger for the cold start.

**Figure 25. Decomposing the Average Fuel Power into the Losses to the Engine Crankshaft**

The different engine efficiencies can be derived from the modal data collected on the engine during the UDDS. Figure 26 shows the engine efficiency data derived from a hot-start UDDS test. The difference between the indicated and brake efficiency represents the mechanical losses. These losses are relatively constant, with a slight increase through the power ranges. As these data are derived from a test cycle, the higher power is typically associated with higher speed, which explains the slight increase in mechanical losses since frictional losses are higher at higher speeds. From the indicated efficiency without pumping losses, the throttling losses are obvious at the lower power levels, where the throttle is more closed.

Figure 26 can also be used to anticipate the engine operation in hybrid mode. If the engine is only used at a power level above 10 kW, the throttle losses are minimal and the brake thermal efficiency is around 30 percent. Since the conventional vehicle is the baseline, a final interesting plot to consider is an engine torque speed contour plot of the amount of energy used, as shown in Figure 27. In hybrid operation, the engine can be decoupled from the wheel load by using the hybrid system. Also notice from Table 9 that 2.22 MJ of kinetic energy is dissipated in heat and could be available from regenerative braking in a hybrid.

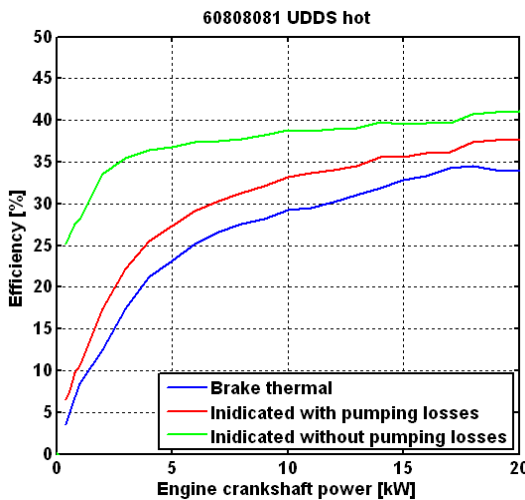


Figure 26. Different Engine Efficiency Lines versus Engine Crankshaft Power

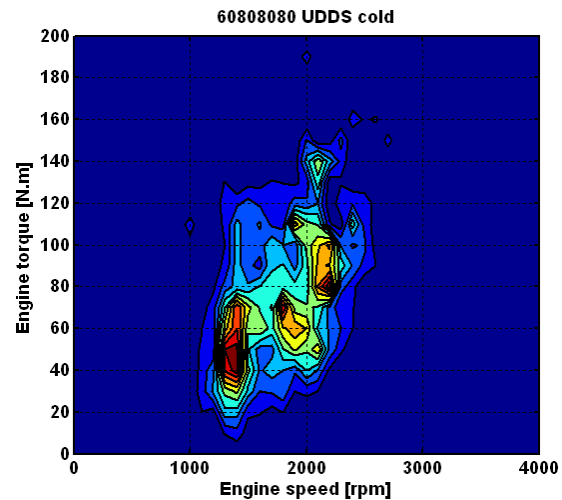


Figure 27. Engine Energy Spent at Different Engine Torque Speed Ranges as a Conventional Vehicle during a UDDS

Further operating losses on conventional vehicle

While the vehicle is stopped during the drive cycles, the engine still consumes fuel while idling, and the launch operation is fairly inefficient. Figure 28 shows both situations.

During a UDDS, the vehicle is stopped over 17 percent of the time. From the data on the hot start, that percentage represents 0.019 gallons of fuel out of the total 0.229 gallons used. So, preventing idling could save 6.9 percent of the fuel, which is possible in a hybrid vehicle.

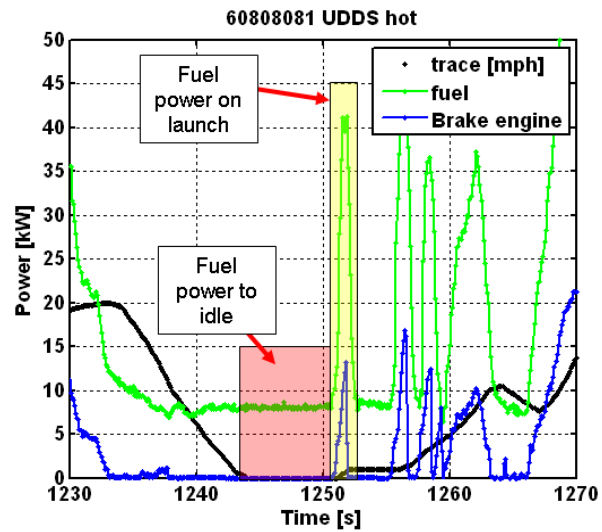


Figure 28. Engine Idle and Launch Losses on the UDDS

The fuel used by the launch is based on average engine cycle efficiency compared to the power to the transmission during the variable torque transfer of the clutch losing. About 0.009 gallons of fuel are used during the launches throughout the UDDS, which represents over three percent of the fuel used.

The “Engine Optimum” Hybrid Vehicle Operation

The emulated hardware

The virtual scalable energy storage and motor module is emulating the JCS 41VLM lithium-ion battery pack and the UQM 75 motor. The vehicle type is the same as in the conventional baseline tests.

Hybrid control strategy

The general philosophy of the hybrid control strategy used in this case is that main vehicle operation is electric only, and upon achieving the driver demand threshold, the engine is clutched in. Once the engine is operating, it is loaded to a preset engine torque speed curve independent of driver demand. The engine is then turned off on the basis of low power request or vehicle speed. When the engine is on, it drives the wheel and charges the batteries. The driver demand threshold is variable, on the basis of the SOC.

“Engine optimum” hybrid vehicle results on UDDS

The test data presented in Table 11 are from a slightly charged gaining test. The fuel economy over the UDDS is 32.9 mpg, which is a 10 percent gain in fuel economy over the conventional vehicle with a hot start. The hydrocarbon emissions are increased by an order of magnitude.

Table 11. “Engine optimum” hybrid vehicle test results on UDDS

Parameter	UDDS (warm start)
Fuel Economy Bag [mpg]	32.9
THC [g/mi]	0.015
NO _x [g/mi]	0.001
SOC init	30.5
SOC end	31.0

During the hybrid operation, the engine came on six times, as shown in Figure 29. This test was run after another hybrid test with about 15 minutes of time to readjust the emissions bench. Thus, the components did cool down some. But even during the test, while the engine is off, the coolant, the catalytic converter, and the engine oil cool off, especially during longer off periods. In this particular hybrid operation, the engine never reaches a thermal steady-state operating regime as compared to the conventional vehicle. The catalyst temperature is of special concern if it cools below the light off temperature, and the conversion efficiency does greatly suffer. At the first engine start, the catalyst is at 200°C, which is slightly below the light off temperature. That engine start generates the major part of the emissions, as shown in Figure 30.

The first start generates the highest emissions because the catalyst temperature is too low and the engine is immediately loaded to a high load. This hybrid control strategy is intended to be the first iteration, and, thus, in future versions, the initial load of the engine should be reduced until the catalyst and the engine oil reach a certain temperature.

The first engine start is shown in Figure 31. The engine does get loaded between 40 and 50 kW, which, at those engine speeds, corresponds to engine torque level of a 140–150 Nm.

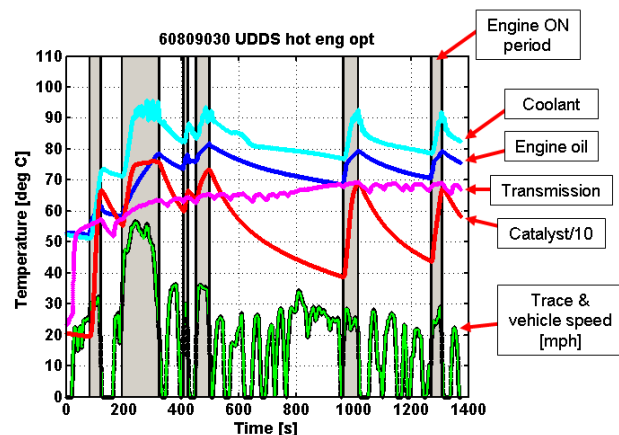


Figure 29. Trace, Engine Operation, and Temperature Information for the ‘Engine Optimum’ Hybrid

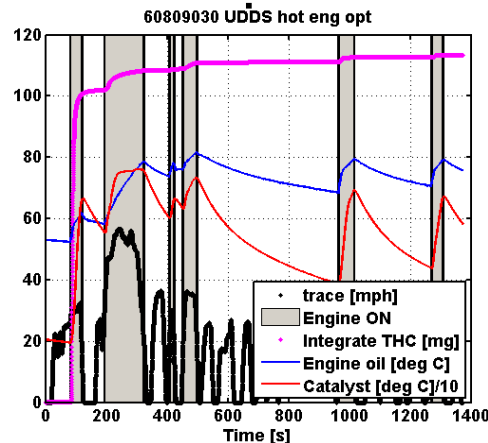


Figure 30. Emission Details for the “Engine Optimum” Hybrid Operation

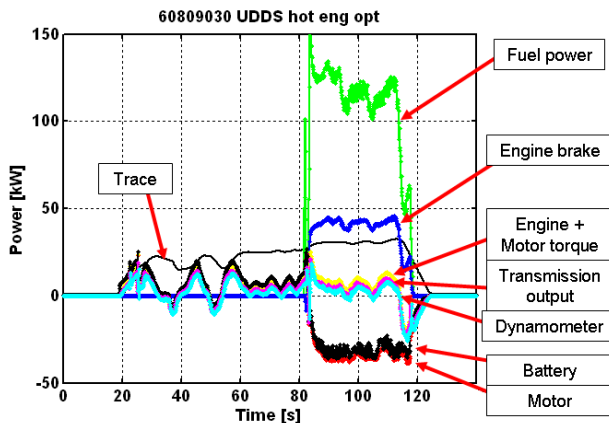


Figure 31. Power Measurements of Components for the First Hill of the UDDS Operating in the “Engine Optimum” Strategy

For the first part of the test, the vehicle operates in electric mode without the engine. After a certain amount of battery energy is used, the driver demand threshold to turn the engine is reached by the driver demand. Then, the engine provides power to the wheels and recharges the batteries. During the deceleration, regenerative braking is achieved by the electric motor, which recharges the batteries. The energy summary is shown in Table 12.

Table 12. Total positive energy measured for the components during the drive cycles in “engine optimum” hybrid mode

Parameter	Energy (MJ) Measured during UDDS (warm start)
Fuel	26.45
Engine crankshaft	9.15
Engine + Motor positive	7.95
Engine + Motor negative	1.44
Transmission positive	5.88
Transmission negative	1.76
Dynamometer positive	4.43
Dynamometer negative	2.17

The average cycle efficiency is 34.6 percent, which is much higher than the 25.3 percent from the conventional hot start. Thus, using the motor and energy storage system to modify the vehicle operation is beneficial to improving overall efficiency. The hybrid system does, however, have its own losses as result of charging and discharging the batteries, as well as losses from the emulated motor efficiencies. Once the 0.82 MJ in auxiliary loads (600 W continuously) is considered, overall hybrid system efficiency is 82.5 percent. Although the high average engine efficiency takes away from the hybrid system efficiency, it is still higher than the average engine efficiency for the conventional engine. Regenerative braking also contributes to the higher overall system efficiency. Table 13 summarizes the efficiencies.

Table 13. Average component efficiency over test cycles

Parameter	Average Cycle Efficiency during [%] UDDS (hot start)
Engine Braking	34.6 %
Overall Hybrid System	82.5 %
Regenerative Energy Recovery	57.4 %

The major advantage thus resides in shifting the engine operation to more efficient areas and eliminating its use in inefficient areas. Figure 32 shows the engine operation. The engine optimum is an extreme hybrid case that optimizes the engine operation. In this hybrid mode for this particular

vehicle emulation, the fuel used on the UDDS is 0.228 gallons compared to 0.276 gallons for the conventional vehicle, which represents petroleum displacement of 17 percent.

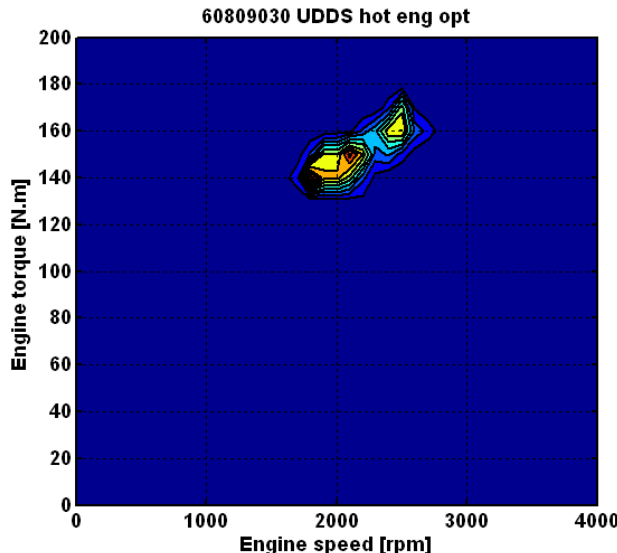


Figure 32. Engine Operation of the “Engine Optimum” Mode

The EV-Capable Plug-In Hybrid Vehicle

This discussion is the continuation of the previous discussion on the “engine optimum” hybrid vehicle. The tests are started with a full state of charge and the vehicle operation is electric only until the state of charge reaches its charge-sustaining SOC threshold.

Summary of all the tests

Figure 33 summarizes the tests for this particular plug-in hybrid test set. The first two urban cycles are covered in electric-only mode. In the third urban cycle, during the higher-speed acceleration in the second mode, the engine turns on for the first time as the SOC reaches the target SOC for the charge-sustaining operation mode. In charge-sustaining mode, the engine oil warms up as the engine is used more frequently. As the charge-sustaining mode is reached, the fuel usage increases and the net battery usage is zero. For the first two cycles, no fuel was used; thus, 100 percent of the petroleum is displaced in this case.

In the charge-sustaining mode, the vehicle operates in the “engine optimum” hybrid strategy presented earlier.

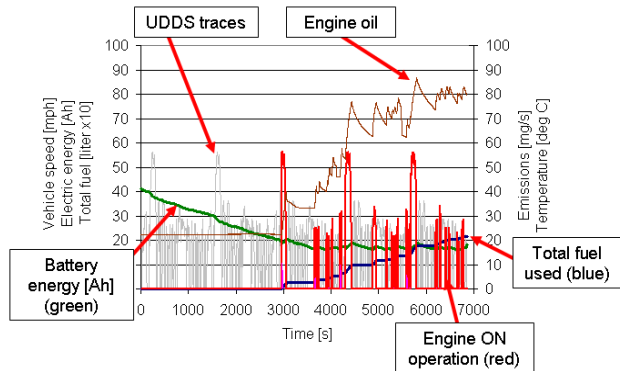


Figure 33. Summary of the Plug-in Hybrid Test Set

Fuel and Electric Consumption Summary

The same test results are summarized in Figure 34. At the start of the first test, the virtual battery is fully charged, and all the hardware components have soaked at ambient temperature for over 12 hours. More electric energy was used during the first cycle than in the second cycle. The mechanical losses in the transmission and tires become lower as components reach their operating temperatures.

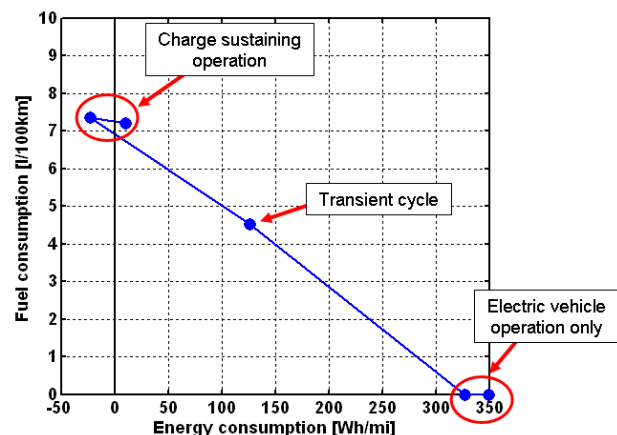


Figure 34. Energy and Fuel Consumption Graph for the “Engine Optimum” Plug-in Hybrid Test

During the transition cycle, the combustion engine comes on for the first time, making that the first cycle with emissions and fuel usage. The two last cycles are in charge-sustaining mode. Table 14 includes the emission information. In fact, the third cycle has the highest emissions because of the engine cold start.

Table 14. Energy consumption and emission summary for the “engine optimum”

Cycle	FE (mpg)	EC (Wh/mi)	THC (g/mi)	NOx (g/mi)
UDDS 1	0	350	N/A	N/A
UDDS 2	0	327	N/A	N/A
UDDS 3	52.6	126	0.022	0.024
UDDS 4	32.3	-23	0.009	0.005
UDDS 5	33.0	10	0.005	0.003

This particular hybrid and plug-in hybrid example shows the capability of MATT. At present, no available PHEV is EV-capable on the UDDS. So, MATT fills that role to generate data for that part of the design space. The data are important to understand the PHEV capabilities and help in the development of the new PHEV test procedures.

The Blended Plug-In Hybrid With a Load-Following Strategy

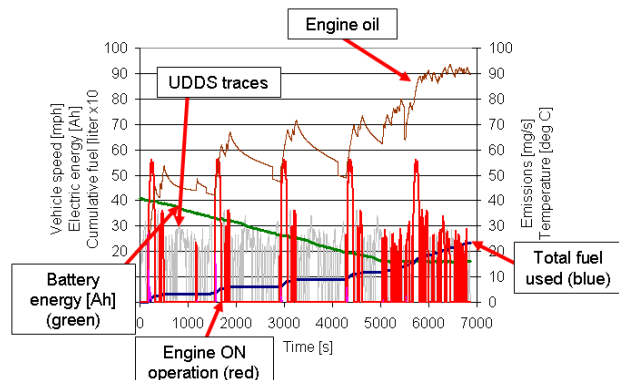
The hybrid control philosophy

In this case, the engine turn-on threshold is much lower compared to the “engine optimum” hybrid strategy both in charge-depleting and charge-sustaining modes. When the engine is operating, it provides the tractive power required to meet the trace but does not excessively charge the batteries. The launch is performed as an electric vehicle, regenerative braking is enabled, and the engine is always off at a stop.

The full charge test results

Figure 35 summarizes the full charge test. The engine is used on the first test, thus making it the cold start test for the engine. The engine is used on the faster and more aggressive hills for the first phase (505) for the UDDS. MATT completes over four urban cycles in the chargedepleting blended mode. The same 41-A•h battery pack is then emulated for the EV-capable test, which only yielded two charge-depleting test cycles. On the charge-sustaining cycle, the engine turns on at almost every mode; this helps the engine to reach a normal operating temperature. At the end of the five UDDS cycles, a total of 0.649 gallons are used, compared to 0.602 gallons used for the EV-capable PHEV. The blended hybrid requires a less-powerful motor, thus cutting cost and packaging issues while still displacing a significant amount of petroleum. The conventional vehicle uses

1.393 gallons of fuel to cover the five urban cycles as a baseline.

**Figure 35. Blended PHEV Test set as a “Load Following” Hybrid**

Fuel and Electric Consumption Summary

The full charge “load following” blended plug-in hybrid test results are summarized in Figure 36. The cold-start cycle is the first cycle. The cold-start losses show a higher electric and fuel consumption compared to the following hot tests. The second and third tests are almost identical because of the automatic driver repeatability. In the fourth cycle, the transition from charge-depleting to charge-sustaining mode occurs. The last test is charge sustaining. Note that the fuel efficiency results of the charge-sustaining test under load following conditions are not as high as those from the engine optimum charge-sustaining test.

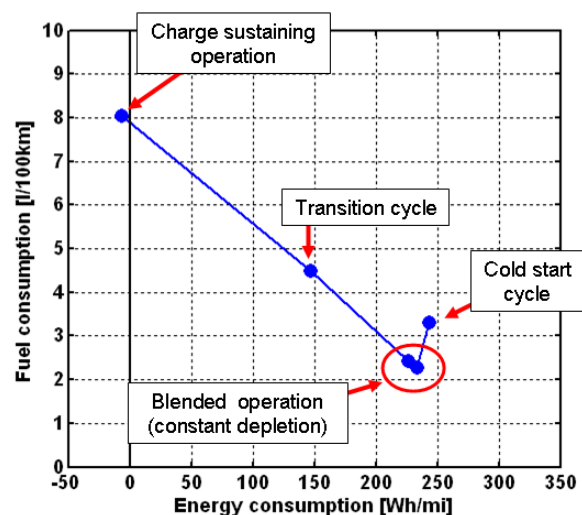
**Figure 36. Energy and Fuel Consumption Graph for the “Load Following” Plug-in Hybrid Test**

Table 15 presents the emissions results. The cold start suffers with high emissions. In fact, emissions are higher than those from the “engine optimum” or conventional cold-start test. A closer look at the time data shows that the catalytic converter does not reach its light-off temperature as fast. The engine optimum control achieves that, thanks to higher engine loads and the conventional vehicle benefits from the engine idle time. The measured emissions then tend to be lower than those from the “optimum control,” which is explained by the lower raw emissions that result when the catalyst reached the appropriate temperature.

Table 15. Energy consumption and emission summary for the “load following” PHEV

Drive Cycle	FE (mpg)	EC (Wh/mi)	THC (g/mi)	NO _x (g/mi)
UDDS 1	71.5	243	0.038	0.006
UDDS 2	104.4	233	0.015	0.014
UDDS 3	98.1	226	0.010	0.002
UDDS 4	52.9	147	0.011	0.002
UDDS 5	29.5	-7	0.003	0.002

The majority of the emissions for all of the cycle occur during the first engine start and operation. Figure 37 shows the details of the emissions for the UDDS 5. Once the catalytic converter is hot, the hydrocarbon emissions are extremely low. Note that the engine reaches a steady operating temperature, but it is still lower than in the conventional vehicle operation.

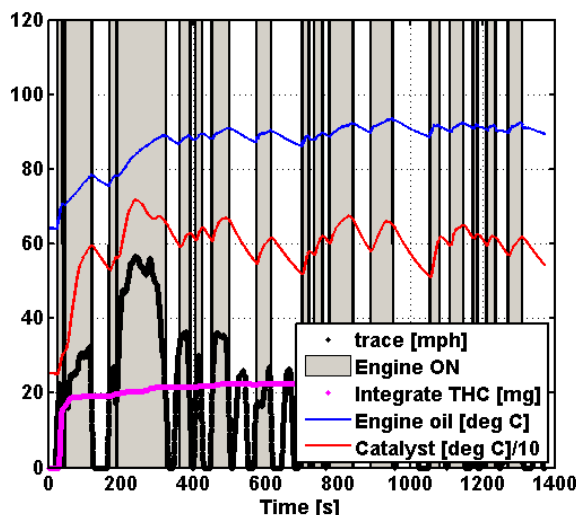


Figure 37. Emission Details for the “Engine Optimum” Hybrid Operation

The engine operation is now more spread across the load range, as shown in Figure 38. Compared to the conventional vehicle, the lower speed range is not used since that is typically covered by the electric launch mode. Once the engine is in use, the control strategy does not add extra load on the engine to optimize engine efficiency. The average engine brake efficiency for charge-sustaining hot start load following the urban cycle is 29 percent. Compared to 25.3 percent for the conventional cycle, the main improvement is the elimination of idling and the lower-speed operating points. The further reduction in fuel consumption compared to the conventional vehicle is explained by the energy recovery resulting from regenerative braking and the electric launch.

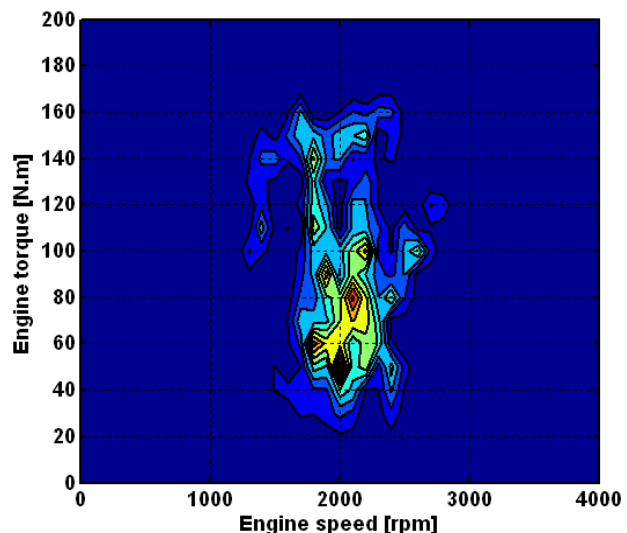


Figure 38. Engine Operation of the “Load Following” Mode

These tests are part of the baseline PHEV test to evaluate the impact of control strategies on emissions and fuel consumption. At first sight, the engine needs to operate at reduced load until the catalyst has reached light off. The major emissions are generated from the first engine start and the first few seconds of engine operation in a cycle. Further work will be performed in this area, including the development of an improved control strategy that includes emissions control.

Further Findings, Investigations, and PHEV Studies

A Special Case for the Conventional Vehicle: Steady-State Speed

With the integrated software, a driver's steady-state speeds are precisely maintained. The power required to maintain a vehicle speed is defined by the vehicle characteristics and that speed. Also, as the load on the engine increases, engine efficiency improves. Thus, at a given speed, the highest possible gear should be selected. Figure 39 confirms that logic through the use of test data. At 30 mph, 3rd, 4th, or 5th gear can be used, and the fuel economy changes from 32 mpg to 49 mpg and 58 mpg, respectively. From a drivability stand point, 5th gear does not give the driver as much torque to accelerate quickly, but the fuel economy, compared to other gears almost doubles.

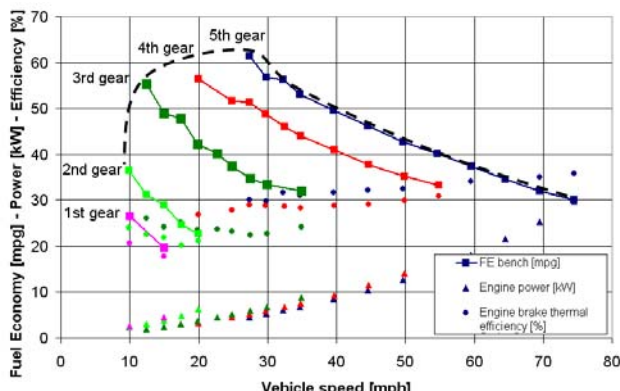


Figure 39. Conventional Vehicle Steady State Speed Results

The peak fuel economy is at 27.5 mph in 5th gear, which is the trade-off point between lower power required at the wheel and engine efficiency.

A Cold-Start Test Compared to a Hot Start for an Electric Vehicle

The losses in a cold driveline are higher because of higher mechanical friction. That effect is demonstrated in Figure 40, which shows that the first cold start of the electric vehicle used more electric energy than the second. By using MATT as an electric vehicle and the manual transmission module, this effect was further investigated, as shown by the data in the Figure.

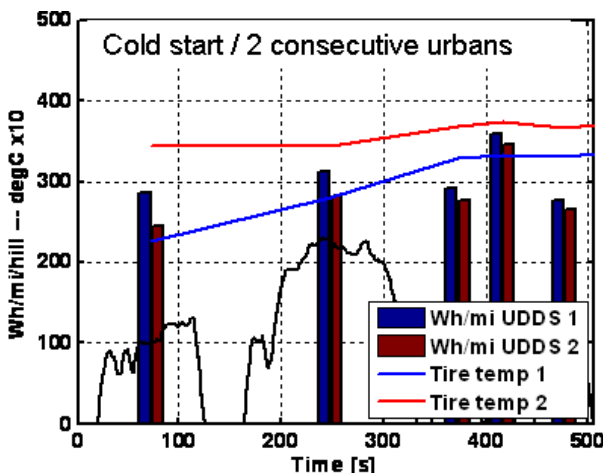


Figure 40. Electric Vehicle Cold Start UDDS Followed by a Second UDDS

The test was started with the first urban cycle as a cold start in the morning after a night in the test cell at 25°C, and the second cycle immediately followed the first. The different losses are apparent upon inspection of the electric consumption on a per-hill basis. The gap between the energy consumption decreases between the first and the second UDDS as the temperature rises. The first urban cycle used 289 Wh/mi, and the second urban cycle performed immediately after the first test used 256 Wh/mi. The electric consumption impact is over 10 percent for a cold-start electric vehicle test over a UDDS.

A few limitations need to be noted. The emulated battery and the emulated motor losses are not temperature dependent since the models are based on hot component data. Thus, this impact is only due to losses associated with the transmission, driveline, and tires. Also, the manual transmission was kept in 3rd gear during both tests and considered as a single-gear electric vehicle setup. In the manual transmission setup, it is possible to recover more regenerative braking energy since full reverse torque is possible through the transmission. The manual transmission is also 96 percent efficient in hot operation.

The First PHEV Investigation: Highway Cycle Cold-Start Correction for Maximum Charge-Depleting Operation

The Proposed Method

Typically for the certification purposes, the highway test cycle for a conventional or charge-sustaining hybrid vehicle requires completing two consecutive highway cycles. The first cycle serves as a warm-up and for the hybrid vehicle to pre-condition the initial state-of-charge of the battery to ensure a second highway is charge sustaining.

For a plug-in hybrid vehicle in a full charge test, all of the energy usage needs need to be taken into account. Thus, highway needs to be considered first. CARB (California Air Resource Board) proposed to use a correction method based using the fuel consumption of a cold-start highway test cycle at a depleted SOC to correct the first full-charge highway cycle. This method does work for a blended PHEV where the engine runs most of the time, but in the case of a maximum depletion PHEV, it may not work. MATT was used to generate data for that case.

For this investigation, the hybrid strategy is designed in such a way that the engine operation is limited during the charge-depletion portion. The engine only supplies the extra power that the motor cannot provide to make the trace. The engine is even less loaded than on the load-following hybrid. In charge-sustaining mode, the engine optimum strategy is applied. This provides a maximum depletion for a blended almost-EV-capable PHEV.

The Full Charge Cold-Start Test Set

The first test is the full-charge cold-start test set. Figure 41 shows some data from the four highway cycles. The first and second highway cycles are the charge-depletion cycle tests. The third highway cycle is the transition cycle to charge sustaining followed by the charge-sustaining test. The engine temperature barely rises during the charge-depleting cycle.

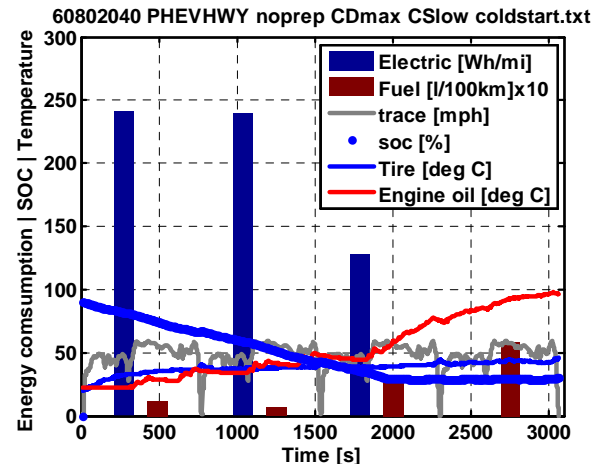


Figure 41. Full Charge Cold-Start Test for Maximum Charge-Depletion Test

Figure 42 summarizes the test set in the energy and fuel consumption plot. The first test, which is the cold-start test, does not align with the rest of the tests because of component and engine inefficiencies. The graph also shows the two proposed calculated fuel consumptions based on utility factor calculations. These calculated fuel consumptions are slightly off the average efficiency line. The cold start correction attempts to adjust that problem.

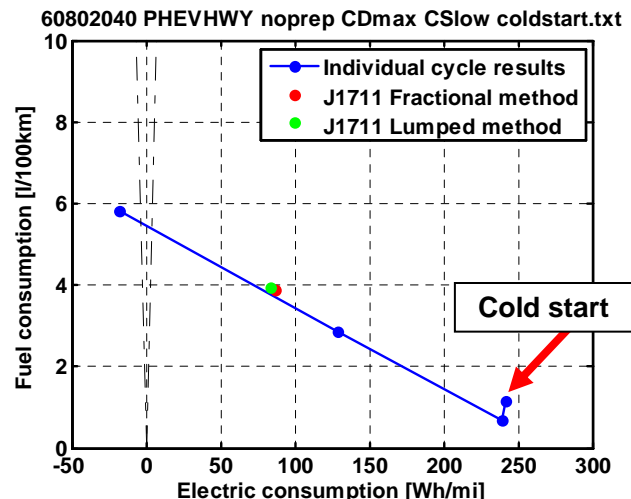


Figure 42. Energy and Fuel Consumption Summary for the Full-Charge Cold Start Test

To correct the cold-start fuel consumption, a correction of less than 0.5 L/100 km needs to be applied. More information on the baseline test is given in Table 16. Note that during charge depletion, the engine is used very little and the average

efficiency is low, which is due to the lower loads applied to achieve maximum charge depletion.

Table 16. Full-charge cold-start test for maximum charge-depletion test

Cycle #	FC (l/100 km)	EC (Wh/mi)	Eng on (%)	Eng eff (%)
HWY 1 (cold start)	1.14	242	12.0	20.3
HWY 2	0.68	239	9.1	24.1
HWY 3	2.8	128	23.4	30.7
HWY 4 (hot test)	5.3	-18	47.1	31.7

The charge-depleted cold-start test set

The second test set is the charge-depleted cold-start test. In this case, the initial state of charge of the batteries is 30 percent, which is the charge-sustaining target SOC. Figure 43 summarizes this test. Note that the operating temperature of the engine is only reached after the third test. In this case, operating as a charge-sustaining hybrid, the second highway cycle is still a transient cycle. As expected, the first cycle consumes more fuel (6.71 L/100 km) than the second cycle (5.8 L/1,000 km).

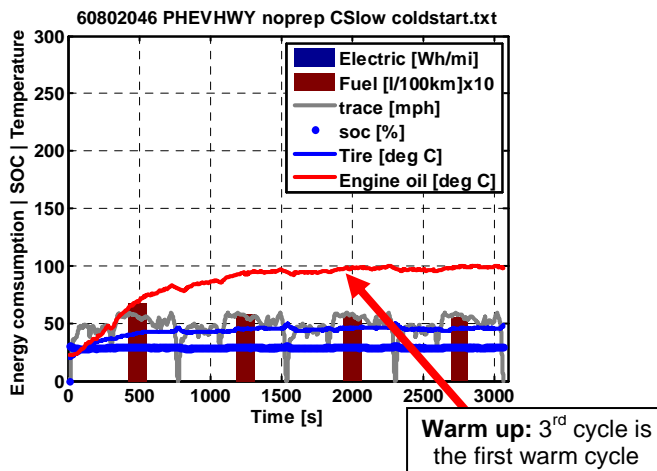


Figure 43. Charge-Depleted Cold-Start Test Summary

The correction factor applied to the first cold-start cycle on the full-charge test is 0.9 L/100 km. That correction factor overestimates the fuel correction, which was estimated at less than 0.5 L/100 km. This is explained by the different engine-on time for the charge-depletion cycles compared to the charge-sustaining cycles. On cold-start charge-depletion, the engine was on for 53 percent of the time at an

average efficiency of 29.2 percent in the engine-optimum hybrid strategy. Therefore, during the charge-depletion cycle (which is providing the correction factor), the engine is used four times more at much higher loads, which results in the overestimation in this particular hybrid case.

The test procedures need to apply to all cases, and thus this correction method is not appropriate.

An Alternate Correction Method: The Charge-Sustaining Switch

If all plug-in hybrids had a charge-sustaining switch, then a preparation cycle could be done in a charge-sustaining mode at full charge to warm up the engine and the driveline before the full-charge test set. An example of this alternate testing is illustrated in Figure 44.

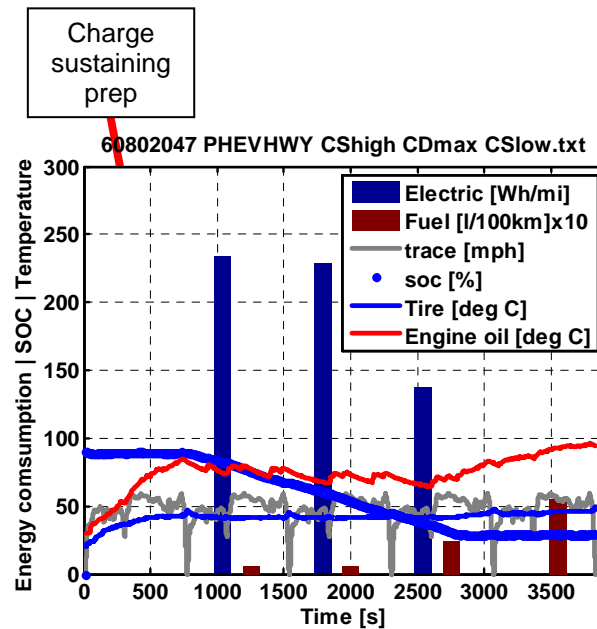


Figure 44. Full-Charge Test Summary with a Prep Cycle

The warm-up cycle in charge-sustaining mode does prevent the cold start offset of the first cycle, as shown in Figure 45.

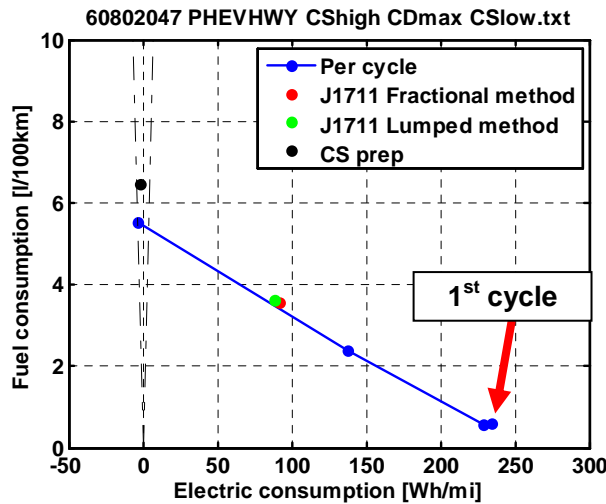


Figure 45. Energy and Fuel Consumption Summary for the Full-Charge Test with Prep cycle

This study was the first highway data set for a maximum-depletion blended-type hybrid available to CARB and the J1711 committee. The test results helped the committee change the proposed cold-start correction method. The open controller feature of MATT was used for this test to obtain a specific hybrid behavior to investigate.

Investigation on Soak Time Between Tests for Plug-In Hybrids

Soak Time between Tests for Plug-in Hybrids

As seen in some earlier PHEV tests, the temperature of the powertrain components have an impact on energy consumption — especially the engine and exhaust after treatment system. The engine operating temperature in PHEV operation is always low compared to the engine operating temperature in conventional vehicle testing. The first engine start seems to dictate the emission for the cycle.

This study aims to determine the impact of the soak time, which is the time from the end of the previous test to the actual start of the next test, on fuel consumption, energy consumption, and emissions.

The Proposed Design of Experiment

The test series involves performing continuous-set charge-depleting urban cycle testing by using varying soak times between the tests. The virtual battery and motor module presents a convenient advantage: immediate recharging of the battery pack to precise

SOC. That feature, along with automatic driver, makes MATT a very repeatable test platform. Figure 46 illustrates the continuous and uninterrupted test plan and test condition.

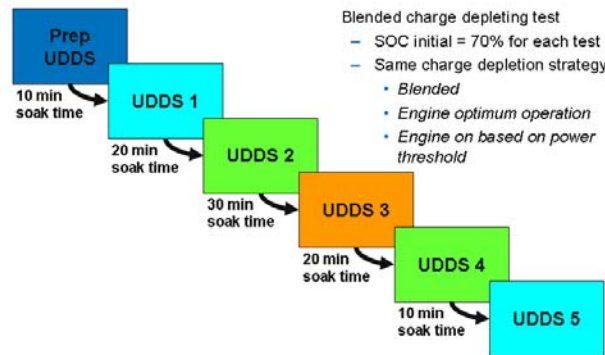


Figure 46. Soak Time Test Matrix

Some Specific Cycle Results

Since it is a charge-depleting test, the engine usage is low, as shown in Figure 47. The major hydrocarbon spike occurs at the first engine start. For the next engine start, the hydrocarbon spikes are low, except for the last engine start after an 800-second cool down.

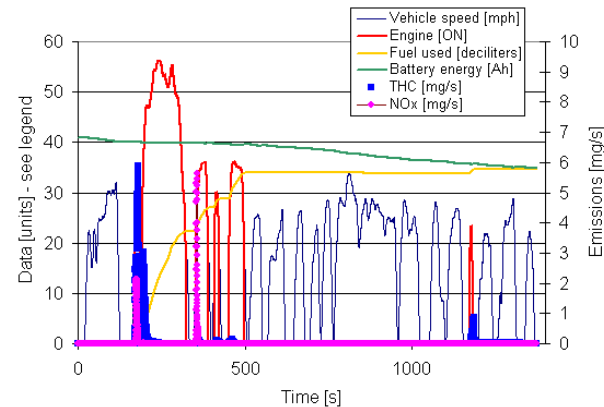


Figure 47. First Test after 10-min Soak

All the important temperatures for the UDDS 1 are shown in Figure 48. The thermostat never opens on these tests; thus, the engine coolant heats fast and stays warm in the block. The engine oil never reaches steady operating temperatures, either. The more interesting temperature to consider is that of the catalytic converter. Light off temperature is between 200 and 300°C, thus explaining the first engine start hydrocarbon emissions. At the last engine start, the catalyst temperature drops below 300°C again, which may explain the more pronounced hydrocarbon slip.

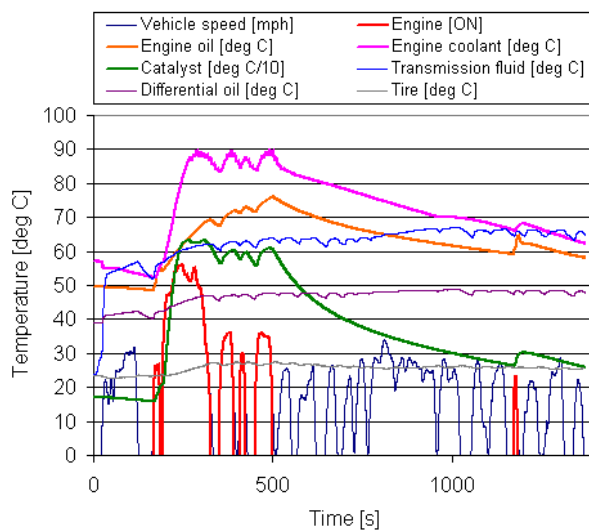


Figure 48. Temperature Information from the First Test after 10-min Soak

Additional interesting information is a thermal image taken at different points for the test set. Figure 49 shows just a few sample pictures. There is an obvious difference in temperature at the end of the 20-min soak time compared to the 10-minute soak time. The catalytic converter insulation is very good since the temperature outside of the can is similar at the end of a test and then 10 or 20 minutes later.

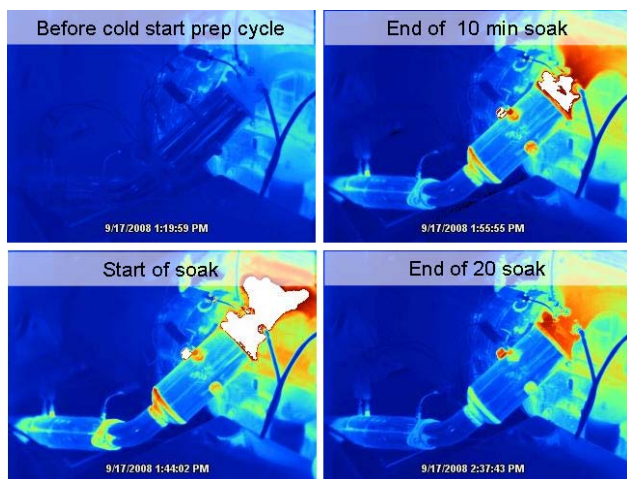


Figure 49. Thermal Images of the Exhaust System on MATT

Throughout the six tests performed, five of the tests are completely identical in terms of engine operation. The test after the first 20-minute soak period had an extra engine start. Despite of the difference, the repeatability of five out of six tests is good. Figure 50 supports the repeatability in the test results.

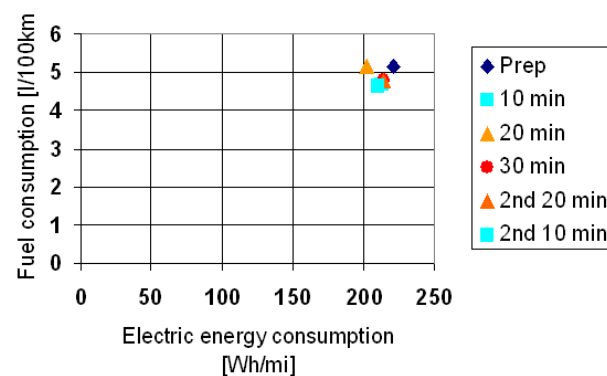


Figure 50. Fuel and Electric Energy Summary for the Soak Time Tests

The prep cycle, which was not a cold start, used the most fuel and electric energy, as expected. The results of the 10-, 20-, and 30-minute soak test are very close. If the one 20-minute soak time test with the extra engine start is set aside, a pattern is visible. The 10-min soak tests use less energy overall, and the longer the soak time, the more fuel and electric energy is used. The difference in the results is not very significant or pronounced.

The emissions results are shown in Figure 51. The prep cycle has the highest emissions, as again expected. After that, all of the tests (except for the one test with the extra engine start) have very similar emissions. Thus, it appears that the soak time has no significant impact on the emissions behavior.

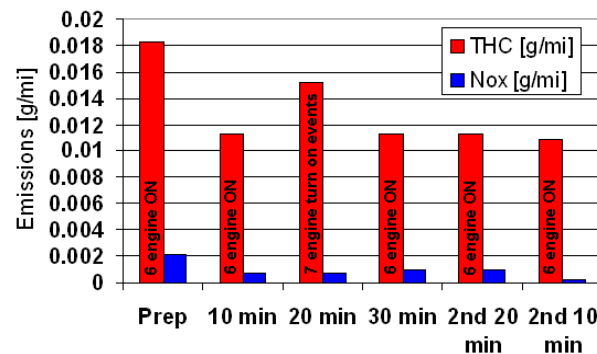


Figure 51. Emissions Summary for the Soak Time Tests

Conclusions

MATT is operational and generating data to answer very specific questions. The hardware has matured to be representative of current hybrid technologies. The engine efficiency and emissions are generated by hardware and thus represent the cold-start effects,

which are difficult to capture in simulation, especially for emissions.

The baseline PHEV hybrid operation has been developed and tested. Some interesting findings on the emissions behavior will result in changes that will be implemented in the control strategy to improve the trade-off between fuel economy and emissions.

A number of studies were performed to serve the hybrid test procedure development. The highway cold-start correction method for PHEVs had a significant impact on the outcome of the proposed standard.

C. Active Combination of Ultracapacitors with Batteries for PHEV ESS

Theodore Bohn (Project Leader)

Argonne National Laboratory

9700 South Cass Avenue

Argonne, IL 60439-4815

(630)-252-6592; tbohn@anl.gov

DOE Technology Manager: Lee Slezak

(202) 586-2335; Lee.Slezak@ee.doe.gov

Objective

Investigate the physical and control limitations of a minimally sized ultracapacitor bank actively coupled via power electronics to an energy density optimized battery for a net reduction in plug-in hybrid vehicle/electric vehicle (PHEV/EV) energy storage system (ESS) size and cost.

Approach

Form a collaborative partnership with the ultracapacitor manufacturer (Maxwell Technologies) to obtain access to the latest component models, industry trends and insights, and robust production-grade hardware.

Create an actively coupled ESS model with an idealized power converter by using the Maxwell reduced order ultracapacitor model and Argonne National Laboratory (ANL) battery models.

Develop capacitor state-of-charge (SOC) regulation control software in Matlab Simulink to maintain usable power delivery and power absorption capability during the dynamic drive cycle demands.

Run simulations, including global optimization of control parameters, to tune the controller software to allow the ultracapacitor/power electronics branch of the ESS to handle rapidly changing current demands and allow the battery to address the slowly changing current demands.

Assemble a full-sized (108 cell) bank of 650 Farad ultracapacitors with instrumentation to track the balance of capacitor voltages and temperature gradients. Run this capacitor bank on the Aerovironment ABC170 power processor as part of the ANL Battery Hardware-in-the-Loop (HIL) test stand. The ABC170 emulates the DC/DC converter that actively couples the ultracapacitor bank to the battery pack.

Implement dSpace-based control system software in the MotoTron stand-alone electronic controller module (ECM) that communicates via CAN with the Brusa BDC412 stand-alone DC/DC converter as an example of actively coupled capacitor/battery ESS.

Accomplishments

Formed a collaborative partnership with Maxwell Technologies. Obtained production capacitor hardware and models.

Constructed an actively coupled capacitor-battery ESS model and four iterations of SOC regulation, including global optimization routines for tuning.

Verified through model results that a compact, 72-Whr (40-lb) ultracapacitor bank could achieve the desired transient decoupling goals under ideal conditions (i.e., a priori knowledge of the drive cycle).

Constructed a full-size (300-V; 72-Whr) ultracapacitor bank with instrumentation. Completed voltage step response checkout tests on the ABC170 test stand.

Obtained a Brusa BDC412 DC/DC converter and MotoTron ECM hardware. Initiated construction of controls and the power lead wiring harness.

Presented papers on this subject at the SAE Congress, the EVS23, the IEEE Vehicle Power and Propulsion Conference, the Advanced Automotive and Ultracapacitor Conference, and the Advanced Capacitor World Summit.

Future Directions

Continue tuning the controller software to balance the SOC window with the aggressiveness of peak power reduction from the battery side of the ESS by relying on insights gained on the Battery HIL test stand and using the ABC170 as the DC/DC converter.

Investigate the limitations of the battery-only ESS at high SOC and low operating temperatures, as well as the estimated reduction in power capability at the end of life. Run the same battery at these conditions with and without the actively coupled ultracapacitor system.

Implement a lower power density, higher energy density battery on the Battery HIL stand with the actively coupled ultracapacitor. The objective is to illustrate the ESS optimized for energy in the battery, and utilize the ultracapacitor array for power via active coupling using power electronics.

Complete implementation of the control software in the MotoTron ECM and Brusa BDC412 DC/DC converter. Run the system with a 300-V, 72-Whr ultracapacitor bank in the PHEV and hybrid electric vehicle. Investigate the impact of cold weather operation and the reduction of system losses to achieve a wider usable battery SOC window (Prius).

Work with the original equipment manufacturer and Tier I suppliers to identify the production cost/size of a DC/DC converter that meets the requirements for an actively coupled ultracapacitor system and an energy-optimized battery for a PHEV the size of a Chevy Volt.

Introduction

A PHEV has a much larger ESS than a charge sustaining hybrid vehicle. One of the main goals of a PHEV is to displace imported petroleum via renewable electricity or off-peak conventional generation resources. A major challenge in building a PHEV that compares with today's conventional vehicles is cost and added mass for the large battery. At 33 kWhr/gal of chemical energy in gasoline, a 10-gal tank can hold the equivalent of 330 kWhr. A PHEV with a 40-mi all electric range requires only a 16-kWhr battery pack, or 48 kg of ideal energy dense cells, based on the gravimetric energy density of some of the best currently available Li-ion battery cells with 250 Whr/kg. This does not include packaging. As a frame of reference, the T-packs shown in Figure 1 are for the Chevy Volt 16-kWhr ESS, weighing 170 kg, or 94-Whr/kg net energy density (Figure 1). The battery in this vehicle is a balance between energy storage capacity and power delivery capability. The battery is also oversized to deliver rated power at end of life (8 kWhr required for 200 Whr/mi*40 mi). The cost of this system is estimated to be in the \$500/kWhr range, or \$8,000.



Figure 1. View of Chevy Volt Battery Pack

The goal of this research is to investigate methods to combine the best attributes of power dense ultracapacitors with energy dense Li-ion batteries to obtain a lower net energy storage system cost than batteries that are a compromise between power and energy density. This is achieved by actively coupling the energy from the ultracapacitors, at a very high rate of charge/discharge, in parallel with the battery. In essence, by using power electronics the ultracapacitors can become the equivalent of "active suspension" to decouple "bumps" from the battery pack during acceleration and braking events. As such, the battery current capability requirements can be

greatly reduced, thus allowing a more energy dense battery to be used in PHEVs of this type.

In addition to reducing power demand stress on the Li-ion battery, the actively coupled ultracapacitor ESS can increase the allowable operating conditions of the Li-ion battery. These include:

1. Operation at low temperatures (at below -20°C , Li-ion batteries generally need to limit the discharge rate to lower than C/5, or only 8 amps for a 41-Ahr/10-kWhr pack);
2. Operation at high SOC (at above 80 percent SOC, most batteries must progressively limit the charge acceptance rate to eventually less than C/2 near 100 percent SOC); and
3. Operation at low SOC (battery impedance increases at low SOC, and internal heat generation/losses increase).

One of the practical benefits of separating the energy storage system for a PHEV into two sections is that the ohmic (I^2R) losses can be relocated into the high current capability ultracapacitors, which have a much lower impedance than batteries and a better surface area for cooling. In other words, the actively coupled capacitor ESS relocates the heat outside the batteries, thus allowing the batteries to be more densely packaged, with thicker electrode material.

As mentioned above, the goal is to reduce the net ESS cost with increased performance and net energy density. The additional cost of the power electronics and ultracapacitors is postulated to be offset by the lower cost, higher energy density batteries.

Another goal of this research is to reduce the total volume of the ESS by cutting the battery size by approximately 50 percent and adding back approximately 30 percent of the volume with ultracapacitors and electronics. Figure 2 shows the JCS VL41M-based 10-kWhr/260-V/41-Ahr liquid-cooled Li-ion battery pack in the rear of a PHEV prototype vehicle. On the right of Figure 2 is the 3-inch-high ultracapacitor bank with the same length and width of the JCS battery pack.



Figure 2. Size Comparison of the Ultracapacitor Array Approach

A collaborative partnership was established with the ultracapacitor manufacturer, Maxwell Technologies. Maxwell provided production grade ultracapacitor hardware, including interconnection bus work and cell protection (voltage balancing/clamping) circuit boards. Maxwell Technologies has moved away from the moment matching technique of ultracapacitor cell and module electronic equivalent circuit representation.

Energy Storage System Component-Level Modeling

A reduced order model that contains the essentials of the moment-matched model is retained along with significant improvements in terms of frequency response and pulse current “ionic tailing.” The simpler model structure along with underlying parameter links to voltage, temperature, and time or cycling exposure round out the model. The nonlinear, voltage-dependent main capacitance element of the moment matched model is retained in the reduced order model, not as the discrete cascade of three time constants, but as a single time constant approximation to double layer capacitance behavior. The equivalent circuit model is shown in Figure 3. This illustrates a reduced order ultracapacitor model for the non-linear relationship of capacitance as a function of voltage simplified implementation of the ultracapacitor behavior into the control software.

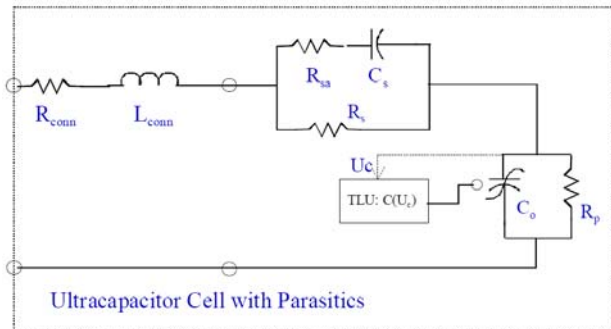


Figure 3. Circuit Diagram of Ultracapacitor Model

A component-level model of the actively coupled ultracapacitor/battery energy storage system was created by using Matlab Simulink and ANL HIL component libraries. The electrical system topology is shown in Figure 4 with the DC/DC converter acting as an “active resistance” to regulate the current sharing of load demand between the battery and ultracapacitor.

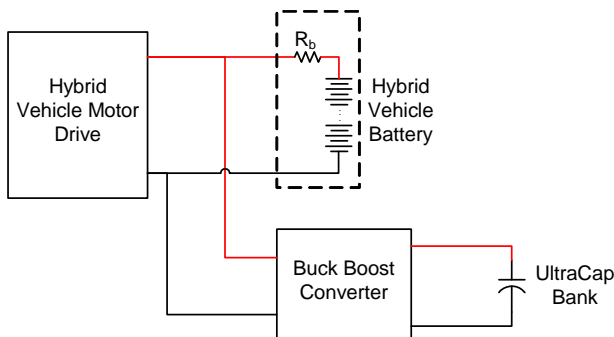


Figure 4. DC/DC Converter Acting as an “Active Resistance”

Control Strategies

As part of the iteration process of experimentation, four different control strategies were implanted in the evolution of control strategy software.

1) Active Resistance (Figure 5)

In this approach, the ultracapacitor behaves as a second battery with significantly lower internal resistance, actively varied as a function of the power electronics.

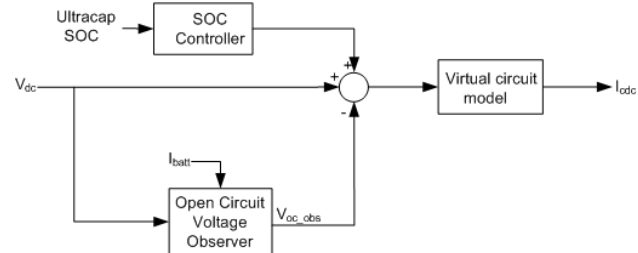


Figure 5. Schematic of “Active Resistance” Circuit

Drawbacks for this method are that it is not as robust as other control methods and is somewhat complex to properly tune. In addition, an open circuit voltage observer requires accurate battery parameter information.

2) State Feedback Partitioning (SFbP) with a Static SOC Set Point (Figure 6)

In this approach, the battery/ultracap current proportions are frequency based, where the fast transient components are handled by the ultracapacitor bank and the slower demand by the battery. The SOC controller attempts to maintain 50 percent SOC to balance power delivery and acceptance capacity. This method, shown below, is easier to tune than the first method.

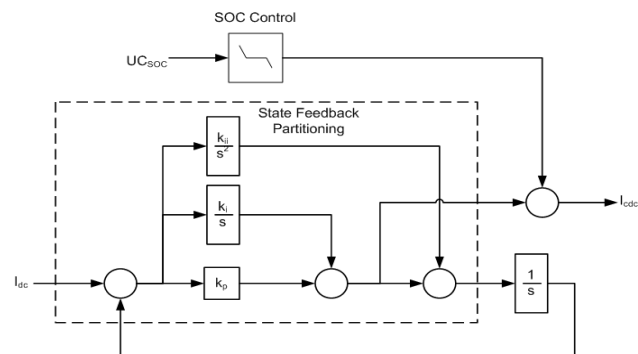


Figure 6. State Feedback Partitioning

3) Global Optimization

This method uses the ideal power model of battery and ultracapacitor, but it requires full knowledge of the future power demands. It also provides a benchmark for the best possible results. The Labview implementation is shown below as a multi-threaded approach leading to fast execution times. The cost function (in global optimization lingo) is assigned to reduce battery root-mean-square (RMS) current, which also leads to reduced ohmic losses. It is based on a simple power-based model.

4) State-Based Feedback Partitioning (SFbP) with a Dynamic SOC Set Point (Figure 7)

Similar to the control block diagram for the second strategy, this control strategy splits the battery/ultracapacitor current based on frequency (i.e., the ultracapacitor for fast current demands and the battery for slower demands). The SOC controller uses vehicle speed to determine the correct ultracapacitor SOC regulation (as a dynamic set point). The vehicle speed input is used to “predict” the next direction for the current command. For example, if the vehicle speed is 60 mph, it is likely that the next current demand will be for regenerative braking, and the capacitor SOC is diminished in anticipation of the incoming charge.

Capacitor/Power Electronics Experiment Hardware

The initial goal was to demonstrate the cost, mass, and volume downsizing from the JCS VL41M 10-kWhr Li-ion battery pack, which is built for PHEV applications. The battery size is 617 mm × 690 mm (24.3 in. × 27.2 in.). As mentioned above, the 108-cell capacitor bank was designed to fit on the top of this battery. “Figure 7 shows the physical capacitor bank.” The net voltage is ~300 V max, and net capacitance is 650 F/108=~6 Farad, for a total stored energy of approximately 72 Whr. The total capacitor mass is 21.6 kg/47 lb.

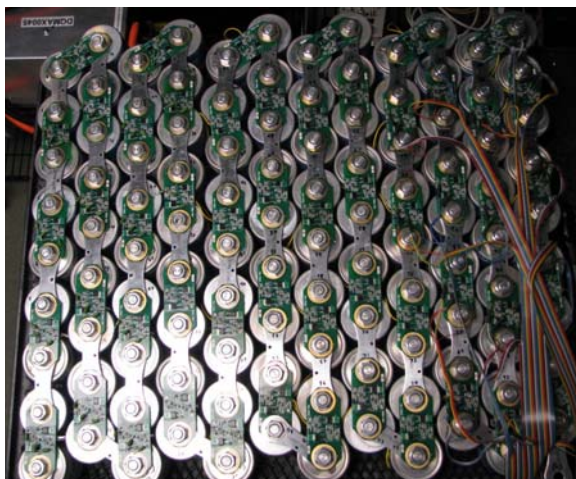


Figure 7. Top View of Ultracapacitor Array

Safety System

The overall ultracapacitor bank is fully monitored via a Keithley 2750 multiplexing DVM, with serial data output to be merged with data collected from dSpace. This 200 channel measures each of the 108 capacitor voltages, as well as 40 thermocouples, to analyze thermal gradients on heat generated in the capacitor bank. The Keithley Model 2750 unit is pictured in Figure 8.



Figure 8. Keithley 2750 Multiplexing DVM Instrument

Battery Hardware-in-the-Loop Test Stand

The ANL Battery HIL stand is shown in Figure 9. The dSpace control rack in the center runs the vehicle models and sends current commands (via CAN) to the ABC170 power-processing unit (shown on the right). The physical JSC VL41M battery is connected to Channel A, and the ultracapacitor bank to Channel B. The thermal chamber on the left can be used for simulating hot or cold operating conditions on the battery or capacitors.



Figure 9. Argonne Battery Hardware-in-the Loop Test Facility

Sensor Locations

Figure 10 shows the location of the branch current sensors and components for this experiment. In this case, the power electronics is the ABC170 Power Processing unit. In later experiments, it will be an automotive-grade stand-alone DC/DC converter. The central control unit is all a part of the Battery HIL stand, located in the dSpace controller. Later experiments will have an automotive-grade control module that outputs CAN messages in the same manner as the dSpace unit.

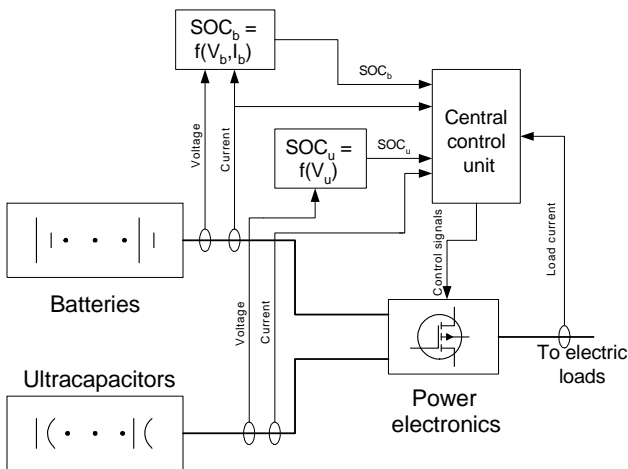


Figure 10. Component Layout for this Experiment

Automotive-Grade Power Electronics/Controller

Figure 11 shows the 60-kW (peak) Brusa BDC412 DC/DC converter. It is an example of high efficiency soft switched state-of-the-art power electronics, with a water-cooled package. The Denso 1,600-W DC/DC converter from the Camry 14-V system is shown on top of the Brusa converter as a power density comparison for air-cooled electronics. The cutaway component to the left of the Brusa converter is the boost inductor from the Prius 21-kW DC/DC converter. In the future work of this research, significant resources will be expended to reduce the size and cost of this boost inductor, which is one of the most bulky and costly components in the system.



Figure 11. 60-kW (peak) Brusa BDC412 DC/DC Converter.

The Toyota Camry 35-kW DC/DC converter, shown in Figure 12, is another example of the packaging density of state-of-the-art automotive-grade power electronics. Incorporating this power electronics package was part of the original experiment plan. After further consideration, there was little to be learned by the 100-amp current limit of this converter.



Figure 12. Toyota Camry 35-kW DC/DC Converter

Results

Hardware: The capacitor bank was assembled and the instrumentation was checked out. Simple ramp commands were executed by the ABC170 to verify the functionality and integrity of instrumentation. Controller strategies will be loaded into the Battery HIL to compare predicted performance with actual capacitor response, and the thermal performance of ultracapacitors will be monitored.

Software: The ultracapacitor-battery ESS model (Figure 13) was constructed with four iterations of SOC regulation controls, including global optimization routines for tuning.

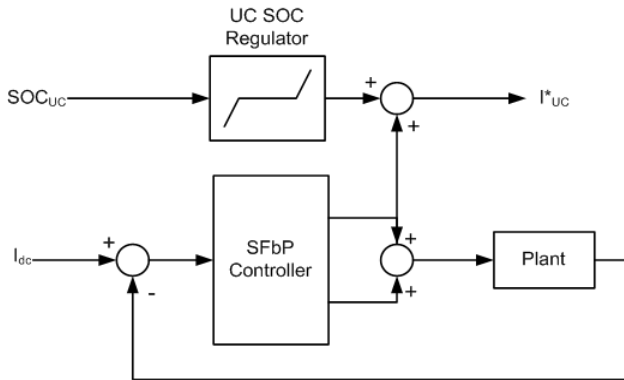


Figure 13. The Ultracapacitor-Battery ESS Model

Simulations of ESS are based on the JCS VL41M Li-ion battery from the Powertrain System Analysis Toolkit (PSAT), the Ultracapacitor models from Maxwell technologies, and the initial power converter. The power converter was assumed to be the ideal response with a single resistance on high side of converter (97 percent full load efficiency).

Simulation Study of Capacitor Sizing

Figure 14 shows that as the capacitor bank size (stored energy) is increased (with the State Feedback Partitioned controller frequency at 0.01Hz and SOC gain at 200A/%), there is a point of inflection around the 100-Whr mark for the various drive cycles in a PHEV the size of a Saturn Vue. This is the point where the system controller can handle all the current requests.

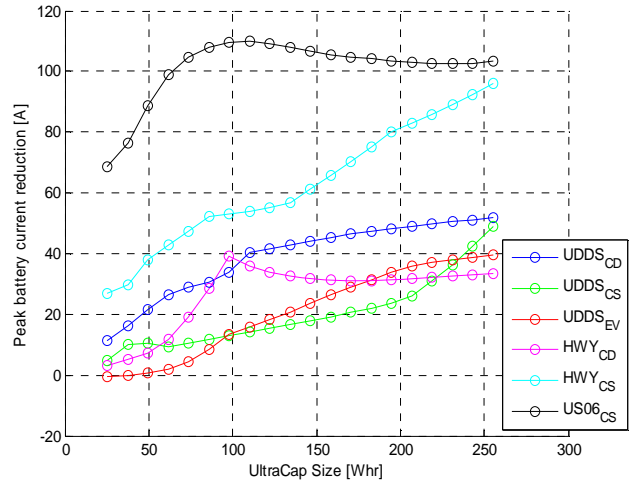


Figure 14. Simulation Study of Capacitor Sizing

Controller Tuning: Further simulation shows that the 64-Whr ultracapacitor bank and 200A/% SOC gain has a cycle-dependent optimal frequency. Figure 15 shows that if the tuning (SFbP) frequency is set too high, there is not much call for this dynamic content. If it is too low, the capacitor bank overcharges or fully discharges.

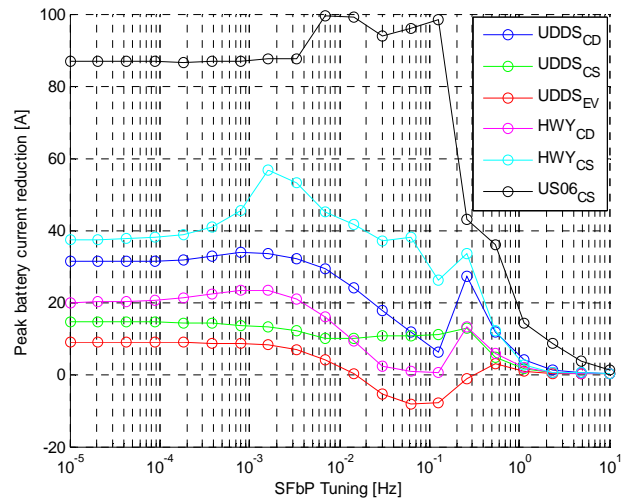


Figure 15. Controller Tuning Exercise

SOC Gain Tuning: The simulation results in Figure 16 show the variation of SOC gain from 0 to 500A/% for the various drive traces and a 64-Whr capacitor bank, with an SFbP gain of 0.01 Hz. It also shows that if the gain is set too high, the SOC window goes unused for these drive traces and is effectively reduced. Further, it shows that SOC gain must be dynamically adjusted (not fixed) to yield consistent results.

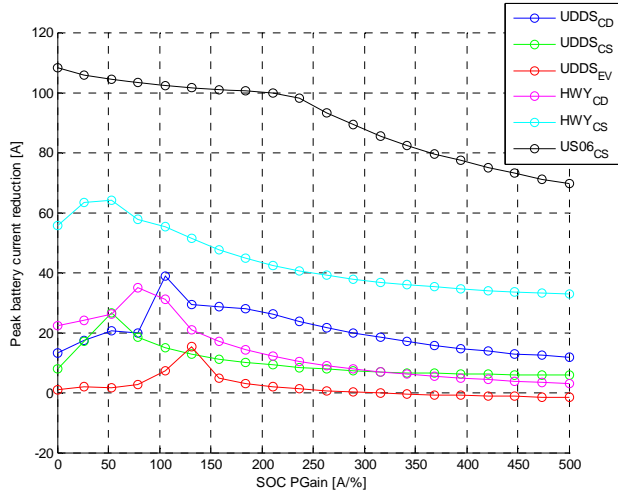


Figure 16. SOC Gain Tuning Exercise

Active Resistance Strategy: Figure 17 shows the composite current sharing of current among the load, battery, and ultracapacitor. The legend shows the dynamic (blue) load trace, taken from a Toyota Prius on the US06 cycle, which is the battery current without the ultracapacitor. The green trace is the equally dynamic capacitor current. The greatly reduced and smoothed red trace is the battery current with the ultracapacitor peak shaving effect.

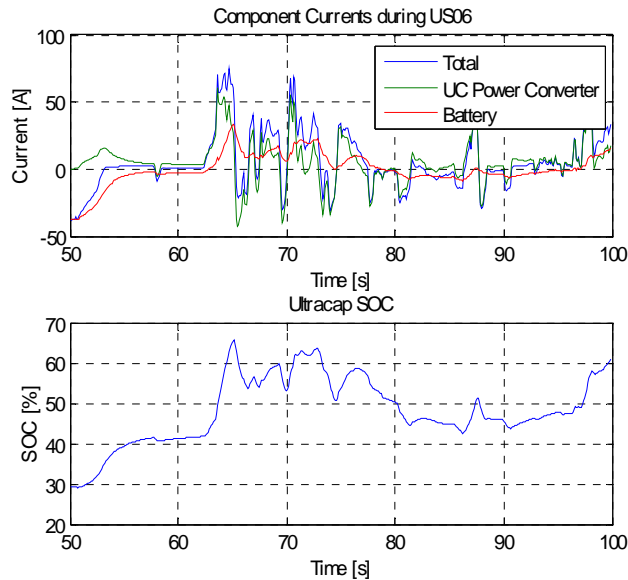


Figure 17. Active Resistance Strategy

Static SOC Gain-Based SFbP Strategy: Figure 18 shows the power profile for the ANL TTR PHEV prototype vehicle (through-the-road parallel, Saturn Vue Greenline Chassis, 75-kW rear drive system). The battery RMS current reduction vs. corner

frequency of the controller plots show that only frequencies below .01Hz are useful. This runs counter to intuition, based on the rate that a person depresses the accelerator in a vehicle. One would think the response would need to be faster.

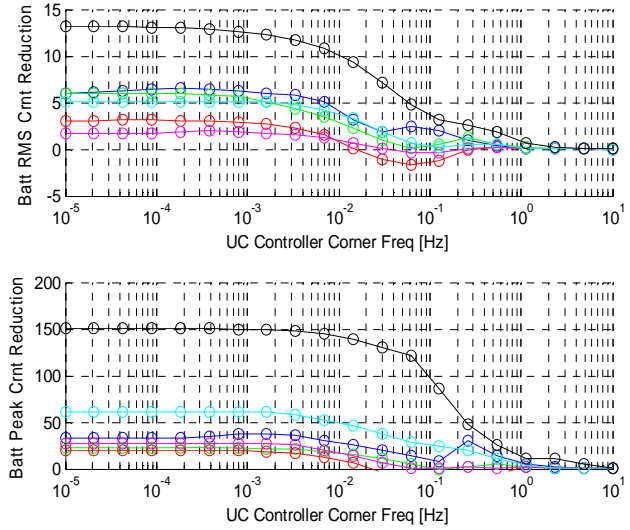


Figure 18. Static SOC Gain-Based SFbP Strategy

Global Optimization Strategy: The global optimization strategy results plot is shown in Figure 19. The preconditioning of the ultracapacitor bank is perfectly optimized, such that the battery current only changes when the ultracapacitor is empty or full. With this strategy the ultracapacitor is full before an acceleration cycle and empty before a regeneration event.

Figure 20 shows that SOC and vehicle speed have good correlation.

State Feedback Partitioned (SFbP) with Speed

Proportional SOC Gain Strategy: Based on the correlation plot in Figure 20, the correlation plot shown in Figure 21 was derived/mapped to constrain SOC to average (50 percent), since the next speed change is not very logical or predictable.

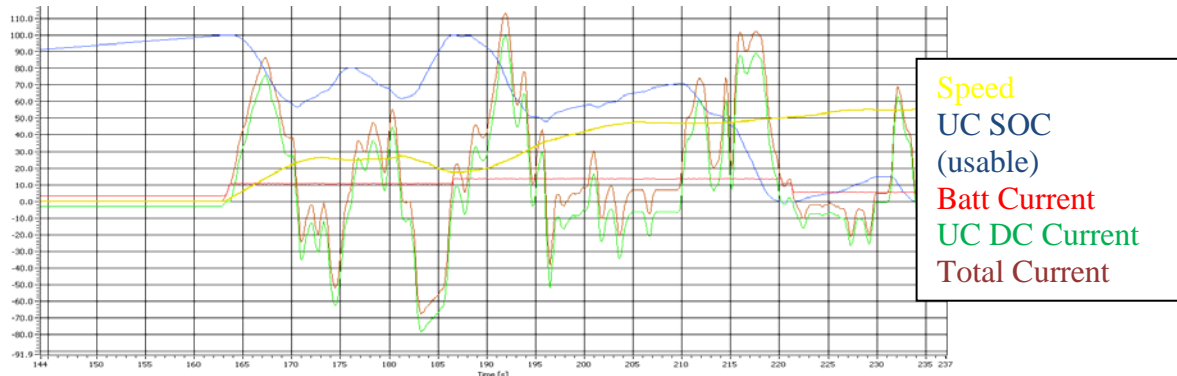


Figure 19. Global Optimization Study

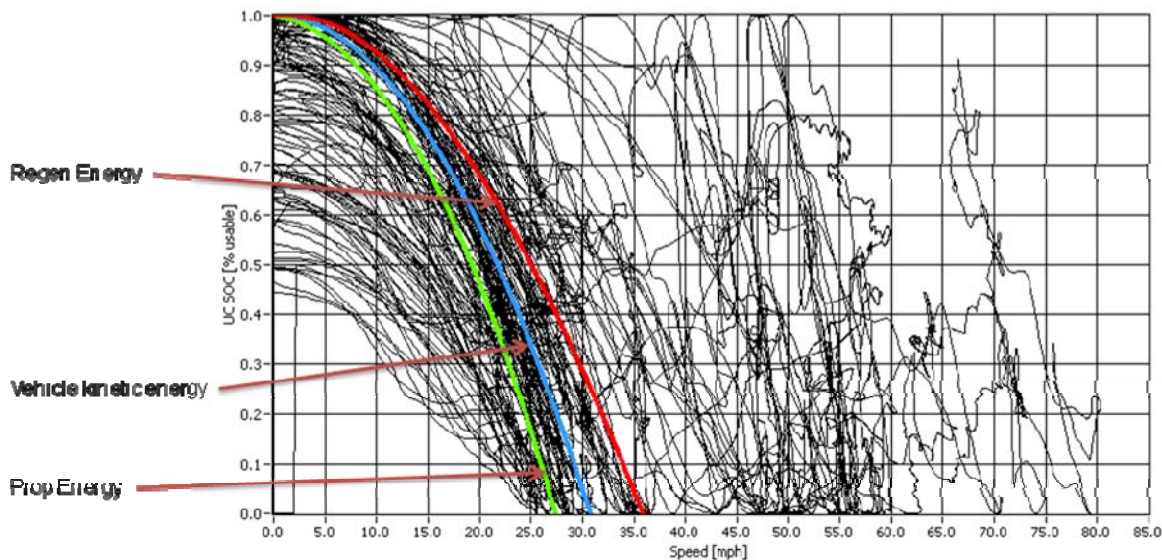


Figure 20. Demonstration of SOC and Vehicle Speed Correlation

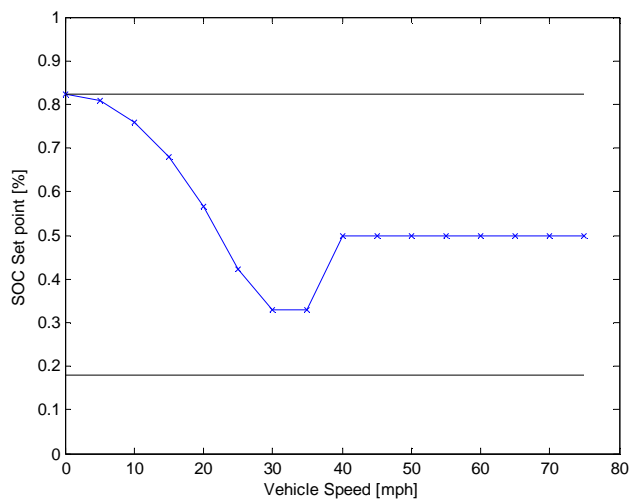


Figure 21. State Feedback Partitioned (SFbP) with Speed Proportional SOC Gain Strategy

Battery RMS Current Reduction with Real World (150 A) Constraint: A summary chart of the RMS current with and without a power converter limit is shown in Figure 22.

As can be seen in Figure 22, the directly paralleled ultracapacitor had marginal benefit in reducing RMS currents. The charge sustaining US06 drive cycle,

which has high dynamic content, had the largest reduction in RMS current via the ultracapacitor bank active combination.

For completeness, the reduction of peak battery currents is shown in Figure 23. There is less of a benefit via this metric, but a notable reduction nonetheless.

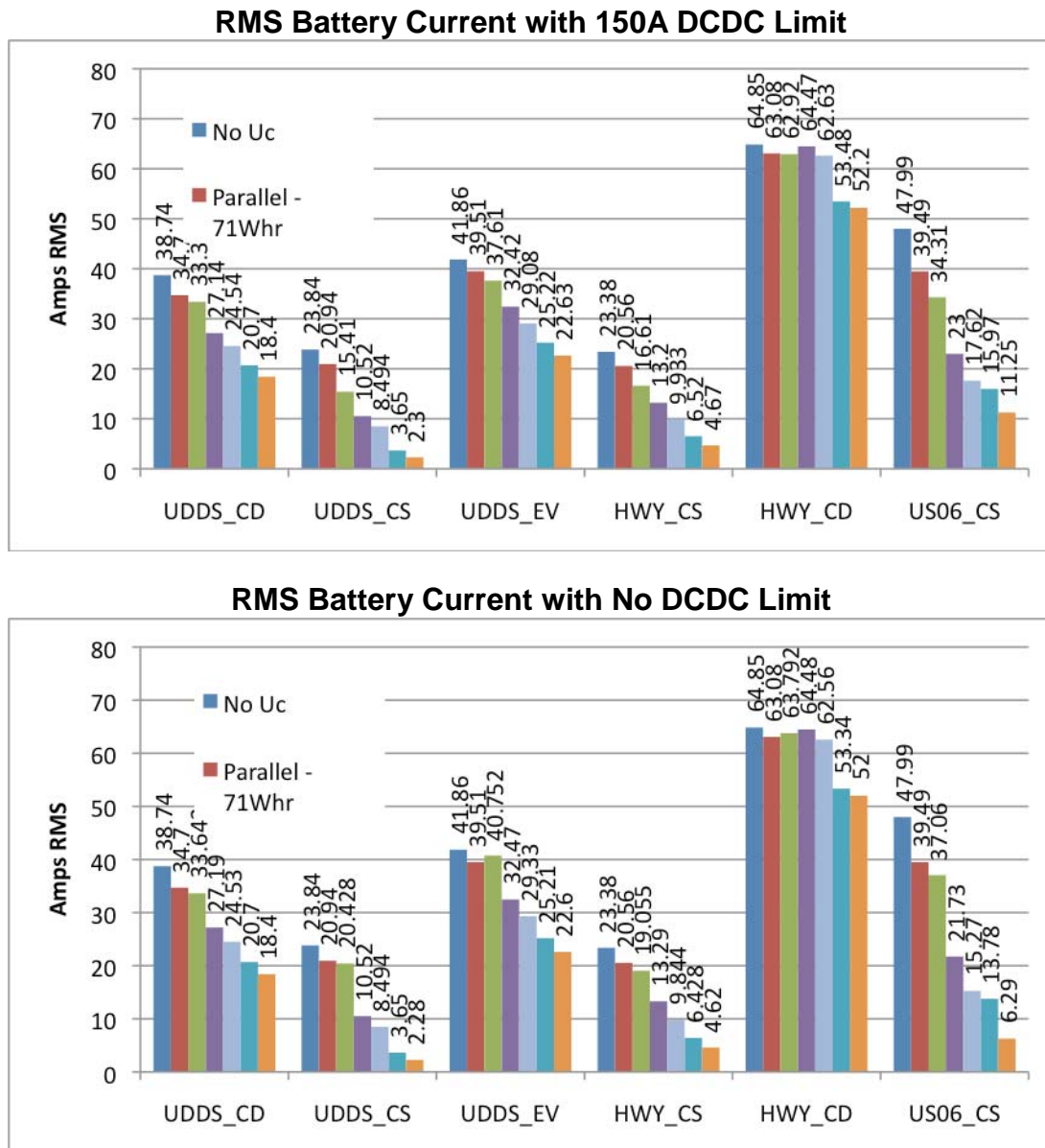


Figure 22. Battery RMS Current Reduction with Real World (150 A) Constraint

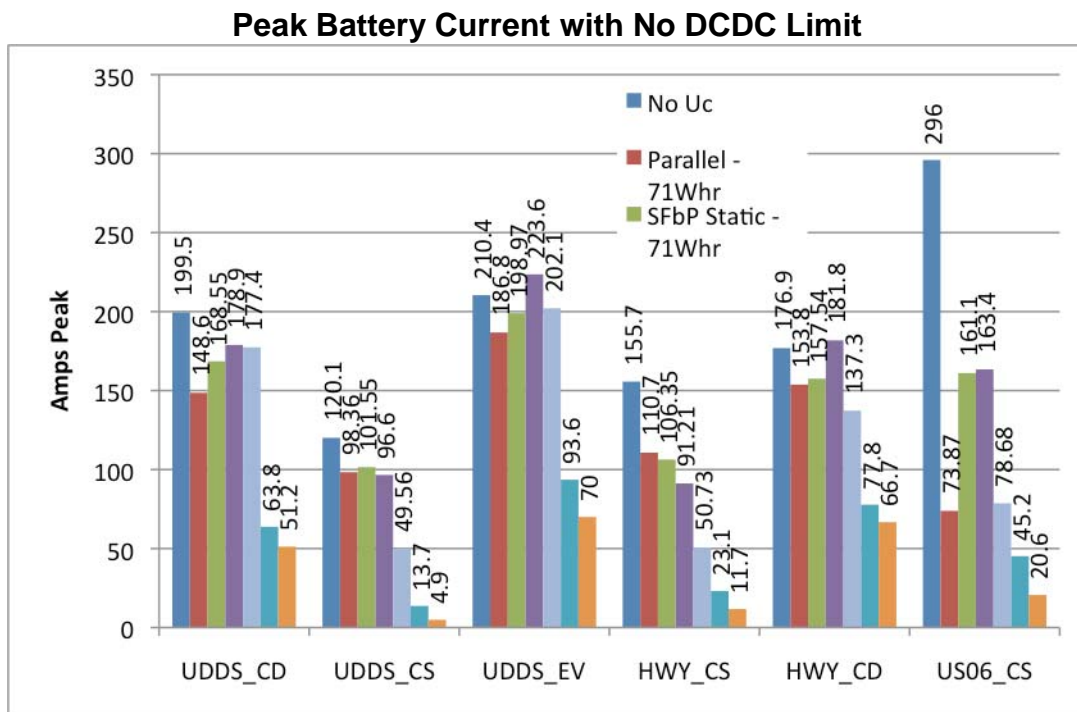


Figure 23. Battery Current Limit with no DC/DC Limit

Summary

A functional current regulator for the active combination of ultracapacitor/battery was developed for this research task. Various control strategies were exercised, and the results were used to iterate on other control strategies. The final vehicle speed-based SOC state feedback portioned control was the most effective.

Also shown is that a 72-Whr total ultracapacitor bank was able to meet most of the goals for reducing RMS battery currents, which could allow for a lower power density battery with higher energy density. This could arguably reduce the net system cost of the PHEV ESS.

Conclusions

A hardware experiment has been constructed and debugged. Voltage step response tests were run on

the ultracapacitor bank, but not the above current decoupling experiments. There have been challenges in getting through the safety approval process at ANL due to the difficulty in locating experts in ultracapacitor ESS safety. This is a relatively new application with new safety concerns related to the high power discharge capabilities of ultracapacitors in the case of a fault. The simulation results above confirm that, in ideal conditions (i.e., a priori knowledge of drive cycle), a compact 72-Whr (40-lb) ultracapacitor bank could achieve the desired transient decoupling goals.

A Brusa BDC412 DC/DC converter and MotoTron ECM hardware have been obtained. Controls and power lead wiring harness construction has been initiated.

D. PHEV Development Platform — Through-the-Road Parallel PHEV

Theodore Bohn (Project Leader)

Argonne National Laboratory

9700 South Cass Avenue

Argonne, IL 60439-4815

(630) 252-6592; tbohn@anl.gov

DOE Technology Manager: Lee Slezak

(202) 586-2335; Lee.Slezak@ee.doe.gov

Objective

Investigate the benefits of plug-in hybrid electric vehicle (PHEV) control strategies and the influences of components on overall vehicle performance. Part of the objective is to create an open controller PHEV platform to achieve this goal, since there are currently no production PHEVs available. Such a platform is also useful in support of the PHEV Test Procedure Development task, as well as the Collaborative PHEV Testing Program with Research/Regulatory Agencies (California Air Resources Board, U.S. Environmental Protection Agency, and Japan Automobile Research Institute).

Approach

Create a through-the-road (TTR) parallel hybrid configuration PHEV prototype based on a Saturn Vue Greenline mild hybrid SUV for the front drive axles and a fully capable electric drive system for the rear axles.

Fully instrument the vehicle, including axle torque sensors for each of the four wheels as well as exhaust temperatures, and include a real-time fuel flow meter. Format CAN-based information for data collection during testing, with tables for calibrated engineering units.

Implement a low-level control system that intercepts and supersedes the CAN messages to the stock vehicle components, such as the engine, starter/alternator, throttle, and brake. A second electronic control system has been implemented via a MotoTron electronic controller module (ECM) to achieve this functionality. Matlab-Simulink software can be compiled and targeted into this ECM via MotoHawk software.

Design, debug, and deploy a high-level vehicle control system, based on the Powertrain System Analysis Toolkit (PSAT) simulation tool existing control blocks. This bridges the low-level controls and sensor information into the vehicle controller, thus allowing the core low-level controls to operate as a separate functional layer. The completed high-level controls allow vehicle simulation of control strategies to be evaluated in a physical vehicle on a somewhat apples-to-apples comparison level.

Fully debug a prototype vehicle on the chassis dynamometer. Conduct performance experiments to evaluate various PHEV components and control strategies.

Accomplishments

Acquired several representative electric drive systems for the TTR parallel PHEV prototype platform, including a 75-kW liquid-cooled permanent magnet motor mated to a low-cost automotive gearbox installed in the rear of the TTR vehicle. Designed an air-cooled 150-kW (peak) AC induction drive system to fit in same rear drive location by using the same motor mounting system and gearbox. No structural modifications were made to the Saturn Vue stock vehicle. Made the addition of installing full axle torque instrumentation.

Mounted a JCS Prototype 10-kW liquid-cooled Li-ion battery system with a battery management system onto vibration isolation mount struts to decouple road fatigue from a non-road-rated battery. Mated a Brusa CAN-based 1.6-kW charger to the battery.

Fabricated a 5-kWhr Panasonic NiMH battery system, along with a cooling system and an E-Vision battery monitor.

Designed a Continental Automotive Battery management module interface; however resources are lacking for non-proprietary software development.

Incorporated a MotoTron CAN-based ECM in the rear of a TTR prototype to override stock Saturn Vue ECM signals to the belt alternator starter (BAS) system, and added sensors to the accelerator and brake signals. Used CAN sensor information/status traffic in a stock Saturn Vue as inputs to ECM.

Developed low-level control system software in Matlab-Simulink and targeted it to the MotoTron ECM by using MotoHawk software and a Greenhills compiler to tie high-level vehicle control software to basic I/O functions. (Debugged and fully developed on the chassis dynamometer.) Integrated a data collection system with low-level software via monitoring and compression of CAN data in engineering units (roots of ARDAQ).

High-level control system software was based on the PSAT simulation tool. Existing control blocks bridge the low-level controls and sensor information into the vehicle controller. The high-level controls allow vehicle simulation of control strategies to be evaluated in a physical vehicle on a somewhat apples-to-apples comparison level (simulation results compared with physical vehicle testing results).

Conducted many weeks of vehicle testing and developed software on the Advanced Powertrain Research Facility (APRF) chassis dynamometer to produce a wide arc of vehicle data and results on this particular powertrain topology (TTR) in a crossover-size SUV, with full electric drive operation for up to 40 miles.

Examined the all-electric-range (AER) capability to test and develop procedures used to minimize the dynamometer test time required for the SAE J1711 PHEV testing standards. Used the vehicle as a baseline for the SAE J1634 (Electric Vehicle Energy Consumption and Range Test), which will undergo renewal/revision in 2008/2009.

Used the PHEV prototype to develop a SmartCharge interactive charging system for the U.S.-Sweden joint PHEV research program. SmartCharge allows communication with utilities to determine the charge rate and the start time of charging to best utilize grid resources.

Used a second drive system and a battery with a spare vehicle chassis (1998 Chevy Geo) to emulate a series hybrid with a performance similar to the Chevy Volt (150-kW air-cooled AC drive, single speed gearbox, bi-direction power flow charger). Future work on engine/generator development is on hold.

Participated in media appearances on local Chicago news stations and Motorweek, as well as with Congresspersons Judy Biggert and Mark Kirk of Chicago. Held a booth at HybridFest 2007.

Future Directions

Continue tuning and rewriting high-level vehicle controller software to maximize vehicle petroleum displacement by optimizing the charge depletion/energy-blending rate from a 10-kWhr Li-ion battery pack.

Continue SmartCharging vehicle interface development for other funded work, as part of the U.S. Department of Energy (DOE)/Google/G.E. collaboration on PHEV charging infrastructure and informatics. This includes supporting the U.S.-Sweden joint research on PHEVs.

Use the platform for simulation-to-physical vehicle (apples-to-apples) evaluation of other energy storage systems (ESSs)/battery chemistries.

Implement and evaluate active combinations of ultracapacitor/Li-ion battery energy storage systems (ESS) for increased dynamic performance and increased operating range (i.e., full power at low temperatures, end-of-life battery, and full power absorption at high SOC).

Continue to support experiments for SAE J1771 and SAE J1634 vehicle testing standards.

Use the TTR PHEV platform as a research tool to compare and complement experiments at Argonne National Laboratory (ANL) that are run on the Battery Hardware-in-the-Loop (HIL) test bed and the MATT-HIL test bed.

Use the platform to evaluate other battery charging systems.

Use the platform as a potential tool to evaluate prototype electric machines in a real-world environment that includes gearbox and thermal constraints. Research funding would be obtained from the DOE Advanced Power Electronics and Electric Machines (APEEM) Project.

Use the series hybrid platform as a tool to emulate the Chevy Volt and investigate the impact of recent advances in small (sub-liter) engine technology in PHEVs.

Introduction

A PHEV has a much larger ESS than a charge-sustaining hybrid. Conversion kits are available to add more electrical storage capability to charge-sustaining (non-PHEV) hybrid vehicles, such as the Toyota Prius and Ford Escape. These vehicles were not designed to operate as electric vehicles over the full speed range needed to run even the Urban Dynamometer Driving Schedule (UDDS) urban drive cycle without starting the engine.

The AER operation is required up to 75 mph or more for experiments running the US06 drive cycle. The TTR parallel powertrain used in this task allows the front of the baseline Saturn Vue Greenline mild (42-V BAS) hybrid vehicle to be used without modification. External control of the engine, starter, and transmission is applied via interrupted CAN bus commands.

The rear of the Saturn Vue is already set to accommodate an all-wheel-drive rear differential and half shafts. These mounting locations and splined rear hubs make it possible to insert a rear electric drive system without modifying the structure of the vehicle. This avoids safety concerns over the crashworthiness of the vehicle when driven on public roads (such as to publicity events for public outreach/education). The rear cargo area of the Saturn Vue CUV is sufficient to carry the extra mass and volume of a 10-kWhr Li-ion battery ESS.

Approach

A simplified Labview component sizing tool was quickly created to examine the all electric driving range to estimate the range for various sized PHEV ESSs. A sample screen of this tool is shown in Figure 1. Vehicle load characteristic coefficients and test weight are inputs, as well as battery capacity and drive system efficiency. A plot of various battery size/range combinations is shown in Figure 2, from zero AER to 40 miles.

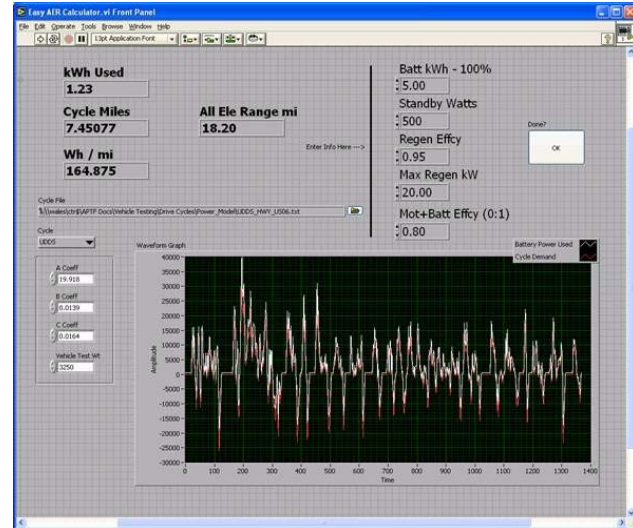


Figure 1. View of Labview Component Sizing Tool

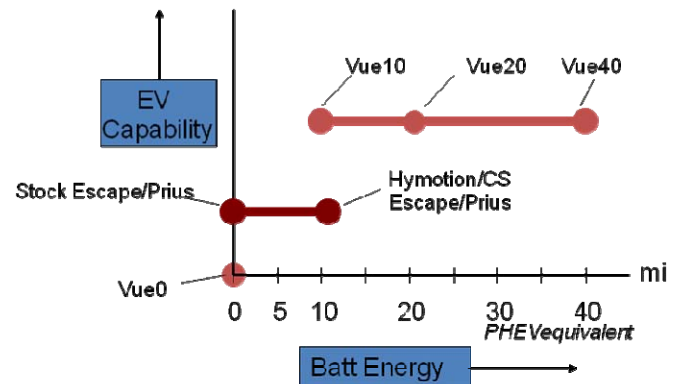


Figure 2. Battery Size and Range Combinations Considered

Even though the initially designed drive system was based on an aggressive 150-kW AC induction drive system, the specifications were altered with consensus among the ANL PSAT modeling group, Battery HIL experimenters, and MATT HIL experimenters. Each of these was emulating a Unique Mobility 75-kW (peak) liquid-cooled surface permanent magnet motor drive system.

One of the goals of the TTR PHEV research platform is to perform apples-to-apples comparisons among the simulation, emulation, and vehicle benchmarking results, on the same simulated and physical hardware.

To meet this goal, the drive system in the TTR platform was changed to the VL41M battery and UQM Powerphase 75-kW motor to match these other experiments.

The gear ratio for the drive system was evaluated and designed by using the above-mentioned simplified tool to calculate the required rear tractive effort in a vehicle this size. The plot of force, in Newtons, is

shown in Figure 2 for the UDDS drive cycle (8:1 overall selected). The vehicle with descriptive decals for public outreach and the 75-kW rear traction motor are also shown in Figure 3.

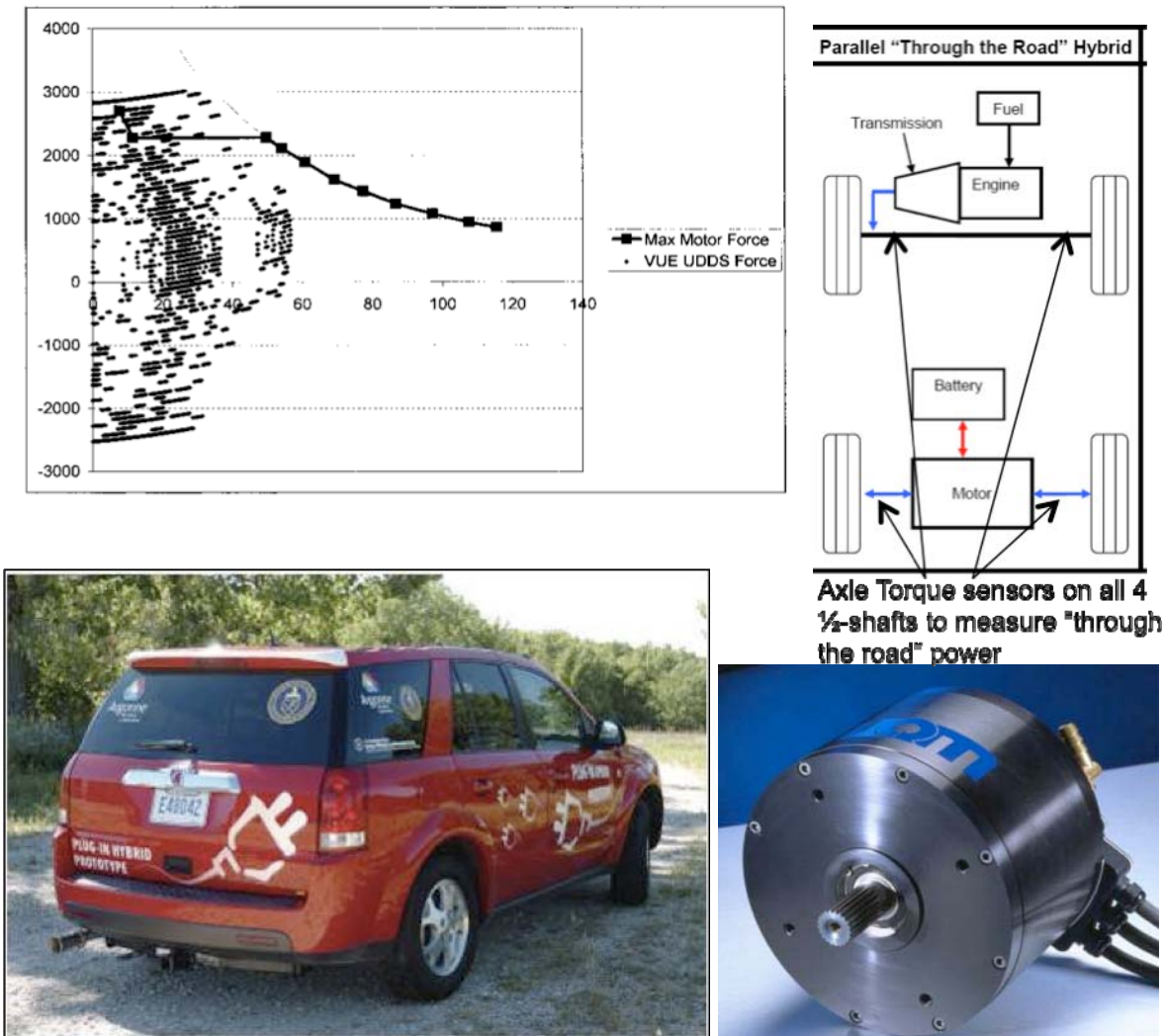


Figure 3. Picture of Prototype Vehicle and 75 kW Electric Motor Selected

The overall view of the stock Saturn Vue Greenline components is shown below in Figure 4, along with the basic block diagram for a TTR parallel hybrid.

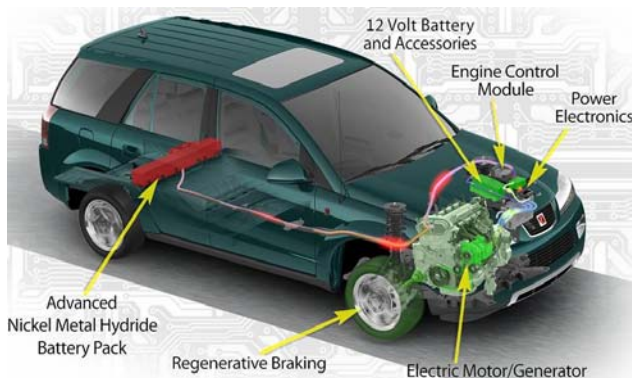


Figure 4. Stock Saturn Vue Greenline Mild Hybrid

Each of the half shafts connected to each wheel is instrumented with an axle torque sensor to measure torque “through-the-road.” One of these axle torque sensors is shown in Figure 5.



Figure 5. Axle Torque Sensor

One of the major constraints in constructing this vehicle was to avoid modifying the vehicle structure. The rear powertrain mounted in the stock Vue rear powertrain cradle is shown in Figure 6 with a UQM Powerphase 75 motor and a Civic SI 5-speed manual gearbox, rated for continuous power and torque above that of the UQM motor. Only two gear ratios—second and third gear range — are reasonable for this vehicle, thus allowing the option to select a gear ratio peak torque vs. high-speed power blending in experiments.

A transmission adapter plate was fabricated to mount the electric motor onto the transmission. Shown also is the custom flexible coupler-to-splined input shaft adapter. The three small bolts used to couple motor power serve as a mechanical fuse to limit torque to the transmission/axles in case of a software command error. This element was sheared early on during software development.



Figure 6.

Energy Storage System

To accommodate a variety of large (in volume and mass) ESSs for this PHEV platform, a large aluminum deck plate was installed in the rear cargo area of the vehicle, with rubber isolator bars for each installation and removal of the battery systems.

Three different ESSs were designed:

- 1) The first, shown in Figure 7, is a liquid-cooled JCS Li-ion 260-V/41-Ahr (10-kWhr) prototype battery that weighs approximately 150 kg.



Figure 7. Through-the-Road Parallel Hybrid Powertrain Design Detail

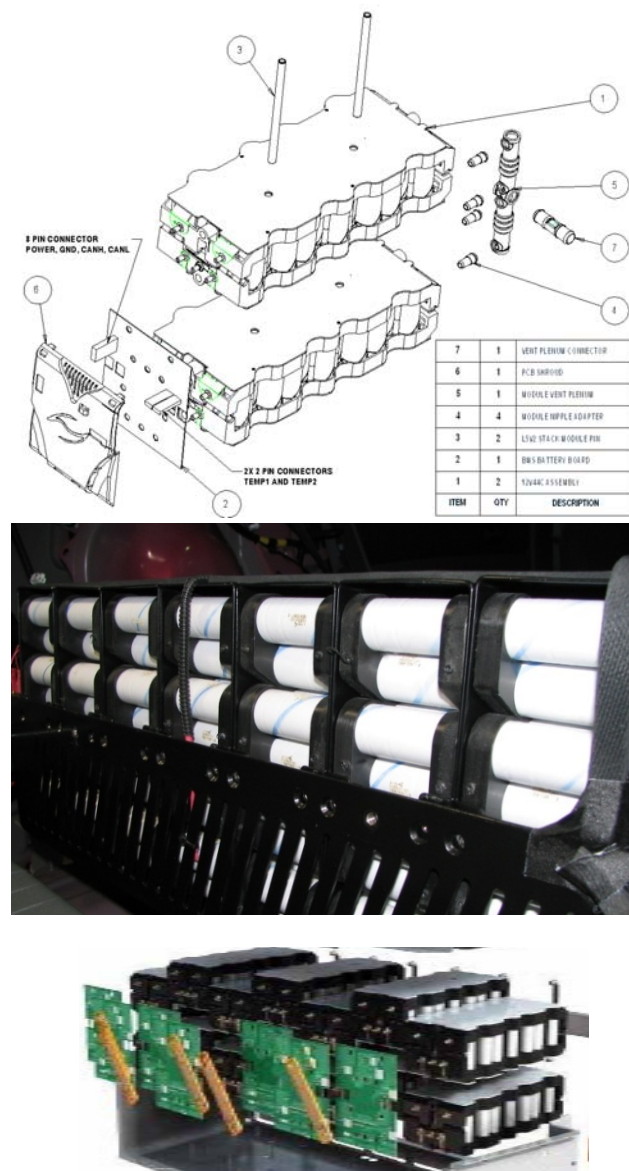


Figure 8. Alternative Battery Pack Design

- 2) The second battery is comprised of A123 Li-ion 2.6-Ahr cells, in sets of 10 in parallel and in plastic modules (shown as a CAD in Figure 8), along with the stack of 8-kWhr/360-V total in series of these modules.
- 3) The third configuration is a 5-kWhr NiMH battery pack Panasonic with 102 modules, 7.2 V each, in 13 Ahr pairs, as shown in Figure 9. A stack of battery modules does not constitute a battery system, which also requires cooling and battery management. This is handled by the E-Vision battery monitor, which is shown in front of the battery stack-right (to track state of charge [SOC]). The Continental Battery Management System (BMS) module, also used in the Chevy Volt, is shown to the left of the E-Vision battery monitor. The Continental BMS module requires proprietary battery software to estimate running SOC.

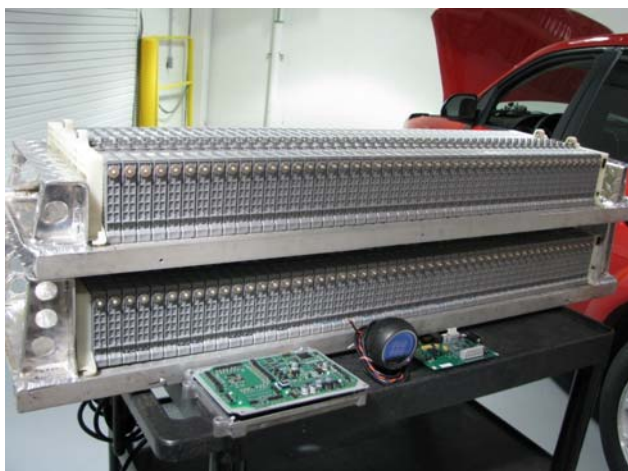


Figure 9. NiMH Battery Pack Configuration

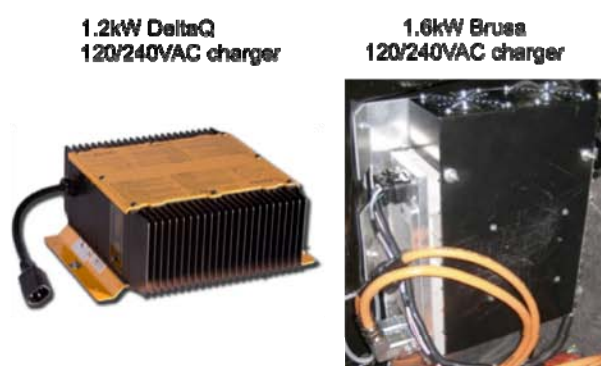


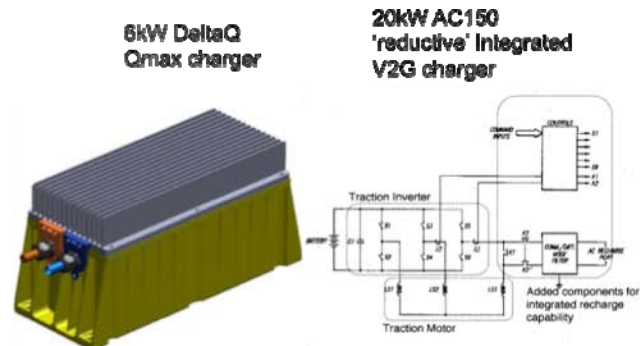
Figure 10. Battery Charger Evaluation/SmartCharge System

Battery Charger Evaluation/SmartCharge System

One of the critical path efficiency components in PHEVs is the battery charging electronics. The TTR PHEV platform can also be used to evaluate battery chargers on real batteries, in a real net-system efficiency context. This platform has the ability to evaluate the chargers shown in Figure 10. They are of three types: unidirectional with serial communication, unidirectional power flow CAN control, and bidirectional power flow.

The basic DeltaQ Quiq charger represents the state-of-the-art for light electric and industrial vehicles (golf-cart-like advanced technology). The Brusa charger, the next level up, has unidirectional power flow and is CAN message controlled. It is Swiss made and costs an unrealistic \$5,000. The DeltaQ Qmax charger to the right of that has the same functionality as the Brusa unit, but it retails for \$500 and offers more power output and simpler packaging in a smaller footprint.

The last charger is part of the AC150 traction electronics that use a method called “reductive” charging, since it reduces component count by using the traction motor as the charger filter inductance. The down side of this method is that the motor frame must be galvanically isolated to avoid leakage currents from the high frequency AC used in the charger. This system allows bi-directional power flow, otherwise known as vehicle-to-grid (V2G), where the battery in the PHEV can be used to power a house, or tasked to support the grid in times of need. This is akin to using PHEVs as energy storage for utilities, or spinning reserve.



The U.S.-Sweden PHEV collaboration used the TTR PHEV platform to develop the SmartCharge system, which allows the utility to communicate with the vehicle to allow the utility to influence when the vehicle initiates charging and rate of charge to best utilize the power grid resources at that moment. Figure 11 shows the SmartCharge control module, Qmax Charger and modem, based on the low-cost robust automotive-grade ARDAQ processing hardware.



Figure 11. Argonne-Designed Smart Charging System for a PHEV

Low-Level Control Electronics and Software

Figure 12 shows the MotoTron ECM, which contains the Matlab-Simulink control software that is compiled in MotoHawk with a Greenhills compiler that targets the low-level interface functions run on the MPC556 processor in the ECM with I/O. In other words, there is a system in place to “connect the hooks” between low-level control code and the I/O functions of the ECM. Shown below the ECM in the photo is a “smart fuse block” used in the TTR platform for the added circuits and loads. This smart fuse block comes from the racing industry and is essentially a CAN-controlled load regulator. Instead of blowing a fuse or circuit breaker, this device has a programmable current limit to keep circuits connected, but not overloaded. This can also be used as a soft start circuit and variable speed motor controller.



Figure 12. MotoTron ECM

High-Level Control Software

Based on Simulink code written for PSAT modeling, a high-level PHEV controller was developed after great efforts to first simulate the vehicle in PSAT. The graphical user interface (GUI) representation is shown in Figure 13.

This resulted in PSAT pulling up the component models listed in Figure 14, from which the high-level controller was based.

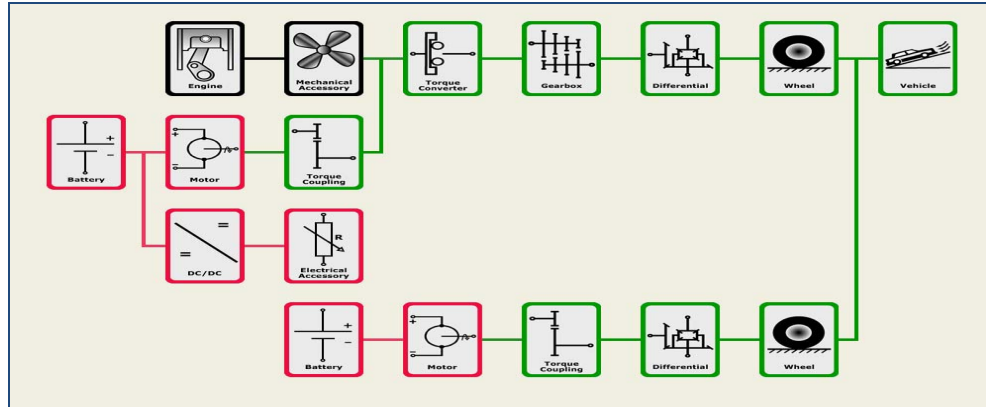


Figure 13. High-Level Control Layout in PSAT

Component	Model	Technology	Initialization File	Scaling File
Driver	for_engine_abc_veh		drv_normal_1000_05	
Mechanical Accessory	constant_pwrloss_trq_in		accmech_0	
Clutch/Torque Converter	torque_converter_map		torqconv_over250Nm	
Energy Storage	pngv_map	nimh	ess_nimh_9_36_PNGVmodel_Cobasys_MY07_Vue	
Energy Storage 2	pngv_map_anc_Pl_cstr	liion	ess_li_41_54_PNGVanl_SattVL41M_Pl_cstr	
Motor 2	map_Pelec_funTW_volt_in	pm	mc_pm_36_75_UQM	mc_s
Motor	map_Pelec_funTW_volt_in	pm	mc_pm_7_14_Accord_ORNL	mc_s
Gearbox	automatic_map_trqloss_funTVratio		gb_4_ae_296_162_1_068_4T45E	
Final Drive 2	map_trqloss_funTW		fd_1_MATT	fd_s
Final Drive	map_trqloss_funTW		fd_1_MATT	
Wheel Axle 2	2wd_abc		wh_0354_P215_70_R16	
Wheel Axle	2wd_abc		wh_0354_P215_70_R16	
Vehicle	curve_fit_josses_dyno_coeff		veh_1160_abc_vus_green_line	
Exhaust Aftertreatment	3way_cat_map	3c	ex_3c	
Power Converter: Electrical Accessory	V2V_constant_eff		pc_095_150	
Electrical Accessory	constant_pwrloss_volt_in		accelec_200	
Engine	map_hot	si	eng_si_2400_126_LAT_2007	
Torque Coupling: Motor 2	map_trqloss_funTW		tc_variable_efficiency	
Torque Coupling: Motor	map_trqloss_funTW		tc_2	

Figure 14.

Alternative PHEV Topology Platform (Series Hybrid, Chevy Volt specs)

As a result of the change in the TTR drivetrain components to match other experiments, the spare set of powertrain components was configured as a series hybrid PHEV topology, equally useful in evaluating PHEV components, in a system-level context. A surplus Chevy Geo chassis, shown in Figure 15, left over from previous engine experiments from that vehicle provided the glider. The configuration and power levels are equivalent to the Chevy Volt PHEV.

The series configuration in this case consists of an electric front-wheel drive system, a PHEV battery in the rear seating area to maintain the center of gravity, and a compact engine/generator in the rear where the spare tire was originally located. Figure 16 shows the vehicle and AC 150 (150-kW AC induction) drive system mounted in the front of the vehicle.



Figure 15. Modifications in Progress to Chevy GEO



Figure 16. Fabrication of Series Hybrid Powertrain Configuration

A custom adapter plate was fabricated to mount this gearbox in the front of the vehicle (Figure 17). This mount and gearbox can also be used to evaluate other candidate PHEV motors without significant rework.

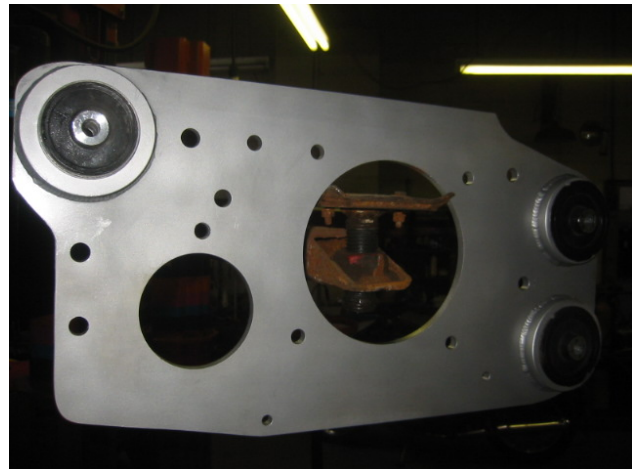


Figure 17. Custom Adapter Plate for Powertrain Mounting

The rear deck area has a large aluminum diamond plate to accommodate various PHEV battery technologies. In the first iteration, a 2-kWhr Lexus RX400h battery pack was used. The photos in Figure 18 show this pack, as well as the 102 module NiMH custom 5-kWhr PHEV pack. The cooling system for this battery is also shown.

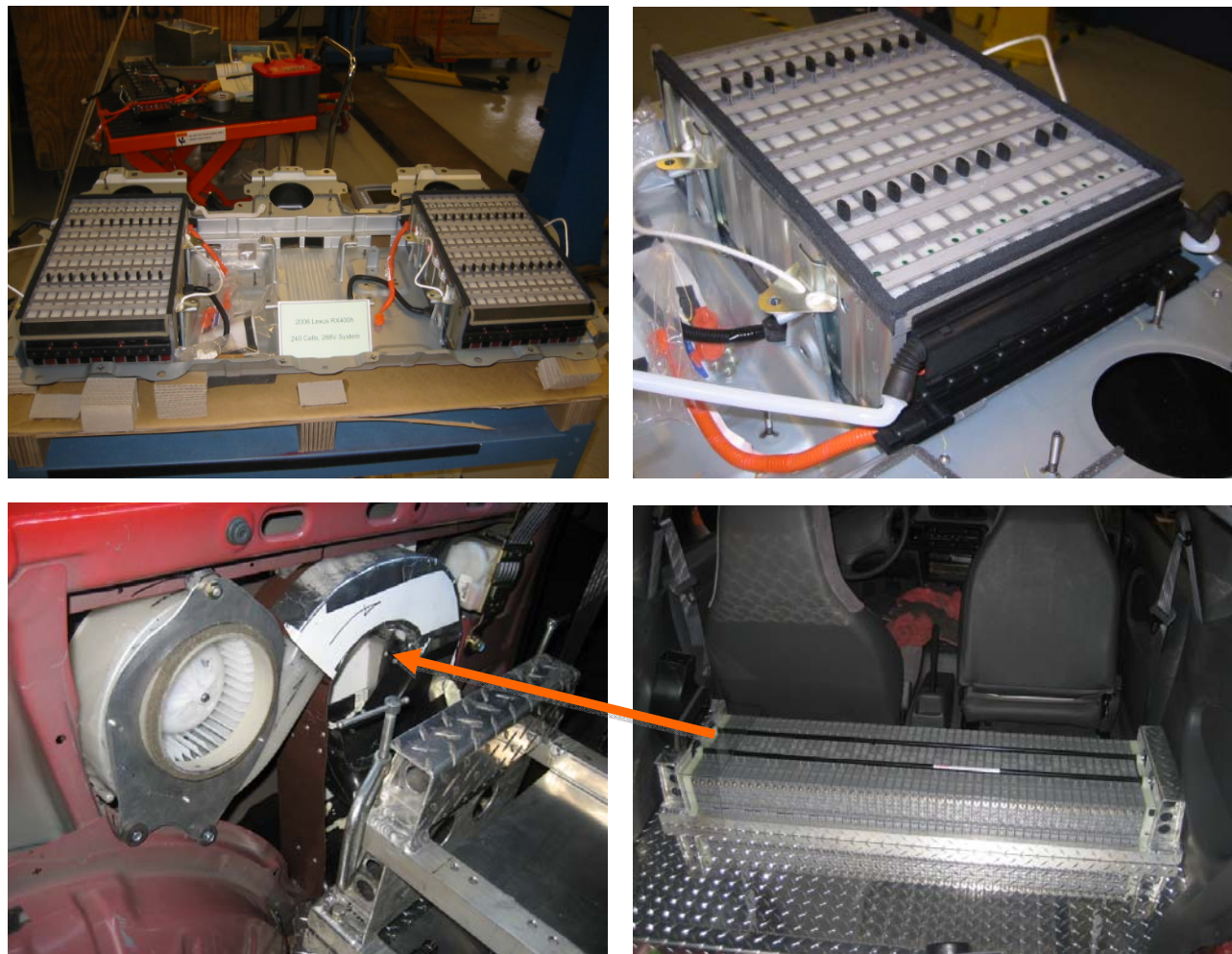


Figure 18. Lexus RX400h battery pack

Rear-Mounted Engine/Generator

Several small engine-mounting systems have been designed for A/B comparison of various technologies for use as rear mounted series power plants.

The first is a German-built 750-cc 2-cylinder Weber MPE750 engine, which weighs less than 40 kg, shown in Figure 19 coupled to a 75-kW UQM motor. The overlay of the engine efficiency curve with the generator efficiency curve. By using an inverter driven generator, optimization studies can be

conducted to compare physical results with model results for engines in series hybrid vehicles.

The engine technology investigation, for future work, could include an electrically driven turbo charger, powered from the electrical output of the generator. Using a higher compression ratio naturally aspirated version of this engine, and the electrically driven turbocharger shown in Figure 20, could be shown to improve overall system efficiency.



Figure 19. Weber 2-Cylinder 750 cc Displacement Engine

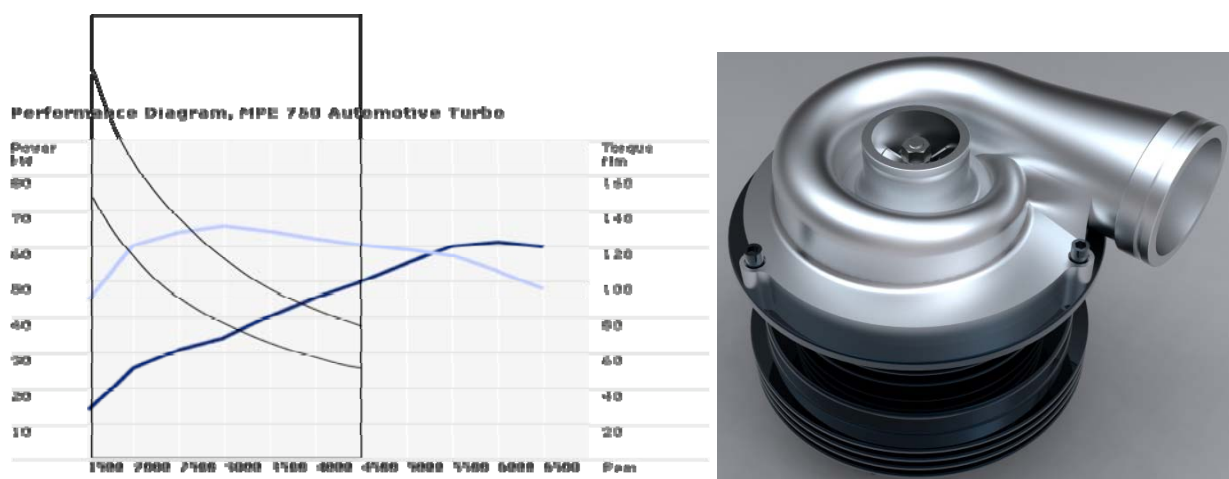


Figure 20. Electricity driven turbocharger and associated performance characteristics

As an extension of the Weber 750 engine, a 1-liter Honda Insight Engine was mounted on an identical coupling, such that the mount points in the rear of the series hybrid platform vehicle accommodate both engine/generator pairs. This area of the vehicle can be used to benchmark other sub-liter or similar engines. The Toyota IQ 1-liter engine is shown in Figure 21 as well, for future consideration.

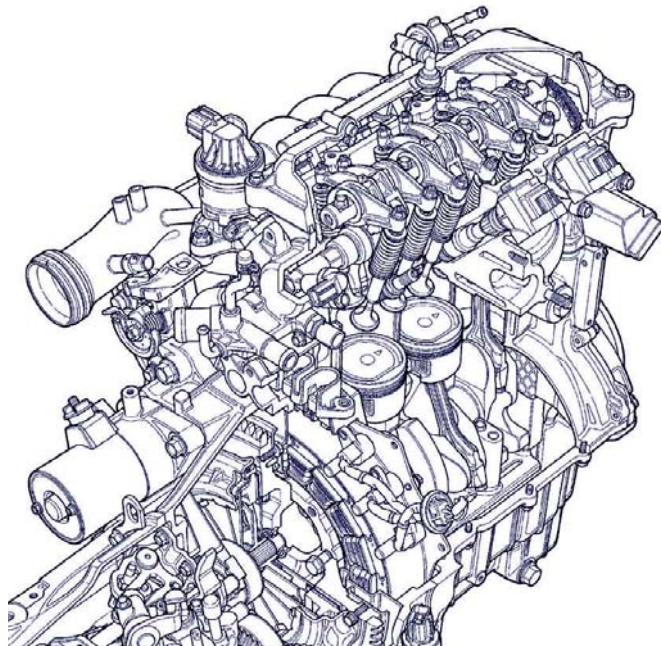
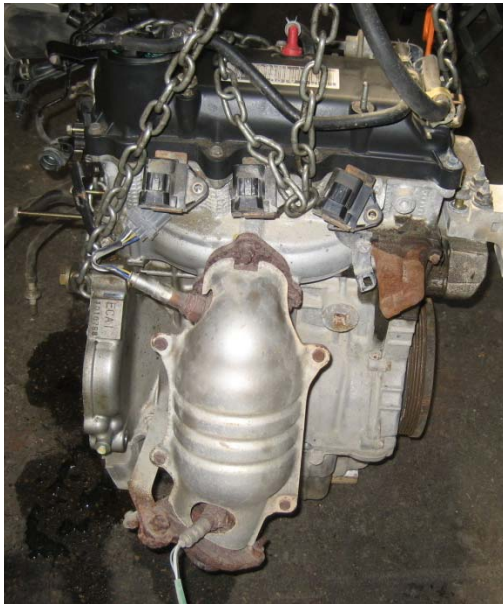


Figure 21. Toyota IQ 1.0-liter Displacement Engine

Results

Dynamometer Debugging and Vehicle Testing

Figure 22 shows the TTR prototype platform on the ANL APRF four-wheel-drive dynamometer. During fiscal year 2008, many weeks were devoted to vehicle testing of the TTR.



Figure 22. Saturn TTR PHEV undergoes testing on Argonne's 4WD Chassis Dynamometer

There was a non-trivial number of component failures while developing and testing the high-level vehicle control software. This included undesirable engine operating modes that led to the premature failure of the catalytic converter in the vehicle. In that case, the modeled vehicle behavior did not match the vehicle actual behavior — more specifically, operating the engine outside the mapped control space (full rich output led to the overheated catalyst).

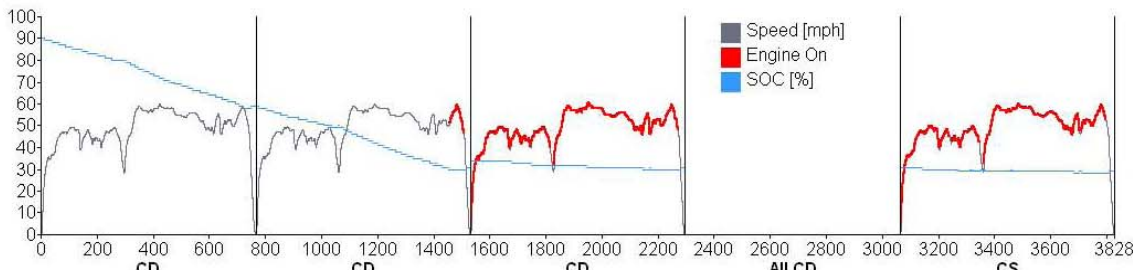
The same held true for accidental instantaneous full torque command to the rear drive system that, due to computational error, led to a sheared “torque fuse” on the motor output coupler.

Eventually, the net result of the software was able to run various blending strategies. Single page test result summaries are shown in Figure 23(a–c). One of the tests included using the Ford Escape PHEV dynamometer coefficients to assess the differences in tuning between the TTR and the Ford-tuned Escape. The labels below show the summary results tests, including blended and all electric operation for various drive cycles.

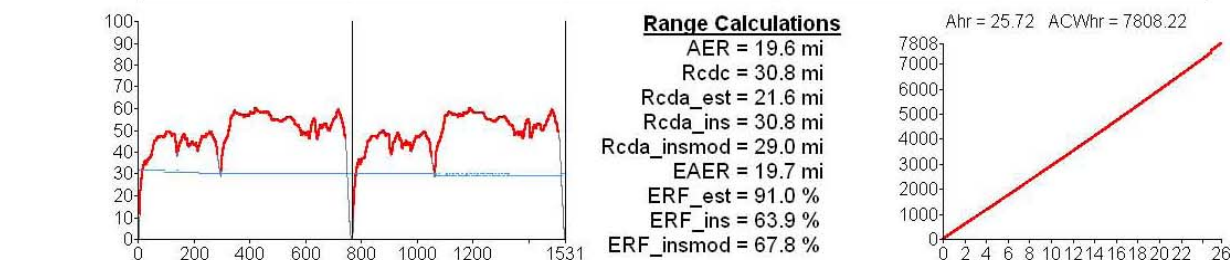


TTR

Escape Road Load Coefficients



	CD	CD	CD	All CD	CS
SOC (st.del.end)	90, 31, 59	59, 28, 31	34, 3, 31	90, 62, 31	31, 2, 29
delta Ahr (1/mi)	12.5 (1.22)	11.8 (1.15)	1.27 (0.12)	25.6 (0.83)	0.65 (0.06)
DCWhr (1/mi)	3259 (318)	2903 (283)	304 (29.6)	6466 (210)	143 (13.9)
ACWhr (1/mi)	3944 (384)	3449 (336)	368 (35.8)	7761 (252)	188 (18.3)
gal (mpg)	0.00 (117784)	0.03 (353)	0.31 (32.9)	0.34 (90.2)	0.31 (33.3)
L (1/100km)	0.00 (0.00)	0.11 (0.67)	1.18 (7.16)	1.29 (2.61)	1.17 (7.07)
FDF	1.00	0.91	0.01	0.64	0.02
Ahr x Vsys (1/mi)	3201 (312)	3010 (293)	326 (31.7)	6537 (212)	167 (16.2)
Ahr x Vsys / Fuel	1161	3.27	0.03	0.60	0.02
OCV	269.9	256.1	255.4	N/A	254.8



	CS Cold	CS Hot	All CS	43/57 CS	Same Trip CS
SOC (st.del.end)	32, 2, 30	30, 0, 30	32, 2, 30	N/A	N/A
delta Ahr (1/mi)	0.56 (0.06)	0.23 (0.02)	0.80 (0.04)	0.37 (0.04)	1.03 (0.03)
DCWhr (1/mi)	126 (12.3)	39.9 (3.89)	166 (8.10)	77.1 (7.52)	206 (6.70)
ACWhr (1/mi)	163 (15.9)	66.9 (6.52)	230 (11.2)	108 (10.6)	297 (9.7)
gal (mpg)	0.32 (32.5)	0.31 (32.6)	0.63 (32.5)	0.32 (32.5)	0.95 (32.6)
L (1/100km)	1.19 (7.24)	1.19 (7.22)	2.39 (7.23)	1.19 (7.23)	3.58 (7.23)
Ahr x Vsys (1/mi)	144 (14.1)	59.3 (5.78)	204 (9.9)	95.9 (9.35)	263 (8.55)
Ahr x Vsys / Fuel	0.01	0.01	0.01	0.01	0.01
OCV	255.8	255.8	N/A	255.8	N/A

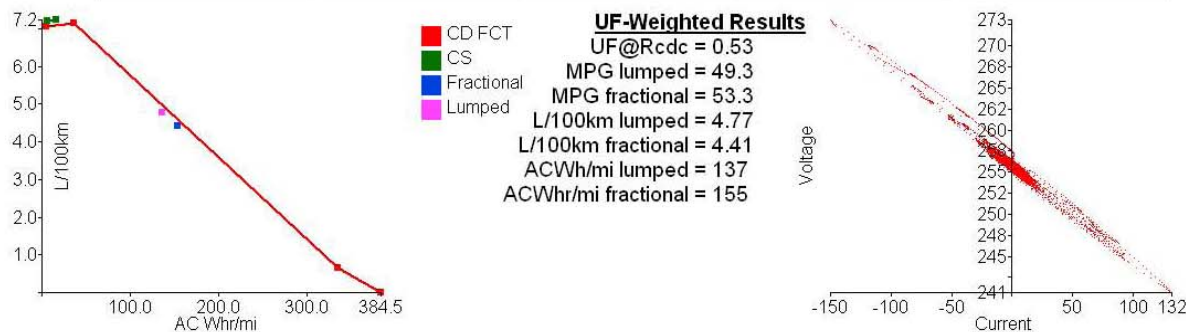
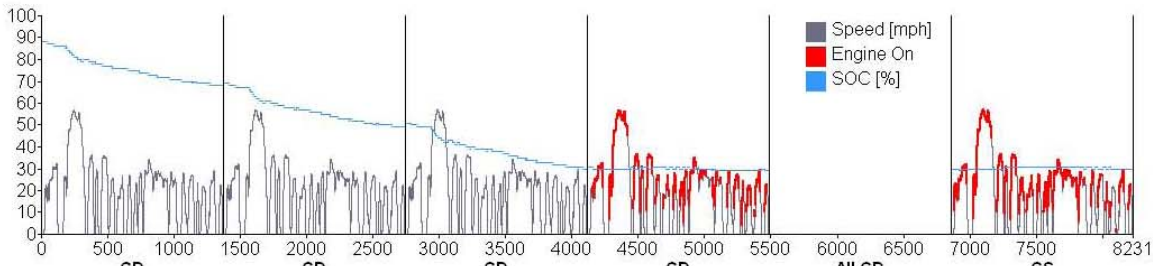


Figure 23a. Highway Cycle with 19.6-mi AER until Charge Sustaining Mode

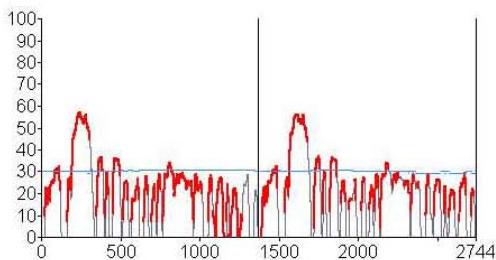


TTR

Escape Road Load Coefficients

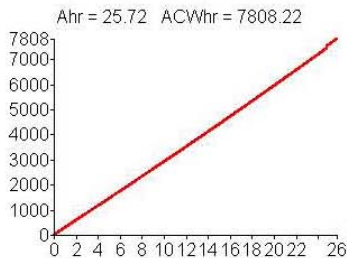


	CD	CD	CD	CD	All CD	CS
SOC (st.del.end)	88, 20, 68	69, 20, 49	51, 21, 30	31, 2, 29	88, 63, 29	30, 0, 30
delta Ahr (1/mi)	8.01 (1.08)	8.08 (1.08)	8.27 (1.11)	0.46 (0.06)	24.8 (0.83)	-0.2 (-0.02)
DCWhr (1/mi)	2107 (283)	2035 (273)	2019 (271)	75.9 (10.2)	6237 (209)	-79 (-11)
ACWhr (1/mi)	2578 (346)	2429 (325)	2410 (323)	133 (17.8)	7549 (253)	-46 (-6.2)
gal (mpg)	0.00 (78221)	0.00 (89457)	0.00 (67688)	0.26 (28.4)	0.26 (113)	0.26 (28.3)
L (1/100km)	0.00 (0.00)	0.00 (0.00)	0.00 (0.00)	0.99 (8.30)	1.00 (2.07)	1.00 (8.31)
FDF	1.00	1.00	1.00	-0.05	0.75	0.17
Ahr x Vsys (1/mi)	2058 (276)	2077 (278)	2125 (285)	118 (15.8)	6378 (214)	-41 (-5.5)
Ahr x Vsys / Fuel	683	786	609	0.01	0.77	-0.00
OCV	273.8	263.4	256.3	255.8	N/A	255.4

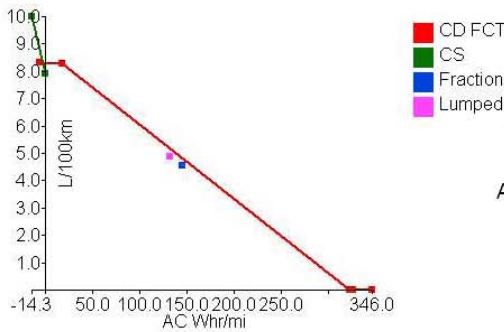


Range Calculations

AER = 22.5 mi
 Rcdc = 29.8 mi
 Rcda_est = 22.6 mi
 Rcda_ins = 28.1 mi
 Rcda_insmod = 22.4 mi
 EAER = 22.0 mi
 ERF_est = 97.3 %
 ERF_ins = 78.4 %
 ERF_insmod = 98.2 %



	CS Cold	CS Hot	All CS	43/57 CS	Same Trip CS
SOC (st.del.end)	30, 0, 30	30, 0, 30	30, 0, 30	N/A	N/A
delta Ahr (1/mi)	-0.4 (-0.05)	0.00 (0.00)	-0.4 (-0.02)	-0.2 (-0.02)	-0.4 (-0.01)
DCWhr (1/mi)	-131 (-18)	-34 (-4.6)	-165 (-11)	-76 (-10)	-234 (-7.9)
ACWhr (1/mi)	-106 (-14)	1.39 (0.19)	-105 (-7.1)	-45 (-6.0)	-103 (-3.5)
gal (mpg)	0.32 (23.5)	0.25 (29.8)	0.57 (26.3)	0.28 (26.7)	1.06 (27.9)
L (1/100km)	1.20 (10.0)	0.94 (7.90)	2.14 (8.95)	1.05 (8.80)	4.03 (8.42)
Ahr x Vsys (1/mi)	-95 (-13)	1.08 (0.15)	-94 (-6.3)	-40 (-5.4)	-91 (-3.1)
Ahr x Vsys / Fuel	-0.01	0.00	-0.01	-0.00	-0.00
OCV	257.0	257.0	N/A	257.0	N/A



UF-Weighted Results

UF@Rcdc = 0.52
 MPG lumped = 48.4
 MPG fractional = 51.8
 L/100km lumped = 4.86
 L/100km fractional = 4.54
 ACWh/mi lumped = 132
 ACWh/mi fractional = 145

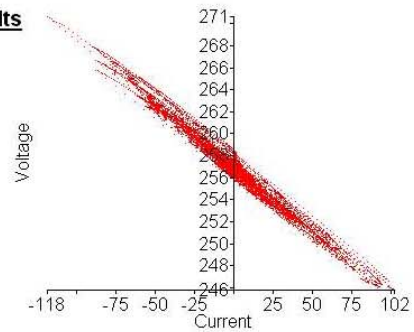
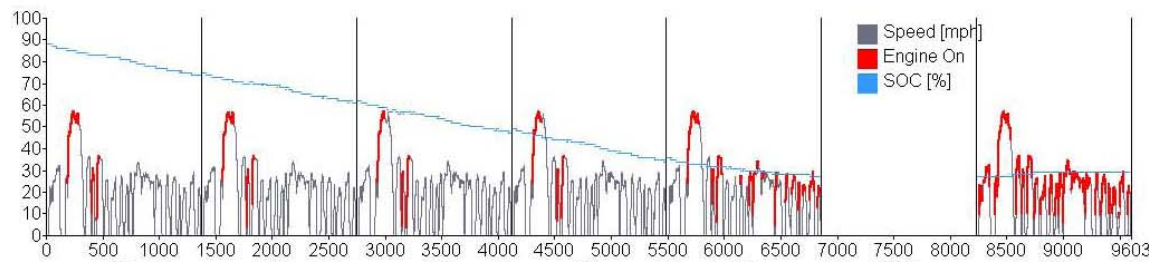


Figure 23b. Urban Drive Cycle and 22.5 mi of AER until Sustaining

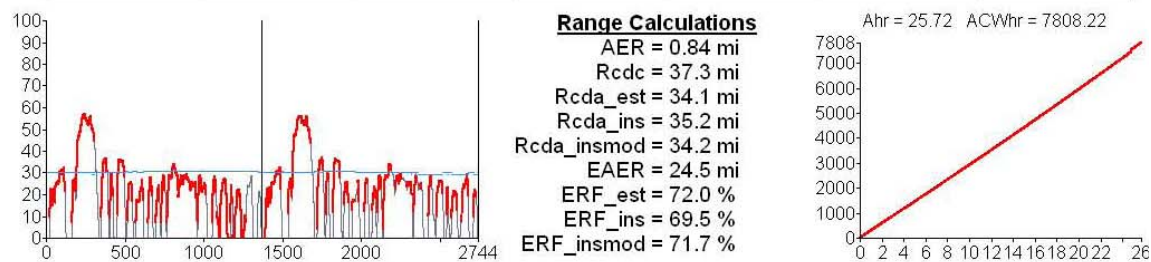


TTR

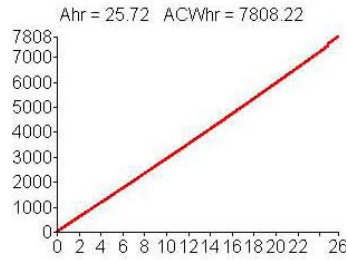
Escape Road Load Coefficients



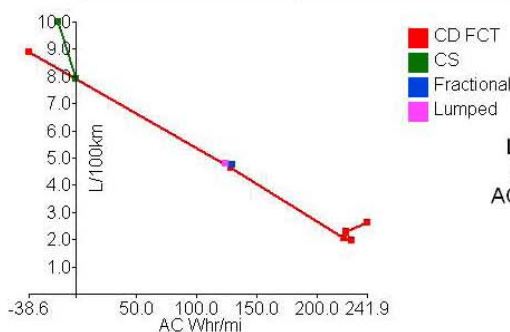
	CD	CD	CD	CD	CD	All CD	CS
SOC (st.del.end)	88, 14, 74	75, 14, 61	62, 15, 47	49, 14, 35	36, 9, 27	88, 66, 27	27, -2, 29
delta Ahr (1/mi)	5.50 (0.74)	5.45 (0.73)	5.75 (0.77)	5.69 (0.76)	3.36 (0.45)	25.7 (0.69)	-1.0 (-0.1)
DCWhr (1/mi)	1469 (197)	1405 (189)	1444 (194)	1402 (188)	799 (107)	6519 (175)	-298 (-40)
ACWhr (1/mi)	1805 (242)	1668 (224)	1711 (229)	1661 (223)	963 (129)	7808 (209)	-295 (-40)
gal (mpg)	0.08 (90.1)	0.07 (103)	0.06 (120)	0.07 (114)	0.15 (50.8)	0.43 (86.9)	0.28 (26.5)
L (1/100km)	0.31 (2.61)	0.27 (2.28)	0.24 (1.96)	0.25 (2.05)	0.56 (4.63)	1.62 (2.71)	1.06 (8.88)
FDF	0.74	0.71	0.75	0.74	0.41	0.67	0.11
Ahr x Vsys (1/mi)	1414 (190)	1400 (188)	1477 (198)	1463 (196)	863 (116)	6615 (177)	-262 (-35)
Ahr x Vsys / Fuel	0.54	0.61	0.75	0.71	0.19	0.49	-0.03
OCV	277.0	269.7	263.1	258.0	255.1	N/A	256.4



Range Calculations
 AER = 0.84 mi
 Rcdc = 37.3 mi
 Rcda_est = 34.1 mi
 Rcda_ins = 35.2 mi
 Rcda_insmod = 34.2 mi
 EAER = 24.5 mi
 ERF_est = 72.0 %
 ERF_ins = 69.5 %
 ERF_insmod = 71.7 %



	CS Cold	CS Hot	All CS	43/57 CS	Same Trip CS
SOC (st.del.end)	30, 0, 30	30, 0, 30	30, 0, 30	N/A	N/A
delta Ahr (1/mi)	-0.4 (-0.05)	0.00 (0.00)	-0.4 (-0.02)	-0.2 (-0.02)	-0.4 (-0.01)
DCWhr (1/mi)	-131 (-18)	-34 (-4.6)	-165 (-11)	-76 (-10)	-269 (-7.2)
ACWhr (1/mi)	-106 (-14)	1.39 (0.19)	-105 (-7.1)	-45 (-6.0)	-101 (-2.7)
gal (mpg)	0.32 (23.5)	0.25 (29.8)	0.57 (26.3)	0.28 (26.7)	1.31 (28.3)
L (1/100km)	1.20 (10.0)	0.94 (7.90)	2.14 (8.95)	1.05 (8.80)	4.97 (8.32)
Ahr x Vsys (1/mi)	-95 (-13)	1.08 (0.15)	-94 (-6.3)	-40 (-5.4)	-90 (-2.4)
Ahr x Vsys / Fuel	-0.01	0.00	-0.01	-0.00	-0.00
OCV	257.0	257.0	N/A	257.0	N/A



UF-Weighted Results
 UF@Rcdc = 0.59
 MPG lumped = 48.9
 MPG fractional = 49.7
 L/100km lumped = 4.81
 L/100km fractional = 4.73
 ACWh/mi lumped = 124
 ACWhr/mi fractional = 130

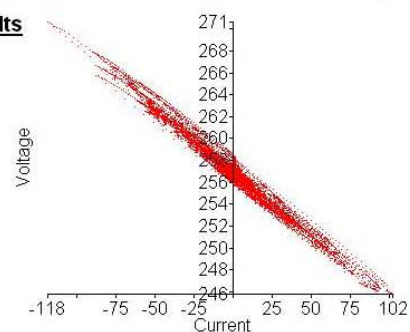


Figure 23c. Blended Mode Operation and Fuel Economy as High as 120 mpg on the Urban Driving Cycle

Figure 24 shows a plot of emissions collected vs. fuel consumed on the highway cycle.

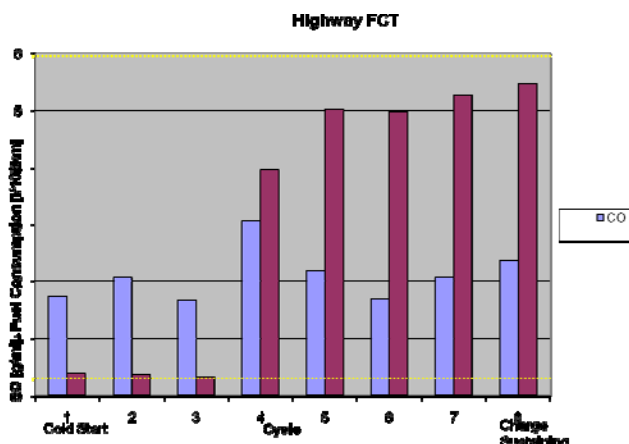


Figure 24. Saturn Vue TTR Emission Testing Result Plotted as a Function of Fuel Consumed

The full electric capability of the TTR prototype platform has been used to test various aspects of the SAE J1711 PHEV test methods and standards. The same is true of the SAE J1634 EV testing standard for the TTR prototype in electric only mode.

Conclusions

A valuable experiment and PHEV controls development platform have been created in the TTR PHEV prototype platform. The vehicle and software function well enough to complete many rounds of dynamometer and (some) on-road testing. This open source controller software platform can be used to investigate blending strategies as well as benchmark PHEV components in a systems-level context. There are several battery packs lined up for fiscal year 2009 evaluation in the TTR platform, as well as other ESSs such as the battery/active ultracapacitor combination systems. Electric machines and power electronics can be readily adapted to this fully capable (strong hybrid) prototype.

Publications/Presentations

1. Neeraj Shidore and Ted Bohn, "Evaluation of Cold Temperature Performance of the JCS-VL41M PHEV Battery Using Battery HIL," presented at the SAE 2008 World Congress conference at Detroit, MI, USA, April 2008.
2. Neeraj Shidore et al., "Quantifying PHEV All Electric Range and Fuel Economy in Charge Sustaining Mode for Low SOC Operation," poster at the EVS-23 Conference, California, USA, Dec. 2008.
3. Aymeric Rousseau, Neeraj Shidore, and Richard "Barney" Carlson, "Impact of Battery Characteristics on PHEV Fuel Economy," presented at the Advanced Automotive Batteries Conference (AABC), Orlando, FL, July 2008.
4. Aymeric Rousseau et al., "PHEV Battery Requirement - Uncertainty Based on Real World Drive Cycles and Impact on Fuel Efficiency," presented at the First Li-ion Battery Conference, Argonne, IL, September 2008.
5. Neeraj Shidore and Henning Lohse-Busch, "Power Train Component and Subsystem Evaluation at Argonne National Laboratory," invited presentation at the dSpace user's conference, Livonia, MI, USA, September 2008.

IV. LABORATORY TESTING AND BENCHMARKING

A. Benchmarking and Validation of Hybrid Electric Vehicles

Michael Duoba (Project Leader)

Argonne National Laboratory
9700 South Cass Avenue

Argonne, IL 60439-4815
(630) 252-6398; mduoba@anl.gov

DOE Technology Manager: Lee Slezak

(202) 586-2335; Lee.Slezak@ee.doe.gov

Objectives

Provide operational data during chassis dynamometer testing by using novel instrumentation for:

2008 GM Tahoe Hybrid (Level 1+)

2007 Nissan Altima Hybrid

Approach

Purchase vehicle, manufacturers' service manuals, and diagnostic tools for the vehicles tested.

In the case of the Level 1 testing, instrument engine speed, battery current, and battery voltage.

In the case of the Level 1+ testing, install a drive shaft torque sensor and use indicated engine torque sensor to determine engine torque from in-cylinder pressure measurement.

Also for level 1+ testing, determine, scale, and record Controller Area Network (CAN) signals through testing as a means of measuring parameters that would otherwise be too difficult or expensive to obtain.

Run tests for cycle fuel economy, performance testing, and steady-state load for all of the vehicles.

Accomplishments

Produced insightful data on the latest hybrid technologies and controls systems from General Motors (GM) by Level 1+ testing a GM Tahoe Hybrid. (This is the first 2-Mode hybrid transmission.)

Successfully conducted Level 1+ testing on a re-saleable vehicle without modification to the vehicle. Conducted a full range of tests with a large number of vital sensors and signals collected.

Developed CAN signal data acquisition for recording signals that the vehicles monitor or use for controls

Future Directions

Further evaluate engine torque measurement instrumentation, which may be a viable and more cost-effective alternative to the time-consuming and expensive addition of an engine flywheel torque sensor.

Investigate upgrading the Advanced Powertrain Research Facility (APRF) to be 5-Cycle compliant by the addition of solar load for the SC03 test, as well as extreme cold climate control for the -7°C FTP.

Introduction

Vehicle benchmarking combines testing and data analysis to characterize efficiency, performance, and emissions as a function of duty cycle, as well as to deduce control strategy under a variety of operating conditions. The data are applicable to virtually every effort in the FreedomCAR partnership, and all of the “Tech Teams” benefit from the data collected in the Advanced Powertrain Research Facility (APRF) at Argonne National Laboratory’s (ANL) Center for Transportation Research.

Approach

Level 2 testing is conducted with sensors throughout the vehicle to determine the energy flow at all critical areas. Level 2 instrumentation includes battery current, voltage, engine torque and speed, fuel flow, temperatures, and many more. Level 2 instrumentation is typically solely installed on DOE-purchased vehicles that are not meant for resale because of the high numbers of sensors that are installed and the amount of modification sometimes required. Level 1 testing is conducted to acquire the high-level data in a reduced time frame. Level 1 testing uses less component instrumentation than Level 2 and does not require that the vehicle be extensively broken down, but it delivers fewer data. Battery current and voltage, engine speed, emissions data, and fuel economy are recorded and analyzed. However, Level 1 testing is a desirable approach for HEVs that do not represent leading-edge technology. Level 1+ instrumentation contains many of the same sensors and signals as Level 2, except for engine torque.

Level 1+ Model Year 2008 GM Tahoe Hybrid

Vehicle Description

The Tahoe is the first full-size SUV Hybrid. It uses a 2-Mode transmission system. This vehicle was tested in cooperation with Idaho National Laboratory (INL) and the Advanced Vehicle Testing Activity (AVTA) by using Level 1+ instrumentation (Figure 1).

The Tahoe Hybrid 2-Mode is a power-split hybrid that has two power-split modes (input split and compound split). The input split mode (“Lo” mode) is designed for high-torque, low-speed operation, while the compound split mode (“Hi” Mode) is designed for lower-torque, higher-speed operation.



Figure 1. GM Tahoe Hybrid Level 1+

The engine used in the Tahoe Hybrid is the GM LFA 6.0-L V8. The Vortec 6000 LFA is a Generation IV small block V8 truck engine. It produces 332 hp at 5100 rpm and 367 lb·ft (498 N·m) at 4100 rpm. The LFA variant is used in GM's hybrid GMT900 trucks and SUVs. It has two valves per cylinder with a “cam in block” design. This engine uses Active Fuel Management, which operates the engine in eight cylinders and four cylinders. Also, variable valve timing is used by advancing the relative position of the camshaft with respect to the crankshaft. The camshaft timing variation ranges from -45 deg to +7 deg relative to the crankshaft. The LFA engine has several special design features that are specific for the hybrid operation. This engine has only one belt-driven accessory, which is the water pump. The rest of the accessories, including power steering, air-conditioner, and alternator, are powered by the battery system. Also, a high-compression ratio of 10.78:1 is used to increase efficiency. With variable camshaft timing, late intake valve closing can also be used to improve engine efficiency.

The Tahoe Hybrid 2-Mode transmission system enables full hybrid operation, and it can still be packaged in the same location as a conventional transmission. The 2-Mode transmission contains two permanent magnet motors, each rated at 60 kW, and three planetary gear sets with four clutches (Figure 2). An advantage of the 2-Mode system over typical power-split hybrids is that it can use smaller electric motors for given performance requirements. The 2-Mode system can operate in two electric-continuously variable transmission (E-CVT) modes with either the Lo or Hi clutch engaged or four discrete gear states through the proper selection of clutch pair applications.

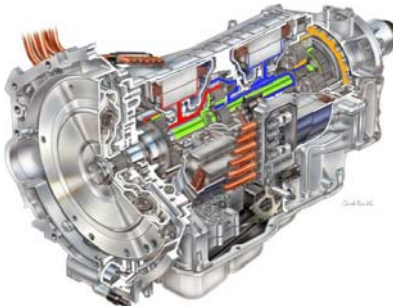


Figure 2. GM Tahoe Hybrid 2-Mode Transmission

The high-voltage battery system in the Tahoe Hybrid is a 1.8-kWh NiMH system that uses the same Panasonic cells as in the Lexus GS450h. In the Tahoe Hybrid, the battery system is located under the rear seat, and it is air-cooled by cabin air. Also, the air-conditioning system is powered from the high-voltage bus. The system is rated up to 6 kW peak, but through testing, only 2 kW peak was observed.

The auxiliary system of the Tahoe Hybrid powers many systems on the vehicle, including some systems typically driven directly from engine power. A 42-V system, generated from a high-voltage DC/DC, is used exclusively on the vehicle to provide power to the electric power steering. The 12-V system of the vehicle powers all of the essential electronics of the vehicle, as well as the power brake booster. Because the engine is off for a large amount time, a vacuum brake booster is not an option. Instead, a hydraulic assist system that is driven by a 12-V pump (similar to an anti-lock brake [ABS] pump) is used to assist the driver with brake pedal force. During dynamometer testing, a typical 12-V auxiliary load of 375 W was measured. Under this condition, only critical accessories are operating.

Testing Results

Fuel Consumption

The Tahoe Hybrid was tested by using a chassis dynamometer to measure fuel consumption and emissions and to determine overall functionality of the powertrain and its subsystems. Typical cycles (including Urban Daily Driving Schedule [UDDS], HWY, and US06 drive cycles) were conducted, and specific tests were undertaken to identify the sensitivity of fuel consumption to speed and acceleration. These tests are UDDS cycles multiplied by a speed multiplier ($\times 0.8$, $\times 1.2$, $\times 1.4$), in which the

speed trace is directly scaled by a factor. The standard cycles (UDDS and HWY) were also conducted with the air conditioner running in recirculation mode. Figure 3 shows a plot of the fuel consumption versus the electrical energy consumption. Data points falling within the “V-shaped” window (around the y-axis) are considered to be charge-sustaining.

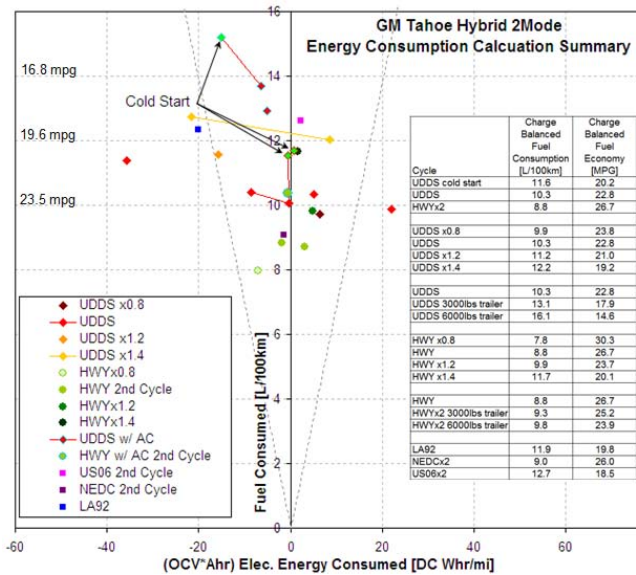


Figure 3. Fuel Consumption Results of Tahoe Hybrid 2 Mode

Table 1. Comparison of Fuel Economy Results

Test Results "New Window Sticker" Adjusted Fuel Economy [MPG]	EPA "Window Sticker" Adjusted Fuel Economy [MPG]	5.3L Tahoe 4Spd Trans Fuel Economy [MPG]
16.9 City	21	14
18.9 Hwy	22	20

For the UDDS cycle, the raw results showed over 20 mpg, but with the window sticker adjustment calculation, the adjusted city fuel economy was 16.9 mpg, which is rather low compared to the 21-mpg city Environmental Protection Agency (EPA) fuel economy shown on the window sticker. This difference is partly due to the Target ABC parasitic loading differences when testing on a chassis dynamometer facility.

Testing was conducted at steady-state speeds and at several grades. These tests were primarily used to

analyze the operating characteristics of the engine, but the steady fuel economy trend also was obtained, which is shown in Figure 4. Note that for any grade, the fuel economy decreases nearly linearly with increasing vehicle speed above 40 mph. At low grades (one and two percent), the maximum fuel economy occurs at speeds slightly lower than 40 mph.

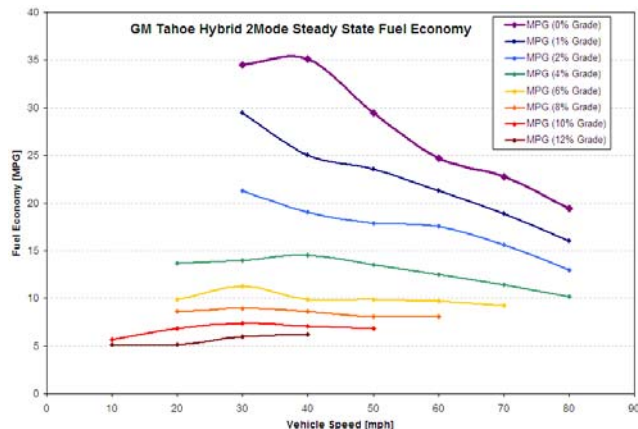


Figure 4. Steady-State Fuel Economy of Tahoe Hybrid at Various Percent Grades

The tailpipe emissions of the Tahoe Hybrid were measured throughout testing. The emissions levels approach those for super ultra-low emission vehicle (SULEV) designation for hot-start UDDS tests, but CO levels exceeded the limit during cold-start UDDS cycles and one hot-start UDDS cycle. It is interesting to note that an aggressive cycle (US06 and LA92) produced very low emissions (less than SULEV), as seen in Figure 5.

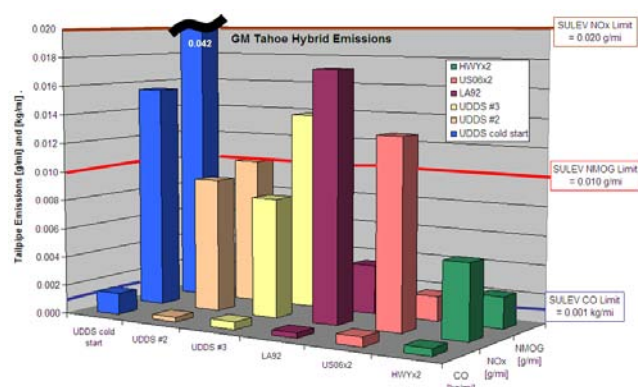


Figure 5. Tailpipe Emissions of Tahoe Hybrid

Engine Operation

The engine in the Tahoe Hybrid uses several advanced technologies to improve efficiency. Two notable technologies used are cylinder deactivation and camshaft phasing.

Cylinder deactivation is used extensively under nearly all driving conditions. Figure 6 illustrates the percent of time the engine operates in four-cylinder and eight-cylinder modes. Note for the HWY cycles at various speed-scaling factors, the percent of time in four-cylinder operation increases greatly with decreasing speed scaling. For the scaled UDDS cycles, note that the eight-cylinder operation is nearly constant through the various scaled UDDS cycles. When the engine starts, it operates in eight-cylinder mode for a minimum of six seconds until enough hydraulic pressure is achieved to deactivate the lifters for the deactivated cylinders. Only then can the engine run in four-cylinder mode.

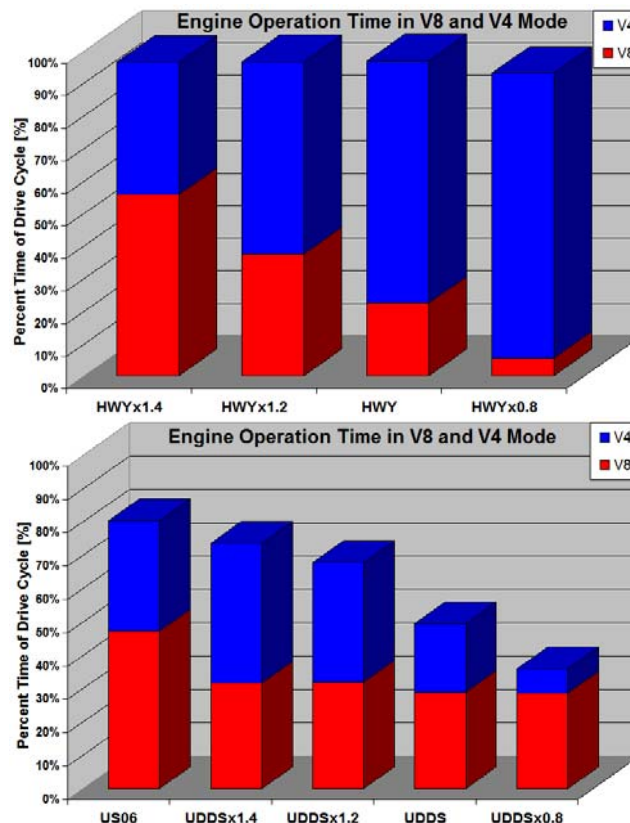


Figure 6. Percentage Time of 4-Cylinder Mode and 8-Cylinder Mode

Camshaft phasing is used in the Tahoe Hybrid engine to improve efficiency by using late intake valve closing in combination with a rather high compression ratio of 10.8:1. This can be considered a Miller cycle. The camshaft phasing also allows advancement of the cam timing to increase volumetric efficiency of the engine at low speeds and mid to light loads. Figure 7 shows the operating map of the camshaft phasing used in the Tahoe Hybrid.

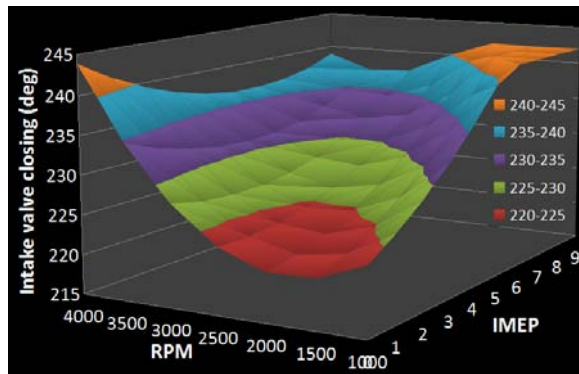


Figure 7. Camshaft Phasing Map

By using the spark plug pressure transducers and engine crankshaft position encoder, as described in a previous section, indicated mean effective pressure (IMEP) engine torque is calculated in real time during testing. This torque measurement is used in eight-cylinder and four-cylinder modes. Figure 8 shows the calculated engine torque over a US06 cycle. Note the distinct regions in blue and red, indicating four- and eight-cylinder operation. Also note the negative torque region of each. The pumping losses of the engine in four-cylinder mode are roughly one-half of the losses in eight-cylinder mode. This is expected because in four-cylinder mode, one-half of the cylinders are closed and therefore act as an air spring.

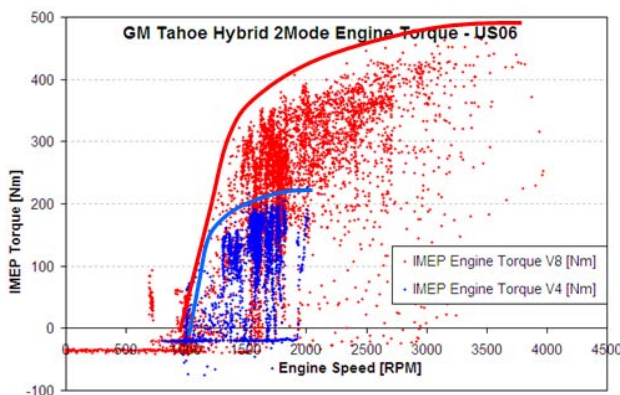


Figure 8. Engine Torque on a US06

The IMEP engine torque, along with the direct fuel flow measurement, can be used to calculate engine efficiency. An efficiency map was calculated for four-cylinder and eight-cylinder modes. These efficiency maps are shown in Figure 9 with engine torque data from a UDDS cycle overlaid on the efficiency map. Note the concentration of engine operation in four-cylinder mode near 1200 RPM. There appears to be a local minimum around 125 Nm and 1200 RPM.

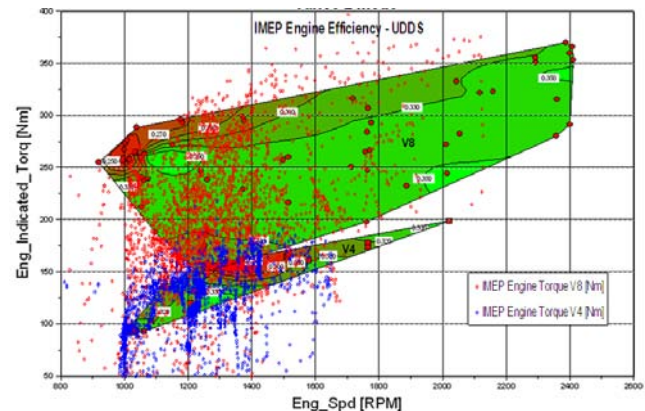


Figure 9. IMEP Engine Efficiency Map

2-Mode Transmission Operation

The 2-mode transmission is able to operate in two E-CVT modes and four discrete gear ratios. The Tahoe Hybrid optimizes the use of the transmission real time to minimize fuel consumption. Figure 10 shows the transmission ratio regions and the four linear fixed-gear regions.

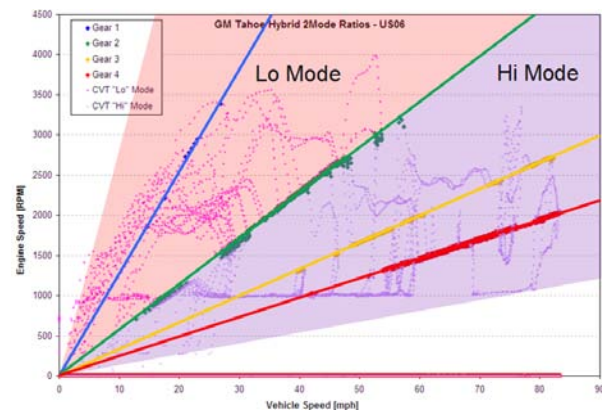


Figure 10. Transmission Ratio Utilization

From zero speed, the vehicle launches in Lo mode and changes ratio as determined by the control system. The transmission will transition to Hi mode at the synchronous point. This is the speed ratio at

which both clutches for Hi mode and Lo mode are at zero slip speed (i.e., it could be in Lo mode or Hi mode at the same time). If both clutches are engaged, the transmission is in fixed second gear. If a different fixed gear state is required, the transmission will change ratio, in Hi mode or Lo mode to the proper ratio; and then the additional clutch is applied to constrain the transmission to the desired fixed gear. A jump shift (non-synchronous shift) from fixed gear to fixed gear is not part of normal operation.

Fixed gear states 2, 3, and 4 are used often in normal driving, but fixed gear state 1 is used only for very heavy accelerations and towing. Lo mode, as the name implies, is used for low-speed, high-torque operation, as well as reverse, while the Hi mode is used for higher-speed operation.

A real-time optimization algorithm is used with the 2-Mode system to minimize losses through the system in every driving condition. This means the control system automatically adjusts ratio, torque from the engine, and two electric motors to meet the driver's demand in the most efficient manner possible.

To gain a better understanding of the advantages of the 2-Mode system, the driveshaft torque is analyzed and compared to vehicle speed, which is shown in Figure 11. This is the same test data as those from Figure 10. Notice in Figure 11 the regions of Lo mode operation during launch transitioning to gear state 2 operation. Also, there is an extensive use of gear state 4. Below 20 mph, engine-off operation (EV operation) is very common during deceleration and initial launch. Figure 11 also shows the characteristic motor torque curve during regenerative braking operation.

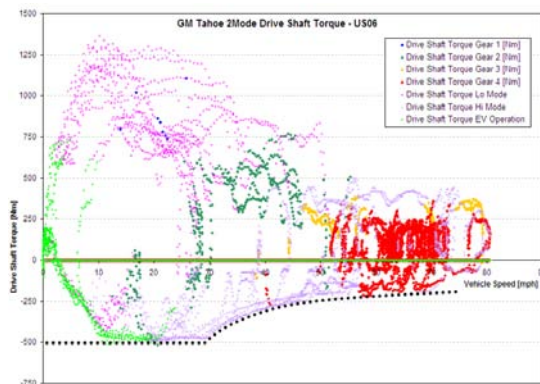


Figure 11. Driveshaft Torque over US06 Drive Cycle

Regenerative braking power is typically limited to 30-kW battery power. Figure 12 shows an aggressive braking maneuver that saturates the regenerative braking. The blue region is the battery power, which is controlled to a limit of 30 kW. The pink region is the losses from the driveshaft to the battery, which includes transmission losses, electric machine losses, and power electronics losses. The green region in Figure 12 is the mechanical braking that is blended with the regenerative braking to provide the driver's desired deceleration rate.

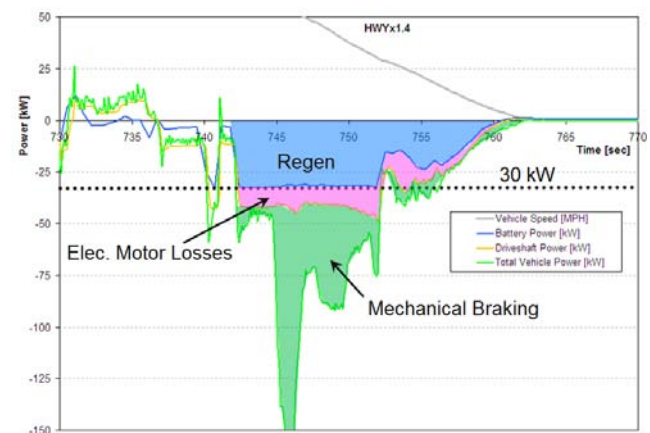


Figure 12. Regenerative Braking Utilization

The Tahoe Hybrid is a rear-wheel-drive (RWD) vehicle, so all of the regenerative braking is recaptured through the rear wheels. GM implemented several safety features to enhance the regenerative braking to ensure vehicle safety and stability. Maximum regenerative braking can only be achieved when the steering wheel is pointed straight forward. Maximum regenerative braking is significantly decreased as the steering wheel is turned away from center to prevent an over-steer condition that can result from turning with significant rear-wheel regenerative braking.

Energy Storage System Utilization

The battery system is controlled to a limit of ± 30 kW under typical operation, but excursions to 60 kW were measured while starting the engine during aggressive EV launch, as seen in Figure 13. Also, the battery utilization can be seen during the fixed-gear operation. The configuration is essentially a parallel hybrid when operating in a fixed-gear state.

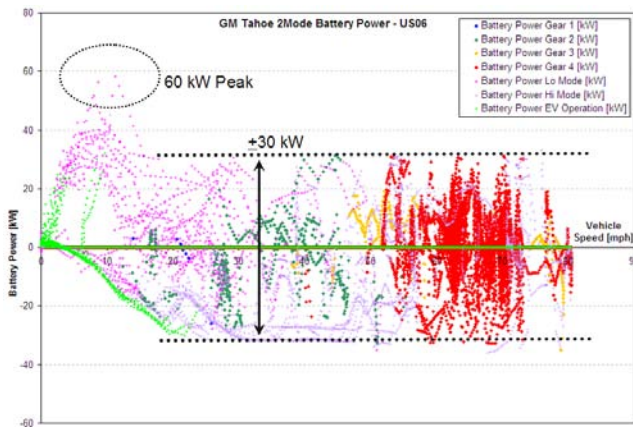


Figure 13. Battery Power over US06 Drive Cycle

Summary

The GM Tahoe Hybrid is the first production full-size hybrid SUV that has significant towing capability. The Tahoe Hybrid uses a large-displacement engine with a 2-Mode transmission that enables full hybrid operation without excessively large electric motors. GM implemented several advanced technologies into the Tahoe Hybrid to maximize fuel economy, including cam phasing in conjunction with a high-compression ratio to operate as a Miller cycle and cylinder deactivation to operate the engine in more efficient regions during low power demands. Nearly all of the engine's belt-driven accessories are powered from the high-voltage system rather than the engine power directly.

The 2-Mode system is expected in future production hybrids, which will enable a reduction in fuel consumption while still satisfying America's need for large vehicles without compromise. PHEV versions of 2-Mode vehicles are also expected, and these vehicles may further reduce fuel consumption by means of petroleum displacement.

Level 1 Model Year 2007 Nissan Altima Hybrid

Vehicle Description

The Nissan Altima Hybrid, shown in Figure 14, was tested by using Level 1 instrumentation. The Altima Hybrid uses the same hybrid transmission system and battery system as in the Camry hybrid. The engines are different but have similar displacements. This vehicle was tested in cooperation with INL and AVTA.



Figure 14. Nissan Altima Hybrid

Dynamometer Testing Results

The Fuel Consumption of the Altima Hybrid, shown in Figure 15, should be very similar to the Camry Hybrid because they use the same hybrid components and battery system. The fuel economy of the Altima Hybrid is better than that of the Camry Hybrid in the City but not the HWY cycle. A summary of this comparison is shown in Table 2. The Altima Hybrid's fuel economy in the City is better than that of the Camry Hybrid mainly because of lower mass and decreased engine-on time. On the HWY cycle, the Camry Hybrid's fuel economy is better than that of the Altima Hybrid mainly because engine efficiency is most likely higher in the Camry because of the higher compression ratio and Miller Cycle operation.

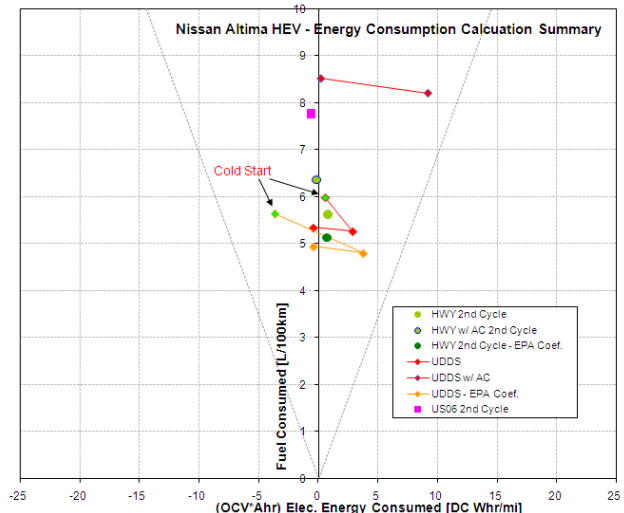
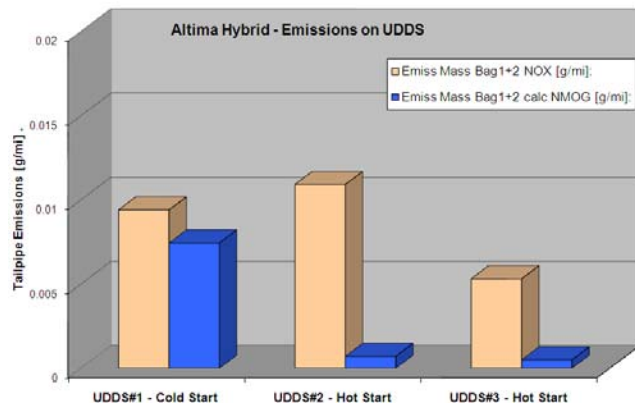


Figure 15. Altima Hybrid Fuel Consumption Dynamometer Testing Results

Table 2. Fuel Economy Comparison of Altima Hybrid and Camry Hybrid

	Altima Hybrid	Camry Hybrid
EPA Reported Fuel Econ (mpg)	35 City 33 Hwy	33 City 34 Hwy
Dyno Test Results Fuel Econ (mpg)	33.5 City 32.3 Hwy	32.9 City 34.3 Hwy
Test Weight (lb)	3750	4000
Engine Size [L]	2.5 L	2.4 L
Engine Comp Ratio	9.6:1	12.5:1
Engine-On Time Hot UDDS [%]	33.3	35.4

Tailpipe emissions from the Altima Hybrid were collected through the dynamometer testing. The vehicle demonstrated SULEV emissions levels, as shown in Figure 16.

**Figure 16. Altima Hybrid Tailpipe Emissions Results**

Conclusions

The APRF at ANL has become a powerful tool for gathering data from the most advanced powertrains at a level of detail not available anywhere else in the industry. The OEM (original equipment manufacturer) partners in FreedomCAR have become close collaborators in terms of sharing time and equipment, and they benefit significantly from the testing programs and studies performed at ANL's Center for Transportation Research. In addition, ANL is constantly introducing new instrumentation methods, like CAN signal data acquisition, which can replace some sensors. This will improve the reliability of data acquisition and reduce the effort and time delays encountered when fabricating and installing intrusive sensors into the vehicle. Such new testing methodologies will also allow us to collect more readings from a larger subset of vehicles being tested.

B. Benchmarking of Plug-In Hybrid Electric Vehicles

Michael Duoba (Project Leader)

Argonne National Laboratory

9700 South Cass Avenue

Argonne, IL 60439-4815

(630) 252-6398; mduoba@anl.gov

DOE Technology Manager: Lee Slezak

(202) 586-2335; Lee.Slezak@ee.doe.gov

Objectives

Provide operational data during chassis dynamometer testing by using novel instrumentation for various converted plug-in hybrid electric vehicles (PHEVs):

Hymotion Escape PHEV – Level 1

Electrovaya Escape PHEV – Level 1

HybridsPlus Escape PHEV – Level 1

Approach

Measure energy usage from the vehicle's battery system(s) by using the Hioki Power Meter, which includes current and voltage sensors. The Hioki meter also calculates real-time ampere-hour (Ahr) and kilowatt-hours (kWh).

Measure tailpipe emissions from the vehicle. Calculate fuel economy from this emissions measurement through use of a carbon balance method.

Collect data from vehicle control signals from the controller area network (CAN) bus.

Test fuel economy and emissions over the Federal Testing Procedure and highway (HWY) cycles.

Test in extreme ambient temperature conditions to determine the effect on fuel consumption.

Accomplishments

Determined results from dynamometer testing for Electrovaya Escape PHEV, Hymotion Escape PHEV, and HybridsPlus Escape PHEV.

Conducted sub-freezing ambient temperature testing on the Hymotion Escape PHEV and a Hymotion Prius PHEV.

Future Directions

Investigate the effect of driving intensity on PHEV fuel consumption in terms of:

Dynamometer testing with more aggressive driving intensity.

Correlation of dynamometer testing to on-road fleet data.

Introduction

Now that plug-in hybrid electric vehicles (PHEVs) are emerging, it is important to test, characterize, and benchmark the variety of PHEV designs and control strategies. Vehicle benchmarking combines testing and data analysis to characterize a vehicle's efficiency, performance, and emissions. The vehicle is tested over many cycles to deduce the control strategy under a variety of operating conditions. The PHEV benchmarking data can be applicable to virtually every effort in the FreedomCAR partnership, and all of the Tech Teams benefit from the data collected in Argonne's Advanced Powertrain Research Facility (APRF).

Approach

Three Escape PHEV conversions were tested in the APRF over cold-start and hot-start urban dynamometer driving schedule (UDDS) and HWY cycles in both charge-depletion and charge-sustaining operation. Full-charge tests, as well as abbreviated tests with the air conditioner operating, were conducted. Charging events were also collected and analyzed. These three Escape PHEVs are owned by the New York State Energy Research and Development Authority (NYSERDA).

During charge-depletion operation, PHEVs use only a fraction of the fuel normally consumed in charge-sustaining operation. For this reason, the accuracy of data collected is of the highest importance. The Advanced Powertrain Research Facility (APRF) is able to produce results within repeatability of one percent. Measurement of fuel consumption and electrical energy consumption are necessary to characterize the operation and impact of each PHEV.

Testing was also conducted in an on-road study at a wide range of ambient temperatures to investigate the effects of temperature on PHEV fuel consumption resulting from battery system temperature.

Vehicles Tested

Electrovaya Escape PHEV Level 1

The Electrovaya Escape PHEV, shown in Figure 1, uses an additional 12-kWh lithium ion (Li-ion) battery pack in addition to the production nickel metal hydride (NiMH) battery system. This Li-ion system is composed of Electrovaya Li-ion cells.



Figure 1. Electrovaya Escape PHEV

The additional Li-ion battery pack sits on top of the production NiMH pack as seen in Figures 2 and 3. It transfers power to the high-voltage bus through a series pass regulator, which is an actively controlled integrated gate bipolar transistor (IGBT) that controls current flow. This device is unidirectional, which means that the Electrovaya battery can supply power, but it cannot accept current, such as during regenerative braking.



Figure 2. Battery System of the Electrovaya Escape PHEV



Figure 3. Inside the Electrovaya Escape PHEV Battery System

Hymotion Escape PHEV Level 1

The Hymotion Escape PHEV, shown in Figure 4, uses an 8-kWh Li-ion battery pack in addition to the stock NiMH pack. An actively controlled direct current (DC)/DC converter is used to transfer power from the Li-ion pack to the high-voltage bus.



Figure 4. Hymotion Escape PHEV

The Hymotion battery system, shown in Figures 5 and 6, is composed of A123 cells and an actively controlled DC/DC converter that controls the power delivered to the high-voltage bus of the vehicle.



Figure 5. Hymotion Escape Battery System



Figure 6. Inside the Hymotion Escape Battery

HybridsPlus Escape PHEV Level 1

The HybridsPlus Escape PHEV, shown in Figure 7, is a battery replacement PHEV system that uses a 12-kWh Li-ion battery pack composed of A123 cells.



Figure 7. HybridsPlus Escape

The HybridsPlus battery system (Figure 8) replaces the production NiMH battery, which reduces vehicle weight but increases control complexity because HybridsPlus must control the battery during all modes of operation, including charge-sustaining operation. In addition, the electrical control unit (ECU) communication must be properly implemented by HybridsPlus to prevent data transfer controller (DTC) or communication errors.



Figure 8. HybridsPlus Escape Battery System

Testing and Analysis

The three Escape PHEV conversions are tested by the energy technology engineering center (ETEC) through a series of on-road tests to determine real-world fuel economy from city and highway driving. The ETEC also performs coastdown testing of the three vehicles to determine the roadload settings to be used during dynamometer testing. Figure 9 shows the dynamometer ABC coefficients used for testing that were obtained by ETEC's coastdown testing. Notice the largest difference between the vehicles is mass.

The HybridsPlus Escape weighs significantly less (by about 250 lbs) than the other two Escape conversions because HybridsPlus is a battery replacement conversion, therefore eliminating the mass of the production battery.

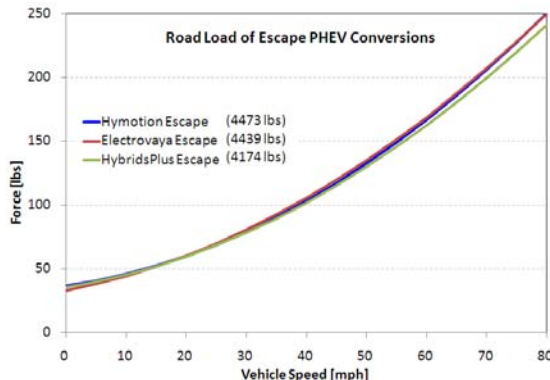


Figure 9. Roadload Settings Used For Dynamometer Testing of the Three PHEVs

All of the Escape PHEV conversions use CAN bus signal manipulation to operate in a charge-depletion control strategy. The Hymotion Escape and the HybridsPlus Escape operate with an essentially constant depletion rate because both are controlled directly. The HybridsPlus Escape control is through the production Escape ECU control by CAN signal manipulation, and the Hymotion Escape DC/DC converter is controlled to deliver a constant depletion rate. The Electrovaya, on the other hand, has a depletion rate that decreases with battery state of charge (SOC). The depletion rate depends mainly on the battery voltage. As the voltage decreases, the depletion rate also decreases. These depletion rates can be seen in Figure 10. Each point on the graph is an individual test cycle. Note the cluster of points for the Hymotion Escape and the HybridsPlus Escape in the middle right-hand side of the graph. These points indicate a constant rate of depletion. The Electrovaya Escape shows a decreasing rate of depletion by successive tests by having increased its fuel consumption and decreased its electrical energy consumption. The graphical points are migrating up and left on the graph.

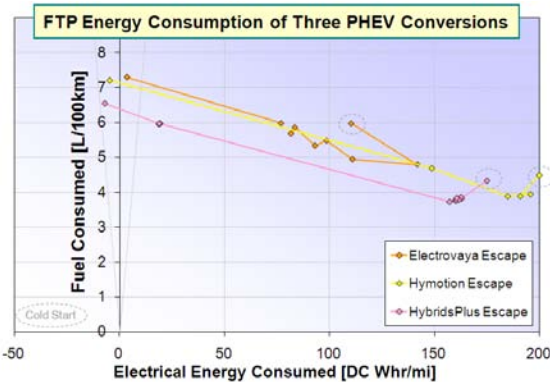


Figure 10. Energy Consumption of the Three Escape Conversions and Four Prius Conversions

The tailpipe emissions from the three Escape PHEVs were below super ultra-low emission vehicle (SULEV) limits. Figure 11 shows the emissions of the three Escape PHEV conversions. While some early Prius PHEV conversions did not meet SULEV because of limited calibration development, all three of the Escape PHEV conversions were shown to be SULEV compliant.

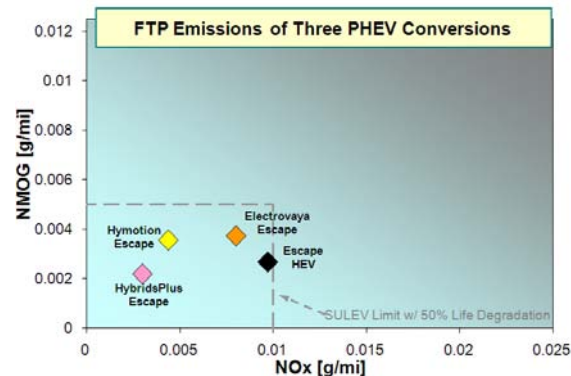


Figure 11. Tailpipe Emissions of Three Escape PHEVs Conversions

Sub-Freezing Ambient Temperature Testing

Testing was conducted at sub-freezing temperatures to determine the impact of battery temperature on fuel consumption of a conversion PHEV. The Hymotion Escape was the vehicle used for this study, which is shown in Figure 12.



Figure 12. Hymotion Escape PHEV at Sub-Freezing Ambient Conditions

This on-road testing was conducted over a prescribed driving route at prescribed speeds and accelerations. Additional testing was conducted to isolate the impact of the battery temperature on the fuel and electrical energy consumption levels. This test was performed by directly comparing two tests, including a baseline test in which the vehicle is cold-soaked overnight in sub-freezing conditions to allow all the systems on the vehicle to approach steady-state ambient temperature. The second test maintains battery temperature to approximately 15°C during the cold-soak period such that the battery begins the test at normal operating temperature. This temperature regulation was accomplished by placing a small heater around the battery (both the Hymotion Li-ion and the production NiMH), which was on only during the soaking period — not during testing. Comparing the results of these two tests will indicate the direct impact of battery temperature on conversion PHEV fuel consumption.

Figure 13 shows the percentage increases in fuel consumption as compared to the steady-state fuel consumption after the vehicle was driven for a long enough amount of time such that all of the vehicle systems reached a steady-state operating temperature in the -5°C ambient temperature. The charge-depleting fuel consumption at this steady-state operating temperature is 4.9 L/100 km, and the electrical energy consumption is 190 Wh/mile.

For the baseline test, the overall increased fuel consumption was 70 percent for the first loop on the on-road cycle, when the entire vehicle starts from -5°C. The successive cycles decrease in fuel consumption because all of the vehicle's systems are warming up. The baseline tests are shown by the blue line.

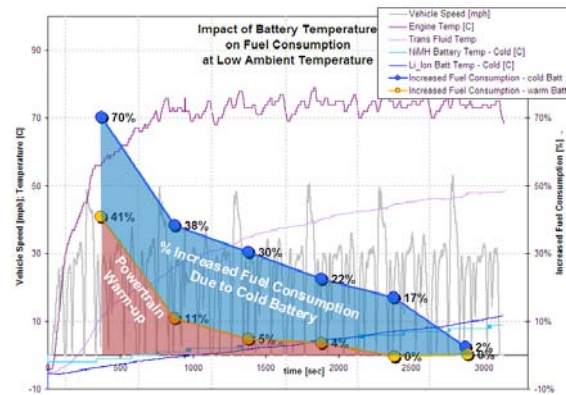


Figure 13. Fuel Consumption Differences between the Cold and Warm Battery Tests

For the experimental tests with the battery temperature maintained above 15°C, the powertrain and driveline reduced efficiency, which accounted for a 41 percent increase in fuel consumption in the first test loop drive cycle. The successive cycles also showed a decreasing impact on fuel economy as the vehicle systems warmed up. These experimental tests are shown by the yellow line.

The area in red in Figure 13 shows the impact of the powertrain and drivetrain, whereas the blue area is the impact resulting from the battery system.

For the baseline test, as the engine quickly warms up, the fuel consumption impact rapidly decreases. Once the engine is at steady-state operating temperature (i.e., after approximately 10 minutes), the transmission and driveline cold inefficiencies caused the remaining impact on fuel consumption as the systems continue to warm up toward the steady-state temperature. In contrast, the increase in the battery system's temperature from -5°C to 10°C was fairly slow — approximately one hour — which made the fuel consumption impact from the battery temperature more significant than the powertrain warm-up impact, and it tapered off over a much longer period of time. Even after the hour of testing, the battery system had not reached a steady-state temperature, but the battery power was operating at normal levels.

The engine on/off operation was nearly the same for the two tests, but the fuel and electrical energy consumption rates were quite different. This difference is likely because the production battery calibration in the Escape powertrain control system protected the battery at sub-freezing conditions. The

NiMH battery system has reduced power capability at sub-freezing temperatures, and the Hymotion system cannot circumvent the calibration used by the hybrid control system even though the cold temperature capability of the Li-ion battery system is more robust.

Summary

Three PHEV Escape conversions were tested on dynamometer drive cycles as well as in sub-freezing ambient conditions. The results from dynamometer testing showed the effectiveness of PHEV conversions for midsize SUVs, along with the feasibility of obtaining SULEV limits. Conversion PHEVs have been shown to possess a few limitations that reduce their ability to displace fuel consumption at a high rate; overall, however, the three PHEV conversions tested show a considerable capability to displace petroleum.

Publications/Presentations

R. Carlson, et al., "Impact of Sub-Freezing Ambient Conditions on PHEV Fuel Consumption," *EVS 24*, May 2009.

C. PHEV Test Methods and Procedures Development

Michael Duoba (Project Leader)

Argonne National Laboratory

9700 South Cass Avenue

Argonne, IL 60439-4815

(630) 252-6398; mduoba@anl.gov

DOE Technology Manager: Lee Slezak

(202) 586-2335; Lee.Slezak@ee.doe.gov

Objectives

Work with SAE by chairing the industry subcommittee to rework the existing SAE J1711 standard for hybrid electric vehicle (HEV) test procedures, to accommodate the testing specifically of plug-in hybrid electric vehicles (PHEVs).

Define the “Utility Factor” for PHEV charge-depleting operation by using 2001 Department of Transportation (DOT) data.

Work with California’s Air Resources Board (CARB) staff to help satisfy their objectives of testing and quantifying PHEV advantages to achieve the goal of finishing a procedure document for certification of PHEVs in California over the summer of 2008.

Approach

Chair the J1711 SAE task force committee, set agendas, and facilitate decision-making.

Hold regular meetings with CARB staff (mostly phone conferences) and attend public staff meetings.

Sponsor a new SAE document (SAE J2841) that defines the “Utility Factor” that will be referenced by CARB legislation

Use the vehicles available through the Advanced Vehicle Testing Activity (AVTA), the Argonne National Laboratory (ANL)-instrumented Prius, the Mobile Advanced Technology Testbed (MATT) platform, and the Through-the-Road (TTR) prototype vehicle for testing various uncertain aspects of the new test procedures.

Accomplishments

The SAE J1711 task force met monthly throughout fiscal year (FY) 2008, starting with a long list of unresolved issues and one by one found data to support a decision or found innovative solutions to remove the roadblocks.

Several key testing issues were addressed by extensive testing in ANL’s Advanced Powertrain Research Facility (APRF). For example, using 4 HWY cycles in a row was recommended after it was discovered during testing that 2 HWY cycles in a row showed unacceptable differences in the second test.

ANL helped CARB successfully create the new hybrid electric vehicle (HEV)/PHEV test procedure document by recommending various procedural changes and coming up with test data to support ANL’s opinions.

Future Directions

Although the SAE J1711 concept was frozen this year, the document still needs to be rewritten and submitted for ballot in the next fiscal year.

ANL has been asked by industry to co-organize the SAE J1634 (battery electric vehicle [BEV] test procedure), with a focus on developing a shortcut method. ANL’s experience with developing a PHEV shortcut method will be useful. Also, electric vehicle (EV) operation of a PHEV must be compatible with results from BEV testing.

The DOE must issue a ruling on the Petroleum Equivalency Factor (PEF) for electricity energy use of BEVs and PHEVs. ANL's experience in test procedures and in doing well-to-wheel analysis (Greenhouse Gases, Regulated Emissions, and Energy Use in Transportation [GREET] model) will be instrumental in providing guidance in its update.

Introduction

In the mid-1990s, the SAE J1711 task force (chaired by GM) developed the original J1711 procedure document. However, at that time, no production hybrid electric vehicles (HEVs) or plug-in hybrid electric vehicles (PHEVs) existed. In fact, procedure validation was performed at General Motors (GM) with student competition vehicles from University of California (UC) - Davis (PHEV) and the University of Maryland (charge-sustaining HEV).

By 2004, the original J1711, like all SAE J-docs after five years, expired. They require reapproval either as-is or after some updating. The fundamental procedures used for HEVs are not in contention; it was the PHEV procedures that drew attention. In the literature and in stakeholder focus groups (like those held at DOE in 2006), many widely accepted assumptions for how PHEVs should be tested deviated from the original assumptions given in the original J1711. Soon after the DOE stakeholder meeting, the industry called upon ANL to chair the SAE J1711 session and make the PHEV section up to date and to support consensus decisions with reliable PHEV data.

The SAE J1711 reissue effort has spanned from late 2006 to the current FY 2008. In 2007, the focus was on developing a "5-Day" PHEV test procedure to test the Advanced Vehicle Testing Activity (AVTA) vehicles that were planned to come to ANL over the next year or two. In FY08, the focus was on helping CARB with their procedures and freezing the J1711 test concept.

Approach

Many of the existing PHEV programs at ANL heavily leverage the test procedure development activity. Because engineers have had over a decade to think about testing PHEVs, conceptually, nothing is new. The only effort that will help in the development is access to new data to support major decision points. Many of the small investigative experiments were aimed at looking at the impact of

various decisions — in other words, asking the question, "How important or sensitive is the outcome if the testing or calculations are conducted on any one of several concept options?"

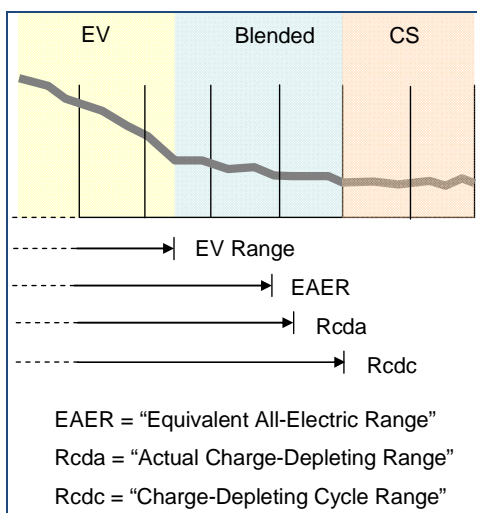
The SAE J1711 document has essentially three different components: (1) definitions and terminology, (2) test sequence and procedure, and (3) data processing and weighting.

Terminology and Definitions

A great deal of time was spent making suitable definitions for PHEVs to satisfy CARB's new rules for PHEVs in their Low Emissions Vehicle program (also known as the "ZEV mandate"). Among other sources of discussion, ANL published and presented data supporting the notion that a "blended" depleting mode is still a viable and worthy technology option that should be included in the CARB credit matrix. CARB did decide to include the vehicle and used a host of terms and definitions, some of which came from ANL procedure development concepts. Over the course of several months in FY08, definitions like "charge-depleting cycle range," "actual charge-depleting range," "electric range fraction," and "equivalent charge-depleting range" were investigated and developed by ANL and CARB through the use of ANL data and modeling. Figure 1 illustrates the various range definitions.

Test Sequence and Procedures

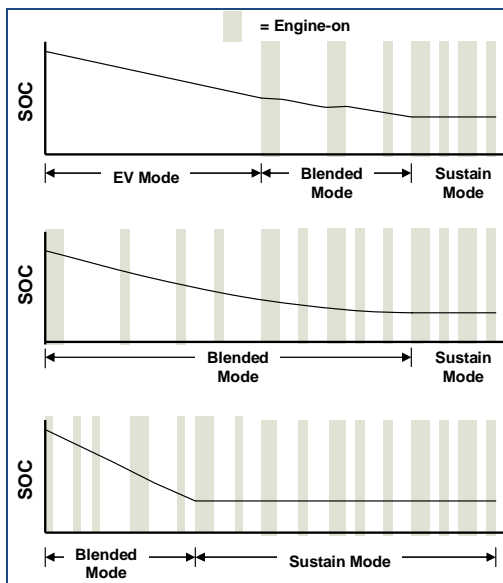
One of the biggest challenges was taking existing legacy test procedures and methodology and applying them to the concept of charge-depleting operation. Although in parts of the conventional vehicles test procedures conditions are defined for stabilized operation, this is never the case in charge-depleting operation in which the vehicle takes much longer to warm up, and eventually the vehicle transitions to sustaining behavior. The implications of this cannot be overstated. An oversight in the procedure concept could, on the one hand, yield a benefit for plug-ins that would inspire all manufacturers of today's

**Figure 1. PHEV Range Definitions**

charge-sustaining hybrids to install a plug on the car for a phantom benefit in emissions or fuel consumption.

The fundamental departure from conventional vehicle tests is testing the vehicle in its charge-depleting mode in what is termed the “Full Charge Test” (FCT).

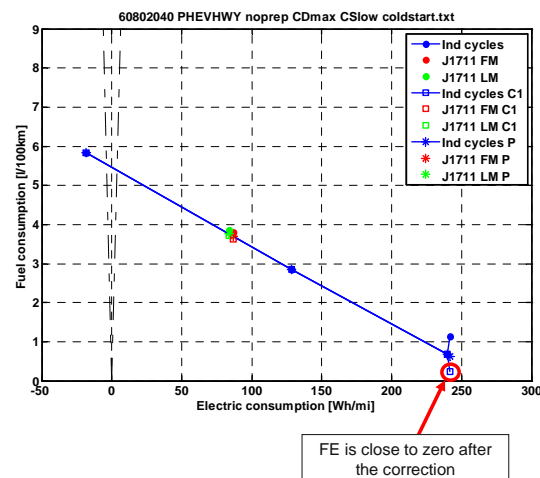
The objective of the FCT is to capture all possible operation of a specific test cycle from full charge to charge-sustaining. Figure 2 shows some operational possibilities of a PHEV.

**Figure 2. Full Charge Test for Various PHEV Operating Strategies**

The highway test is particularly challenging when using the model of the FCT. The legacy test condition is a thermally stabilized condition in which two cycles are run in series, with the first acting as the “prep” cycle for the second. Only the second cycle counts. For a vehicle in which every depleting kWh counts, the throwing away the first cycle was not an option.

CARB had suggested a “cold-start” correction to account for the inefficient operation that was previously never included in highway cycle testing. This method was included in the draft CARB procedure documents. ANL investigated the robustness of this technique and predicted that it may be prone to unacceptable errors if the vehicle had a very high electric range fraction (ERF). ANL employed the now-mature MATT platform tool to investigate the issue. Conceptual experiments or modeling alone cannot address issues of thermal conditions and its impact. Real hardware with an open controller (such as MATT) was a perfect research tool for the job. The experiment prescribed various levels of ERF in depleting operation tests by adjusting control parameters.

Indeed, an analysis of the experimental data (in Figure 3) revealed that the correction methodology did distort the correction to the point where zero (or even negative) fuel consumption was the conceivable output of the correction. CARB may be changing the policy on cold-start highway correction.

**Figure 3. Results of MATT Experiments Showing Cold-Start Highway Correction Data**

MATT's flexible design employs an emulated battery and electric drive system (based on state-of-the-art models of real hardware) that runs off the grid and not an actual battery. Test conditions can be easily repeated to study very specific aspects of the test procedure. One such J1711 experiment that exploited this capability was the soak time experiment.

Limitations in test cell hardware prevent testing that can run all day without interruption. How sensitive are the intra-test pause lengths to the results? ANL's experiment showed that blended operation actually runs the engine at much lower temperatures than conventional vehicles, and so the changes in soak times were less sensitive than originally thought.

Data Processing and Weighting

The fundamental concept behind processing PHEV results is using in-use driving pattern statistics applied to the PHEV operating ranges found in the test to weight the two fundamental operating modes: depleting and sustaining.

The J1711 committee decided that a separate document that specifically addresses the "Utility Factor" (UF) would be helpful for CARB because their pending legislation required a document to reference. This document was sponsored by ANL staff and is called J2841, "Utility Factor Definitions for Plug-In Hybrid Electric Vehicles Using 2001 U.S. DOT National Household Travel Survey Data." In the analysis, it was found that the original UF curves from 1995 data were processed incorrectly, and the new results from the 2001 data show a more favorable UF for PHEVs. This document was finished and will go to ballot at the beginning of the next fiscal year.

Conclusions

ANL's 12 years of expertise in fuel economy and emissions testing of HEVs and PHEVs are unmatched in the DOE system, if not the world. This is the reason industry requested that ANL lead the J1711 effort. Challenges that have not been overcome for a decade were addressed by the committee with a fresh look and with data from operational PHEVs never before available.

There are high-profile questions as to whether the announced GM Volt will get a label fuel economy of over 100 mpg, and ANL staff is doing everything it

can to provide the expertise in test procedure development to cope with these questions.

ANL is working very hard on-line in the committee and off-line with original equipment manufacturers (OEMs) and suppliers. Several OEMs have brought their protected and secret vehicles to ANL to ensure that they get data that are the best anywhere in the world. Access to state-of-the-art resources has been one reason this project has been so successful.

ANL will continue this effort next fiscal year by co-chairing the EV test procedure rewrite, J1634, "Electric Vehicle Energy Consumption and Range Test Procedure." A related effort is the redevelopment of DOE's Petroleum Equivalency Factor (written in 1995), which defines the way in which electric energy is counted toward petroleum use in CAFE regulations.

Publications/Presentations

Duoba, M., et al., "Test Procedures and Benchmarking Blended-Type and EV-Capable Plug-In Hybrid Electric Vehicles," paper published in EVS-23, Anaheim, CA, Dec. 2–5, 2007.

Duoba, M., et al., "SAE J1711 PHEV Test Procedure Development," HEV Symposium Presentation, San Diego, CA, Feb. 13–14, 2008.

Duoba, M., et al., "Test Procedure Development for 'Blended Type' Plug-In Hybrid Vehicles," SAE 2008-01-0457, SAE Congress, April 2008.

Duoba, M., et al., "On Measuring The Fuel Economy and Emissions of HEVs and PHEVs," Transportation and Energy Panel, Host: BP, Naperville, March 20, 2008.

D. Advanced Hydrogen Vehicle Benchmarking

Michael Duoba (Project Leader)

Argonne National Laboratory

9700 South Cass Avenue

Argonne, IL 60439-4815

(630) 252-6398; mduoba@anl.gov

DOE Technology Manager: Lee Slezak

(202) 586-2335; Lee.Slezak@ee.doe.gov

Objectives

Prepare test facilities and test procedures to take advantage of testing more optimized hydrogen internal combustion engines (H-ICE) and vehicles that will be available for testing in fiscal year (FY) 2007.

Capitalize on the opportunity to use Argonne National Laboratory's (ANL) Advanced Powertrain Research Facility (APRF) test lab to implement its current test procedures and analysis capability whenever a fuel cell vehicle becomes available for testing; report all findings.

Continually work on obtaining accurate and verifiable emission measurements as test vehicles approach zero emissions capability. Alternatively, introduce more refinement and optimization of the existing hydrogen measurement hardware and validate with hydrogen vehicle testing.

Approach

Collect hydrogen-fueled vehicle data by using ANL's 4-wheel drive (WD) chassis dynamometer. For more details about the test facility, refer to the efforts described in Section 4.1 Benchmarking and the validation of hybrid electric vehicles (HEVs).

Adapt testing methods to measure fuel consumption of non-hydrocarbon-based fuels (such as hydrogen).

Conduct repeat tests, if available, to ensure robustness and accuracy.

Perform mathematical analysis to verify quality control of the data.

Accomplishments

Completed biannual one-week sessions of testing on two Chevrolet Silverado H-ICE vehicles as part of a hydrogen engine durability program.

Tested a fuel-cell-powered hybrid crossover SUV built by the University of Waterloo for the advanced vehicle student competition.

Tested and benchmarked a BMW 7-series H-ICE vehicle. Measured near zero emissions. Integrated and utilized a new water balance fuel consumption technique and compared to mass flow measurements.

Future Directions

Test new and unique vehicles that utilize hydrogen as a fuel source, if available.

Report analysis and findings to DOE.

Introduction

Research continues into the use of hydrogen as a vehicle fuel to resolve existing economic, technical, and social barriers. ANL

supports the testing of prototype and proof-of-concept hydrogen vehicles to better understand fuel consumption, emissions, performance, and testing methods. ANL tested a dedicated fuel cell hybrid conversion, two H-ICE-powered BMW 7-series vehicles, and two H-ICE-powered Silverados converted by Electric Transportation Engineering Corporation (eTec) and Roush.

Last year, a new fuel consumption measurement technique that measures the water content of the exhaust was integrated into the laboratory. In an effort to improve the quality of the data collected on hydrogen-powered vehicles, ANL collaborated with BMW engineers to incorporate water-based fuel consumption calculations into the APRF. This metric is directly proportional to fuel consumed by the vehicle and is advantageous while requiring no modification to or interruption of the fuel system to measure fuel consumption. Results of testing the system are presented in the Hydrogen BMW 7-Series testing section. Results for both of the H-ICE Chevrolet Silverados, as well as a fuel-cell-powered Chevrolet Equinox, are also presented.

Approach

H-ICEs can achieve near-zero regulated tailpipe emissions. However, early concepts of H-ICE demonstrated significant challenges associated with NO_x production while still maintaining a reasonable specific power of the engine. With additional development over the past four years, H-ICE-powered vehicles are now achieving lower NO_x and are continuing to increase specific power of the engine. It is therefore critical for super ultra-low emission vehicle (SULEV) and sub-SULEV tailpipe concentrations to have equipment and accuracy sufficient to characterize the emissions and efficiency of such powertrains.

Figure 1 shows one of the two truck-based hydrogen vehicles tested that are part of a demonstration fleet being run by eTec under DOE's Advanced Vehicle Testing Activity (AVTA). These vehicles return to ANL twice a year for fuel consumption, emissions,

and performance testing as part of a hydrogen engine durability study.



Figure 1. Hydrogen-Converted Truck Undergoing Tests at the APRF

For testing of the Silverado, fuel flow was measured directly through the APRF H₂ fuel flow supply and measurement system. The facility connects into the gaseous hydrogen fuel line of the truck. This method of measuring fuel consumption utilizes a mass flow meter based on the Coriolis effect. For hydrogen vehicles with a cryogenic hydrogen fuel system, it is not possible to connect the APRF fuel system to the car. In those situations, the water balance measurement method was applied to the BMW H-ICE vehicle testing. The APRF is the first test laboratory in North America to perform this kind of measurement. Both measurement techniques were used on the hydrogen trucks to validate the water balance method as compared to the more traditional mass flow measurement.

H-ICE Silverado Results

Both of the H-ICE Silverados were tested in March and August of 2008. Cumulative miles at the onset of testing for the Red Silverado were 18,948, while the white Silverado accumulation was 11,932 miles. Both vehicles were tested over the standard three-bag Federal Test Procedure (FTP), as well as the US06 cycle. Coastdown coefficients were collected for both test periods and compared to ensure consistency.

Emissions results are shown for the cold start FTP test in Figure 2, while results for the US06 cycle are shown in Figure 3.

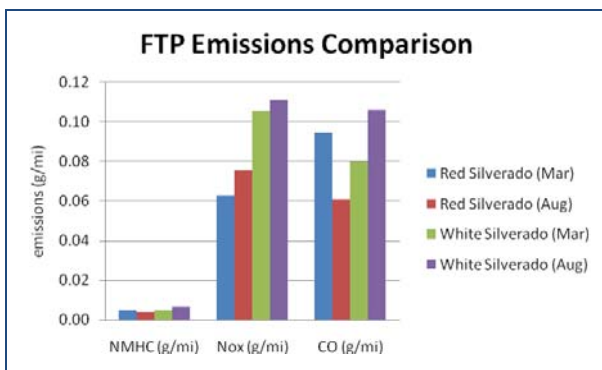


Figure 2. Comparison of FTP Emissions between March/April 2008

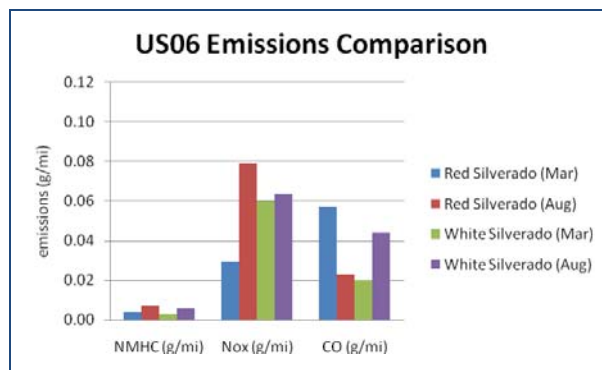


Figure 3. Comparison of US06 Emissions between March/April 2008

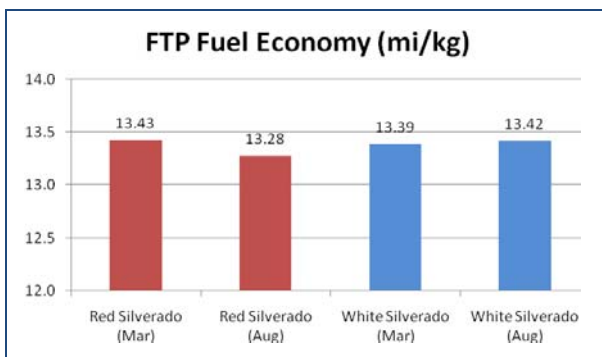


Figure 4. Comparison of FTP Fuel Economy between March/April 2008

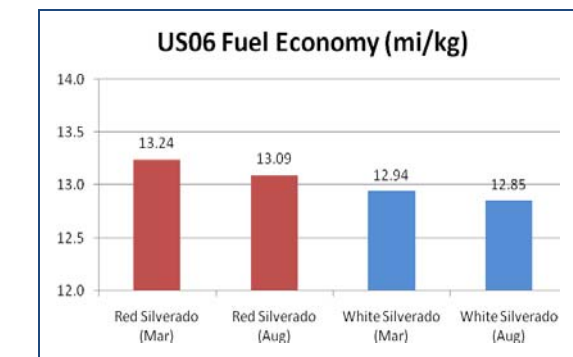


Figure 5. Comparison of US06 Fuel Economy between March/April 2008

From both Figures 2 and 3, it may be seen that the nonmethane hydrocarbons (NMHCs) and carbon monoxide (CO) emissions levels for both vehicles are well below regulated SULEV limits. However, nitrogen oxide (NO_x) emissions are near or slightly under ULEV standards. NO_x emissions for the US06 test cycle are lower than that for the FTP cycle, an interesting phenomenon given that the loading for the US06 is greater than the FTP. These are raw emissions because these vehicles do not use any exhaust after-treatment system, such as a catalyst.

Fuel economy results for both vehicles are compared for the FTP and US06 cycles in Figures 4 and 5. For both vehicles, there was a slight degradation in fuel economy from March to August. The hydrogen flow meters are accurate to within ± 0.35 percent of the total hydrogen flow rate; therefore, the trends are most likely real within the variation of vehicle testing or actual behavior as a function of mileage accumulation in the vehicles.

Performance metrics of the vehicles were also tested. The 0–60 maximum effort acceleration tests were conducted; the results are displayed in Figure 6. In general, the white Silverado is slightly faster as it is 500 pounds lighter than the red Silverado.

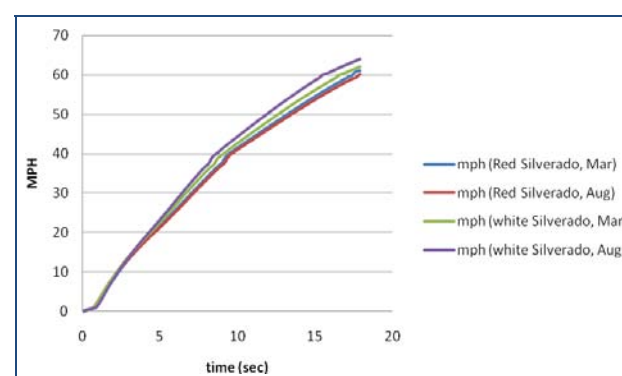


Figure 6. The 0–60 mph Maximum Effort Acceleration between March/April 2008

Fuel Cell Equinox Results

The University of Waterloo converted a Chevrolet Equinox into a hydrogen fuel cell HEV (Figure 7). Two 30-kilowatt (kW) hydrogenics stacks are packaged with the auxiliary support system, such as a cooling system and air blower packaged in the vehicle. All-wheel-drive (AWD) propulsion is provided by two electric motors. A battery pack is used in this series hybrid as the energy and power buffer.



Figure 7. Hydrogen Fuel Cell HEV Test at the APRF

The hybrid control strategy is thermostatic load following. In other words, the fuel cell system provides power to charge the batteries to a higher state of charge (SOC) target. Then the battery provides power until a lower SOC target is reached, and the fuel cell charges again. Under heavy acceleration, both the fuel cell and the battery provide the power to the traction motors. Figure 8 shows the battery usage and control strategy.

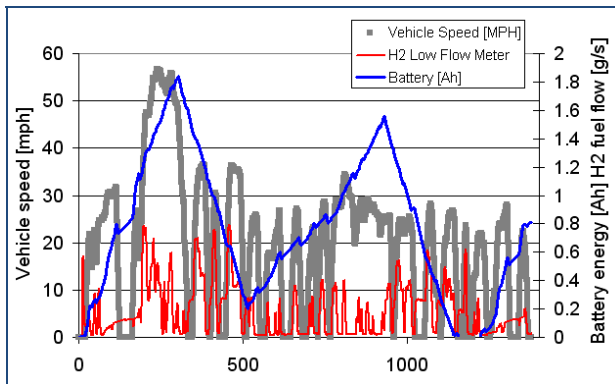


Figure 8. Battery Energy Usage and Fuel Flow on an Urban Cycle

Because of the control, a charge-sustaining urban dynamometer driving schedule (UDDS) cycle was not guaranteed. So several urban cycles (hot and cold) were completed, and the fuel economy results are provided in Figure 9.

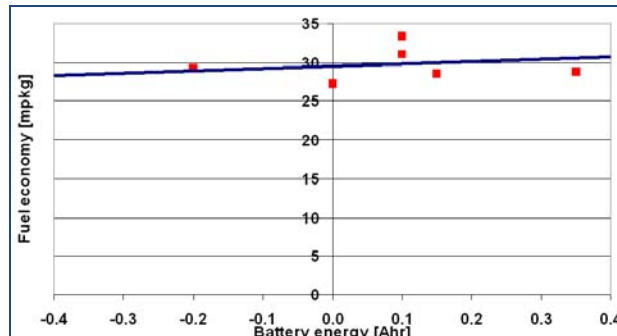


Figure 9. Fuel Economy as a Function of Battery Usage

The charge-sustaining fuel economy for this fuel cell HEV is around 30 miles per kilogram of hydrogen. The stock Chevrolet Equinox is 18.5 mpg on a cold-start UDDS and at 22.4 mpg on a hot start. This fuel cell conversion improved the fuel economy by more than 30 percent on an energy equivalent basis.

The fuel cell system efficiency may explain this improvement. Figure 10 shows the fuel cell system efficiency as being between 40 percent and 50 percent. The average fuel cell system efficiency on the UDDS cycle is around 48 percent.

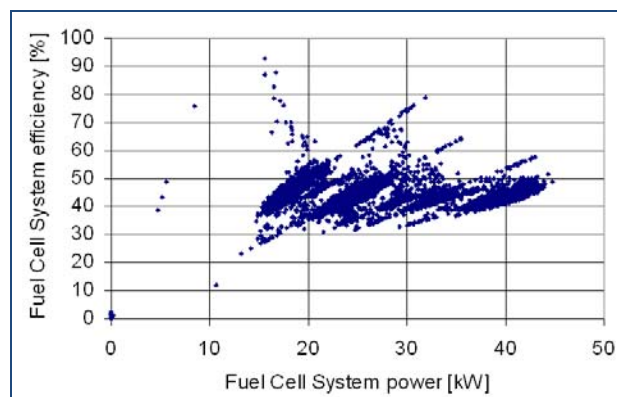


Figure 10. Fuel Cell System Efficiency as a Function of Fuel Cell Power Output

Water Balance Method of Hydrogen Fuel Consumption Measurement

This approach requires measurement of intake air and dilution air humidity as well as water and hydrogen content in the diluted exhaust. On the basis of these numbers, the fuel consumption can be back-calculated by applying a water-balance and using calculations similar to those used for carbon balance with conventional fuels.

Figure 11 is a schematic of the setup used to verify the accuracy of the water balance. For this approach, the fuel consumption of a hydrogen Silverado was measured directly by using a Coriolis mass flow meter and comparing it to the results of the water balance.

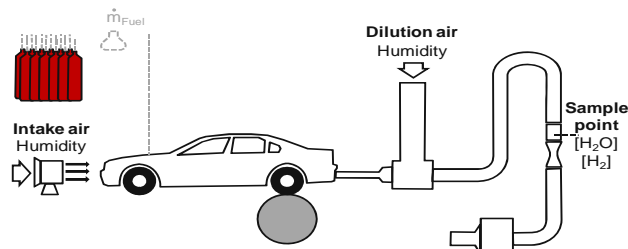


Figure 11. Schematic of Setup for Validation of Water Balance for Fuel Consumption Measurement on Hydrogen Vehicles

A sample result for several steady-state operating points is shown in Figure 12. The hydrogen fuel flow determined with both methods, the direct measurement as well as the water balance, and the relative difference are plotted versus test time. During the steady-state phases at various fuel flow rates, the differences between the direct measurement and calculated results based on water balance are very small. It is also apparent that during the load changes the differences become more pronounced. Because of the applied concept, the water balance is not designed to measure highly dynamic fuel consumption. However, the overall fuel consumption during a drive cycle is expected to match closely even with deviations during highly dynamic operation. This expectation was confirmed by running a Japan 10–15 test cycle. The overall fuel consumption of the direct fuel measurement using a Coriolis meter deviated less than 2 percent from the water balance measurement — confirming that the water balance provides accurate hydrogen fuel consumption values.

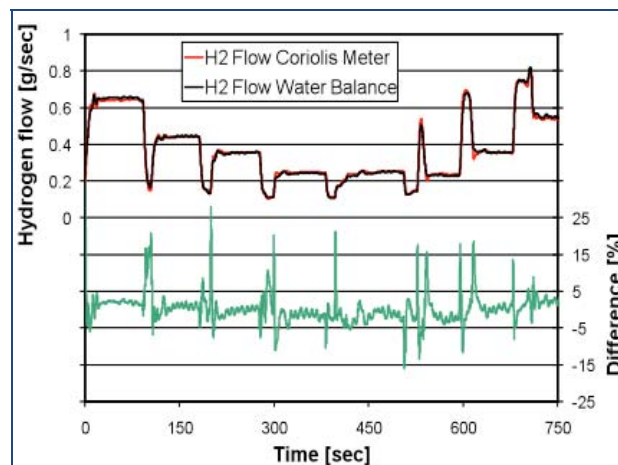


Figure 12. Correlation between Fuel Consumption Measurement Methods for Steady-State Operating Points

BMW H2 7-Series Results

The BMW Hydrogen 7 Mono-Fuel demonstration vehicles were tested for fuel economy as well as emissions on the FTP-75 cold start test as well as the highway test.

The fuel economy numbers on the FTP-75 test were 3.7 kg of hydrogen per 100 kilometers (km), which, on an energy basis, is equivalent to a gasoline fuel consumption of 17 miles per gallon (mpg). Fuel economy numbers for the highway cycle were determined to be 2.1 kg of hydrogen per 100 km or 30 miles per gallon of gasoline equivalent (GGE).

The emissions results (Figure 13) show that these vehicles achieve emissions levels that are only a fraction of the SULEV standard for NO_x and CO emissions. For NMHC emissions, the cycle-averaged emissions are actually 0 g/mile, which requires the car to actively reduce emissions as compared to the ambient concentration (Figure 14).

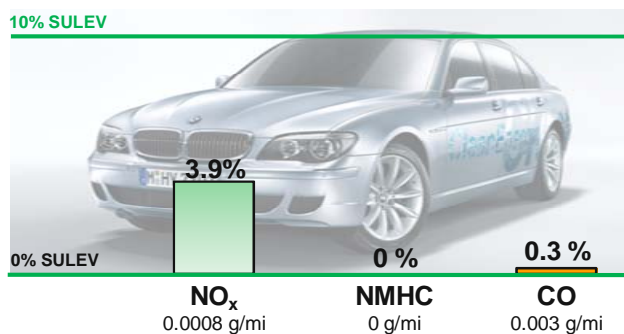


Figure 13. Hydrogen 7 Emissions Results Compared to SULEV Limits

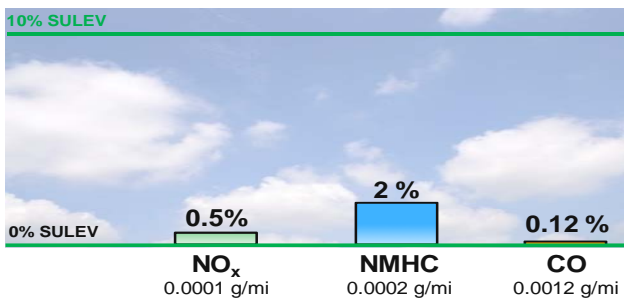


Figure 14. Emissions Signature When Sampling Ambient Air through an Imaginary Vehicle

In addition to cycle-averaged emissions and fuel economy numbers, time resolved (modal) emissions as well as air/fuel ratio data are analyzed to further investigate the root causes of the remaining emissions traces. The BMW Hydrogen 7-series vehicles employ a switching strategy with lean engine operation at low engine loads and stoichiometric operation at high engine loads that avoids the NO_x emissions critical operating regime with relative air/fuel ratios between $1 < \lambda < 2$ (Figure 15).

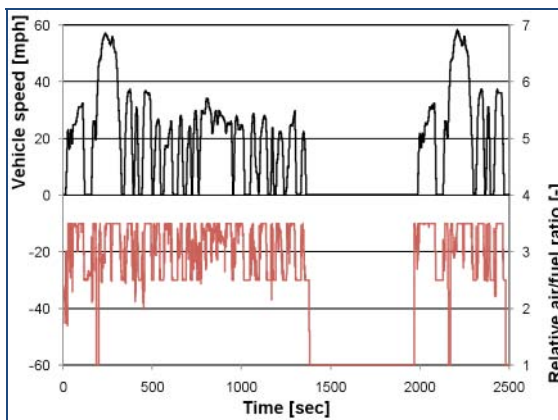


Figure 15. Relative Air/Fuel Ratio during FTP-75 Test

The switching between these operating modes was found to be a major source of the remaining NO_x emissions (Figure 16).

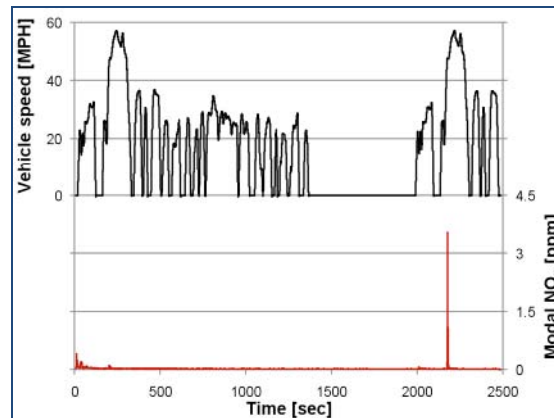


Figure 16. Modal NO_x Emissions During FTP-75 Test

Conclusions

In FY08, three H-ICE vehicles and one dedicated H2 fuel cell vehicle were successfully tested at the APRF, increasing both our knowledge about hydrogen-powered vehicles and our database information. Overall vehicle efficiencies and performance metrics were recorded that may be used as a comparison or benchmark against future vehicles.

Finally, the APRF has demonstrated a unique capability and functionality that very few laboratories in the world currently possess, and it will serve as a critical resource for required hydrogen testing.

E. Maintain an On-Line HEV Test Results Database

Mike Duoba (Project Leader)

Argonne National Laboratory

9700 South Cass Avenue

Argonne, IL 60439-4815

(630) 252-9359; SGurski@anl.gov

DOE Technology Manager: Lee Slezak

(202) 586-2335; Lee.Slezak@ee.doe.gov

Objectives

Design and construct a web-based database for the repository of hybrid vehicle test data. Enable access from industry and the general public.

Upload new data from Argonne National Laboratory's (ANL) Advanced Powertrain Research Facility (APRF) chassis dynamometer, along with the existing APRF data.

Perform critical analyses of the data available to DOE and industry partners.

Approach

Collect vehicle data by using ANL's 4WD chassis dynamometer.

Perform mathematical analysis to verify quality control of the data and to reduce the data for upload onto the publicly available Internet site.

Upload data to an ANL web applet server, after which it will be linked into the database to provide search and reference capabilities.

Calculate and visualize summary data, especially those for plug-in hybrid vehicles (PHEVs), to bring context to the long test procedure data.

Accomplishments

Continued to maintain the on-line downloadable database with search capabilities that is currently available (https://webapps.anl.gov/vehicle_data/).

Uploaded 42 new test folders to the website for download. The vehicles shown include Nissan HEV, General Motors (GM) Tahoe 2-mode, Hymotion Escape PHEV, and Electrovaya Escape PHEV.

Developed an advanced graphical/table calculation tool for PHEV test results calculations. This tool uses all of the new parameters for PHEVs addressed by California's Air Resources Board (CARB) regulations and SAE J1711.

Future Directions

Refine quality control (QC) procedures and continue to upload data to the website.

Provide more summary data and analysis for uploaded data.

Add a log-in function to download extensive "Level 2" data.

Introduction

Vehicle benchmarking combines testing and data analysis to characterize efficiency, performance, and

emissions as a function of duty cycle, as well as to deduce control strategy under a variety of operating conditions. The valuable data obtained from this effort have been placed in an Internet-accessible

database that provides a unique resource not previously available to researchers, students, and industry. This website is available at:
https://webapps.anl.gov/vehicle_data/.

Benchmarking data are useful to nearly all aspects of the FreedomCAR partnership, and the Tech Teams also benefit from the data collected in the Advanced Powertrain Research Facility (APRF). It has also become important for test procedure and policy development for DOE, SAE, CARB, EPA, DOT, and NHTSA. Test procedures, label fuel economy, and CAFE regulations all depend on these data for development. The importance of maintaining this database is paramount because no other government entity or company has such a data resource available.

Approach

For each of the vehicles tested at ANL's APRF, a set of data is generated. Depending upon the level and depth of testing, a stream of 50 to 200 different data is collected at the facility standard of 10-Hz data rate.

After testing, all of the data must be inspected, and it must be determined if the data are complete, thorough, and representative of the vehicle being tested. We use a set of tools that compare and contrast data relative to time and use of the first law of thermodynamics. Because this is a repetitive process, a template to define the time and first law relationships between data is generated. Each new set of data is run against these predefined relationships and set up for visual analysis and comment (Figure 1).

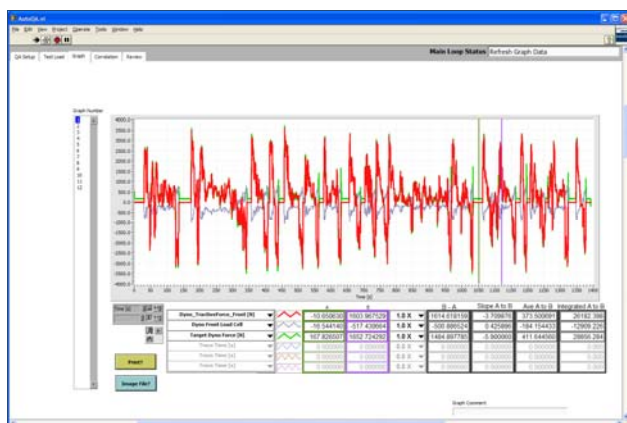


Figure 1. Standard APRF QC Analysis Tool

Once the data are thoroughly checked, the data are saved and reduced to a predefined subset of data. Each set of data includes:

Phase Information: Summary data for each phase of the test; items include fuel economy and emissions (gm/mi), for example.

Test Information: Summary of testing conditions needed to replicate the work at similar vehicle testing facilities; items include road load, dynamometer setting, and test cell environmental conditions, for example.

Main Summary: A one-page test summary with aspects of the phase information, test information, and 10-Hz data combined into a presentable sheet.

10-Hz Data: The raw 10-Hz data for each signal in the vehicle.

After the data quality control step has been performed, data are uploaded to the D3 website (Figure 2). The term D3 is an abbreviation for Downloadable Dynamometer Database. It is in this html interface where the relational and searchable database provides functionality. This website is available at: https://webapps.anl.gov/vehicle_data/.

The current interface is designed so that users can easily find data, which are organized either by vehicle or by a virtual project binder. Users have the ability to search the entire database by vehicle, project, test cycle, date of collection, or a predefined search. After the user has completed searching for the requested data, all of the data are sent via http download in a single compressed data file (zip).

Forty-two new test folders have been uploaded to D3 over the year (there are more ready to go live; the backlog will be filled over the next month or two into FY09). As of September 2008, D3 now has 14 advanced vehicles with over 130 sets of data that can be downloaded.

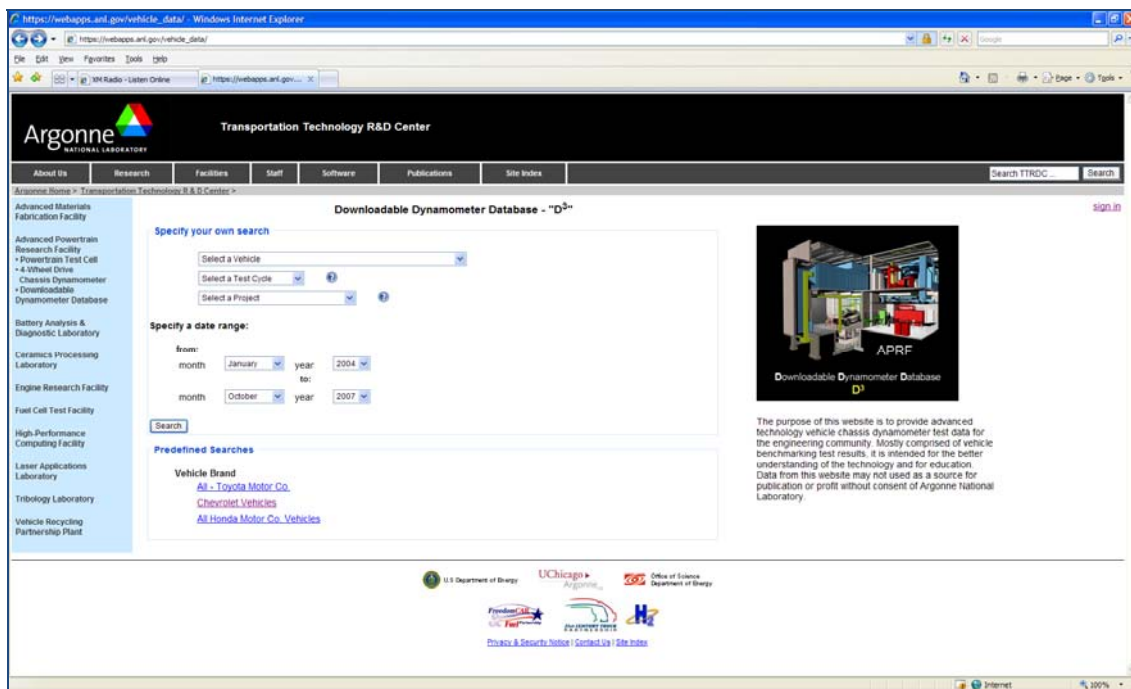


Figure 2. Downloadable Dynamometer Database Homepage

New this year is an automatic one-page reporting tool that visualizes and runs the critical PHEV calculations. Many new parameters unique to PHEVs have been developed in the SAE J1711 and CARB ZEV mandate procedures. They relate to energy consumption rates, various definitions of the depleting range, and equivalent electric vehicle (EV) range. The tool also uses Utility Factors to weight the final results. An example of one example printout is shown in Figure 3.

Conclusions

The ANL D3 allows our industry, academic, and government partners access to high-quality vehicle chassis testing data. The D3 is a simple and easy-to-use tool that allows for the transfer of useful data for analysis and education.

Publications/Presentations

Keller, G., and Gurski, S., et al., "D3 Website," September, VSATT Review, 2007.

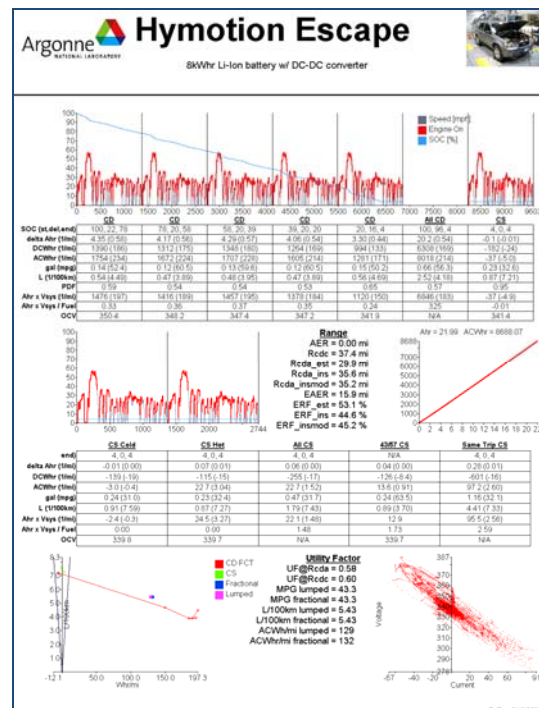


Figure 3. PHEV 1-Page Calculation Printout

V. OPERATIONAL AND FLEET TESTING

A. Hybrid Electric Vehicle Testing

James Francfort (Principal Investigator), Timothy Murphy (Project Leader)

Idaho National Laboratory

P.O. Box 1625

Idaho Falls, ID 83415-3830

(208) 526-6787; james.francfort@inl.gov

DOE Program Manager: Lee Slezak

(202) 586-2335; Lee.Slezak@ee.doe.gov

Objective

Benchmark commercially available hybrid electric vehicles (HEVs).

Provide HEV testing results to vehicle modelers and technology target setters.

Reduce the uncertainties about HEV battery and vehicle life.

Approach

Perform baseline performance and accelerated tests on 14 HEV models to date.

Operate at least two of each HEV model over 36 months to accumulate 160,000 miles per vehicle in fleets to obtain fuel economy, maintenance, operations, and other life-cycle related vehicle data under actual road conditions.

Test HEV batteries when new and at 160,000 miles.

Accomplishments

Accelerated testing for the HEV fleet, consisting of 39 HEVs and 14 models, exhibited varying fuel economies:

37.6 mpg for the 4 Generation (Gen) I Honda Civics

41.0 mpg for the 6 Gen I Toyota Prius

45.2 mpg for the 6 Honda Insights

28.1 mpg for the 2 Honda Accords

44.2 mpg for the 2 Gen II Prius

17.9 mpg for the 2 Chevrolet Silverado HEVs

26.7 mpg for the 2 Ford Escapes

23.4 mpg for the 3 Lexus RX400h

24.4 mpg for the 2 Toyota Highlanders

33.6 mpg for the 2 Toyota Camry

39.0 mpg for the 2 Gen II Honda Civics

26.5 mpg for the 2 Saturn Vues

30.6 mpg for the 2 Nissan Altimas

22.3 mpg for the 2 Chevrolet Tahoes.

As of September 2008, accumulated 4.1 million HEV test miles.

Provided HEV testing results to the automotive industry, the U.S. Department of Energy (DOE), and other national laboratories via the DOE Vehicle Technologies Program's Vehicle Simulation and Analysis Technical Team.

Future Activities

Benchmark new HEVs available during fiscal year (FY) 2009, including new 2-mode HEVs.

Ascertain HEV battery life by accelerated testing at the end of 160,000 miles.

Continue testing coordination with industry and other DOE entities.

Introduction

Today's light-duty hybrid electric vehicles (HEVs) use a gasoline internal combustion engine (ICE) and electric traction motor with approximately 1 kWh of onboard energy storage that is never connected to the grid for charging the battery. The HEV batteries are charged by the onboard ICE-powered generator, as well as by a regenerative braking system. Thirteen of the 14 HEV models in testing use nickel metal hybrid chemistries as the onboard traction battery. Only one HEV model, the 2004 Chevrolet Silverado, uses a lead acid battery. Future HEVs may use lithium battery technologies.

In addition to providing benchmark data to modelers and technology target setters, the Advanced Vehicle Technology Activity (AVTA) benchmarks and tests HEVs to compare the advantages and disadvantages of each technology, and also provides testing results to the public and fleet managers.

Approach

As of the end of FY08, the AVTA has performed, or is performing, accelerated and fleet testing on 39 HEVs, comprised of 14 HEV models:

- Generation (Gen) I Toyota Prius
- Gen II Toyota Prius
- Honda Insight
- Honda Accord
- Chevrolet Silverado
- Gen I Honda Civic
- Gen II Honda Civic
- Ford Escape
- Lexus RX400h
- Toyota Highlander
- Toyota Camry

- Saturn Vue
- Nissan Altima
- Chevrolet Tahoe.

Baseline performance testing has been completed on all 14 HEV models. Note that the difference between fleet and accelerated testing is that some vehicles are placed in fleet operations without a deliberate effort to place maximum miles on a vehicle (fleet testing). While in accelerated testing, two of each HEV model will each accumulate 160,000 on-road miles in approximately 36 months.

All testing has been completed on the following HEV models:

- Generation (Gen) I Toyota Prius
- Gen II Toyota Prius
- Honda Insight
- Honda Accord
- Gen I Honda Civic
- Ford Escape
- Lexus RX400h.

Results

As of the end of FY08, the 39 HEVs have accumulated 4.1 million total accelerated and fleet test miles (Figure 1). During FY08 the HEVs accumulated a total of 936,000 miles, averaging 78,000 test miles per month (Figure 2). The fuel economies ranged from 17.9 to 45.2 mpg in the on-road fleet and accelerated testing (Figure 3). All of the HEVs that have been on-road tested to date exhibit some seasonal variations in fuel economy (Figure 4). The impact from using the air conditioning is evident from the baseline performance testing results (Figure 5) when average fuel use decreases by 9 mpg when the air

conditioning is on during dynamometer testing. The air conditioning impact varies from 14.6 percent for the Vue to 28.4 percent for the Gen II Civic, with an average negative impact of 23 percent (Figure 6).

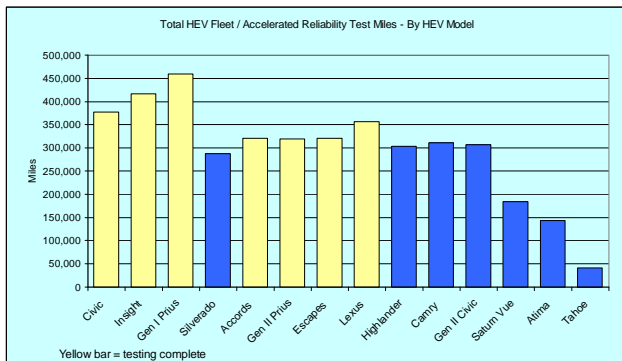


Figure 1. Total HEV Test Miles by Vehicle Model.

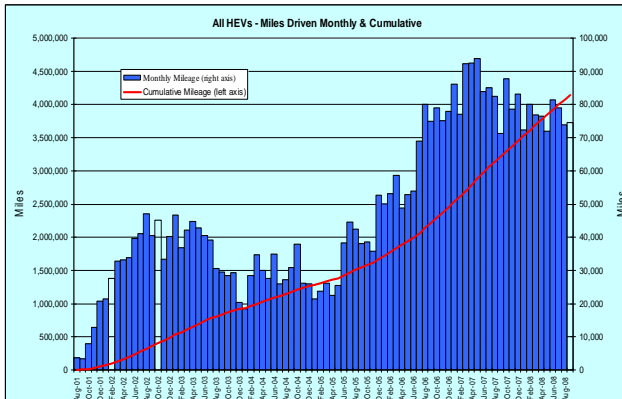


Figure 2. Monthly HEV Test Mile Accumulation during Fleet and Accelerated Testing: The graph runs from August 2001 until September 2008.

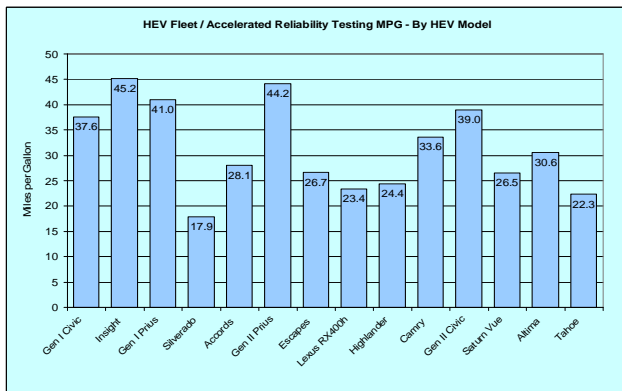


Figure 3. HEV Fuel Economy (mpg) Test Results for each HEV Model in Fleet and Accelerated Testing

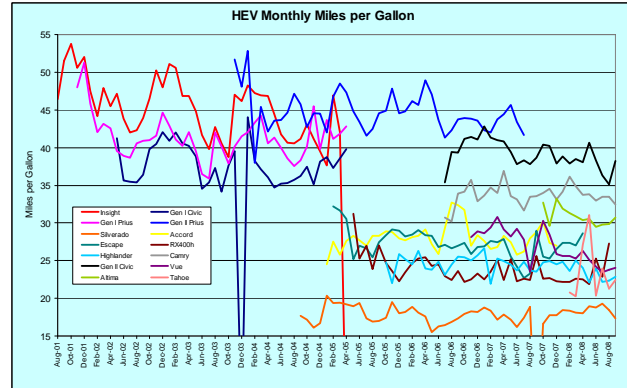


Figure 4. Monthly Fuel Economy Testing Results by HEV Model, August 2001 through the end of September 2008

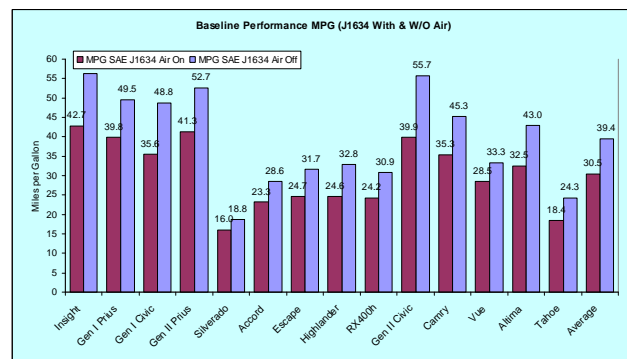


Figure 5. Baseline Performance Fuel Economy Test Results for SAE J1634 Drive Cycle Testing with the Air Conditioning On and Off

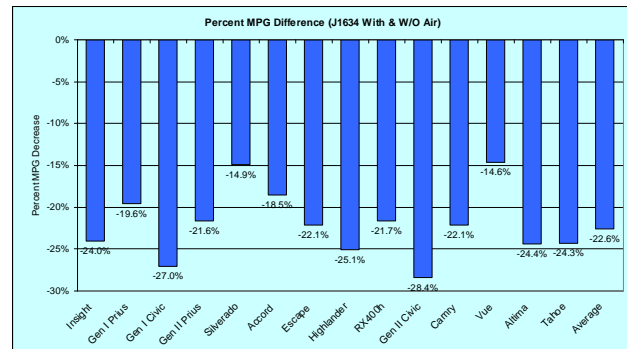


Figure 6. Percentage Decrease in Baseline Performance Fuel Economy Test Results for SAE J1634 Drive Cycle Testing when the Air Conditioning is Turned on during the Testing

In addition to the HEV fuel economy and total test miles data being collected, all maintenance and repair events, including the costs or if under warranty, dates and vehicle miles when an event occurred, is collected to compile life-cycle vehicle costs. This data are presented on the AVTA's Worldwide Web pages as both a maintenance fact sheet (Figure 7) and an HEV fact sheet, which includes miles driven, fuel economy, mission, and life-cycle costs on a per-mile basis (Figure 8).

The Environmental Protection Agency (EPA) has implemented new test methods (<http://www.fueleconomy.gov/feg/ratings2008.shtml>) for estimating mpg ratings for all light-duty vehicles. Figure 9 shows both the original EPA mpg estimates (light yellow bars) for HEVs the AVTA has tested,

and mpg figures the EPA has published if the same vehicles were tested or calculated to the new test methods (blue bars). The EPA numbers are displayed as the average for both city and highway results. Results for the AVTA fleet testing also are graphed (red bars) to show comparison to the old and new EPA estimates. The HEVs are displayed by all-wheel, two-wheel, and four-wheel drive in order to match EPA test categories. Note that the average AVTA fleet testing mpg is 30.1 mpg, which is close to the new EPA test method average of 31.2 mpg (3.6 percent higher than results for the AVTA fleet testing). The older EPA test method results averaged 36.8 mpg (22.2 percent higher than results for the AVTA fleet testing). Given all the variety in driving speeds, weather, terrain, and driving habits, 3.6 percent is extremely accurate.

HEV Fleet Testing
Advanced Vehicle Testing Activity
Maintenance Sheet for 2007 – Toyota Camry Hybrid

VIN # JTNNB46K773007129

Date	Mileage	Description	Cost
8/7/2006	5,122	Changed oil	\$38.74
10/28/2006	10,144	Changed oil	\$39.15
12/3/2006	12,234	Changed oil	\$24.34
2/8/2007	17,019	Changed oil	\$40.51
2/15/2007	17,750	Installed LoJack antitheft system	\$625.00
5/18/2007	31,339	Changed oil, changed air filter and oil filter and changed transmission oil	\$145.96
5/30/2007	37,210	Changed oil	\$32.41
6/19/2007	42,365	Changed oil and replaced two tires	\$263.21
7/16/2007	48,006	Changed oil	\$58.67
8/9/2007	53,373	Changed oil	\$30.54
9/12/2007	59,519	Changed oil	\$41.47
10/18/2007	69,769	Changed oil and replaced filter	\$35.96
11/6/2007	73,043	Replaced tire pressure sensor, rear struts, rear shocks and aligned wheels	\$819.10
11/16/2007	75,320	Changed oil, replaced air filter and replaced transmission oil	\$63.48
12/12/2007	80,605	Changed oil and rotated tires	\$35.98
1/4/2008	85,717	Changed oil and replaced air filter	\$49.50
1/23/2008	90,403	Changed oil and replaced filter	\$35.98
2/13/2008	95,734	Changed oil, inspected brakes and replaced brake pads	\$176.76
3/19/2008	103,825	Changed oil, replaced and balanced two tires, inspected brakes	\$226.39
5/29/2008	119,700	Changed oil and replaced filter	\$27.48
6/13/2008	123,756	Changed oil and filter, and replaced and balanced two tires	\$198.91
7/28/2008	135,369	Changed oil and filter	\$27.48
8/14/2008	140,448	Changed oil and replaced air filter	\$51.27

Figure 7. An Example of an HEV Maintenance Sheet

FREEDOMCAR & VEHICLE TECHNOLOGIES PROGRAM

HEV Fleet Testing Advanced Vehicle Testing Activities



2005
Honda Accord
VIN #
JHMCN36495C000657

Fleet Performance

Description:
This vehicle is operated throughout the valley of Phoenix, Arizona by JP Morgan Chase Bank of Arizona's courier fleet. It is operated six days a week, transferring documents between branches and a central processing center on city streets and urban freeways as well as intrastate courier routes.

Major Operations & Maintenance Events:
Repaired electrical door lock @ 79,722
Cost: \$321.17

Operating Cost:
Purchase Cost: \$32,945 (12/04)*
Kelly Used Vehicle Price: \$16,935 (1/07)
Sale Price: In Operation
Maintenance Cost: \$0.038/mile
Operating Cost: \$0.13/mile
Total Ownership Cost: \$0.32/mile

Operating Performance:
Total miles driven: 103,646
Cumulative MPG: 29.5

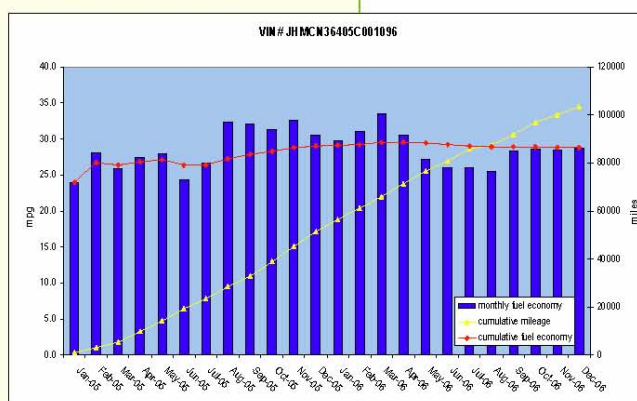
Vehicle Specifications

Engine: i-VTEC V6
Electric Motor: 11.9 kW
Battery: Nickel metal hydride
Seatbelt Positions: Five
Payload: 952 lbs
Features: Front wheel drive, regenerative braking

See HEVAmerica Baseline Performance Fact Sheet for more information.

FreedomCAR & Fuel Partnership

A Strong Energy Portfolio for a Strong America
Energy efficiency and clean, renewable energy will mean a stronger economy, a cleaner environment, and greater energy independence for America. Working with a wide array of state, community, industry, and university partners, the U.S. Department of Energy's Office of Energy Efficiency and Renewable Energy invests in a diverse portfolio of energy technologies.



For more information contact:
EERE Information Center
1-877-EERE-INF (1-877-337-3463)
www.eere.energy.gov

* Purchase includes dealer price with options plus taxes. It does not include title, license, registration, extended warranty or delivery fee costs. Gas figured at \$2.45/gallon.

U.S. Department of Energy
Energy Efficiency and Renewable Energy
Bringing you a prosperous future where energy is clean, abundant, reliable, and affordable

Figure 8. An Example of an HEV Fact Sheet

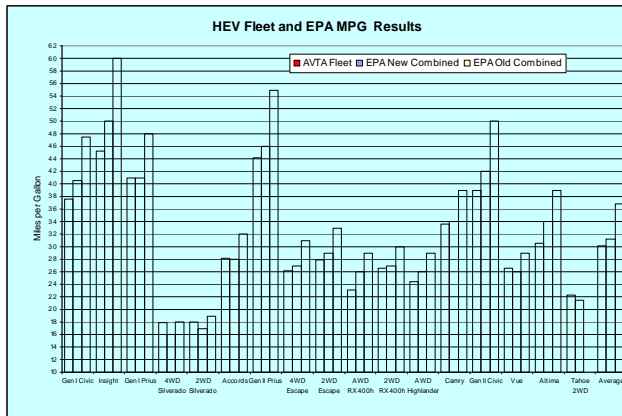


Figure 9. Results for the AVTA Fleet Testing compared to the results for the old and new EPA mpg testing: The 14 HEV models are broken out into two-wheel, four-wheel, and all-wheel drive categories to match EPA vehicle categories.

Conclusions

The largest single impact on fuel economy is from the use of the air conditioning with these early HEV models during the summer months. The HEV battery packs appear to be robust; as of the end of FY08 and 4.1 million test miles, there were two nickel metal hydride (NiMH) traction battery failures. One NiMH failure was due to a battery controller failure and should not be attributed as a pack failure. The second NiMH pack failed at 147,000 miles. Therefore, a single high-mileage failure out of 4.1 million test miles suggests the NiMH HEV batteries are very robust.

Future HEV onboard energy storage systems may include combinations of multiple battery technologies employing different charge and discharge methods, and ultracapacitors. Future HEVs may operate on alternative fuels such as hydrogen, methane, compressed natural gas (CNG), ethanol, or blends of hydrogen and CNG. If these technologies or combinations of these technologies appear, they will be introduced into the HEV testing activity.

The AVTA has partnered with private fleets to conduct the high mileage HEV testing, as these other fleets have provided at no charge to the AVTA more than \$5 million in driver costs.

Future Activities

New HEVs available from U.S., Japanese, and European manufacturers will be benchmarked during FY09, as will new 2-mode HEVs. Most new HEVs will be tested to reduce uncertainties about HEV technologies, especially the life and performance of their batteries and any other onboard energy storage systems.

Publications

Approximately 110 HEV baseline performance, fleet and accelerated testing fact and maintenance sheets, reports, and presentations have been generated by the AVTA and all are available on the AVTA's World Wide Web (WWW) pages. The HEV baseline performance testing procedures and vehicle specifications were also updated and republished on the WWW. New HEV reports and papers published during FY08 are listed below. In addition to the below testing fact sheets and paper, maintenance requirements and fuel use fact sheets are generated every three months for all of the HEVs. All of these documents can be found at:

<http://avt.inl.gov/hev.shtml> and
http://www.eere.energy.gov/vehiclesandfuels/avta/light_duty/hev/hev_reports.shtml.

2008 Chevrolet Tahoe HEVAmerica baseline performance testing fact sheet.

http://avt.inel.gov/pdf/hev/fact_sheet08Tahoe.pdf

2007 Nissan Altima HEVAmerica baseline performance testing fact sheet.

http://avt.inel.gov/pdf/hev/fact_sheet7982.pdf

2007 Saturn Vue HEVAmerica baseline performance testing fact sheet.

<http://avt.inel.gov/pdf/hev/factSaturnVue.pdf>

B. Plug-in Hybrid Electric Vehicle Testing by DOE's Advanced Vehicle Testing Activity (AVTA)

James Francfort (Principal Investigator), Timothy Murphy (Project Leader)

Idaho National Laboratory

P.O. Box 1625

Idaho Falls, ID 83415-3830

(208) 526-6787; james.francfort@inl.gov

DOE Program Manager: Lee Slezak

(202) 586-2335; Lee.Slezak@ee.doe.gov

Objective

Benchmark early production and prototype plug-in hybrid electric vehicles (PHEVs) from vehicle conversion companies and original equipment manufacturers (OEMs).

Reduce the uncertainties about vehicle and battery performance and life, as well as document fuel (petroleum and electricity) use over various distances.

Document PHEV charger performance (profile and demand), charging times, and infrastructure needs, as well as operator behavior impact on charging times and frequencies.

Provide PHEV testing results to vehicle modelers, technology target setters and industry stakeholders.

Approach

Use the PHEV testing specifications and procedures developed by the Advanced Vehicle Testing Activity (AVTA) that are reviewed by industry, national laboratories, and other interested stakeholders.

Obtain PHEVs for testing to the reviewed PHEV testing specifications and procedures.

Perform baseline performance track and laboratory tests, accelerated on-road tests, and fleet demonstrations on PHEVs.

Place limited numbers of PHEVs in demonstration fleet environments for vehicle, infrastructure, and operator testing.

Leverage DOE funding resources with other organizations' resources.

Prepare testing and data collection methods in preparation for the testing of PHEVs from additional OEMs in support of the Department of Energy's (DOE) PHEV Technology Advancement and Demonstration Activity (TADA) that will support PHEV deployment.

Accomplishments

Obtained and tested two PHEVs from OEMs and seven PHEVs from five PHEV conversions companies. These nine PHEVs in testing and demonstrations represent all PHEV models that were viable and operating test candidates in North America during fiscal year (FY) 2008.

Conducted a PHEV charging infrastructure review.

Began conducting cooperative PHEV testing with non-DOE groups to provide testing access to PHEVs operating in demonstration fleets along with testing and demonstration partners lead by: National Rural Cooperative Association (NRECA), New York State Energy Research Development Agency (NYSERDA), City of Seattle, King County, Port of Chelan, Port of Seattle, Puget Sound Clean Air Agency, Tacoma Power, University of California at Davis, and PHEV conversion companies Hymotion and EnergyCS.

As of the end of FY08, the AVTA had 75 PHEV testing partners operating 95 PHEVs.

Conducting geographically and mission diverse PHEV testing and demonstration activities in 17 states and three Canadian provinces, including Arizona, California, Georgia, Indiana, Kentucky, Minnesota, New York, North Carolina, North Dakota, Ohio, Oregon, South Carolina, Texas, Vermont, Virginia, Washington, and Wisconsin, as well as Manitoba, Toronto, and British Columbia.

Evaluated PHEV data loggers and data logging systems for use onboard PHEVs.

Total PHEV fleet demonstration cost sharing to date of \$400k to the DOE/AVTA and \$3.1 million in non-DOE/AVTA costs.

Performed due diligence on other PHEV models to determine suitability as test candidates.

Future Activities

Initiated processes to implement additional PHEV testing and demonstrations in Hawaii.

Continue performing due diligence on potential PHEV suppliers and obtain PHEVs for testing as appropriate.

Adding up to 79 additional PHEVs to fleet demonstrations in early fiscal year 2009, including 34 PHEVs in British Columbia at no cost to DOE.

Continue to assess value of fleet requests to provide PHEV fleet data to the AVTA.

Obtain future PHEV models and battery technologies for testing.

Develop additional PHEV demonstration relationships and support the deployment of PHEVs in these testing fleets.

Coordinate PHEV and charging infrastructure testing with industry and other DOE entities.

Introduction

Current hybrid electric vehicles (HEVs) combine internal combustion engines (ICEs) and battery storage devices to increase performance and/or fuel efficiency. The batteries commonly used in HEVs have approximately 1 kWh of onboard energy capacity and they are recharged by onboard energy sources such as regenerative braking and motor/generators powered by the onboard ICEs. Many companies and groups are proposing, planning, and have started the introduction of plug-in hybrid electric vehicles (PHEV). Most of the PHEVs currently available use a HEV as the base vehicle, and add additional or replacement battery packs with 5 to 10 kWh of energy storage to the base HEVs. PHEV control systems and power electronics are also added to the base vehicle to complete the upgrade. These larger additional or replacement battery packs are sometimes recharged by the onboard systems, but all of them must also use onboard chargers connected to the off-board electric grid to fully recharge the PHEV battery packs.

The concept of additional onboard energy storage and grid-connected charging raises questions that include the life and performance of these larger batteries, the

charging infrastructure required, how often the vehicles will actually be charged, and the actual amount of petroleum displaced over various missions, drive cycles, and drive distances.

Approach

The U.S. Department of Energy's (DOE) Advanced Vehicle Testing Activity (AVTA) supports the introduction of PHEVs by testing the emerging group of PHEV products and documenting vehicle and battery performances, as well as electricity and petroleum use in cost shared ways. As a first step, the AVTA developed a 400-page test plan for inspection, dynamometer, test track, accelerated and fleet testing of PHEVs. In addition, nine PHEV models have been obtained and used in various demonstrations and testing missions, with additional candidate test PHEVs being considered for testing. The AVTA has conducted a PHEV charging infrastructure and power electronics study and the documenting report was being completed as FY08 ended. The AVTA has also signed testing, demonstration, and data collection agreements with several non-DOE fleets that operate PHEVs, and the AVTA will collect performance and charging data to characterize the performance of the PHEVs and the charging infrastructure.

Results

The 400-page draft test plans were completed during FY06, and they were submitted for review by other National Laboratory groups. During FY07, the plans were further reviewed by a larger group of PHEV industry and stakeholders, and the resulting comments addressed. During FY08, further refinement of the test procedures were waiting on a final SAE J1772 procedure that will be used to update the AVTA's PHEV dynamometer testing procedures. A total of nine PHEV models were in testing during FY08; the baseline performance (track and dynamometer) and accelerated testing results are discussed below.

The nine PHEVs that were tested during FY08 included:

Renault Kangoo (Figure 1), with a nickel cadmium battery pack

Ford Escape E85 PHEV (from Ford), with a lithium battery pack and its unique charge port (Figure 2)

Toyota Prius converted by EnergyCS, with a lithium battery pack (Figures 3 and 4)

Toyota Prius converted by Hymotion, with a lithium pack (Figures 5 and 6)

Ford Escape converted by Hymotion, with a lithium battery pack (Figure 7)

Ford Escape converted by Electrovaya, with a lithium battery pack (Figure 8)

Ford Escape converted by Hybrids Plus, with a lithium battery pack (Figure 9)

Toyota Prius converted by Hybrids Plus, with a lithium battery pack

Toyota Prius converted by Manzanita

As with all vehicles that are baseline performance tested, testing fact sheets are developed for each PHEV (Figure 10).



Figure 1. Renault Kangoo PHEV



Figure 2. Ford E85 PHEV Escape's unique 120-Volt Charge Port Located in the Front Left Side Fender, in Use



Figure 3. Lithium Ion Battery Pack used in EnergyCS Conversion of a Toyota Prius



Figure 4. Lithium Ion Battery Pack Placement in the EnergyCS conversion of a Toyota Prius: The pack is in the black box. Note the 110-volt connector cord in the bottom left of the picture.



Figure 7. A123 Lithium Ion Battery Pack Placement in the Hymotion conversion of a Ford Escape: The pack sits close the back site of the Escape in the rear storage area. A PHEV suitable charging infrastructure extension cord is in the back storage area. The pack is topped by the silver colored metal



Figure 5. Prius being converted to a PHEV by Hymotion Staff



Figure 8. Electrovaya Lithium Battery Pack in a Ford Escape converted by Electrovaya: The pack takes up the entire rear storage area.



Figure 6. A123 Lithium Ion Battery Pack Placement in the Hymotion conversion of a Toyota Prius: The pack sits between the rear of the vehicle and the original Prius battery, which is retained and used. (The Prius battery is to the right of the bright orange cables and only the upper rear side is visible as bright metal.)



Figure 9. Hybrids Plus PHEV conversion of a Ford Escape: The Hybrids Plus battery pack is under the metal cover, allowing full use of the rear storage area.

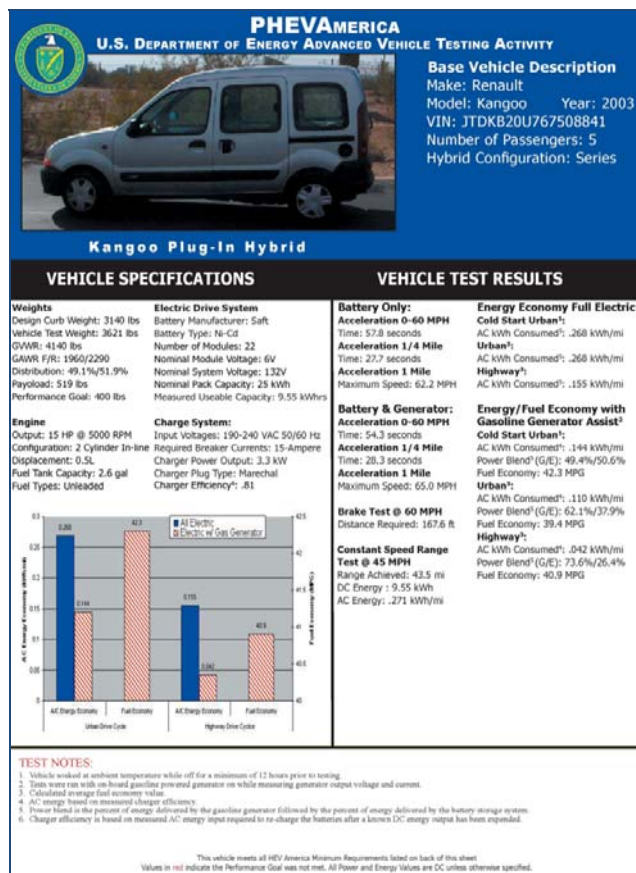


Figure 10. An Example of a Baseline Performance Testing Fact Sheet

EnergyCS PHEV Testing - The Prius converted by EnergyCS (Monrovia, CA) completed baseline performance testing during FY07, which included dynamometer testing (conducted by Argonne National Laboratory for the AVTA). However, the results obtained in FY07 for several vehicles are repeated in this FY08 report to allow the reader to compare these testing results to subsequent baseline performance testing results obtained during FY08.

This testing includes Urban Dynamometer Drive Schedule (UDDS: 1,372 seconds) testing, during which the EnergyCS PHEV demonstrated gasoline mpg results exceeding well over 100 mpg for each of the first four UDDS test cycles (Figure 11). Note that each UDDS test cycle is 7.48 miles in distance. The test cycles are repeated while the test PHEV continues to operate in charge-depleting mode (pulling electricity out of the PHEV battery pack) until it operates in two charge-sustaining modes (no more additional electricity can be pulled out of the

PHEV battery pack). The charge-sustaining results are repeated in the graphs to show the cumulative fuel-use effects if the vehicle were tested for additional cycles.

The EnergyCS Prius is also subjected to Highway Fuel Economy Driving Schedule (HWFEDS; 764 seconds) on the dynamometer, during which the gasoline mpg results were greater than 80 mpg for the first of the three 10.25 mile long test cycles (Figure 12). As with the UDDS cycles, the testing is repeated in charge-depleting mode and then repeated again for at least two charge-sustaining modes.

During FY08, the EnergyCS Prius completed accelerated testing, during which the EnergyCS PHEV Prius is driven with a dedicated driver over a series of 10-mile city and 10-mile highway loops. These two loops are repeated in different combinations that range from 10- to 200-mile individual test cycles, which are each followed by a battery recharging period (Table 1). As Table 2 shows, the EnergyCS PHEV exhibited significant higher mpg test results when driven on the road compared to the 44-mpg results for the stock Prius HEV that the AVTA measured after 320,000 test miles. This is especially true for the 10-mile cycle (128.1 mpg) and the 60 mile cycle (103.7). The initial three 40-mile cycles were originally only 200 mile cycles, but after the first round of EnergyCS Prius testing, it was recognized that 600 miles are needed for each 40-mile cycle to ensure a larger sample of gasoline use since as little as 1.4 gallons of gas was being used during the 200 miles. However, during these initial tests, this vehicle exhibited from 86 to 146 mpg. When the 20-mile cycle was conducted, it was identified that towards the end of the testing the vehicle was only receiving minimal recharge, which was the first indication of problems with the battery pack. When the 40-mile cycles were repeated (Table 3) to 600 miles, it became evident that there were problems with the Valance battery pack used in this conversion and the results were only in the 42.7 to 56.1 mpg range. Even with the battery problems, the weighted average fuel use for this vehicle during accelerated testing was 73 mpg. It should be noted that this is 66 percent higher mpg than the AVTA's testing results of 44 mpg for the two "normal" Toyota Prius hybrid electric vehicles (HEV) driven for 320,000 miles.

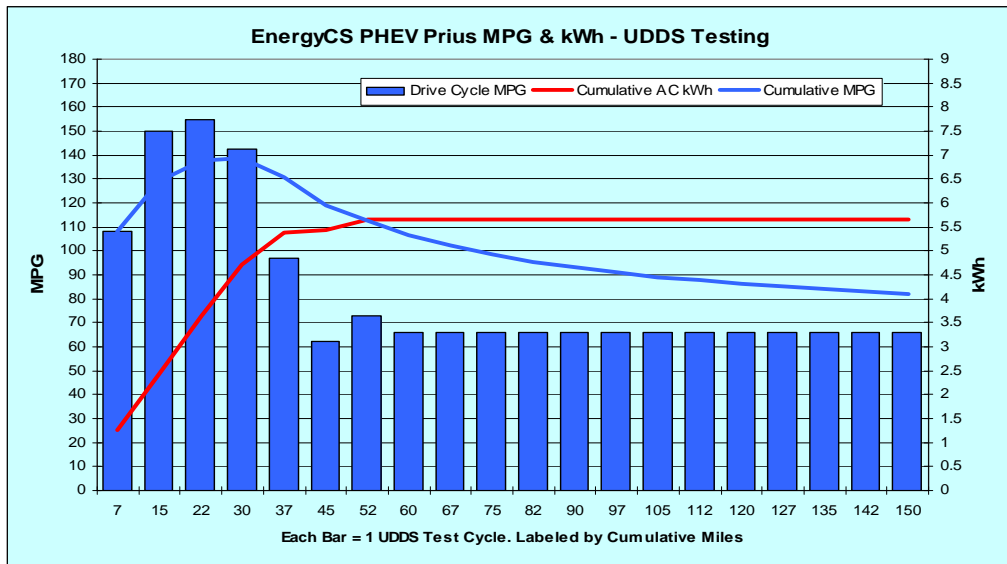


Figure 11. EnergyCS PHEV Prius conversion UDDS testing results. (The blue line is the cumulative mpg and the red line is the cumulative kWh use.)

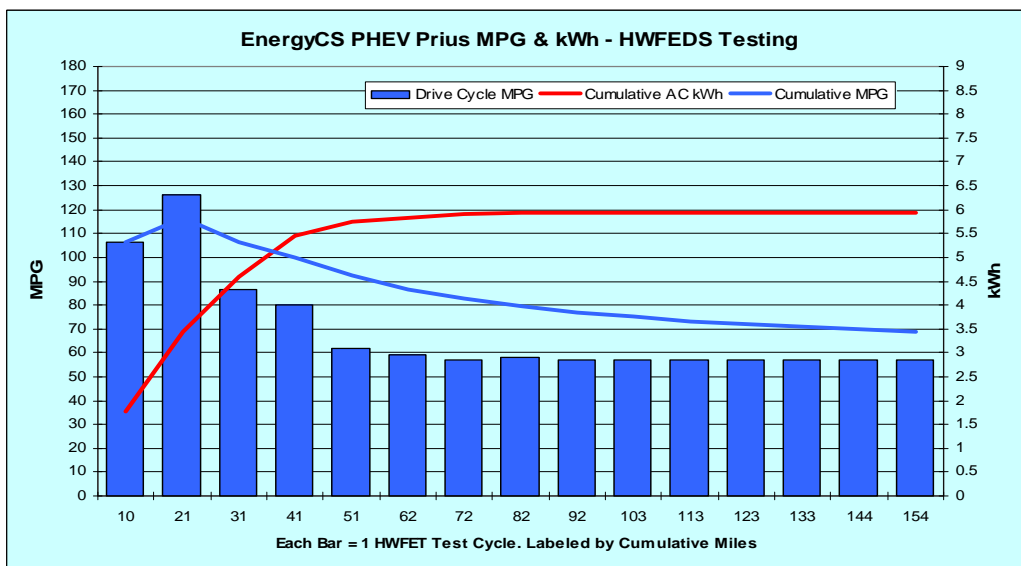


Figure 12. EnergyCS PHEV Prius conversion HWFEDS testing results. (The blue line is the cumulative mpg and the red line is the cumulative kWh use.)

Table 1. Revised PHEV accelerated testing distances as of the end of FY08.

Cycle (mi)	Urban (10 mi)	Highway (10 mi)	Charge (hours)	Repetitions (N)	Total (mi)	Repetitions (%)	Miles (%)	Cumulative (mi)
10	1	0	4	60	600	37%	11%	600
20	1	1	8	30	600	19%	11%	1,200
40	4	0	12	15	600	9%	11%	1,800
40	2	2	12	15	600	9%	11%	2,400
40	0	4	12	15	600	9%	11%	3,000
60	2	4	12	10	600	6%	11%	3,600
80	2	6	12	8	640	5%	12%	4,240
100	2	8	12	6	600	4%	11%	4,840
200	2	18	12	3	600	2%	11%	5,440
Total	2,340	3,100	1,344	162	5,440			5,440
Average	43%	57%	8.3	18.0				

Table 2. EnergyCS PHEV accelerated testing results to date. Note that when this vehicle started testing, the three 40-mile cycles were only going to be for 200 miles each. These 200-mile distances have been subsequently changed to 600-mile distances each as seen in Table 1. However, the 40-mile cycles are presented below as they were completed as of the end of FY07. Note that each total distance was slightly greater than 200, 600 or 640 test miles.

Cycle (mi)	Urban (10 mi)	Highway (10 mi)	Charge (hours)	Reps (N)	Total (mi)	Electricity		Gasoline	
						kWh	Gals	MPG	
10	1	0	4	60	600	115.58	4.78	128.1	
20	1	1	8	30	600	86.21	7.95	77.9	
40	4	0	12	15	200	17.37	1.61	126.4	
40	2	2	12	15	200	29.00	1.42	145.1	
40	0	4	12	15	200	30.00	2.43	85.5	
60	2	4	12	10	600	65.00	5.90	103.7	
80	2	6	12	8	640	39.04	10.09	65.8	
100	2	8	12	6	600	22.67	8.81	70.8	
200	2	18	12	3	600	12.98	10.46	57.8	
Total	1,740	2,500	984	132	4,240	Weighted Average		88.8	

Table 3. EnergyCS PHEV accelerated testing results at completion of repeating the accelerated testing to 600 miles for the three 40-mile test loops. Note that each total distance was slightly greater than 600 or 640 test miles.

Cycle (mi)	Urban (10 mi)	Highway (10 mi)	Charge (hours)	Reps (N)	Total (mi)	Electricity		Gasoline	
						kWh	Gals	MPG	
10	1	0	4	60	600	115.58	4.78	128.1	
20	1	1	8	30	600	86.21	7.95	77.9	
40	4	0	12	15	600	25.00	14.29	42.7	
40	2	2	12	15	600	31.52	11.05	56.1	
40	0	4	12	15	600	32.44	11.36	55.5	
60	2	4	12	10	600	65.00	5.90	103.7	
80	2	6	12	8	640	39.04	10.09	65.8	
100	2	8	12	6	600	22.67	8.81	70.8	
200	2	18	12	3	600	12.98	10.46	57.8	
Total	1,740	2,500	984	132	5,440	Weighted Average		73.1	

Hymotion Prius PHEV Testing with the Version I Battery – This section discusses the testing results using the Version I Hymotion (owned by A123 Systems, Boston, MA). Prius PHEV conversion battery. Subsequent to the completion of crash testing conducted by Hymotion (not part of the Vehicle Technologies Program activities), Hymotion redesigned the original Version I battery and replaced all of the Version I Prius PHEV batteries with their crash-tested Version II Prius battery. This section discusses testing results for Prius with the Version I battery conversion.

The Version I Prius converted by Hymotion has completed baseline performance testing, which includes dynamometer and track testing. As with the EnergyCS Prius, the Hymotion Prius testing included UDDS testing, during which the Hymotion PHEV demonstrated gasoline mpg results exceeding 140 mpg for each of the first three UDDS test cycles (Figure 13). The UDDS results are graphed similarly to the EnergyCS results, with the Hymotion results shown in charge depleting modes and charge sustaining modes, with the sustaining results repeated to show cumulative energy use over longer distances.

The Version I Hymotion Prius is also subjected to HWFEDS testing on the dynamometer, during which the gasoline mpg results were greater than 80 mpg for the first of the three 10.25-mile test cycles (Figure 14). As with the UDDS cycles, the HWFEDS testing is repeated in charge-depleting mode and then repeated again for at least two charge-sustaining modes.

During FY08, the Version I Hymotion Prius completed accelerated testing (Table 4) and the test results were from 101.1 to 127.2 mpg for the shorter first four test cycles. After completing the 5,440 miles of accelerated testing with no apparent battery problems, the vehicle had weighted average fuel use of 79.5 mpg, 81 percent higher than the 44 mpg results for the stock Prius HEV that the AVTA measured after 320,000 test miles.

Hymotion Prius PHEV Testing with the Version II Battery – As FY08 ended, the Hymotion Prius conversion with the crash tested Version II battery pack had just started accelerated testing, with four loops completed (Table 5). The gasoline use was similar to the Version I vehicle, with the mpg results higher for two loops and lower for the other two

loops. During FY09, this vehicle will also be baseline performance tested.

Renault Kangoo - Both the EnergyCS and Hymotion PHEVs use the Prius's parallel HEV design, which allows both the electric motor and the gasoline engine to propel the vehicle. The third PHEV model tested is the Renault (France) Kangoo, which uses a series HEV design. In Renault series design, an electrical generator is powered by an internal combustion engine, and the generator charges the vehicle traction battery pack. The generator is not connected directly to the electric drive motor. In a parallel design, electricity can also be generated directly by a fuel cell, but again, it can only be used to charge the battery, it is not connected directly to the electric drive motor. This type of series design is the same design that General Motors has announced for its future Volt PHEV.

While the Kangoo is not of an overly sophisticated design, it is the first, and to date only, series PHEV available. Therefore, the AVTA has benchmarked the performance of the Kangoo and its electric-only selectable mode. To date, none of the other currently available PHEVs allow the driver to switch to an electric-only mode until the traction battery pack is deleted and the vehicle is propelled by the gasoline-powered generator. Therefore, the Kangoo has been tested in both electric-only and electric-assist modes, where during several baseline performance tests (Table 6) the Kangoo exhibited energy efficiencies of 0.155 to 0.268 alternating current (AC) kWh per mile in electric-only mode. In electric assist mode, the Kangoo exhibited 0.042 to 0.144 AC kWh per mile, and 39 to 42 mpg (both the electric motor and gasoline engine propelled the Kangoo).

During accelerated testing, the Kangoo was able to operate on electricity only for 40 miles during the first four test cycles (Table 7). It should be noted that the Kangoo did not complete the 100- and 200-mile cycles due to gasoline engine and inverter failures. The nearest authorized dealer is in Brussels, Belgium, so the vehicle was sold.

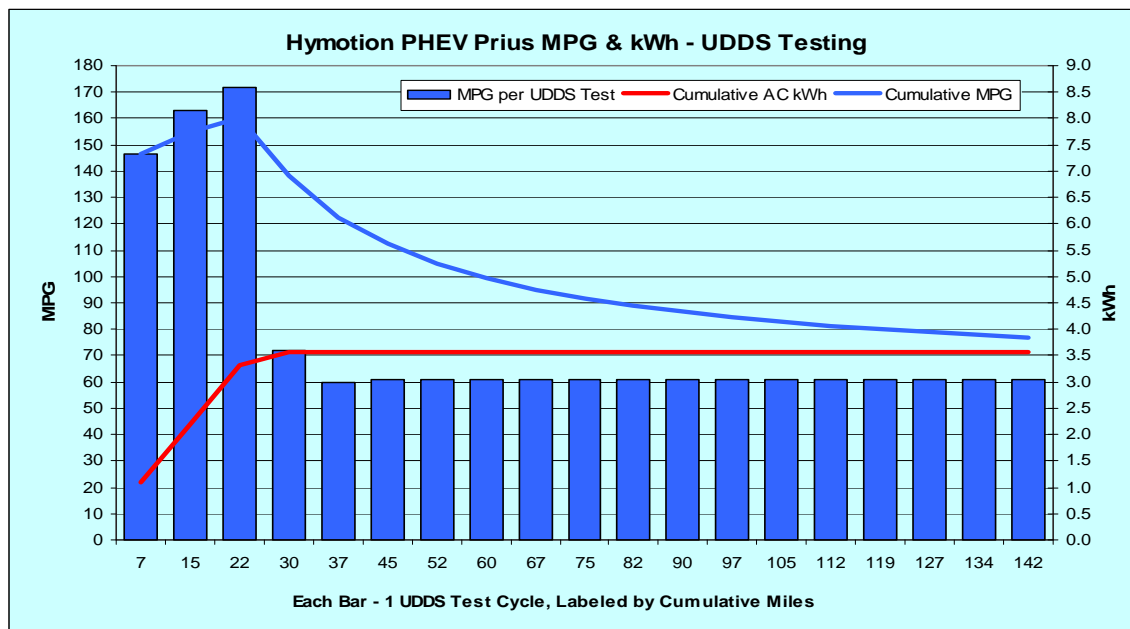


Figure 13. Hymotion Battery Version I PHEV Prius conversion UDDS testing results.
(The blue line is the cumulative mpg and the red line is the cumulative kWh used.)

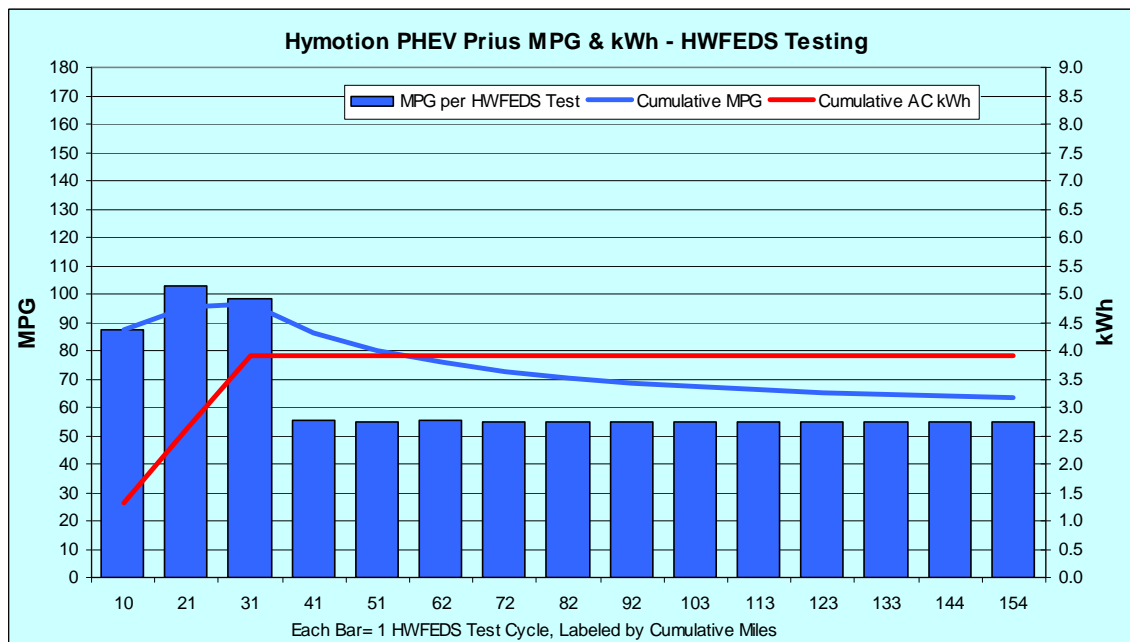


Figure 14. Hymotion Battery Version I PHEV Prius conversion HWFEDS testing results.
(The blue line is the cumulative mpg and the red line is the cumulative kWh used.)

Table 4. Hymotion Prius PHEV with the Version I battery pack accelerated testing results.

Note that each total distance was slightly greater than 600 or 640 test miles.

Cycle	Urban (mi)	Highway (10 mi)	Charge (hours)	Reps (N)	Total (mi)	Electricity kWh	Gasoline Gals	Gasoline MPG
10	1	0	4	60	600	136.33	4.81	127.2
20	1	1	8	30	600	122.02	5.37	115.9
40	4	0	12	15	600	84.10	6.05	101.1
40	2	2	12	15	600	87.22	5.78	106.9
40	0	4	12	15	600	79.82	8.54	73.1
60	2	4	12	10	600	55.33	8.98	68.9
80	2	6	12	8	640	43.99	11.36	58.3
100	2	8	12	6	600	35.98	8.43	73.2
200	2	18	12	3	600	15.0	11.02	54.8
Total	1,740	2,500	984	132	5,440	Weighted Average		79.5

Table 5. Initial Hymotion Prius PHEV with the Version II battery pack accelerated testing results.

Only four test cycles were completed at the end of FY08. Note that each total distance was slightly greater than 600 or 640 test miles.

Cycle	Urban (mi)	Highway (10 mi)	Charge (hours)	Reps (N)	Total (mi)	Electricity kWh	Gasoline Gals	Gasoline MPG
10	1	0	4	60	600	111.43	5.205	117.6
20	1	1	8	30	600			
40	4	0	12	15	600			
40	2	2	12	15	600			
40	0	4	12	15	600			
60	2	4	12	10	600			
80	2	6	12	8	640	41.38	10.71	61.8
100	2	8	12	6	600	26.48	10.91	56.5
200	2	18	12	3	600	16.01	10.41	57.7
Total	1,740	2,500	984	132	5,440	Weighted Average		

Table 6. Energy use test results for the Renault Kangoo baseline performance testing and the onroad 10-mile accelerated test cycle

Test Cycle	kWh AC per Mile	Miles per Gallon
Battery only—UDDS	0.268	
Battery only—HWFEDS	0.155	
Battery only at constant 45 mph	0.271	
Battery and ICE cold start UDDS	0.144	42.3
Battery and ICE hot start UDDS	0.110	39.4
Battery and ICE hot start HWFEDS	0.042	40.9
Sixty - Battery Only 10-mile Accelerated Test Cycle	0.481	

Table 7. Renault Kangoo PHEV accelerated testing results. Note that each total distance was slightly greater than 600 or 640 test miles.

Cycle (mi)	Urban (10 mi)	Highway (10 mi)	Charge (hours)	Reps (N)	Total (mi)	Electricity		Gasoline	
						AC kWh	Mi/kWh	Gals	MPG
10	1	0	4	60	600	359.60	1.7	0	
20	1	1	8	30	600	131.96	4.6	0	
40	4	0	12	15	600	35.18	5.6	0	
40	2	2	12	15	600	33.22	6.0	0	
40	0	4	12	15	600	28.60	7.0	0	
60	2	4	12	10	600	57.96	10.4	13.3	45.1
80	2	6	12	8	640	44.62	14.4	16.6	38.6
100	2	8	12	6	600	Deleted*			
200	2	18	12	3	600	Deleted*			
Total	1,740	2,500	984	132	3,040				

* Testing ended when gasoline engine and inverter failed.

Hymotion Escape PHEV Testing – During the UDDS dynamometer portion of the baseline performance testing, the Hymotion PHEV conversion (owned by A123 Systems, Boston, MA) of a Ford Escape demonstrated gasoline mpg results of approximately 60 mpg during the warm-start second, third, and fourth test cycles. During the cold-start first cycle and the fifth cycle when the vehicle was entering charge sustaining mode, the vehicle still exhibited test results greater than 50 mpg (Figure 15) while using a total of 7.2 AC kWh while in charge depleting mode. This vehicle is owned by the NYSERDA and it was tested in partnership between DOE’s AVTA and NYSERDA in support of NYSERDA’s leadership efforts to support the development of the PHEV industry.

During the HWFEDS dynamometer testing (Figure 16), the Hymotion Escape exhibited two cycles over 65 mpg while using a total of 6.8 AC kWh for all four cycles in charge depleting mode.

The Hymotion Escape conversion has completed accelerated testing (Table 8) with no battery issues. The testing results for the nine test cycles ranged from 33.5 mpg for the 200-mile cycle to 53.1 mpg of the 10-mile cycle. The weighted average result was 43.3 mpg. It should be noted that this is a 61 percent higher mpg than the AVTA’s testing results of 27 mpg for the two “normal” Ford Escape HEVs driven for 320,000 miles.

Electrovaya Escape PHEV Testing – During the UDDS dynamometer portion of the baseline performance testing, the Electrovaya (Toronto, Canada) PHEV conversion of a Ford Escape never achieved 50 mpg on the UDDS test cycle (Figure 17) as the vehicle had difficulty operating properly. This vehicle is owned by the NYSERDA and it was tested in partnership between DOE’s AVTA and NYSERDA in support of NYSERDA’s leadership efforts to support the development of the PHEV industry.

During the HWFEDS dynamometer testing (Figure 18), the Electrovaya Escape again had difficulty operating at its maximum potential and it only had two test cycle results over 40 mpg, as it only used 2.4 kWh of its 12 kWh pack.

The Electrovaya Escape conversion is approximately 80 percent of the way through the accelerated testing (Table 9) but it has had some problems operating on the road. The individual test cycle results to date have ranged from 29.2 to 43.1 mpg. The weighted average result at the end of FY08 was 35.3 mpg. It should be noted that this is 31 percent higher mpg than the AVTA’s testing results of 27 mpg for the two “normal” Ford Escape HEVs driven for 320,000 miles.

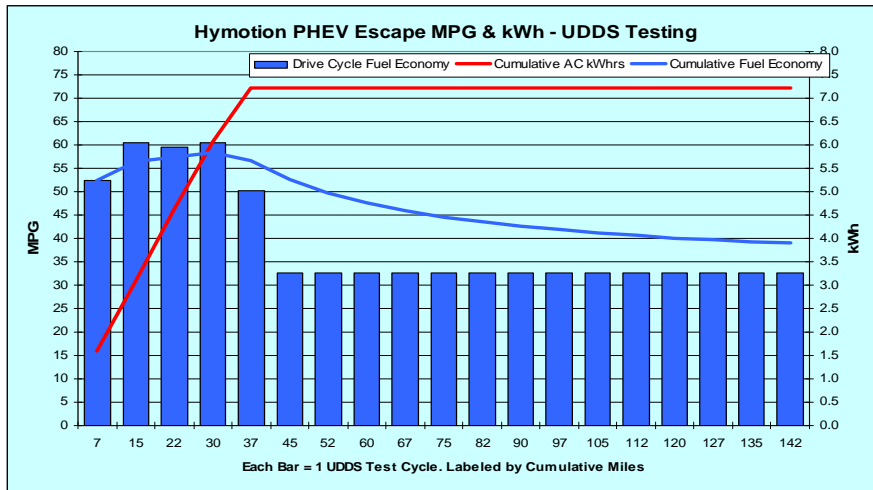


Figure 15. Hymotion Escape PHEV conversion UDDS testing results.
(The blue line is the cumulative mpg and the red line is the cumulative kWh used.)

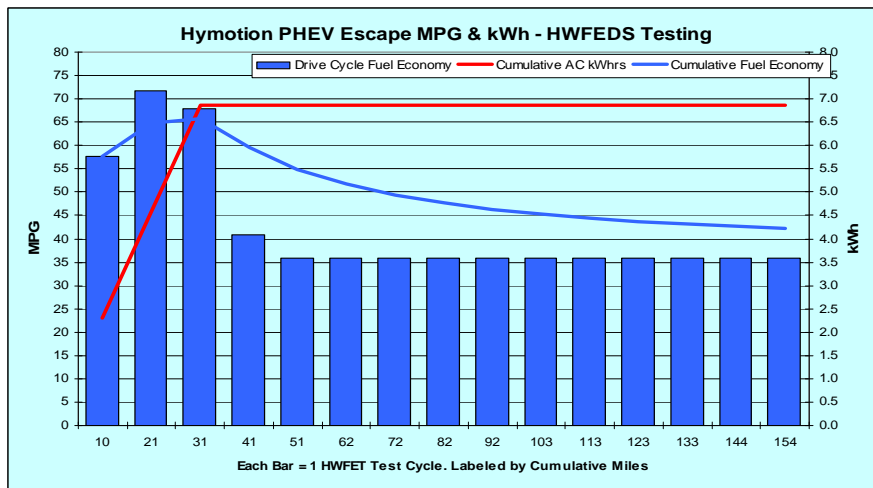


Figure 16. Hymotion Escape PHEV conversion HWFEDS testing results.
(The blue line is the cumulative mpg and the red line is the cumulative kWh used.)

Table 8. Hymotion Escape Prius PHEV conversion accelerated testing results.
Note that each total distance was slightly greater than 600 or 640 test miles.

Cycle (mi)	Urban (10 mi)	Highway (10 mi)	Charge (hours)	Reps (N)	Total (mi)	Electricity kWh	Gasoline	
							Gals	MPG
10	1	0	4	60	600	198.93	11.52	53.1
20	1	1	8	30	600	163.29	13.51	45.7
40	4	0	12	15	600	57.51	14.91	41.1
40	2	2	12	15	600	76.29	15.99	38.7
40	0	4	12	15	600	114.14	11.92	51.5
60	2	4	12	10	600	97.18	13.70	45.3
80	2	6	12	8	640	77.69	16.05	41.3
100	2	8	12	6	600	58.64	15.69	39.8
200	2	18	12	3	600	26.09	17.72	33.5
Total	1,740	2,500	984	132	5,440	Weighted Average	43.3	

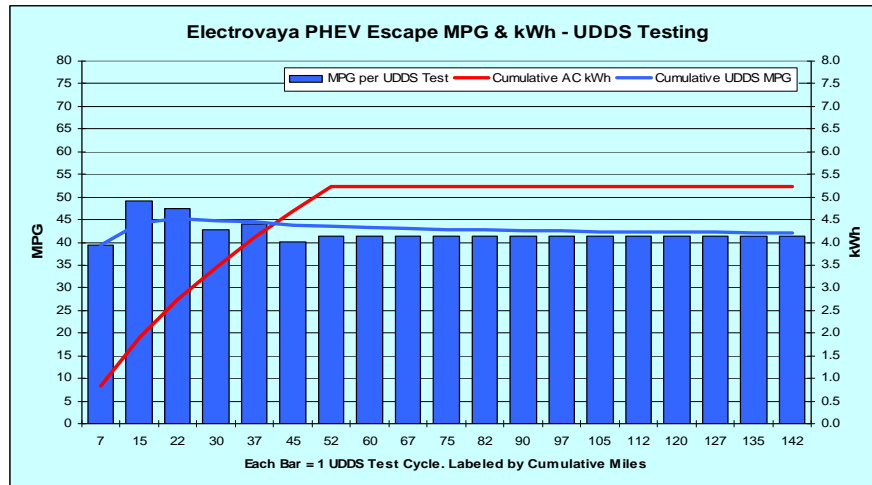


Figure 17. Electrovaya Escape PHEV conversion UDDS testing results.
(The blue line is the cumulative mpg and the red line is the cumulative kWh used.)

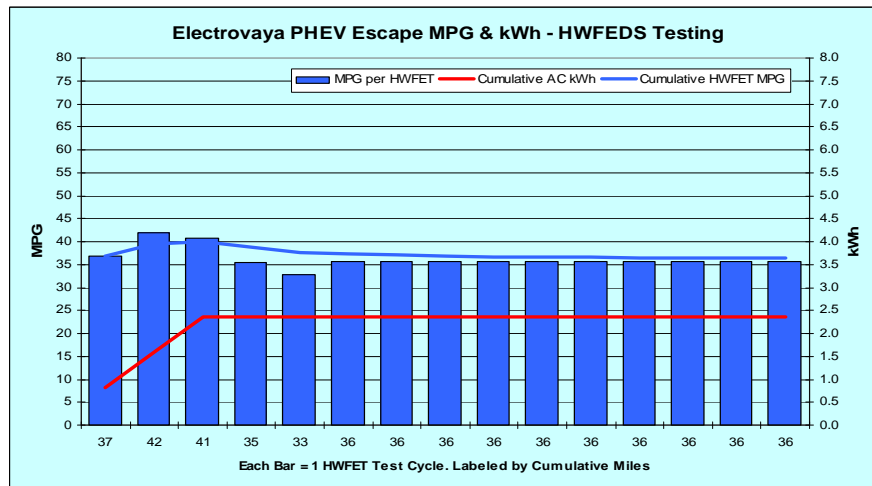


Figure 18. Electrovaya Escape PHEV conversion HWFEDS testing results.
(The blue line is the cumulative mpg and the red line is the cumulative kWh used.)

Table 9. Electrovaya Escape Prius PHEV conversion accelerated testing results.
Note that each total distance was slightly greater than 600 or 640 test miles.

Cycle	Urban (10 mi)	Highway (10 mi)	Charge (hours)	Reps (N)	Total (mi)	Electricity		Gasoline	
						kWh	Gals	MPG	
10	1	0	4	60	600				
20	1	1	8	30	600	In testing			
40	4	0	12	15	600	71.3	16.42	37.3	
40	2	2	12	15	600	69.8	14.34	43.1	
40	0	4	12	15	600	55.84	20.73	29.8	
60	2	4	12	10	600	44.79	16.64	37.3	
80	2	6	12	8	640	42.72	16.30	40.8	
100	2	8	12	6	600	20.85	21.17	29.2	
200	2	18	12	3	600	13.31	19.01	30.9	
Total	1,740	2,500	984	132	5,440	Weighted Average			

Hybrids Plus Escape PHEV Testing – During the UDDS dynamometer portion of the baseline performance testing, the Hybrids Plus (Boulder, CO) PHEV conversion of a Ford Escape achieved over 54 mpg during the cold start first cycle on the UDDS test cycle (Figure 19) and greater than 60 mpg over the next 7 cycles while in charge depleting mode. After 60 miles of testing, the cumulative fuel use was 61 mpg while using 8.7 AC kWh. In charge sustaining mode, it achieved 36 mpg. For the first 60 miles of dynamometer testing, there was a cumulative increase of 69 percent in mpg.

This vehicle is owned by the NYSERDA, and it was tested in partnership between DOE's AVTA and NYSERDA in support of NYSERDA's leadership efforts to support the development of the PHEV industry.

During the HWFEDS dynamometer testing (Figure 20), the Hybrids Plus PHEV Escape conversion had two of its six charge depleting test cycle results over 72 mpg and at 62 miles of testing after six HWFEDS cycles, the cumulative mpg was 61 mpg, a 56 percent improvement over the charge sustaining result of 39 mpg. The vehicle used a total of 9.7 AC kWh during this testing.

The accelerated on-road testing for this vehicle was still suspended as FY08 ended after completing only 550 miles of its first test cycle due to safety concerns after a Hybrids Plus Prius PHEV conversion experienced a battery fire four months earlier.

Other PHEV Test Vehicles – The AVTA has three other PHEV models/conversions in various forms of testing and demonstrations. The status of each is discussed below.

The single Hybrids Plus Prius PHEV conversion (lithium battery) in the test fleet was involved in a thermal anomaly that rendered the vehicle inoperable for any further testing. At the end of FY08, there were no plans to obtain access to another Hybrids Plus Prius conversion.

Two Manzanita Prius PHEV conversions with lead acid batteries were operating with AVTA data loggers. However, the battery in one of these two

PHEVs exhibited signs of swelling and venting during charging and is not active. While the Manzanita was one of the earliest PHEV conversions, the per vehicle conversion cost is higher than the lithium battery equipped Hymotion Prius conversion costs. In addition, the rear suspensions in the base Prius must be reinforced in the Manzanita conversions due to the lead acid battery weight. In fleet operations, the two Manzanita conversions were averaging about 46 mpg after the first 9,400 miles of data collection. There are no current plans to perform baseline performance or accelerated testing on the Manzanita conversions.

The Ford PHEV Escape that is E85 capable was used by DOE and the AVTA as a demonstration PHEV from an OEM in the Washington, DC area during the last quarter of FY08. Many Federal agencies were able view and drive this vehicle in order to understand the capabilities of PHEVs when they are available as a Federal Fleet option in the future.

Fleet Testing – As of the end of FY08, there were approximately 250 PHEVs operating in North America, and most of these were in the United States. In order to collect data on PHEVs in fleet operations, at the beginning of FY08 the AVTA partnered with the two PHEV conversion companies that had performed the most PHEV conversions to date. As FY08 ended, the AVTA has now partnered with 75 organizations in the United States and Canada, and the mix of organizations includes:

- 36 Electric utilities (some via NRECA)
- 6 City governments
- 2 County governments
- 2 State governments
- 8 Universities and colleges
- 2 Clean air agencies
- 7 Private companies and advocacy organizations
- 3 Governments of Canadian provinces
- 1 Sea port and 1 U.S. military organization
- 2 PHEV conversion companies

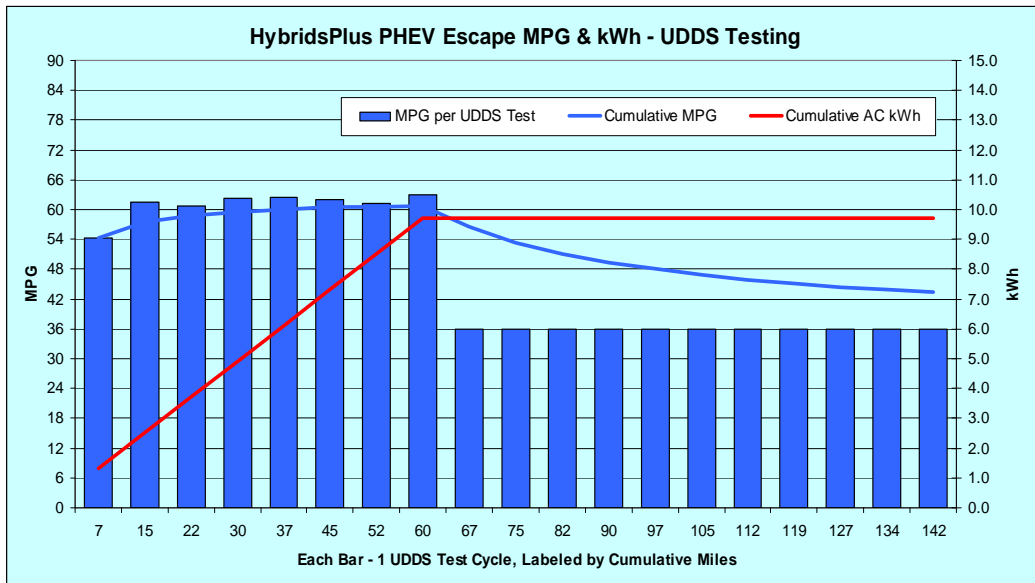


Figure 19. Hybrids Plus Escape PHEV conversion UDDS testing results.
(The blue line is the cumulative mpg and the red line is the cumulative kWh used.)

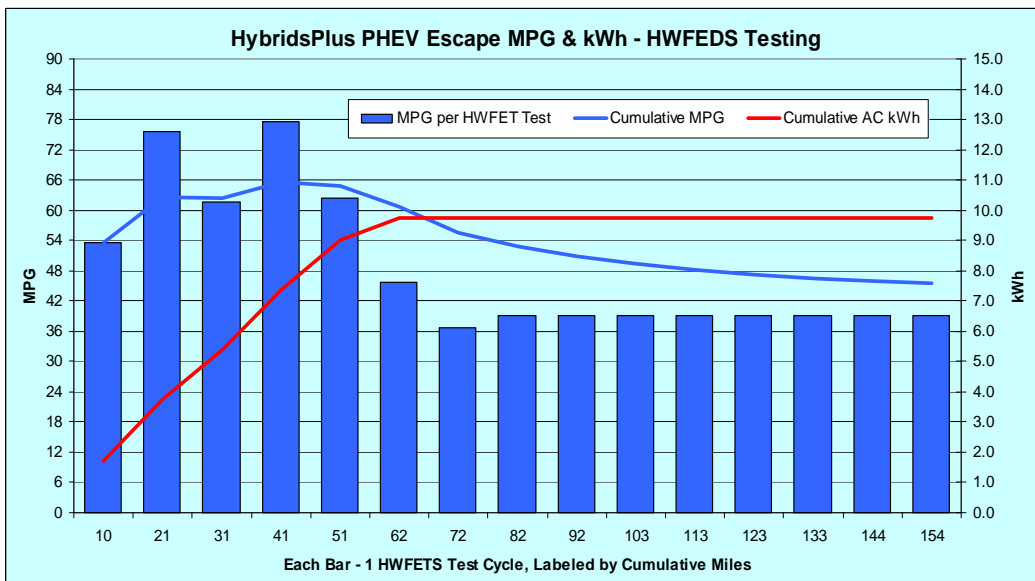


Figure 20. Hybrids Plus Escape PHEV conversion HWFEDS testing results.
(The blue line is the cumulative mpg and the red line is the cumulative kWh used.)

The above 75 PHEV fleet testing partners are operating 95 PHEVs in 17 states and three Canadian provinces (Figure 21) as FY08 ended, with another 79 PHEVs to be added early in 2009, for a total of 154 PHEVs in fleet testing.

The initial 50 vehicles used Kvaser data loggers, which only include a data logger and a memory card that must be either physically mailed to the INL or

uploaded via the Internet. However, the additional 104 fleet PHEVs are all using V2Green onboard data loggers, GPS units, and cellular communications due to the low cost of collecting data via wireless communications, and data collection accuracy.



Figure 21. Locations of the PHEVs in North American fleet operations from which the AVTA is collecting onboard data.

About 125 of the 154 PHEVs are Hymotion PHEV conversions of Toyota Priuses, an additional 12 are EnergyCS conversions of Toyota Priuses, and approximately 10 more are Hybrids Plus conversions of Priuses and Ford Escape HEVs. The remaining PHEVs are a mixture of a couple of lead acid PHEV conversions or a couple of Hymotion Escape conversions. The heavy concentration of Hymotion Prius PHEVs reflects the fact that approximately 75 percent of all PHEVs in North America are Hymotion Prius conversions.

The first AVTA PHEV test fleet is in the Seattle/Tacoma, Washington State area, with 15 PHEVs in the fleets of:

- City of Seattle/Seattle City Light,
- King County,
- Port of Seattle,
- Puget Sound Clean Air Agency, and
- Tacoma Power (City of Tacoma).

Another AVTA PHEV Washington State demonstration of 14 PHEVs is lead by the Port of Chelan. The University of California at Davis has 13 PHEVs in a test fleet with public drivers that are providing data to the AVTA.

The AVTA also has a testing support agreement with NYSERDA to support fleet testing of 20 PHEVs in New York State fleets; however, deployment was only just starting as FY08 ended. A testing agreement with the National Rural Electric Cooperative

Association was providing onboard data access to six PHEVs, with four more to be added. AVTA access to six PHEVs to be placed into operations in Hawaii was being arranged as FY08 ended.

A sample of the types of data that are being accumulated from the PHEV fleet testing and demonstrations can be seen in the three-page summary report for the North American PHEV Demonstration in Figures 22 through 24. The summary is for the thirty Hymotion Prius with Kvaser data loggers that provided data from January to June 2008.

As can be seen in Figure 22, these PHEVs were driven a total of 77,000 miles during this period. The vehicle operations are broken down into three operations modes:

Charge Depleting Mode (CD): During each entire trip there is electric energy in the battery pack to provide either all electric propulsion or electric assist propulsion during which the electric motor and gasoline engine propel the vehicle.

Charge Sustaining Mode (CS): During a trip there is no electrical energy available in the Hymotion A123Systems PHEV battery pack to provide any electric propulsion support.

Combined (or Mixed) CD and CS (CD/CS) Mode: There is electric energy in the Hymotion A123Systems battery pack available at the beginning of a trip but during the trip the battery is depleted and the battery charge is sustained only as the trip is completed.

It should be noted that the only way to recharge the Hymotion A123Systems battery packs is to plug the vehicle in. This PHEV design does not accept energy for recharging during regenerative braking or from the onboard electric generator. The Hymotion design keeps the stock Toyota Prius HEV battery and only this battery can accept onboard energy from recharging or regenerative braking.

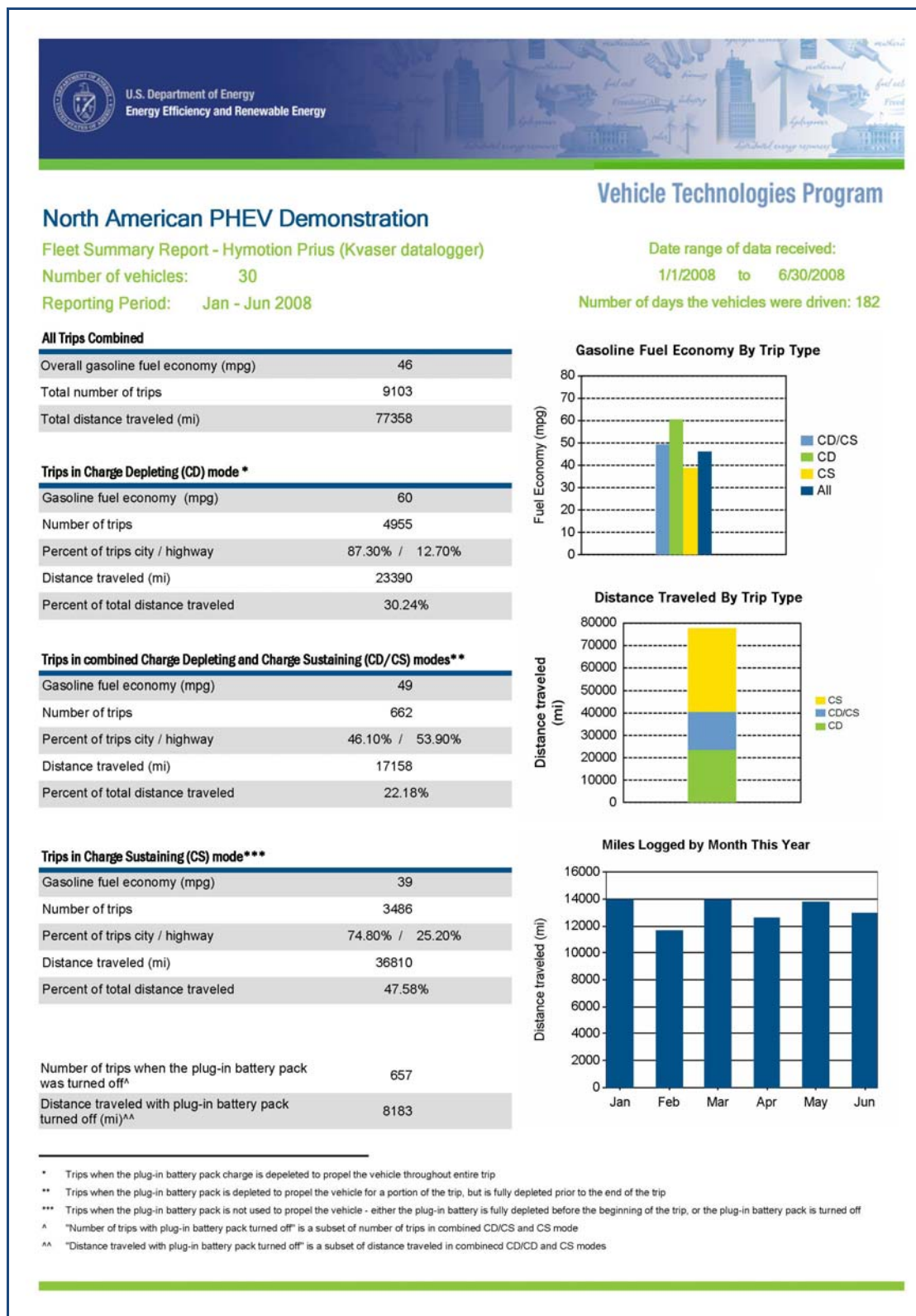


Figure 22. Page 1 of 3 for the PHEV Summary Report for 30 PHEVs operating January – June 2008 with onboard Kvaser data loggers

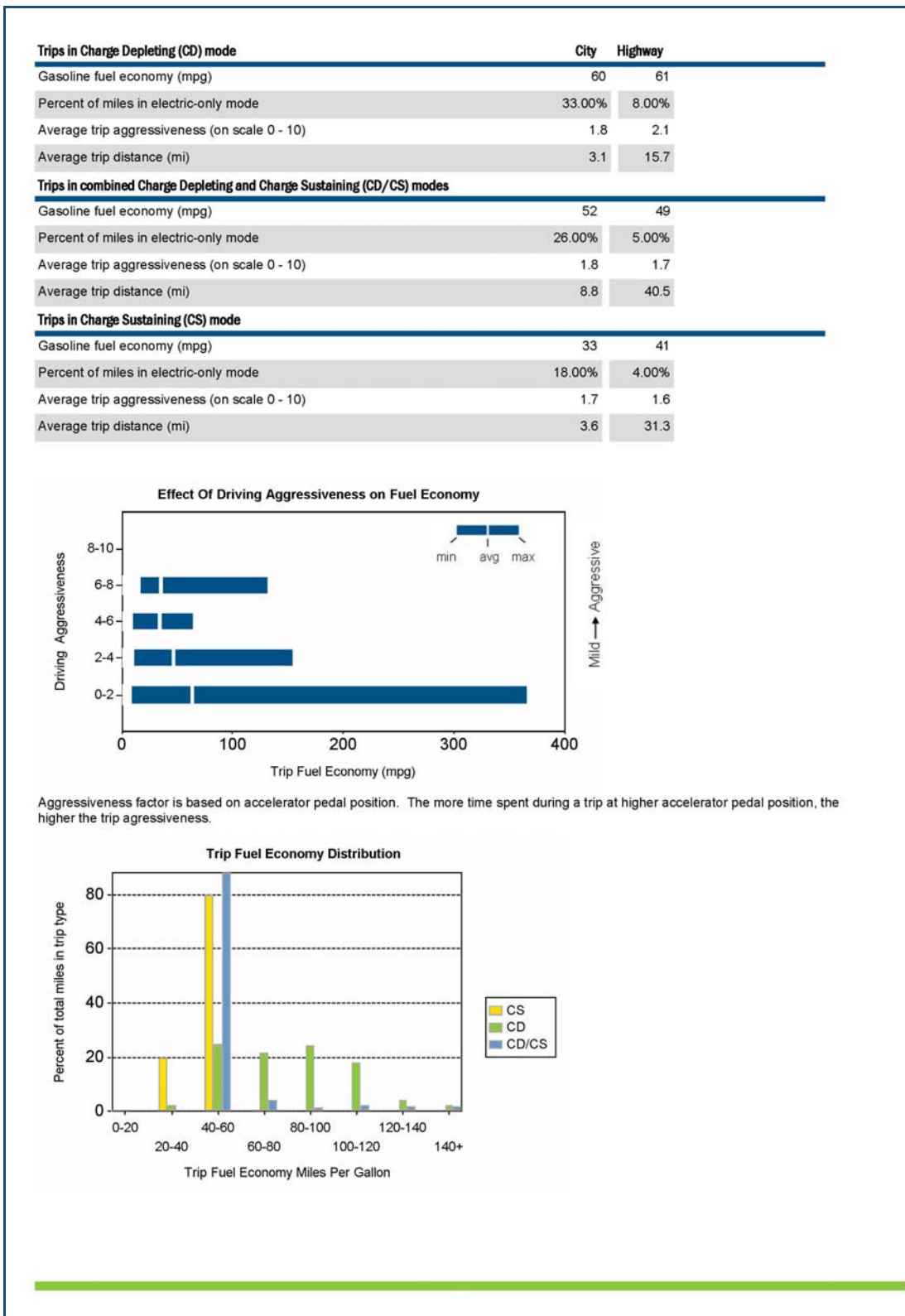


Figure 23. Page 2 of 3 for the PHEV Summary Report for 30 PHEVs operating January – June 2008 with onboard Kvaser data loggers

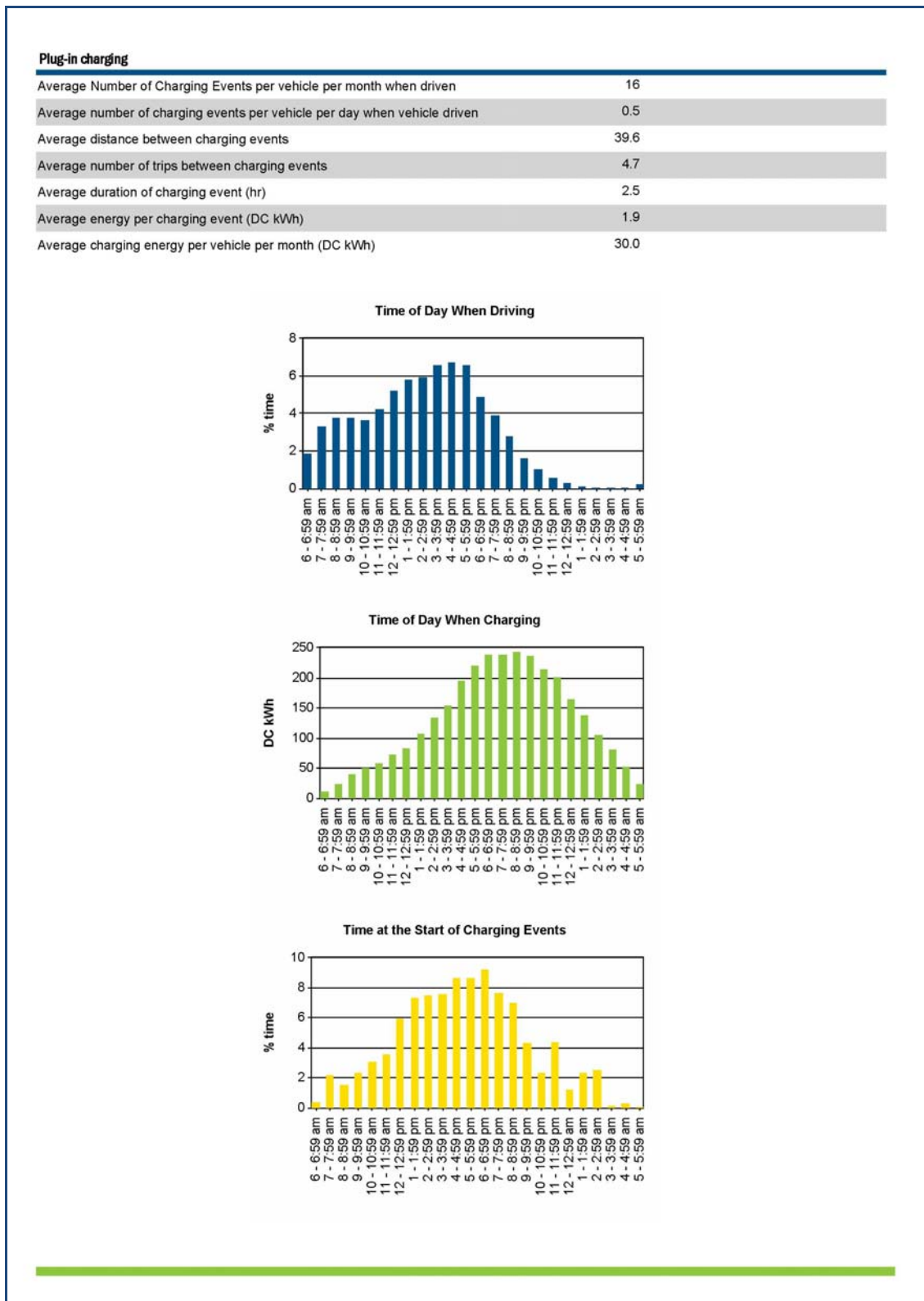


Figure 24. Page 3 of 3 for the PHEV Summary Report for 30 PHEVs operating January – June 2008 with onboard Kvaser data loggers

As can also be seen in the first page of the summary sheet (Figure 22), the overall fuel economy for the 9,103 trips was 46 mpg, but for the 4,955 trips in CD mode, it was 60 mpg, a 50 percent improvement over the 39 mpg for the 3,486 trips taken in CS mode.

As can be seen on page two of the summary sheet (Figure 23), the fuel economy is broken down by city and highway trips, which is binned by average speeds, number of stops per mile, amount of time accelerating, number of stops per mile, number of acceleration events per mile, and the number of seconds cruising per mile. Figure 23 also shows the impacts on PHEV mpg when drivers drive more aggressively. This is measured by the accelerator pedal position and the amount of time spent during a trip at a higher accelerator pedal position. The higher position is how far down the pedal is pushed by the driver; if the pedal is pushed to the floor, it is in the 100 percent position – the most aggressive position. In the graph on page two titled “Effect of Driving Aggressiveness on Fuel Economy,” the bottom 0-2 bar represents all trips driven when the pedal position was at 40 percent or more for only 20 percent or less time of each individual trip, and the average fuel economy was about 60 mpg. Note that some individual trips had fuel economies between 300 to almost 375 mpg per trip.

The third page (Figure 24) provides recharging information and patterns. The average number of charging events per day when a vehicle is driven was 0.5 charges, the vehicles were driven an average of 40 miles between charging events, with 4.7 trips per charging event, and the average charge was for 2.5 hours, and the average energy charged was 1.9 DC kWh.

Figure 24 also shows that the peak drive time was between 4 and 5 p.m. (first graph on page three, Figure 24), with the peak time of day when charging as measured by DC kWh use as between 6 and 10 p.m. (second graph on page three), and the peak start of charging between 6 and 7 p.m. (third graph on page three). It should be noted that most of these vehicles are operating in fleets and most of the driving would occur during work hours, with most of the charging occurring either during breaks, or at the end of the work day.

The impact on PHEV fuel economy from aggressive driving can also be seen in Figure 25. This figure

represents a set of individual trips, the mpg for each trip, and the percentage of time the pedal position is above 40 percent. Generally, when the pedal position is in the aggressive position (40 percent or higher) for 20 percent of the trip or less, the fuel economy for each trip can exceed 100 mpg when the entire trip is taken in CD mode. Some CD-mode trips get lower mpg, but these trips are generally for short durations during which a cold engine start occurs.

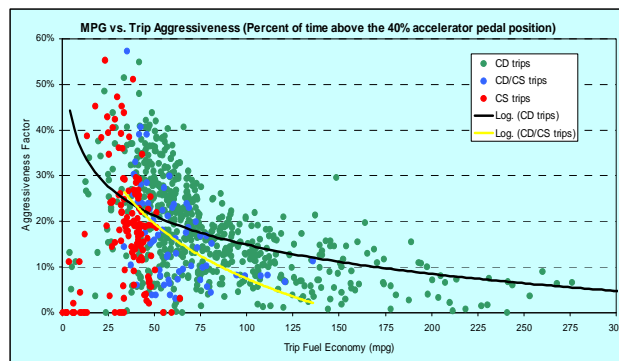


Figure 25. Miles per gallon impacts from aggressive driving patterns, from 13 Hymotion Prius PHEV conversions.

Conclusions

The PHEV industry is still very much in its infancy, with less than 250 light-duty PHEVs deployed in the United States as of the end of FY08. Total independent test miles on any single PHEV battery pack is very limited, so the high-mileage life of PHEV battery packs is unknown. Initial testing of PHEVs suggests there is great potential for reducing petroleum consumption, however, the current cost to convert a HEV to a PHEV ranges from \$10,000 to \$40,000 per vehicle plus the base cost of the HEV. Therefore, on an economic basis, the cost to the vehicle operator to reduce petroleum consumption with PHEVs is currently considerable. However, the future incremental cost to convert HEVs to PHEVs, or the cost of ground-built PHEVs from OEMs, is unknown but is anticipated to be lower.

There is also discussion about PHEVs being able to provide electricity back to the electric grid during periods of peak demand. However, the current group of PHEVs is using 110-volt connectors for recharging from the grid, so this concept may remain theoretical at least for the near future due to limits in the amount of electric energy that can be transferred quickly. Another limiting factor may be battery life, as it is

currently unknown what PHEV battery cycle life will be, and if sending electricity back to the grid may significantly lower battery life.

The eventual control systems that will be used by future PHEVs is also unknown, as some in this infant industry support all-electric ranges while others support greater use of additional electric assist, which will theoretically help maximize battery life.

Regardless of these questions, the few PHEVs currently in operation have demonstrated the significant potential of PHEVs to reduce the use of petroleum for personnel transportation.

Future Activities

The AVTA will continue to test new PHEV models as they become available as well as previously tested PHEV models that have had significant modifications such as new battery designs or chemistries that are believed to provide significant performance enhancements.

In addition to continued testing of vehicle performance, PHEV charging patterns, demands, and the human influence on charging patterns will be documented on the micro level to better understand charging demands and costs at the individual branch circuit, building, and local distribution network levels.

Consideration is being given to testing additional PHEVs in various modes of operation and battery state of charge (SOC) to determine battery life and vehicle performance if the vehicle is charged in scenarios such as every other day, or less often; if the battery is continuously discharged and then charged from 50 percent, 20 percent, or some other SOC; or if the vehicle is continuously operated at very low SOC and rarely charged. These and other operational modes will be considered for additional testing to examine vehicle and battery performance and life.

Developing additional PHEV testing partnerships will be pursued that support the objectives of testing PHEVs in diverse geographic and electric generation regions in order to support a greater understanding of vehicle and battery maintenance needs, functionality, operational life, and life-cycle costs.

Some of the specific testing that the AVTA was initiating or concluding as FY08 ended includes:

Hot weather testing of the Version II Hymotion A123Systems PHEV battery for Prius conversions.

Three recharging studies at commercial facilities to measure the amount of energy and power at a facility that will be required to recharge PHEVs.

Bidirectional vehicle to grid charging at the 6-kW and 20-kW levels.

In addition, all of the AVTA's testing of PHEV conversions to date has resulted in the development of PHEV testing methods, specifications, and procedures for use when the first OEM PHEVs are available starting in 2009. During FY08, DOE announced that Ford, General Motors, and Chrysler all were selected for negotiations for funding to support the development of PHEVs as part of DOE's PHEV Technology Assistance and Demonstration Activity (TADA). The first PHEV models delivered from the TADA will be tested by the AVTA.

The AVTA's fleet testing of PHEVs has been conducted in a highly cost-shared manner; the AVTA's fleet testing costs have been approximately \$400,000 in data logger and conversions costs, while the non-DOE fleets have contributed over \$3 million in base vehicles, conversions, data loggers, and vehicle operations costs.

Publications

Given the infancy of the PHEV industry, there have only been limited numbers of PHEV publications to date generated by the AVTA. The PHEV baseline performance testing procedures and vehicle specifications are listed below and are available on the World Wide Web. PHEV reports and papers published during FY08 are listed below. All of these documents can be found at
<http://avt.inl.gov/hev.shtml> and
http://www.eere.energy.gov/vehiclesandfuels/avta/light_duty/hev/hev_reports.shtml.

2003 Renault Kangoo PHEV America Baseline Performance Testing Fact Sheet:
<http://avt.inel.gov/pdf/phev/KangooFact.pdf>

2007 Hymotion Prius conversion Accelerated Testing Fact Sheet:
<http://avt.inel.gov/pdf/phev/HymotionPriusAccelTestingResultsReport.pdf>

Fleet Demonstrations Testing Results Summary Sheet:
http://avt.inel.gov/pdf/phev/Hymotion_Prius_Kvaser_Jan-June_2008.pdf

PHEV Testing Results and Fleet Demonstration - Plug-in 2008, San Jose, CA:
http://avt.inel.gov/pdf/phev/Plug_In_2008_San_Jose_Presentation.pdf

PHEV Testing Results and Fleet Demonstrations - Power Up Summit. May 2008:
http://avt.inel.gov/pdf/prog_info/PHEV_Testing_Wenatchee_Summit_May_08.pdf

DOE Merit Review - 2008 PHEV Vehicle Evaluations and Data Collection:
http://avt.inel.gov/pdf/prog_info/DOE_Merit_Review_08_PHEVs.pdf

HEV and PHEV Testing - EVS-23 Presentation December 2007 at EVS conference in Anaheim, California:
http://avt.inel.gov/pdf/prog_info/HEVandPHEVtesting_EVS23_presentation.pdf

C. Hydrogen Internal Combustion Engine (ICE) Vehicle Testing

James Francfort (Principal Investigator), Timothy Murphy (Project Leader)

Idaho National Laboratory

P.O. Box 1625

Idaho Falls, ID 83415-3830

(208) 526-6787; james.francfort@inl.gov

DOE Program Manager: Lee Slezak

(202) 586-2335; Lee.Slezak@ee.doe.gov

Objectives

Assess the safety, and operating characteristics of 100 percent hydrogen fueled internal combustion engine (ICE) vehicles.

Identify any engine and vehicle system degradations when operating ICE vehicles on 100 percent hydrogen.

Perform independent testing on candidate 100 percent hydrogen ICE vehicles.

Approach

Use the Integrated Waste Hydrogen Utilization Project (IWHUP) in Vancouver, British Columbia, as a source of inexpensive and high volume hydrogen to fuel eight 100 percent hydrogen ICE pickups converted from natural gas fuel to 100 percent hydrogen fuel operations.

Perform baseline performance (closed test track and dynamometer) testing on appropriate test vehicles.

Accomplishments

Fleet testing of eight vehicles fueled at the IWHUP demonstrated no safety problems during vehicle fueling and operations as the vehicles demonstrated consistent, reliable behavior.

The fleet vehicles demonstrated faster exhaust gas oxygen sensor degradation and an increased presence of water in the engine oils.

Future Directions

Continue to document the operations of the eight vehicles and fuel use, vehicle performance, and any effects hydrogen has on vehicle subsystems.

Continue to evaluate candidate test vehicles and when appropriate, perform baseline performance and fleet testing on them.

Introduction

In past fiscal years, the Advanced Vehicle Testing Activity (AVTA) was very actively involved in monitoring the Arizona Public Service Alternative Fuel Pilot Plant (Figure 1) and testing 100 percent hydrogen ICE vehicles as well as ICE vehicles operating on blends of hydrogen and compressed natural gas (CNG). Seven different hydrogen ICE models have been tested, including:

- Roush/Chevy Silverado, 100 percent hydrogen
- Ford F150 32 Valve, 100 percent hydrogen
- Ford F150 16 Valve, 100 percent hydrogen
- Ford F150 CNG, up to 50 percent hydrogen
- Ford F150 CNG, up to 30 percent hydrogen
- Dodge RAM Wagon Van CNG with 15 percent hydrogen
- Mercedes Sprinter Van, 100 percent hydrogen.

It should be noted that no original equipment manufacturers (OEMs) were involved in converting these vehicles to operate on hydrogen.

Approach and Results

Given the decreased interest in hydrogen, this vehicle technology has not been an area of major research for the AVTA. However, the AVTA has continued to collect data on the eight Roush pickups operating at IWHUP in Vancouver, as this is a very low-cost testing activity.



Figure 1. APS Alternative Fuel (Hydrogen) Pilot Plant, with fuel dispensing island in the foreground

The eight vehicles are all compressed natural gas Chevy Silverado base vehicles converted to operate on 100 percent hydrogen fuel by Roush Industries. The vehicle is of a “crew cab” configuration, with six seat belt positions. It uses three Dynetek carbon-fiber-wrap aluminum-lined tanks installed in the bed of the pickup (Figure 2) for onboard hydrogen storage. The nominal pressure is 5,000 psi (at 25°C) with a maximum pressure of 6,350 psi. The total fuel capacity is 10.5 GGEs. In addition to the fuel tanks, other modifications included a supercharger, hydrogen fuel rails, hydrogen injectors, and significant engine control testing and modifications.

The eight vehicles have been operated for approximately 56,000 miles. Based on the onboard data loggers, they are averaging about 13 miles per gasoline gallon equivalent (mpgge) of hydrogen. The vehicles have been driven on 4,300 trips, during which they had an average trip distance of 12.9 miles (Figure 3). The average speed per trip is in the 15 to 25 mile per hour range (Figure 4).



Figure 2. Dynetek Hydrogen Fuel Tanks in the Bed of the Pickup

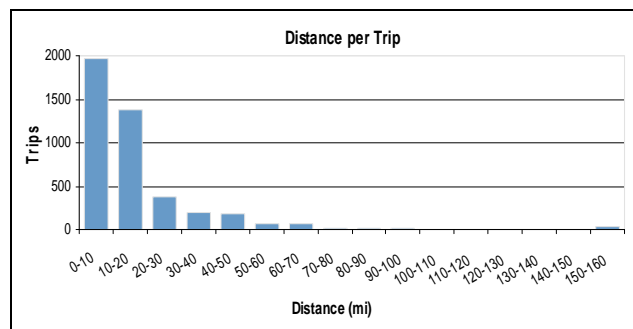


Figure 3. Average Distance per Trip for the Eight Hydrogen ICE Vehicles at IWHUP

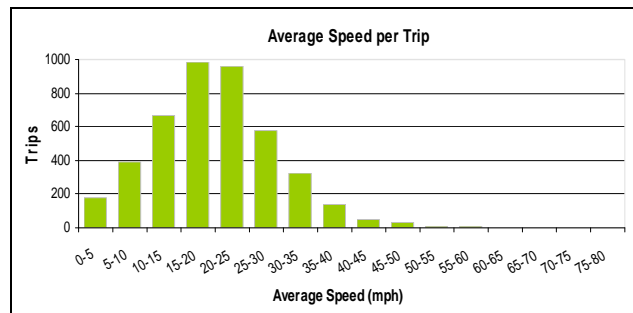


Figure 4. Average Speed per Trip for the Eight Hydrogen ICE Vehicles at IWHUP

Normal fleet operations and vehicle subsystem examinations have identified several consequences from lean-burn operations. Given hydrogen's very wide flammability limits, very lean burn is used to minimize the presence of NO_x in the exhaust stream. This large use of intake air relative to hydrogen results in cooler engine operations. As a believed result, water is appearing in the engine oils, which has the potential to shorten engine life. A second finding is the short life of exhaust gas oxygen sensors, the operation of which is required for California Air Resources Board (CARB) certification. It is unknown whether the cooler exhaust gas is failing to burn off contaminants; this is one possible theory.

The fleet testing of the hydrogen vehicles in Canada has been very highly leveraged as the AVTA only invested in data loggers (\$24,000). The testing partners invested in the base vehicles, conversions requirements for hydrogen operations, as well as provided the drivers, fuel, insurance and maintenance, at a cost of more than \$1 million.

Publications and Presentations

Various publications document pre-fiscal year 2008 hydrogen ICE testing as well as the hydrogen station design and monitoring efforts. These reports can be found at: <http://avt.inel.gov/hydrogen.shtml>.

D. Neighborhood Electric Vehicle Testing

James Francfort (Principal Investigator), Timothy Murphy (Project Leader)

Idaho National Laboratory

P.O. Box 1625

Idaho Falls, ID 83415-3830

(208) 526-6787; james.francfort@inl.gov

DOE Program Manager: Lee Slezak

(202) 586-2335; Lee.Slezak@ee.doe.gov

Objective

Support Federal and other fleet requirements for quality test data on neighborhood electric vehicle (NEV) models.

Support the California Air Resources Board's (CARB) decision requiring that all NEV models sold in California be tested by the Advanced Vehicle Testing Activity (AVTA) in order to be eligible for CARB incremental funding and credits.

Maintain documented test procedures and capabilities to support the continued introduction and operations of neighborhood electric vehicles in fleet environments, and expand the NEV test base.

Approach

Answer all CARB questions regarding NEV testing history, test procedures development, conduct of testing, and AVTA objectives.

Conduct NEV testing as requested by industry and other NEV stakeholders.

Results

Supported CARB's requirement that all NEV models sold in California be tested to the AVTA NEV America baseline performance testing procedures

Conducted NEV America baseline performance testing on five new NEV models from three NEV manufacturers during fiscal year (FY) 2008, for a total of 19 NEV models tested to date.

Responded to questions and inquiries from numerous NEV manufacturers and prospective manufacturers as to the testing process, costs, and schedules.

Future Activities

Given the potential of this market and the expanding use of NEVs, the AVTA will continue to test suitable new entrants as manufacturers introduce additional NEVs. As FY08 ended, the AVTA was in discussion with six NEV manufacturers regarding testing additional NEVs.

Introduction

Neighborhood Electric Vehicles (NEVs) are defined by the National Highway Traffic Safety Administration as low-speed electric vehicles with attainable speeds of more than 20 mph, but not more than 25 mph. NEVs are generally allowed to operate on public streets with posted speeds up to 35 mph and are licensed as a motor vehicle.

NEVs are growing in popularity among fleets and the public because of improvements in technology and their inherently low operating costs. In response to this increasing popularity, the AVTA continued to maintain testing procedures and to update them based on past testing experience.

Approach

Support was given to CARB regarding its process to adapt the NEV America test procedures as its standard requirement. NEV inquiries as to testing processes, schedules and costs were answered. NEV America baseline performance testing was conducted on five NEVs from three manufacturers, including:

- 2007 GEM (Global Electric Motorcars) eL XD, two-passenger extended bed NEV;
- 2007 GEM e6, six-passenger NEV;
- 2008 Zenn Cars Zenn two-passenger NEV
- 2008 Miles Electric Vehicles Miles ZX40S-AD four passenger NEV; and
- 2008 Miles Electric Vehicles Miles ZX40ST two-passenger short bed NEV.

Results

The above five NEV models are discussed here along with the other 14 NEV models tested to date (total of 19 NEV models tested) for comparison purposes.

Per FMVSS 500 (Federal Motor Vehicle Safety Standard), the top speed of NEVs cannot exceed 25 mph. As seen in Figure 1, the most recently tested five NEVs have top speeds of either 24.9 or 25 mph, while the previously tested vehicles had an average top speed of 23.5 mph.

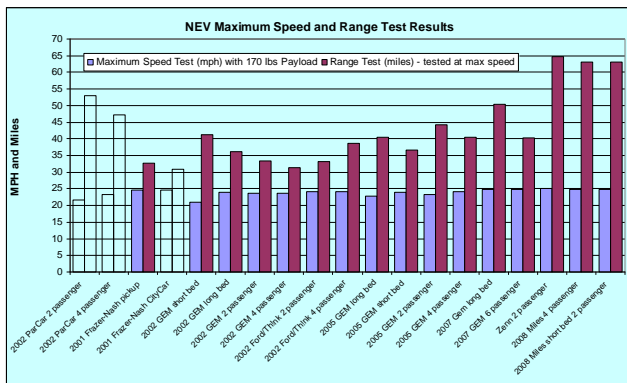


Figure 1. NEV Maximum Speed as Tested on a Closed Test Track, with the accelerator pedal held to the floor (“brick test”) and the range per charge also conducted on a closed track during the “brick test” method

As also seen in Figure 1, three of the five NEVs have test ranges in excess of 60 miles per charge. The average for all 19 models is 43 miles per charge. It should be recognized that actual “real-world” miles

per charge will be lower generally by about 25 percent.

Figure 2 shows the time required to recharge each NEV to 100 percent state of charge and the battery capacity of each NEV. All of the graphed testing results are for 110 volt charging. The recharge times for the two Frazier-Nash NEVs are not graphed as these vehicles were charged by a Level 3 charger. The Frazier-Nash sedan was recharged in 0.93 hours and the Frazier-Nash pickup was recharged in 0.97 hours. Recharge times for the graphed 17 NEVs ranged from 6 to 11.3 hours, with an average recharge time of 9 hours. The 19 NEV models had from 5.3 to 10.8 kWh of onboard storage (Figure 2), with an average onboard storage of 6.4 kWh.

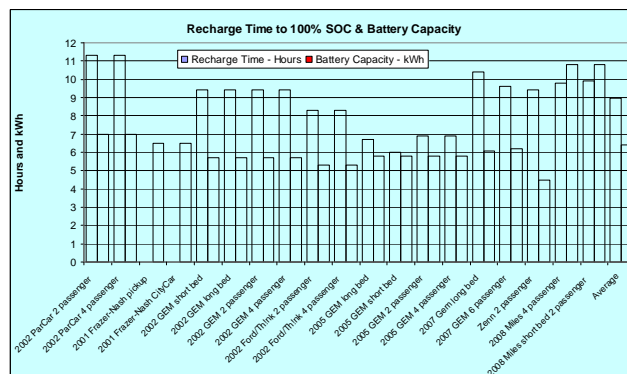


Figure 2. NEV Recharge Times to 100 percent state of charge (SOC) and battery capacity for each NEV: All testing results are for 110 volt charging (Level 1 Charging). The time to recharge for the two Frazier-Nash NEVs is not given because these vehicles were charged by a Level 3 charger. The Frazier-Nash sedan was recharged in 0.93 hours and the pickup was recharged in 0.97 hours.

Figure 3 shows the acceleration from 0 to 20 mph testing results. The most recent five NEVs tested during FY08 had an average acceleration time of 4.9 seconds while the average for the previous 14 test models was 8.1 seconds, which was influenced by the results for the first two NEVs tested and their acceleration times over 16 seconds each. All 19 NEV models have an average acceleration time of 7.2 seconds.

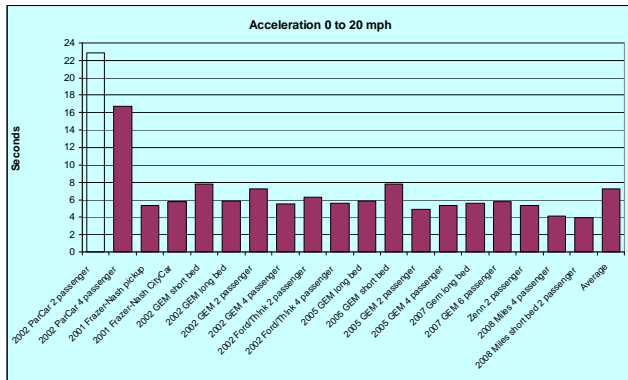


Figure 3. NEV Acceleration Test Times in Seconds to Accelerate from 0 to 20 mph

Figure 4 shows the charging efficiency for 17 of the NEV models as measured at the charger in AC Wh per mile. The overall average for the 17 NEVs was 168 AC Wh per mile while the average for the five recent NEVs tested was 206 AC Wh per mile. The average charging efficiency for the first 12 NEVs tested was 152 AC Wh per mile. This 152 to 206 increase in charging efficiency per mile is likely related to the increase in vehicle weight. The first 12 NEVs tested with charging efficiency results weighed an average of 1,312 pounds while the FY08 test vehicles weighed an average of 1,992 pounds each.

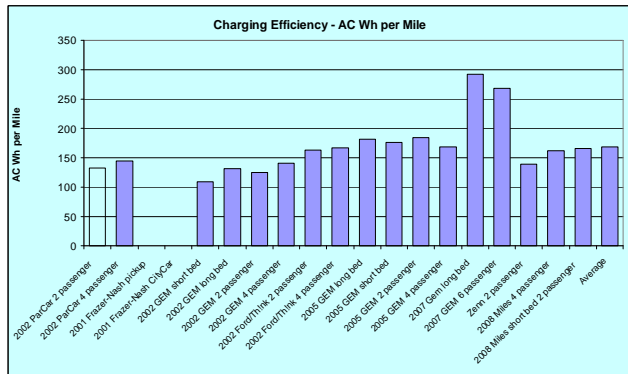


Figure 4. NEV Charging Efficiency, in AC Wh per mile, for the 17 NEV models. The two Frazier-Nash NEVs were charged at Level 3, and the 2002 data for charging efficiency are not available. The 17 NEVs were all charged at 110 volts (Level 1 charging).

Figure 5 shows the miles per AC kWh efficiency for the 17 NEVs charged at 110 volts. NEVs can be a fairly fuel efficient transportation option given the average efficiency of 6.3 miles per kWh. Using the national average price of electricity of 10 cents per kWh, the average price of fuel would be 1.5 cents per mile.

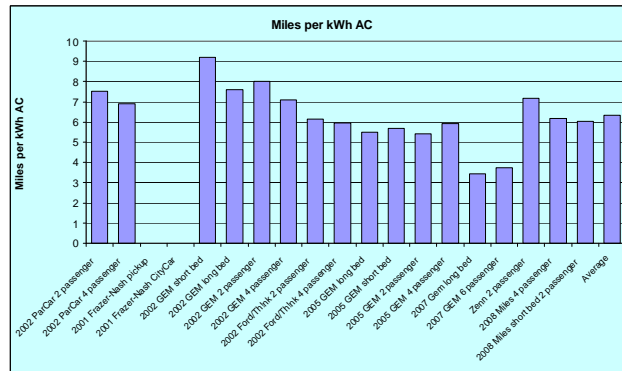


Figure 5. NEV Vehicle Efficiency, as measured in miles per kWh AC when the vehicles are charged at 110 volts (Level 1 Charging). The two Frazier-Nash NEVs were charged at Level 3, and the 2002 data for charging efficiency are not available. The 17 other NEVs were all charged at 110 volts.

Future Plans

As FY08 ended, the AVTA has been approached by six additional NEV manufacturers for information on testing their NEVs. It is anticipated that NEVs will continue to be tested by the AVTA.

Publications

The 18 NEV testing specifications and procedures used for the NEVAmerica testing can be found at: <http://avt.inel.gov/nev.shtml>.

NEVAmerica testing reports published by the AVTA during FY08 are listed below.

2008 Miles 2 Passenger pickup NEVAmerica baseline performance testing fact sheet.
<http://avt.inel.gov/pdf/nev/Miles2008ZX40ST.pdf>

2008 Miles 4 passenger sedan NEVAmerica baseline performance testing fact sheet.
<http://avt.inel.gov/pdf/nev/Miles2008ZX40S.pdf>

2008 ZENN 2 passenger sedan NEVAmerica baseline performance testing fact sheet.
<http://avt.inel.gov/pdf/nev/Zenn2008.pdf>

2007 GEM 6 passenger sedan NEVAmerica baseline performance testing fact sheet.
<http://avt.inel.gov/pdf/nev/gem2007e6.pdf>

2007 GEM long bed NEVAmerica baseline performance testing fact sheet.
<http://avt.inel.gov/pdf/nev/gem2007elXD.pdf>

E. Advanced Technology Medium and Heavy Vehicles Testing

Kevin Walkowicz (Principal Investigator)

National Renewable Energy Laboratory

1617 Cole Blvd.

Golden, CO 80401

(303) 275-4492; kevin_walkowicz@nrel.gov

DOE Technology Manager: Lee Slezak

(202) 586-2335; Lee.Slezak@ee.doe.gov

Objective

Validate the performance and costs of advanced technologies in medium- and heavy-duty applications.

Provide results to interested parties to further optimize and improve the systems.

Facilitate purchase decisions of fleet managers by providing needed information.

Approach

Work with fleets to collect operational, performance and cost data for advanced technologies.

Analyze performance and cost data over a period of one year or more.

Produce fact sheets on advanced heavy-duty vehicles in service.

Provide updates on current applications to the Department of Energy (DOE) and other interested organizations, as needed.

Accomplishments

Published final results on ISE Hybrids operating in the city of Long Beach, CA.

Published final results on 2nd Generation of Orion VII / BAE Hybrid Electric Buses operating in New York City.

Completed six months of data collection and completed a draft report for an evaluation with UPS and Eaton Corporation to evaluate a Lithium Battery Hybrid Electric Vehicle (HEV) Delivery Truck in Phoenix, AZ.

Completed six months of data collection and completed a draft report for plug-in hybrid electric school buses manufactured by IC Corporation in two locations.

Completed and demonstrated the 1st iteration of a fleet duty cycle creation and analysis tool.

Future Activities

Complete evaluations on current fleet vehicles, initiate new evaluations.

Coordinate modeling and testing activities with other DOE projects such as 21st Century Truck Partnership (21st CTP) and the Advanced Heavy Hybrid Propulsion Systems (AH²PS) Project.

Monitor and evaluate promising new technologies and work with additional fleets to test the next-generation of advanced vehicles.

Introduction

Understanding how advanced technology vehicles perform in real-world service, and the associated costs, is important to enable full commercialization and acceptance in the market. The Advanced Vehicle Testing Activity (AVTA) works with fleets that operate these vehicles in medium- and heavy-duty applications. AVTA collects operational, performance, and cost data for analysis. The data analyzed typically cover one year of service on the vehicles to capture any seasonal variations. Because of this, evaluation projects usually span more than one fiscal year. The AVTA team also works on shorter term projects designed to provide updates on current applications to DOE and other interested organizations.

Approach

The AVTA activities for 2008 included:

- Fleet evaluations
- Short term technology development – Fleet Duty Cycle Creation Tool

Fleet Evaluations

In FY 2008, AVTA worked with 3 fleets to evaluate the performance of advanced technologies in service. They are:

1) *New York City Transit (NYCT)* has been investigating clean fuel technologies for several years. NYCT purchased 325 hybrids in two initial orders. The first order of 125 (Gen I) is an upgrade from the fleet's prototype Orion VI hybrids. The second order of 200 (Gen II) has several additional modifications to further improve system performance.

In fiscal year (FY) 2008, AVTA completed its work with this fleet, evaluating the second-generation (Gen II) Orion VII/BAE hybrid electric bus and published a final National Renewable Energy Laboratory (NREL) Technical Report. In order to compare the evolution of Orion/BAE hybrid bus technology, this report compares both generations of hybrids during their first year of operation. To assess any deterioration in performance or increase in operation costs, the report also compares Gen I hybrid bus performance over two years of evaluation. In addition, AVTA published a SAE paper,

representing a compilation of transit bus technology evaluations at NYCT. Highlights of the NREL Technical Report are as follows:

- **Usage:** NYCT quickly integrated the Gen II hybrid buses into the fleet, achieving a similar usage rate of approximately 2,100 monthly miles per bus. The Gen I hybrids averaged about 2,400 miles per month per bus, mainly due to depot speed differences.
- **Reliability:** The Gen II hybrid buses exhibited high reliability, as measured by miles between road calls (MBRC). Gen II hybrids measured 5,445 MBRC, while Gen I measured 5,188 MBRC (Evaluation Year 1) and 6,250 MBRC (Evaluation Year 2). These reliability results are better than NYCT's requirement of 4,000 MBRC. These results indicate acceptable reliability among Gen I and II hybrids, and increasing reliability over time for the Gen I hybrids.
- **Fuel Economy:** The fuel economy realized by Gen II hybrids was 3.00 mpg, or 5.9 percent lower than Gen I hybrids in their first year of evaluation. This decrease can be attributed to exhaust gas recirculation system (EGR)-equipped engines used by the Gen II hybrids, as well as moderate hardware and software differences between the two generations. The fuel economy exhibited by the Gen I hybrids increased 1 percent from evaluation years one to two. Although this difference is statistically insignificant, it does indicate that the lead-acid traction battery pack degradation is not occurring. (See Figure 1.)

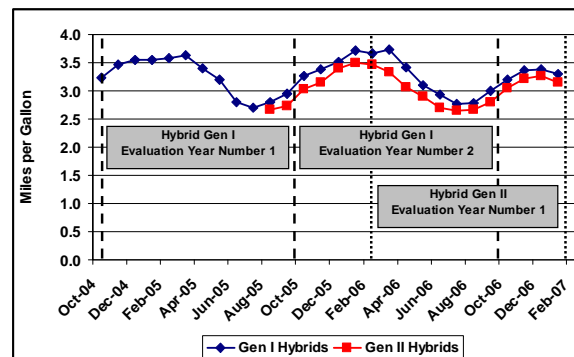


Figure 1. Fuel Economy Summary of Gen I and Gen II Bus Groups

- **Maintenance Costs:** The Gen II hybrids exhibited a lower maintenance cost per mile than Gen I hybrids – \$0.75/mile versus \$1.23/mile. Several improvements made to the Gen II hybrids, as well as greater familiarity of maintenance staff are the primary reason for this difference. Buses had an average total maintenance cost higher than that of the hybrid buses: Propulsion-only maintenance costs for the Gen II hybrids were \$0.16/mile. Gen I hybrid maintenance costs increased slightly over two evaluation years, from \$1.23/mile to \$1.42/mile. However, this increase was not due to the hybrid propulsion system, which accounted for a stable \$0.36 mile to \$0.34/mile over two years.
- **Regenerative Braking Benefit:** Gen I hybrids were compared to compressed natural gas (CNG) buses as baseline with respect to miles to first brake reline. Gen II hybrids had not yet accumulated sufficient mileage to require a brake reline event, and provide this comparison. NYCT expects non-hybrid buses to have a four-wheel brake reline every 18,000 miles. The Gen I hybrids accumulated an average of twice the mileage of the CNG buses before requiring a brake reline.
- **Traction Battery Performance:** The lead-acid traction batteries used in this hybrid system area characterized by a three-year life expectancy and 6-month conditioning interval. During the evaluation period, the Gen II hybrids exhibited zero battery failures. The Gen I hybrids exhibited a 4.8 percent failure rate in the first year of evaluation, and a 3.3 percent failure rate in the second year. This improvement within the generation, as well as from Gen I to Gen II, can be attributed to improved battery management software applied by BAE.

2) PHEV School Bus – Enova/IC Corporation Gasoline Hybrid – In 2008 AVTA began to work with three fleets to evaluate gasoline hybrid buses that are currently operating in 14 different locations around the country. Wake County, NC, and Manatee, FL, school districts were chosen due to their data collection capabilities. One additional site will be added in FY09 for a total of three. The buses, manufactured by IC Corporation, a division of International Truck and Engine Corporation, are

33.5 t front engine school buses with a gross vehicle weight (GVW) of 29,800 lbs. The buses are equipped with International VT365 engines and have the Enova ‘post transmission’ hybrid system added. A 330VDC lithium battery pack is utilized. The data collection activity will summarize one school year’s worth of data (from approximately September 2007 through May 2008).

In September 2008 a draft interim report was submitted to DOE to document six months worth of data collected at the two sites. These buses were compared with the conventional diesel buses that were also in operation in the fleets. A final published report is expected by September 2009. Highlights of the draft interim report are as follows:

- **Fuel Economy:** Figures 2 and 3 show the fuel economy comparison between the hybrid and diesel buses in Wake County and Manatee. When compared to the conventional diesel buses, the results show an overall increase of 30 percent for the Manatee hybrids and 17 percent overall increase for the Wake County hybrids in fuel economy

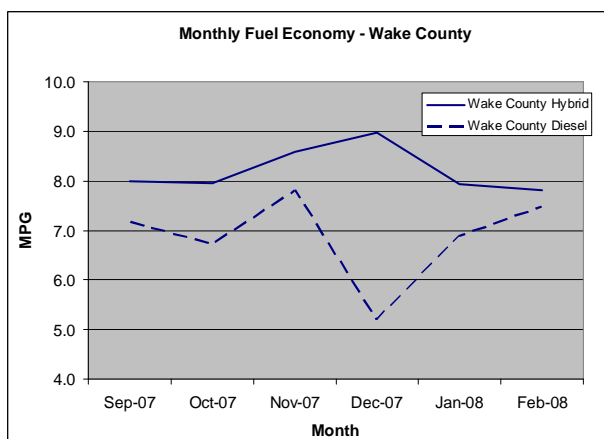


Figure 2. Fuel Economy for Hybrid and Diesel Buses at Wake County School District

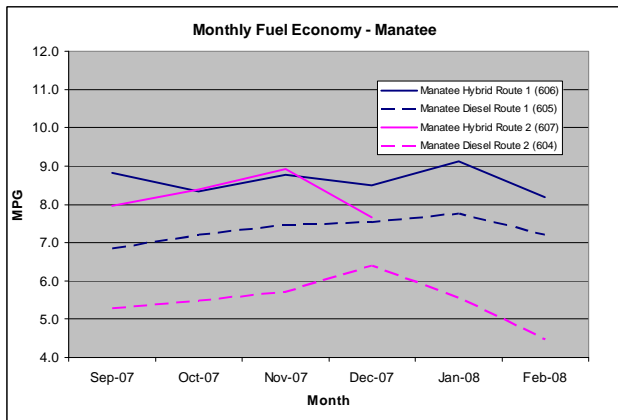


Figure 3. Fuel Economy for Hybrid and Diesel Buses at Manatee School District

- **Energy Storage:** Enova chose to use lithium ion batteries for energy storage instead of nickel metal hydride (NiMH) or lead acid batteries more commonly used in hybrid buses. The lithium ion batteries work well for the larger state-of-charge (SOC) variations associated with plug-in hybrid electric vehicle (PHEV) duty cycles. In addition, the lithium ion batteries have a longer life expectancy compared to other battery types. IC Corporation has a two-year warranty for the batteries. The battery pack used in these charge depleting vehicles are charged overnight using a 220V, 30 amp, single-phase circuit. Full charge will take approximately four hours with the 220V circuit. A 110V option is also available and will approximately double the charge time to eight hours.

During the first year of service and a portion of the evaluation period for some buses, a manufacturing issue was identified. It was discovered that the packaging of the battery pack was improper as it was locating the battery pack on one side of the bus chassis. Not having a split battery pack, IC Corporation corrected the issue with another equally weighted ballast on the opposite side of the chassis, which added extra weight. Once a split battery back was available from the battery supplier (Valence), the ballast was removed and the split/balanced mass pack was installed in the buses. This added retrofit activity does show up in the downtime on some of the buses. Figure 4 is a photo of this battery pack.



Figure 4. Enova PHEV Battery Pack

- **Usage:** Figures 5 and 6 show the miles per month usage for both bus groups. The hybrids in Manatee averaged 1,663 and 994 miles/month for routes 1 and 2 respectively. The Manatee diesels averaged 1,933 and 1,155 miles/month respectively for the same routes. The Wake County hybrids averaged 2,535 miles per month and the diesels averaged 2,133 miles/month.

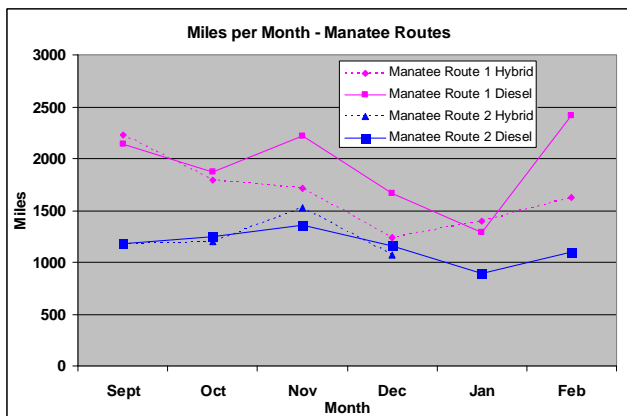


Figure 5. Manatee Miles per Month

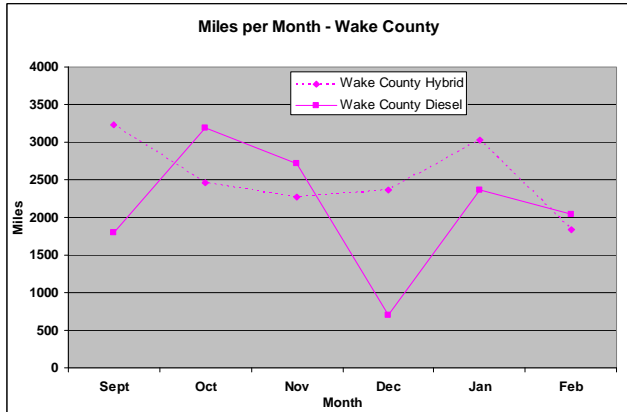


Figure 6. Wake County Miles per Month

- Operational Costs:** Total operational costs for the diesel buses (fuel and maintenance costs) were \$0.42 per mile and \$0.37 per mile for Manatee and Wake County respectively. The total operational costs for the hybrid buses were \$0.35 per mile and \$0.32 per mile. There was 17 percent decrease overall for the hybrids in Manatee and a 13 percent decrease for the hybrids in Wake County.
- Overall, the school districts have been satisfied with the buses.
- Laboratory emissions testing is planned for early 2009.

3) *Long Beach, CA – ISE Gasoline Hybrid* – AVTA has finished its work with Long Beach Transit (LBT) fleet to evaluate 10 of the gasoline hybrid buses which are currently operating in the city of Long Beach, CA. LBT currently has forty-seven 40-ft hybrid gasoline-electric buses equipped with Maxwell ultracapacitors for energy storage. These buses arrived between June and August 2005. They were expected to operate more cost effectively than CNG buses in terms of infrastructure, fuel economy, and maintenance savings and offer a clean option for LBT as gasoline was qualified as an alternative fuel for transit buses by the California Air Resources Board (CARB).

In June 2008, AVTA published a final project report for 24 months of data on the buses in service (June 2005 – June 2007). These buses were compared with the conventional diesel buses that were also in operation in the LBT fleet. A final report was published in December 2007. Highlights of this report are as follows:

- Fuel Economy:** Figure 7 shows the fuel economy comparison between the hybrid and diesel buses. When compared to the conventional diesel buses, the results show an overall decrease of 4.3 percent in fuel economy (on a straight per gallon basis) and an 8.5 percent increase in fuel economy (if the fuel consumption is adjusted for the energy content on a volumetric basis).

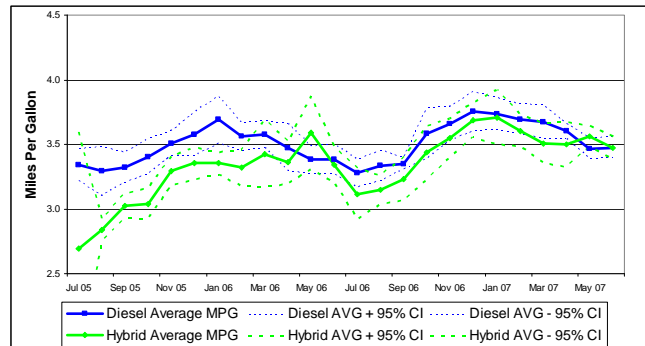


Figure 7. Fuel Economy for Hybrid and Diesel Buses at LBT in Similar Duty Cycle.

- Maintenance Cost:** Figure 8 shows the total maintenance cost and propulsion system maintenance cost for both types of buses. For total maintenance cost, the hybrids averaged \$0.31/mile and the diesels averaged \$0.54/mile – a 42 percent decrease in costs for the hybrids. For propulsion system only maintenance costs, the hybrids averaged \$0.08/mile and the diesels averaged \$0.19/mile – a 63 percent decrease. These propulsion system costs do not include any warranty related costs.

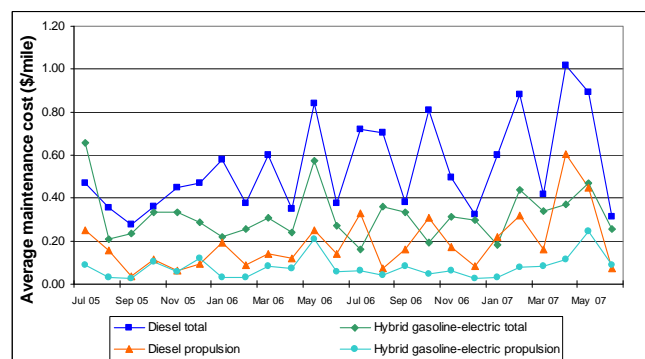


Figure 8. Maintenance Costs per Mile

- Brake Maintenance:** Figure 9 shows the average time to the first front and rear brake relines for both types of buses. All of the hybrid buses have more miles on them than any diesel bus had by the time of its first rear reline. On average, the hybrid buses have doubled the mileage to first rear brake reline and are approaching the mileage the diesel buses averaged for their first front reline. Maintenance costs for the brakes on the baseline diesel buses were 10 times greater than the costs for the hybrids: 0.0036 \$/mile for the hybrids vs. 0.0356 \$/mile for the diesels.

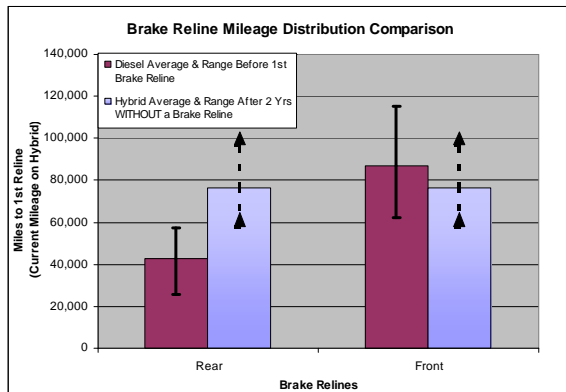


Figure 9. Brake Reline Mileage Distribution Comparison

- **Ultracapacitors:** During the evaluation period a manufacturing issue was identified; acetonitrile was leaking from some of the ultra-capacitors. ISE corrected the issue with a warranty campaign based on serial numbers of suspect batches of ultracapacitors. The correction was to apply an epoxy coating over the ultracapacitors, sealing them. Two incidents of ultra-capacitor dry cell overheating were attributed to this leakage within the fleet, but were not part of the study group.



Figure 10. Maxwell Ultracapacitor Pack

- **Reliability:** Figure 11 shows the MBRC for both bus groups for all systems and also for propulsion system only. Total MBRC for the hybrids averaged 9,000 miles and the diesels averaged 11,040 miles (an 18 percent decrease in MBRC for the hybrids). For the propulsion system MBRC for the hybrids averaged 15,000 miles and the diesel buses averaged 19,118 miles (22 percent less MBRC for the hybrids).

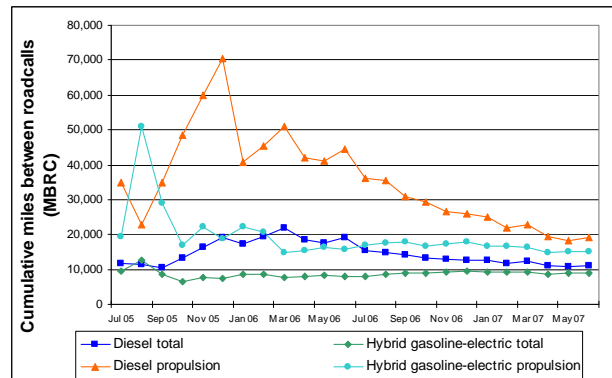


Figure 11. MBRC for Both Bus Groups

- **Operational Costs:** Total operational costs for the diesel buses (fuel and maintenance costs) were \$1.19 per mile. The total operational costs for the hybrid buses were \$1.05 per mile – a 12 percent decrease overall for the hybrids.
- Overall, LBT Transit has been satisfied with the buses.

4) **UPS Hybrid Package Delivery** – A new fleet evaluation was initiated in FY2007. AVTA was to be evaluating trucks in a UPS fleet in Dallas, TX, to evaluate the performance of their MD package delivery vehicles equipped with an advanced battery powered Eaton parallel hybrid system. An evaluation to assess the performance and feasibility of this technology was initiated. However in the spring of 2008 UPS informed NREL that Dallas was not a good location to study from their point of view due to numerous reasons that made it not representative of their fleet and they requested changing the study location. A new group of vehicles was selected in Phoenix, AZ, for the study and detailed evaluation was restarted. The intent of the project is to compare these lithium battery parallel hybrid trucks with conventional diesel powered trucks. Duty cycle data acquisition was completed in August 2008 in Phoenix.

In September 2008, AVTA produced a draft interim project report for six months of data on the trucks in service (January 2008 through June 2008). A final published report is expected in March 2009. Highlights of the draft interim report are as follows:

Delivery Van Use and Duty Cycle: The hybrids had a usage rate that was 14 percent less than that of the diesel vans. Van average usage did not change

significantly during the first six months of the evaluation period. The hybrids consistently were driven a fewer number of miles throughout the evaluation period. In general, the hybrids spent more time idling and operating at slower speeds than the diesels did, and the diesels spent slightly more time operating at greater speeds; this resulted in the hybrids' fewer monthly miles.

Fuel Economy: The six-month average fuel economy for the hybrid vans is 13.06 mpg; 27.2 percent greater than that of the diesel vans (two-tailed P value = 0.0015). Figure 12 shows the average monthly mpg for each van group and the cumulative average mpg as well.

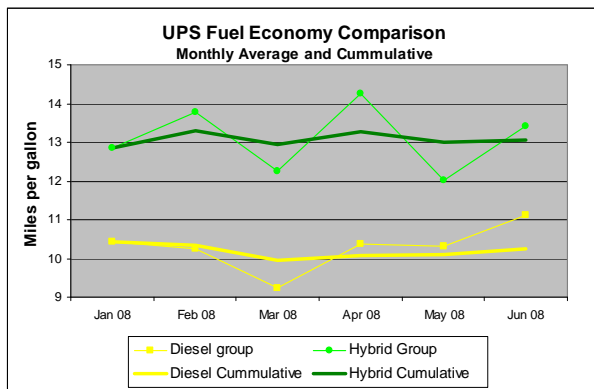


Figure 12. Average Monthly Fuel Economy

Maintenance Costs: The total maintenance cost per mile was 30 percent less for the hybrid vans than for the diesel vans. The propulsion related maintenance cost per mile was 23 percent less for the hybrid vans than for the diesel vans. Total maintenance costs were 40 percent less for the hybrids over the first six months of evaluation.

Short Term Technology Evaluations:

Fleet Duty Cycle Creation and Analysis Tool – The AVTA team has identified a need by fleet operators and researchers to quickly and accurately assess what type of drive cycle vehicles are operating on. In response to this need, the AVTA team has initiated an effort to devise a computational tool that is capable of analyzing user acquired GPS time-speed data and creating a compressed 'custom' duty cycle based on the inputs. An eight-hour 1-Hz data set is quickly and easily compressed down to a 30-minute test cycle for vehicle testing or modeling activities. An additional function of this tool will be to provide comparative data, which will allow the user to assess

which 'standard' duty cycle is closest to the data provided. Additional output will include statistics on various parameters of interest. Figure 13 shows a general screen shot of the output of this tool.

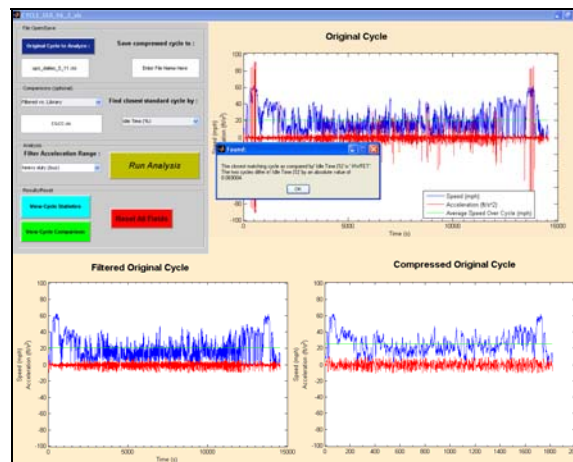


Figure 13. Screen Shot of Duty Cycle Analysis and Creation Tool

Additional work is being done in FY09 to refine the analysis functions and validate the results. A limited use trial run with a controlled group of users is scheduled for late FY09.

Overall AVTA Results

Results from AVTA fleet evaluations have been anticipated and well received by the industry. Specific results for each evaluation are described as a part of the project sections above.

Future Plans

The team will continue working with fleets to investigate the latest technology in medium duty and heavy-duty vehicles. The team will track the latest developments in advanced vehicles and select those with the most promise for further study. Future plans include working with simulation and modeling teams at the DOE labs to ensure that relevant vehicle data are collected to verify and enhance the various simulation models.

FY2008 Publications / Presentations

Barnitt, R. A. (June 2008). In-Use Performance Comparison of Hybrid Electric, CNG, and Diesel Buses at New York City Transit. SAE Paper No. 2008-01-1556. 10 pp.; NREL Report No. CP-540-42534.

Barnitt, R. (March 2008). BAE/Orion Hybrid Electric Buses at New York City Transit: A Generational Comparison (Revised). 31 pp.; NREL Report No. TP-540-42217.

Lammert, M. (September 2008). UPS: Draft Interim Evaluation of Diesel-Electric Hybrid Delivery Vans. 18 pp.; NREL Report No. TP-540-40134.

Walkowicz, K. (September 2008). Case Study (Interim): In-Use Performance and Laboratory Testing of Plug-In Hybrid Electric School Buses. 22 pp.; NREL Report No. CP-540-44104.

Barnitt, R.A. (March 2008). In-Use Performance of Orion BAE Hybrid Buses at New York City Transit (Presentation). 18 pp.: Presented at the Diesel Technology Forum Webinar.

Lammert, M. (March 2008). Long Beach Transit Two-Year Hybrid Gasoline Electric Evaluation - Final. 26 pp.: NREL Report No. TP-540-4222.6

Walkowicz, K (September 2008). Progress Review - Fleet Duty Cycle Creation and Analysis Tool (Milestone Presentation). Presented to DOE September 16, 2008.

Walkowicz, K (May 2008). U.S. Department of Energy's MD/HD Hybrid Evaluations (Presentation). 12 pp.: Presented at the Alternative Fuels Vehicle Institute Annual Conference in Las Vegas, NV.

VI. AERODYNAMIC DRAG REDUCTION

A. DOE Project on Heavy Vehicle Aerodynamic Drag

Project Principal Investigator: K. Salari

Co-Investigator: J. Ortega

Lawrence Livermore National Laboratory

P.O. Box 808, Livermore, CA 94551-0808

(925) 424-4635; salari1@llnl.gov

DOE Technology Manager: Lee Slezak

(202) 586-2335; Lee.Slezak@ee.doe.gov

Contractor: Lawrence Livermore National Laboratory

Contract No.: W-7405-ENG-48, W-31-109-ENG-38, DE-AI01-99EE50559

Objective

Class 8 tractor-trailers consume 11-12% of the total US petroleum use. At highway speeds, 65% of the energy expenditure for a Class 8 truck is used in overcoming aerodynamic drag. The project objective is to improve fuel economy of Class 8 tractor-trailers by providing guidance on methods for reducing drag by at least 25%. This 25% reduction in drag would present a 12% improvement in fuel economy at highway speeds, equivalent to about 130 midsized tanker ships per year. The specific goals of this project include:

Provide industry with design guidance and insight into aerodynamic drag reduction of heavy vehicles.

Develop innovative drag reduction concepts that are operationally and economically sound.

Establish a database of experimental, computational, and conceptual design information for drag reduction concepts and devices.

Establish an experimental data base for understanding the key drag producing flow structures around heavy vehicles.

Develop the ability to simulate and analyze the key aerodynamic flow structures around heavy vehicles.

Investigate the potential of aerodynamic devices for full-scale fuel economy that target the trailer base, tractor-trailer gap, and underbody.

Demonstrate the full-scale fuel economy potential of these devices.

Approach

Simulate and analyze the aerodynamic flow around heavy vehicles using advanced computational fluid dynamics (CFD) tools and experiments.

Investigate aerodynamic drag reduction devices (e.g., base flaps, tractor-trailer gap stabilizers, underbody skirts, wedges and fairings, and blowing and acoustic devices).

Generate an experimental database for understanding the drag producing flow phenomena.

Provide industry with design guidance and insight into the flow physics of heavy vehicles from experiments and computations.

Accomplishments

Completed the test plan, design of the holding frame to move the truck into the 80'x120' wind tunnel test section, and mounting requirements for the full-scale experiment of Class 8 heavy vehicles at the National Full-Scale

Aerodynamics Complex (NFAC) wind tunnel facility located at NASA's Ames Research Center. This effort is in partnership with International Truck and Engine Corporation and Michelin Americas Research & Development Corporation.

Various new tractor-trailer underbody skirts, wedges, and fairings have been evaluated for their drag reduction capability.

Future Direction

Getting devices on road.

Conduct a full-scale wind-tunnel test at the NFAC 80'x120' full-scale wind-tunnel with coloration of International Truck and Engine Corporation and Michelin Americas Research & Development Corporation.

Seek collaborative feedback and demonstrations of drag reduction devices from fleet owners and operators.

Develop and transfer technology and information to industry.

Identify the need for experimental and computational methods to evaluate design options for improved fuel efficiency.

Improve the thermal coupling of a Class 8 heavy vehicle engine to the internal and external cooling flow because of the new 2010 EPA emission requirements. Current engine-flow coupling approaches are empirical, ad hoc, one-dimensional, and insufficient to meet the more restrictive requirements. A fully coupled engine-flow modeling capability with first principle heat and flow physics and combustion modeling is needed to significantly improve the current modeling capability.

Contouring the tractor hood provides a reduction in drag, but also reduces the grille area and coolant air flow. Since additional underhood cooling may be required to meet EPA regulations, we are including underhood flow in the aerodynamic drag simulations and in the planning for the 80'x120' wind-tunnel tests. This will allow us to provide additional insight into this coupled (thermal, fluid) flow phenomena.

Economic/duty cycle evaluation with PSAT (ANL's system model).

Provide mechanistic data: strong variation in the drag coefficient with yaw, air speed, geometry/devices, environmental turbulence, etc.

Acknowledgments

- This work was performed under the auspices of the U.S. Department of Energy by Lawrence Livermore National Laboratory in part under Contract W-7405-Eng-48 and in part under Contract DE-AC52-07NA27344.
-

B. Investigation of a Trailer Underbody Fairing for Heavy Vehicle Aerodynamic Drag Reduction

Jason Ortega, Kambiz Salari

Lawrence Livermore National Laboratory

7000 East Ave, L-098, Livermore, CA 94551

925-423-0958, Fax 925-422-3389, mccallen1@llnl.gov

DOE Technology Manager: Lee Slezak

(202)586-2335; Lee.Slezak@ee.doe.gov

Technical Program Manager: Jules Routbort

(630) 252-5065; routbort@anl.gov

Contractor: Lawrence Livermore National Laboratory

Contract No.: W-7405-ENG-48

Objective

Although trailer side skirts have been shown to reduce the aerodynamic drag of heavy vehicles, they have not been accepted on a wide-scale basis throughout the heavy vehicle industry due to a number of operational concerns. The shipping fleets that have tested the skirts found that their design limited the ground clearance of the vehicle and, as a result, the skirts were often damaged when the vehicle passed over railroad crossings or backed into sunken loading docks. In the more northern shipping routes, the skirts tended to collect a substantial amount of ice, which increased the overall weight of the vehicle and, therefore, required the drivers to remove the accumulated ice before entering truck weigh stations. While some of these operational issues can be overcome either by arching or actively retracting the skirts so as to increase their ground clearance or by enhancing the robustness of the skirts, the heavy vehicle industry has remained reluctant to employ such alternative trailer skirt designs.

However, with rising fuel costs, potentially unstable fuel supplies, and global warming, there are much greater incentives today to further reduce heavy vehicle fuel usage and, consequently, trailer underbody devices may be the means by which this goal can be achieved. Yet, to gain the acceptance of the heavy vehicle industry, these devices must be developed in a manner that not only yields aerodynamic drag reduction, but also provides designs that are operationally practical.

Approach

In accordance with this criterion, the present study investigates the drag reduction performance of a trailer underbody fairing using computational fluid dynamics (CFD) simulations.

Accomplishments

From the simulations, the drag coefficient, C_d , of the baseline vehicle is computed to be 0.641, where the majority (0.429) of this value is due to drag on the tractor. The remaining portion of the drag is divided about equally between the trailer cargo box and the trailer wheel assembly. Installation of two different types of trailer underbody fairings (Figures 2 and 3) of varying length reduces the drag coefficient below this baseline value (Figure 4). For the T1 fairings, C_d decreases in a roughly monotonic fashion as the fairing length is increased, with the longest fairing yielding a C_d of 0.617. For the T2 fairings, the drag coefficient also decreases as the fairing length is increased. However, for the 9.2 m long T2 fairing, C_d is reduced even more substantially to a value (0.599) that is even less than that (0.605) of trailer side skirts. Additional details on the fairing performance can be found at the end of this section in a paper that was presented at the Society of Automotive Engineers 2008 Commercial Vehicle Engineering Congress and Exhibition.

Near Term Direction

Collaborate with International Truck and Engine Company to perform small-scale wind tunnel measurements of various fairing designs.

Far Term Direction

Collaborate with International Truck and Engine Company to perform full-scale wind tunnel measurements of various fairing designs.

Introduction

As described within the recent reviews of Cooper [1,2], a number of drag reduction devices were designed in the late 1970s and 1980s to reduce the aerodynamic drag of heavy vehicles. The result of this effort led to the development of a number of designs, such as cab-mounted air deflectors, fairings, side extenders, and front-end rounding, that significantly improved the aerodynamics and, hence, the fuel efficiency of heavy vehicle tractors. These devices were accepted by the heavy vehicle industry because they required modification only to the tractors. Furthermore, the tractor owners could recover their investment in these devices from the subsequent fuel cost savings. In addition, a number of second-generation devices were developed to reduce the aerodynamic drag of heavy vehicle trailers. One of these devices, trailer side skirts, was constructed from flat plates suspended on either side of the trailer underbody. The skirts reduced the vehicle drag by shielding the trailer wheel assembly from the high speed, cross-stream flow that passed beneath the trailer when the vehicle operated within a crosswind. Some designs also included additional skirts that were located behind the trailer wheels and were shaped to conform to the drag reduction devices placed on the trailer base [2].

Although the trailer side skirts reduced aerodynamic drag, they were not accepted on a wide-scale basis throughout the heavy vehicle industry due to a number of operational and economic concerns. The shipping fleets that tested the skirts found that their design limited the ground clearance of the vehicle and, as a result, the skirts were often damaged when the vehicle passed over railroad crossings or backed into sunken loading docks. In the more northern shipping routes, the skirts tended to collect a substantial amount of ice, which increased the overall weight of the vehicle and, therefore, required the

drivers to remove the accumulated ice before entering truck weigh stations. Lastly, the trailer side skirts suffered from two economic disadvantages common to all of the second-generation drag reduction devices: first, the installation of the skirts required modification to the trailers, which were greater in number than the tractors, thus resulting in a greater initial investment; and, second, because the trailers were often client-owned, there was no incentive for the client to spend money on fuel-saving options that provided no direct financial benefit to them [2]. While some of these operational issues could have been overcome either by arching or actively retracting the skirts so as to increase their ground clearance [3] or by enhancing the robustness of the skirts, the heavy vehicle industry has remained reluctant to employ such alternative trailer skirt designs.

However, with rising fuel costs, potentially unstable fuel supplies, and global warming, there are much greater incentives today to further reduce heavy vehicle fuel usage and, consequently, trailer-mounted devices may be the means by which this goal can be achieved. Yet, to gain the acceptance of the heavy vehicle industry, these devices must be developed in a manner that not only yields aerodynamic drag reduction, but also provides designs that are operationally practical. In accordance with these criteria, the present study investigates the drag reduction performance of a trailer underbody fairing (Figure 1), which could potentially overcome some of the operational issues associated with trailer side skirts. In particular, we address the following questions in this study using computational fluid dynamics (CFD) simulations. Does the trailer underbody fairing reduce the drag of a heavy vehicle? Can the fairing produce as large of a drag reduction as that of trailer side skirts? What are the overall changes in the trailer underbody flow field following the installation of the fairing? And, how

do these changes contribute to the reductions, if any, in the drag coefficient?

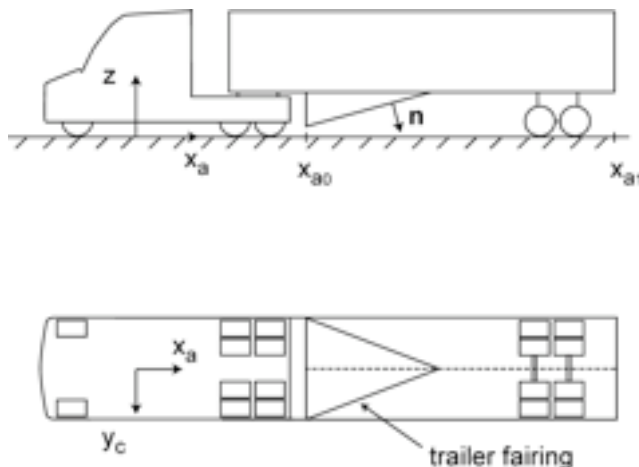


Figure 1. Trailer Underbody Fairing

Computational Setup

To address these questions, we perform CFD simulations on a full-scale heavy vehicle, which is a representation [4] of a Freightliner Columbia tractor [5] and a 13.7 m long freight van (Figure 2a). The tractor geometry is simplified by sealing the engine grill and cooling air intakes, a modification which has been shown in full-scale wind tunnel tests to have a negligible effect upon the drag of the vehicle [6]. Furthermore, the trailer landing gear is removed from the trailer, allowing us to more readily identify changes in the flow field arising from the presence of the underbody fairing. Two types of trailer underbody fairing designs, T1 and T2, are investigated within this study (Figure 2b, 3a). The T2 fairing is similar to the T1 fairing, except for a 0.97 m wide channel that runs the length of the T2 fairing. The resulting ground clearances halfway between the rear tractor drive wheels and the front trailer wheels are 1.2, 1.1, 0.9, and 0.7 m for the 2.3, 4.6, 6.9, 9.2 m long fairings, respectively. To provide a performance comparison with the trailer underbody fairings, traditional trailer side skirts, which have a length of 7.8 m and ground clearance of 0.4 m, are also modeled (Figure 3b).

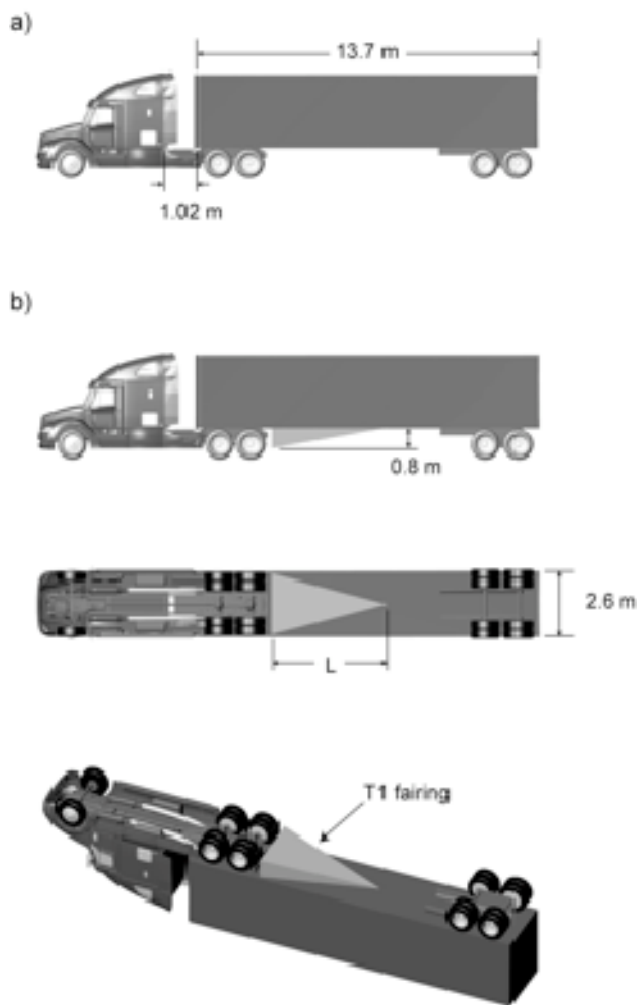


Figure 2. a) Baseline Heavy Vehicle Geometry (The side extenders located on the tractor base have a width of 0.38 m.) b) T1 Fairing, where $L = 2.3, 4.6, 6.9, 9.2$ m

The simulations are performed within a computational domain that is $98\text{ m} \times 49\text{ m} \times 128\text{ m}$ (Figure 4), such that the heavy vehicle cross-sectional area is 0.2% of the domain cross-sectional area. To model the crosswind velocity, U_w , which is typically 3.1 m/s at the vehicle mid-height [7], while the vehicle travels at a ground speed, U_g , of 29.1 m/s, the tractor and trailer are yawed to $\theta = \tan^{-1}(U_w/U_g) = 6.1^\circ$ and a velocity of $(U_g^2 + U_w^2)^{1/2} = 29.3$ m/s, is specified at the inlet to the computational domain. The inlet turbulent intensity and length scale are 2% and 2 m, respectively, values which are within the range commonly experienced by road vehicles [8]. The resulting vehicle width-based Reynolds number, $Re = rUgw/m$, is 5,000,000, where r and m are the density and viscosity, respectively, of air and w is the trailer width, 2.6 m. Beneath the heavy vehicle, a no-slip, moving ground plane boundary condition is

prescribed at a velocity of U_g and a yaw angle of 6.1° . The no-slip surfaces of the tractor and trailer tires, which rotate at an angular velocity of 53 s^{-1} , intersect the ground plane, producing a tire contact patch that has a swept angle of 20° [9]. A slip boundary condition and a zero gradient boundary condition are specified along the walls and outlet, respectively, of the computational domain. Since the purpose of this study is to highlight the general performance trends of the fairings, we solve the steady Reynolds averaged Navier-Stokes (RANS) equations [10] for the flow about the heavy vehicle using a finite-volume code [11], an approach which reduces both the computational time and data storage requirements. The k-w SST turbulence model [12] with a wall function [13] is employed in these simulations. A previous study by Pointer [14] demonstrated that this approach can adequately capture the drag coefficient of a heavy vehicle at width-based Reynolds numbers on the order of 106. However, it should be noted that the use of this approach in the context of highly unsteady, massively separated flows may call into question the specific details of the flow field about the vehicle. In future experimental investigations, we will have the opportunity to confirm the findings presented in the current computational study.

To extract the resulting drag force on the heavy vehicle, we average the drag coefficient, C_d , over 10,000–20,000 iterations, where $C_d = D/(\frac{1}{2}\rho U_g^2 A_0)$, D is the drag force, and A_0 is the cross-sectional area of the vehicle. Due to a possible lack of local mesh resolution or to the numerical scheme, the drag coefficient tends to oscillate slightly about its average value, an example of which is shown in Table 1. To ensure that the computed flow fields are adequately independent of the grid resolution,

Table 1. Drag coefficient of the baseline vehicle (Figure 2a) as a function of the grid resolution

Cells	C_d
4.1×10^6	0.674 ± 0.004
11.2×10^6	0.651 ± 0.004
26.5×10^6	0.641 ± 0.004
34.5×10^6	0.637 ± 0.005

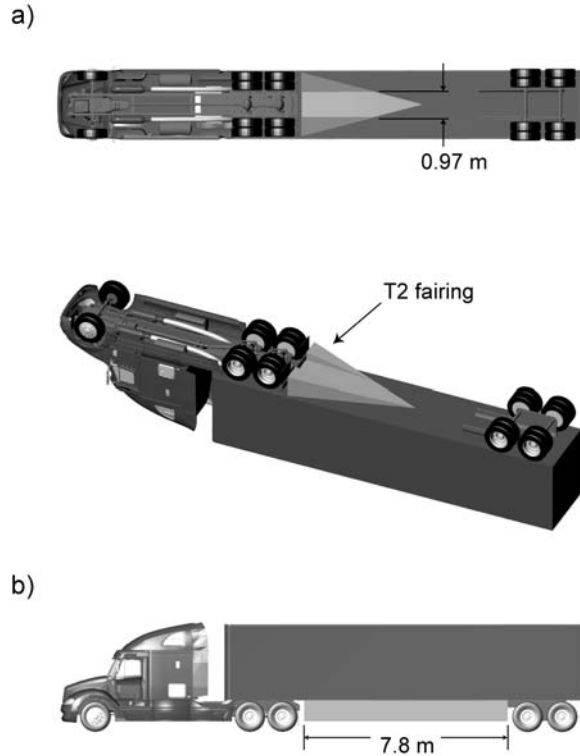


Figure 3. a) T2 Fairing and b) Trailer Side Skirts Geometries

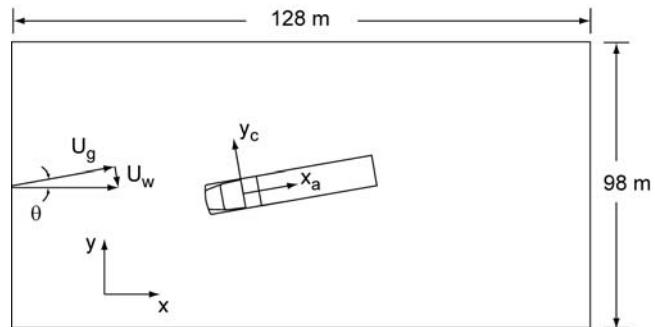


Figure 4. Computational Domain

simulations of the baseline tractor-trailer geometry (Figure 2a) are repeated on four grids having sizes of 4.1×10^6 , 11.2×10^6 , 26.5×10^6 , and 34.4×10^6 cells. Upon refining the grids, the relative difference in the drag coefficients decreases, indicating a trend towards convergence. Therefore, grids with spatial resolutions similar to that of the 26.5×10^6 grid are employed in the subsequent simulations.

Results and Discussion

From these simulations, the drag coefficient of the baseline vehicle is computed to be 0.641, where the majority (0.429) of this value is due to drag on the tractor. The remaining portion of the drag is divided about equally between the trailer cargo box and the trailer wheel assembly. Installation of the trailer underbody fairings reduces the drag coefficient below this baseline value (Figure 5). For the T1 fairings, C_d decreases in a roughly monotonic fashion as the fairing length is increased, with the longest fairing yielding a C_d of 0.617. For the T2 fairings, the drag coefficient also decreases as the fairing length is increased. However, for the 9.2 m long T2 fairing, C_d is reduced even more substantially to a value (0.599) that is even less than that (0.605) of trailer side skirts.

The means by which the fairings reduce the drag of the heavy vehicle can be understood by examining the trailer underbody flow physics. Without the fairing, the baseline flow beneath the trailer is composed of a large recirculation zone that separates from the tractor drive wheels and underbody, both of which form a pseudo backward facing step onto the lower surface of the trailer. The recirculation zone extends approximately 5.7 m downstream of the tractor drive wheels and mud flaps (Figure 6a). Due to the cross stream velocity and the interaction of the underbody flow with the trailer wheel assembly, this zone is skewed in the -y direction, thereby increasing the exposure of the windward trailer wheels to higher fluid velocities, while decreasing the exposure of the leeward trailer wheels (Figure 6c). In addition, the recirculation zone produces a relatively low pressure coefficient of $C_p \approx -0.18$ on the tractor mud flaps and drive wheels, which, in turn, contributes to the vehicle drag, where $C_p = (p-p_0)/(1/2\rho U_g^2)$ and p_0 is the free stream pressure. On the other hand, the fairings provide a surface to which the underbody flow can reattach, thereby either reducing the size of the recirculation zone or, for the longest fairings, nearly eliminating it altogether (Figures 6b,d).

To determine how the underbody pressure field responds to these flow changes, C_p is computed over the fairing surface. Since the component of pressure that acts in the body axis direction, x_a , of the vehicle is solely responsible for the pressure drag on the fairing, C_p is multiplied by the inner product of \mathbf{n}_a and \mathbf{n} , to give $C_{pa} = C_p \mathbf{n}_a \cdot \mathbf{n}$, where \mathbf{n} is the surface normal of the vehicle and \mathbf{n}_a is the unit normal vector in the body axis direction, x_a . Plots of C_{pa} along the centerline of the fairings (dashed line in Figure 1) demonstrate that the underbody flow reattachment to the fairing surface generates surface pressures that are greater than that present on the mud flaps and drive wheels of the baseline vehicle (Figure 7a,b), hence leading to a reduction in drag. The longer fairings, which are more conducive to flow reattachment due to their smaller inclination angle relative to the free stream, generally produce greater values of C_{pa} than those of the shorter fairings, which explains why the longer fairings yield a larger reduction in drag than the shorter fairings. Across the entire downstream facing surface of the fairings, the average values of C_{pa} for the T2 fairings are consistently greater than those of the T1 fairings of equal length (Figure 7c). The reason for this is that the channel that runs the length of the T2 fairings allows the underbody flow to pass between the tractor drive wheels over the center of the channel, which has a smaller angle of inclination relative to the free stream. This allows the underbody flow to more attach more readily to the T2 fairing surface. Without the channel, the flow between the tractor drive wheels impinges upon the front of the T1 fairings (Figure 7d,e), which not only increases the average pressure coefficient on the front surface of the fairing, hence increasing the vehicle drag, but also causes the underbody flow to lose momentum in the x_a direction, making it more difficult for the flow to subsequently reattach to the fairing surface. As a result, the drag force on the T1 fairings is consistently greater than that of T2 fairings, which, in fact, generate a net thrust force for each fairing length (Figure 7f).

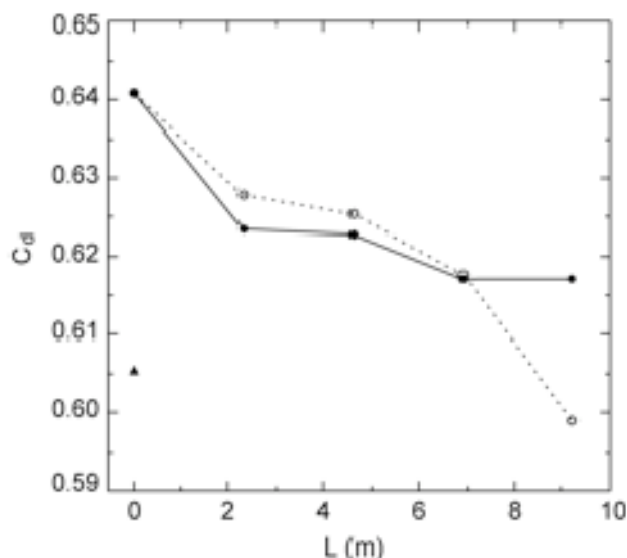


Figure 5. Drag Coefficient of the Vehicle at 6.1° yaw, as a function of the fairing length for the T1 (solid line) and T2 (dashed line) fairings; drag coefficient of the vehicle with trailer side skirts, solid triangle.

In spite of this, the $L = 2.3, 4.6$, and 6.9 m T2 fairings do not perform better than the T1 fairings in reducing the overall vehicle drag, which is due to the influence that the fairings have upon the local drag coefficients of other portions of the vehicle. Consider, for example, the $L = 4.6$ m T1 and T2 fairings. Both fairings result in similar drag coefficients on the tractor ($C_d = 0.431$ and 0.429 for the T1 and T2 fairing configurations, respectively) and the trailer cargo box/fairing components ($C_d = 0.082$ for the T1 and T2 fairing configurations). Yet, the T1 fairing is slightly more effective in reducing the overall vehicle drag than the T2 fairing even though the net drag force on the T2 fairing is less than that of the T1 fairing (see Figures 5 and 7f). This disparity primarily arises from the increased drag that the T2 fairing produces upon the trailer wheel assembly ($C_d = 0.110$ and 0.115 for the T1 and T2 fairing configurations, respectively). In this case, the T2 fairing produces an average trailer underbody velocity in the x_a direction that is greater than that of the T1 fairing ($U_{a-\text{avg}} = 11.9$ and 13.6 m/s for the T1 and T2 fairing configurations, respectively), where the average underbody velocity, $U_{a-\text{avg}}$, is computed in the volume beneath the projected area of the trailer cargo box from x_{a0} to x_{a1} (see Figure 1). As a result, the trailer wheel

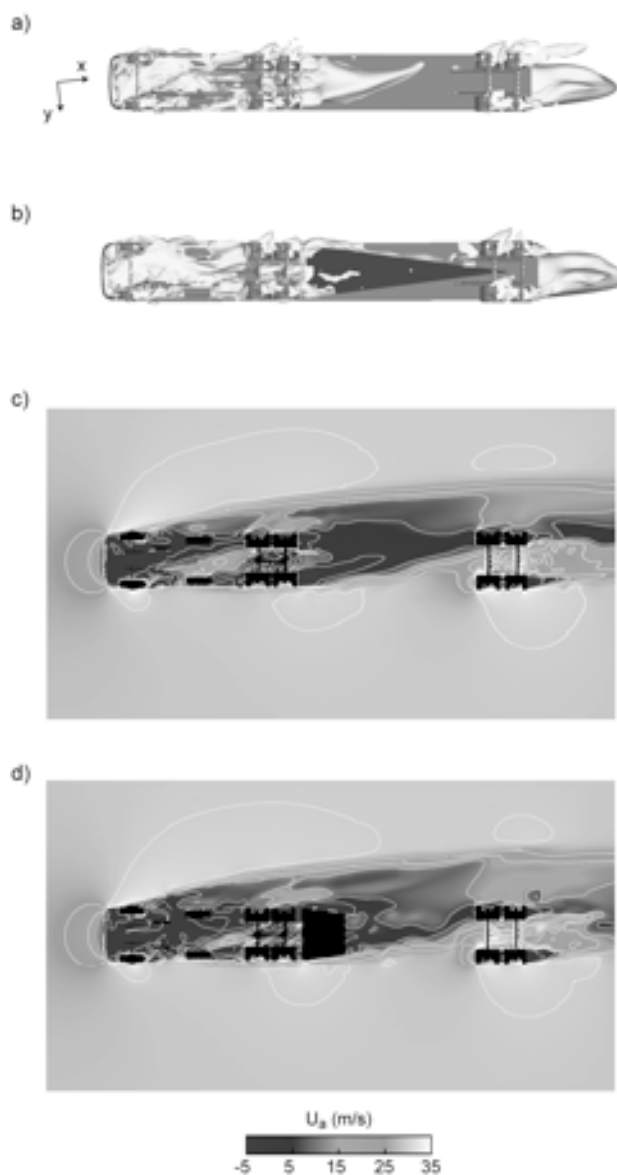


Figure 6. Iso-surface of $U_a = -0.001$ m/s for the a) baseline vehicle and the b) $L = 9.2$ m T1 fairing configurations, where U_a is the component of velocity in the x_a direction (see Figure 1). b) Contours of U_a within a horizontal plane ($z = 0.56$ m) that passes through the axles of the c) baseline vehicle and d) $L = 9.2$ m T1 fairing configuration.

assembly downstream of the T2 fairing is exposed to a higher fluid velocity, which, in turn, increases the drag coefficient of the trailer wheel assembly above that of the T1 fairing configuration. A qualitatively similar trend also occurs for the $L = 2.3$ and 6.9 m T1 and T2 fairing configurations (Figure 8).

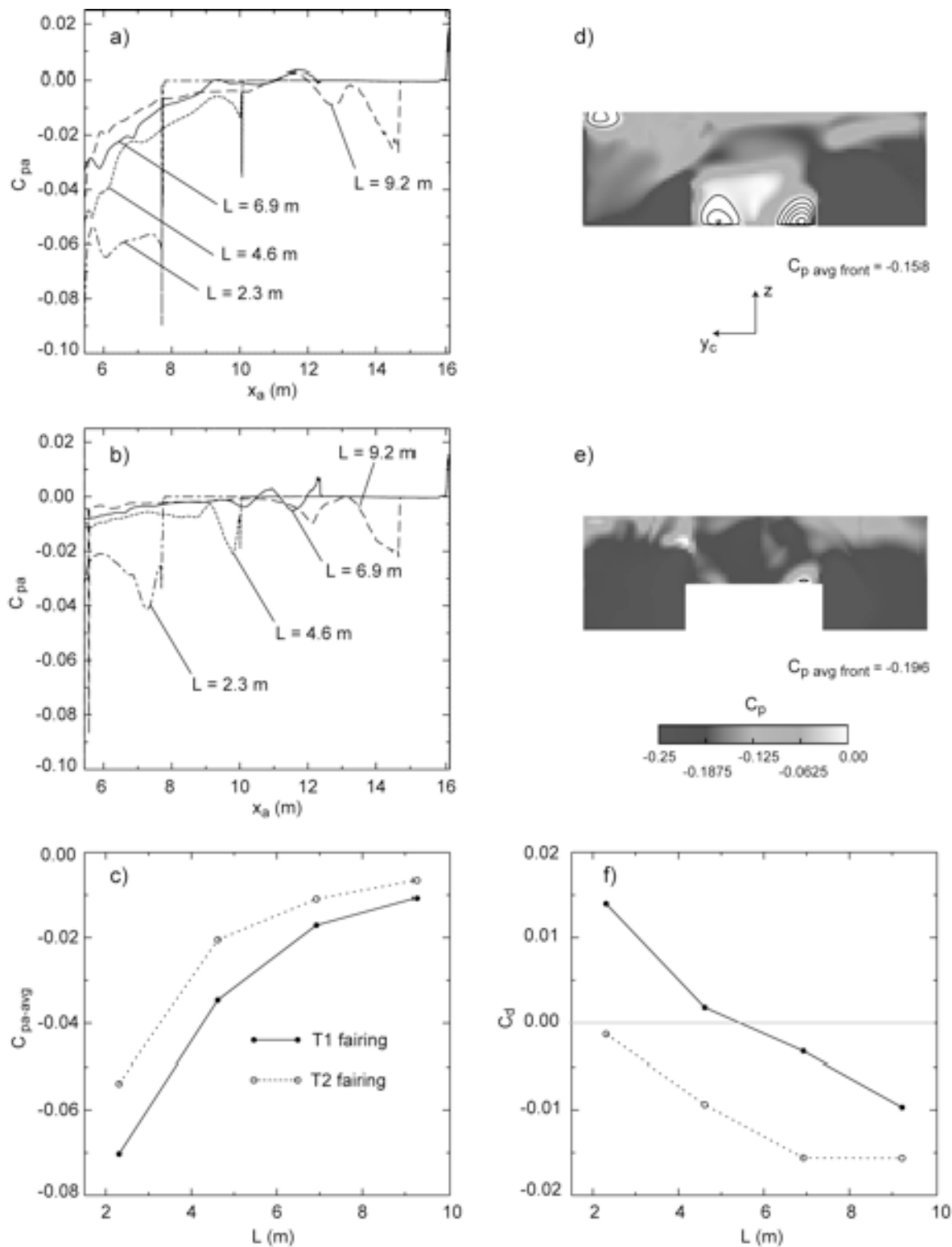


Figure 7. Distribution of C_{pa} along the centerline of the a) T1 and b) T2 fairings. c) Average pressure coefficient on the downstream facing surface of the T1 and T2 fairings as a function of the fairing length. Pressure coefficient contours on the front of the L = 6.9 m d) T1 and e) T2 fairings. The contour lines indicate areas with positive values of C_p . f) Drag coefficient of the T1 and T2 fairings as a function of the fairing length.

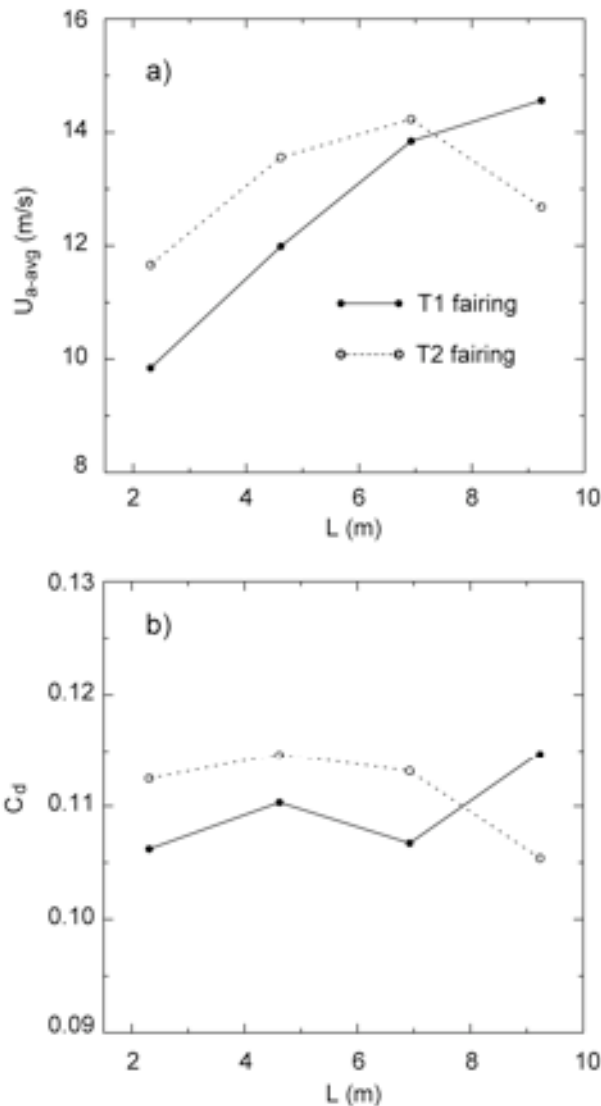


Figure 8. a) Average trailer underbody velocity and b) trailer wheel assembly drag coefficient for the T1 and T2 fairings as a function of the fairing length.

However, the $L = 9.2$ m T2 fairing is different than the other configurations in that it outperforms the T1 fairing of equal length ($C_d = 0.617$ and 0.599 for the T1 and T2 fairings, respectively, from Figure 5). Unlike the shorter fairings, the $L = 9.2$ m T2 fairing decreases $U_{a\text{-avg}}$ below that of the T1 fairing (Figure 8a). In particular, the T2 fairing alters the underbody flow so as to produce a distinct minimum in the velocity field that persists to the front of the leeward trailer wheels, an effect which is indicated in the velocity profile plots shown in Figure 9. This reduces the exposure of the leeward trailer wheels to higher fluid velocities and, as a result, yields a smaller trailer wheel assembly drag

coefficient than that of the T1 fairing ($C_d = 0.115$ and 0.105 for the T1 and T2 fairing configurations, respectively, from Figure 8b). (Note that the remainder of the drag savings of the T2 fairing compared to the T1 fairing stems from a relative reduction of the trailer cargo box/fairing drag coefficient.)

Conclusion

By performing a series of CFD simulations, we have investigated the drag reduction capability of several trailer underbody fairings. For the baseline vehicle, the flow beneath the trailer is composed of a large recirculation zone, which reduces the pressure on the tractor drive wheels and mudflaps and, hence, increases the vehicle drag. The simulation results indicate that the fairings function by reducing the size of this zone, if not eliminating it nearly altogether. As the fairing length is increased, the average pressure coefficient across the fairing surface also increases, leading to a larger reduction in the vehicle drag. Although fairings that incorporate a longitudinal channel consistently yield larger fairing surface pressure coefficients, they typically do not outperform fairings that lack this channel.

Examination of the trailer underbody flow reveals that fairings with a channel increase the average trailer underbody velocity, which leads to an increase in the drag force on the trailer wheel assembly located downstream of the fairing. An exception to this observation occurs for the longest channeled fairing, which not only produces greater fairing surface pressure coefficients, but also reduces the fluid velocities to which the trailer wheels assembly is exposed. In this case, the channeled fairing, which has a mid-trailer ground clearance of 0.7 m, reduces the drag coefficient by 0.042 , a value that is greater than that of the trailer side skirts modeled in this study.

The interplay between the trailer wheel assembly and the flow field produced by the fairing suggests that further reductions in drag may be achieved by aerodynamically shaping both the region immediately downstream of the tractor drive wheels and the trailer wheel assembly. Clearly, a successful design must not only eliminate the trailer underbody recirculation zone, but must also minimize the resulting drag of the trailer wheel

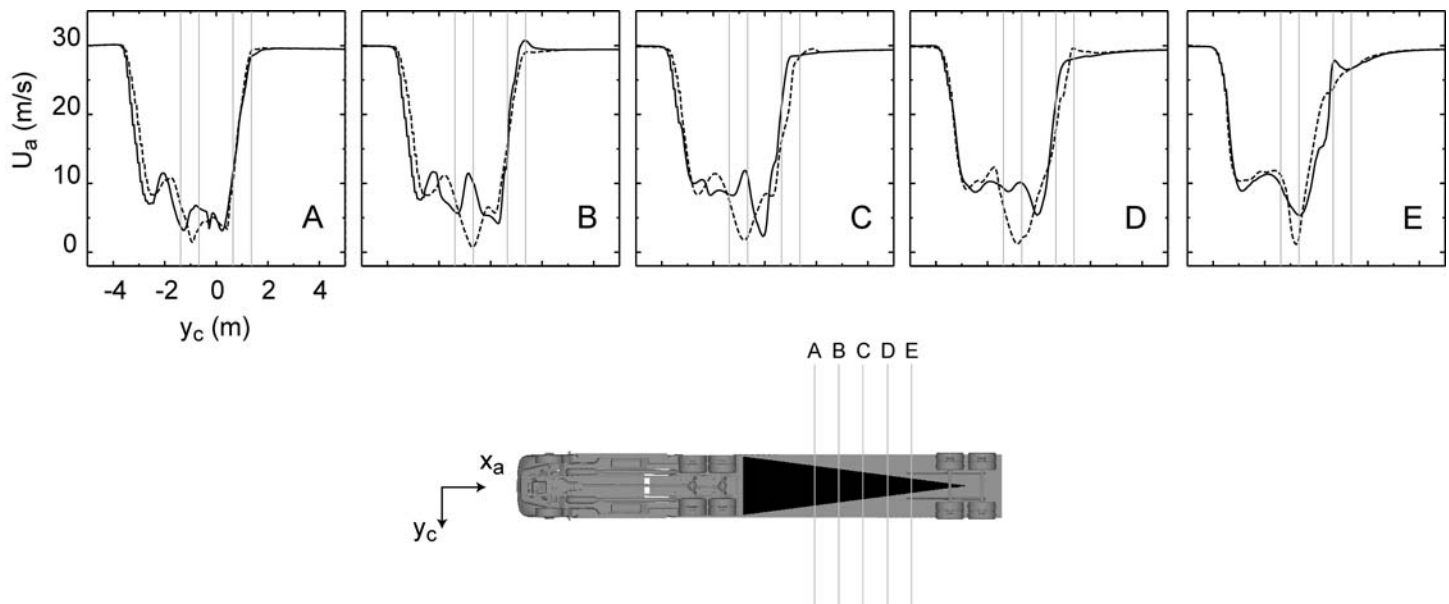


Figure 9. Trailer underbody velocity profiles of U_a for the $L = 9.2$ m T1 (solid line) and T2 fairings (dashed line). The profiles are located at $z = 0.56$ m (axle height) with a 1 m spacing in the x_a direction ending 1 m upstream of the trailer tires. The grey vertical lines in each plot denote the edges of the windward and leeward trailer tires.

assembly, while still maintaining an adequate trailer ground clearance. Perhaps, a first step to achieving this would be to employ a trailer underbody fairing in conjunction with another device, such as a trailer bogie fairing or a trailer wheel fairing, which reduces the drag coefficient of the trailer wheel assembly [6]. In future computational and experimental studies, we will have the opportunity to evaluate such an approach and to determine whether or not additional drag savings can be achieved from this combination of devices.

Acknowledgments

This work performed under the auspices of the U.S. Department of Energy by Lawrence Livermore National Laboratory under Contract DE-AC52-07NA27344. UCRL-CONF-402275.

References

1. Cooper, K. R., "Commercial Vehicle Aerodynamic Drag Reduction: Historical Perspective as a Guide," in *The Aerodynamics of Heavy Vehicles: Trucks, Buses, and Trains*, McCallen, R., Browand, F., and Ross, J. (eds.), Lecture Notes in Applied and Computational Mechanics, Vol. 19, 2004, 9-28.
2. Cooper, K. R., "Truck Aerodynamics Reborn - Lessons from the Past," SAE 2003-01-3376, SAE International Truck and Bus Meeting and Exhibition, Fort Worth, Texas, November 10-12, 2003.
3. Schoon, R. E., "On-Road Evaluation of Devices to Reduce Heavy Truck Aerodynamic Drag," SAE 2007-01-4294, 2007.
4. Turbo Squid, www.turbosquid.com, 2006.
5. Freightliner, www.freightlinertrucks.com/trucks/find-by-model/columbia/, 2007.
6. Leuschen, J. and Cooper, K. R., "Full-Scale Wind Tunnel Tests of Production and Prototype, Second-Generation Aerodynamic Drag-Reducing Devices for Tractor-Trailers," SAE 06CV-222, 2006.
7. "SAE Wind Tunnel Test Procedure for Trucks and Buses," SAE J1252, SAE Recommended Practice, 1979.
8. Cooper, K. R. and Watkins, S., "The Unsteady Wind Environment of Road Vehicles, Part One: A Review of the On-road Turbulent Wind Environment," SAE 2007-01-1236, 2007.

9. Axon, L., Garry, K. P., and Howell, J., "An Evaluation of CFD for Modeling the Flow around Stationary and Rotating Isolated Wheels," SAE 980032, SAE International Congress and Exhibition, Detroit, Michigan, February 23-26, 1998.
10. Tennekes, H. and Lumley, J. L., *A First Course in Turbulence*, MIT Press, Cambridge, England, 1992.
11. STARCCM+, v.2.10.017, CD-Adapco, www.cd-adapco.com, 2008.
12. Menter, F. R., "Zonal Two Equation k- ω Turbulence Models for Aerodynamic Flows," AIAA 93-2906, Proc. 24th Fluid Dynamics Conf., Orlando, Florida, USA, July, 6-9, 1993.
13. Reichardt, H., "Vollstaendige Darstellung der turbulenten Geschwindigkeitsverteilung in glatten Leitungen," *Z. Angew. Math. Mech.*, **31**(7), 208-219, 1951.
14. Pointer, W. D., "Evaluation of Commercial CFD Code Capabilities for Prediction of Heavy Vehicle Drag Coefficients," AIAA-2004-2254, 34th AIAA Fluid Dynamics Conference and Exhibit, Portland, Oregon, June 28 – July 1, 2004.

VII. THERMAL MANAGEMENT

A. Efficient Cooling in Engines with Nucleate Boiling

Principal Investigator: W. Yu (coworkers: David M. France and Roger K. Smith)

Argonne National Laboratory

9700 South Cass Avenue, Building 212, Argonne, IL 60439

(630) 252-7361; fax: (630) 252-5568; e-mail: wyu@anl.gov

Technology Development Manager: Lee Slezak

(202) 586-2335, Lee.Slezak@hq.doe.gov

Technical Program Manager: Jules Routbort

(630) 252-5065, routbort@anl.gov

Contractor: UChicago Argonne, LLC

Contract No.: DE-AC02-06CH11357

Objectives

Investigate the potential of two-phase flow in engine cooling applications.

Determine limits on two-phase heat transfer (occurrence of critical heat flux or flow instability).

Approach

Experimentally determine heat transfer rates and critical heat fluxes in small channels with water and a mixture of 50 percent ethylene glycol in water.

Perform experiments over a large concentration range of ethylene glycol in water.

Experimentally determine heat transfer characteristics for subcool flow boiling of water and ethylene glycol/water mixtures.

Perform experiments with alternative fluids to conventional coolants.

Accomplishments

Completed experimental tests and data analysis for the two-phase pressure gradients and boiling heat transfer coefficients of horizontal flows to water and ethylene glycol/water mixtures.

Developed a new procedure to analytically calculate the boiling temperature along the test section and, subsequently, the local heat transfer coefficients. This procedure is based on ideal-mixture and equilibrium assumptions along with Raoult's law.

Developed a pressure drop correlation modified from Chisholm's correlation with a concentration factor to better predict pressure drops for ethylene glycol/water mixtures.

Developed a general correlation of boiling heat transfer coefficients, modified from Argonne National Laboratory's (ANL) boiling heat transfer correlation, with a concentration factor for the prediction of heat transfer rates of flow boiling in small channels, including refrigerants, water, and ethylene glycol/water mixtures.

Fabricated a new vertical experimental test section, calibrated the instruments attached to the test section, and modified the test facility and test monitoring program for vertical-flow boiling tests. Rewired the interfacial connection device between the instruments attached to the horizontal and vertical test sections and the data acquisition computer system for easy switching between the horizontal- and vertical-flow test sections.

Completed single-phase calibration tests for vertical flow on the nucleate boiling test facility. Performed preliminary experimental tests and data analysis for two-phase vertical-flow boiling to pure water.

Prepared an extensive Environment, Safety, and Health Plan for the experimental facility.

Participated in an onsite inspection and safety review of the experimental facility.

A paper from the project, published in the prestigious *International Journal of Multiphase Flow*, was one of the most cited articles for the years 2002 to 2005 with over 60 citations (as recently identified by the journal).

Future Directions

Subsequent to the preparation of the Environment, Safety, and Health Plan and the onsite inspection and safety review, complete 32 changes/modifications to the experimental facility as directed by the ANL, Energy Systems Division, Safety Committee.

Continue systematic two-phase heat transfer experiments of water and ethylene glycol/water mixtures with vertical flows to provide essential information for design of a nucleate-boiling cooling system.

Study the effect of vertical versus horizontal flows on two-phase heat transfer.

Experimentally determine heat transfer characteristics for subcool flow boiling of water and ethylene glycol/water mixtures.

Perform systematic experiments with alternative fluids.

Introduction

Analyses of trends in the transportation sector indicate that future engine cooling systems may have to cope with greater heat loads because of more powerful engines, more air conditioning, more stringent emissions requirements, and additional auxiliary equipment. Also, reducing the size of cooling systems can reduce vehicle weight, reduce coolant pumping power, and lead to improved aerodynamic profiles for vehicles all of which contribute to reduced fuel consumption. To achieve these benefits, researchers need to design cooling systems that occupy less space, are lightweight, have reduced fluid inventory, and exhibit improved performance. Among various new cooling systems proposed, nucleate boiling has great potential to meet these challenges. Order-of-magnitude higher heat transfer rates can be achieved in nucleate-boiling cooling systems when compared with conventional, single-phase, forced-convective cooling systems. However, successful design and application of nucleate-boiling cooling systems for engine applications require that the critical heat flux and flow instabilities not be reached. Therefore, a fundamental understanding of flow boiling mechanisms under engine application conditions is

required to develop reliable and effective nucleate boiling cooling systems.

Cooling engine areas such as the head region often contain small metal masses that lead to small coolant channels. This geometry, in turn, leads to low mass flow rates that minimize pressure drop. Although significant research has been performed on boiling heat transfer and the critical heat flux phenomenon, results applicable for engine cooling systems are limited. The purpose of the present study is to investigate the characteristics of coolant boiling, critical heat flux, and flow instability under conditions of small channel and low mass fluxes.

The test apparatus used in this investigation was designed and fabricated to study boiling heat transfer, two-phase pressure drop, critical heat flux, and flow instability of flowing water, ethylene glycol, and aqueous mixtures of ethylene glycol at high temperature (up to 250°C) and low pressure (<345 kPa). Figure 1 shows a schematic of the apparatus.

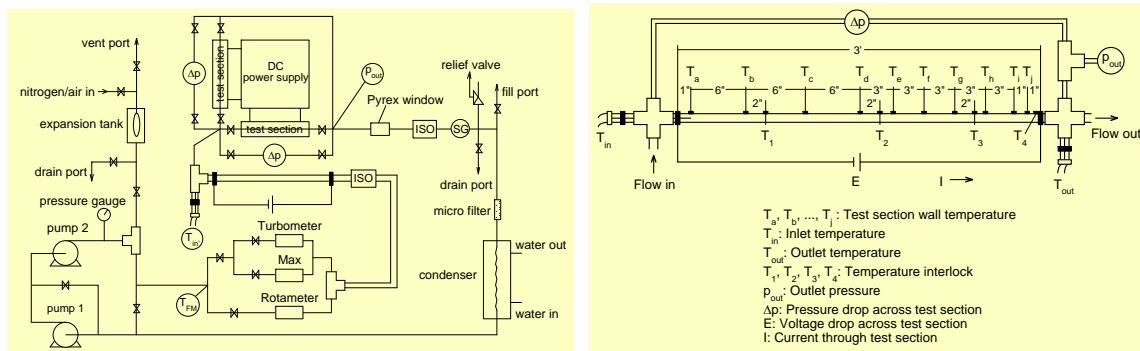


Figure 1. Schematic diagram of nucleate-boiling cooling test apparatus (left) and horizontal test section (right)

The apparatus is a closed loop that includes two serially arranged pumps with variable speed drives, a set of flowmeters, an accumulator, a preheater, a horizontal test section, a vertical test section, and a condenser. The flowmeter set, including various types and sizes, was chosen to cover a large range of flow rates and was calibrated traceable to the National Institute of Standards and Technology (NIST). The estimated uncertainty in the measurements of flow rates was ± 3 percent. The bladder-type accumulator allows for stable control of the system pressure. The preheater provides a means to set the inlet temperature of the test sections at various desired levels. Both the preheater and test sections were resistance-heated with controllable direct current (DC) power supplies. Provisions were made to measure temperatures along the test section for calculating heat transfer coefficients. The pressures and temperatures at the inlet and outlet of the test section were also measured. Pressure transducers and thermocouples were calibrated against standards traceable to NIST. The estimated uncertainty in the measurements of pressures and temperatures were ± 3 percent and $\pm 0.2^\circ\text{C}$, respectively. As a safety precaution, both the preheater and test sections were provided with high-temperature limit interlocks to prevent them from overheating. After leaving the test section, the two-phase flow was condensed into a single-phase flow, which returned to the pumps to close the system.

To switch between the horizontal- and vertical-flow test sections, an interfacial connection was fabricated (shown in Figure 2). This device establishes a connection between the test-section sensor instruments and the data-acquisition computer system, and allows for precision switching between

the horizontal and vertical test sections, which share the rest of the test loop.

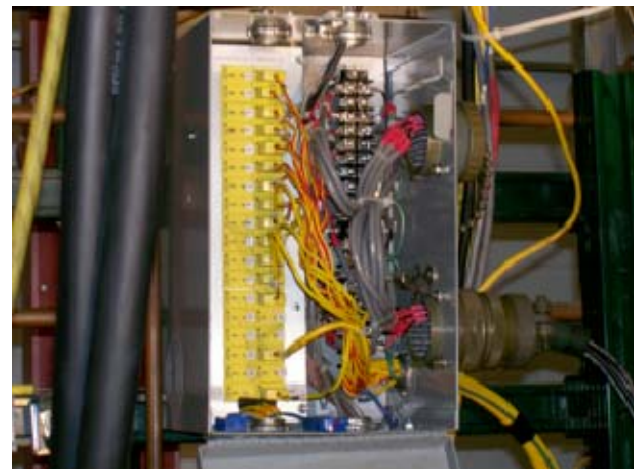


Figure 2. Interfacial connection

A data acquisition system consisting of a computer and a Hewlett-Packard multiplexer was assembled to record outputs from all sensors. A data acquisition program, which includes all calibration equations and conversions to desired engineering units, was written. The data acquisition system provides not only an on-screen display of analog signals from all sensors and graphs of representative in-stream and wall-temperature measurements, but also a means of recording temperature and pertinent information such as input power (voltage across the test section and current through the test section), mass flux, outlet pressure, pressure drop across the test section, and outlet quality for further data reduction.

Results and Discussion

To calculate local boiling heat transfer coefficients of an ethylene glycol/water mixture, the water-vapor mass fractions, mixture vapor mass qualities, and mixture temperatures along the experimental test section must be determined. Researchers have used various approaches in making these determinations. Perhaps the simplest approach is to assume that the mixture boiling temperature is constant along the test section and equal to the mean of the zero quality temperature and the temperature at the test section outlet. This approach is not conducive to the determination of local heat transfer coefficients along the length of the test section, as done in the present study. Assuming a linear mixture temperature distribution along the test section can increase accuracy. Another approach is to utilize a mixture equation of state, such as the hard-sphere equations. However, ideal mixture and equilibrium assumptions along with Raoult's law are sufficient to calculate the boiling temperature along the test section and, subsequently, the local heat transfer coefficients with the highest degree of accuracy among the approaches presented. This ideal mixture calculation approach was developed and adopted in this study. Assuming an ideal mixture and applying Raoult's and Dalton's laws to it, one can derive the following equations for determining the water vapor mass fraction F_v , mixture vapor mass quality x , and mixture temperature. T_m

$$F_v = \frac{9p_w(p_m - p_{EG})}{31p_m(p_w - p_{EG}) - 22p_w(p_m - p_{EG})}$$

$$x = \frac{31F_m(p_w - p_{EG}) - (9 + 22F_m)(p_m - p_{EG})}{31F_v(p_w - p_{EG}) - (9 + 22F_v)(p_m - p_{EG})}$$

$$T_{mi} = T_{mo} - \frac{\dot{q}/\dot{m} + [F_{vi} i_{fgWi} + (1 - F_{vi}) i_{fgEGi}] x_i - [F_{vo} i_{fgWo} + (1 - F_{vo}) i_{fgEGo}] x_o}{[F_m C_{pWI} + (1 - F_m) C_{pEGI}]}$$

where P is the pressure, T is the temperature, F is the mass fraction, x is the mass quality, C_p is the specific heat, i_{fg} is the latent heat of vaporization, \dot{q} is the heat transfer rate, and \dot{m} is the mass flow rate.

Horizontal Flow Boiling

Both experimental tests and data analysis for two-phase boiling heat transfer of horizontal flows to water and ethylene glycol/water mixtures have been completed. The main results are reported below.

Boiling Curve. Figure 3 shows the heat flux as a function of wall superheat for boiling of water and ethylene glycol/water mixtures in small channels. As can be seen from Figure 3, generally, the saturation boiling in small channels can be divided into three boiling regions, namely, convection dominant, nucleation dominant, and the transition between the two.

Both convective heat transfer and boiling heat transfer exist in all three regions, but their proportions are different in these regions. In the convection-dominant-boiling region, the wall superheat is low, usually less than a few degrees centigrade. Although there is boiling heat transfer, the dominant mechanism is convective heat transfer. As a result, the mass quality and heat transfer rate are quite low compared with those in the other two regions. In the nucleation-dominant-boiling region, the wall superheat is higher than that in the convection-dominant-boiling region but lower than certain upper limits that depend on mass flux. Opposite to the convection-dominant boiling, the boiling heat transfer in the nucleation-dominant boiling is so developed that it becomes dominant, and the heat transfer rate is much higher than that in convection-dominant boiling. As can be seen from Figure 3, the heat flux in this region is independent of mass flux and can be predicted with a power-law function of wall superheat. This characteristic was used in correlating the heat transfer data. In the transition-boiling region, the wall superheat is relatively high. The heat flux in this region is also high and close to the critical heat flux. The boiling in this region is unstable, and a small change in the heat flux will result in a large change in wall superheat. If the heat flux increases further, it is possible for the system to reach a critical point, producing an undesirably large increase in the wall superheat.

The above discussion shows that nucleation-dominant boiling is desired in engineering applications for both high heat transfer rate and stable flow boiling without reaching the critical point.

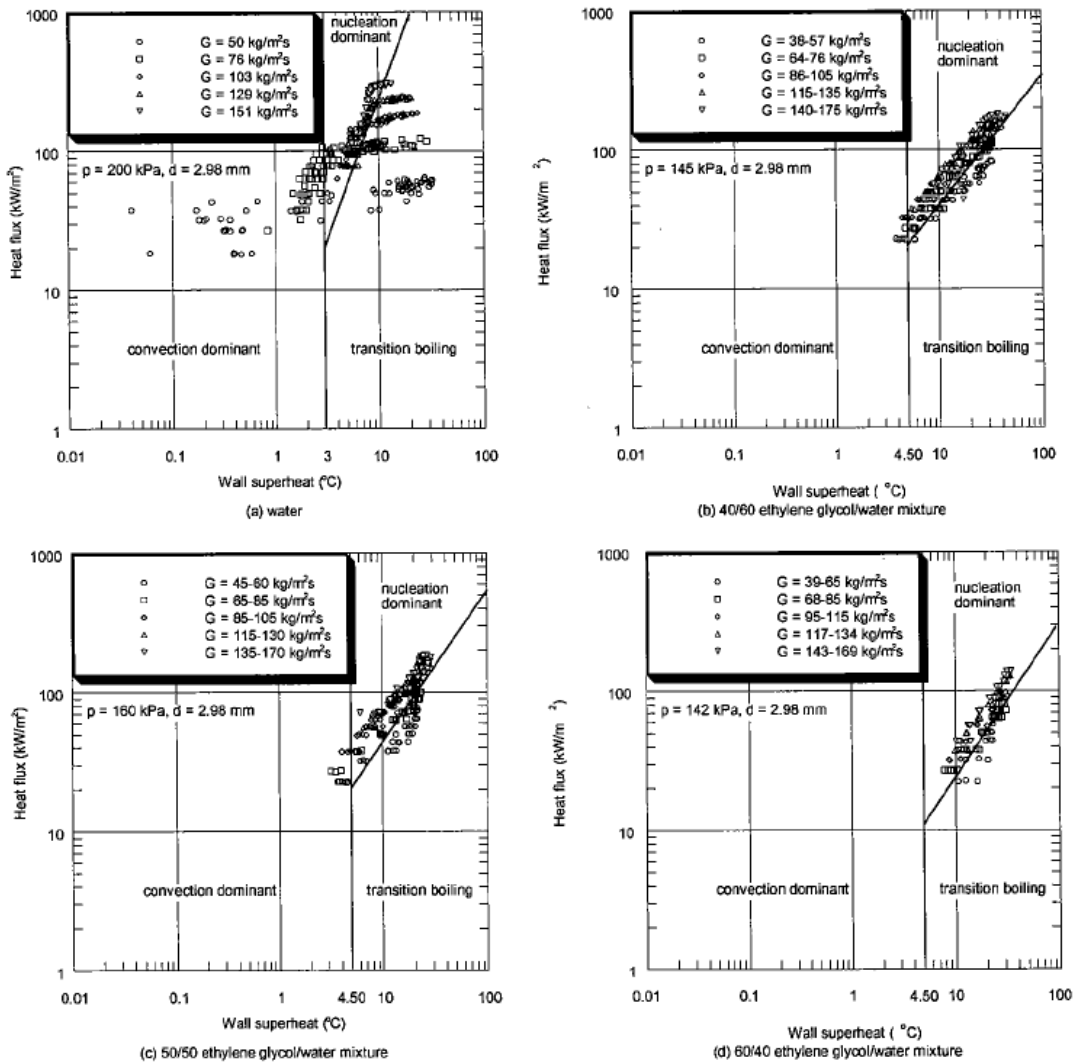


Figure 3. Heat flux as a function of wall superheat

Two-Phase Pressure Drop. The concept of two-phase multipliers proposed by Lockhart and Martinelli and the correlation of those multipliers by Chisholm were used to compare predictions with the present experimental data. As can be seen from Figure 4, the experimental data are in reasonable agreement with the Chisholm predictions both in values and trends, although the Chisholm correlation slightly over-predicts the experimental data.

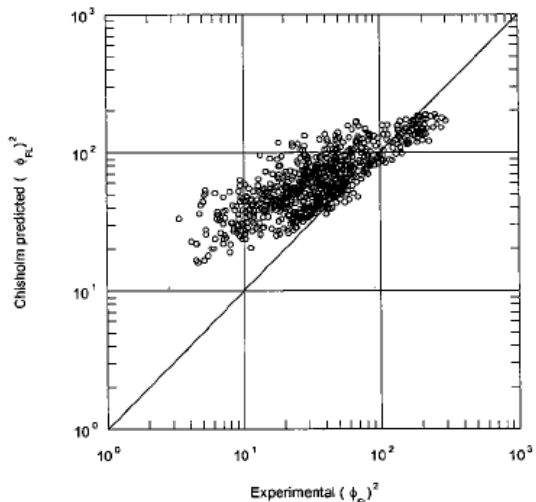


Figure 4. Two-phase frictional pressure gradient

To better predict the experimental data and to take the concentration factor into account, the constant parameter $C = 12$ in Chisholm's correlation was modified into a function of the volume concentration (v) of ethylene glycol/water mixtures, and Chisholm's correlation then becomes

$$\phi_{FL}^2 = 1 + \frac{12[1 - 2.8v(1-v)]}{X} + \frac{1}{X^2}$$

This correlation reduces to Chisholm's correlation for both pure water ($v = 0$) and pure ethylene glycol ($v = 1$). In Figure 5, the experimental data are compared with the predictions of the modified Chisholm's correlation. This modification improves the predictions both in values and trends.

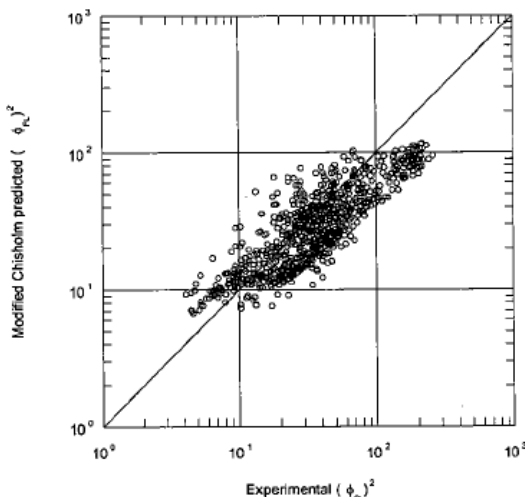


Figure 5. Two-phase frictional pressure gradient

Heat Transfer Coefficient. In the present study, the nucleation-dominant boiling data have the following characteristics.

- (a) Although both convective heat transfer and nucleate-boiling heat transfer exist, the dominant heat transfer mechanism is nucleate boiling. Since the nucleate-boiling heat transfer rate is much higher than the convective heat transfer, the latter can be neglected.
- (b) As shown in Figure 3, the boiling heat transfer is dependent on heat flux but almost independent of mass flux. This finding means that, for a specific fluid, the boiling heat transfer coefficient can be expressed as a function of heat flux.
- (c) The heat transfer coefficients have different dependence on heat flux for different fluids. Therefore, deriving a general correlation for boiling heat transfer coefficients requires fluid properties in the correlation.
- (d) ANL researchers employed the dimensionless parameter combinations in the form of boiling number, Weber number, and liquid-to-vapor density ratio in developing different predicted correlations for boiling heat transfer coefficients with different fluids, and the predicted results are quite good.

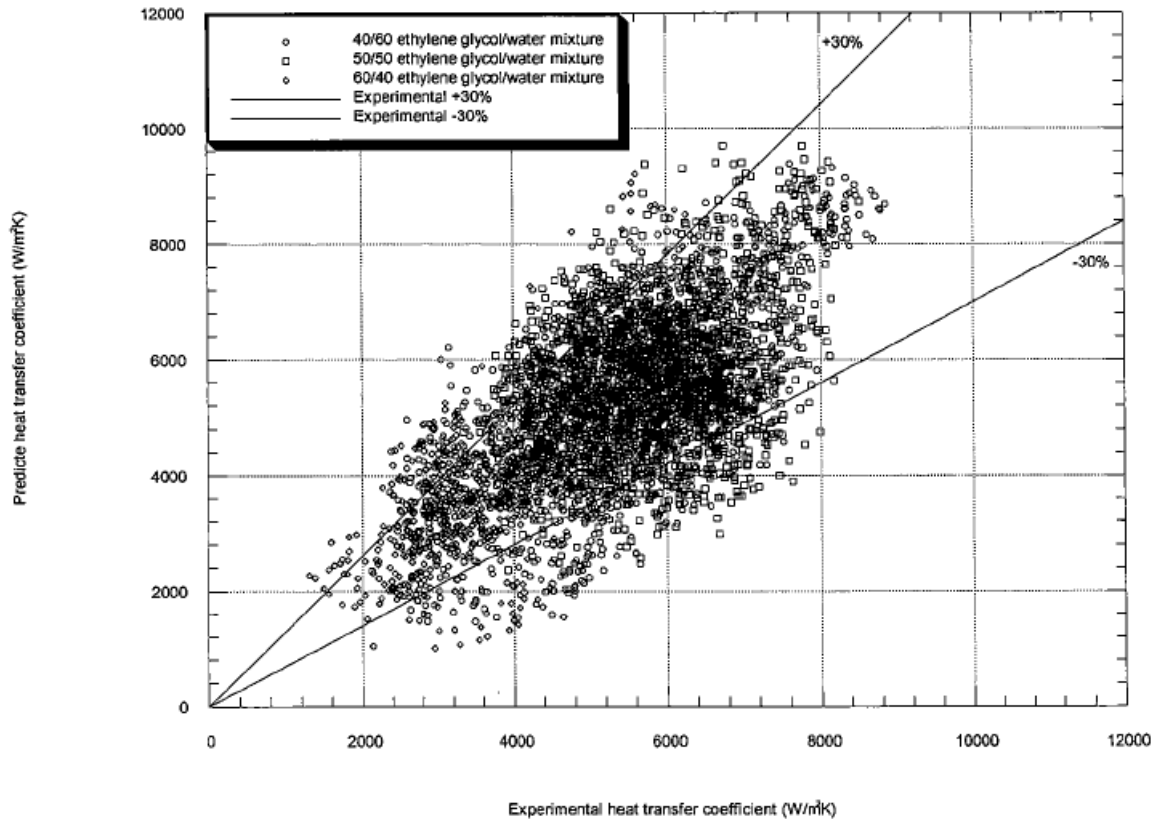


Figure 6. Heat transfer coefficient comparisons (nucleation-dominant-boiling region)

Based on the above facts, ANL extended the dimensionless property term parameter to include the liquid-to-vapor viscosity ratio, which produced good correlation of boiling heat transfer data (h) for water, 50/50 ethylene glycol/water mixture, refrigerant 12, and refrigerant 134a.

$$h = 135000(BoWe_l^{0.5})^{0.5} \left[(\rho_l/\rho_v)^{-0.5} (\mu_l/\mu_v)^{0.7} \right]^{1.5}$$

In the above equation, ρ is the density, μ is the viscosity, and the boiling number Bo and the Weber number We_l are defined, respectively, as

$Bo = q''/(Gi_{fg})$ and $We_l = G^2 D / (\rho_l \sigma)$, where q'' is the heat flux, i_{fg} is the latent heat of boiling, G is the mass flux, D is the diameter, and σ is the surface tension. For this heat transfer equation to be used for the prediction of experimental data for ethylene glycol/water mixtures with concentrations other than 50/50, ANL further modified it with a concentration correction factor, which reduces to one for concentrations of $v = 0$ and $v = 0.5$. The new correlation can be expressed as

$$h/h^* = [1 + 6v(v - 0.5)](BoWe_l^{0.5})^{0.5} \left[(\rho_l/\rho_v)^{-0.5} (\mu_l/\mu_v)^{0.7} \right]^{-1.5}$$

where h^* is a characteristic heat transfer coefficient of 135 kW/m²·K for all of the data.

Figure 6 shows the experimental data and the predicted values obtained with the correlation for ethylene glycol/water mixtures. The predictions are in good agreement with the experimental data, and most are within ± 30 percent of the data. Note that the comparisons are only for the data within the nucleation-dominant-boiling region. The success of the correlation in predicting the heat transfer coefficients of fluids boiling in small channels is directly related to the trend, as presented in Figure 3, that the heat transfer data are dependent on heat flux but not mass flux. The fact that the equation is also heat-flux but not mass-flux dependent is in accord with the experimental data.

Vertical Flow Boiling

In the application of engine cooling, both horizontal and vertical flows exist. Therefore, it is necessary to

investigate the impact of vertical versus horizontal flows on two-phase heat transfer.

Experimental Test Section. The design of the vertical experimental test section was similar to the existing horizontal section. The instruments attached to the vertical test section include thermocouples and pressure transducers that were calibrated against NIST-traceable standards to ensure accurate measurements of temperatures and pressures. The test facility and test-monitoring program were also modified to adapt to both horizontal and vertical flows. Figure 7 is a picture of the vertical test section before it was insulated.



Figure 7. Vertical experimental test section

Single-Phase Calibration. Single-phase heat transfer for vertical flow has been carried out in the test facility, and the results are compared to the predictions of the Gnielinski equation in Figure 8. All experimental data are within 20 percent of predictions. This agreement serves as a validation of the accuracy of the instrumentation, measurements, data acquisition, and data reduction procedures. These single-phase heat transfer tests are an “end-to-end” final validation of the test apparatus.

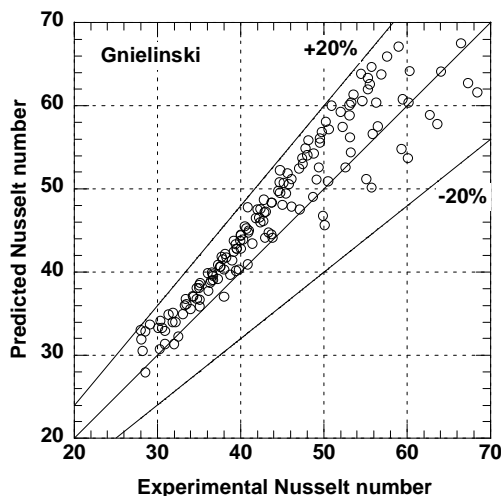


Figure 8. Single-phase Nusselt number

Preliminary Boiling Tests. Systematic vertical flow experiments are planned for two-phase boiling heat transfer with water and ethylene glycol/water mixtures. The tests are expected to provide essential information for the design of nucleate-boiling cooling systems. Preliminary vertical-flow boiling tests have been carried out, and the results are reported below.

Figure 9 shows heat flux as a function of wall superheat for boiling water at $100 \text{ kg/m}^2\text{s}$ mass flux and ambient inlet temperature. Vertical with horizontal flow boiling results are also compared in Fig. 9 under the same test settings. As can be seen in the figure, the curve for vertical flow boiling follows the same trend as that for horizontal flow boiling. However, to reach the same wall superheat, the heat flux (and, in turn, the critical heat flux) for vertical flow boiling is higher than for horizontal flow boiling. This result is expected because the vapor distribution for vertical flow boiling is more uniform than that for horizontal flow boiling due to the influence of gravity. This phenomenon is important for the design of nucleate boiling cooling systems. Because a practical cooling system usually contains both horizontal and vertical channels, the design of a nucleate boiling cooling system will be too conservative if based only on the horizontal-flow boiling data and too optimistic if based only on the vertical-flow boiling data.

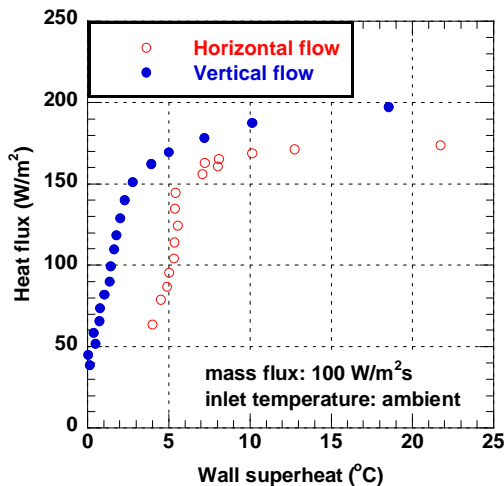


Figure 9. Horizontal and vertical boiling curve

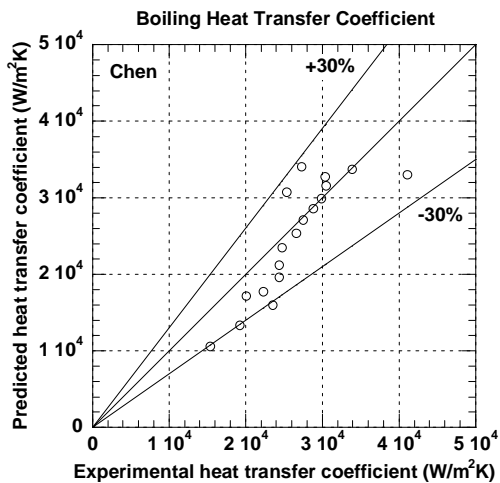


Figure 10. Heat transfer coefficient comparisons

Figure 10 compares the heat transfer coefficient data of the two-phase vertical flow boiling for 100 W/m^2 mass flux and ambient inlet temperature with the predictions of the Chen correlation that was developed based on water boiling data. The limited data show a reasonable agreement between the experimental data and predictions, and most of the predictions are within ± 30 percent of the experimental data. Note that the comparisons are only for the data within the nucleation-dominant-boiling region and that further experiments are necessary to confirm this trend.

Conclusions

Excellent progress has been made on the experiments and analysis for this project.

(a) A new procedure has been developed that can analytically calculate the boiling temperature along the test section and, subsequently, the local heat transfer coefficients by using ideal-mixture and equilibrium assumptions along with Raoult's law. This procedure can be easily used for designing cooling systems with flow boiling.

(b) Two-phase frictional pressure gradients of ethylene glycol/water mixtures follow similar trends as those of water. The results are in reasonable agreement with the predictions of Chisholm's correlation. A modification has been made to Chisholm's correlation, which reduces to Chisholm's correlation for concentrations $v = 0$ and $v = 1$. This modified Chisholm's correlation improves the predictions of pressure drop for ethylene glycol/water mixtures.

(c) The experiments show a high heat transfer rate with ethylene glycol/water mixtures, which is a positive result for engine cooling. ANL developed a general correlation based on data for water, ethylene glycol/water mixtures (concentrations 40/60, 50/50, and 60/40), and refrigerants. This correlation predicts the experimental data quite well, and most of the predicted values are within ± 30 percent of the experimental data.

(d) It was found that the boiling heat transfer of ethylene glycol/water mixtures is mainly limited by flow instability rather than critical heat fluxes that usually constitute the limits for water boiling heat transfer. Tests show that stable, long-term, two-phase boiling flow is possible for ethylene glycol/water mixtures as long as the mass quality is less than a certain critical value (approximately < 0.2). The heat transfer rate at this mass quality is significantly higher than that of conventional, single-phase, forced-convective heat transfer.

(e) The single-phase tests in vertical flow have confirmed the validation of the vertical test section and data reduction process. Preliminary experimental tests of vertical flow boiling to water show the same trend of wall superheat increasing with heat flux except that, to reach the same wall superheat, the heat flux for vertical flow boiling is higher than that for horizontal flow boiling. The results imply that the critical heat flux for vertical flow boiling is higher than that for horizontal flow boiling. The heat transfer coefficient data for vertical flow boiling are

predicted reasonably well by the Chen correlation, and most of the predictions are within ± 30 percent of the experimental data. These preliminary results will be verified by ongoing systematic tests of vertical flow boiling. Water and ethylene glycol/water mixtures will be used for two-phase boiling heat transfer experiments of vertical flows. The tests are expected to provide essential information for the design of nucleate-boiling cooling systems.

(f) Progress was made on the re-certification of the experimental test facility after the addition of the vertical test section. An extensive Environment, Safety, and Health Plan was completed for the experimental facility. An onsite inspection and safety review of the experimental facility was conducted, and, as a consequence, changes/modifications to the experimental facility are underway. These will be completed before testing is resumed.

B. Erosion of Materials in Nanofluids*

*This project is jointly funded by Propulsion Materials and Heavy Vehicle Systems Optimization

Principal Investigators: J. L. Routbort and D. Singh (coworker: Roger Smith)

Argonne National Laboratory

9700 S. Cass Avenue, Argonne, IL 60439-4838

(630) 252-5065; fax: (630) 252-5568; e-mail: routbort@anl.gov

DOE Technology Manager: Lee Slezak

(202) 586-2335, Lee.Slezak@ee.doe.gov

Contractor: UChicago Argonne, LLC

Contract No.: DE-AC03-06CH11357

Objective

Determine if the use of fluids containing a variety of nanoparticles result in erosive damage to radiator materials and coolant pumps.

If damage occurs, develop models to predict the erosive damage.

Approach

Develop an experimental apparatus to measure erosive loss.

Conduct experiments to study erosive damage of fluids containing various types and sizes of nanoparticles on typical radiator materials.

Develop methods to characterize nanofluids and analyze erosion results.

Accomplishments

Observed little erosion damage to a typical radiator material, aluminum Al3003, in experiments performed using CuO nanoparticles in ethylene glycol having impact angles of 30 and 90° and velocities up to 10 m/s for impact for a total time of 3620 hrs. Particle concentration varied between 0.1 and 0.85 vol %.

Utilized small-angle x-ray scattering technique to measure nanoparticle size, distribution, and shape.

Determined that polymeric gears are degraded by a SiC/water nanofluid.

Modified erosion apparatus to avoid excessive wear in polymeric gears.

Determined that an SiC/water nanofluid does not degrade aluminum Al3003.

Designed apparatus to measure wear in an automotive water pump.

Future Direction

Measure erosion of typical radiator materials using fluids containing a variety of well-characterized nanoparticles, varying the angle, size of the nanoparticles, impact velocity, nanoparticle volume percent, and temperature.

If erosion occurs, develop a predictive model.

Build apparatus to measure wear in an automotive pump.

Perform erosion tests using an actual automotive coolant pump.

Forward

Efforts have shifted away from the in-house production of nanofluids, to development of advanced characterization techniques and establishment of working relationships between companies that produce nanofluids. As commercial nanofluids become available, Argonne National Laboratory (ANL) will measure their thermal properties. Fluids that show promise from a heat transfer perspective will then be characterized by measuring the viscosity, thermal conductivity, and heat transfer coefficients while particle sizes will be measured by small-angle X-ray scattering (SAXS) and Dynamic Laser Scattering (DLS). Finally, liquid erosion tests will be performed to determine if the nanofluid will damage radiator materials.

Introduction

Many industrial technologies face the challenge of thermal management. With ever-increasing thermal loads due to trends toward greater power output for engines and exhaust gas recirculation for diesel engines, cooling is a crucial issue in transportation. The conventional approach for increasing cooling rates is use of extended surfaces such as fins and microchannels. Reducing radiator size will reduce the frontal area and hence the aerodynamic drag. However, current radiator designs have already stretched these approaches to their limits. Therefore, an urgent need exists for new and innovative concepts to achieve ultra-high-performance cooling. Nanofluids seem to show enormous potential as a coolant for radiators. Literature has many examples of increased thermal conductivity of fluids by the addition of nanoparticles (see review by Yu, et al. (1). Indeed a CFD (computational fluid dynamics) calculation of a Cummins 500 hp diesel engine using an ideal nanofluid as coolant has shown that the radiator size could be reduced five percent [2], reducing weight and size, and hence aerodynamic drag.

In order for the enhanced thermal conductivity to be utilized it must be shown that liquid erosion of typical radiator materials will be tolerable. If nanofluids result in excessive erosive wear, they cannot be used. Hence, the Vehicle Technologies (VT) Program funds an investigation on liquid erosion of radiator materials using nanofluids.

Results and Discussion of Erosion

It is important to understand the fluid flow and model the interaction of the fluid jet/target interactions in the liquid erosion apparatus. This was modeled by Tanju Sofu using a STAR-CD for 90° impacts. The results (Figure 1) are presented as the near-wall velocity as a function of distance from the center of the target at various velocities. The results agree very well with the actual imprint of the jet impinging the target. The picture shown in Figure 2 was obtained by painting the surface of the target. One observes the stagnation point and that the maximum damage occurs about 5 mm from the center in accord with the maximum wall velocity, as predicted by the CFD calculation.

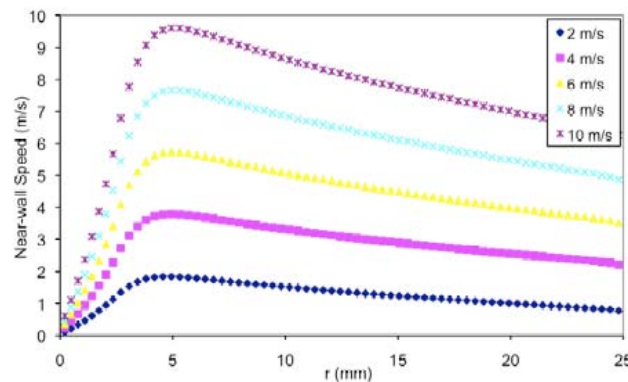


Figure 1. Result of a STAR-CD calculation showing the near-wall speed as a function of position from the center of the target for various velocities

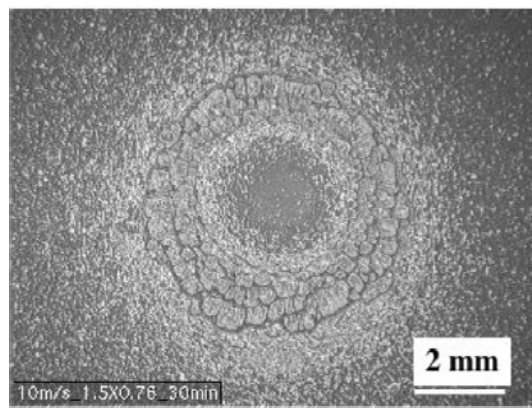


Figure 2. Imprint pattern of water jet impacting a painted aluminum 3003 target

SiC is a very promising nanoparticle. It will not oxidize and has a relatively high thermal conductivity, over five times greater than CuO. SiC nanoparticles in water were supplied to ANL by

Saint-Gobain with 4.0 and 7.3 vol. % concentrations. The SiC particles were not a uniform size and contained two peaks in the DLS: one centered at 31 nm and the other at 179 nm. The DLS results are shown in Figure 3. The results are in very good agreement with the SAXS results.

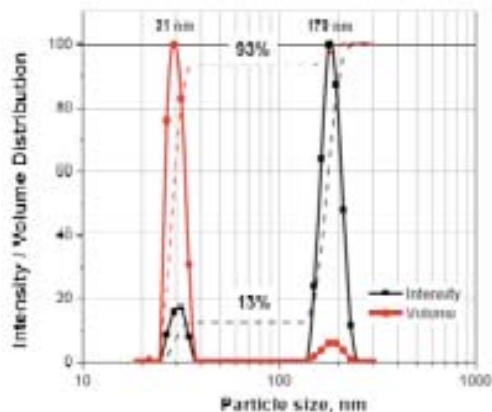


Figure 3. Dynamic Laser Scattering results on SiC/water nanofluid

Damage is likely to be more severe as the kinetic energy of the impacting particle is increased. Hence one would expect that at the same velocity and mean diameters, the SiC (density \approx 3.2 g/cc) nanofluid would result in more erosion than resulted from the CuO (density \approx 2.7 g/cc) [3]. Additionally, SiC is considerably harder than CuO and the concentration of SiC (2 vol.%) was higher than that of the CuO in ethylene glycol/water (\approx 1 vol.%). Hence all of these factors would indicate that the water containing SiC nanoparticles would be a severe test of damage caused by the nanofluid and would be expected to result in more erosion.

Recall that the CuO/ethylene glycol nanofluid did not cause any damage to the target for velocities between 8 and 10.5 m/s at 30, 50, and 90° impact angles for tests lasting between 200-300 hrs. Damage to the polymeric gears was restricted to $\leq 0.5\%$ weight loss at 10 m/s for 500 hrs [3].

By comparison the 2 vol.% SiC nanoparticles in water resulted in $\approx 4\%$ weight loss to the polymeric gears after 700 hrs of testing at 5 m/s. A photograph of the erosion damage is shown in Figure 4. The fact that the polymeric gears were eroded resulted in an impact velocity that continually decreased over time as the pump gears became worn. Hence a peristaltic pump was used to replace the gear pump. Some

problems were encountered with fatigue of the rubber tubing resulting in cracks that required moving the rubber hose 10 to 15 cm each day.



Figure 4. Photograph of the erosion of the polymeric gears after 700 hrs of testing with water containing 2 vol.% SiC nanoparticles

However, after 750 hrs of testing the 2 vol.% SiC/water nanofluid at 8 m/s and at an impact angle of 30°, there was no erosion damage to the aluminum 3003 target. This is most encouraging from an engineering viewpoint, but disappointing from a modeling point of view.

The above observation was obtained at one condition and does not represent the most severe conditions. Hence, it would be premature to conclude that nanofluids will cause no damage in cooling systems.

Issues & Future Direction

It is recognized that the erosion tests conducted so far were designed to accurately and reproducibly control the important erosion parameters, namely velocities, impact angles, and particle size, material, concentration, and the fluid. However, conditions in an actual pump are quite different. Hence we have redesigned the erosion apparatus to serve not only to supply fluid under controlled conditions, but also to determine if nanofluids will damage an actual automotive radiator pump. The new system will be calibrated during the first quarter of fiscal year 2009. It consists of the same chamber with the target as used before, and the same motor, controller, a magnetic-type flow meter, and a 5-liter reservoir, but instead of a gear pump, we have obtained a water pump used in automotive applications. The aluminum impeller of the pump can be removed

periodically to measure its weight loss and to inspect the damage. Hence we will accumulate not only engineering data on the erosion of the pump, but also more controlled data on the effect of nanofluids on the erosion of the target that are vital to developing predictive models. Additionally, we will obtain data on clogging of piping and pumps resulting from heavily loaded nanofluids.

The new apparatus will be used to investigate ethylene glycol fluids containing different nanoparticles and different vol. % nanoparticle loadings. We intend to test a 4 vol.% SiC nanofluid as well as EG/water containing intermetallic nanoparticles.

Conclusions

No severe erosion damage of aluminum 3003 has been observed to date. However, the nanofluids tested thus far were not the extremes. We have designed and are building an apparatus that will not only allow continuation of the well-controlled tests designed to develop the data required to model erosive damage, but will closely replicate “real world” conditions in an automotive water pump.

References

W. Yu, D. M. France, J. Routbort, S.U.S. Choi, “Review and Comparison of Nanofluid thermal Conductivity and Heat Transfer Enhancements, Heat Transfer Engineering, **29**, 432-460 (2008).

S. K. Saripella, W. Yu, J. L. Routbort, D. M. France, and Rizwan-uddin, “Effects of Nanofluid Coolant in a Class 8 Truck Engine,” SAE Technical Paper 2007-01-21413.

Annual Report (FY07), Propulsion Materials, pgs. 152-157.

C. Integrated Underhood and Aerodynamic Analysis

Principal Investigator: Tanju Sofu

Argonne National Laboratory

9700 S. Cass Avenue, Argonne, IL 60439-4838

(630) 340 2380; tsofu@anl.gov

DOE Technology Manager: Lee Slezak

(202) 586-2335; lee.slezak@ee.doe.gov

Agreement number 16625/17812: ANL CRADAs with Cummins and Caterpillar: (\$340K)

Objective

Develop a novel simulation technique to predict diesel engine thermal performance and to identify potential hot-spots in engine compartments of heavy-duty trucks.

Optimize engine thermal system and cooling package leading to improvements in energy efficiency of heavy vehicle systems.

Approach

Develop a conjoined 1-D thermal-fluid model and 3-D CFD model for a prototypical heavy vehicle underhood thermal system of a diesel engine.

Build the underhood thermal model and predict engine compartment temperatures, flow field distribution, and engine thermal performance under the specified test conditions.

Achieve fuel efficiencies through cooling system optimization and radiator size reductions.

Accomplishments

A conjoined 1-D and 3-D underhood thermal simulation package of a diesel engine with exhaust gas recirculation (EGR) was developed.

Thermal-fluid model was created with engine metal structure, underhood air, lubrication oil, and coolant circuits (cabin heater, EGR, and radiator subsystems).

CFD model was developed to simulate the underhood air temperatures and the component surface heat transfer rates between ambient air and engine metal structure.

Simulation package was validated for tests of engine speeds 1200 and 1700 rpm. The simulation package predicts the temperatures and distributed heat rejection rates with reasonable accuracy.

Future Direction

Thermal-fluid model needs to be improved by including air-conditioning loop and adding more components to the existing subsystems of cabin heater, EGR, radiator-fan, and charge air cooler.

CFD model needs to be refined to account for the local heat transfer effects from heat exchanger, radiator, and charge air cooler with fan under operation.

Combined use of thermal-fluid and CFD models should be expanded to study the sizes and the relative placements of radiator, charge air cooler, and fan to maximize the cooling efficiency.

Need/Problem Addressed

An optimal design of vehicle thermal systems is important for energy efficiency since less than one-third of the total fuel energy provides useful mechanical work (remainder is lost through the exhaust system and heat rejection). Determination of accurate temperature distributions in and around the engine allows redesign of a heavy-vehicle underhood configuration and helps achieve fuel efficiencies through cooling system optimization. Specific issues related to emission control technologies needed to meet the new diesel engine emission requirements further highlight the need for a predictive analytical capability to address unique heavy-vehicle underhood thermal control challenges.

Engine makers like Cummins and Caterpillar work very closely with original equipment manufacturers (OEMs) for engine installation issues as well as cooling system optimizations. Fuel efficiency considerations also tie their work to external aerodynamics of different heavy vehicle designs. As a result, they need a comprehensive analytical capability to make C_D assessments for different design options in addition to their traditional focus on underhood thermal management.

Approach

A typical thermal-control challenge is to avoid component overheating due to tighter packaging. Since high temperatures can reduce component durability and life, the assessment of temperature distributions under the hood is an important element of a design cycle. In addition to the need to identify hot-spots, determining the temperature distributions under the hood is also critical to achieve fuel efficiencies through cooling system optimization and radiator size reduction. A predictive analytical capability can help to redesign an underhood configuration while keeping the aerodynamic considerations in perspective to meet energy efficiency and emissions reduction targets.

The objective of the proposed activities (in collaboration with engine makers like Cummins and Caterpillar) is to provide a methodology to fully characterize thermal-flow conditions in the underhood compartment of a heavy vehicle based on combined use of thermo-fluids system models and computational fluid dynamics (CFD) techniques for

both the underhood and external aerodynamics analyses. This methodology will help OEMs address design challenges related to emission control technologies needed to meet the new diesel engine emission requirements by providing a predictive capability to shorten component design and test cycles with a validated high-fidelity (but also a practical) simulation tool.

Progress

CFD, although computationally intensive, is the tool of choice for simulations of the entire vehicle in 3-D. When coupled with 1-D systems models to represent the engine and cooling system response, CFD can be used to fully characterize thermal-flow conditions in the underhood compartment of heavy vehicles. Combined use of CFD and system models offers unique advantages. System model accounts for thermal energy balance and heat distribution inside the engine through 1-D network of flow loops. The CFD model addresses multi-dimensional flow and heat transfer effects wherever needed. The combined model needs basic ambient conditions and component performance curves by exchanging data between 1-D and 3-D models.

In 2006, a network of 1-D representation of a Cummins engine internal flow loops has been developed combined with a lumped-parameter approach to characterize thermal interactions between them through the engine structure as major conduction paths. This thermo-fluids system model, developed using commercial software Flowmaster, simplifies the complex engine system by discretization based on known heat transfer paths under equilibrium conditions. It can predict the complete engine thermal system performance by analyzing the interactions of the engine with the coolant, oil, and ventilation air loops, and accounts for thermal energy balance by considering the heat generated from combustion to be transferred to various discrete component surfaces (e.g., cylinder head, valve cover, front cover, engine block, cylinder head, ECM) through specified conduction paths.

In 2007 and through the first half of 2008, the work on CFD modeling of the underhood compartment of a generic class-8 heavy vehicle, and its coupling with the 1-D systems model was completed. The results of the coupled CFD and network flow models are compared with the test data from Cummins for

validation. Similar to the earlier experience with a Caterpillar off-road vehicle engine, a very good agreement between the model results and test data has been achieved. For the second half of 2008, an agreement is being pursued with Cummins Inc. to start the first implementation of integrated underhood and external aerodynamics simulations for a prototypical heavy-vehicle configuration.

Future (FY 2009) Activities

As an extension to ongoing work (expected to start in FY 2008), the integrated underhood thermal and external aerodynamics analyses will be performed to address issues related to cooling system optimizations. Industrial partner, Cummins Inc., will identify a realistic heavy-vehicle configuration to be studied and provide technical information to help prepare the CFD models. In the final stage, both the Contractor and the Participant will build the analytical models and conduct simulations to assess changes in aero-drag forces in response to cooling system design changes. The final product will be an experimentally validated analysis methodology for performing external aerodynamics simulations of realistic heavy vehicle geometries using commercial CFD software. The best practice guidelines to be established as a result of this study will be made available to the consortium of OEMs participating in the Department of Energy (DOE) program.

Deliverables

Milestone	Deadline
Develop underhood CFD model of the selected heavy vehicle configuration	Completed: December 2007
Complete the integrated model assessments using the experimental data from Cummins	Completed: March 2008
Report the model development and assessment results as final CRADA document	September 2008
Start the extension of the underhood work to external aerodynamics analyses	2008-2009

D. CoolCab – Truck Thermal Load Reduction Project

Ken Proc (Principal Investigator)

National Renewable Energy Laboratory

1617 Cole Blvd.

Golden, CO 80401

(303) 275-4424; kenneth_proc@nrel.gov

DOE Technology Manager: Lee Slezak

(202) 586-2335; Lee.Slezak@ee.doe.gov

Objectives

Investigate the potential to reduce truck cabin thermal load through testing and analysis.

Develop a tool to help predict heating, ventilating, and air conditioning (HVAC) load reduction in truck tractor sleeper cabins.

Approach

Work with industry to identify specific needs and development projects in heavy trucks.

Perform baseline truck testing, data analysis, and model validation work.

Key Milestones

Engineering Test Report: Infrared Image Field Test at Schneider National, July 2005.

Status Report: CoolCab Testing with Volvo Truck, September 2006.

Interim Report on CoolCab Activity, August 2007.

Presentation of Results of Industry Meetings and Tool Specifications, September 2008.

Future Activities

SAE paper on results of baseline truck testing and CFD modeling.

Proof-of-concept tool with initial validation case.

Develop working prototype of HVAC load calculation tool.

Introduction

The trucking industry is faced with increased costs from rising fuel prices, higher maintenance costs, and driver turnover. In addition, excessive idling has been identified as a source of wasted fuel and an unnecessary cost. Survey estimates report sleeper trucks idle an average of more than 1,400 hours annually [1]. Engine idling consumes more than 800 million gallons of fuel annually in long-haul (>500 miles/day) trucks [2]. Trucks typically idle to run cabin climate control (heating, cooling, and dehumidification) during driver rest periods and to

provide electric power for other amenities. Reducing the amount of truck engine idling can significantly reduce fuel consumption, save money, and reduce tailpipe emissions.

The U.S. Department of Energy's (DOE) Advanced Vehicle Testing Activity (AVTA) initiated a study of diesel truck engine idle reduction technologies in 2002 [3]. This study consisted of several projects that evaluated existing on-board idle reduction technologies, including diesel-fired and electric heaters, electric air conditioning systems, and an auxiliary cab cooler using phase change material.

This evaluation demonstrated measured idle reduction and fuel savings with some of the technologies but identified the following issues in meeting driver and operator requirements:

Energy storage capacity: Battery powered and other stored energy cooling systems lacked capacity to meet mandatory driver rest periods in warm ambient temperatures (above 85°F).

Driver comfort: Drivers noted areas within the truck cab where excessive heat penetrated the cabin walls from the environment and the engine exhaust system.

Cost: Some of the technologies tested required significant installation time to retrofit an existing truck. This installation cost, in addition to the hardware cost, was too high to provide sufficient technology payback to the fleets.

To address the identified cost issue, DOE solicited proposals for cost-shared projects to integrate an on-board idle reduction technology at a truck original equipment manufacturer (OEM) [3]. International Truck and Engine Corporation was awarded a contract, and the design and factory installation work is currently underway. This work, however, is not addressed in this report.

To address the capacity and comfort issues identified, DOE, through the National Renewable Energy Laboratory (NREL), launched the CoolCab project. This project conducted a qualitative study of truck tractor cabins to identify potential areas for improvement. Working with Schneider National, two tractors were analyzed using infrared images to investigate heat loss [4]. This exploratory work noted several areas for improvement in the truck cab insulation, including driver and passenger footwells, sunroof and ceiling pad areas, and the rear of the upper bunk (Figure 1).

The CoolCab project continues to quantify truck cab heat loss and further investigate reducing the thermal load of the truck heating, ventilating, and air conditioning (HVAC) system during driver rest periods. Working with truck OEMs Volvo and International, CoolCab tested and analyzed two trucks at NREL's outdoor test facility; this work is the focus of this report.

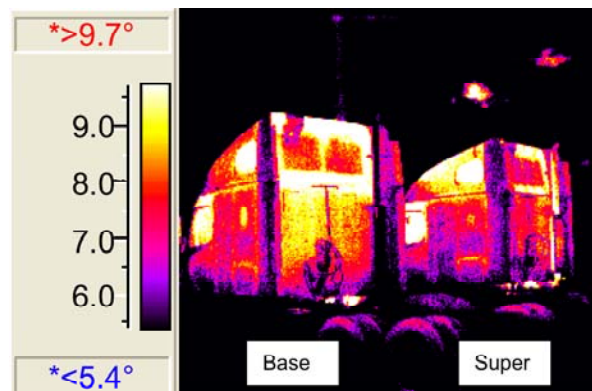


Figure 1. Upper Sleeper Bunk Infrared Image

Objective

The main objective of the CoolCab project is to identify design opportunities to reduce the thermal load inside truck tractor cabs. Reducing the heating or cooling load is the first step in improving system efficiency to reduce fuel consumption. Reducing this load will enable existing idle reduction technologies and allow more efficient technologies to keep truck drivers comfortable during rest periods.

A secondary objective of reducing cabin thermal load is to decrease heating and cooling loads while a truck or other vehicle is traveling. This load reduction may provide further gains in reducing fuel consumption and improving fuel economy. In addition, with a trend toward hybrid powertrains in vehicles, energy required for HVAC and other accessories will be at a premium. Load reduction will help reduce these energy demands and help extend vehicle range and efficiency in both light and heavy vehicles.

Approach

Truck Testing

Truck testing was conducted outdoors at NREL's test facility. Two trucks were tested with a third truck tractor used as a control for comparison and baseline data (Figure 2). All trucks were fully instrumented and subjected to a series of four tests to help measure heat transfer and identify high heat loss areas: Co-heat tests, solar soak, air exchange, and infrared (IR) imaging.



Figure 2. Test Truck and Control Truck Parked for Testing

Co-Heat Tests

Testing began with establishing a baseline for truck cab insulation. By measuring the amount of heat required to maintain a given temperature, an overall heat transfer coefficient, or UA, for the cabin can be calculated from the expression

$$Q = UA\Delta T, \text{ where } Q \text{ is the heat transfer rate.}$$

From UA, an 'R-value' can be derived from a known area for the truck cab from the equations

$$R = 1/U \text{ and } U = UA/A, \text{ where } A \text{ is the truck cabin interior surface area.}$$

UA tests were performed to quantify the heat transfer rate in both the test and control trucks. By using a control truck but only modifying the test trucks, it was possible to quantify changes in performance under variable conditions encountered at the outdoor test site. A correction factor was applied to the test data based on data obtained from the control truck (which was not modified). Once the baseline testing of the trucks was completed, simple modifications (insulating windows, applying a sleeper isolation curtain, etc.) were made to the test tractors to help understand heat loss paths.

Solar Soak

Testing also included daytime heat soak tests to help quantify solar gains. Interior temperatures were measured in both test trucks with and without window insulation to understand the effects of the glass areas. Once again, the control truck was used to

obtain correction factors for variable conditions. The data obtained in the daytime heat soak tests were also used to validate the accuracy of a Fluent Inc. model of the cab previously developed by NREL and International.

Air Exchange

An air exchange test was also conducted on the trucks by measuring the decay rate of a known gas injected into the cab interiors. This test provided data on the amount of overall air leakage in the truck cab relative to other vehicles.

IR Imaging

Additionally, infrared images of both the interiors and exteriors of the trucks were used to identify higher heat loss areas (hot spots) in the truck cabs. The images provided more insight to areas that could be improved to reduce measured heat loss.

Modeling

A numerical model of the International sleeper cab was developed using Fluent CFD software and RadTherm thermal analysis software. International provided the volume and surface mesh file of the sleeper cab interior. The model volume mesh comprises approximately 4.4 million cells; the surface mesh in RadTherm was approximately 105,000 elements. RadTherm models the solar load on the vehicle, convection losses on the interior and exterior surfaces, and conduction through the surfaces. Fluent CFD software was used to model the convective heat transfer and fluid flow in the cabin. During the analysis, RadTherm and Fluent interacted in the following way: RadTherm provided surface temperature boundary conditions to Fluent, and Fluent provided heat transfer coefficients and fluid temperatures to RadTherm. Several exchanges between RadTherm and Fluent were needed to achieve a consistent solution. Figure 3 shows Fluent-predicted air temperatures on a centerline of the cabin. Figure 4 shows RadTherm-predicted surface temperatures. Both figures show a baseline cool down configuration with a curtain partitioning the cabin.

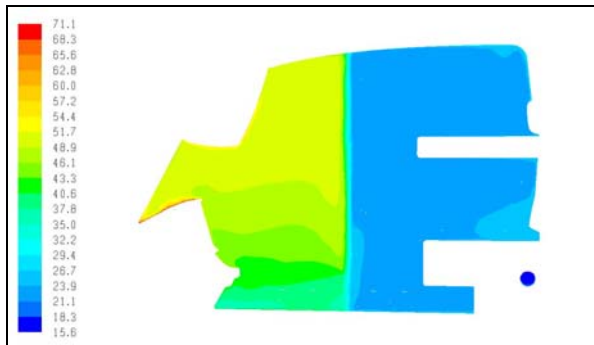


Figure 3. Fluent Predicted Air Temperature (°C)

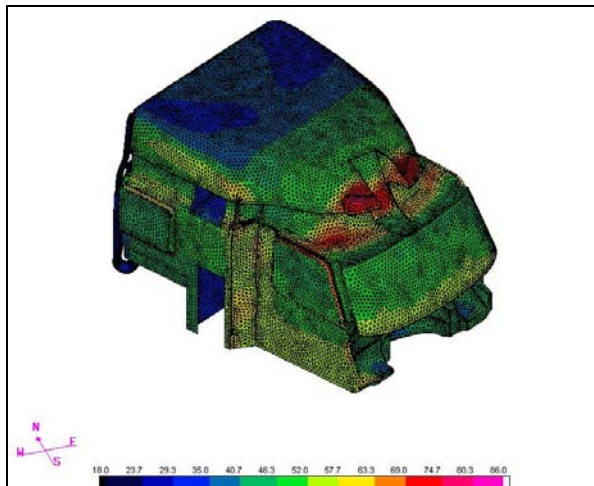


Figure 4. RadTherm Predicted Surface Temperatures (°C)

The model was first validated against quasi steady state soak data from several days of soak tests. The soak tests represented several configurations of the cabin; for example, some tests were with a curtain and others were without. Figure 5 shows a comparison of the average cabin air temperatures predicted by the model to test data for the sleeper cab. Figure 6 shows a comparison of the average surface temperatures predicted by the model to test data for the sleeper cab. In both Figures 5 and 6, ambient temperature is also shown for reference. Several factors, such as uncertainty in temperature measurement locations, material properties, and vehicle orientation, could have contributed to the differences between measured temperatures and the model-predicted temperatures. Overall, the results show agreement within 3°C to 4°C. The validated model was then used to simulate the vehicle cool down.

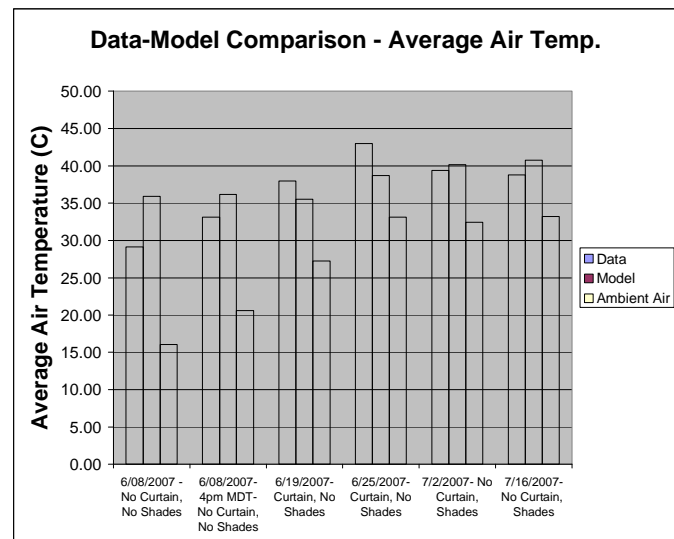


Figure 5. Model Air Temperatures Compared to Test Data

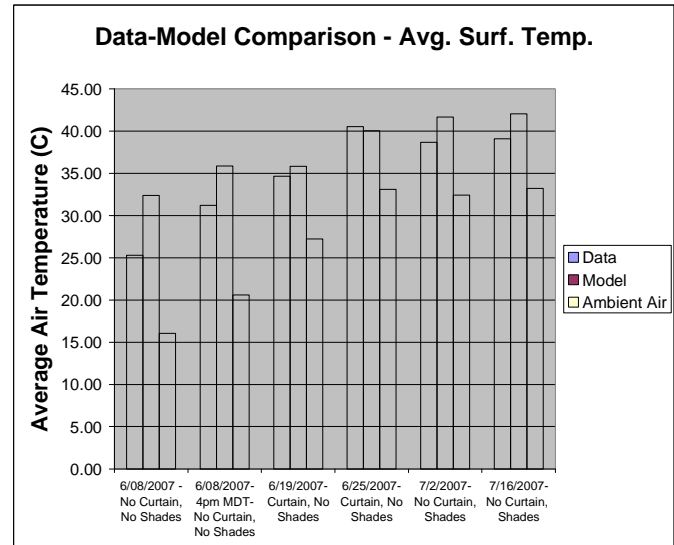


Figure 6. Model Surface Temperatures Compared to Test Data

Results

Co-Heat Tests

The co-heat tests were run with two electric heaters installed in the sleeper bunk area of the truck tractor cab. Truck interiors were heated to 40°C to simulate a typical cab temperature differential in a test ambient of about 15°C. Truck interiors were temperature-soaked overnight (about six hours) to stabilize temperatures ($\pm 0.5^\circ\text{C}$ of set point) before logging data. To calculate the UA value, power usage (logged

voltage and current to the heaters) was recorded to determine the heat transfer rate.

Figure 7 shows interior and exterior (ambient) temperatures of the control truck during a typical co-heat test. Temperatures were very stable during the data recording period from 3 a.m. to 5 a.m.

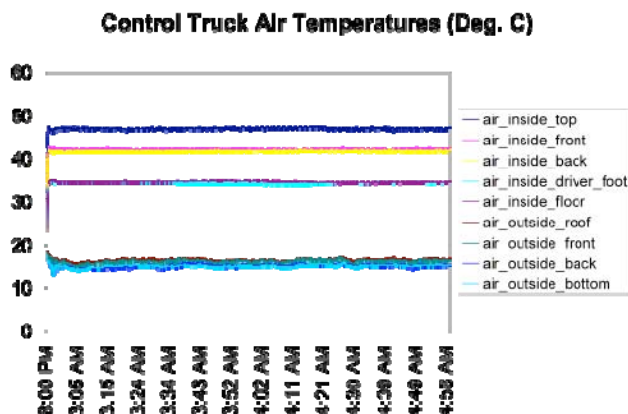


Figure 7. Measured Inside and Outside Truck Air Temperatures

Typically five runs of each configuration were conducted to obtain three valid runs (stable temperatures and little or no wind). Three valid runs were averaged to calculate the UA value for each configuration. Simple modifications were made to the test trucks to help understand heat loss paths. The different configurations for the UA test were the base case (no modifications), sleeper curtain closed and window shades applied, and windows insulated. The sleeper curtain configuration applied the factory-supplied snap-in window shades and sleeper privacy curtain during testing to measure the effects of isolating the sleeper compartment. The windows-insulated configuration included the application of foiled bubble insulation on the inside of the cab windows to estimate the amount of heat lost through the window glass (Figure 8). The factory sleeper curtain and shades were not applied in this configuration. A fourth configuration was also tested in the second test vehicle, which replaced the standard curtain with a foam-insulated or arctic curtain in the closed position (standard window shades applied).



Figure 8. Insulated Windows on Test Truck

The measured UA for the first test truck in the base configuration was 65 W/K. Therefore, in a typical overnight cab heating case with an ambient temperature of 0°C, heating the cab to 20°C would require 1,300 W ($Q = UA\Delta T$). Closing the sleeper curtain and applying the window shades lowered the UA to 54 W/K for the sleeper area, a 16 percent reduction from the base case. The sleeper-curtain-closed configuration yielded a 21 percent reduction in the second test truck. Insulating the windows reduced the UA 16 percent in the first test vehicle from the base case and 14 percent in the second. Insulated window shades could further reduce heat loss when used in conjunction with the sleeper curtain, but this configuration was not tested. Although the 16 percent or 21 percent reduction from insulating the windows is significant, it is important to note that a large portion of the heat loss was through the cabin walls and other heat loss paths (door seals, vents, etc.) and was investigated through modeling and other testing detailed in this report. The results of UA tests are summarized in Table 1.

Table 1. Summary of UA Test Results (Reductions from Base)

	Base or Unmodified Case	Sleeper Curtain Closed	Arctic Curtain Closed	Windows Insulated
UA Test Truck 1	65 W/K	-16 percent	N/A	-16 percent
UA Test Truck 2	51 W/K	-21 percent	-26 percent	-14 percent

Solar Soak

Testing also included daytime heat soak tests to help quantify solar gains. Interior temperatures were measured in both trucks with and without window insulation to understand the effects of the glass areas. Once again, a control truck was used to obtain any correction factors for variable conditions. The data obtained in the daytime heat soak tests were also used to validate the accuracy of a Fluent model of the cab previously developed by NREL and International.

The soak tests were run in a similar manner to the co-heat tests, using the same temperature data acquisition set-up but not using electric heaters. Trucks were faced south to maximize sun exposure with soak temperatures recorded to capture peak sun intensity from about noon to 2 p.m. The truck interior air temperatures and the outside ambient temperatures were used to calculate an average interior cab temperature above ambient. Three valid runs (stable solar irradiance and little or no wind) were averaged to calculate the average temperature rise above ambient for the same configurations as the co-heat tests.

The interior temperature rose 13°C above ambient on average for the first test truck and 11°C for the second test truck. For the second test truck, closing the standard sleeper curtain and installing the window shades reduced the temperature rise above ambient by about 1°C and 3°C with the arctic curtain. Covering the windows with foil insulation (windows-insulated configuration) reduced the temperature rise in the truck cab by 8°C in the first test truck 4°C in the second truck. The results of the soak testing are summarized in Table 2. The greater reduction in temperature rise in the windows-insulated configuration (and the greater ΔT in the base case) for the first test truck can be attributed to a larger glass area that included a sunroof. (There was no sunroof in the second test truck).

**Table 2. Summary of Solar Soak Test Results
(Reductions from Base)**

	Base or Unmodified Case	Sleeper Curtain Closed	Arctic Curtain Closed	Windows Insulated
Soak Test Truck 1	$\Delta T = 13^\circ\text{C}$	N/A	N/A	-8°C
Soak Test Truck 2	$\Delta T = 11^\circ\text{C}$	-1°C	-3°C	-4°C

Air Exchange

To calculate the air exchange of the truck tractor cabins, the decay rate of a known gas in the cab was measured. Sulfur hexafluoride (SF6) gas was injected into the truck cab and a tracer gas analyzer was used to record the decay data. From the measured concentration over a given period, the air exchange rate was calculated in air changes per hour (ACH).

The first test truck averaged 0.8 ACH over the test period, while the second truck averaged 0.7 ACH. Figure 9 shows the results of the air exchange testing. Both truck cabins had less than one air change per hour and were considered relatively well sealed. No additional investigation on air leakage as a source of thermal load reduction was considered.

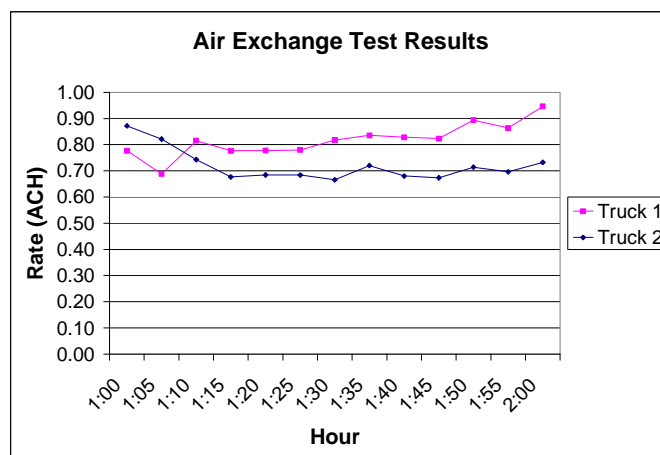


Figure 9. Results of Air Exchange Testing

Infrared Imaging

Infrared images were taken of the test trucks to help identify potential sources of high heat loss. An infrared radiometer was used to capture images while truck interiors were heated during the co-heat tests.

The nighttime images revealed expected heat loss around door and window seals in both trucks as well as at the seam joining the roof to the lower cab (Figure 10). Some heat loss was also noted at the roof structural members where insulation may have been lacking. The higher exterior temperatures in the image indicated the areas of higher heat loss than the surrounding areas.

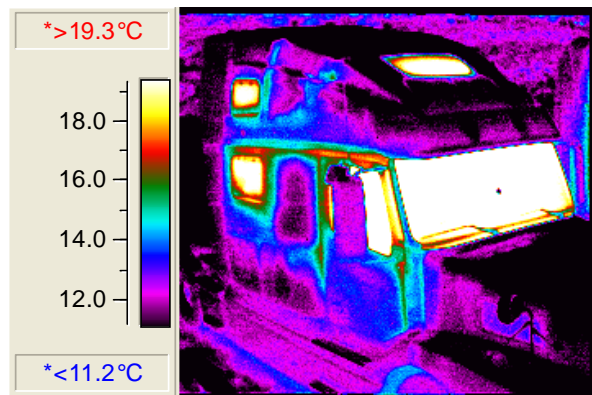


Figure 10. Infrared Image of Test Truck 1

Infrared images of the second test truck revealed higher temperature areas in the upper left and right corners at the rear of the truck cab (Figure 11). This heat loss could be the result of lacking or missing insulation in air duct areas at the rear corners of the cab.

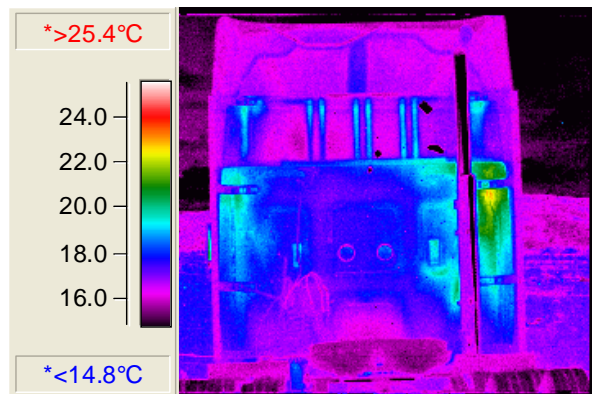


Figure 11. Infrared Image of Test Truck 2

Modeling

For the cool-down model only the rear air-conditioning (A/C) unit was simulated with a fixed airflow of 0.156 kg/s (264 cfm). As a worst-case scenario, daytime ambient and solar conditions were chosen to be an August day in Phoenix. The temperature of the air inlet to the cabin was adjusted

to achieve equal cabin volume average air temperature. For the configurations without a divider curtain, the average air temperature of the entire cabin was compared. For the configurations with a divider curtain, only the sleeper portion of the cabin was considered. The duty of the A/C unit was then calculated as the sensible heat gain of the air being circulated through the A/C system. Recirculation of cabin air and moisture removal was not considered and would affect the size and duty of the A/C system. The heat due to cabin occupants and cabin equipment, such as electronics, was also not considered. The duty or heat gain of the air circulating in the A/C system was then compared to judge the effectiveness of the various configurations.

Figure 12 shows the effect of both the curtain partitioning the cabin and increasing insulation. As expected, partitioning the cabin and only cooling part of the air will take less energy. The model predicted this would decrease the duty of the A/C system by 30 percent. Additional insulation shows a case of decreasing returns. With the sleeper curtain open, doubling the insulation reduces the A/C duty by approximately 35 percent. With the curtain closed, doubling the insulation reduces duty by 25 percent (54 percent from the base configuration with no curtain). However, doubling the insulation again only resulted in approximately 6 percent less duty.

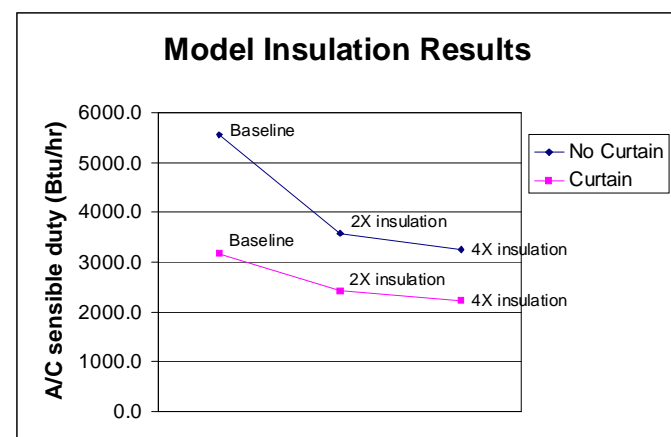


Figure 12. Effect of Increased Insulation

Covering the windows with insulated reflective shades was also simulated. The model shows that covering the windows will reduce the A/C duty by 34 percent with the curtain open and 14 percent with the curtain closed. The reduction with the curtain is much less than without it because the shades

primarily keep the solar load out of the front of the cabin where most of the glass area is.

Conclusions

Through truck testing and thermal modeling, opportunities to reduce thermal load were identified and quantified. Vehicle testing demonstrated reductions in heating loads from standard configurations (sleeper curtain and window shades) as well as some optional configurations (insulated curtain and window insulation). Vehicle modeling predicted reductions in cooling loads from improved cab insulation and covered windows. The opportunities for thermal load reduction are as follows:

Applying the standard sleeper privacy curtain and shades reduced heating load for the sleeper area by up to 21 percent. An insulated sleeper curtain further reduced the load to 26 percent over the base configuration. Covering the windows in the truck cab reduced the heating load by up to 16 percent over base and could further reduce heating in the sleeper curtain configurations.

Insulating the truck cab windows also reduced daytime solar temperature gains by up to 8°C, which reduced predicted cooling load by 34 percent with the sleeper curtain open. Doubling the insulation alone would reduce the cooling load by about 35 percent with the sleeper curtain open and a total of 54 percent with the sleeper curtain closed.

Infrared images identified other potential areas to reduce heat loss, such as areas around window and door seals, at body and structural seams, and areas where insulation may be lacking around air circulation ducts.

References

1. The American Transportation Research Institute. "Idle Reduction Technology: Fleet Preferences Survey." February 2006.
2. Stodolsky F., Gaines L., Vyas A. "Analysis of Technology Options to Reduce the Fuel Consumption of Idling Trucks." Argonne National Laboratory, ANL/ESD-43, June 2000.
3. Proc K. "Idle Reduction Technology Demonstrations." NREL, DOE/GO-102004-1993, November 2004.
4. Rugh J., Farrington R. "Vehicle Ancillary Load Reduction Project Close-Out Report." NREL, NREL/TP-540-42454, January 2008.

VIII. FRICTION AND WEAR

A. Boundary Lubrication Mechanisms

Principal Investigators: O. O. Ajayi, C. Lorenzo-Martin, R.A. Erck, J. Routbort, and G. R. Fenske

Argonne National Laboratory

9700 South Cass Avenue, Argonne, IL 60439

(630) 252-9021; fax: (630) 252-4798; e-mail: ajayi@anl.gov

DOE Technology Manager: Lee Slezak

(202) 586-2335; Lee.Slezak@ee.doe.gov

Technical Program Manager: Jules Routbort

(630) 252-5065; routbort@anl.gov

Contractor: Argonne National Laboratory, Argonne, Illinois

Contract No.: DE-AC02-06CH11357

Objective

Develop a better understanding of the mechanisms and reactions that occur on component surfaces under boundary lubrication regimes with the ultimate goal of friction and wear reduction in oil-lubricated components and systems in heavy vehicles. Specific objectives are as follows:

Determine the basic mechanisms of catastrophic failure in lubricated surfaces in terms of materials behavior. This knowledge will facilitate the design of components and systems with higher power density.

Determine the basic mechanisms of chemical boundary lubrication. This knowledge will facilitate lubricant and surface design for minimum friction.

Establish and validate methodologies for predicting the performance and failure mechanisms of lubricated components and systems.

Integrate coating and lubrication technologies for maximum enhancement of lubricated-surface performance.

Transfer the technology developed to OEMs of diesel engine and vehicle components and systems.

Approach

Characterize the dynamic changes in the near-surface material during scuffing.

Formulate a material-behavior-based scuffing mechanism and prediction capability.

Determine the chemical kinetics of boundary film formation and loss rate by in-situ X-ray characterization of tribological interfaces at the Advanced Photon Source (APS) of Argonne National Laboratory (ANL).

Characterize the physical, mechanical, and tribological properties of tribochemical films, including the failure mechanisms.

Integrate the performance and failure mechanisms of all the structural elements of a lubricated interface to formulate a method for predicting performance and/or failure. This task will include incorporation of surface coatings.

Maintain continuous collaboration with original equipment manufacturers (OEMs) of heavy vehicle systems to facilitate effective technology transfer.

Accomplishments

Conducted extensive characterization of microstructural changes during scuffing of 4340 steel, using scanning electron microscopy (SEM) and energy dispersive X-ray (EDX) analysis.

For metallic materials, developed a model of scuffing initiation based on an adiabatic shear instability mechanism and scuffing propagation based on a balance between heat generation and heat dissipation rates.

Characterized the mechanical properties and scuffing resistance of a graded nanocrystalline surface layer produced by severe plastic deformation resulting from the scuffing process.

Conducted preliminary evaluation of scuffing mechanisms in ceramic materials.

Extended study of scuffing mechanisms into ceramic/metal contact pairs.

Using X-ray fluorescence, reflectivity, and diffraction at the APS, demonstrated the ability to characterize tribocorrosion films generated from model oil additives.

Designed and constructed an X-ray accessible tribo-tester for in-situ study of boundary film formation and loss rates.

Future Direction

Experimentally validate the comprehensive scuffing theory for various engineering materials, including ceramics.

Develop and evaluate methods and technologies to prevent scuffing in heavily loaded oil-lubricated components and systems.

Using X-ray based and other surface analytical techniques, continue to characterize tribocorrosion films formed by model lubricant additives.

Characterize the physical, mechanical, and failure mechanisms of tribocorrosion films with nano-contact probe devices.

Evaluate the impact of various surface technologies, such as coating and laser texturing, on boundary lubrication mechanisms.

Develop a technique to measure actual contact temperature needed for tribocorrosion film formation.

Introduction

Many critical components in diesel engines and transportation vehicle systems such as gears and bearings are lubricated by oil. Satisfactory performance of these components and systems in terms of efficiency and durability is achieved through the integration of materials, surface finish, and oil lubricant formulations, often based on an Edisonian trial-and-error approach. Experience is likely the sole basis for new designs and methods to solve failure problems in lubricated components. Because of the technology drive to more efficient and smaller systems, more severe operating conditions are invariably expected for component surfaces in advanced engines and vehicle systems. The trial-and-error approach to effective lubrication is inadequate and certainly inefficient. Departure from this approach will require a better understanding of

the fundamental mechanisms of boundary lubrication and surface failure in severely loaded lubricated components.

Another major technical thrust for the Department of Energy (DOE) in the development of diesel engine technology for heavy vehicles is emissions reduction. With the higher efficiency of diesel engines compared to gasoline engines, significant reduction in emissions will facilitate greater use of diesel engines for automotive applications. Unfortunately, some essential components in oil lubricants and diesel-fuel additives (such as sulfur, phosphorus, and chlorine) are known to poison the catalysts in emission-reducing after-treatment devices used in diesel engines. Reduction or elimination of these additives will make emission after-treatment devices more effective and durable; it will, however, make the surfaces of many lubricated components more

vulnerable to catastrophic failure. An effective replacement for these essential lubricant additives is being sought. Such an endeavor requires a better understanding of the mechanisms of boundary lubrication and the failures therein.

Increases in vehicle efficiency will require friction reduction and an increase in power density in the engine and powertrain systems. Higher power density translates to increased severity of contact between many tribological components. This condition will compromise the reliability of various critical components, unless they are effectively lubricated. The efficacy of oil additives in reducing friction and in protecting component surfaces depends on the nature and extent of the chemical interactions between the component surface and the oil additives. In addition to reliability issues, the durability of lubricated components also depends on the effectiveness of oil lubrication mechanisms, especially under boundary conditions. Components will eventually fail or wear out by various mechanisms, including contact fatigue. Wear is the gradual removal of material from contacting surfaces, and it can occur in many ways, such as abrasion, adhesion, and corrosion. Repeated contact stress cycles to which component contact surfaces are subjected can initiate and propagate fatigue cracks and, ultimately, lead to the loss of a chunk of material from the surface. This damage mode by contact fatigue is often referred to as "pitting." Wear and contact fatigue are both closely related to boundary lubrication mechanisms. Anti-wear additives in lubricants are designed to form a wear-resistant protective layer on the surface. The role of lubricant additives in contact fatigue failure is not fully understood, although it is clear that the lubricant chemistry significantly affects contact fatigue. Again, lack of a comprehensive understanding of the basic mechanisms of boundary lubrication is a major obstacle to a reasonable prediction of the durability of lubricated systems.

Significant oil conservation benefits would accrue by extending the drain interval for diesel engine oil, with an ultimate goal of a fill-for-life system. Successful implementation of the fill-for-life concept for the various lubricated systems in heavy vehicles requires optimization of surface lubrication through the integration of materials, lubricant, and, perhaps, coating technologies. Such an effort will require an

adequate fundamental understanding of surface material behavior, chemical interactions between the material surface and the lubricant, and the behavior of material and lubricant over time.

Some common threads run through all of the challenges and problems in the area of effective and durable surface lubrication of components in efficient and high-power-density systems. The two key ones are (1) lack of adequate basic and quantitative understanding of the failure mechanisms of component surfaces and (2) lack of understanding of the basic mechanisms of boundary lubrication, i.e., how lubricant chemistry and additives interact with rubbing surfaces, and how this affects performance in terms of friction and wear.

To progress beyond the empirical trial-and-error approach for predicting lubricated component performance, a better understanding is required of the basic mechanisms regarding the events that occur on lubricated surfaces. Consequently, the primary objective of the present project is to determine the fundamental mechanisms of boundary lubrication and failure processes of lubricated surfaces. The technical approach taken differs from the usual one of posttest characterization of lubricated surfaces; instead, it includes developing and applying in-situ characterization techniques for lubricated interfaces that will use the X-ray beam at the Advanced Photon Source (APS) located at Argonne National Laboratory (ANL). Using a combination of different X-ray-based surface analytical techniques, we will study, in real time, the interactions between oil lubricants and their additives and the surfaces they lubricate. Such a study will provide an improved understanding of the basic mechanisms of boundary lubrication. In addition to surface chemical changes, the materials aspects of various tribological failure mechanisms (starting with scuffing) will be studied.

Results and Discussion

Scuffing Mechanisms

Effort during fiscal year (FY) 2008 was devoted to continued development of tribological components for high-power-density systems, i.e., material pairs with high scuffing resistance. Our evaluation of steel and structural ceramic contact pairs showed significantly higher scuffing resistance, as shown in Figure 1, which plots the contact severity index (CSI)

for scuffing between hardened steel and different ceramics. The CSI is the product of the friction coefficient, the sliding velocity, and the normal load and is a measure of frictional energy input to cause scuffing at a contact interface. The higher the CSI, the higher the scuffing resistance. In some ceramic materials [tetragonal-zirconia polycrystal (TZP) and partially stabilized zirconia (PSZ)], scuffing did not occur. When scuffing did occur, the CSI was two to four times that of steel, which reflects a substantial increase in power density.

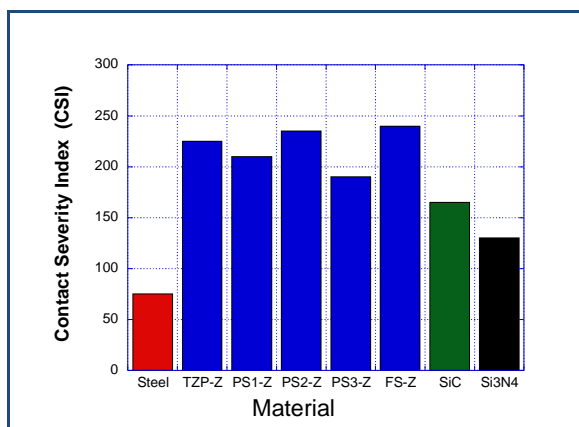


Figure 1. Contact Severity Index (CSI) for Different Ceramic-Steel Contact Pairs

In the steel/ceramic contact pair, scuffing occurred only when extensive metal transfer from steel onto the ceramic surface had occurred, as illustrated in Figure 2.

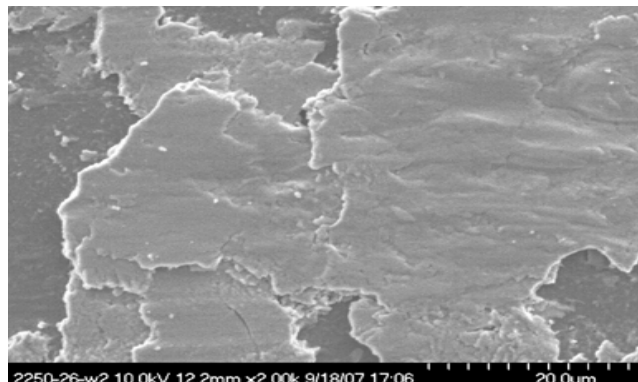


Figure 2. SEM Micrograph of Scuffed SiC Showing Extensive Metal Transfer

Because of the significance/role of metal transfer in the scuffing of ceramics, effort was devoted to elucidate the processes and mechanisms involved in metal transfer. Scanning electron microscopy (SEM) of ceramic surfaces subjected to severe sliding

contact in scuffing tests revealed highlighting of the grain boundary, as illustrated in Figure 3. This phenomenon, which we termed “tribo-mechanical etching,” is the precursor to the formation of a metal transfer layer. In addition to etching, micro-fracture in the vicinity of grain boundaries also occurred (Figure 3c). Figure 3b also shows the nucleation of material transfer.

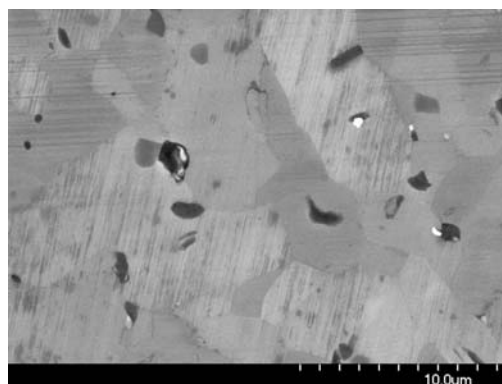


Figure 3a. SiC material

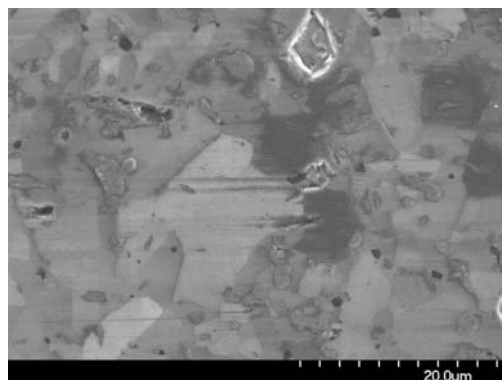


Figure 3b. SiC showing metal transfer initiation

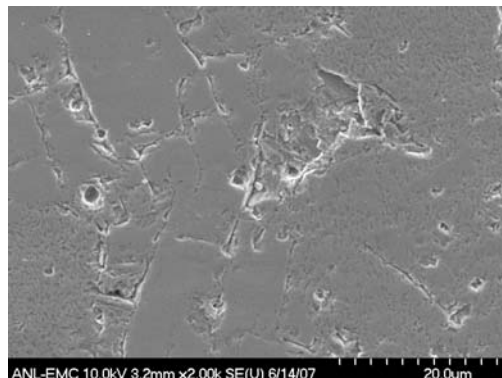


Figure 3c. PSZ material showing grain boundary microfracture and etching

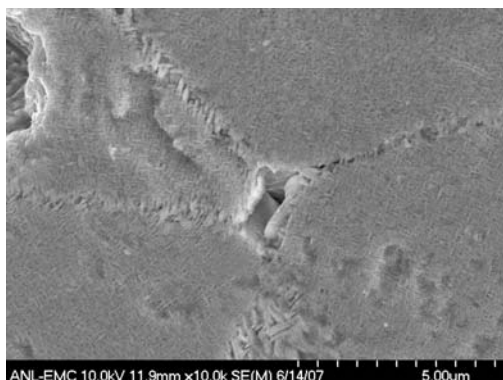


Figure 3d. PSZ showing tetragonal precipitat

Figure 3. SEM Micrograph Showing Tribo-Mechanical Etching of Different Ceramic Materials

Based on these observations, we propose that several mechanisms occur during scuffing of ceramic materials: anisotropic plastic deformation; uneven metal transfer from grain to grain due to differences in surface energy; thermal etching; and different wear rates in different phases. Once metal transfer initiates, it will continue to grow with increasing contact severity imposed by the scuffing test. At a critical metal transfer level, macro-scuffing occurs as a result of shear instability between the transfer layer and the steel counterpart.

Tribochemical Film Analysis

The main focus of this task is friction reduction under the boundary regime through the formation of low-shear-strength boundary films. Once such films are identified, various characterization techniques are applied to determine the structure, composition, and properties of the films. During FY 2008 low-friction boundary films were produced from both model additives and fully formulated lubricant. Figure 4 shows an example of significant friction reduction under the boundary lubrication regime with a formulated oil at 100°C. A boundary friction as low as 0.04 was achieved as compared to the typical value of 0.1 upon the formation of these films. Post-test analysis conducted on the low-friction boundary films included SEM and EDX. Figure 5 shows the secondary electron image (SEI) of the film and the EDX spectrum of the lower-friction boundary film. In addition, focused ion beam (FIB) analysis was conducted on the film to assess the thickness through use of the cross-sectional view of the film shown in Figure 6. The plan is to extract a transmission

electron microscopy sample with the FIB so as to determine the structure and composition of the low-friction boundary films.

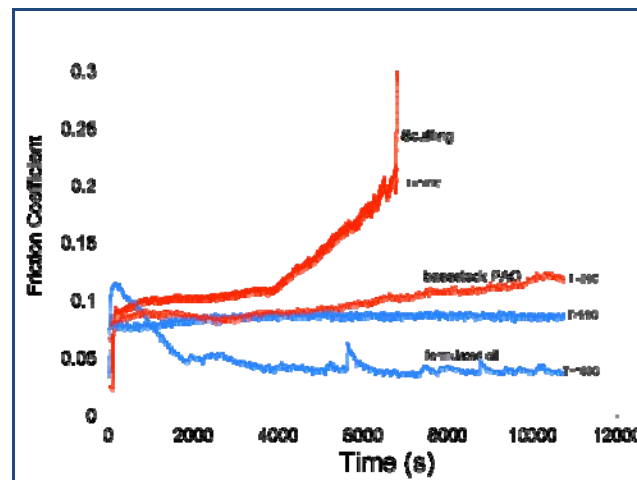


Figure 4. Variation of Friction Coefficient with Time Showing Effect of Boundary Films in Tests with Poly-alpha Olefin (PAO) and Formulated Oil at Room Temperature and 100°C

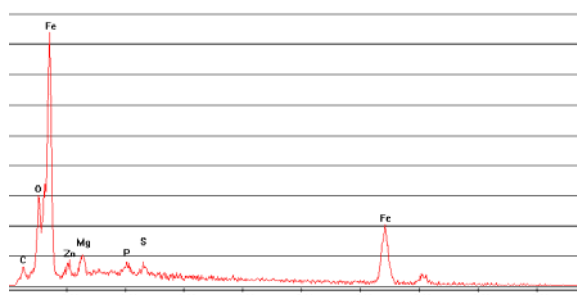
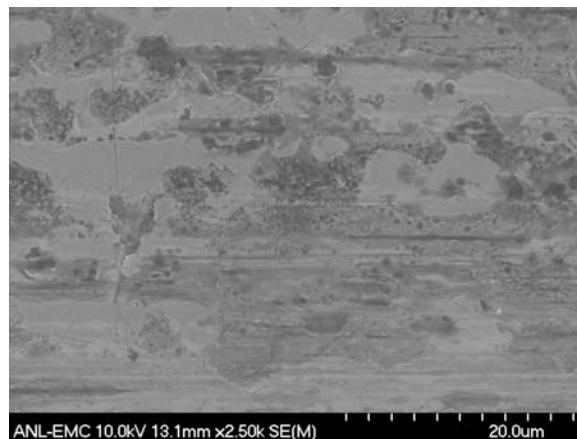


Figure 5. SEM Micrograph and EDAX Spectrum of Low-Friction Boundary Film produced from a Fully Formulated Lubricant

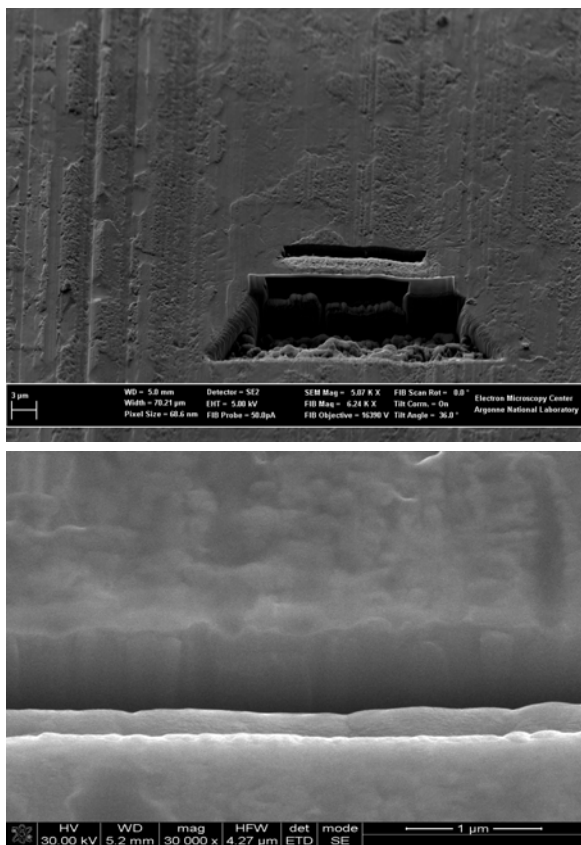


Figure 6. FIB Analysis of Low-Friction Boundary Films for Cross-Sectional Examination

Conclusions

Significant progress was made in the two major tasks of this project during FY 2008. In the first task, material pairs with a high CSI (indicative of scuffing resistance) were evaluated. The mechanisms for scuffing in these material pairs were elucidated, providing a pathway for further improvement in scuffing resistance. The development of materials with enhanced scuffing resistance will facilitate the development of high-power-density components and systems.

The second task involved characterization of low-friction boundary films produced from a model lubricant and fully formulated lubricant. Post-test analysis of the films by SEM, EDX, and FIB is ongoing. These analyses will provide information on the thickness, composition, and structure of highly desirable low-friction boundary films.

Publications

C. Lorenzo-Martin, O.O. Ajayi, D. Singh, J.L. Routbort, and R.A. Erck, "Mechanism of Scuffing in Oil-Lubricated Structural Ceramic and Metallic Material Contact," Presented at KC Ludema International Symposium, STLE Annual Meeting, Cleveland, OH, May 18-22, 2008.

O.O. Ajayi, "Mechanism of Scuffing for Lubricated Metallic Near-Surface Material," Presented at KC Ludema International Symposium, STLE Annual Meeting, Cleveland, OH, May 18-22, 2008.

R.A. Erck, O.O. Ajayi, and J. Hernandez-Cintron, "Friction of Steel Sliding under Boundary Lubrication Regime in Commercial Gear Oils at Elevated Temperatures," Presented at STLE Annual Meeting, Cleveland, OH, May 18-22, 2008.

C. Lorenzo-Martin, O.O. Ajayi, R.A. Erck, and J.L. Routbort, "Tribo-mechanical Etching of Structural Ceramic Materials during Lubricated Severe Sliding Contact," *Wear* (in press).

B. Parasitic Energy Loss Mechanisms

Principal Investigators: George Fenske, Robert Erck, and Nicholaos Demas

Argonne National Laboratory

Argonne, IL 60439

(630) 252-5190 ; fax: (630) 252-4798 ; e-mail: gfenske@anl.gov

DOE Technology Manager: Lee Slezak

(202) 586-2335; Lee.Slezak@ee.doe.gov

Participants

Oyelayo Ajayi, Argonne National Laboratory

Zoran Fillipe, University of Michigan

Contractor: Argonne National Laboratory

Contract No.: DE-AC02-06CH11357

Objective

Develop and integrate mechanistic models of engine friction and wear to identify key sources of parasitic losses as functions of engine load, speed, and driving cycle.

Develop advanced tribological systems (lubricants, surface metrology, and component materials/coatings) and model their impact on fuel efficiency with a goal to improve vehicle efficiency by three percent in fiscal year (FY) 2012.

Develop engine component maps to model the impact on fuel efficiency for use in analytical system toolkits.

Develop database of friction and wear properties required for models of mechanistic friction and wear of coatings, lubricant additives, and engineered surface textures.

Validate mechanistic models by performing instrumented, fired-engine tests with single-cylinder engines to confirm system approaches to reduce friction and wear of key components.

Approach

Predict fuel economy improvements over a wide range of oil viscosities using physics-based models of asperity and viscous losses.

Model changes in contact severity loads on critical components that occur with low-viscosity lubricants.

Develop and integrate advanced low-friction surface treatments (e.g., coatings, surface texturing, and additives) into tribological systems.

Measure friction and wear improvements on advanced laboratory rigs and fired engines to confirm model calculations.

Develop component maps of parasitic energy losses for heavy-vehicle system models.

Accomplishments

Modeled the impact of low-friction coatings and low-viscosity lubricants on fuel savings (up to four percent) and predicted the impact of low-viscosity lubricants on the wear and durability of critical engine components.

Developed experimental protocols to evaluate the friction and wear performance of advanced engine materials, coatings, and surface treatments under prototypical piston-ring environments.

Evaluated the impact of a commercial additive on the friction properties of base fluids and commercial heavy-duty engine lubricants.

Developed protocols to deposit low-friction coatings on piston rings and evaluated their impact on the friction of a fully formulated engine lubricant.

Modified a single-cylinder diesel test stand to measure cylinder-bore friction under motored and fired conditions.

Developed lab technique to simulate piston-skirt/liner friction using prototypic components.

Future Direction

Apply superhard and low-friction coatings on actual engine components and demonstrate their usefulness in low-viscosity oils.

Optimize coating composition, surface finish, thickness, and adhesion to achieve maximum fuel savings.

Evaluate the impact of advanced lubricant additives on asperity friction.

Introduction

Friction, wear, and lubrication affect energy efficiency, durability, and environmental soundness of critical transportation systems, including diesel engines. Total frictional losses in a typical diesel engine may alone account for more than 10 percent of the total fuel energy (depending on the engine size, driving condition, etc.). The amount of emissions produced by these engines is related to the fuel economy of that engine. In general, the higher the fuel economy, the lower the emissions. Higher fuel economy and lower emissions in future diesel engines may be achieved by the development and widespread use of novel materials, lubricants, and coatings. For example, with increased use of lower viscosity oils (that also contain lower amounts of sulfur- and phosphorus-bearing additives) the fuel economy and environmental soundness of future engine systems can be dramatically improved. Furthermore, with the development and increased use of smart surface engineering and coating technologies, even higher fuel economy and better environmental soundness are feasible.

The integration of advanced lubricant chemistries, textured/superfinished surfaces, and advanced component materials and coatings necessitates a systems approach. Changes in one system component can readily change the performance of other components. For example, application of a hard coating on a liner to improve its durability may decrease the durability of the mating rings. Also, lowering the viscous drag will cause certain components (e.g., bearings) to operate under boundary lubrication regimes not previously encountered, resulting in accelerated degradation. A

systems approach is required to not only identify the critical components that need to be addressed in terms of energy savings, but also to identify potential pitfalls and find solutions.

The main goal of this project is to develop a suite of software packages that can predict the impact of smart surface engineering technologies (e.g., laser dimpling, near frictionless carbon, and superhard coatings) and energy-conserving lubricant additives on parasitic energy losses from diesel engine components. The project also aims to validate the predictions by comparison with experimental friction and wear data from Argonne National Laboratory (ANL). Such information will help identify critical engine components that can benefit the most from the use of novel surface technologies, especially when low-viscosity engine oils are used to maximize the fuel economy of these engines by reducing churning and/or hydrodynamic losses. A longer-term objective is to develop a suite of computer codes capable of predicting the lifetime and durability of critical components exposed to low-viscosity lubricants.

Starting in 2003, ANL and Ricardo, Inc. have collaborated to identify engine components that can benefit from low-friction coatings and/or surface treatments. The specific components have included rings, piston skirt, piston pin bearings, crankshaft main and connecting rod bearings, and cam bearings. Using computer codes, Ricardo quantified the impact of low-viscosity engine oils on fuel economy. Ricardo also identified conditions that can result in direct metal-to-metal contacts, which, in turn, can accelerate engine wear and asperity friction. Efforts were also initiated to identify approaches to validate the predictions under fired conditions.

ANL has focused on the development and testing of low-friction coatings under a wide range of sliding conditions with low- and high-viscosity engine oils. These coatings (such as near frictionless carbon) as well as laser-textured surfaces were subjected to extensive friction tests using bench-top rigs. The test conditions (i.e., speeds, loads, and temperatures) were selected to create conditions where direct metal-to-metal contacts will prevail, as well as situations where mixed or hydrodynamic regimes will dominate. Using frictional data generated by ANL, Ricardo estimated the extent of potential energy savings in diesel engines and identified those components that can benefit the most from such low-friction coatings and/or surface treatments. ANL developed a test rig to simulate engine conditions for piston rings sliding against cylinder liners – one of the major sources of parasitic energy losses identified in Ricardo's studies. The test rig is being used not only to identify candidate technologies (e.g., coatings and additives) that can provide the level of friction reduction assumed in the Ricardo models, but also to provide information on the impact of the technologies on material and component wear/durability.

During FY 2008, ANL modified the lab ring-on-liner test rig to accommodate piston-skirt-on-liner tests. Ricardo and the University of Michigan continued modifications to their single-cylinder Hydra test engine and initiated motored tests in advance of fired tests scheduled for FY 2010.

Results

Phase I and II activities for this project focused on modeling the impact of low-friction surfaces and low-viscosity engine lubricants on friction losses and fuel economy. Figure 1 [1-3] summarizes the results of Ricardo's calculations on the impact of boundary friction and engine lubricant viscosity on the fuel economy of a heavy-duty diesel-powered vehicle. These curves are based on detailed calculations of the friction mean effective pressure for the piston rings and skirt, valve-train components, and engine bearings under a range of driving conditions. The results predicted fuel savings up to four to five percent, depending on lubricant viscosity grade and asperity friction.

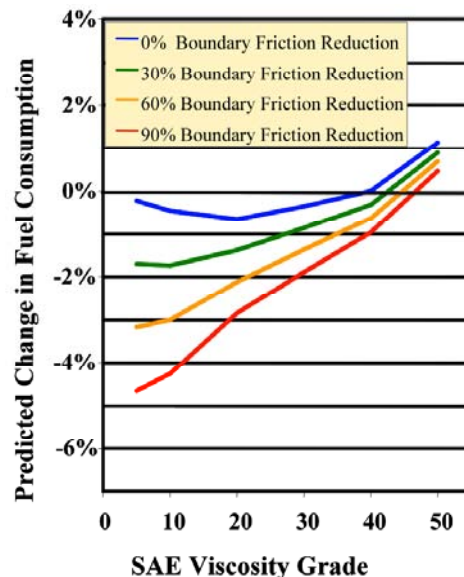


Figure 1. Graph of Predicted Change in Fuel Economy as a Function of Engine Lubricant Viscosity and Boundary Friction

A phase III activity was initiated to validate the calculations by tests using a non-fired diesel engine. The instrumentation for direct measurement of piston assembly friction in a motored, compression engine is based on the *fixed sleeve* methodology, where the friction force acting on the inner liner is transferred to the outer fixed sleeve instrumented with strain gauges. The technique is robust and facilitates easy swapping of pistons or rings for testing of multiple combinations of coated/uncoated components. The instrumentation has been completed for the University of Michigan/Ricardo single-cylinder Hydra engine and a cylinder bore of 84 mm.

ANL activities focused on measurements of the friction properties of candidate low-friction technologies in a reciprocating test rig that simulated ring-on-liner conditions. Figure 2 shows a photograph of the test rig. The test system uses segments of rings and liners obtained from standard rings and liners. The liner diameters are currently 128 mm, 137 mm, and 145 mm, which are comparable to diameters modeled by Ricardo and in common use in heavy-duty diesel engines. The system is capable of applying loads up to 2000 N, speeds up to 10 Hz, strokes up to 37 mm, and temperatures to 300°C. Data recorded during the tests include friction forces, temperature, ring position, and contact resistance (between the ring and liner) at rates in excess of 2000 Hz. High data

acquisition rates (above 2000 Hz) are used to obtain “flash shots” of the friction, position, and contact resistance during each stroke. Such information provides the detailed data required to determine which lubrication regime (boundary, mixed, or hydrodynamic) is dominant during the stroke.

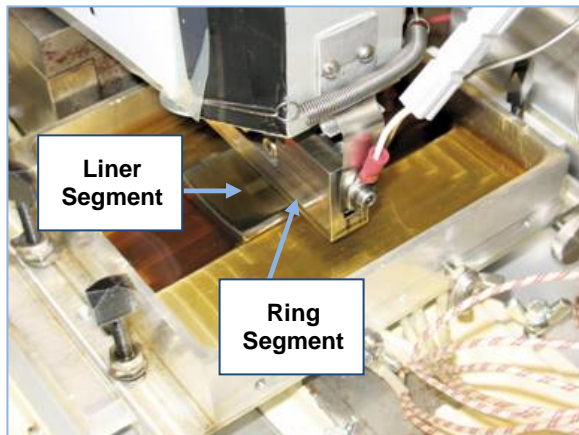


Figure 2. Ring-on-Liner Test Rig Used to Simulate Reciprocating Motion between a Ring Segment and Liner Segment

Figure 3 shows data obtained during a typical run, which can last up to 10 days, for poly-alpha olefin (PAO) 10 with a commercial boric-acid-based additive. The test temperature was cycled between room temperature and 100°C to simulate engine conditions. The blue curve (average friction coefficient from 20 measurements) changes with time (and temperature). The friction at the start of the first heating ramp to 100°C started out high (around 0.1), then rapidly decreased to 0.08 as the additive reacted with the surface to form a low-friction tribofilm. When the test temperature decreased, the viscosity increased, leading to greater fluid film separation and, hence, lower friction. The contact resistance can be used to qualitatively assess the formation of tribological films at the interface. A low contact resistance indicates metal-to-metal contact, while high resistance indicates formation of either a full fluid film separating the ring and liner, or an insulating tribofilm on the ring and/or liner surface. As the sample cooled, the friction decreased, and the minimum friction continued to drop with each cycle – indicating break-in of the ring and liner surfaces. The contact resistance data indicate the formation of a tribofilm at elevated temperatures. At room temperature, the contact resistance dropped,

suggesting the film had been removed by the sliding action.

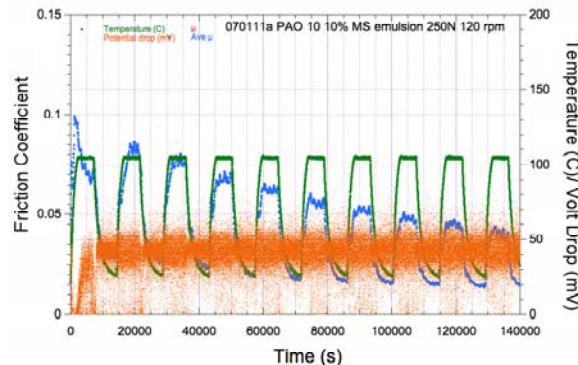


Figure 3. Friction Response of Prototypic Heavy-Duty Ring and Liner Segments, during laboratory tests with PAO 10 and a commercial boric-acid-based additive.
Blue: 20-point running average of friction;
Green: temperature; and Orange: contact resistance.

The example shown in Figure 3 used a pure base oil (PAO 10) that contained an emulsified commercial additive. The friction coefficient for this fluid decreased over time at room temperature and 100°C. The friction at 100°C decreased from 0.1 at the start to 0.04 at the end of the run. The room-temperature friction dropped from 0.03 at the start to less than 0.02 at the end. False-color 3D imaging of the ring segment used in these tests suggests the low-friction behavior in Figure 3 can be attributed to the smoothening that occurred during these runs as part of normal wear-in or accelerated wear-in of the surface [4].

Efforts were also initiated to develop protocols to deposit near frictionless carbon and superhard nanocomposite coatings on ring and liner segments. Discussions with MAHLE indicated that it is critical to develop processing conditions that minimize ring distortion and warpage. Detailed measurements of the ring dimensions, including ring gap separation before and after deposition, were carried out with an optical microscope. The superhard nanocomposite coating [5] was used to deposit MoCuN coatings on as-received rings (cast iron, nitrided steel, and CrN-coated nitrided steel prepared by physical vapor deposition). The ring gaps showed no appreciable changes in length – all changes were less than 0.1 mm – well below the 0.5-mm limit specified by MAHLE.

During FY 2008, ANL activities also focused on extending measurements of the friction properties of candidate low-friction from piston-ring/liner to piston-skirt/liner conditions. Figure 4a is a photograph of a piston showing the regions of the piston where test pieces are sectioned. Figure 4b is a photograph of the test rig. The rig uses segments of 128-mm diameter skirts and liners—comparable to those modeled by Ricardo and in common use in heavy-duty diesel engines. The system is capable of applying loads up to 2000 N, speeds up to 10 Hz, strokes up to 37 mm, and temperatures to 300°C. Data recorded during the tests include friction forces, temperature, ring position, and contact resistance (between the ring and liner) at rates in excess of 2000 Hz. High data acquisition rates (above 2000 Hz) are used to obtain “flash shots” of the friction, position, and contact resistance during each stroke. Such information provides the detailed data required to determine which lubrication regime (boundary, mixed, or hydrodynamic) is dominant during the stroke.

Figure 5 shows data obtained during a typical run. The test was conducted at room temperature. The blue curve (average friction coefficient) changes with time and reciprocating speed. At 60 s the load was decreased. The friction was nearly identical whether high load or low load, but generally decreased with increasing reciprocating speed. This finding is attributed to greater oil entrainment and, therefore, oil film thickness at higher speeds.

When the test temperature was increased to 100°C (Figure 6), friction was again nearly identical whether high load or low load, but generally increased with increasing reciprocating speed.

The contact resistance can be used to qualitatively assess the formation of tribological films at the interface. A low contact resistance indicates metal-to-metal contact, while high resistance indicates formation of either a full fluid film separating the ring and liner, or an insulating tribofilm on the ring and/or liner surface. The friction traces indicate that sliding is in the boundary lubrication regime at room temperature, and that no tribofilm forms. At 100°C a small amount of tribofilm may have formed, but when the load was reduced, the contact resistance indicated a near absence of metal-to-metal contact.

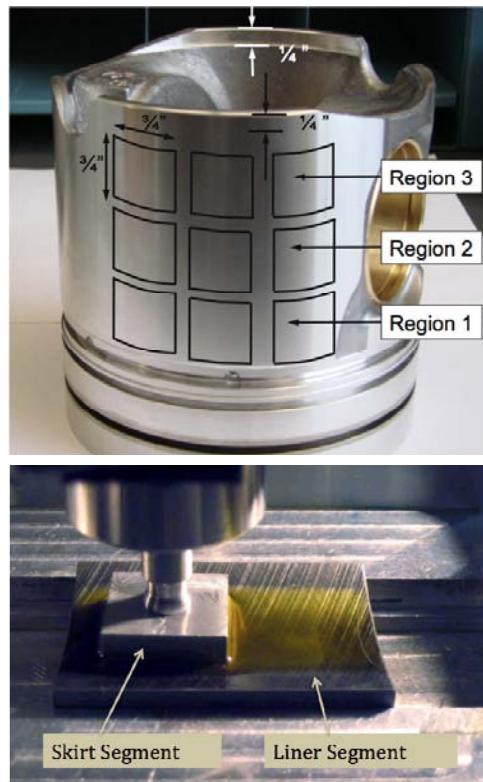


Figure 4. a) Photograph of Piston Prior to Sectioning and b) Skirt-on-Liner Test Sliding System Used to Simulate Reciprocating Motion between a Piston Skirt and Liner Segment in Oil Bath

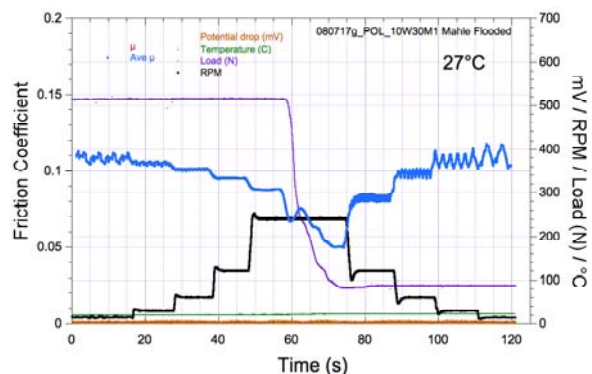


Figure 5. Friction Response of Unmodified Piston Skirt Sliding on Liner, during laboratory tests with formulated synthetic engine oil (10W-30) at room temperature. Black – reciprocating speed; Purple – load; Blue – running average of friction; Green – temperature; and Orange – contact resistance.

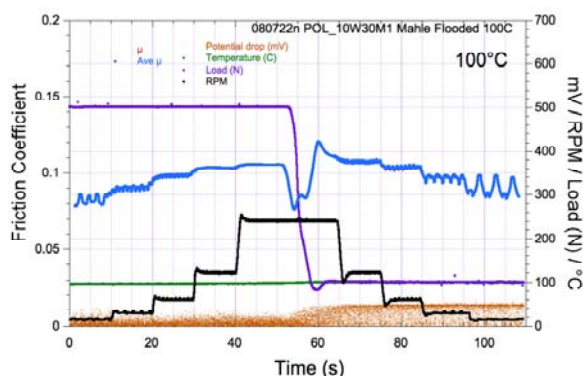


Figure 6. Friction Response of Unmodified Piston Skirt Sliding on Liner, during laboratory tests with formulated synthetic engine oil (10W-30) at 100°C. Black – reciprocating speed; Purple – load; Blue – running average of friction; Green – temperature; and Orange – contact resistance.

This result is attributed to tribofilm formation. The viscosity of the oil was much smaller at 100°C than room temperature, and comparing Figures 5 and 6 ruled out the formation of a hydrodynamic-oil insulating layer.

Figure 7 shows a “snapshot” graph of several sliding cycles at 100°C, with red showing the instantaneous friction coefficient. This test was performed in commercial motor oil. Unlike ring friction, in which the friction is highest at the low sliding speed where the oil film thickness and the lambda ratio are small, the skirt exhibits the highest friction in mid-stroke.

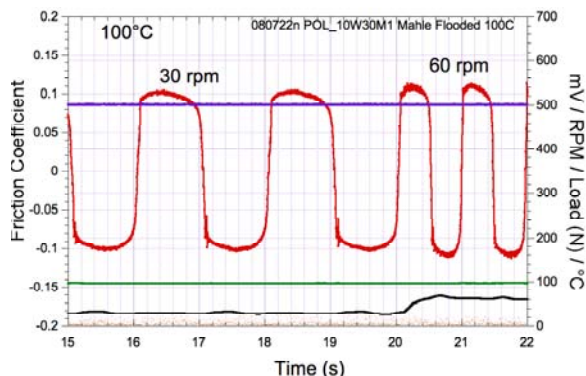


Figure 7. Instantaneous Friction Response of Unmodified Piston Skirt Sliding on Liner, during laboratory tests with formulated synthetic engine oil (10W-30) at 100°C. Black – reciprocating speed; Purple – load; Red - friction; Green – temperature; and Orange – contact resistance.

Figure 8 shows false-color 3D images of the skirt segment used in the tests. The top shows the texture of an as-received, unworn skirt. The skirts are finished with strong circumferential machining marks. The bottom of Figure 8 shows a much smoother surface and illustrates how wear can occur.

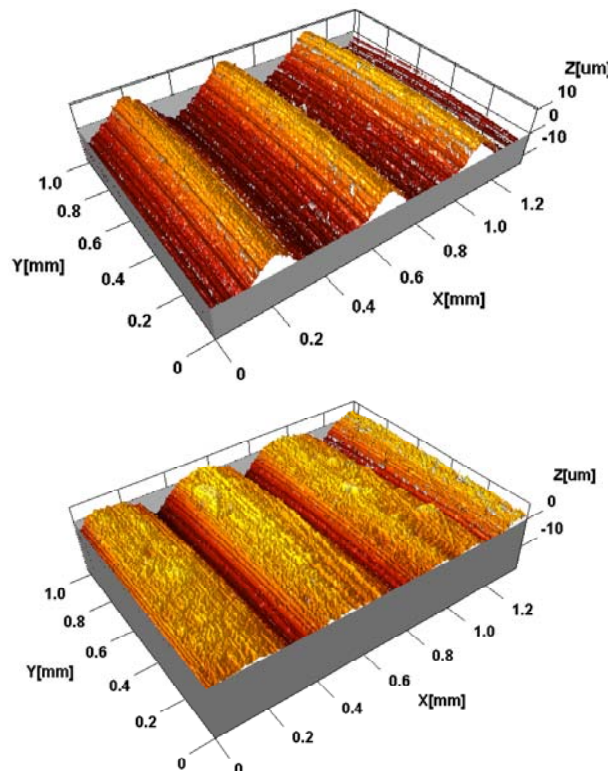


Figure 8. False-Color 3D Image of Skirt Segment Showing As-Received Surface Texture (top) and Polished Texture (bottom) caused by Wear

Summary

Computer simulations of parasitic energy losses in diesel engines indicate that fuel savings up to five percent can be achieved through the use of low-viscosity engine lubricants and low-friction surface treatments. Work is underway to experimentally validate the models by tests with a fired, single-cylinder diesel rig outfitted with an instrumented fixed-sleeve to measure the friction forces continuously as a function of crank angle.

A piston component test rig was developed and brought on-line to validate the friction coefficient data used to model the parasitic friction losses, as well as to optimize advanced surface modification technologies for engine applications. Tests are underway to evaluate two technologies: a boric-acid-

based lubricant additive and a surface texturing technique. Laboratory tests using the ring-on-liner rig indicated that friction can be significantly reduced by using boric-acid based additives. Further tests are in progress to evaluate tribological test results for piston skirt segments, both uncoated and coated with a solid film, in low-viscosity engine lubricants. Use of additives and surface texturing, in addition to low-friction coatings, will be further examined and optimized in FY 2009 in preparation for fired engine tests on the instrumented Hydra test engine in FY 2010.

FY 2009 activities with the instrumented Hydra engine will establish baseline friction data for comparison to low-friction technologies. Part of this task will involve in-situ friction measurements of unformulated base fluids (at two viscosities) with and without low-friction additives. Subsequent tasks will concentrate on measurements of low-friction technologies (e.g., low friction coatings, superfinishing, textured surfaces, and low-friction additives).

References

- 1) I. Fox, Numerical Evaluation of the Potential for Fuel Economy Improvement due to Boundary Friction Reduction within Heavy-Duty Diesel Engines, ECI International Conf. on Boundary Layer Lubrication, Copper Mountain, CO, Aug. 2003.
- 2) George Fenske, Parasitic Energy Loss Mechanisms, FY 2006 Progress Report for Heavy Vehicle Systems Optimization.
- 3) George Fenske, Parasitic Energy Loss Mechanisms: Impact on Vehicle System Efficiency, U.S. Department of Energy Heavy Vehicle Systems Review, April 18-20, 2006, Argonne National Laboratory, Argonne, Illinois.
- 4) George Fenske, Parasitic Energy Loss Mechanisms, FY 2007 Progress Report for Heavy Vehicle Systems Optimization.
- 5) A. Ozturk, K.V. Ezirmik, K. Kazmanli, M. Urgen, O.L. Eryilmaz, and A. Erdemir, Comparative Tribological Behaviors of TiN-, CrN- and MoN-Cu Nanocomposite Coatings, *Tribo. Int.* 41(1): 49-59 (2008).

Acknowledgments

Argonne is managed by UChicago Argonne, LLC, for the U.S. Department of Energy under contract DE-AC02-06CH11357.

C. Superhard Coatings

Principal Investigators: A. Erdemir, O. Ajayi, and O. Eryilmaz

Argonne National Laboratory

Energy Systems Division, Argonne, IL 60439

(630) 252-6571; fax: 630-252-4798; e-mail: erdemir@anl.gov

DOE Technology Manager: Lee Slezak

(202) 586-2335; Lee.Slezak@ee.doe.gov

Contractor: Argonne National Laboratory

Contract No.: DE-AC02-06CH11357

Objective

Design, develop, and implement superhard and low-friction coatings to increase the durability, fuel economy, and environmental compatibility of engine systems.

Characterize and verify superhard and low-friction coatings performance (bench-top and engine studies).

Elucidate friction and wear-reducing mechanisms using surface analytical techniques.

Confirm performance under severe running conditions of fired engines.

Demonstrate commercial-scale production of such coatings.

Transfer demonstrated technology to end users (both engine and coating companies).

Approach

Obtain, inspect, and prepare test samples and components for coating deposition.

Develop optimized deposition protocols that can consistently produce superhard coatings on these samples and components.

Characterize coating adhesion, thickness, and surface roughness.

Test and demonstrate superior friction and wear performance under a wide range of conditions using bench-top test machines and actual engines.

Analyze the test data and determine coating performance and benefits.

Prepare reports.

Accomplishments

During fiscal year (FY) 2008, installed a pulsed DC power source that resulted in higher deposition rates and a much denser coating with stronger adhesion to substrate materials.

Used this new power source and further optimized the deposition conditions to produce superhard coatings on a variety of test samples and actual engine components.

Confirmed the extreme resistance of these coatings to wear and scuffing failures.

Demonstrated the superior friction-reducing abilities of the coatings under a wide range of sliding conditions.

Employed surface analytical tools to better understand their friction and wear mechanisms.

Two industrial partners signed option-to-license agreements with Argonne National Laboratory (ANL) for the commercialization of this technology.

One of the largest industrial coating manufacturers in the world is currently scaling up and will offer this coating to many engine companies and part suppliers.

Another surface engineering company started licensing discussions with ANL.

Future Direction

Validate structural, mechanical, and tribological properties of superhard coatings produced by industrial partners in production-size deposition systems.

Determine the coatings' long-term friction and wear performance under actual engine conditions (motored/fired).

Confirm durability.

Concentrate on technology transfer.

Increase collaboration with engine company partners.

Demonstrate cost competitiveness.

Demonstrate fuel-saving and emission-reducing benefits.

Finalize licensing talks and commercialize the coatings.

Introduction

Higher energy efficiency, longer durability, and lower emissions are highly desired attributes in future transportation systems. However, without further improvements in the surface mechanical and tribological properties of sliding, rolling, or rotating engine components, these attributes will be very difficult to realize. In particular, higher loads, speeds, temperatures, and other harsh operating conditions in future engine systems will render most traditional materials useless. Accordingly, the aim of this project is to design, develop, and implement novel superhard and low-friction coatings that can result in higher energy efficiency, longer durability, and lower emissions in future engines.

During FY 2008, much effort was directed toward further optimization, scale-up, and commercialization of our superhard coating technology. Specifically, a world-renowned coating company was selected to produce these coatings in a production-scale deposition system. Potential end users were involved, as they applied these coatings on their engine parts to be used for long-duration performance and durability tests.

Optimization and Characterization of Coatings

During FY 2008, optimization studies continued with emphasis on controlling coating microstructure and chemistry as well as thickness, hardness, and surface roughness. The control of surface roughness was particularly important for the initial or break-in frictional behavior of coated parts. To optimize the structural morphology and chemistry of superhard coatings, a number of deposition trials were pursued. In one of these, the target bias was changed, while in another the rotational speed of the sample holder was changed. Yet in another case, the location and/or orientation of samples with respect to the sputtering targets were changed. These studies indicated that the target bias and the rotational speed of samples were most important in improving coating morphology and chemistry. Studies on deposition temperature also yielded important information. Deposition at higher temperatures (i.e., above 300°C) always resulted in much denser coating morphology, but also a higher degree of internal stresses. These coatings were much harder (i.e., more than 30 GPa) than those deposited at lower temperatures. As for the control of surface roughness, higher rotational speeds and lower deposition temperatures were most effective. The use of higher bias voltage also had some positive effects. It resulted in a much smoother surface finish, and hence, a lower friction and wear during tribological tests. These coatings exhibited excellent bonding to

the substrate materials mainly because of the formation of a larger graded interface, which often results from greater inter-diffusion at or near the interface.

Optimizing the chemical composition of nanocomposite coatings is extremely important not only for tribological performance but also compatibility with lubricants, as we emphasized in previous reports. During last year's studies, it was suspected that the presence of very small amounts of oxygen in nanocomposite coatings might be beneficial to the frictional behavior of such coatings under boundary-lubricated sliding conditions. During FY 2008, more effort was devoted to investigating that possibility, and in the end, the conclusion was reached that oxygen may indeed have some beneficial effects on the frictional performance. The presence of oxygen within the film appears to result in smaller grains and denser film morphology, as well as smoother surface finish, which in turn result in better tribological behavior during sliding tests. Oxygen may also improve the responsiveness of coatings to the lubricants.

Based on the knowledge gained from the above studies, a series of smooth and dense coatings were produced and their friction and wear performance was determined in bench-top test machines. Figure 1 shows the frictional performance of an optimized coating under lubricated sliding conditions. As is clear, the friction coefficient of this coating is very low from the beginning, mainly because of its smooth surface finish and optimized chemical composition.

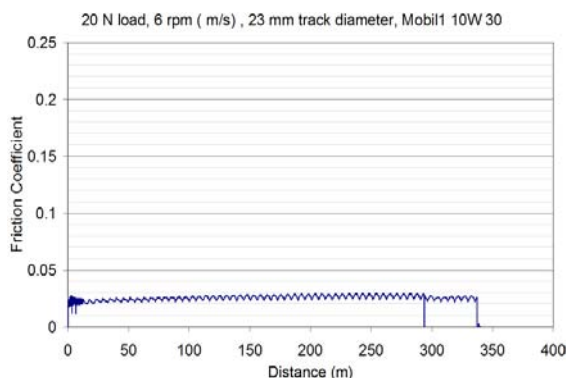


Figure 1. Friction Coefficient of a Smooth Superhard Nanocomposite Coating under Lubricated Sliding Conditions

Scale-up and Commercialization Activities

As part of our scale-up and commercialization activities, an industrial coating company was closely involved. The company was interested in the technology and in offering it for large-scale applications in transportation fields. The effort included teaching them how to produce the coating in their commercial-scale deposition system. A post-deposition characterization was also conducted and the coated parts were evaluated, and the deposition protocol was optimized. As part of this collaboration, coating company representatives have visited us several times for licensing talks, and teleconferences were held almost weekly to discuss the progress being made and what to do next. Initial trials in their large deposition systems were not successful. The produced coatings had several problems. Specifically, they had the undesirable columnar morphology shown in Figure 2. Their deposition rate was somewhat lower than that achieved at ANL. The amount of Cu in the coatings was much lower than that needed for ideal tribochemistry during sliding. As a result, the coatings exhibited low hardness (less than 20 GPa); their adhesion to substrate material was poor; and most importantly, their tribological performance was inferior to the coatings that we have been producing at ANL.

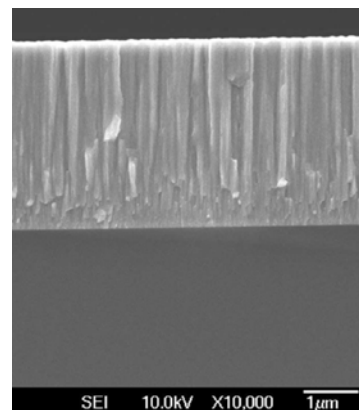


Figure 2. Structural Morphology of an initial MoN-Cu Coating Produced by the Industrial Coating Company

As a result, the decision was made to pursue a more systematic approach. To solve the problem associated with Cu deficiency, the company was asked to switch to a Mo/Cu composite target from two monolithic targets (one for Mo, one for Cu). To achieve more uniform Cu distribution within the coating, the company was instructed to increase the rotational

speed of the sample holder. To increase the deposition rate, it was asked to apply lower bias voltages to the substrate holders and higher power to the sputtering targets. To improve hardness, to the company increased the deposition temperature, which also fixed the problems associated with chemical stoichiometry.

After each deposition trial, the samples were recovered. Some of the recovered samples were shipped to us for chemical, mechanical, and tribological characterization. Others were subjected to the coating company's tests for hardness, adhesion, thickness, etc. The results from these studies were compared and discussed in detail during our weekly teleconferences. After several rounds of coating trials, films could be deposited at the coating company that looked almost the same as the ones that had been produced at ANL. Figure 3 shows the structural morphology of the latest coating produced by the coating company using their commercial-scale deposition system. Compared with the earlier coatings (Figure 2), this coating looked dense and essentially free of the columnar morphology. The coatings produced in the beginning had a columnar morphology and were not hard enough. The coating produced after several rounds of optimization studies was essentially featureless and had the same morphological character as our original superhard coating.

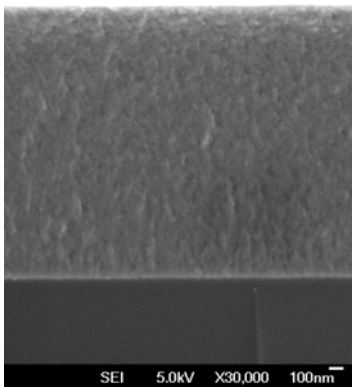


Figure 3. Structural Morphology of the Latest Coating from Coating Company

Tribological Studies

Tribological testing of the optimized superhard coatings produced by the coating company is being carried out at ANL and at potential end-user companies. The tests at ANL are carried out in pin-

on-disk and block-on-ring type systems to determine the friction, wear, and scuffing behaviors of coated samples. All of these tests are performed under severe loading conditions to achieve a boundary-lubricated sliding regime. As mentioned earlier, the initial coatings failed to provide low friction and wear, and they could not be tested under heavy loadings of the block-on-ring test machine. Because of poor adhesion, these coatings would fracture or delaminate from the rubbing surfaces.

The latest coatings are resistant to wear and scuffing (perhaps due to their superhardness of about 40 GPa), but their frictional performance needs further improvement. Specifically, the friction coefficients of these latest coatings either change during the course of sliding tests (i.e., low to start with but increase toward the end of test) or are somewhat higher than those of the coatings we have been producing in our deposition system. Using surface analytical tools, we plan on examining the sliding surfaces of these coatings and determining whether there is a boundary film. If so, the nature of the tribochemical films forming on the surface will be analyzed and compared to those typically found on the sliding surfaces of our films.

Using the block-on-ring test machine, we performed a series of scuffing tests on some of the coatings provided by the outside company. Most of these coatings passed the scuffing tests and endured the severe loading conditions. In a few cases, some coating delamination or wear was observed, but most of the coatings exhibited scuffing behavior similar to that of the original coatings.

In recent months, superhard coatings have been applied to tappets and piston rings and subjected to performance tests at engine companies. These coatings performed extremely well in the wear and scuffing tests and resulted in 75 percent reduction in friction in the case of tappets. The company that provided the tappets was very impressed with the test results and will continue to do more tests before reaching a decision for large-scale applications. If the friction coefficients of these coatings can be reduced even further (preferably to the same level as shown in Figure 1), then the full-scale production of superhard coatings should be possible in commercial deposition systems, and these coatings could then be used in actual engines.

Conclusions

During FY 2008, efforts were directed toward further optimization and scale-up of the superhard coating technology. Specifically, with the help of a commercial coating company, these coatings were produced in commercial-scale deposition systems and extensive tests were performed to determine their mechanical and tribological properties. Surface and structure analytical studies were also performed on these coatings to determine their structural morphology and chemical compositions. Tribological tests of such coatings in our laboratory confirmed their extreme resistance to wear and scuffing, although the friction coefficients of these coatings were somewhat higher than those of the original coatings. In FY 2009, effort will be in part concentrated on further reducing the friction coefficient of these coatings. However, the main focus will be on applying these coatings to a large variety of engine components (tappets, valve lifters, fuel injectors, piston rings, etc.) and testing them in actual engines. Currently, work is being conducted with several engine companies and with the coating company in order to apply the coating to their parts.

Patents and Publications

During FY 2008, a patent application was filed in the U.S. Patent and Trademark Office. In addition, several papers were published and/or presented on the work that was performed under this project:

Erdemir, A.; Eryilmaz, O.; Urgen, M.; Kazmanli, K., "Development of Multi-functional Nano-composite Coatings for Advanced Automotive Applications," Invited Plenary Paper, 16th International Colloquium on Tribology: Automotive and Industrial Lubrication, Stuttgart/Ostfildern, Germany, January 15-17, 2008.

Erdemir, A.; Eryilmaz, O.L.; Urgen, M.; and Kazmanli, K., "Lubricant-Friendly MoN-Cu Coatings for Extreme Tribological Applications," AVS 54th International Symposium and Exhibition, Seattle, WA, October 14-19, 2007.

Erdemir, A.; Urgen, M.; Eryilmaz, O.; Kazmanli, K.; Ezirmik, V., "Tribological Behaviors of $\text{MoN}_x\text{-Cu}$ and -Ag Nanocomposite Coatings under Boundary Lubricated Sliding Conditions," International Conference on Metallurgical Coatings and Thin Films, San Diego, CA, April 28, 2008 - May 2, 2008.

Ezirmik, V.; Kazmanli, K.; Eryilmaz, O.L.; Erdemir, A.; Urgen, M., "Friction and Wear Behavior of Nanocomposite Mo-N-Ag Coatings under Boundary Lubricated Sliding Conditions," STLE Annual Meeting, Cleveland, OH, May 18-22, 2008.

Erdemir, A.; Eryilmaz, O. L., "Lubricant-Friendly, Super-hard and -Low Friction Coatings by Design: Applications in Engines," 14th Diesel Engine-Efficiency and Emissions Research Conference, Dearborn, MI, Aug. 4-7, 2008.

Erdemir, A.; Eryilmaz, O.L., "Development of MoN-Ag-based Nanocomposites Films for Severe Tribological Applications," AVS 55th International Symposium and Exhibition, Boston, MA, Oct. 19-24, 2008.

Ajayi, O.; Erck, R.; Erdemir, A.; Fenske, G., "Effect of EGR on Diesel Engine Oil Degradation and Impact on Wear," 14th Diesel Engine-Efficiency and Emissions Research Conference, Dearborn, MI, Aug. 4-7, 2008.

Erdemir, A.; Eryilmaz, O.L.; Urgen, M.; Kazmanli, K., "Development of self-Lubricating Nano-composite Coatings," Plenary Lecture, International Conference on Functional Coatings, Budapest, Hungary, March 30-April 2, 2008.

D. Residual Stresses in Thin Films*

*This project is jointly funded by Propulsion Materials and Heavy Vehicle Systems Optimization

Principal Investigators: D. Singh and J. L. Routbort (coworker: Cinta Lorenzo-Martin)

Argonne National Laboratory

9700 S. Cass Avenue, Argonne, IL 60439-4838

(630) 252-5009; dsingh@anl.gov

DOE Technology Manager: Lee Slezak

(202) 586-2335; lee.slezak@ee.doe.gov

Contractor: UChicago Argonne LLC

Contract No.: DE-AC03-06CH11357

Objective

Measure residual stresses in thin films and coatings as a function of film thickness, and relate stresses to film properties such as hardness, fracture toughness, and adhesion energy to relate to film processing variables and to predict durability.

Use techniques developed for measurements of residual stresses in thin films and coatings to measure residual stresses in layered structures produced by joining by high-temperature deformation and to improve their mechanical properties.

Approach

Develop X-ray technique to measure change of lattice parameter of coating constituents as a function of depth and hence to calculate the lattice strains and stresses.

Develop indentation technique to measure hardness, fracture toughness, and adhesion energy of films and coatings.

Relate stresses, properties, and processing conditions to film durability.

Accomplishments

Advanced Photon Source (APS) used to measure stresses in 3- μm thick thin films of nanocrystalline MoN and MoCuN deposited on silicon and steel substrates as a function of depth.

Stresses were found to be sensitive to deposition conditions and thermal annealing.

Preliminary coating/film adhesion energies measured using indentation.

Demonstrated that by proper selection of materials the fracture strength of a composite is increased.

Future Directions

Develop indentation technique to measure film adhesion.

Investigate stresses in superhard, nanocrystalline MoCuN films as a function of deposition conditions and Cu concentration on steel substrates as well as investigate other coatings systems applicable for engine applications.

Introduction

Plastic-joining has been applied successfully to various advanced ceramic and intermetallic materials [1-2]. However, some limitations arise when dissimilar materials are joined because of the residual stresses generated upon cooling as a result of the coefficient of thermal expansion (CTE) mismatches.

Mora et al. [3-4] studied the development of residual stresses in zirconia toughened alumina (ZTA) composites. Because zirconia has a higher CTE than alumina, stresses develop upon cooling during the sintering process resulting in compression of the alumina phase. In addition to the stresses in the monolithic materials, additional thermal residual stresses arise when different compositions of ZTA materials are joined by plastic deformation.

Gutierrez-Mora et al. [3-4] showed that the tensile stress peak is at a short distance away from the joint interface, and coincided with the fracture location during the flexural tests [4]. In general, the presence of residual tensile stresses may pose a detrimental effect on the mechanical properties of joined components.

The intent of this study is to demonstrate that residual stresses, produced during joining by high-temperature plastic deformation, can be utilized effectively for the enhancement of the mechanical properties. The role of residual stresses generated from high-temperature plastic joining is considered for two different compositions (and CTE) of ZTA composites. These composites were joined by plastic deformation to produce a layered structure.

Compressive stresses generated in the low CTE phase material are shown to contribute to a strength enhancement. Magnitudes of the residual stress were experimentally measured and correlated to the increase in strength. It is proposed that such an approach can be used for enhancing strength and reliability of as-fabricated components as well as of existing structures.

Material Design

In this study, the proposed approach is to fabricate a layered structure (as shown in Figure 1) in which a material, A, with a specific thermal expansion is sandwiched between a different material, B, with a different CTE. Materials A and B can be selected with the appropriate CTE and high-temperature

deformation characteristics. To generate compressive residual stresses in the outer layers (A), CTE of material B needs to be higher than that of material A.

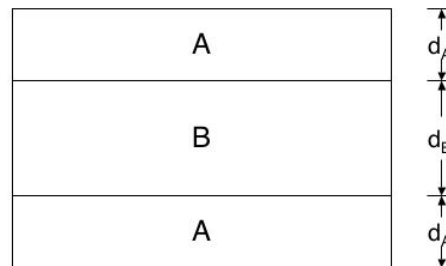


Figure 1. Schematic of the layered structure fabricated by plastic deformation.

For a perfectly joined interface, the average residual stresses generated in the layers A and B can be given as [5]:

$$\sigma_A = \frac{-E_A E_B d_B \Delta \varepsilon_o}{(1-\nu)(2E_B d_A + E_A d_B)} \quad (1)$$

$$\sigma_B = \frac{2E_A E_B d_A \Delta \varepsilon_o}{(1-\nu)(2E_A d_A + E_B d_B)} \quad (2)$$

E_A , E_B are Young's modulus for materials A and B, respectively, ν is the Poisson's ratio, and $\Delta \varepsilon_o$ is the difference in the strain between the two layers and can be given in terms of the CTE of the two materials and the cool down temperature range (ΔT) over which the stresses are generated:

$$\Delta \varepsilon_o = \Delta \alpha \Delta T = (\alpha_A - \alpha_B) \Delta T \quad (3)$$

It should be noted that from simple force balance,

$$\sigma_B(d_B) + \sigma_A(2d_A) = 0 \quad (4)$$

From (1), assuming $E_A = E_B$, surface compressive stress in outer layer A can be given as:

$$\sigma_c = -\frac{d_B E \Delta \varepsilon_o}{(1-\nu)(2d_A + d_B)} \quad (5)$$

where, $(2d_A + d_B)$ the total thickness of the layered composite.

Assuming that the failure occurs at the outer surface A, fracture stress can be given simply as [5]:

$$\sigma_f = \sigma_{fA}^o - \sigma_c \quad (6)$$

where, σ_{fA}^o is the fracture stress for monolithic material A, and σ_c is the compressive stress in material A given by (5). Upon substitution,

$$\sigma_f = \sigma_{fA}^o + \frac{d_B E (\alpha_A - \alpha_B) \Delta T}{(1 - \nu)(2d_A + d_B)} \quad (7)$$

To demonstrate the fracture strength enhancement from residual stresses/strains generated from joining by high-temperature plastic deformation, layered composite system of ZTA is considered in which outer layers have 60 vol. % alumina and middle layer has 40 vol. % alumina. The material properties for these materials are taken from Gutierrez-Mora et al. [4] and are listed in Table 1.

Table 1. Material Properties of ZTA Composites

Material	ZT60A	ZTA40A
E (Gpa)	320	320
CTE (10^{-6})	10.22	10.68
s_f^o (Mpa)	580	700
ν	0.26	0.26

Based on the material properties for ZT60A and ZTA40A as listed in Table 1 and a cooling temperature, ΔT , of 1350 °C, the residual stresses generated in the surface layers, obtained from Equation 2, as a function of the outer layer (A) thickness are plotted in Figure 2. In these calculations, the inner layer thickness was kept constant at a value of 3.5 mm, and the thickness of outer layer varied from 0.1 mm to 0.4 mm. As shown in the plot, residual compressive stresses increase with decreasing outer layer thickness. By changing the relative thicknesses, d_A and d_B , and the CTEs of materials A and B, it is envisioned that the residual stresses can be manipulated and consequently the fracture behavior of the layered composite structure.

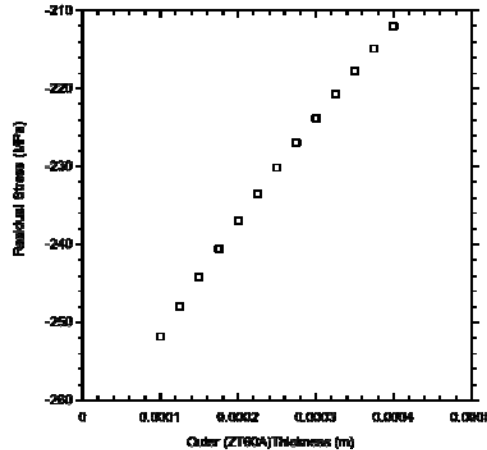


Figure 2. Residual stresses generated as a function of outer layer thickness for ZT60A/ZT40A/ZT60A layered structure

The predicted fracture strength (Equation 7) for failure at the surface is shown in Figure 3 as a function of outer layer thickness. As one would expect, the strength values decrease with increasing surface layer. Nevertheless, the increase in strengths achieved can be greater than 830 MPa or greater than 20 percent by introducing surface compressive stresses.

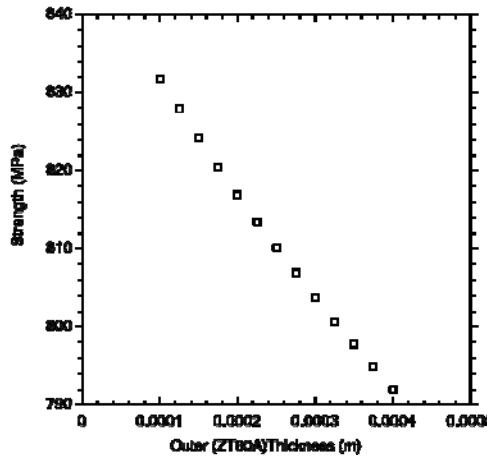


Figure 3. Predicted Strength for ZT60A/ZT40A layered composites as a function of outer layer (ZT60A) thickness for surface failure

Based on the analysis presented, it is possible to enhance the fracture strength of ZTA composites by surface compressive stresses introduced during joining by high-temperature plastic deformation. Strength enhancements of 20 percent can be expected for the composite ZT60A/ZT40A/ZT60A used in the

analysis and are experimentally demonstrated in this paper.

Experimental Procedures

Sample fabrication

Zirconia toughened alumina with compositions of 40 vol.% and 60% alumina (ZT40A and ZT60A respectively) were made from commercial powders: Al₂O₃ from Malakoff Industries, Malakoff, TX (average particle size 0.7 μm), and 3 mol% Y₂O₃-stabilized ZrO₂ from Tosoh Corporation Ceramics, Bound Brook, NY (average particle size 0.3 μm). Powders were ball-mixed in a solution of isopropanol alcohol with 2 ml of Witco Emphos PS-21A and 2% wt. of an organic binder for 12 hours. The resultant mixture was dried and then milled with pestle and mortar and subsequently sieved through a 60 mesh. Rectangular pellets were cold pressed at 250 MPa, and sintered in air at 1450 °C for 4 hours. The heating rate was 40°C/hour up to 400°C and 120°C/hour until sintering temperature was reached. Samples were cooled down at 120°C/hour to room temperature. Dense (~95%) pellets of approximately 26 mm x 5 mm x 5 mm were obtained. In order to reveal the microstructure, samples of each composition were polished up to 1 μm diamond paste and thermally etched for 30 minutes at 1200 °C for microstructural evaluation.

Joining

Joining experiments were carried out on as-sintered samples in a constant crosshead speed on a universal testing system (Instron Model 1125, Canton, MA) equipped with a high-temperature furnace. Two ZT60A bar samples were placed in the furnace chamber such that they sandwiched the ZT40A bar. Joining tests were performed in argon atmosphere at 1350°C and at a strain rate of $5 \times 10^{-6} \text{ s}^{-1}$ up to a final strain of 4 to 5 percent. Typical stresses reached during joining process were 30 to 40 MPa. Test conditions were chosen to guarantee plastic flow without grain growth. After joining, layered samples were ground and polished such that the outer layers (ZT60A) had a nominal thickness of 0.4 mm, whereas inner layer (ZT40A) was 3.5 mm.

Microstructural and phase evaluations

After flexural tests, sample sections taken far away from failure locations were cross-sectioned and polished up to 1 μm diamond paste, followed by thermal etching for 30 minutes at 1200 °C. Finally the sample was coated with carbon for microstructural observation by Electron Scanning Microscopy (SEM) using a Hitachi Model S-4700-II (Tokyo, Japan).

X-Ray diffraction scans, using an analytical x-ray diffractometer model Philips X'Pert MPD System (The Netherlands), were carried out on each composite sample in order to ensure that no phase changes occurred in the composite constituents, particularly, zirconia, as a result of sample preparation. As-sintered, ground, and thermally etched samples of each type were analyzed. Cu_{ka} radiation was used for analysis and samples were scanned over 20 to 90° range at an interval of 0.001°.

Flexural test

Fracture tests using a 4-point-bend method were performed at room temperature on the ZT40A, ZT60A, and layered composites, at a constant crosshead speed on an Instron universal testing system (Model 4505, Canton, MA) using hardened steel fixtures. The inner and outer loading spans were 10 mm and 20 mm, respectively. The imposed loading rate was 0.5 mm/min. A total of 3 to 4 samples were tested for each material type and the fracture strength was calculated using the maximum load at failure. To identify the flaws that nucleated failure in the layered structure, fractographic analysis was conducted using an SEM.

Residual stresses measurement

X-ray micro-diffraction was performed on beamline 20-ID of the Advanced Photon Source, Argonne National Laboratory. A 10 keV x-ray beam was selected by a double-crystal Si (111) monochromator and then focused by a Kirkpatrick-Baez mirror. The focused x-ray beam ($1 \times 1 \mu\text{m}^2$) was incident on the cross-section plane of the layered sample. The x-ray beam was parallel to the interface between the layered sample. The angle between the sample cross-section plane and the incident x-ray beam was 12°. The sample was scanned in the vertical direction with a line-scan step size of 20 μm. The diffracted x-rays

at different locations along the cross section were collected by a two-dimensional charge-coupled device (CCD) x-ray detector, which was placed 150 mm away from the sample. An x-ray fluorescence detector was also used to examine the chemical elements in the layered sample. Fluorescence signal from trace Cu impurities in the sample was used to locate the boundary between two adjacent layers.

Results

Microstructural and x-ray analysis

Microstructures of the as-fabricated ZT40A and ZT60A samples are shown in Figure 4. Average grain sizes for zirconia (lighter phase) and alumina (darker phase) were 0.3 and 0.7 μm respectively. As shown in these micrographs, the samples are close to being fully dense.

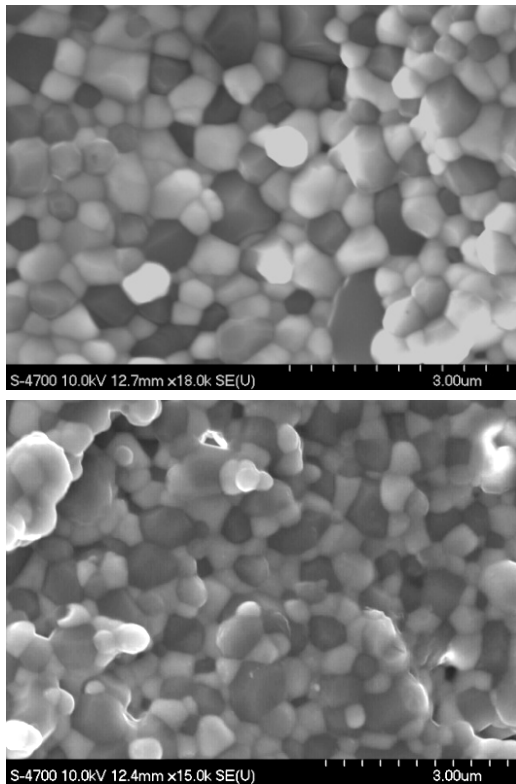


Figure 4. Microstructures of (top) zirconia toughened 40 vol.% alumina and (bottom) zirconia toughened 60 vol.% alumina

Figure 5 shows the interface of the sample after joining. Arrows indicate the interface. The joint is dense and has no visible residual porosity. Closer examination reveals that the grains on the joining

surfaces interpenetrate to accomplish the joining process.

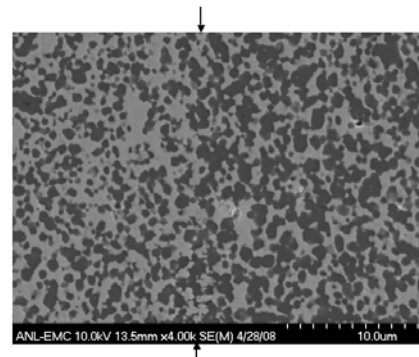


Figure 5. SEM micrograph of the joined interface of ZT40A (left) and ZT60A (right). Arrow indicates the location of the interface. Darker phase is alumina.

A typical XRD pattern for an as-fabricated ZT40A sample is shown in Figure 6. Peaks for both zirconia and alumina are present. Further, for zirconia phase, both tetragonal and cubic phases are present. Ratio of tetragonal to cubic zirconia phases was estimated to be 3:1 [6]. However, as a result of sample preparation (grinding and polishing) there was emergence of monoclinic zirconia phase and its content was estimated as approximately 8 percent. It should be noted that similar XRD patterns are obtained for ZT60A with stronger alumina peaks.

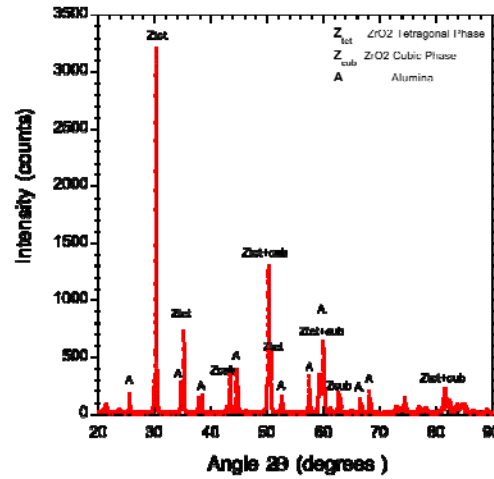


Figure 6. XRD pattern of ZT40A composite sample

Flexural test

Four-point-bend tests were carried out on the ZT40A, ZT60A, and joined ZT60A/ZT40A/ZT60A samples at ambient temperatures. Outer layers of the joined material were ground down to the chosen layer

thicknesses (0.45 mm) with a constant (3.5 mm) inner layer prior to the flexural testing. The average fracture strengths for layered ZT60A/ZT40A/ZT60A samples were 707 ± 81 MPa versus 480 ± 45 MPa for ZT40A and 410 ± 120 MPa for ZT60A and are shown in Figure 7.

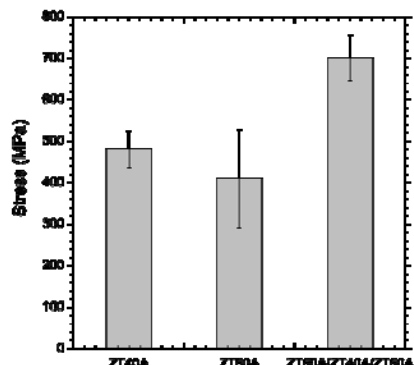


Figure 7. Flexural strength of ZT40A, ZT60A, and layered ZT60A/ZT40A/ZT60A samples

Fractographic analysis of the layered samples after flexure tests showed no evidence of failure initiation at the interface in any of the samples. Figure 8 shows a fractured layered structure with a fracture initiation from the outer (ZT60A) surface. In addition, location of the ZT40A/ZT60A interface can also be seen.

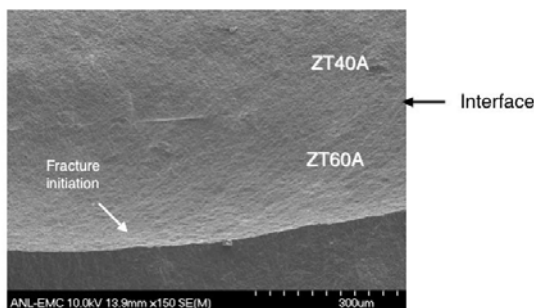


Figure 8. SEM of ZT60A/ZT40A/ZT60A layered structure tested in flexure showing fracture initiation from the surface of ZT60A outer layer.

Residual Stress

Figure 9 shows a typical 2-D micro-diffraction pattern of the layered sample collected by the CCD detector. Partial rings shown in the image were formed by x-rays diffracted from different crystal planes of tetragonal zirconia. The (103) diffraction ring was selected for analysis due to its more uniform intensity distribution. To calculate the residual strain on the sample, two segments of the ring (around $f = 0^\circ$ and 50°) were selected as shown in Figure 8,

where ϕ is the azimuth angle. Integration of the ring segments gives diffraction peaks from which the lattice spacings (d) for specific f can be obtained. The d -versus- $\sin^2\psi$ method was used to calculate the deviatoric strain, where ψ is the angle between the specimen and the crystal coordinate systems [7]. The azimuth angle f is related to ψ according to the simple geometric relationship between the incident x-rays, sample, and x-ray detector. In the d -versus- $\sin^2\psi$ plot, d values obtained at $\psi = 0^\circ$ and 90° give the out-of-plane and in-plane lattice spacings, respectively. The strain-free lattice spacing can be obtained by taking the d value at $\psi = 63^\circ$, assuming a Poisson's ratio of 0.26 for the sample. These three d values were used to calculate the deviatoric in-plane and out-of-plane strains.

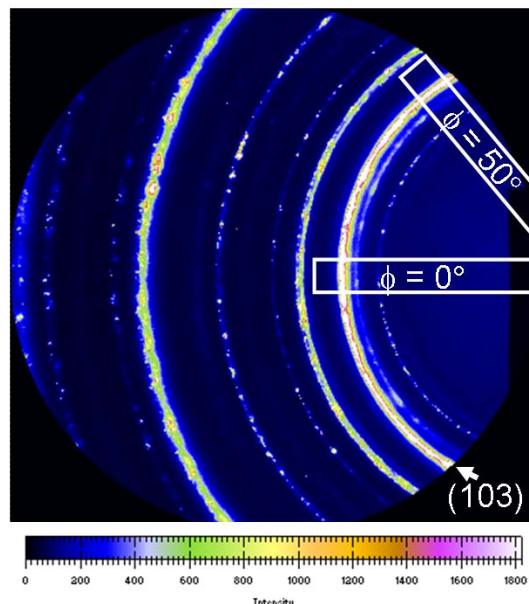


Figure 9. A typical x-ray microdiffraction pattern of the layered sample.

Figure 10 shows the distribution of in-plane residual strain at different locations along the cross section of the layered sample. An interesting feature can be observed near the joint of the top and the middle layers. In the top layer (ZT60A) near the joint, the strain is compressive, while in the middle layer (ZT40A) near the joint the strain is tensile. There is a sharp transition from compressive to tensile strain at the interface. The magnitude of the maximum strain in both cases was about 0.1 percent, and the estimated error in strain was ± 0.05 percent. In both the top and the middle layer, the magnitude of strain decreases as the location moves away from the joint,

and it becomes a constant at about 100 μm away from the joint interface.

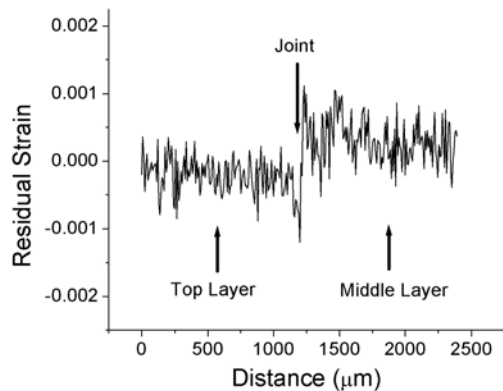


Figure 10. Distribution of deviatoric in-plane strain along the cross section of the layered sample.

Discussion

Flexural strength tests on the ZT60A/ZT40A/ZT60A layered structure fabricated by plastic joining show higher strengths over the bend strengths of ZT60A and ZT40A composites individually. The strength enhancement (707 MPa) is close to 47 percent over the higher strength ZT40A phase (480 MPa) and 70 percent over than the ZT60A composite (410 MPa). As discussed in the Material Design section, the strength enhancement is attributed to the compressive residual stresses generated in the outer layer. Figure 11 shows the strength prediction based on Equation 7 as a function of outer layer thickness and the measured bend strength of the layered structure. This prediction uses the actual thicknesses of the layers in the samples tested and the measured strengths for ZT40A and ZT60A in this study. The predicted value, at an outer layer thickness of 0.0045 m, is 615 MPa. The experimentally observed values were 707 MPa, which exceeds the prediction by 15 percent. It should be noted that the scatter in the measured value of the layered structure is ± 81 MPa. Further, there may be errors introduced from the assumptions in material parameters (E , v , CTE) used for the calculations.

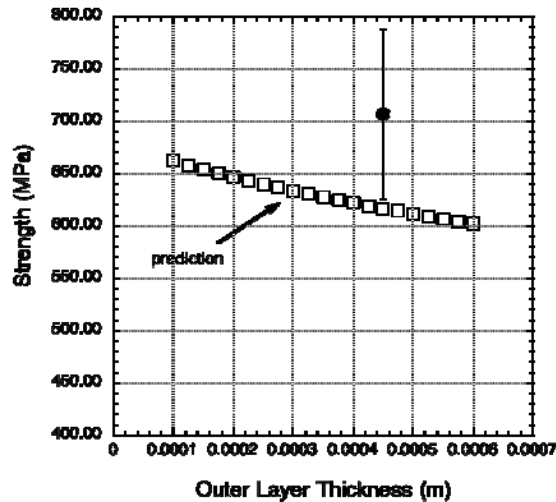


Figure 11. Comparison of experimentally measured flexural strength with the prediction for the layered structure as a function of the outer layer thickness

Since the failure location is at the surface of the outer layer, compressive residual stresses counteract the applied tensile stresses during the bend test. From the residual strain measurements, it appears that the strain difference between ZT40A and ZT60A is large (0.0008) near the interface and drops to about 0.0005 at regions away from the interface. It should be noted that these in-plane strains are estimated only from the shift in the diffraction peak of zirconia phase only. Using elastic modulus for ZT60A as 320 GPa (Table 1), compressive stress in the ZT60A layer is estimated as 280 MPa close to the interface and 160 MPa at regions away from the interface. These values bound the calculated value (from Equation 5) of about 213 MPa for a similar geometry of the layered structure.

Gutierrez-Mora et al. [3] estimated residual stresses across the interface in joined ZT20A/ZT80 sample using a micro-indentation technique. They measured residual stresses parallel (in-plane) as well as tensile stresses perpendicular to the interface as a function of distance from the interface. Their values for in-plane residual compressive stresses were as high as 300 MPa near the interface but were reduced to about 200 MPa at 200 μm away from the interface in ZT80A. These higher values are probably the result of large CTE mismatch between the joined ZT20A and ZT80A samples and the larger differences in their Young's moduli.

As evidenced by the SEM micrograph of Fig. 8, failure location in the joined layered structures was at the surface. The failure appears to initiate from a surface flaw resulting from sample surface preparation. Thus, for qualitative assessment of fracture strength of ZT60A in the layered structure, residual compressive stress of 160 MPa can be superimposed on the ZT60A strength of 410 MPa. This yields a value of 570 MPa, which is lower than the average strength of 707 MPa observed for the layered structure. The discrepancy between predicted and observed strengths for ZT60A could be because of different fracture causing flaw population in the ZT60A composite and the ZT60A outer layer in the joined layered structure.

The fracture strength in ZTA composites increases monotonically with zirconia content. This behavior has been reported in the literature for ZTA composites materials [4]. The fracture strength values obtained through this work are lower than the ones reported by Gutierrez-Mora et al. for the monolithic ZT40A and ZT60A composites. This might be due to lower density (95 percent of theoretical) observed in this study as compared to density (greater than 99 percent of theoretical) reported by Gutierrez-Mora et al. [4]. These differences could be introduced during the material fabrication from batch to batch. Nevertheless, it is important to note that the enhancement of greater than 40 percent for the fracture strength over just ZT40A, the higher strength constituent.

Finally, strength or toughness enhancement in zirconia ceramic systems can result from the tetragonal to monoclinic phase transformation. However, XRD analysis for the phases in ZT60A composite and ZT60A in the layered structure showed similar phases with the presence of small fraction of monoclinic zirconia. Thus, it appears the strength enhancements observed in this study are entirely due to the compressive residual stresses.

Conclusions

We have taken techniques and results from two projects, joining by plasticity, and measurements of residual stresses in superhard, nanocrystalline coatings and applied lessons learned to a graded composite structure. Residual stresses arising from thermal expansion mismatches can be used positively in strength and reliability enhancements of structural

ceramics and composites. Zirconia toughened alumina composites with two different compositions (40 vol. % alumina and 60 vol. %) were joined by a plastic deformation process to produce a layered structure. Residual compressive stresses in the outer 60% vol. alumina layer resulted in strength improvements of 60 percent over bulk zirconia containing 60 vol.% alumina. Results were explained on the basis of a stress analysis and measurement of residual stresses. Experimentally measured strength increase of the layered structure agrees, with the experimental scatter, with the calculations. The strategy for materials design discussed here can be utilized in producing high reliability ceramic components as well as in the repair of existing components.

Future Direction

We will continue to develop the indentation technique to measure surface adhesion energies. We will also explore the applicability of using residual stresses to increase fracture strength at elevated temperatures, but below the stress relaxation temperatures.

References

1. K.C. Goretta, D. Singh, N. Chen, F. Gutierrez-Mora, M. de la Cinta Lorenzo-Martin, A. Dominguez-Rodriguez, J. L. Routbort, *Matls. Sci. Eng. A* 498, 12-18 (2008).
2. T. Nagano, F. Wakai. *J. Mater Sci.* 28, p5793 (1993)
3. F. Gutierrez-Mora, K.C. Goretta, S. Majumdar, J.L. Routbort, M. Grimdisch, A. Dominguez-Rodriguez, *Acta Materialia* 50, p3475 (2002)
4. F. Gutierrez-Mora, D. Singh, N. Chen, K.C. Goretta, J.L. Routbort, S.H. Majumdar, A. Dominguez-Rodriguez. *J. of European Ceramic Society*, 26 961-965 (2006)
5. A. V. Virkar, J. L. Huang, and R. A. Cutler, *Journal of the American Ceramic Society*, 70 [3], p 164 (1987)
6. C.J. Howard, P.J. Hill. *Journal of Materials Science* 26, p127, (1991)
7. V. Hauk, *Structure and Residual Stress Analysis by Nondestructive Methods* (Elsevier, Amsterdam, 1997), Chap. 2, pp. 132–215.

This document highlights work sponsored by agencies of the U.S. Government. Neither the U.S. Government nor any agency thereof, nor any of their employees, makes any warranty, express or implied, or assumes any legal liability or responsibility for the accuracy, completeness, or usefulness of any information, apparatus, product, or process disclosed, or represents that its use would not infringe privately owned rights. Reference herein to any specific commercial product, process, or service by trade name, trademark, manufacturer, or otherwise does not necessarily constitute or imply its endorsement, recommendation, or favoring by the U.S. Government or any agency thereof. The views and opinions of authors expressed herein do not necessarily state or reflect those of the U.S. Government or any agency thereof.

A Strong Energy Portfolio for a Strong America

Energy efficiency and clean, renewable energy will mean a stronger economy, a cleaner environment, and greater energy independence for America. Working with a wide array of state, community, industry, and university partners, the U.S. Department of Energy's Office of Energy Efficiency and Renewable Energy invests in a diverse portfolio of energy technologies.

For more information contact:
EERE Information Center
1-877-EERE-INF (1-877-337-3463)
www.eere.energy.gov